SYNTHESIS, CHARACTERIZATION AND BIOLOGICAL APPLICATIONS OF COMPLEXES OF BISTHIOSEMICARBAZONES WITH TRANSITION METALS (Co, Ni, Cu, Zn)

Thesis Submitted for the Award of the Degree of

DOCTOR OF PHILOSOPHY

in

Chemistry

By

QURAT UL AIN

Registration Number: 11919634

Supervised By

Dr. Rekha Sharma

Department of Chemistry,
School of chemical engineering and physical sciences
Lovely Professional University, Punjab

Co- Supervised By

Dr. Kamaldeep Paul

Department of Chemistry and Biochemistry,
Thapar Institute of Engineering and
Technology, Patiala Punjab

LOVELY PROFESSIONAL UNIVERSITY, PUNJAB

2024

DECLARATION

I, hereby declared that the presented work in the thesis entitled "Synthesis, characterization and biological applications of complexes of bisthiosemicarbazones with transition metals (Co, Ni, Cu, Zn)" in fulfillment of degree of **Doctor of Philosophy (Ph.D.)** is the outcome of research work carried out by me under the supervision of Dr. Rekha Sharma, working as Professor, in the Department of Chemistry, School of Chemical Engineering and Physical Sciences, Lovely Professional University, Punjab, India. In keeping with the general practice of reporting scientific observations, due acknowledgements have been made whenever the work described here has been based on the findings of other investigator. This work has not been submitted in part or full to any other University or Institute for the award of any degree.

(Signature of Scholar)
Qurat Ul Ain
Registration No.:11919634
Department of Chemistry,
School of Chemical Engineering and Physical Sciences,
Lovely Professional University, Punjab, India

CERTIFICATE

This is to certify that the work reported in the Ph. D. thesis entitled "Synthesis, characterization and biological applications of complexes of bisthiosemicarbazones with transition metals (Co, Ni, Cu, Zn)" submitted in fulfillment of the requirement for the reward of degree of **Doctor of Philosophy (Ph.D.)** in the Department of Chemistry, School of Chemical Engineering and Physical Sciences, Lovely Professional University, is a research work carried out by Qurat Ul Ain, 11919634, is bonafide record of her original work carried out under my supervision and that no part of thesis has been submitted for any other degree, diploma or equivalent course.

(Signature of Supervisor)

Dr. Rekha Sharma
Professor
Department of Chemistry,
School of Chemical Engineering and Physical Sciences,
Lovely Professional University, Punjab India

DEDICATION

This doctoral thesis is whole-heartly dedicated to my parents

Mr. Nazir Ahmad Najar

And

Mrs. Shakeela Begum

Whose Prayers, efforts and wishes are an inspiration for me and make me able to get such success and honor. Along with hard work, gracious consideration and affection towards me of my supervisor **Dr. Rekha Sharma**.

ACKNOWLEDGEMENT

Completing a PhD is an extraordinary accomplishment, one that I still struggle to fully comprehend. It feels surreal to realize that I have reached this monumental milestone in my academic journey at School of Chemical Engineering and Physical Sciences, Lovely Professional University. Firstly, I offer all praises and thanks to ***Allah*** *for His blessings and strength that have enabled me to complete this thesis. I extend my heartfelt gratitude to my supervisor,* ***Dr. Rekha Sharma*** *for her unwavering guidance and support throughout this journey, which allowed me to deepen and refine my research. The results presented in my thesis would have been impossible without their guidance. Her constructive feedback and invaluable suggestions during the experimental phase and thesis writing process have greatly contributed to the success of this research. Besides my supervisor, I am with immense gratitude to my co-supervisor* ***Dr. Kamaldeep Paul*** *from School of Chemistry and Biochemistry, Thapar Institute of Engineering and Technology, Patiala for his expertise in this field and provision of necessary facilities for my research work. My gratitude extends to* ***Dr. Iqubal Singh*** *for their tremendous advice and support during the duration of my research. I am also grateful to* ***Dr. Kailash Chandra Juglaan****, HOS, School of Chemical Engineering and Physical Sciences, Lovely Professional University, Punjab, for allowing me to become a scholar and providing the necessary facilities for my research.*

I would like to express my heartfelt appreciation to all the faculty members of the Department of Chemistry of School of Chemical Engineering and Physical Sciences, Lovely Professional University. I would also like to express my sincere appreciation to the non-teaching staff of the department. I am grateful to all of my teachers and well-wishers particularly Dr. Umar who provides his good time to help in formatting my thesis, Dr. Rameez, Aiman sherwani and Dr. Aaliya for their support and encouragement during my career both intentionally and unintentionally.

I would especially like to thank my roommates Shaakira Malik and Mankomal Arora for spending these research years together and the restless nights we spent prior to deadlines. It would not have been possible to carry out this research without their emotional support and invaluable assistance. I must extend my sincere thanks to all my dear friends especially Aasima Firdous, Sabreen Bashir, Tanzeela Qadir and Nancy George for their consistent encouragement, timely support, unconditional love, and spiritual support during this hard time. I would like to thank my colleagues Mir irtiqa and Sheikh insha for their timely help and cooperation.

Last but not least, I am heartly thankful to my parents Mrs. and Mr. Nazir Ahmad Najar who made this thesis journey beautiful and are constant support for my success. This acknowledgment extends heartfelt thanks to all my family members especially my brothers Mr. Arif nazir, Javid nazir, Irshad nazir, Zubair nazir and Owais Amin who have been a pillar of support and encouragement. Their unwavering belief in my capabilities and understanding during challenging times were instrumental. I am grateful to my Bhabhi's who are not less than sisters have contributed much during this journey. Heart touching thanks to my nieces who lowers the research stress by their sweetly actions.

(***Qurat Ul Ain***)

Date: 01-05-2024

Place: Lovely Professional University, Punjab

GLOSSARY OF ABBREVATIONS

KBr	Potassium bromide
FTIR	Fourier Transfer Infra-Red
^{1}H NMR	Proton Nuclear Magnetic Resonance
^{13}C NMR	Carbon Nuclear Magnetic Resonance
DMSO	Dimethyl sulfoxide
TMS	Tetramethyl silane
2,3bitsc, $H^{1}L$	2,3-isatin bisthiosemicarbazone
2,3bitsc N-Me, $H^{2}L$	2, 3-isatin bis-N-methyl thiosemicarbazone
2,3bitsc N-Ph, $H^{3}L$	2,3-isatin bis-N-phenyl thiosemicarbazone
2,5bttsc, $H^{4}L$	2,5 thiophene dicarboxaldehyde Bisthiosemicarbazone
2,5 H_2bttsc N-Me, $H^{5}L$	2,5 thiophene dicarboxaldehyde bis-N-methylthiosemicarbazone
2,5 H_2bttsc N-Ph, $H^{6}L$	2,5 thiophene dicarboxaldehyde bis-N-phenylthiosemicarbazone
2,5 H_2bptsc, $^{7}H_2L$	2,5-Piperazine bisthiosemicarbazone
2,5 H_2bptsc N-Me, $^{8}H_2L$	2,5-Piperazine bis N-methyl thiosemicarbazone
2,5 H_2bptsc, $^{9}H_2L$	2,5-Piperazine bis N-phenyl thiosemicarbazone
2,6 H_2bdptsc, $^{10}H_2L$	2,6 Diacetyl pyridine bisthiosemicarbazone
2,6 H_2bdptsc N-Me, $^{11}H_2L$)	2,6 Diacetyl pyridine bis N-methyl thiosemicarbazone
2,6 H_2bdptsc N-Ph, $^{12}H_2L$	2,6 Diacetyl pyridine bis N-phenyl thiosemicarbazone
PyBTSC	Pyruvaldehyde Bis N-Methyl thiosemicarbazone.

Tri.BTSC	3,5-diacetyl-1,2,4 triazole bis(4N-p-chlorophenyl thiosemicarbazone).
BNMeBTSC	Benzil N-methyl bisthiosemicarbazone.
GTSM2	Glyoxal Bis4,4-Dimethyl-3-thiosemicarbazone.
GTSCM	Glyoxal Bis4-Cyclohexyl-4methyl-3-thiosemicarbazone.
PyTSM2	2,2′-Pyridil Bis4,4-Dimethyl-3-thiosemicarbazone.
PGTSM2	Phenylglyoxal Bis4,4-Dimethyl-3-thiosemicarbazone.
2,3 TBTSC	2,3 thiophene dicarboxaldehyde bisthiosemicarbazone.
CHMTSC	Cyclohexane-1,2-Bis4-methyl-3-thiosemicarbazone.
H2Pu4M4E	Pyruvaldehyde 2-N(4)-methyl and N(4) ethyl bisthiosemicarbazone.
H2Pu4E4M	PyruvaldehydeN(4)-ethyl and 2-N(4)-methyl bisthiosemicarbazone.
H2Pu4M4DE	Pyruvaldehyde2-N(4)-methyl or N(4)-ethyl Bis thiosemicarbazone.
H2Pu4Mpip	PyruvaldehydeN(4)-methyl piperidyl Bis thiosemicarbazone.
H2Pu4Mhex	Pyruvaldehyde hexamethylene iminyl Bis thio-semicarbazone.
PTSM	Pyruvaldehyde-bis(N4-methylthiosemicarbazone).
ATSM	Di-acetyl-bis(N4-methylthiosemicarbazone).
H2Pg4DE	Phenylglyoxal bis N-diethylthiosemicarbazone.

H4DA-PTsz-Me	2,6 diacetylpyridine bis 4-N-methyl thiosemicarbazone.
LMe2H4	Benzil bis4-methyl-3-thiosemicarbazone.
ATS	Diacetyl bisthiosemicarbazone.
PTS	Pyruvaldehyde bisthiosemicarbazone.
GTS	Glyoxal bisthiosemicarbazone.
ATSM2	Biacetyl bis(4,4-dimethyl-3-thiosemicarbazone).
MGTSM2	Methyl glyoxal bis(4,4-dimethyl-3-thiosemicarbazone).
GTSM	Glyoxal bis(4-methyl-3-thiosemicarbazone)
2,5 H_2bttsc, $^{1}H_2L$	2,5 thiophene dicarboxaldehyde bisthiosemicarbazone
2,5 H_2bttsc N-Me, $^{2}H_2L$	2,5 thiophene dicarboxaldehyde bis-N-methyl thiosemicarbazone
2,5 H_2bttsc N-Ph, $^{3}H_2L$	2,5 thiophene dicarboxaldehyde bis-N-phenyl thiosemicarbazone
bitsc, $^{4}H_2L$	Isatin bisthiosemicarbazone
bitsc N-Me, $^{5}H_2L$	Isatin bis-N-methyl thiosemicarbazone
bitsc N-Ph, $^{6}H_2L$	Isatin bis-N-phenyl thiosemicarbazone
2,5bttsc, $^{7}H_2L$	2,5 thiophene dicarboxaldehyde bisthiosemicarbazone
2,5 H_2bptsc, $^{7}H_2L$	2,5-Piperazine bisthiosemicarbazone
2,5 H_2bptsc N-Me, $^{8}H_2L$	2,5-Piperazine bis N-methyl thiosemicarbazone
2,5 H_2bptsc, $^{9}H_2L$	2,5-Piperazine bis N-phenyl thiosemicarbazone
2,6 H_2bdptsc, $^{10}H_2L$	2,6 Diacetyl pyridine bisthiosemicarbazone
2,6 H_2bdptsc N-Me, $^{11}H_2L$)	2,6 Diacetyl pyridine bis N-methyl thiosemicarbazone

2,6 H_2bdptsc N-Ph, $^{12}H_2L$	2,6 Diacetyl pyridine bis N-phenyl thiosemicarbazone
M.P.	Melting point
MS	Mass spectrometry
ESR	Electron spin resonance
VSM	Vibrating sample magnetometer
XRD	X-ray diffractometer
ppm	Parts per million
amu	Atomic mass unit
m	Medium
s	Sharp
w	Weak
t	Triplet
d	Doublet
s	Singlet
Ms	Saturation magnetization
Mr	Remanence magnetization
Hc	Coercivity magnetization
emu	Electromagnetic unit
m/z	Mass/charge
nm	Nanometre
RT	Room temperature
µg/ml	Microgram per milliliter
$Ni(OAc)_2$	Nickel acetate
$Cu(OAc)_2$	Copper acetate

$Co(OAc)_2$	Cobalt acetate
$Zn(OAc)_2$	Zinc acetate
MIC	Minimal inhibitory concentration
Anti-TB	Anti-tuberculous
MABA	Microplate alamar blue assay
S	Sensitive
R	Resistant
IC_{50}	Half-maximal inhibitory concentration
DNA	Deoxyribonucleic acid
HSA	Human serum albumin
ASP	Aspartic acid
PRO	Proline
TYR	Tyrosine
PHE	Phenylalanine
MET	Methionine
GLY	Glycine
ILE194	Isoleucine
SER	Serine
VAL	Valine
ALA	Alanine
TRP	Tryptophan

LIST OF CONTENTS

Abstract

This present thesis illustrates the synthesis and characterization using various spectroscopic techniques of **12** different ligands and their metal complexes **48** with Cobalt ^{II}, Nickel ^{II}, Copper ^{II} and Zinc ^{II}. The synthesized ligands and their metal complexes were characterized by M.P., FTIR, NMR (^{1}H and ^{13}C NMR), ESR (for Cu and Co), VSM (Ni), XRD (Zn) and evaluated against M. tuberculosis H37RV for anti-tubercular activity. Thiosemicarbazide is reacted with different aldehydes or ketones in 2:1 molar ratio to form bisthiosemicarbazones, (2,5 H_2bttsc, ^{1}**H_2L**), (2,5 H_2bttsc N-Me, ^{2}**H_2L**), (2,5 H_2bttsc N-Ph, ^{3}**H_2L**), (2,3bitsc, ^{4}**H_2L**), (2,3 H_2bitsc-N-Me, ^{5}**H_2L**), (2,3 H_2bitsc-N^{-}Ph, ^{6}**H_2L**), (2,5 H_2bptsc, ^{7}**H_2L**), (2,5 H_2bptsc N-Me, ^{8}**H_2L**), (2,5 H_2bptsc N-Ph, ^{9}**H_2L**), (2,6 H_2bdptsc, ^{10}**H_2L**), (2,6 H_2bdptsc N-Me, ^{11}**H_2L**) and (2,6 H_2bdptsc N-Ph, ^{12}**H_2L**). All the synthesized ligands were characterised by M.P., FTIR, NMR (^{1}H and ^{13}C NMR). Reaction of cobalt(II) acetate with ^{1}**H_2L**-^{12}**H_2L** yielded complexes of stoichiometry, [Co(L)] **1-12** molar ratio in 1:1. All the complexes have m/z values in well agreement with proposed stoichiometry. The existence of free electrons in the ground term, $d_{x^2-y^2}$ in tetrahedral environment is confirmed by a larger $g_{\parallel}$ value than $g_{\perp}$. The anti-T.B activity of ligands generally get enhanced upon complexation. It has been noted that enhancing the hydrophobicity of a ligand via substitutions at the N^1 atom typically boosts its anti-T.B activity. For example, the anti-T.B efficacy of ^{1}**H_2L**, which has an (MIC =6.25 µg/ml), is significantly increased when complexed with Co(II) **1**, reducing the (MIC=1.6 µg/ml). Drug-protein binding studies of compounds using (HSA) were conducted utilising ultraviolet-visible and fluorimetry spectroscopy to investigate pharmacokinetics, or the efficient transport of molecules to their target locations. Strong binding interactions were exhibited by the ligand ^{1}**H_2L** and complex (**1)** with HSA. Furthermore, the experimental data is supported by the molecular modeling studies. Low binding energy obtained (-5.8) ^{1}**H_2L**, (-6.68) **1** Kcal/ mol, indicate strong interaction.

Reaction of Nickel (II) acetate with ^{1}**H_2L**-^{12}**H_2L** yielded complexes of stoichiometry, [Ni(L)] **13-24** in molar ratio1:1. All the complexes were characterised using FTIR, Mass, UV-visible and VSM studies. All the complexes have m/z values in well agreement with proposed stoichiometry. The magnetic moment found experimentally was in the range of 2.8-4.62 B.M for complexes **13-24** confirms the tetrahedral geometry. The anti-TB activity of ^{10}**H_2L** (MIC = 50µg/ml) was more increased on complexation with Ni(II) **34** (MIC=12.5µg/ml). The drug-protein binding study of ligand ^{10}**H_2L** and complex (**34)** exhibited strong binding interactions values with HSA. The

minimal binding energies obtained using molecular modelling (PDB ID: 2H7M) is obtained is (-6.4) ^{1}**H$_2$L**, (-7.0) **1** Kcal/ mol, indicate strong interaction, which also supports the experimental data. The reaction of Copper(II) acetate with **^{1}H$_2$L-^{12}H$_2$L** yielded complexes of stoichiometry, [Cu(L)] **25-36** in molar ratio 1:1. All the complexes have m/z values in well agreement with proposed stoichiometry. The square planar geometry for complexes was confirmed from g and *f* (empirical parameter) values obtained from ESR spectra. The anti-TB activity of ^{2}**H$_2$L** and ^{4}**H$_2$L** (MIC = 3.12, 50µg/ml) get enhanced on complexation through Cu(II) (MIC=1.6, 25µg/ml). The most potent ligand ^{2}**H$_2$L,** ^{4}**H$_2$L** and complex **26, 28** have strong binding interactions constant values indicates significant binding interactions with HSA. The experimental data is also supported by the significant intermolecular interaction of these compounds shown by molecular modeling studies with smallest binding energy -5.8 (^{2}**H$_2$L**), -7.6(^{4}**H$_2$L**), -6.6 (**26**) and -8.7 (**28**) Kcal/ mol, Reaction of Zinc(II) acetate with ^{1}**H$_2$L-^{12}H$_2$L** yielded complexes of stoichiometry, [Zn(L)] **37-48** in molar ratio 1:1. All the complexes have m/z values in well agreement with proposed stoichiometry. It was observed that crystalline complexes (**37-39,43-48**) has good crystal size as compared to amorphous complexes (**40-42**) and belongs to different crystal systems. The anti-tubercular activity of ^{9}**H$_2$L** (MIC = 3.12µg/ml) get more enhanced-on complexation with Zinc(II) **45** (MIC=0.8µg/ml). The interaction of ligand with Zinc(II) was more confirmed by the HSA studies. The ligand ^{9}**H$_2$L** and complex (**45)** exhibit high binding interactions with values 3.13×10^{5} M^{-1} and 9.34×10^{5} M^{-1}. In addition, Low binding energy obtained from molecular modelling (-9.1) ^{9}**H$_2$L**, (-12.4) **45** Kcal/ mol, indicate strong interaction, which also supports the experimental data.

CHAPTER- 1

INTRODUCTION

1.1 Introduction of bisthiosemicarbazones

Coordination chemistry, a vital aspect of inorganic chemistry, encompasses a broad range of research focusing on coordination compounds. These compounds exhibit diverse properties across various metals in the periodic table, spanning different coordination numbers and oxidation states. The versatility in their preparation has led to widespread applications in numerous fields, including pharmaceuticals, polymers, paints, fungicides, and more [1]. Additionally, coordination compounds play significant roles in natural processes, exemplified by their presence in chlorophyll, hemoglobin, Vitamin-B complex, and enzymes. Schiff bases, are known for their versatile coordination chemistry, contribute significantly to this realm and further expand the scope and potential applications of coordination compounds [2,3]. Schiff bases exhibit versatile applications across various fields, including separation processes, metallic deactivation, bioinorganic chemistry, catalysis, electrochemistry, and environmental chemistry [4–8]. They are also employed in purifying carbonyl and amino compounds and protecting these groups during complex or sensitive reactions. Furthermore, Schiff bases serve as fundamental units in certain dye compositions [9]. In organic synthesis, reactions involving Schiff base formation are instrumental in establishing carbon-nitrogen bonds. Additionally, Schiff bases serve as crucial intermediates in numerous enzymatic reactions, particularly those involving the interaction between an enzyme and an amino or carbonyl group on the substrate. Notably, catalytic mechanisms in biochemical processes often entail the condensation of a primary amino group of an enzyme, typically a lysine residue, with a substrate's carbonyl group to form an imine [10]. Rising scope of Schiff bases in biological system made them a key area of investigation [11–13]. Schiff bases generated from thiosemicarbazide are one of the examples with lot of pharmacological activities like, antibacterial, antifungal, antitumor, anticancer and antiviral [14–21]. Thiosemicarbazones (I) containing nitrogen, sulfur donor atoms have established notable interests and extensive study scope through variety of bonding modes [22–26], capability of ion-sensing [27–29], catalytic properties [30–33] and biological applications like anti-malarial, anti-viral, radioprotective, trypanocidal, anti-inflammatory, anti-bacterial, anti-fungal, anti-tumor, and anti-amoebic activities [34–38]. Biological significance of thiosemicarbazones increased when its two units are connected by aromatic or aliphatic rings to form bis(thiosemicarbazone) and gets coordinated with transition metals [39,40]. Apart from the various coordination geometries, additional interest in thiosemicarbazone chemistry includes cyclometallation and analytical application [41–43].

Thiosemicarbazones have major biological applications when they form complexes with metal ions because they create chelate N, S-binding pockets that allow metals to be coordinated, which affects biological activity [44–61].

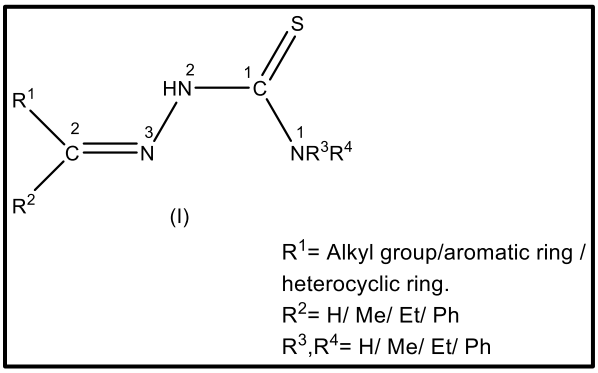

Scheme 1. Chemical structure of thiosemicarbazone

The flexibility of thiosemicarbazones coordination capacity towards various metals twigs from the ease with which R groups at the C^2 and N^1 atoms of thio-ligands might deviate [62], which is also the reason for variable bonding modes exhibited by them. Thiosemicarbazones are divided into two categories: (i) Monothiosemicarbazones; (ii) bisthiosemicarbazones [63].

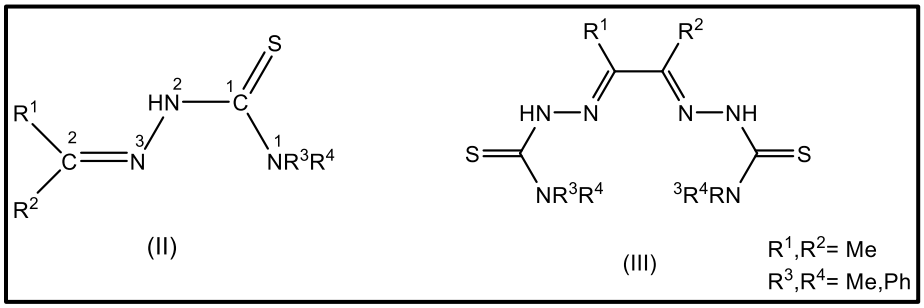

Scheme 2. Structure of (i) Monothiosemicarbazone (II); (ii) bisthiosemicarbazone (III).

As the name suggests, monothiosemicarbazones carry only one thiosemicarbazone moiety, while bisthiosemicarbazones contain two moieties associated by means of their imine nitrogens [64]. A detailed review covering monothiosemicarbazones has already been reported [23,63,65,66].Thus, the current review aims to focus on bisthiosemicarbazones only. Bisthiosemicarbazones have been known for more than 50 years for their significance in anti-tumor, anti-biotic and anti-viral

properties [67]. In the times that followed, it has become apparent that they may also bestow with a suitable way of tagging biologically active molecules, by using metallic radionuclides and fluorescence. Bisthiosemicarbazones, having the two thiosemicarbazone moieties positioned in such a way that the molecule is capable of acting as a tetradentate ligand, are excellent chelating agents. The more importance of these ligands is in the field of biological systems due to the heteroatoms present in the ring. These heteroatoms contain elements such as nitrogen, oxygen, sulphur, and more. Heterocycles have a similar structure to cyclic organic compounds made entirely of carbon atoms. However, replacing one or more carbon atoms with heteroatoms results in distinct physicochemical properties that distinguish them from all-carbon rings. Heterocyclic compounds are highly useful in chemistry and industry due to their unique properties. Heterocycles are a crucial class of chemical molecules having significant applications in various scientific fields. Heterocycles are a fascinating subject of study due to their unique characteristics and structural diversity in chemistry. Heterocycles are essential for sustaining life, playing a vital role in biology by encoding genetic information. The nitrogenous bases adenine and guanine in DNA, and uracil and cytosine in RNA, are heterocyclic molecules. These bases are essential for storing and transmitting genetic information, highlighting the importance of heterocycles in sustaining life. Heterocycles play an important role in both pharmacology and medicine. Many medications and pharmaceuticals on the market incorporate heterocyclic motifs in their structures. The astounding accomplishments highlight the wide range of medicinal uses of these substances. They are flexible targets for synthesis and essential structural components in both medicinal chemistry and chemical synthesis because of their fascinating biological functions. The pharmaceutical industry has demonstrated a great deal of interest in the diverse uses of heterocycles. Thus, heterocyclic molecules are essential in chemistry and can lead to innovation in various fields when complexation with metals.

1.2. Transition metals with bisthiosemicarbazones

Transition elements can be broadly categorized as elements or ions with partially filled d or f sub-shells. However, in a broader context, any element exhibiting partially filled d or f shells in any oxidation state is considered a transition element [68] and d-block elements, often known as transition metals, include elements like Co^{II}, Ni^{II}, Cu^{II} and Zn^{II}. Typically, stable compounds arise from interactions between soft acids and soft bases, as well as hard acids and hard bases [69]. Metals play an important role in biological redox reactions because of their relative stability in

various oxidation states [70]. In addition, due to their broad range of reactivity in permitting different chemical transformations, transition metal catalysts have gained widespread acceptance as practical instruments in contemporary synthetic organic chemistry. Since supporting ligands have been developed, the chemistry has expanded and now has a major impact on the stability and reactivity of metal complexes in the main coordination system [71].

Copper has been used to create bioactive compounds because of its low toxicity. Mycobacterium tuberculosis H37RV strain was significantly inhibited by a number of copper(II) complexes [72–77]. Copper(II) bis(thiosemicarbazone) complexes are of most significance due to their use as anticancer drugs [78],[79]. Anticancer activity of bisthiosemicarbazone can be correlated by i) Cu(II) chelation [80]; ii) its ability to release coordinated Cu(II) inside the cell [17,18]. Since the heterocyclic structure can donate hydrogen or electrons to the acceptors (i.e., DPPH) to decrease the generation of free radicals, their presence in a molecule made them important candidates for investigation of their antioxidant studies. The radio labelled copper complexes have been made possible by short synthesis times, allowing for simultaneous diagnosis and treatment [81–83]. Hamsters with human GW39 colon cancer tumors have been treated with radiolabeled ^{64}Cu(ATSM), which has considerably increased their survival time (6 times)[84]. Bisthiosemicarbazones provided an advantage for the development of kits to support clinical diagnosis and treatment by containing a copper isotope in the radionuclide[68,85]. Cobalt (II) complexes of thiosemicarbazones have been extensively researched and synthesised due to their diverse characteristics. All mammals have cobalt, an essential trace element that functions as a cofactor of vitamin B12, allowing it to control DNA synthesis and preserve normal nervous system and brain function [14]. The production and reactivity of Schiff base ligand cobalt complexes have long been of interest to inorganic chemists [86,87]. For example, cobalamin (B12) coenzymes, dioxygen transporters, and oxygen activators have all been extensively mimicked by cobalt complexes containing tetradentate Schiff base ligands [78,88]. They are also employed as antibacterial agents and for enantioselective reduction [88,89]. Nickel (II) Schiff base complexes with sulphur donors have been studied due to their presence in biological nickel centres, including the active sites of ureases, methyl-S-coenzyme-M-methyl reductase, and hydrogenases [90]. Transition-metal-ion complex Zinc(II), have been extensively studied due to their diverse therapeutic applications, including antiviral and anticancer properties. Zinc(II) compounds of bis(thiosemicarbazone) have shown promise as anti-tubercular and anticancer drugs [91–94].

A number of gallium and indium complexes of bisthiosemicarbazones are also known to be used as potential imaging agents [95–97]. Optical properties shown by thiosemicarbazones get increased in bisthiosemicarbazones due to its capacity to create a number of five-membered chelate rings. This makes that more likely their pharmacological characteristics and coordinated behaviour towards the transition metals is extensively researched [99–102]. Bisthiosemicarbazones are also used as sensors to detect heavy metals [102–105].

1.3. Preparation of bisthiosemicarbazones

Bisthiosemicarbazones can be prepared by condensation of aldehydes or ketones with thiosemicarbazide in 1: 2 molar ratio (IV) [106].

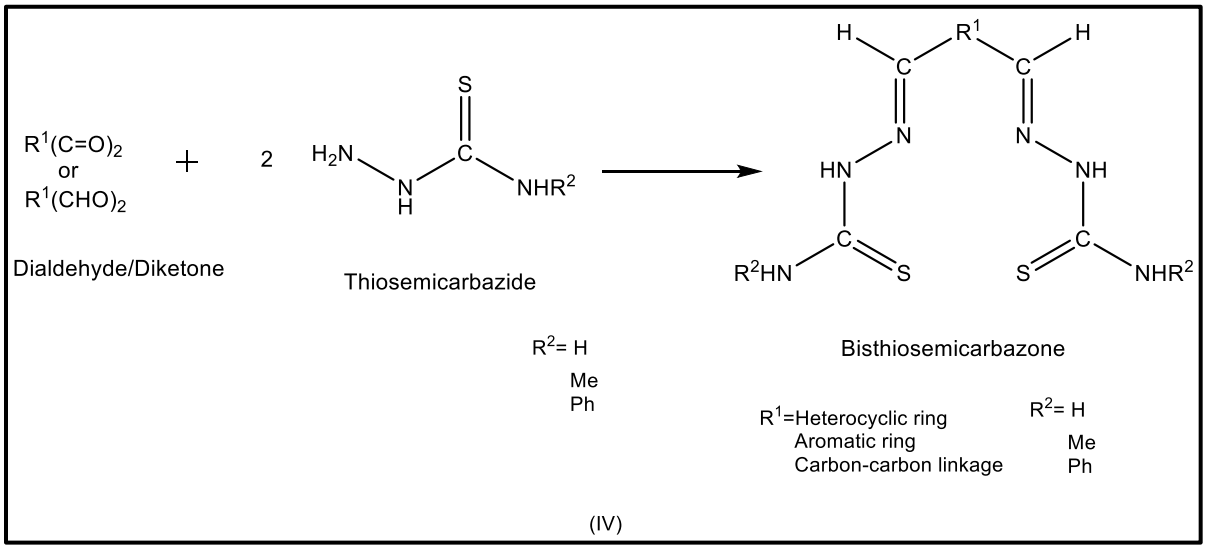

Scheme 3. Schematic representation of bisthiosemicarbazone

1.4. Bonding modes of bisthiosemicarbazones

Bisthiosemicarbazone can coordinate to a metal ion in both neutral and anionic forms, exhibiting a variety of bonding modes. These modes are as follows: i) tetradentate coordinating through two azomethine nitrogen and thin/thiolate sulphur (V); ii) bidentate-cum-bridging coordinative via azomethine nitrogen and thione/thiolate sulphur of one arm to one of the metal atom and second arm to second metal atom (VI); iii) two azomethine nitrogen and one thiolate sulphur binding to one metal atom and second metal atom thus forming sulfur bridge (VII); iv) in the existence of other donor atom, pentadentate (VIII); vii) pentadentate-cum-sulfur bridging (IX) [108,109]. All of the above-mentioned modes have been identified by X-ray crystallography, and in certain cases,

density functional theory (DFT) simulations have also verified the structural description [109–111].

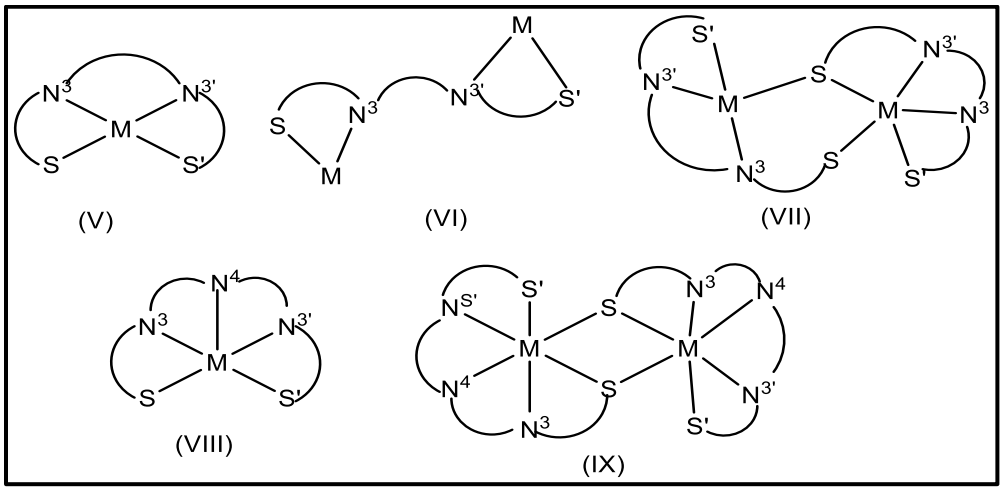

Scheme 4. Bonding modes of bisthiosemicarbazones

CHAPTER- 2

REVIEW OF LITERATURE

2. Review of Literature

It was observed from the literature that a large number of monothiosemicarbazones have already known,[5,112–120] whereas the number of bisthiosemicarbazone reported in literature are comparatively less and can be divided into following types:

2.1 Types of bisthiosemicarbazones: Depending upon the linkage between two thio- moieties, bisthiosemicarbazones can be divided into three different broad categories.

i) Bisthiosemicarbazones with C-C linkage between two thio- moieties

ii) Bisthiosemicarbazones with an aromatic group linking two thio- moieties

iii) Bisthiosemicarbazones with heterocyclic group linking two thio- moieties

2.1.1 Type I. Bisthiosemicarbazones with C-C linkage between two thio- moieties: A number of bisthiosemicarbazones are known with various substituents on carbon atoms of the C-C linkage and amino nitrogen [39,78,82,109,111,121–137]. The ligands with methyl, ethyl or phenyl substituents on C-C linkage are known (**A1**-**A32**). These ligands were prepared by refluxing thiosemicarbazide and diketone in 2:1 molar ratio [121,125] (Table 2.1).

Table 2.1: A list of bis-thiosemicarbazones with C-C linkage between two thio- moieties

1	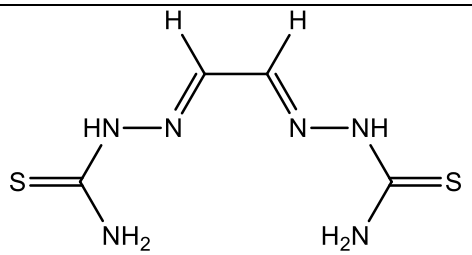 **A1**	2	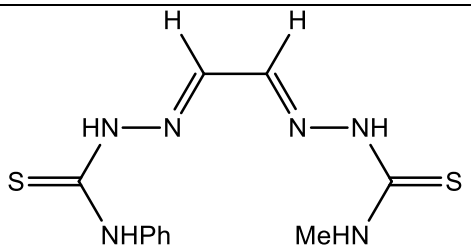 **A2**
3	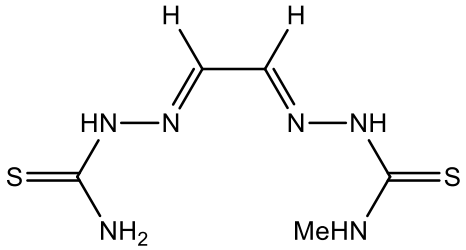 **A3**	4	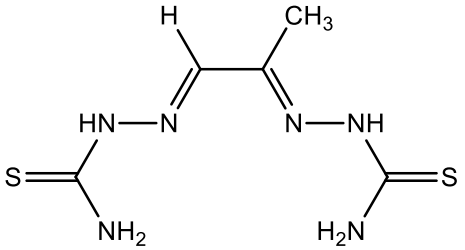 **A4**

5	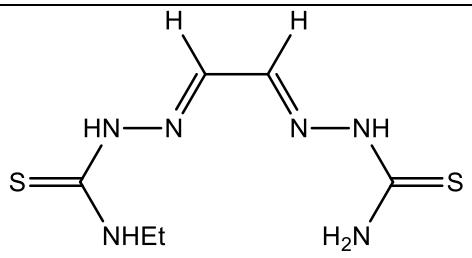 **A5**	6	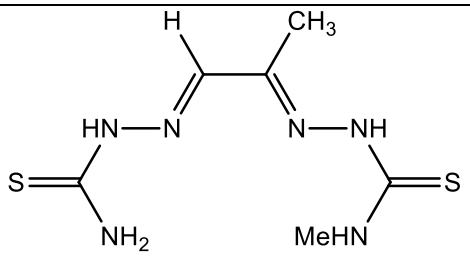 **A6**
7	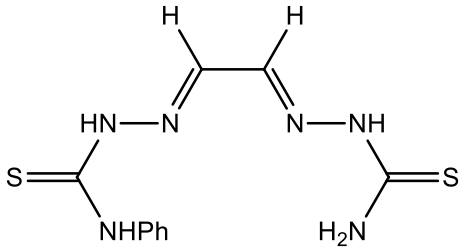 **A7**	8	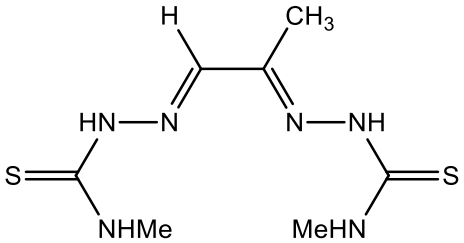 **A8**
9	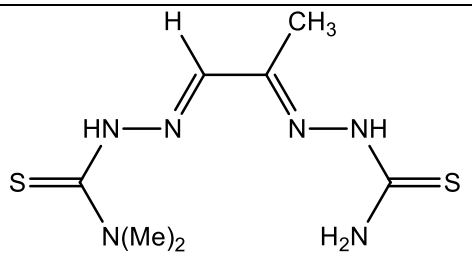 **A9**	10	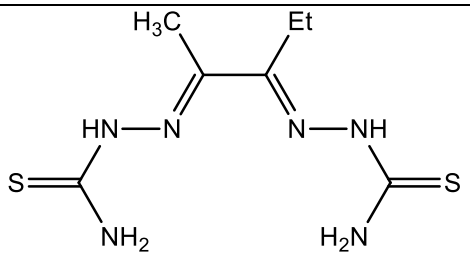 **A10**
11	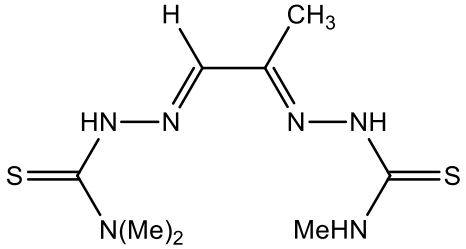 **A11**	12	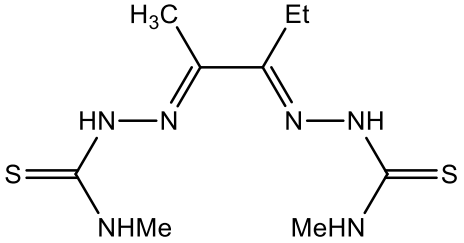 **A12**
13	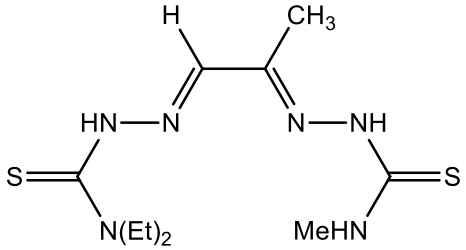 **A13**	14	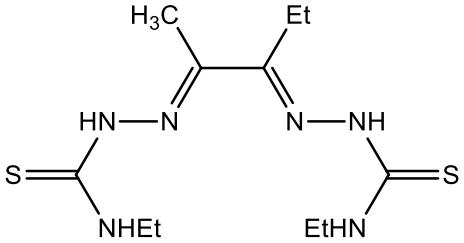 **A14**

15	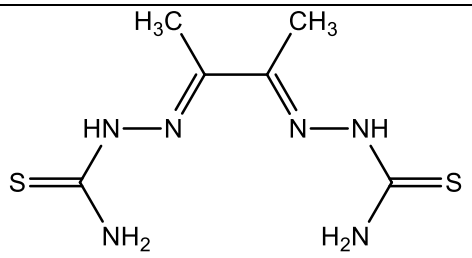 **A15**	16	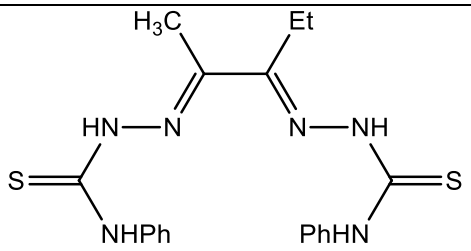 **A16**
17	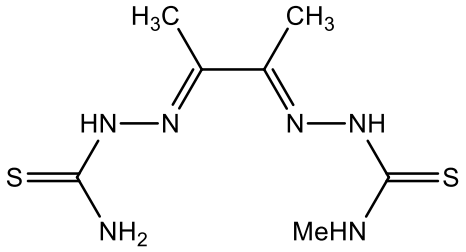 **A17**	18	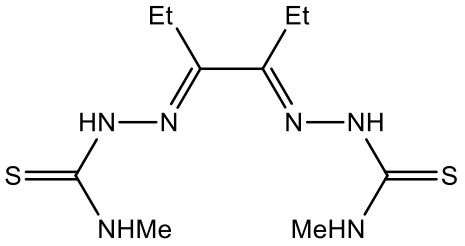 **A18**
19	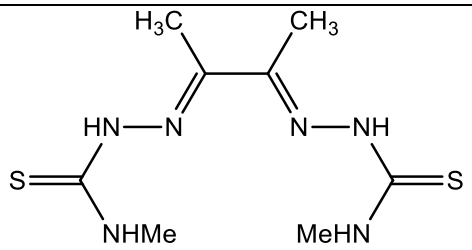 **A19**	20	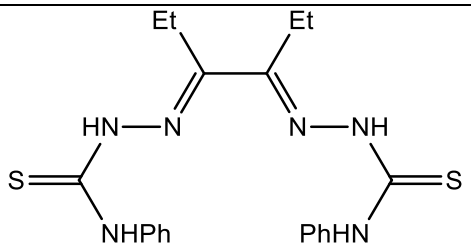 **A20**
21	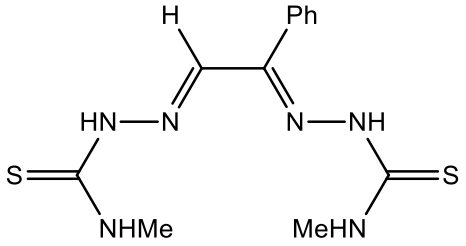 **A21**	22	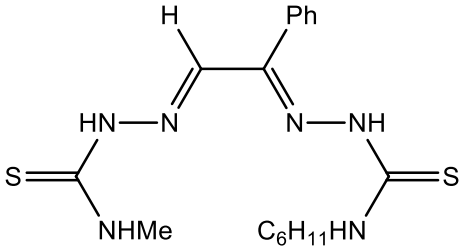 **A22**
23	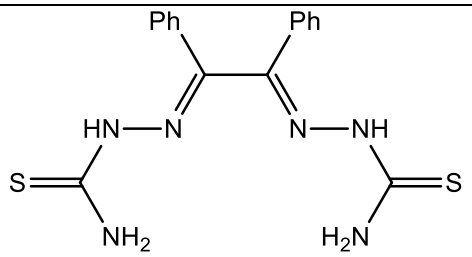 **A23**	24	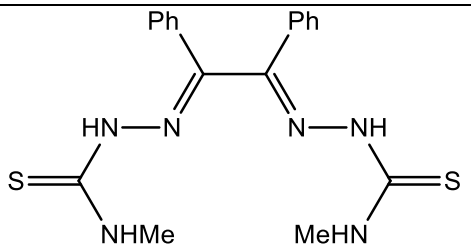 **A24**

25	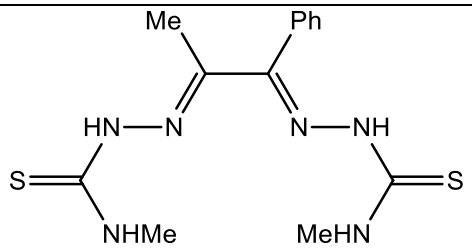 **A25**	26	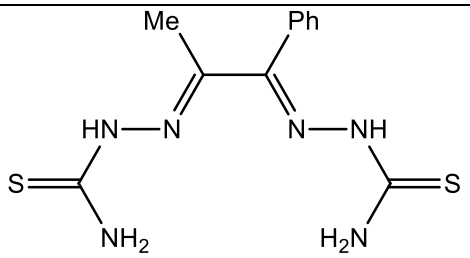 **A26**
27	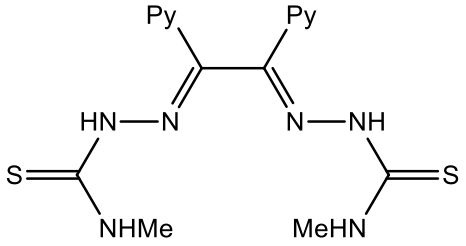 **A27**	28	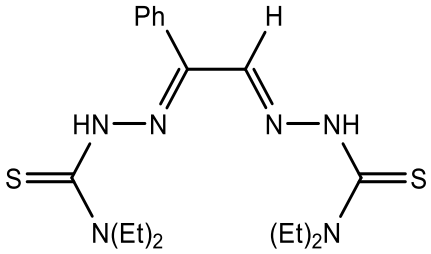 **A28**
29	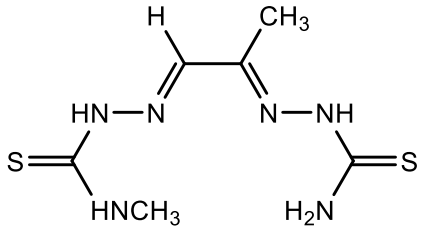 **A29**	30	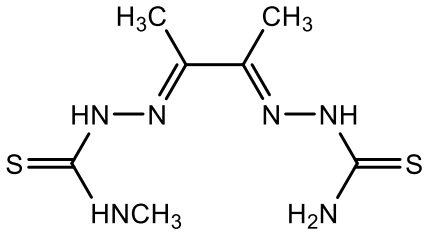 **A30**
31	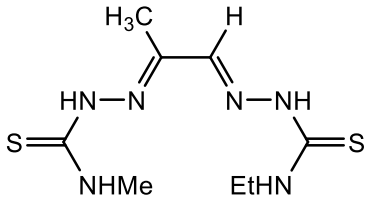 **A31**	32	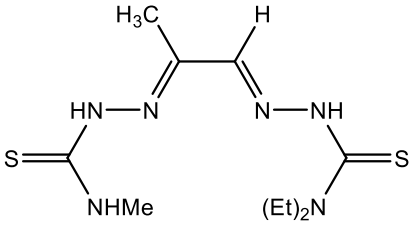 **A32**

2.1.2. Type II. Bisthiosemicarbazones with an aromatic ring linking two thio- moieties: In this type of bisthiosemicarbazone, two thio-moieties are connected through aromatic rings [129–131]. Aromatic rings can be a single benzene ring or two benzenes fused together with one cyclic ring (**B1**-**B8**). Two thio-moieties are connected to benzene ring at 1,4 positions (**B1**-**B3**, **B5**), at 1,6 positions (**B4**) and at 2,6 positions (**B6**, **B7**). Ligands **B5**-**B6**, have either one or two hydroxyl

groups at benzene ring. B4 contains a hydroxyl group on carbon 2 (C2) of bisthiosemicarbazone (Table **2.2**). These ligands were prepared by condensation of dialdehydes (**B1**-**B7**) or diketone (**B8**) with two moles of thiosemicarbazide.

Table 2.2: A list of bis-thiosemicarbazones with aromatic ring linking two thio- moieties

1	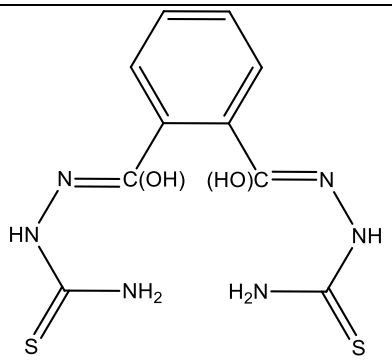 **B1**	2	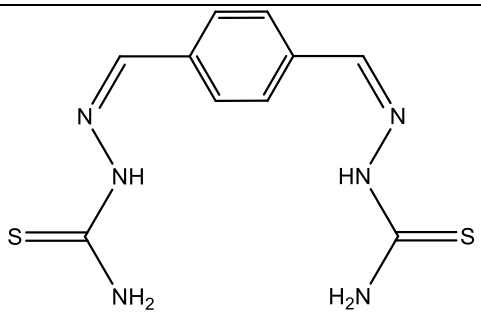 **B2**
3	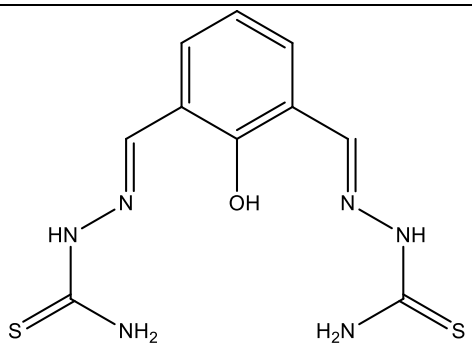 **B3**	4	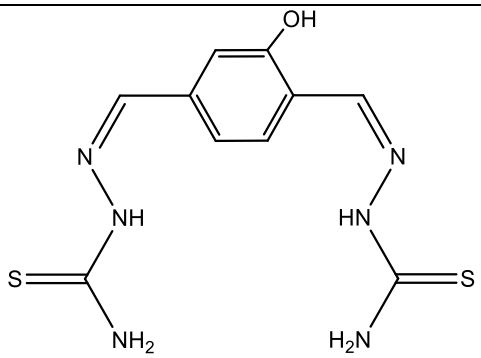 **B4**
5	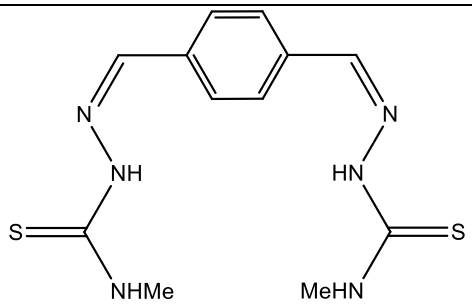 **B5**	6	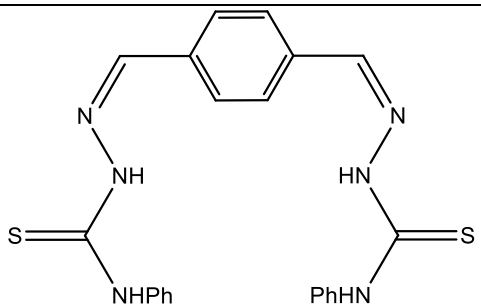 **B6**

7	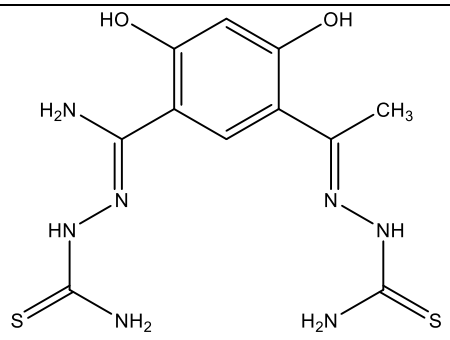 **B7**	8	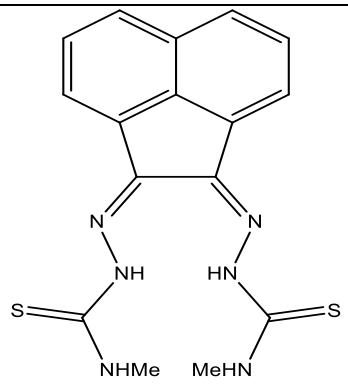 **B8**

2.1.3 Type III. Bisthiosemicarbazones with heterocyclic ring linking two thio-moieties:

In this category of bisthiosemicarbazone ligands, two thio-moieties are connected through a heterocyclic ring (**C1-C17**) [11][130][132–144]. Heterocyclic rings can be five- or six-membered. Rings with one or three heteroatoms are also known. Some ligands contain fused heterocyclic ring (one phenyl and one five membered ring). The bis-ligands with pyridine ring linking the two thio-moieties (C1-C7) in meta with various substituents at the terminal end of both thio-arms. Only one bisthiosemicarbazone containing a five membered heterocyclic ring connecting two thio-moieties (**C8**) is known. The two arms are attached in ortho at the 2,3 positions of thiophene ring [145]. Using a modified procedure, aldehydes are converted into radicals by Fenton type reaction and then reacted with 1,4 pyrazine to form pyrazine-2,5-carbaldehydes. The prepared carbaldehyde was then condensed with two moles of thiosemicarbazide to form corresponding bisthiosemicarbazones [153]. Bisthiosemicarbazone with two thio-arms connected by a phenanthroline ring (C14) and a triazole ring (C15, C16) is also known. These ligands were prepared using the general condensation method (Table 2.3).

Table 2.3: List of bithiosemicarbazones with two thio-moieties joined by heterocyclic rings

1	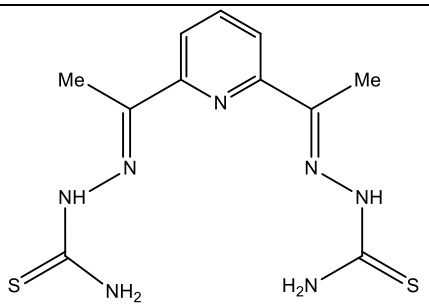 **C1**	2	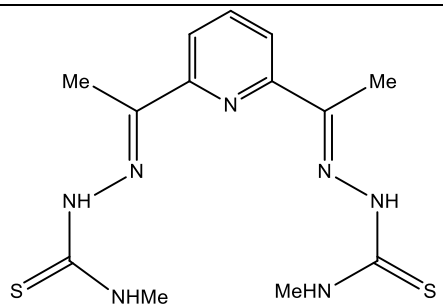 **C2**
3	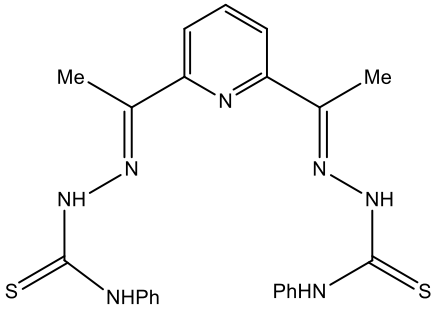 **C3**	4	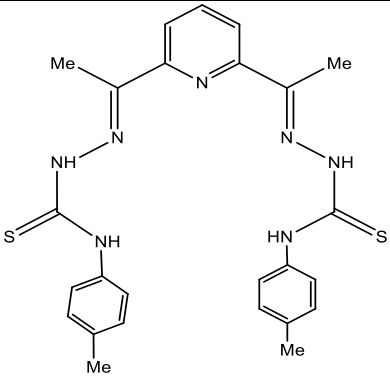 **C4**
5	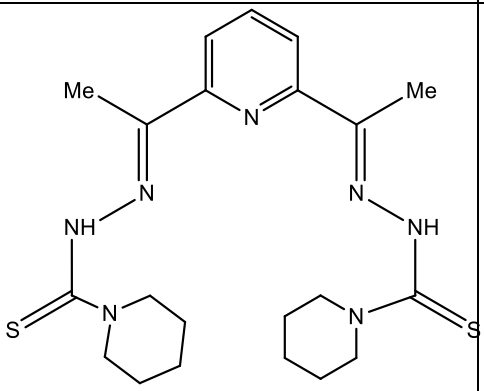 **C5**	6	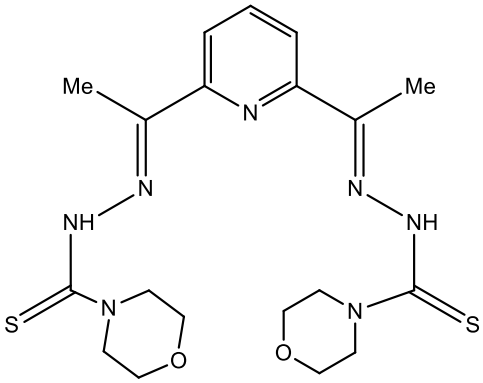 **C6**

7	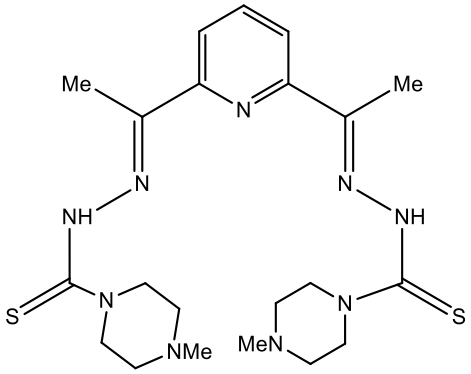 **C7**	8	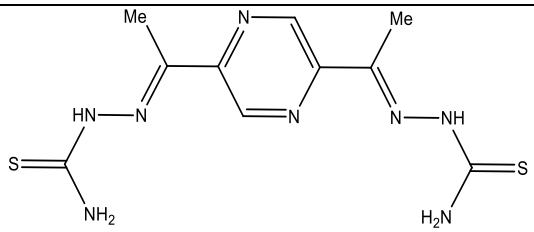 **C8**
9	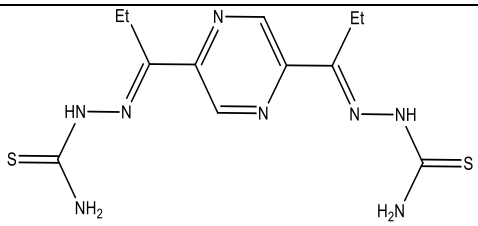 **C9**	10	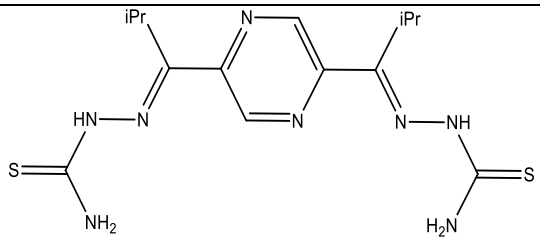 **C10**
11	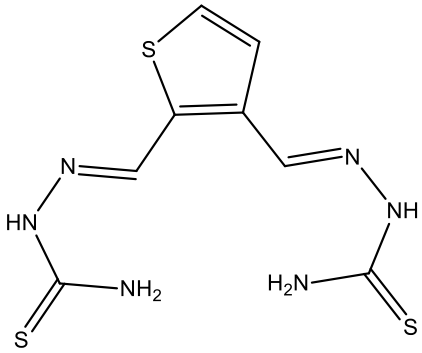 **C11**	12	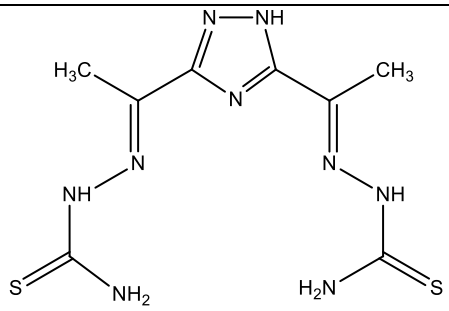 **C12**

13	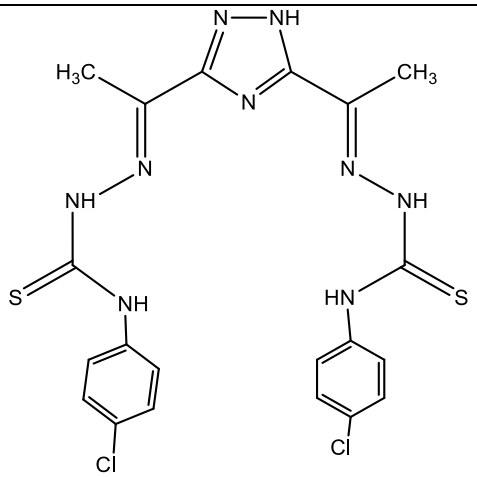 **C13**	14	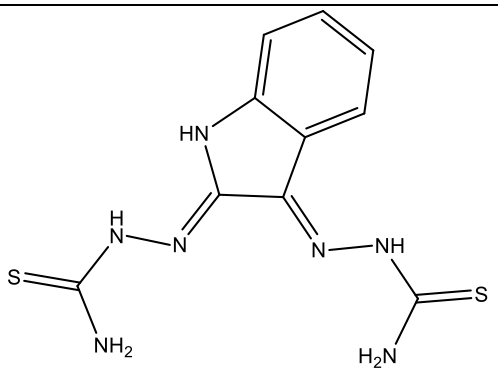 **C14**
15	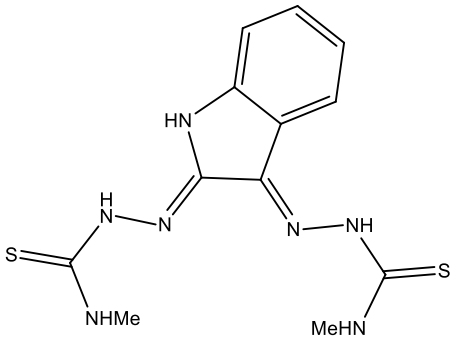 **C15**	16	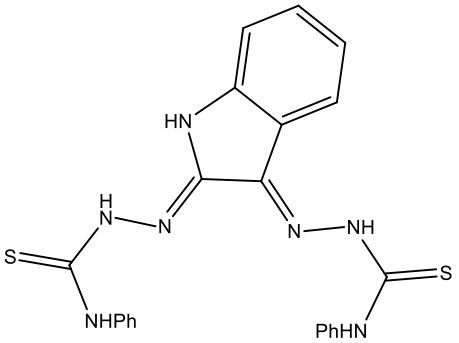 **C16**
17	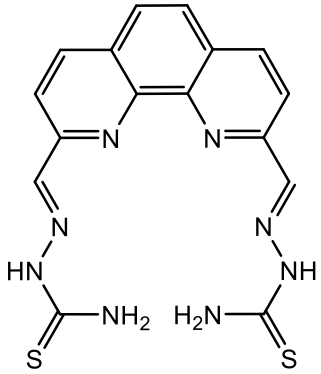 **C17**		

The condensation of thiosemicarbazide with cyclohexane-1,2-dione and (4,10-Dimethyl-1,4,7,10-tetraazacyclododecane-1,7-diyl) bis (propan-2-one, respectively, yields bisthiosemicarbazones with cyclohexane rings (D1, D2) and macrocyclic rings (D3) (Chart 1) [142].

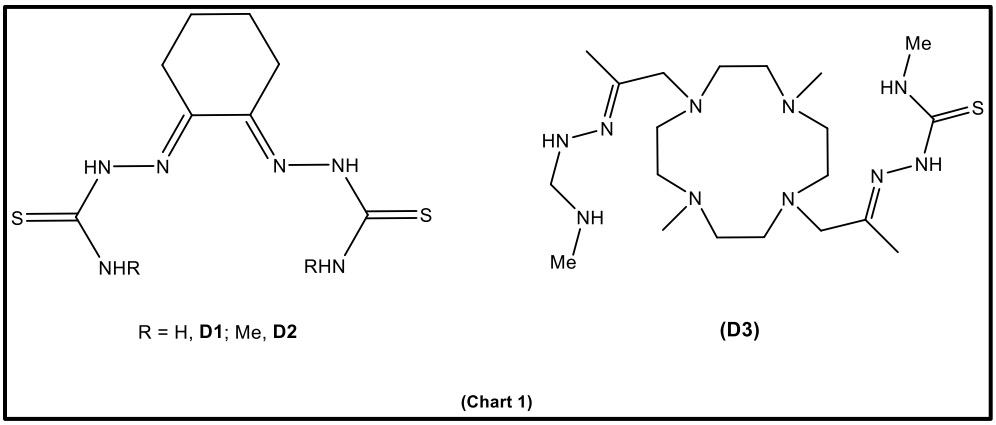

(Chart 1)

It has been observed that, generally for the synthesis of ketone based bisthiosemicarbazone, acidic condition had to be maintained by adding few drops of acid [88], whereas in case of aldehyde based bisthiosemicarbazone, condensation of aldehyde and thiosemicarbazide can take place without addition of acid [145].

2.2. Spectroscopic Techniques

Various spectroscopic techniques like IR, UV-visible, NMR and ESR were used to characterize the bisthiosemicarbazones and their complexes. IR and UV-Visible spectroscopy, ESR, ^{31}PNMR, ^{59}Co NMR, ^{119}Hg NMR etc. of compounds was discussed in text wherever applicable. Only ^{1}H and ^{13}C NMR are discussed in brief in current section. The numbering used to mention the various protons in NMR spectra is given in structure X.

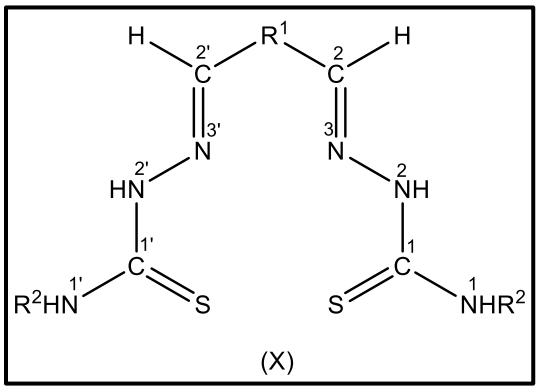

(X)

The NMR spectra of some representative bisthiosemicarbazones and metal complexes with neutral as well as anionic ligands have been discussed to understand the basic pattern of signals and effect of complexation on these signals. Important chemical shifts in ^{1}H and ^{13}C NMR are given in Table **2.4** and Table **2.5** respectively.

Table 2.4: ^{1}HNMR chemical shifts (δ, ppm) of ligands and metal complexes.

Ligands	**N^2H**	**N^1H_2**	**CH_3**	**C^2H**	**Ring proton**	**Reference**
PyBTSC	10.80	10.20	2.50	-	8.55-7.09	[149]
Tri.BTSC	11.30	10.23	2.45-2.44	-	7.68-7.28	[152]
BNMeBTSC	9.85	8.89	3.01	-	7.72-7.38	[129]
$GTSM_2$	11.06	-	3.2	-	7.90	[39]
GTSCM	10.99	-	3.02	-	7.88	[39]
$PyTSM_2$	15.39	-	3.25	-	8.70-7.87	[39]
$PGTSM_2$	13.23	-	3.42- 3.31	-	8.57-7.47	[39]
2,3 TBTSC	11.61	8.35	-	-	7.67	[145]
CHMTSC	10.6	8.06	3.0	-	1.7-2.4	[151]
$H_2Pu4M4E$	11.70 10.36	8.53 8.45	2.17	7.67	-	[154]
$H_2Pu4E4M$	11.72 10.28	8.51 8.40	2.14	7.64	-	[154]
$H_2Pu4M4DE$	9.13 8.79	7.58	2.05	7.33	-	[154]
$H_2Pu4Mpip$	9.15 8.80	7.57	2.04	7.32	-	[154]
$H_2Pu4Mhex$	9.25 8.83	7.58	2.04	7.36	-	[154]
H4DA-PTsz-Me	10.35	8.73	3.05-2.43	-	8.40-7.83	[155]

LMe_2H_4	9.85	8.89	3.01	-	7.72-7.38	[136]
Complexes	**N^2H**	**N^1H_2**	**CH_3**	**C^2H**	**Ring protons**	**Reference**
[Pd(PyBTSC)]	-	10.75	2.72-2.62	-	8.43-7.34	[149]
[Pt(PyBTSC)]	-	11.00	2.78-2.71	-	8.56-7.70	[149]
[Pd(Tri.BTSC)]	12.93	11.40	2.46	-	7.68-6.88	[152]
[Pt(Tri.BTSC)]	13.00	11.35	2.49	-	7.72-7.0	[153]
[Pd(BNMe BTSC)]	-	8.0	2.68	-	7.18-7.13	[129]
[Zn(PyTSM$_2$)]	-	-	3.19	8.07-8.05	7.78-7.09	[39]
[Zn(PGTSM$_2$)]	-	-	3.22	8.12-7.38	-	[39]
$CdCl_2$(2,3BTSC)	11.62 11.54	8.35 7.63	-	-	8.30-7.63	[145]
$CdBr_2$(2,3BTSC)	11.62 11.55	8.52 7.63	-	-	8.30-7.63	[145]
[Cd(CHMTSC)(NO_3)]NO_3.CH_3CN (45)	11.36	8.85	3.09	-	1.75-2.87	[151]
[Zn(CHMTSC)Cl] Cl.CH_3CN(44)	10.63	8.87	2.98-2.08	-	1.68-2.87	[151]
[Ni(Pu4M4E)]	-	8.03 7.75	1.88	7.09	-	[156]
[Ni(Pu4E4M)]	-	7.94 7.79	1.87	7.09	-	[156]
[Ni(Pu4M4DE)]	-	5.12	1.89	6.64	-	[156]
[Ni(Pu4Mpip)]	-	5.13	1.90	6.67	-	[156]
[Ni(Pu4Mhex)]	-	5.10	1.89	6.65	-	[156]
Zn(H_2DAPTsz-Me)	-	6.87	2.75-2.41	8.21-7.58	-	[155]

Pb(H_2DAPTsz-Me)(H_2O)	-	7.21	2.89-2.39	8.18-7.21	-	[155]
Hg(LMe_2H_4)(ONO_2)$_2$	9.55	8.19	2.95	-	7.82-7.25	[136]

Table 2.5: ^{13}CNMR chemical shifts (δ, ppm) of ligands and metal complexes.

Ligands	**C^1**	**C^2**	**CH_3**	**Ring carbon atoms**	**References**
BNMeBTSC	178.6	140.4	31.5	133.2-126.8	[129]
CHMTSC	179.5	138.3	33.9	27.5-21.6	[151]
H4DA-PTsz-Me	178.5	156.4	30.8	147.5-120.5	[155]
LMe_2H_4	178.6	140.4	31.5	133.2-126.8	[136]
Complexes	**C^1**	**C^2**	**CH_3**	**Carbon Ring Proton**	**References**
[Pd(BNMeBTSC)]	179.0	156.1	33.8	131.4-127.5	[129]
Cd(CHMTSC)(NO_3) NO_3.CH_3CN	178.53	145.22	30.22	19.16-29.63	[151]
[Zn(CHMTSC)Cl]Cl. CH_3CN	178.67	146.15	32.52-30.13	20.14-29.90	[151]
Hg(LMe_2H_4)(ONO_2)$_2$	174.7	146.6	33.3	128.5-130.1	[136]

2.3 Complexes of bisthiosemicarbazones: Although several bisthiosemicarbazone complexes with metals have been described, only a small number of them have structural details. The description of complexes that are structurally characterized using x-ray crystallography is given below:

2.3.1 Group 7 (Manganese): Manganese(II) salt with the ligand (H_2L) formed complex of stoichiometry, [Mn(L)(EtOH)$_2$] **1** (Chart 2) [39]. The complex was synthesised using electrochemical method, where ligand was dissolved in acetonitrile containing tetramethylammonium perchlorate and used as supporting electrolyte. The cathode of electrochemical cell was made of platinum wire, whereas a metal plate is placed as anode.

Geometry exhibited by complex **1** is pentagonal bipyramidal by two imine nitrogen atoms, two thiolate Sulphur atoms and one pyridine atom occupying corner of a pentagon, whereas axial positions are taken by two oxygen atoms from two molecules of ethanol. Bisthiosemicarbazone is acting as a di-anionic pentadentate ligand.

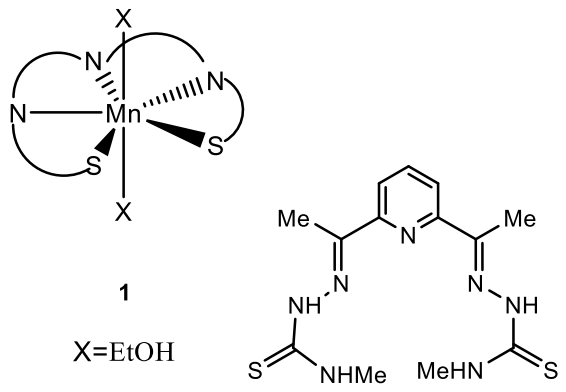

Chart 2

Manganese (II) acetate to a methanolic solution of tetraazacyclododecane (H_2L) resulted in the formation of the complex, $[MnHL]^+$, which was then precipitated as the tetraphenylborate salt $[Mn(H_2L)(BPh_4)]$**2** (Figure 2.1), by adding $NaBPh_4$[157]. The complex **2** is high spin and showed a magnetic moment of 5.82 BM corresponding to five unpaired electrons. The ligand is coordinated to metal centre through sulfur and azomethine nitrogen of one arm of bis ligands and four nitrogens of macrocyclic rings to form distorted octahedral geometry. Second arm of bis ligand remains uncoordinated.

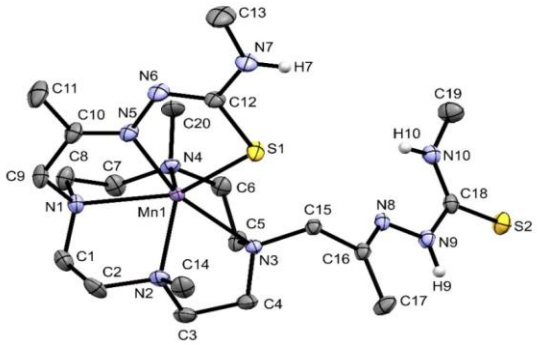

Figure 2.1: Molecular structure of $[MnHL]^+$ {adapted from reference [157]}

2.3.2 Group 8 (Iron): 2,6-diacetylpyridine bisthiosemicarbazone(^1H_2L) and 2,6-diacetylpyridine bis(phenyl thiosemicarbazone) (^2H_2L) were reacted with anhydrous $FeCl_3$ in dry methanol under a N_2 atmosphere to form complexes of formula, $[H_2L(FeCl_2)]Cl$ (HL = ^1H_2L **3**; ^2H_2L **4**) (Chart 3) [121]. The thio- ligand is attached to metal centres via two nitrogen atoms, two sulphur atoms and pyridine nitrogen. The axial positions in complexes **3** and **4** are occupied by chlorine atoms thus, acquiring pentagonal bipyramidal geometry.

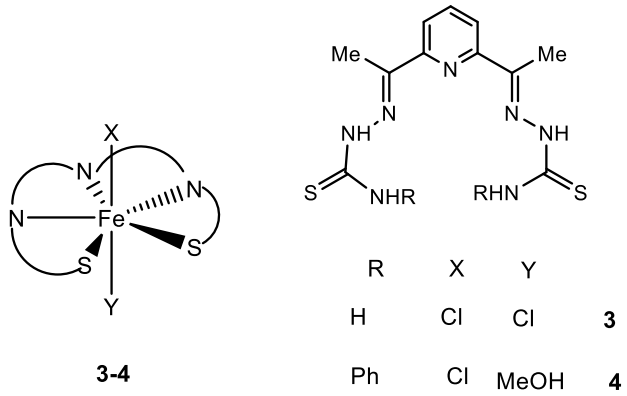

Chart 3

An unexpected structure is obtained when ^2H_2L was reacted with $Fe(ClO_4]_3$ to form complex, $[Fe(^2L)_2]ClO_4$ **5** (Chart 4)[121]. In complex **5**, two bis ligands are attached to metal center. One arm attached to pyridine ring remains intact and bind to metal through pyridine nitrogen, azomethine nitrogen and sulfur atoms, whereas the second arms get partially hydrolyzed.

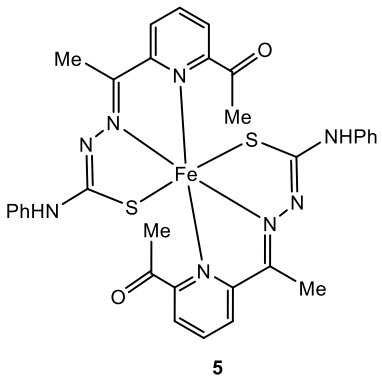

Chart 4

2.3.3 Group 9 (Cobalt): Instead of a monomer with iron (II) 2,6-diacetylpyridine bis phenyl thiosemicarbazone (H_2L) reacted with cobalt perchlorate to form the dimeric pentagonal

bipyramidal complex, $[(H_2L)\ Co(CH_3CN)]_2(ClO_4)_4$ **6** (Figure 2.2, a) [121]. Magnetic measurement of the complex 5 are similar to that of high spin Co(II) complexes showing orbital contribution towards magnetism ranging from 4.7-5.2 [121,122]. Similar reaction of H_2L with $Co(NO_3)_2$ formed an dimeric octahedral complex of formula, $[(L_2)Co]_2(NO_3)_2$ **7** (Figure 2.2, b). In complex **6**, each cobalt atom is bonded with pentadentate, neutral ligand with donor atoms occupying corner of a pentagon. One of the axial positions is taken by acetonitrile and other by sulfur atom of second ligand to form a symmetric $Co(\mu\text{-}S)_2Co$ core. In complex **7**, five donor atoms of one ligand and sulfur from second ligand provide octahedral sphere around each cobalt atom.

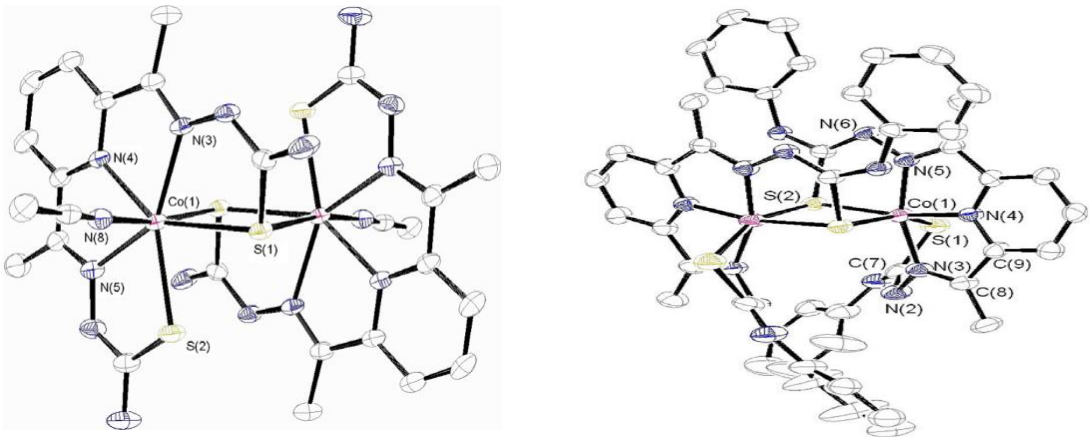

(a) **(b)**

Figure 2.2: Molecular structure of a) $[(H_2L)Co(CH_3CN)]_2(ClO_4)_4$ **6** and b)$[(L_2)Co]_2(NO_3)_2$ **7**{adapted from reference [121]}

The reaction of cobalt(II) nitrate with diacetyl bisthiosemicarbazone (^1H_2L) and glyoxal bisthiosemicarbazone (^2H_2L) yielded complexes of the stoichiometry, $[Co(L)(X)_2]NO_3$(L = ^{1}L, X= (NH_3) **8**; ^{2}L, X = imidazole (Im) **9** benzylamine (BnA) **10** (Chart 5)[111]. All these complexes have shown similar feature during cyclic voltammetry studies. An upfield shift is observed in ^{59}Co NMR spectra on changing equatorial ligand from diacetyl bisthiosemicarbazone to glyoxal bisthiosemicarbazone and axial ligand changes from imidazole to benzylamine.

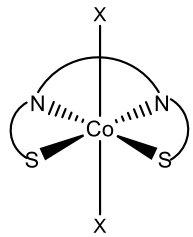

8 - 10

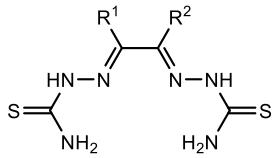

R^1	R^2	X	
Me	Me	NH_3	**8**
H	Me	Im	**9**
H	H	BnA	**10**

Chart 5

Addition of cobalt(II) acetate in methanolic solution of tetraazacyclododecane (H_2L) resulted into formation of complex, $[CoHL]^+$, which was then precipitated as tetraphenylborate salt $[Co(HL)](BPh_4)$ **11** (Figure 2.3), by adding $NaBPh_4$ [157]. The formation of complex cation was confirmed from the peak at m/z = 544.22 in mass spectrum. Two discrete diastereomeric units, $[Co1(HL)]^+$ and $[Co2(HL)^+$ are crystallized in complex **11** and present as racemic mixture (Figure 2a and 2b). The pentadentate ligand coordinated via sulfur, azomethine nitrogen of one arm and four nitrogens from macroyclic ring to form six five-membered chelate rings. Due to the steric bulk of macrocyclic ring, sulfur and azomethine nitrogen of second arm of bisthiosemicarbazone remains uncoordinated. The complex **11** is high spin and showed magnetic moment of 4.24 BM corresponding to three unpaired electrons.

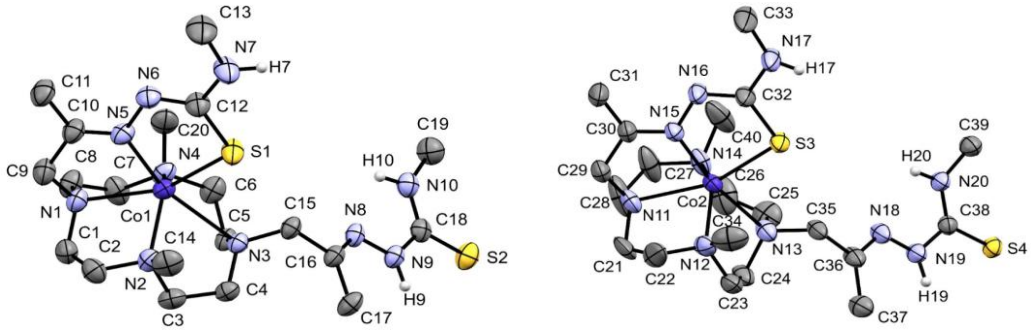

(a) **(b)**

Figure 2.3: Molecular structure of a) $[Co1HL]^+$ and b)$[Co2HL]^+$ {adapted from reference[157]}

2.3.4 Group 10 (Nickel, Palladium and Platinum)

Nickel:

The reaction of nickel(II) acetate with a number of substituted bisthiosemicarbazones (H_2L) having symmetric arms (same group at both amino nitrogen) and asymmetric arms yielded complexes of stoichiometry, [Ni(L)] **12-15** (Chart 6)[79,147].The $\nu(N^2H)$ band in free ligands appeared in the range, at 3133 – 3228 cm^{-1},which disappeared on complexation indicate deprotonation of ligands. The $\nu(C=S)$ band (807-811cm^{-1}) in free ligands shifted to lower energy (739-763 cm^{-1}) on complexation supporting the binding of ligand to metal centre in thiolate form. In these complexes, nickel is coordinated with two imine nitrogen atoms and two thiolate sulfur atoms of bisthiosemicarbazone, thus acting as tetradentate, dianionic ligand. In the electronic spectrum of **14** and **15**, a single d→d band at 14000 cm^{-1} is observed supporting planer structure of these complexes.

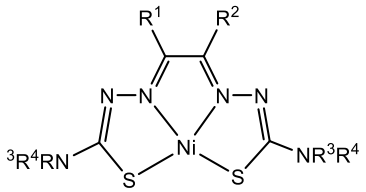

12-15

R^1	Me	H	H	H
R^2	Me	Ph	Me	Me
R^3, R^4	Me	Et	Me, H	Me, H Et
	12	**13**	**14**	**15**

Chart 6

The reaction of nickel(II) chloride with thiophene 2,3-dicarboxaldehyde bisthiosemicarbazone (H_2L) under refluxing condition yielded complex of formula, [Ni(HL)]Cl **16** (Chart 7) [145].Complex **16** is a cationic complex having one chloride ion outside the coordination sphere. The $\nu(NH)$ band of free ligand appeared at 3378 cm^{-1} in IR spectrum, which get shifted to low energy region in complex **16** (3346 cm^{-1}), whereas a high energy shift has been obtained for complex (1607 cm^{-1}) as compared to free ligand (1597 cm^{-1}). Bisthiosemicarbazone showed non-

symmetrical coordination through azomethine nitrogen atoms of both the arms and the sulfur atom (in thione form) of one arm and thiolate form of second arm to give distorted square planar geometry. Thiophene ring is disordered in crystal structure. Both the ligand and its Ni(II) complex were tested for their antifungal activity against, *candida glabrata* and observed that complex showed good antifungal activity ($MIC_{80,}$ 62 μg/mL)vis-à-vis free ligand ($MIC_{80,}$ 250 μg/mL).

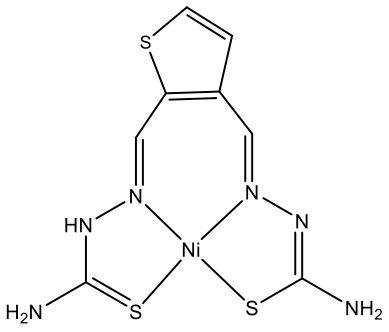

16

Chart 7

The reaction of nickel(II) acetate with acenapthenequione N-methyl bisthiosemicarbazone(H_2L^1) and acenapthenequione N-ethyl bisthiosemicarbazone (H_2L^2) yielded complexes of stiochiometry, [Ni(L)] (L = L^1,**17**; L^2, **18**) (Chart 8) [95].In these complexes, bisthiosemicarbazones are acting as tetradentate, dianionic ligand, coordinating to metal center via N_2S_2 donor atoms to give square planar geometry.

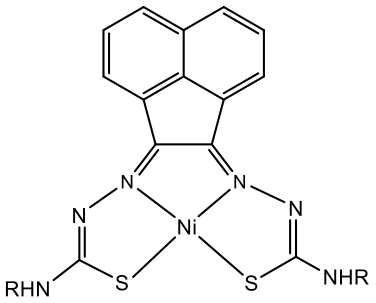

R= Et **(17)**, Me **(18)**

Chart 8

Palladium and Platinum:

1-Phenylglyoxal bis{N(3)diethyl thiosemicarbazone}(H_2L) reacted with K_2PdCl_4 with the addition of triethylamine to form complex, [Pd(L)]**19** (Chart 9). The ligand coordinated to Pd (II) in different manner. The phenyl arm coordinates with thiolate sulfur and thioamide nitrogen atoms

to form four membered rings, whereas the second arm coordinate through thiolate sulfur and azomethine nitrogen atoms to form five membered chelate ring. Due to different coordination modes of two arms, the geometry around the palladium atom is more towards rectangular than square [156].

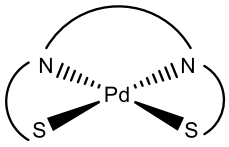

19

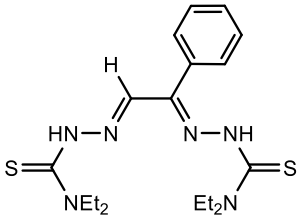

Chart 9

Terephthaldehyde bisthiosemicarbazone (H_2L) reacted with [$PdBr_2(Ph_3P)_2$] and Et_3N in toluene to form a complex of formula, [$Pd_2(L)Br_2(PPh_3)_2$]**20** (Chart 10). One arm of bis- ligands is coordinated to the metal ion via the azomethine nitrogen and the thiolate sulphur atoms to give five-membered chelate ring and the second arm is coordinated to a second palladium ion in similar way to give a dimer. The other two coordination sites of the both the palladium ions are occupied by bromide ion and phosphorous atom of Ph_3P molecule. Catalytic activity of complex was tested for Mizoroki -Heck cross-coupling reaction of aryl chloride with a number of olefins and found that the complex can act as competent homogenous catalyst [154].

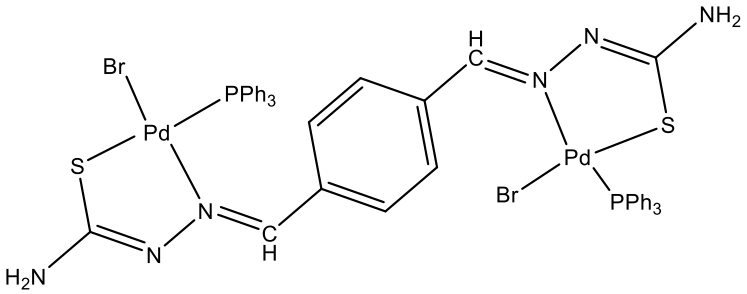

20

Chart 10

The metal ion, $[MCl_4]^{2-}$ reacted with 3,5-diacetyl-1,2,4 triazole bis(^{4}N-p-chlorophenyl thiosemicarbazone) (H_3L) to form dimeric compounds of formula, $[M(\mu\text{-}HL)]_2$ (M = Pd, **21**; Pt, **22**) (Chart 11) [153].To each metal ion the ligands are coordinated through one triazole nitrogen, one azomethine nitrogen, one thiolate sulfur of deprotonated arm of one ligand molecule and thione sulfur of neutral arm of other ligand molecule. Thus, deprotonated arm of ligand coordinated as tridentate and neutral as monodentate forming bridge between the two palladium ions. Ligand has shown excellent antiproliferative activity, whereas complexes low cellular growth inhibition.

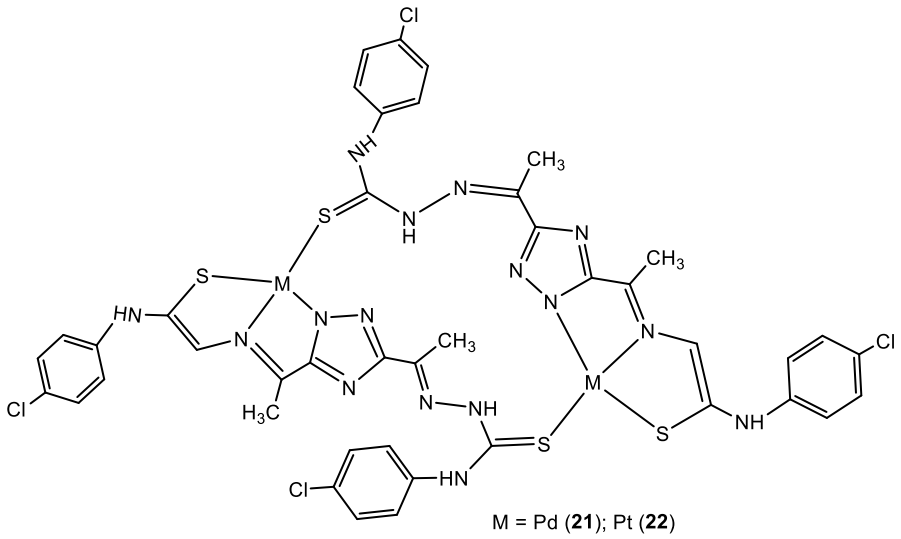

Chart 11

The reaction of 2,6-Diacetyl pyridine bis(4N-pchlorophenyl thiosemicarbazone) (H_2L) with $[MCl_2(Ph_3P)_2]$ (M= Pd, **23**; Pt, **24**) in toluene, in the presence of triethylamine yielded complexes of stoichiometry, [Pd(L)] and [Pt(L)]**23-24** (Chart 12) [149]. Inspite of symmetrical deprotonation, asymmetric coordination by ligand is observed in **23** and **24**. One arm of ligand form bonds with metal ion through azomethine nitrogen and thione sulfur, whereas other arm coordinate through the hydrazine nitrogen atom only. The fourth coordination site is occupied by pyridine nitrogen to form square planar geometry around the metal ion and results into formation of one five membered ring and one six membered rings.

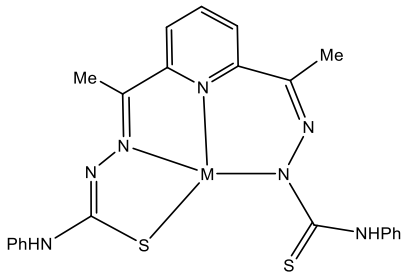

M=Pd (**23**); Pt(**24**)

Chart 12

Benzil bis 4-methyl thiosemicarbazone (H_2L) reacted with K_2PdCl_4, generated by *in situ* reaction of $PdCl_2$ and LiCl, yielded complex of formula, [PdL] **25**, (Figure 2.4) whereas the similar reaction in the presence of $LiOH{\cdot}H_2O$ gave another complex, $[Pd_2(\mu\text{-}L)_2]{\cdot}2DMF$ **26** (Figure 2.5). However, the reaction of H_2L with K_2PtCl_4 in the presence of $LiOH{\cdot}H_2O$ gave two complexes, [PtL] **27** and $[Pt_2(\mu\text{-}L)_2]{\cdot}2DMF$ **28** (Chart 13). In complexes **25** and **27**, ligand is doubly deprotonated coordinating to metal center via two azomethine nitrogen and two thiolate sulfur atoms to form three five membered chelate rings. Complexes **26** and **28** are dimeric and each bis ligand is attached to two different metal ions. One arm of bis thiosemicarbazone is metalated at ortho position along with bonding through imine nitrogen and thiolate sulfur, whereas the second arm is attached to second metal through thione sulfur only to form distorted square planar geometry [129].

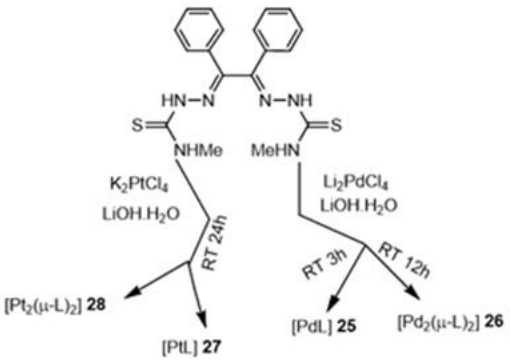

Chart 13

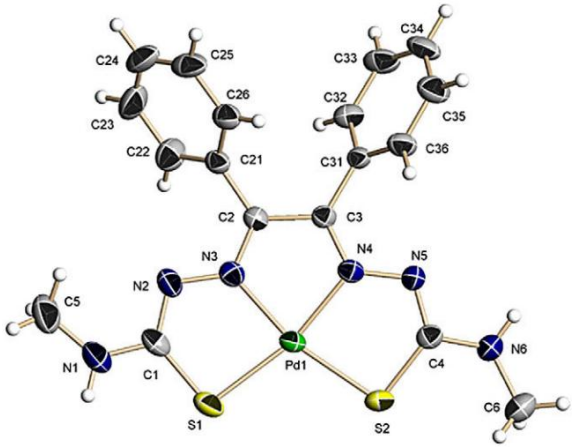

Figure 2.4: Molecular structure of [PdL] **25**{adapted from reference[98]}

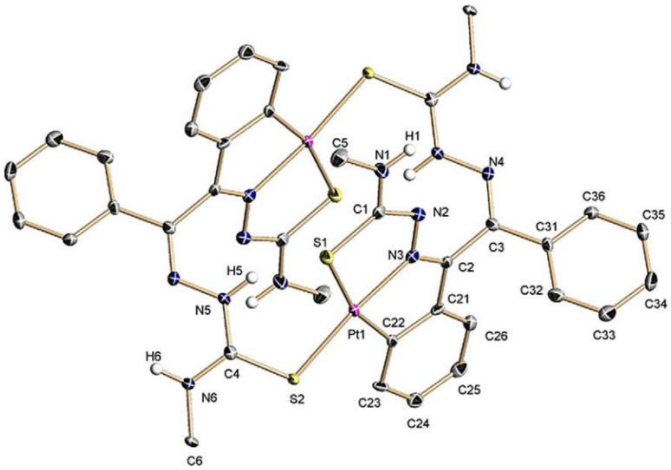

Figure 2.5: Molecular structure of $[Pt_2(\mu\text{-}L)_2]$ **28**{adapted from reference[98]}

2.3.5 Group 11 (Copper, Gold)

Copper:

The reaction of copper(II) acetate with a series of substituted bisthiosemicarbazones produced complexes of stoichiometry, [Cu(L)] Where, L= glyoxal bis(4,4-Dimethyl-3-thiosemicarbazone) ($GTSM_2$), glyoxal bis-(4-Cyclohexyl-4-methyl-3-thiosemicarbazone) (GTSCM), pyridil bis-(4,4-dimethyl-3-thiosemicarbazone) ($PyTSM_2$), acetyl propinoyl bis-(4,4-dimethyl-3-thiosemicarbazone) ($EMTSM_2$), phenylglyoxal bis-(4,4-dimethyl-3-thiosemicarbazone) ($PGTSM_2$) **29-33** (Chart 14) [39]. The thio-ligand is attached to metal centre via two sulphur and two nitrogen atoms thus acts as a tetradentate ligand and form three five membered chelate rings.

The geometry exhibited by the metal centre is distorted square planar. Cyclic voltammetry studies indicate quasi-reversible behavior of metal in all these complexes. Complexes **29-33** were tested for their antiproliferative activity against SK-N-MC Neuroepithelioma cells. Complex [Cu(GTSM$_2$)] was found to be most effective with IC$_{50}$ value of 0.44μM and 9.8 μM respectively.

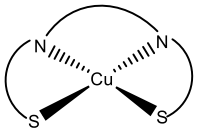

29-33

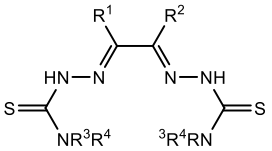

R^1	R^2	R^3	R^4	
H	H	Me	Me	**29**
H	H	Me	C_6H_{11}	**30**
C_5H_4N	C_5H_4N	Me	Me	**31**
Me	C_2H_5	Me	Me	**32**
H	C_6H_5	Me	C_6H_{11}	**33**

Chart 14

Similarly, biacetyl-bis(4-pyrrolidinyl-3-thiosemicarbazone) (ATSC), benzil-bis(4-pyrrolidinyl-3-thiosemicarbazone) (BTSC) and glyoxal-bis(4-methyl-4-phenythiosemicarbazone) (GTSC) reacted with copper acetate to form complexes, [Cu(L)] **34-36** (Chart 15). The metal ion has a distorted square planar geometry and the ligand coordinates to the metal ion through two Sulphur atoms and two nitrogen atoms. Cytotoxic activity of copper complexes were checked against human cancer cell lines and was found that the copper complexes were inactive (>100 μM) except for complex Cu(BTSCH)ClO_4 which was highly toxic (2.36 μM) against HepG2 cells .It has also been found that the ligand BTSCH$_2$ is moderately less toxic to the cancer cells than their copper complexes [123].

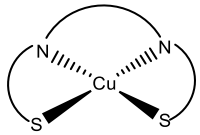

34- 36

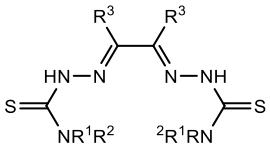

R^1	R^2	R^3	
CH_2-CH_2	CH_2-CH_2	Me	**34**
CH_2-CH_2	CH_2-CH_2	Ph	**35**
Me	H	Me	**36**

Chart 15

The reaction of copper(II) with substituted bisthiosemicarbazones yielded the complexes, [Cu(H_2L)],[1]L= pyruvaldehyde bis (N-methyl thiosemicarbazone),[2]L=Diacetyl bis(4-methyl-3-thiosemicarbazone) **37**-**42** (Chart 16), and the geometry exhibited by the complexes is square planar. The thio-ligand is coordinated to two sulfur and two nitrogen atoms [78,156].

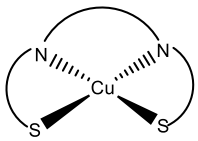

37- 42

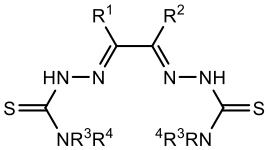

R^1	R^2	R^3	R^4	
H	Me	Me	Me	**37**
Me	Me	Me	H	**38**
C_2H_5	C_2H_5	H	H	**39**
Me	Me	Me	Me	**40**
H	Ph	Et	Et	**41**
Me	Me	Me	H	**42**

Chart 16

Copper(II) complexes of formula, [Cu(L)] (L = L^1, **43**; L^2, **44**) with acenapthenequione N-methyl bisthiosemicarbazone(H_2L^1) and acenapthenequione N-ethyl-bisthiosemicarbazone (H_2L^2) were obtained by transmetallation of [Zn(L)] (L = L^1**43**; L^2 **44**) (Chart 17) [95]. Transmetallation was confirmed by reverse phase HPLC with R_f = 24.2 (**43**) and 20.3 min for 40 as compare to R_f = 19.3

and 17.1min for their respective Zn precursors. In these complexes, the bisthiosemicarbazone is coordinating to metal ion through two sulphur and two nitrogen donor atoms to give square planar geometry, thus acting as tetradentate, dianionic ligand. Cyclic voltametric studies of complexes indicate the reversible reduction (Cu^{II}/Cu^{I}). The different g value in ESR spectra, along three coordinates ($g_{xx,}$ 2.036; $g_{yy,}$ 2.036; $g_{zz,}$ 2.139 (**43**) and $g_{xx,}$ 2.031; $g_{yy,}$ 2.035; $g_{zz,}$ 2.137 (**44**) confirmed asymmetric environment around Cu centre.

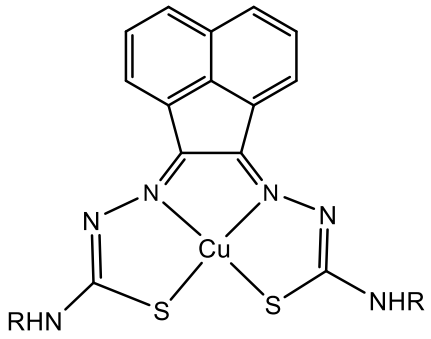

R= Et **(43)**, Me **(44)**

Chart 17

Gold:

The ethanolic solution of $NaAuCl_4{\cdot}2H_2O$ was sonicated with a solution of diacetyl-bis(N^4–methyl thiosemicarbazone (H_2L^1) and diacetyl-bis(N^4-ethylthiosemicarbazone (H_2L^2) to form complexes of stoichiometry, $[Au(H_2L)]AuCl_4$ (H_2L^1, **45;** H_2L^2, **46)** (Chart 18) [135]. In these complexes, the Au (III) is in the center of a square plane (N_2S_2), molded by two iminium nitrogen atoms and two thiolate sulfur atoms of ligand. Steric bulk and chelating moieties provide sufficient stability to Au(III) for their in vivo applications.

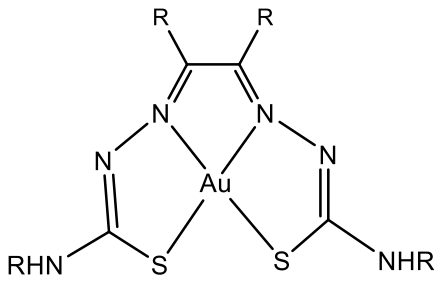

R = Me (**45**); Et (**46**)

Chart 18

2.3.6 Group 12 (Zinc, Cadmium, Mercury)

Zinc(II) acetate reacted with a series of bisthiosemicarbazones having methyl / ethyl/ allyl / pyridyl substituents at amino nitrogen to form complexes, [Zn(L)X] **47-50** (Chart 19) [39]. Geometry of Zn(II) in these complexes is square pyramidal. Bisthiosemicarbazone coordinates through two nitrogen and two sulfur atoms to form the complexes, whereas axial position is occupied by oxygen atom of H_2O (**47**) or DMSO (**48**, **49**) or CH_3OH (**50**).

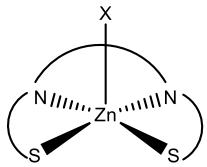

47- 50

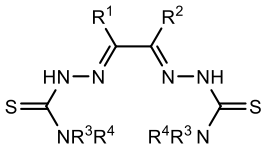

R^1	R^2	R^3	R^4	X	
Me	Me	Me	Me	DMSO	**47**
C_5H_4N	C_5H_4N	Me	Me	DMSO	**48**
H	C_6H_5	Me	Me	H_2O	**49**
Me	Me	Et	allyl	CH_3OH	**50**

Chart 19

The similar reaction of Zinc(II) with bisthiosemicarbazone having methyl group at amino nitrogen of one arm and NH_2 group at amino nitrogen of other arm (asymmetric) formed a polymeric complex **51** (Chart 20) [82]. In this complex, axial position is taken by terminal amino group of the second ligand.

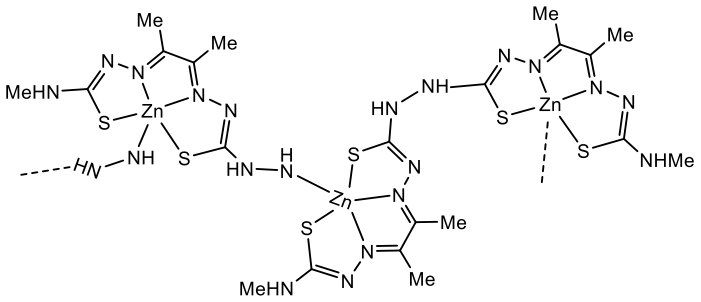

51

Chart 20

Addition of zinc(II) acetate in methanolic solution of tetraazacyclododecane (H_2L) resulted into the formation of complex, $[ZnHL]^+$, which was then precipitated as tetraphenylborate salt $[Zn(HL)](BPh_4)$ **52** (Figure 2.6), by adding $NaBPh_4$ [157].The complex has a distorted octahedral geometry. The formation of complex cation was confirmed from the peak at m/z = 549.22 in mass spectrum. The ligand is coordinated to metal ion through sulfur and azomethine nitrogen atoms of one arm of bis ligands and four nitrogen atoms of macrocyclic rings to form distorted octahedral geometry. Second arm of bis ligand remains uncoordinated.

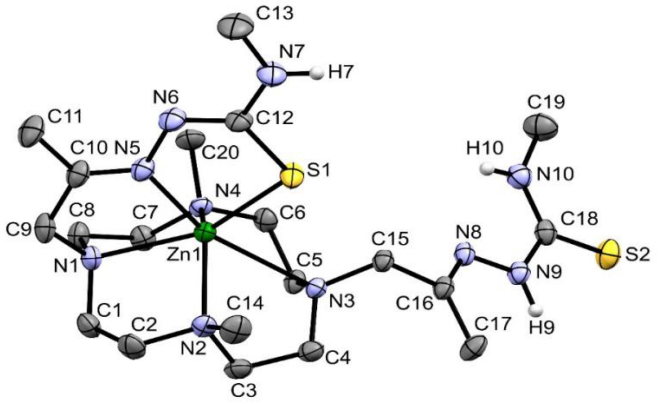

Figure 2.6: Molecular structure of $[ZnHL]^+$ {adapted from reference[110]}

The reaction of cyclohexane-1,2-bis (4-methyl-3-thiosemicarbazone) (H_2L) with $ZnCl_2$ and $Cd(NO_3)_2$ formed complexes, $[ZnCl(L)]Cl{\cdot}CH_3CN$ **53** and $[Cd(L)(NO_3)]NO_3.CH_3CN$ **54**, respectively (Chart 21) [151]. The geometry of Zn(II) in **53** is square pyramidal, with two nitrogen and two sulfur atoms of bis-ligand forming a plane and the axial position is occupied by a chlorine atom. Complex **54** is seven coordinated. Monomeric unit of complex **54**, consist of planar ligand and two oxygen atoms of nitrate group. Each monomeric unit is connected through one of the oxygens of bidentate coordinated nitrate group.

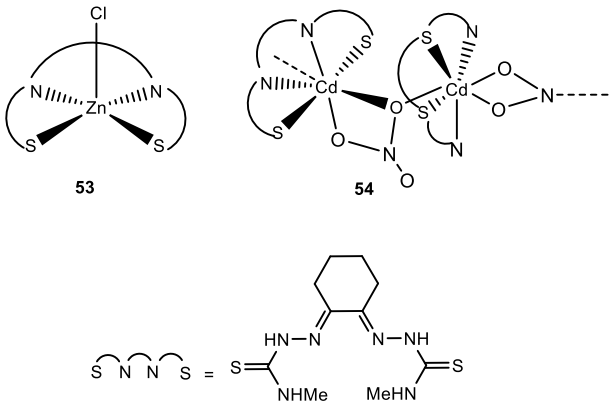

Chart 21

The reaction of mercury nitrate with benzil bis 4-methyl-3-thiosemicarbazone yielded complexes of stoichiometry, [Hg(L)(ONO_2)] **55** (Chart 22) [158]. The ligand is coordinated to metal centre through two nitrogen atoms and two sulphur atoms, two monodentate nitro groups are also coordinated to metal centre and attains the octahedral geometry. In ^{199}Hg NMR one signal appeared at -917.8ppm in DMSO and other signal at -898.3ppm in DMF or $CDCl_3$, in accordance to four coordinated mercury complexes. The weaker bond between Hg-ONO_2 is broken in these above-mentioned solvents and it is supported by the conductivity measurements also.

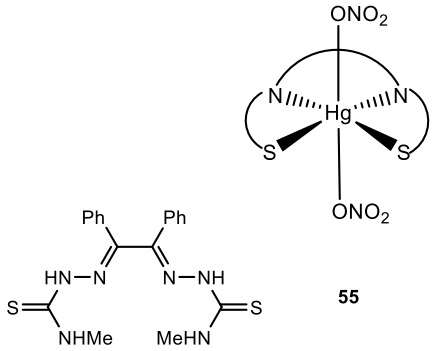

Chart 22

2.3.7 Group 13 (Indium): Reaction of indium chloride with a series of substituted bis-thiosemicarbazones (H_2L) in the presence of sodium methoxide in anhydrous methanol in inert environment yielded complexes of formula, [In(L)Cl] **56-59** (Chart 23) [116]. The thio-ligand is attached to indium centre via two azomethine nitrogen atoms and two thiolate sulfur atoms making a plane with chloride ion occupying axial position of square pyramidal geometry. THF (**56**), EtOH (**57)**, CH_2Cl_2 (**58**) are present as solvent of crystallization, whereas no solvent of crystallization is

observed in **59.** Steric hindrance by aliphatic substituents in **59** may be the reason for absence of any solvent of crystallization. Complex **58** was studied for fluoride exchange in the coordination sphere, which was confirmed by presence of a signal at δ -73.4 ppm in its ^{19}F NMR spectrum.

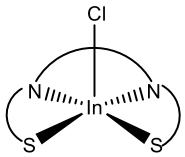

56-59

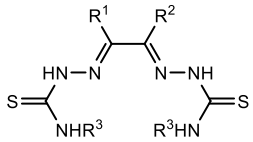

R^1	R^2	R^3	
Et	Me	Ph	**56**
Et	Et	Ph	**57**
Ph	Ph	Me	**58**
Et	Et	Me	**59**

Chart 23

2.3.8 Group 14

Tin and lead

2,6-Diacetyl pyridine bis (4-phenyl thiosemicarbazone) (H_2L) was reacted with $^nBu_2Sn$ to form complex, $[^nBu_2Sn(L)]\cdot(Me_2CO)_{0.5}$ **60** (Chart 24). In this complex, metal ion is hepta-coordinated. Two butyl groups are present above and below the pentagon plane, thus forming pentagonal bipyramidal geometry around the central metal atom. The ^{119}Sn Mossbauer spectrum of complex **60** has shown isomer shift (δ) of 1.43(1) mms^{-1} and quadrupole splitting (Δ) of 3.51 mms^{-1}, which support a distorted pentagonal bipyramidal geometry [128].

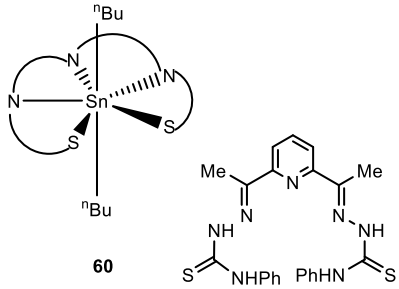

60

Chart 24

Lead:

Lead (II) complex of bis 2,6- diacetyl pyridine N-methyl thiosemicarbazone (H_2L), [Pb(L)] **61** (Chart 25) was prepared in electrochemical cell. In the electrochemical cell, zinc plate was used

as anode and the suspension of the ligand H_2L in acetonitrile containing tetramethylammonium perchlorate was electrolyzed using 10 mA current. Due to the hydrated nature of cofmplex, ν(N-H) band merged with ν(OH) band and appeared at 3310 cm^{-1}. Presence of ν(C=S) band at 1075 cm^{-1} and 802 cm^{-1} and non-appearance of ν(SH) band in the range between 2600-2500 cm^{-1} indicate that ligand is coordinated in thione form rather than thiole form. The pyridyl nitrogen, two azomethine nitrogens and two thiolato sulfur atoms coordinate to metal centre to give an unprecedent distorted pentagonal geometry. Apical position is vacant due to the stereo-chemically active lone pair on lead. This lone pair may be responsible for non-spherical distribution of charge around the lead [159].

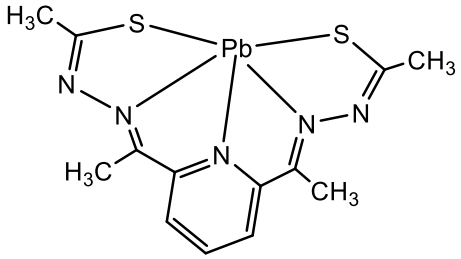

61

Chart 25

2.4 Structure – Activity relationship

A structure-activity relationship can be drawn for antiproliferative activity of unsubstituted and substituted diimine bisthiosemicarbazone against *SK-N-MC Neuroepitheliama Cells*.

Table 2.6 List of substituted and unsubstituted bisthiosemicarbazone along with IC_{50} values (μM) against *SK-N-MC Neuroepitheliama Cells*

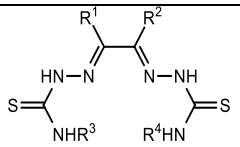

R^1	R^2	R^3	R^4	Ligand	IC_{50}
H	H	H	H	GTS	0.021±0.002
Me	H	H	H	PTS	0.017±0.003
Me	Me	H	H	ATS	≥12.5
H	H	Me	Me	GTSM	0.90±0.12

H	H	Me	C_6H_{11}	GTSCM	0.87±0.03
Me	H	Me	Me	$MGTSM_2$	2.28±0.13
Me	Me	Me	Me	$ATSM_2$	6.16±0.11
Me	Et	H	H	CTS	≥12.5
Me	Et	Me	Me	CTSM	11.2±0.82
Et	Et	H	H	DTS	≥12.5
Et	Et	Me	Me	DTSM	≥12.5

Bisthiosemicarbazones with un-substituted diimine backbone have shown maximum antiproliferative activity (Table **2.6**). A larger decrease in the activity was observed on substitution of hydrogen atom with alkyl group (methyl or ethyl). As the carbon chain at C-C backbone increases, lipophilicity increased thus antiproliferative activity decreased and thus for getting maximum activity, diimine backbone of bisthiosemicarbazone must remain unsubstituted. However, the substituent at terminal atom (N-atom) had not played a significant role in determining the activity of these ligands. The activity of some of these ligands get enhanced on complexation with Cu(II) (Table **2.7**). The enhancement can be attributed to the ability of GSH synthesis inhibitor to act contrary to NAC [39], Actually the cytotoxicity of complexes can be due to the combination of many factors like total copper taken by cell, lipophilicity, cellular compartmentalization and redox activity.

Table 2.7 Comparison of antiproliferative activity of ligand with their Cu(II) complexes

Compound	**IC_{50} (μM)**	
	Ligand	**Cu(II) complex**
GTSM	0.90 ± 0.12	0.19 ± 0.01
GTSCM	0.87 ± 0.03	> 10
$ATSM_2$	6.16 ± 0.11	0.75 ± 0.25
$MGTSM_2$	2.28 ± 0.13	2.27 ± 0.08
CTSM	11.2 ± 0.82	4.20 ± 0.99

The ligands GTS, PTS and ATS were tested for their cytotoxic effects under normoxic and hypoxic conditions for HeLa and A549 cell lines and compared with their Co(III) complexes having two axial co-ligands [111]. IC_{50} values for ligands and their complexes are given in Table **2.8.**

Table 2.8: IC_{50} values (μM) for ligands and their cobalt complexes

Compound	**HeLa**		**A549**		**Cellular uptake of complexes in A549**	
	normoxia	**hypoxia**	**normoxia**	**hypoxia**	**Co/Protien (pg / μg) normoxia**	**Co/Protien (pg / μg) hypoxia**
ATS	> 20	> 20	16.4 ± 0.87	17.5 ± 2.7	-	-
$[Co(ATS)(NH_3)_2]^+$	> 500	> 500	> 500	> 500	55 ± 1	70 ± 3
$[Co(ATS)(Im)_2]^+$	> 500	> 500	> 500	> 500	50 ± 2	57 ± 4
$[Co(ATS)(BnA)_2]^+$	> 500	> 500	> 500	> 500	64 ± 1	82 ± 1
PTS	0.027 ± 0.002	0.055 ± 0.001	0.06 ± 0.03	0.09 ± 0.03	-	-
$[Co(PTS)(NH_3)_2]^+$	≈ 22	≈ 15	≈ 16.9	≈ 21.8	32 ± 1	32 ± 3
$[Co(PTS)(Im)_2]^+$	≈ 28	≈ 17	≈ 4.2	≈ 8.6	18±0.3	30±1
$[Co(PTS)(BnA)_2]^+$	≈ 8.6	≈ 8.8	≈ 7.1	≈27	29± 1	33± 1
GTS	0.067 ± 0.008	0.094 ± 0.010	0.02 ± 0.01	0.04 ± 0.01	-	-
$[Co(GTS)(NH_3)_2]^+$	21 ± 2.9	15 ± 4.6	12 ± 1.4	9.2 ± 1.4	27 ± 1	17 ± 0.1
$[Co(GTS)(Im)_2]^+$	7.4 ± 2.4	3.7 ± 2.3	2.6 ± 0.4	2.9 ± 0.7	15 ± 1	20 ± 1
$[Co(GTS)(BnA)_2]^+$	7.3 ± 1.5	6.3 ± 0.76	5.8 ± 0.95	8.2 ± 1.9	22 ± 1	22 ± 1

From the above table, it is clear that cytotoxicity of complexes depends on equatorial bis(thiosemicarbazone) ligand with GTS showing maximum and ATS having least cytotoxicity, however the cellular uptake follows reverse pattern. This may be due to the highly negative redox potential of complexes. From the results, a mechanism can be proposed, where complexes enter

into the cell, undergo ligand substitution reaction (increase redox potential), transmetalate with copper(II) or release bisthiosemicarbazone. The axial ligands are not showing any profound effect on cytotoxicity. Generally, complexes containing benzylamine and imidazole are more active than those having ammonia but not applicable for all complexes.

3,5-diacetyl-1,2,4triazolbis(^{4}N-p-chlorophenyl thiosemicarbazone) (H_3L) was tested for antiproliferative activity against human NCI-H460 (non small lung cancer), T-47D (breast cancer), A2780 and A2780cisR (epithelial ovarian cancer) cell lines and found to exhibit excellent activity even more than cisplatin except in A2780 (Table **2.9**)[143].

Table 2.9: Antiproliferative activity of H_3L [39,126,149]

IC_{50}±SD (μM)					**Resistance Factor**
Compound	**A2780**	**A2780cisR**	**NCI-H460**	**T-47D**	**IC_{50} in A2780cisR / IC_{50} in A2780**
H_3L	3.10 ±0.02	3.51 ±0.03	7.07 ±0.07	3.37 ±0.1	1.1
Cisplatin	0.88 ±0.01	7.71 ±0.10	7.25 ±0.56	12 ±1	8.8

Resistance factor of 1.1 (H_3L) versus 8.8 (cisplatin) is of main importance, as a value < 2 indicates non-cross resistance. Mechanism of ability to overcome cisplatin resistance in A2780cisR cell involves reduced drug transport, increased DNA repair and GSH level [39,126,149].

It is reported that organic compounds containing heterocyclic rings are currently gaining more importance due to their interesting biological and pharmacological applications [160–162]. Thiosemicarbazones containing heterocyclic rings are another important category of ligands with N, S donor atoms, which can chelate to transition metal ions and alter their biological properties [163–165]. The position at which thio-moiety is attached to heterocyclic ring and the type of donor atoms in the heterocyclic ring had significant impact on the activity of these compounds [163,166]. The two thiosemicarbazone moieties attached to heterocyclic ring are of importance these days due to their structural similarities to natural biological compounds, flexibility, selectivity, and sensitivity to the central metal atom. Keeping these points in consideration, in current thesis the synthesis of heterocyclic bisthiosemicarbazones and complexes with Cobalt ^{II}, Nickel ^{II}, Copper ^{II} and Zinc ^{II} has been carried out.

2.5 Aims and objectives: From the above literature survey, it has been observed that a number of complexes with type I bis-thiosemicarbazones are structurally characterized as compare to type II

and type III ligands. Thus, to explore the coordination chemistry of bis-thiosemicarbazones of type III, the following objectives has been designed:

1. Synthesis and characterization of bisthiosemicarbazone ligands based upon heterocyclic moieties.
2. Synthesis and characterization (IR, NMR and X-ray (wherever possible) of complexes of Ni(II), Cu(II), Zn(II) and/or Co(III) with the bisthiosemicarbazone ligands.
3. Biological activities of synthesized ligands and their metal complexes.
4. Biomolecular interaction studies of synthesized biologically active ligands and their metal complexes.

CHAPTER -3

MATERIALS AND METHODS

3.1 Chemicals and reagents:

Thiosemicarbazide, 4-methyl thiosemicarbazide, 4-Phenyl thiosemicarbazide, 2,5 thiophene dicarboxaldehyde, Isatin, 2,5 Piperazine dione, 2,6 diacetylpyridine are procured from Sigma-Aldrich chemicals. Cobalt acetate, nickel acetate, copper acetate and zinc acetate are procured from Loba chemicals.

3.2 Instrumentation:

3.2.1 Melting Point: The melting point of synthesized ligands were determined with electrically heated apparatus.

3.2.2 Infrared spectroscopy: Infra-red (IR) spectra was recorded using KBr pellets by SHIMADZU FTIR 8400S, Fourier Transform, Infrared spectrophotometer.

3.2.3 NMR spectroscopy:

A BRUCKER ADVANCE III NMR Spectrophotometer operating at 500 MHz in DMSO was used to record ^{1}H NMR spectra, with TMS serving as the internal reference.

3.2.4 Mass spectroscopy:

The mass spectra were acquired using an LCMS Spectrometer.

3.2.5 ESR Spectroscopy:

The JEOL, JES - FA200 ESR Spectrometer was used to record ESR spectra. The X band is used for study at room temperature and low temperature.

3.2.6 UV-visible spectroscopy: HSA binding studies were carried out using SHIMADZU UV-1800 Spectrometer.

3.2.7 Fluorescence spectroscopy: HSA binding studies were also carried out using fluorescence Spectrometer (Perkin Elmer LS6500).

3.2.8 Vibrating Sample Magnetometer (VSM): VSM studies of complexes was done on Lakeshore VSM7410 at room temperature.

3.2.9 Powder X-Ray Diffractometer (XRD): The powder XRD spectrum was obtained from BRUKER D8 X-ray diffractometer using Cu K α radiation with λ= 1.5405Å.

3.3 Experimental Methods:

3.3.1 ESR spectroscopy

ESR spectroscopy is well established method for figuring out the electronic structure of paramagnetic metals like copper(II) (one unpaired electron). The spin Hamiltonian (H) can be used to jointly express the energy changes (Equation-1).

$$H = \beta e.\ S \cdot g \cdot B_0 + h\ S \cdot A \cdot I \quad \textbf{(1)}$$

βe is the electron Bohr magneton, S is the electron spin operator, and g is the electronic g-tensor. I is nuclear spin operator 3/2 for ^{63}Cu. A is the hfc tensor, h is Planck's constant.

The shape of the spectrum reflects the ligand field's symmetry. The g value is commonly expressed as g_x, g_y, or g_z, depending on which way the g tensor is pointing. A single line with the equation $g_x = g_y = g_z$ is obtained in the case of an isotropic symmetric ligand field, signifying a coordination environment with cubic symmetry. A tetragonal field is indicated in the case of axial symmetry by the equation $g_x = g_y g_z$, and potential geometries are extended octahedral, square pyramidal, or square planar. When an asymmetric field exists, rhombicity is indicated by g_x g_y g_z. G value can be used to identify a variety of parameters, including electron delocalization, covalency, and crystal-field splitting.

3.3.2 Anti-Tuberculosis Activity

The anti-tubercular activity was recorded using literature method (Blue Almar method) [167-168]. [169].

3.3.3 Human Serum Albumin binding studies:

3.3.3.1 UV-visible spectroscopic study

The UV-visible absorption of HSA (7 μM) was recorded with the incremental additions of ligands (0-5 μM) complexes (0-9 μM). The absorption spectra of HSA with the most potent compounds measured in the range, 200-800 nm. The binding constant (K_b) of HSA and compound was calculated by employing the benesi-Hildebrand (Equation-2):

$$\frac{A_0}{(A-A_0)} = \frac{\varepsilon_f}{(\varepsilon_b - \varepsilon_f)} + \frac{\varepsilon_f}{(\varepsilon_b - \varepsilon_f)K_b\ [\text{ligand or complex}]} \ldots\ldots (2)$$

In this equation, A_o and A indicate the HSA absorption in the unrestricted form and presence of ligands or complexes respectively, while ε_f and ε_b denote the molar extinction coefficients of HSA in the unrestricted form and presence of ligands or complexes respectively. The ratio of intercept to the slope was used as $A_o/(A-A_o)$ versus 1/[ligand or complex] plots to calculate the K_b value.

3.3.3.2 Fluorescence study

Fluorescence titrations have been carried out using HSA (7 μM) with incremental additions of ligands (0-8 μM) and complexes (0-16 μM) in phosphate buffer having *p*H 7.4 at 298 K. All spectra were recorded by varying the wavelength in the range of 200-800 nm using 280 nm as excitation wavelength.

Stern-Volmer equation was used to calculate quenching constant (Equation -3).

$\frac{F_0}{F} = 1 + K_{sv}\,[Analyte] = 1 + K_q\tau_o[ligand\ or\ complex]$ …….. (3)

Where, F_o and F signify the HSA's emission intensity in unrestricted form and the existence of ligands or complexes, respectively. Quenching constant (K_{sv}) was determined from the plots of F_o/F versus [ligand or complex]. Further binding constants (K_b) and No. of binding sites (n) were computed using modified Stern-Volmer equation (Equation -4)

$log\frac{F_0-F}{F} = logK_b + nlog[ligand\ or\ complex]$…….. (4)

The values of K_b and n were determined from intercept and slope, respectively from log {(F_o-F)/F versus log [ligand or complex]} plots. Whereas, F_o and F are the same as in equation -3.

3.3.4 Molecular Modelling

The molecular docking studies of ligands their complexes, respectively with PDB ID: 2H7M were performed using Auto Dock software package (vina). To configure every ligand-mycobacterium tuberculosis enoyl reductase interaction, Auto Dock Tools (1.5.6rc3) was utilised. Water molecules were removed and polar hydrogen atoms were supplied. Nonpolar hydrogen atoms were combined with carbon atoms after the gasteiger charges were calculated. To optimise the 3D structure of ligands, the Gaussian 09W programme was used and the results were saved in PDF format. The incomplete charges of the PDF files for the ligands, and their complexes respectively were changed by employing the ADT programme (version 1.5.6rc3), and the resulting file was kept in Pdbqt format. The dimensions of grid box representing the (x, y, and z) directions-60 Å, 60 Å, 60 Å-were maintained throughout the docking process. The grid was employed with a spacing of 0.375 Å.

3.4 Synthesis of Ligands:

Reactions was carried out for 6-7 hours. The clear solution after filtration was kept for crystallization. After two days the compound was collected.

For ^{1}H NMR and ^{13}C NMR DMSO was selected as solvent because it is an ideal solvent for a wide range of organic and inorganic substances and allowing for clearer detection of the proton and carbon resonances due to complete solubility of the sample in it.

3.4.1 (2,5 H_2bttsc, $^{1}H_2L$):

To a solution of thiosemicarbazide (0.6g, 7.1mmol) in 40 ml of methanol, was added a 10 ml solution of 2,5 thiophene dicarboxaldehyde in methanol (0.5g, 3.5mmol), and was refluxed for 6-7 hours. Brown compound was collected from the brown-coloured solution after two days. Yield: 83%, Main FTIR peaks (neat, cm^{-1}), $\upsilon(NH_2)$ 3409m, 3277; υ(–NH–) 3155m; υ(C=N) 1600s; υ(C=C) 1583m, $\delta(NH_2)$ 1535s; υ(C=S) 826s. ^{1}H NMR (500 MHz, DMSO-D_6, δppm): 11.60s (2H, -N^2H-); 8.32s, 7.52s (4H, N^1H_2); 8.19s (2H, C^2H); 7.41s (2H, $C^{4,5}H$). ^{13}C NMR (125 MHz DMSO-D_6, δppm): 178.35($C^{1,1'}$); 141.17($C^{2,2'}$); 137.39 ($C^{3,3'}$), 131.46 (C^4), 114.96 (C^5).

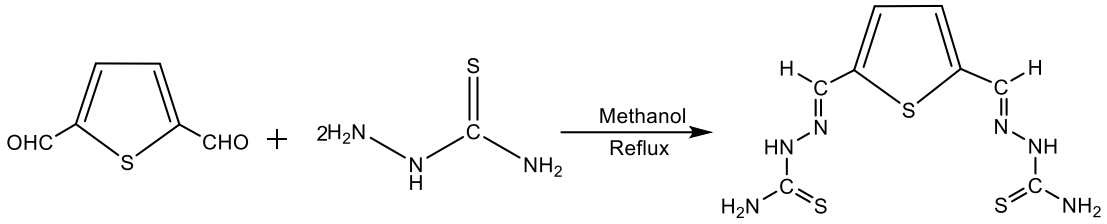

2,5 thiophene dicarboxaldehyde thiosemicarbazide 2,5 thiophene dicarboxaldehyde bisthiosemicarbazone, H_2bttsc

3.4.2 (2,5 H_2bttscN-Me, $^{2}H_2L$):

To a solution of N-methyl thiosemicarbazide (0.75g, 7.13mmol) in 40 ml of methanol, was added 10ml solution of 2,5 thiophene dicarboxaldehyde (0.5g, 3.56mmol) in methanol, and was refluxed for 6-7 hours. Brown compound was collected after two days from the brown coloured solution Yield: 80%, M.P. 220-222°C, Main FTIR peaks (neat, cm^{-1}): $\upsilon(NH_2)$ 3373m; υ(–NH–) 3155w; υ(C=N) 1594s; υ(C=C) 1462m; $\delta(NH_2)$ 1428s; υ(C=S) 801s. ^{1}HNMR (500 MHz, DMSO-D_6, δppm): 11.62s (2H, -N^2H-); 8.20s (2H, -N^1H); 8.14s (2H, $C^{2,2'}H$); 7.41s (2H, $C^{4,5}H$); 3.02s (CH_3).^{13}C NMR (125 MHz DMSO-D_6, δppm): 177.75 ($C^{1,1'}$); 140.70 ($C^{2,2'}$); 137.01 ($C^{3,3'}$); 131.20 ($C^{4,5}$); 31.37(CH_3).

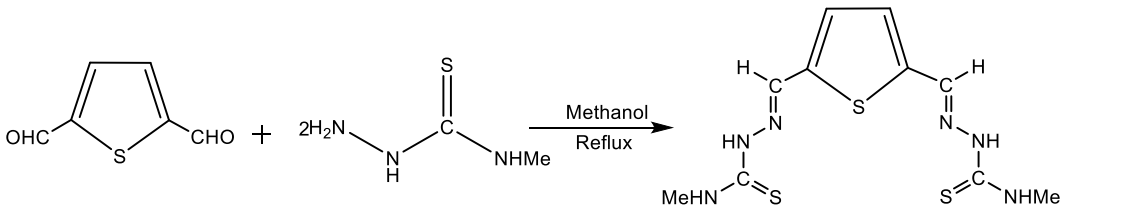

2,5 thiophene dicarboxaldehyde N-methylthiosemicarbazide 2,5 thiophene dicarboxaldehyde N-methylbisthiosemicarbazone, H_2bttsc N-Me

3.4.3 (2,5 H_2bttsc N-Ph, ^3H_2L):

To a solution of N-phenyl thiosemicarbazide (1.19g, 7.12mmol) in 40 ml of methanol, was added 10 ml solution of 2,5 thiophene dicarboxaldehyde in methanol (10 ml) (0.5g, 3.5mmol and was refluxed for 6-7 hours. Creamish compound was collected after two days from the light brown coloured solution. Yield: 85%, Main FTIR peaks (neat, cm^{-1}): $\upsilon(NH_2)$ 3303m; υ(–NH–) 3156w; υ(C=N) 1636s; υ(C=C) 1594m; $\delta(NH_2)$ 1524s; υ(C=S) 836s. ^{1}H NMR (500 MHz, DMSO-D_6, δppm): 10.36s (2H, -N^2H-); 9.83s (2H, -N^1H); 9.16s (2H, C^2H); 7.66 -7.14 m (10H, ring protons).^{13}C NMR (125 MHz DMSO-D_6/$CDCl_3$, δppm):179.89 ($C^{1,1'}$); 139.43 ($C^{2,2'}$); 128.69-123.30 (ring carbon).

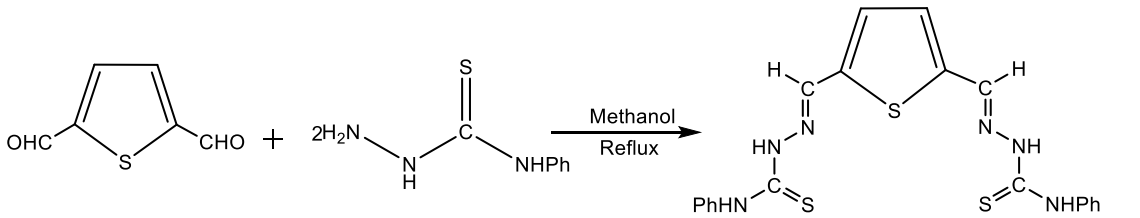

2,5 thiophene dicarboxaldehyde N-phenylthiosemicarbazide 2,5 thiophene dicarboxaldehyde N-phenyl bisthiosemicarbazone, H_2bttsc-N-Ph

3.4.4 (2,3bitsc, ^4H_2L):

To a solution of thiosemicarbazide (2.46g, 26.99 mmol) in 60 ml of methanol, was added a solution of isatin in methanol (10 ml) (2g, 13.59 mmol), and was refluxed for 6-7 hours. Orange compound was collected from the yellow coloured solution after two to three days. Compound was filtered and dried in vacuo. Yield: 88%, Main FTIR peaks (neat, cm^{-1}), $\upsilon(NH_2)$ 3332m, 3259m, υ(–NH–) 3156m,υ(C=N) 1618s, υ(C=C)1587m, $\delta(NH_2)$1457s, υ(C=S) 851s. ^{1}H NMR (500 MHz,DMSO-D_6; δppm): 12.47s (2H,-$N^{2,2'}$H), 11.20s (1H, N^4H_{isatin}), 9.04, 8.68s (2H, $N^{1,1'}H_2$), 7.37t (1H, C^7H, J=7.5Hz), 7.11t (1H, C^6H, J=7.5Hz); 6.94d (1H, C^5H, J= 7.5Hz),7.64d (1H, C^8H ,J= 7.5Hz). ^{13}C

NMR (125 MHz DMSO-D_6, δppm):179.16 ($C^{1,1'}$), 163.19(C^2), 142.82 (C^3), 132.65(C^9), 131.18(C^7), 122.49(C^5), 121.03 (C^6), 119.87(C^8), 111.50 (C^4).

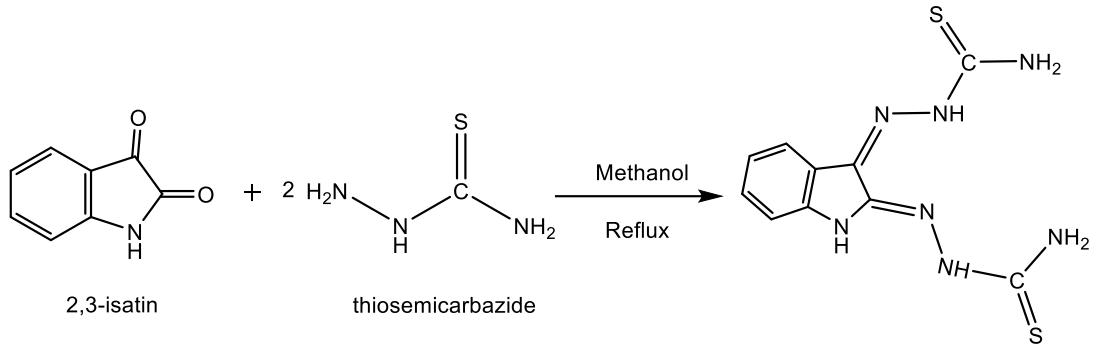

3.4.5 (2,3 H_2bitsc-N^1-Me, ^5H_2L):

To a solution of N-Methyl thiosemicarbazide (2.85g, 27.10 mmol) in 60 ml of methanol, was added a solution of isatin in methanol (10 ml) (2g, 13.59 mmol), and was refluxed for 6-7 hours. Dark red compound was collected from the orange-coloured solution after two to three days. Compound was filtered and dried in vacuo. Yield: 71%, Main FTIR peaks (neat, cm^{-1}), υ(NH_2) 3461m, 3207m,υ(C-H) 2976, υ(C=N)1546s, υ(C=C) 1458m,υ(C=S) 831s. ^{1}H NMR (500 MHz , DMSO-D_6, δppm): 12.60s (2H,-$N^{2,2'}$H), 11.21s (1H, N^4H_{isatin}), 9.25s (2H, $N^{1,1'}$HMe), 7.38t (1H, C^7H, J= 7.5Hz), 7.12t (1H, C^6H, J=7.5Hz), 7.66d (1H, C^8H, J=7.5Hz), 6.93d (1H, C^5H, J=8Hz), 3.12s (3H, CH_3).^{13}C NMR (125 MHz DMSO-D_6, δppm):179.58($C^{1,1'}$), 162.78($C^{2,2'}$), 143.21(C^3), 132.97(C^9), 131.58(C^7), 123.56(C^5),121.35 (C^6),120.28(C^8), 111.50 (C^4),39.53(CH_3).

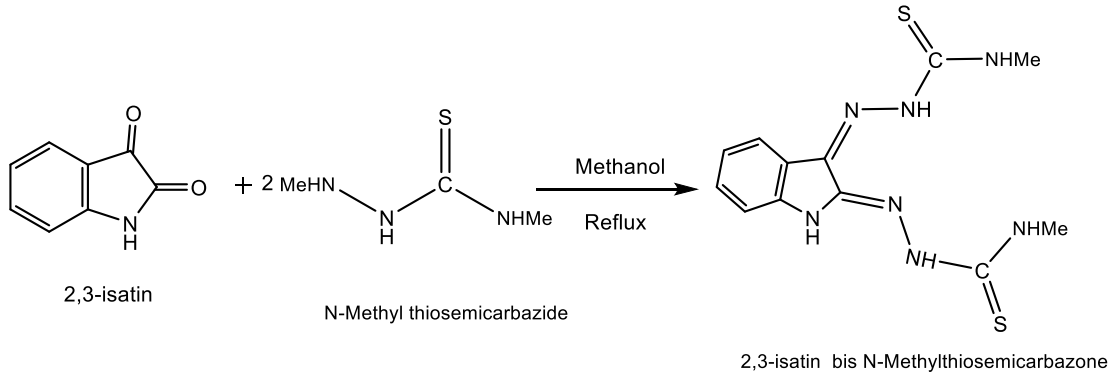

3.4.6 (2,3 H_2bitsc-N^1-Ph, ^6H_2L):

To a solution of N-phenyl thiosemicarbazide (4.54g, 27.0 mmol) in 60 ml of methanol, was added a solution of isatin in methanol (10 ml) (2g, 13.59 mmol), and was refluxed for 6-7 hours. Dark red compound was collected from the dark orange coloured solution after two to three days. Compound was filtered and dried in vacuo. Yield: 84%, Main FTIR peaks (neat, cm^{-1}), $\upsilon(NH_2)$ 3290m, υ(–NH–) 3173m, υ(C=N) 1591s, υ(C=C) 1533m, υ(C=S) 827s. ^{1}H NMR (500 MHz, DMSO-D_6, δppm): 12.80 (s, 2H, $N^{2,2'}$H-), 11.28 (s, 1H, N^4H_{isatin}), 10.84 (s, 2H, $N^{1,1'}$HPh), 7.79-6.95 (m, ring protons).^{13}C NMR (125 MHz DMSO-D_6, δppm):176.49($C^{1,1'}$), 162.64 (C^2), 142.27(C^3), 138.25-111.03(Ring carbons).

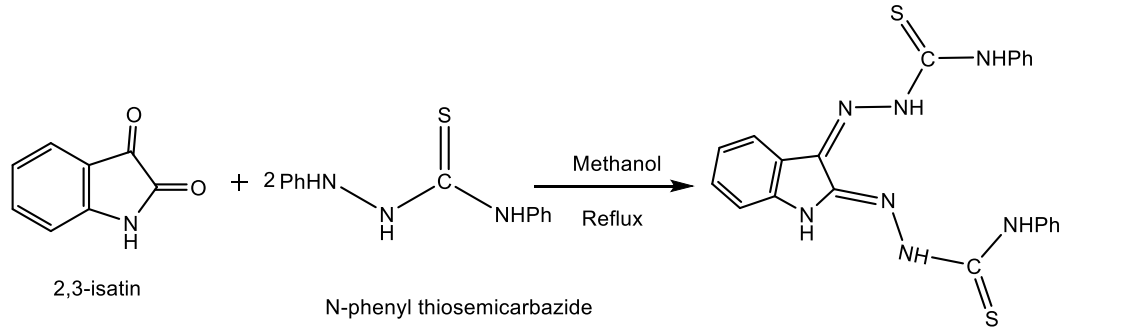

3.4.7 (2,5 H_2bptsc, ^7H_2L):

To a solution of thiosemicarbazide (2.46g, 26.99 mmol) in 60 ml of methanol, was added a solution of 2,5-Piperazinedione in methanol (10 ml) (2g, 13.59 mmol), and was refluxed for 6-7 hours. White compound was collected from the white-coloured solution after two to three days. Yield: 89%, Main FTIR peaks (neat, cm^{-1}), $\upsilon(NH_2)$ 3356m, 3253m; υ(–NH–) 3166m; υ(C=N) 1640; υ(C=C) 1615; $\delta(NH_2)$ 1526; υ(C=S) 895s. ^{1}H NMR (400 MHz, DMSO-D_6, δppm): 8.65s (2H, N^2H), 8.04s (1H, N^4H_{Pip}); 7.57, 7.21s (4H, N^1H_2); 4.57 (4H, $C^{3,3'}$H). ^{13}C NMR (100 MHz DMSO-D_6, δppm): 181.42 ($C^{1,1'}$); 166.54 ($C^{2,2'}$); 45.12 ($C^{3,3'}$).

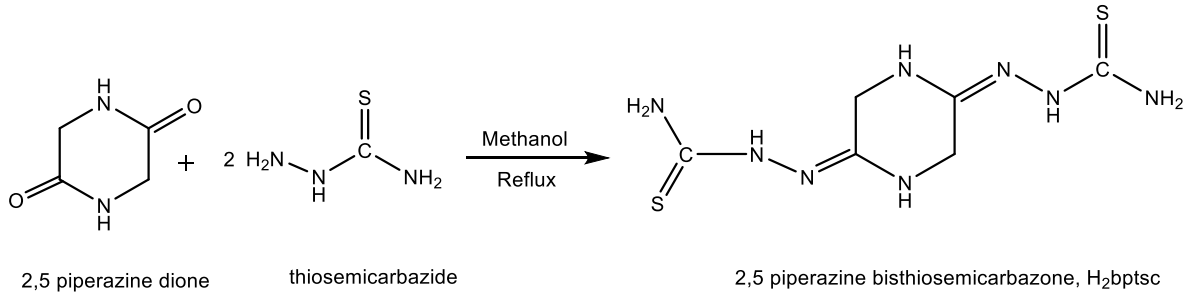

3.4.8 (2,5 H_2bptsc N-Me, ^8H_2L):

To a solution of N-methyl thiosemicarbazide (2.46g, 26.99 mmol) in 60 ml of methanol, was added a solution of 2,5-Piperazinedione in methanol (10 ml) (2g, 13.59 mmol), and was refluxed for 6-7 hours. White compound was collected from the white-coloured solution after two to three days. Yield: 88%, Main FTIR peaks (neat, cm^{-1}), υ(NH_2)3282m; υ(–NH–) 3198m; υ(C=N) 1639; υ(C=C) 1549; υ(C=S) 807s.

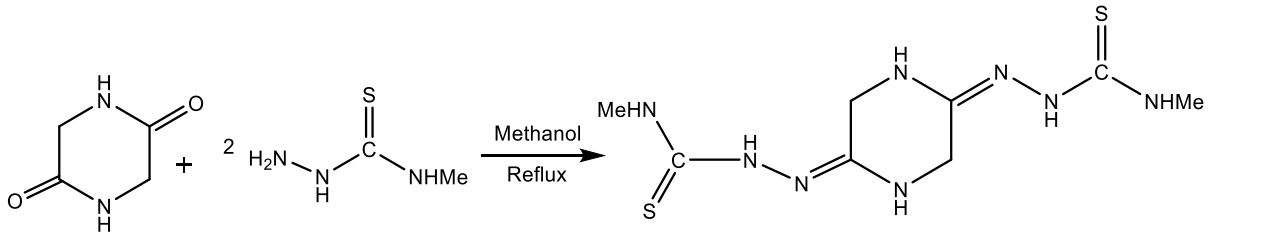

2,5 piperazine dione

N-methyl thiosemicarbazide

2,5 piperazine N-methyl bisthiosemicarbazone, H_2bptsc,N-Me

3.4.9 (2,5 H_2bptsc N-Ph, ^9H_2L):

To a solution of N-phenyl thiosemicarbazide (2.46g, 26.99 mmol) in 60 ml of methanol, was added a solution of 2,5-Piperazinedione in methanol (10 ml) (2g, 13.59 mmol), and was refluxed for 6-7 hours. White compound was collected from the white-coloured solution after two to three days. Compound was filtered and dried in vacuo. Yield: 90%, Main FTIR peaks (neat, cm^{-1}), υ(NH_2) 3301m; υ(–NH–) 3158m; υ (C=N) 1639; υ (C=C) 1466; δ(NH_2) 1437; υ(C=S) 829s. ^{1}H NMR (400 MHz , DMSO-D_6, δppm): 9.10s (2H, N^2H), 9.61, 8.03s (2H, N^1H_2); 4.75s (1H, N^4H_{Pip}); 7.63-7.10 (10H, Ring protons).^{13}C NMR (100 MHz DMSO-D_6, δppm): 180.30 ($C^{1,1'}$); 166.82 ($C^{2,2'}$); 139.48-123.78 (Ring carbon); 45.09 ($C^{3,3'}$).

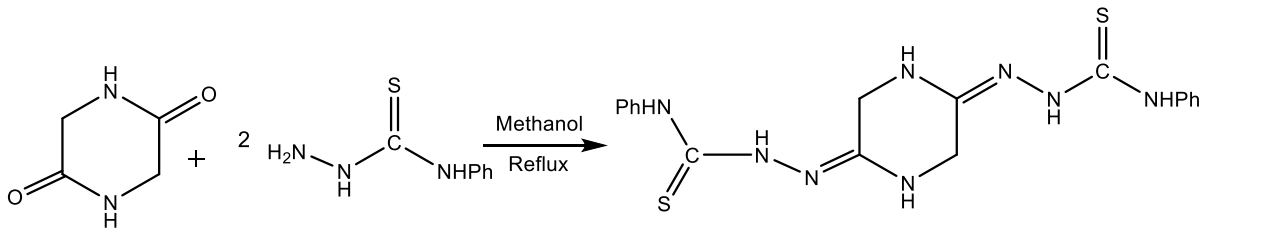

2,5 piperazine dione

N-phenyl thiosemicarbazide

2,5 piperazine N-phenyl bisthiosemicarbazone, H_2bptsc,N-Ph

3.4.10 (2,6 H_2bdptsc, $^{10}H_2L$):

To a solution of thiosemicarbazide (0.6g, 7.1mmol) in 40 ml of methanol, was added a solution of 2,6 diacetyl pyridine in methanol (10 ml) (0.5g, 3.5mmol), and was refluxed for 6-7 hours. Brown compound was collected from the light brown coloured solution after two to three days. Yield: 88%, Main FTIR peaks (neat, cm^{-1}), υ(NH_2) 3423m, 3209; υ(–NH–) 3158m; υ(C=N) 1606; υ(C=C) 1536 δ(NH_2) 1513s; υ(C=S) 827s. ^{1}H NMR (500 MHz, DMSO-D_6, δppm): 10.32s (2H, -N^2H-); 8.42s (4H, N^1H_2); 8.16s (2H, $C^{4,4'}$H); 7.83s (1H, C^5H); 2.43 (6H CH_3). ^{13}C NMR (125 MHz DMSO-D_6, δppm): 179.09($C^{1,1'}$); 154.09($C^{3,3'}$); 148.60($C^{2,2'}$); 139.69 (C^5); 122.15 ($C^{4,4'}$);12.37(CH_3).

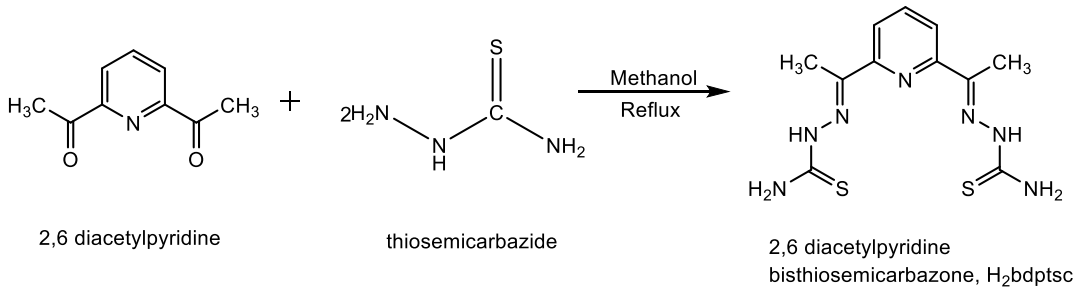

3.4.11 (2,6 H_2bdptsc N-Me, $^{11}H_2L$):

To a solution of N-methyl thiosemicarbazide (0.6g, 7.1mmol) in 40 ml of methanol, was added a solution of 2,6 diacetyl pyridine in methanol (10 ml) (0.5g, 3.5mmol), and was refluxed for 6-7 hours. Dark brown compound was collected from the brown-coloured solution after two to three days. Yield: 90%, M.P. 210-212°C, solubility: soluble on acetonitrile and methanol and partially soluble in chloroform. Main FTIR peaks (neat, cm^{-1}), υ(NH_2) 3450m, 3329m; υ(–NH–) 3190; υ(C=N) 1634; υ(C=C) 1555; δ(NH_2) 1518s; υ(C=S) 836s. ^{1}H NMR (500 MHz, DMSO-D_6, δppm): 10.34s (2H, -N^2H-); 8.70s (2H, N^1H); 8.55s (2H, $C^{4,4'}$H); 7.85s (1H, C^5H); 3.05 (N^1HCH_3); 2.43 (6H CH_3). ^{13}C NMR (125 MHz DMSO-D6, δppm): 179.47 ($C^{1,1'}$); 154.37 ($C^{3,3'}$); 148.0 ($C^{2,2'}$); 136.70 (C^5); 121.53 ($C^{4,4'}$); 31.59 (N^1HCH_3); 12.27(CH_3).

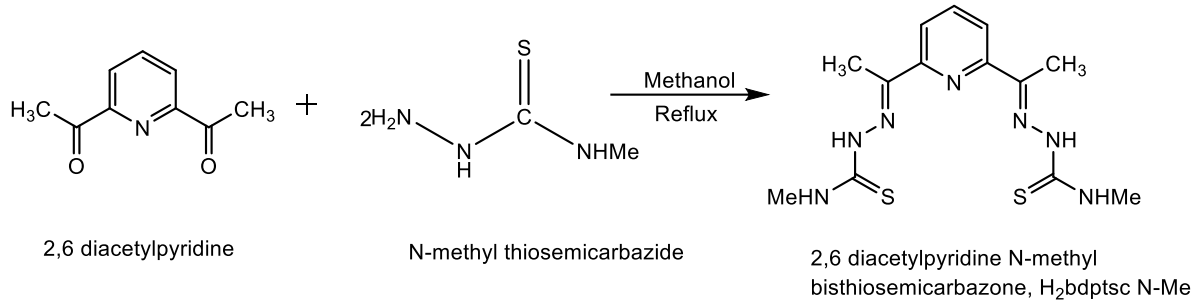

3.4.12 (2,6 H_2bdptsc N-Ph, $^{12}H_2L$):

To a solution of N-phenyl thiosemicarbazide (0.6g, 7.1mmol) in 40 ml of methanol, was added a solution of 2,6 diacetyl pyridine in methanol (10 ml) (0.5g, 3.5mmol), and was refluxed for 6-7 hours. White compound was collected from the white-coloured solution after two to three days. Yield: 87%, Main FTIR peaks (neat, cm^{-1}), $\upsilon(NH_2)$ 3303m; υ(-NH-) 3156; υ(C=N) 1636; υ(C=C)1594; υ(C=S) 896s. ^{1}H NMR (500 MHz, DMSO-D_6, δppm): 10.69s (2H, -N^2H-); 10.23s (2H, N^1H); 8.55s (2H, $C^{4,4'}$H); 7.84s (1H, C^5H); 7.49-7.26 (Ring protons); 2.51 (6H CH_3).

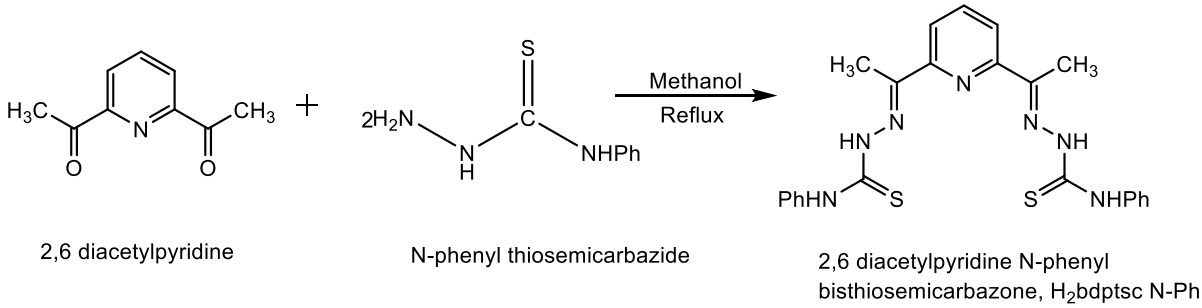

3.4.13 Physical parameters of ligands (^1H_2L to $^{12}H_2L$)

S. No	Melting point	Solubility
1.	213-215°C	Soluble in acetonitrile, methanol and partially soluble in chloroform.
2.	220-222°C	Soluble in acetonitrile, methanol and partially soluble in chloroform.

3.	218-220˚C	Soluble in acetonitrile, methanol and partially soluble in chloroform.
4.	204-206°C	Soluble in acetonitrile, methanol and partially soluble in chloroform.
5.	208-210˚C	Soluble in acetonitrile, methanol and partially soluble in chloroform.
6.	210-212˚C	Soluble in acetonitrile, methanol and partially soluble in chloroform
7.	200-204°C	Soluble in acetonitrile, methanol and partially soluble in chloroform.
8.	206-208°C	Soluble in acetonitrile, and partially soluble in chloroform.
9.	212-214°C	Soluble in acetonitrile, methanol and partially soluble in chloroform.
10.	215-216˚C	Soluble in acetonitrile, methanol and partially soluble in chloroform.
11.	210-212˚C	Soluble in acetonitrile, methanol and partially soluble in chloroform.
12.	216-218˚C	Soluble in acetonitrile, methanol and partially soluble in chloroform.

3.4.14 LCMS values for ligands ($^{1}H_2L$ to $^{12}H_2L$)

S. No	Ligand	m/z
1.	$^{1}H_2L$	285.20
2.	$^{2}H_2L$	313.11
3.	$^{3}H_2L$	440.32
4.	$^{4}H_2L$	294.95
5.	$^{5}H_2L$	319.06
6.	$^{6}H_2L$	445.05
7.	$^{7}H_2L$	261.12
8.	$^{8}H_2L$	288.94
9.	$^{9}H_2L$	413.26
10.	$^{10}H_2L$	311.16
11.	$^{11}H_2L$	339.17
12.	$^{12}H_2L$	372.00

3.5 Synthesis of complexes: Cobalt (II) Complexes

3.5.1 [Co(2,5 bttsc)] 1.

To a solution of 2,5 thiophene dicarboxaldehyde bisthiosemicarbazone (0.028g, 0.097 mmol), was added $Co(OAc)_2$ (0.025g, 0.097mmol) in ethanol. The reddish coloured solution was refluxed for 4 hours. After two to three days brown coloured compound was obtained and dried in vaco. Yield: 79%, M.P. 222-224˚C. Main FTIR peaks (neat, cm^{-1}); $\upsilon(NH_2)$ 3301; υ(–NH–) 3175w; υ(C=N) 1609s; υ(C=C) 1478m; $\delta(NH_2)$ 1334s; υ(C=S) 656s. ESR data (g, gauss): $g_{\parallel}$ 2.27; $g_{\perp}$ 2.07. Mass spectra: m/z$[Co(C_8H_8N_6S_3)]^+$: 340.28 (parent ion peak), 338.34 (Loss of two hydrogens), 274.27 (Loss of one arm of bisthiosemicarabzone)

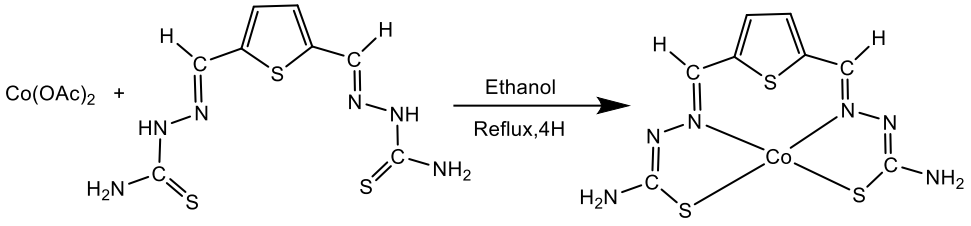

2,5 thiophene dicarboxaldehyde bisthiosemicarbazone [Co(2,5-bttsc)]

3.5.2 [Co(2,5 bttsc N-Me)] 2.

To a solution of 2,5 thiophene dicarboxaldehyde N-methyl bisthiosemicarbazone (0.039g, 0.098 mmol), was added $Co(OAc)_2$ (0.025g, 0.098mmol) in ethanol. The reddish coloured solution was refluxed for 4 hours. After two to three days brown coloured compound was obtained and dried in vaco. Yield: 78%, M.P. 233-235˚C. Main FTIR peaks (neat, cm^{-1}); $\upsilon(NH_2)$ 3339; υ(C=N) 1500s; υ(C=C) 1403m; υ(C=S) 766s. ESR data (g, gauss): $g_{\parallel}$ 2.22; $g_{\perp}$ 2.12. Mass spectra: m/z$[Co(C_{10}H_{12}N_6S_3)]^+$: 373.16 (parent ion peak).

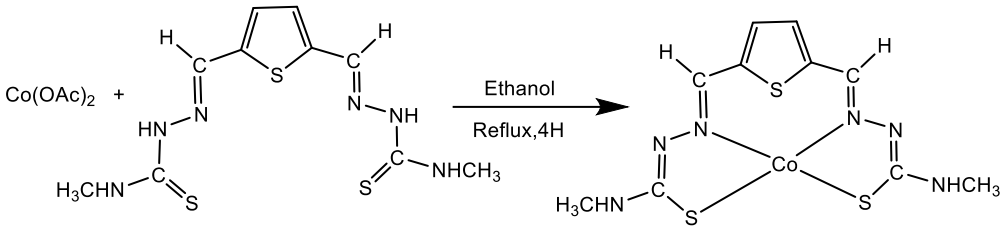

2,5 thiophene dicarboxaldehyde N-methyl bisthiosemicarbazone [Co(2,5-bttsc N-Me)]

3.5.3 [Co(2,5 bttsc N-Ph)] 3.

To a solution of 2,5 thiophene dicarboxaldehyde N-phenyl bisthiosemicarbazone (0.025g, 0.057 mmol), was added $Co(OAc)_2$ (0.014g, 0.057mmol) in ethanol. The reddish coloured solution was refluxed for 4 hours. After two to three days brown coloured compound was obtained and dried in vaco. Yield: 81%, M.P. 228-230˚C. Main FTIR peaks (neat, cm^{-1}); $\upsilon(NH_2)$ 3251; υ(C=N) 1592s; υ(C=C) 1534m; υ(C=S) 748s. ESR data (g, gauss): $g_{\parallel}$ 2.25; $g_{\perp}$ 2.08 Mass spectra: m/z$[Co(C_{20}H_{16}N_6S_3)]$: 492.07(parent ion peak).

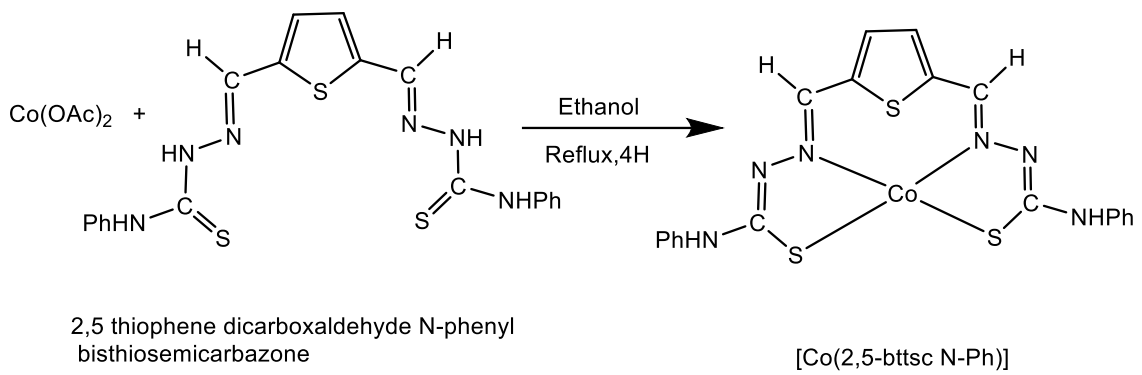

3.5.4 [Co(bitsc)] 4.

To a solution of 2,3-isatin bisthiosemicarbazone (0.058g, 0.20mmol) was added $Co(OAc)_2$ (0.050g, 0.20mmol) in ethanol. The reddish coloured solution was refluxed for 4 hours. After two to three days brown coloured compound was obtained and dried in vaco. Yield: 80%, M.P. 220-222˚C. FTIR bands (neat, cm^{-1}); $\upsilon(NH_2)$ 3276m; $\upsilon(C = N)$ 1640s; $\upsilon(C = C)$ 1589m; δ (NH_2) 1540s; $\upsilon(C = S)$ 773s. ESR data (g, gauss): $g_{\parallel}$ 2.18; $g_{\perp}$ 2.11 Mass spectra: m/z$[Co(C_{10}H_9N_7S_2)]^+$: 355.06 (parent ion peak).

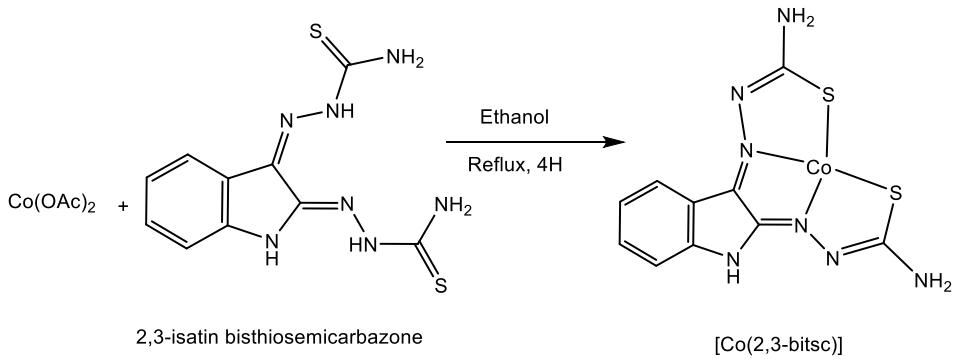

3.5.5 [Co(bitsc-N-Me)] 5.

To a solution of 2,3-isatin-N-methyl bisthiosemicarbazone (0.064g, 0.20mmol) was added $Co(OAc)_2$ (0.050g, 0.20mmol) in ethanol. The reddish coloured solution was refluxed for 4 hours. After two to three days brown coloured compound was obtained and dried in vaco. Yield: 81%, M.P. 232-234˚C, Main FTIR bands (neat, cm^{-1}); υ (NH_2) 3220m; $\upsilon(C=N)$ 1643s; $\upsilon(C = C)$ 1593m; δ (NH_2) 1532s; υ $(C=S)$ 743s. ESR data (g, gauss): $g_{\parallel}$ 2.31; $g_{\perp}$ 2.09. Mass spectra: m/z$[Co(C_{12}H_{13}N_7S_2)]^+$: 382.07(parent ion peak).

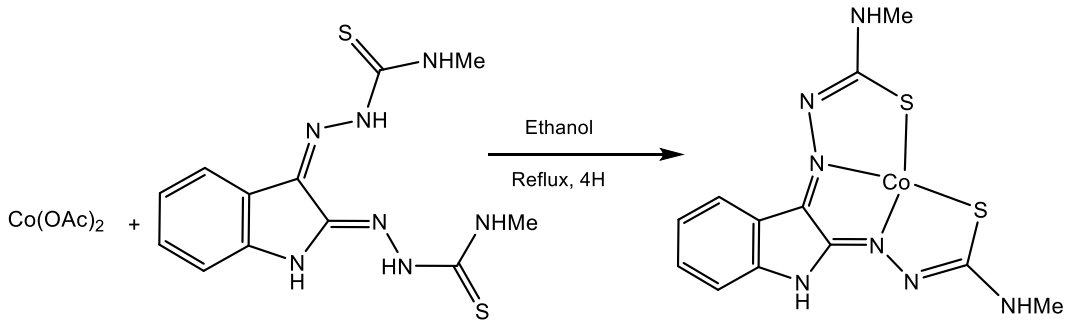

2,3-isatin N-methyl bisthiosemicarbazone

[Co(2,3-bitsc N-Me)]

3.5.6 [Co(bitsc-N-Ph)] 6.

To a solution of 2,3-isatin-N-phenyl bisthiosemicarbazone (0.089g, 0.20mmol) was added $Co(OAc)_2$ (0.050g, 0.20mmol) in ethanol. The reddish coloured solution was refluxed for 4 hours. After two to three days brown coloured compound was obtained and dried in vaco. Yield: 78%, M.P. 216-218°C. Main FTIR bands (neat, cm^{-1}); $\upsilon(NH_2)$ 3217m; $\upsilon(C=N)$ 1654s; $\upsilon(C=C)$ 1513m; δ (NH_2) 1450s; $\upsilon(C=S)$ 743s. ESR data (g, gauss): $g_{\parallel}$ 2.20; $g_{\perp}$ 2.12. Mass spectra: m/z$[Co(C_{24}H_{25}N_7S_2)]^+$: 519.07amu (parent ion peak).

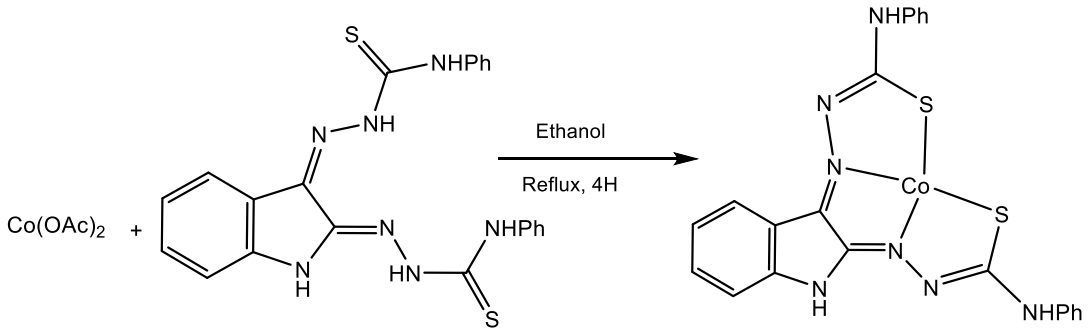

2,3-isatin N-Phenyl bisthiosemicarbazone

[Co(2,3-bitsc N-Ph)]

3.5.7 [Co(2,5 bptsc)] 7.

To a solution of 2,5 piperazinedione bisthiosemicarbazone (0.064g, 0.2mmol), was added $Co(OAc)_2$ (0.050g, 0.2mmol) in ethanol. The reddish coloured solution was refluxed for 4 hours. After two to three days brown coloured compound was obtained and dried in vaco. Yield: 88%, M.P. 224-226°C. Main FTIR peaks (neat, cm^{-1}); $\upsilon(NH_2)$ 3491m, 3262m; $\upsilon(C=N)$ 1643s; $\upsilon(C=C)$ 1533m; $\delta(NH_2)$ 1438s; $\upsilon(C=S)$ 812s. ESR data (g, gauss): $g_{\parallel}$ 2.35; $g_{\perp}$ 2.17. Mass spectra: m/z$[Co(C_6H_{12}N_8S_2)]^+$: 318.34amu (parent ion peak).

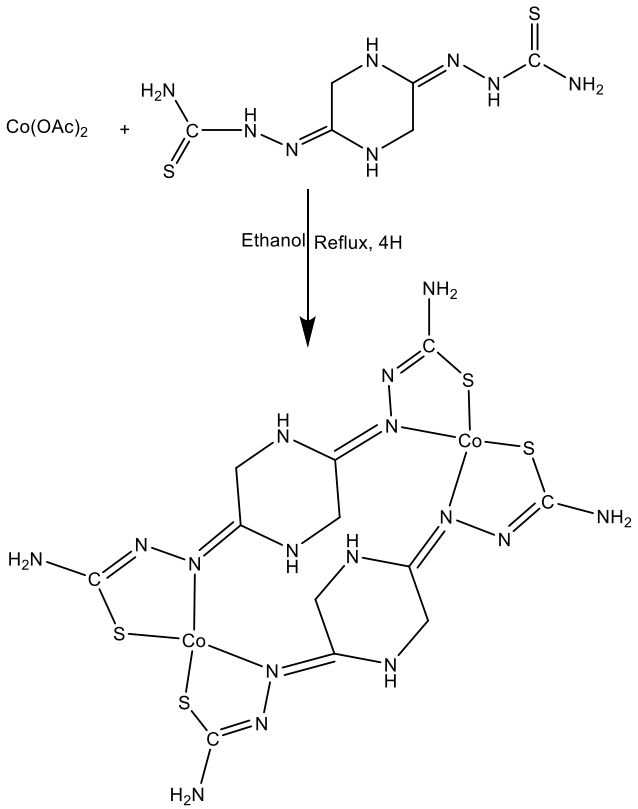

3.5.8 [Co(2,5 bptsc N-Me)] 8.

To a solution of 2,5 piperazinedione N-methyl bisthiosemicarbazone (0.057g, 0.2mmol), was added $Co(OAc)_2$ (0.050g, 0.2mmol) in ethanol The reddish coloured solution was refluxed for 4 hours. After two to three days brown coloured compound was obtained and dried in vaco. Yield: 90%, M.P. 234-236°C. Main FTIR peaks (neat, cm^{-1}); $\upsilon(NH_2)$ 3290m, 3202m; υ(C=N) 1643s; υ(C=C) 1545m; $\delta(NH_2)$ 1424s; υ(C=S) 743s. ESR data (g, tensor, A, gauss): $g_{\parallel}$ 2.58; $g_{\perp}$ 2.06. Mass spectra: m/z$[Co(C_8H_{16}N_8S_2)]^+$: 347.21amu (parent ion peak).

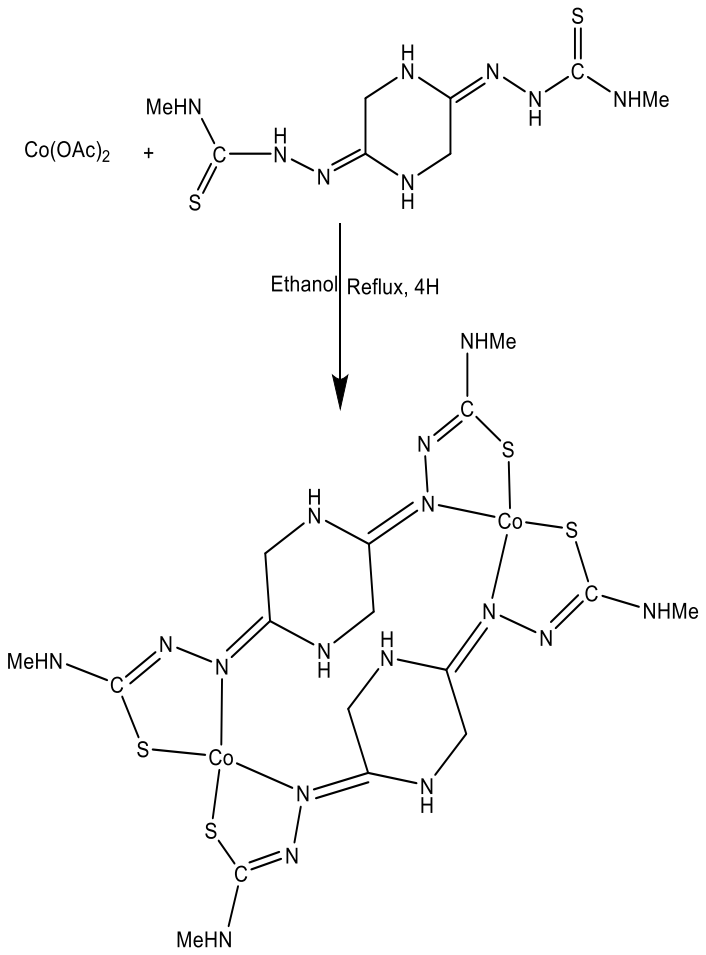

3.5.9 [Co(2,5 bptsc N-Ph)] 9.

To a solution of 2,5 piperazinedione N-phenyl bisthiosemicarbazone (0.102g, 0.2mmol), was added $Co(OAc)_2$ (0.050g, 0.2mmol) in ethanol. The reddish coloured solution was refluxed for 4 hours. After two to three days brown coloured compound was obtained and dried in vaco. Yield: 88%, M.P. 244-246°C. FTIR bands (neat, cm^{-1}); $\upsilon(NH_2)$ 3479m; $\upsilon(C = N)$ 1577s; $\upsilon(C = C)$ 1488m; $\upsilon(C=S)$ 753s. ESR data (g, gauss): $g_{\parallel}$ 2.34; $g_{\perp}$ 2.14. Mass spectra: m/z$[Co(C_{18}H_{22}N_8S_2)]^+$: 471.28amu (parent ion peak).

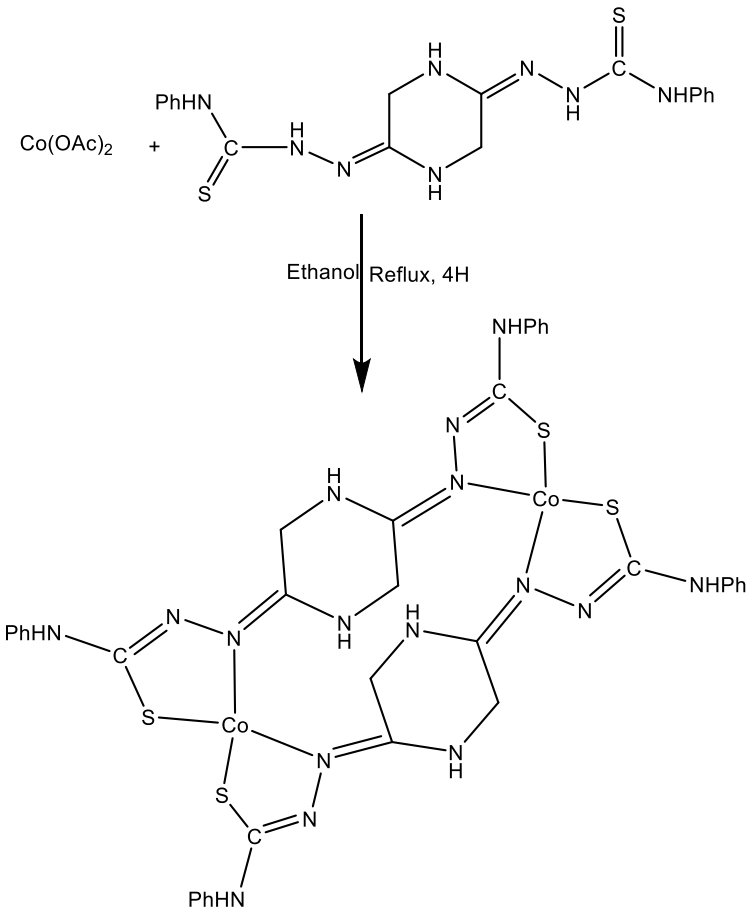

3.5.10 [Co(2,6 bdptsc)] 10.

To a solution of 2,6 Diacetyl pyridine bisthiosemicarbazone (0.025g, 0.8mmol), was added $Co(OAc)_2$ (0.020g, 0.8mmol) in ethanol The reddish coloured solution was refluxed for 4 hours. After two to three days brown coloured compound was obtained and dried in vaco. Yield: 85%, M.P. 242-244°C. Main FTIR peaks (neat, cm^{-1}); $\upsilon(NH_2)$ 3285, $\upsilon(C=N)$ 1590s, $\upsilon(C=C)$ 1487m, $\delta(NH_2)$ 1447s, $\upsilon(C=S)$ 793s. ESR data (g, gauss): $g_{\parallel}$ 2.22; $g_{\perp}$ 2.05. Mass spectra: m/z$[Co(C_{11}H_{13}N_7S_2)]^+$: 367.08amu (parent ion peak).

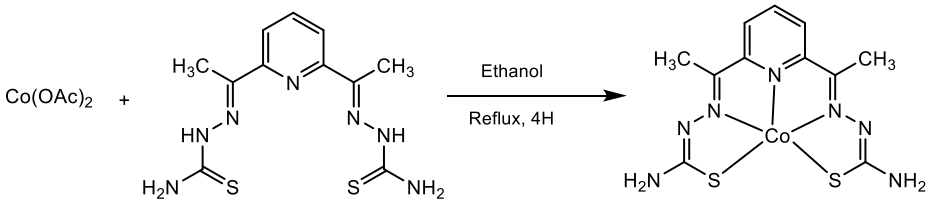

3.5.11 [Co(2,6 bdptsc N-Me)] 11.

To a solution of 2,6 Diacetyl pyridine N-methyl bisthiosemicarbazone (0.025g, 0.7mmol), was added $Co(OAc)_2$ (0.018g, 0.7mmol) in ethanol. The reddish coloured solution was refluxed for 4 hours. After two to three days brown coloured compound was obtained and dried in vaco. Brown coloured compound was collected after two days and dried in vaco. Yield: 86%, M.P. 235-237°C. Main FTIR peaks (neat, cm^{-1}); $\upsilon(NH_2)$ 3265m; υ(C=N) 1619s; υ(C=C) 1508m; υ(C=S) 810s. ESR data (g, tensor, A, gauss): $g_{\parallel}$ 2.28; $g_{\perp}$ 2.22. Mass spectra: m/z [Co $(C_{13}H_{17}N_7S_2)]^+$: 394.29amu (parent ion peak).

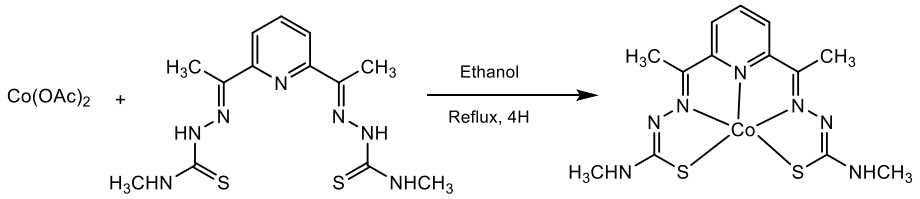

3.5.12 [Co(2,6 bdptsc N-Ph)] 12.

To a solution of 2,6 Diacetyl pyridine N-phenyl bisthiosemicarbazone (0.025g, 0.5mmol), was added $Co(OAc)_2$ (0.013g, 0.5mmol) in ethanol. The reddish coloured solution was refluxed for 4 hours. After two to three days brown coloured compound was obtained and dried in vaco. Yield: 88%, M.P. 247-249°C. Main FTIR peaks (neat, cm^{-1}); $\upsilon(NH_2)$ 3385m, 3200m; υ(C=N) 1604s; υ(C=C) 1477m; υ(C=S) 749s. ESR data (g, tensor, A, gauss): $g_{\parallel}$ 2.45; $g_{\perp}$ 2.31. Mass spectra: m/z$[Co(C_{23}H_{21}N_7S_2)]^+$: 518.13amu (parent ion peak).

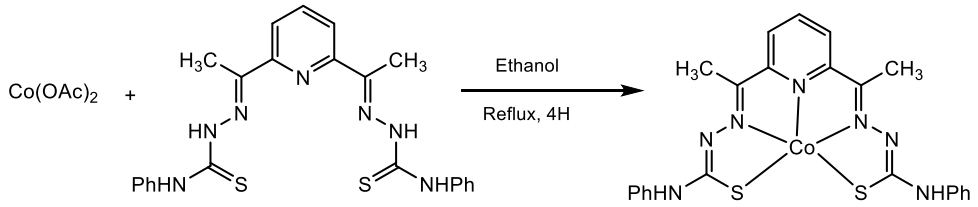

3.6 Complexes of Nickel (II)

3.6.1 [Ni(2,5 bttsc)] 13.

To a solution of 2,5 thiophene dicarboxaldehyde bisthiosemicarbazone (0.035g, 0.12 mmol), was added $Ni(OAc)_2$ (0.025g, 0.12mmol) in ethanol. The dark red coloured solution was refluxed for 4 hours. After two to three days dark brown coloured compound was obtained and dried in vaco.

Yield: 81%, M.P. 226-228°C. Main FTIR bands (neat, cm^{-1}); $\upsilon(NH_2)$ 3419, 3302m; $\upsilon(C = N)$ 1598s; $\upsilon(C = C)$ 1495m; δ (NH_2) 1436s; $\upsilon(C=S)$ 698s. Magnetic moment μ_{eff} (BM)= 3.22. Mass spectra: m/z$[Ni(C_8H_{10}N_6S_3)]^+$: 342.94amu (parent ion peak), 229.14amu (Loss of $(NH_2\text{-}S)_2C$, 137.00amu (Loss of both arms of bisthiosemicarbazone).

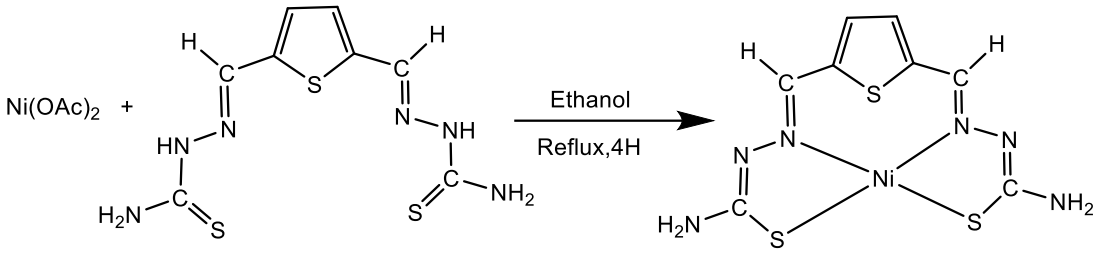

3.6.2 [Ni(2,5 bttsc N-Me)] 14.

To a solution of 2,5 thiophene dicarboxaldehyde N-methyl bisthiosemicarbazone (0.039g, 0.14 mmol), was added $Ni(OAc)_2$ (0.025g, 0.14mmol) in ethanol. The dark red coloured solution was refluxed for 4 hours. After two to three days dark brown coloured compound was obtained and dried in vaco. Yield: 81%, M.P. 232-234°C. Main FTIR bands (neat, cm^{-1}); $\upsilon(NH_2)$ 3314; $\upsilon(C = N)$ 1647s; $\upsilon(C = C)$ 1508m; $\delta(NH_2)$ 1401s; $\upsilon(C=S)$ 797s. Magnetic moment μ_{eff} (BM)= 3.63. Mass spectra: m/z$[Ni(C_{10}H_{12}N_6S_3)]^+$: 370.97amu (parent ion peak).

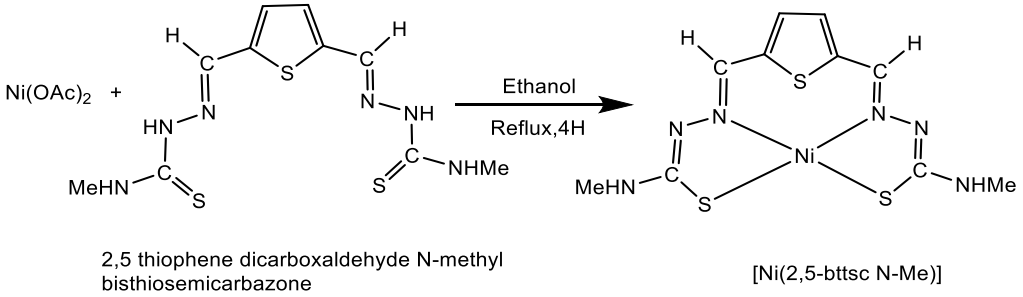

3.6.3 [Ni(2,5 bttsc N-Ph)] 15.

To a solution of 2,5 thiophene dicarboxaldehyde N-phenyl bisthiosemicarbazone (0.025g, 0.57 mmol), was added $Ni(OAc)_2$ (0.014g, 0.57mmol) in ethanol. The dark red coloured solution was refluxed for 4 hours. After two to three days dark brown coloured compound was obtained and

dried in vaco. Yield: 86%, M.P. 233-235°C. Main FTIR peaks (neat, cm^{-1}); υ(NH_2) 3297,3217; υ(C=N) 1590s; υ(C=C) 1509m; δ(NH_2) 1429s; υ(C=S) 751s. Magnetic moment μ_{eff} (BM)= 3.10. Mass spectra: m/z[$Ni(C_{20}H_{16}N_6S_3)]^+$: 502.37 amu (parent ion peak).

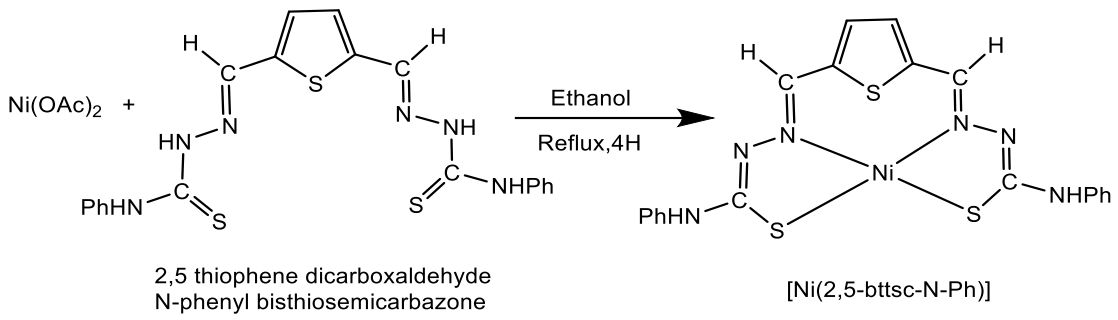

3.6.4 [Ni(bitsc)] 16.

To a solution of 2,3-isatin bisthiosemicarbazone (0.058g, 0.20mmol) was added $Ni(OAc)_2$ (0.050g, 0.20mmol) in ethanol. The dark red coloured solution was refluxed for 4 hours. After two to three days dark brown coloured compound was obtained and dried in vaco. Yield: 82%, M.P. 230-232°C. Main FTIR bands (neat, cm^{-1}); υ (NH_2) 3423, 3229m; υ(C=N) 1652s; υ(C=C) 1509m; υ(C=S) 790s. Magnetic moment μ_{eff} (BM)= 3.17. Mass spectra: m/z[$Ni(C_{10}H_9N_7S_2)]^+$: 355.03 amu (parent ion peak).

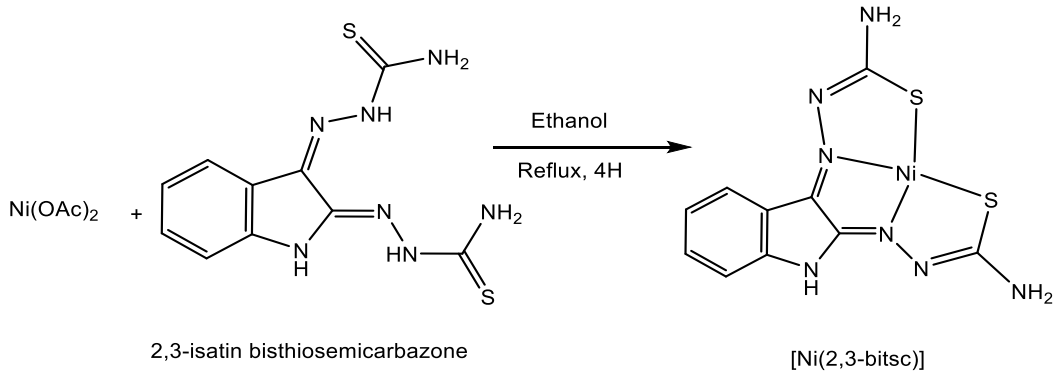

3.6.5 [Ni(bitsc-N-Me)] 17.

To a solution of 2,3-isatin-N-methyl bisthiosemicarbazone (0.064g, 0.2mmol) was added $Ni(OAc)_2$ (0.050g, 0.2mmol) in ethanol. The dark red coloured solution was refluxed for 4 hours. After two to three days dark brown coloured compound was obtained and dried in vaco. Yield: 85%, M.P. 222-224°C, Main FTIR bands (neat, cm^{-1}); υ(NH_2) 3220m; υ(C=N) 1655s; υ(C=C)

1515s; υ(C=S) 776s. Magnetic moment μ_{eff}(BM)= 3.07. Mass spectra: m/z$[Ni(C_{12}H_{13}N_7S_2)]^+$: 393.36 (parent ion peak).

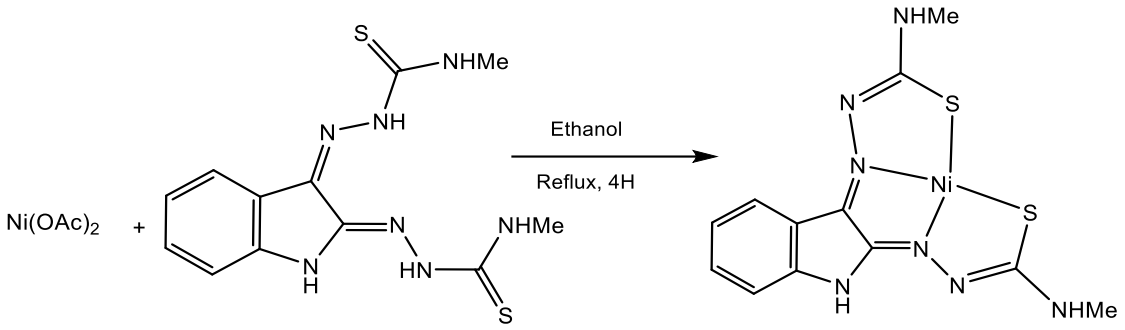

3.6.6 [Ni(bitsc-N-Ph)] 18.

To a solution of 2,3-isatin-N-phenylbisthiosemicarbazone (0.089g, 0.2mmol) was added $Ni(OAc)_2$ (0.050g, 0.2mmol) in ethanol. The dark red coloured solution was refluxed for 4 hours. After two to three days dark brown coloured compound was obtained and dried in vaco. Yield: 78%, M.P. 225-227°C. Main FTIR peaks (neat, cm^{-1}); υ(NH_2) 3281m; υ(C = N) 1669s; υ(C = C) 1525s; υ(C=S) 746s. Magnetic moment μ_{eff} (BM)= 3.32. Mass spectra, m/z: $[Ni(C_{22}H_{17}N_7S_2)]^+$: 500.08 amu (parent ion peak).

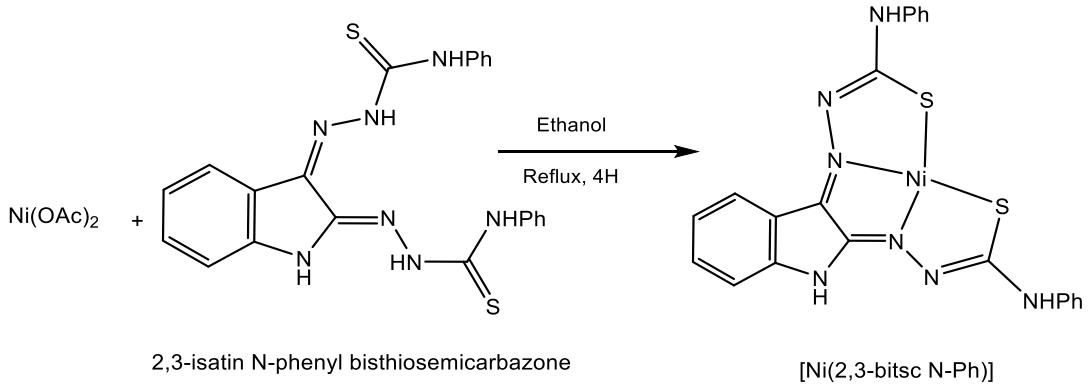

3.6.7 [Ni(2,5 bptsc)] 19.

To a solution of 2,5 piperazinedione bisthiosemicarbazone (0.050g, 0.20mmol), was added $Ni(OAc)_2$ (0.0518g, 0.2mmol) in ethanol. The dark red coloured solution was refluxed for 4 hours. After two to three days dark brown coloured compound was obtained and dried in vaco. Yield: 85%, M.P. 222-224°C. Main FTIR peaks (neat, cm^{-1}); υ(NH_2) 3328m, 3204m; υ(C=N) 1659s;

υ(C=C) 1458m; δ(NH_2) 1329s; υ(C=S) 772s. Magnetic moment μ_{eff} (BM)= 3.53. Mass spectra: m/z [$Ni(C_6H_{12}N_8S_2)$]:318.34 amu (parent ion peak).

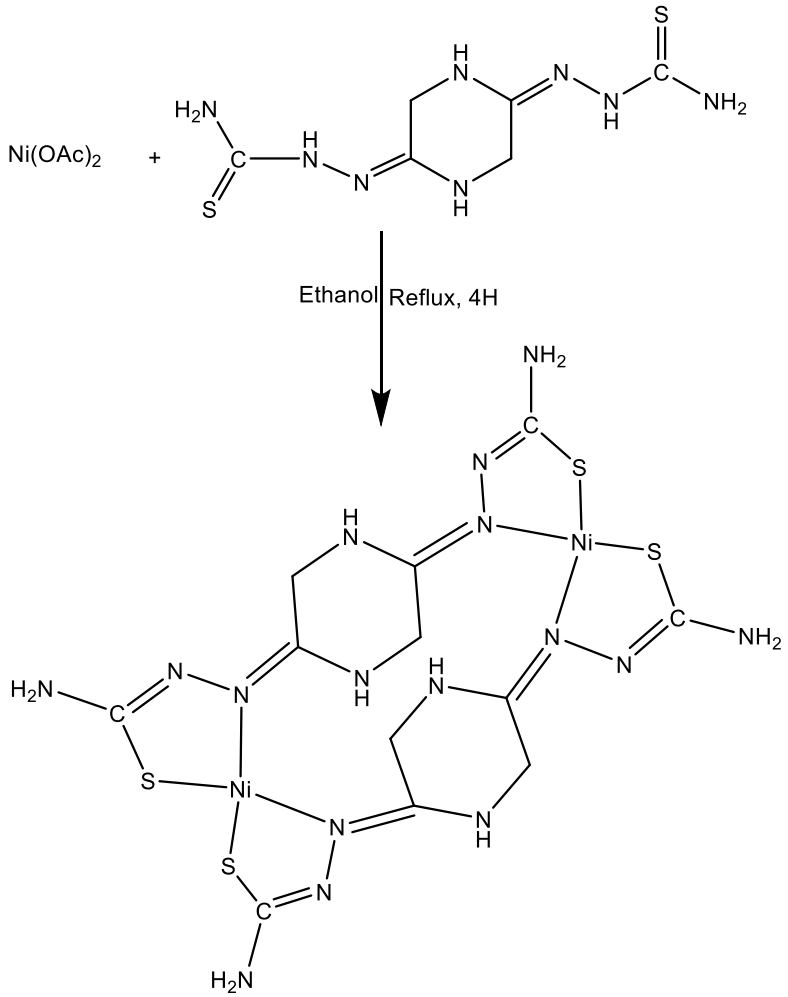

3.6.8 [Ni(2,5 bptsc N-Me)] 20.

To a solution of 2,5 piperazinedione N-methyl bisthiosemicarbazone (0.050g, 0.20mmol), was added $Ni(OAc)_2$ (0.041g, 0.20mmol) in ethanol. The dark red coloured solution was refluxed for 4 hours. After two to three days dark brown coloured compound was obtained and dried in vaco. Yield: 89%, M.P. 220-222°C. Main FTIR peaks (neat, cm^{-1}); υ(NH_2) 3272m; υ(C=N) 1562s; υ(C=C) 1410m; υ(C=S) 725s. Magnetic moment μ_{eff} (BM)= 3.45. Mass spectra: m/z [$Ni(C_8H_{16}N_8S_2)$]: 347.21amu (parent ion peak).

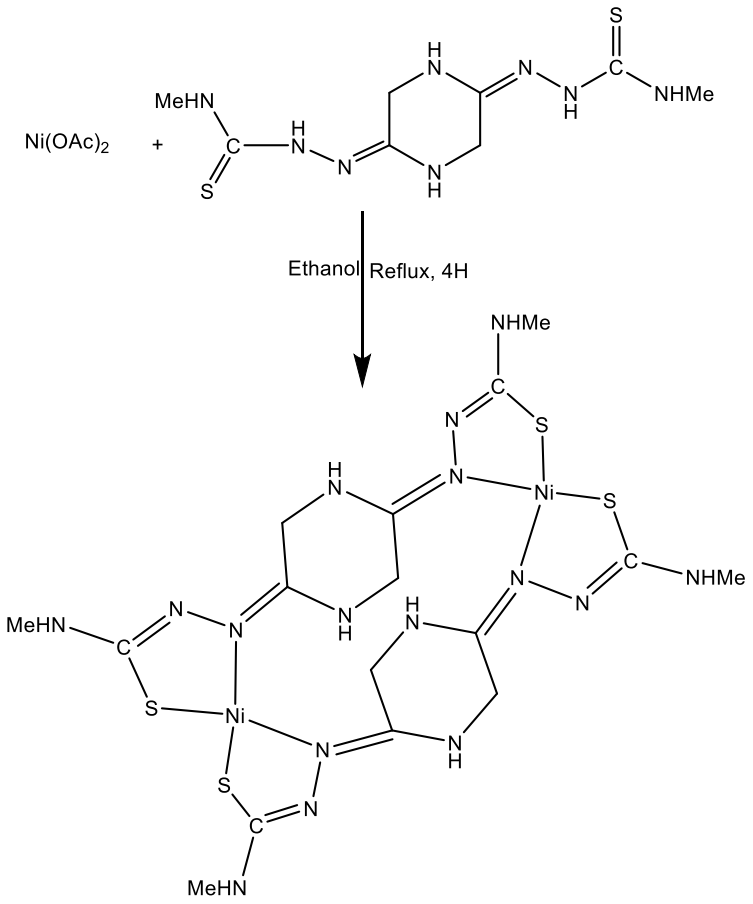

3.6.9 [Ni(2,5 bptsc N-Ph)] 21.

To a solution of 2,5 piperazinedione N-phenyl bisthiosemicarbazone (0.081g, 0.2mmol), was added $Ni(OAc)_2$ (0.050g, 0.2mmol) in ethanol. The dark red coloured solution was refluxed for 4 hours. After two to three days dark brown coloured compound was obtained and dried in vaco. Yield: 88%, M.P. 248-250°C. Main FTIR peaks (neat, cm^{-1}); $\upsilon(NH_2)$ 3292m,3204m; υ(C=N) 1666s; υ(C=C) 1467m; υ(C=S) 798s. Magnetic moment μ_{eff}(BM)= 4.62. Mass spectra: m/z$[Ni(C_{18}H_{22}N_8S_2)]^+$: 545.48 amu (parent ion peak).

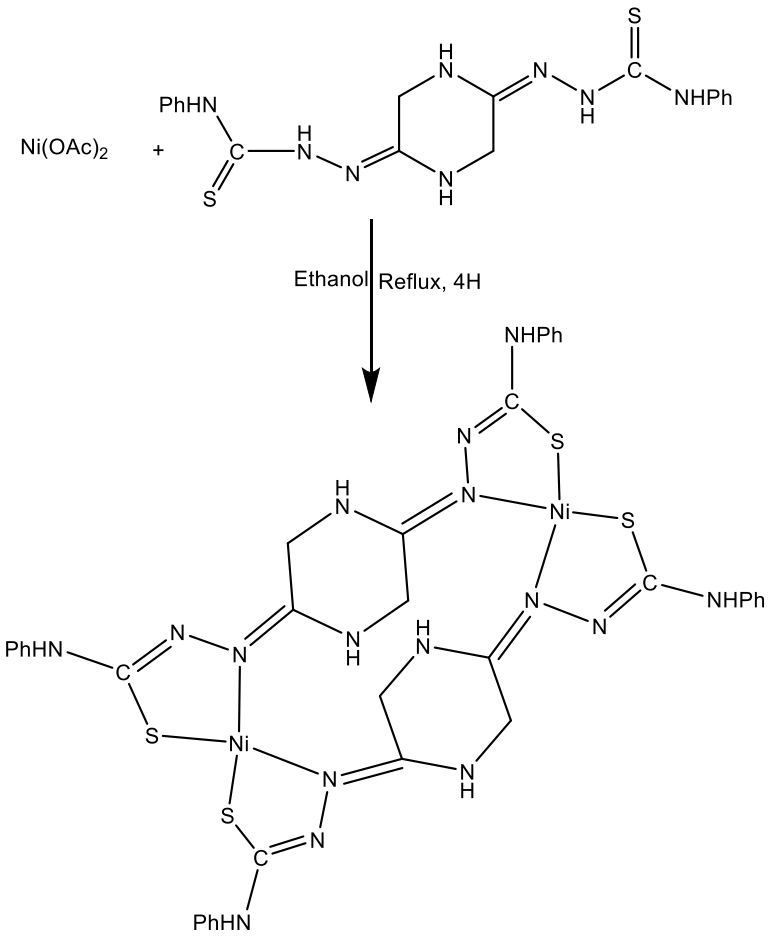

3.6.10 [Ni(2,6 bdptsc)] 22.

To a solution of 2,6 Diacetyl pyridine bisthiosemicarbazone (0.025g, 0.80mmol), was added $Ni(OAc)_2$ (0.020g, 0.80mmol) in ethanol. The dark red coloured solution was refluxed for 4 hours. After two to three days dark brown coloured compound was obtained and dried in vaco. Yield: 90%, M.P. 245-247°C. Main FTIR peaks (neat, cm^{-1}); $\upsilon(NH_2)$ 3285, $\upsilon(C=N)$ 1590s, $\upsilon(C=C)$ 1487m, $\delta(NH_2)$ 1447s, $\upsilon(C=S)$ 793s. Magnetic moment μ_{eff}(BM)= 3.53. Mass spectra: m/z$[Ni(C_{11}H_{13}N_7S_2)]^+$: 365.99 amu (parent ion peak).

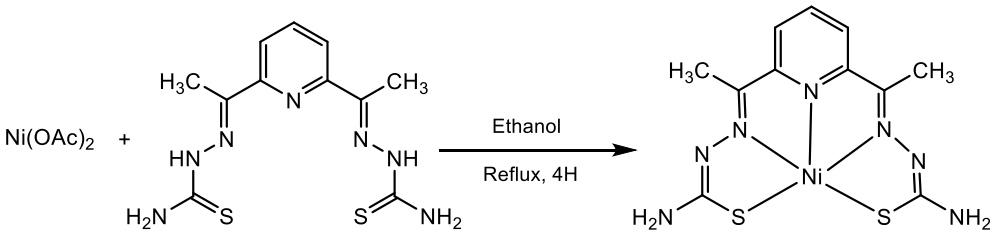

2,6 diacetylpyridine bisthiosemicarbazone [Ni(2,6-bdptsc)]

3.6.11 [Ni(2,6 bdptsc N-Me)] 23.

To a solution of 2,6 Diacetyl pyridine N-methyl bisthiosemicarbazone (0.025g, 0.2mmol), was added $Ni(OAc)_2$ (0.018g, 0.2mmol) in ethanol. The dark red coloured solution was refluxed for 4 hours. After two to three days dark brown coloured compound was obtained and dried in vaco. Yield: 85%, M.P. 232-234˚C. Main FTIR bands (neat, cm^{-1}); $\upsilon(NH_2)$ 3290m; υ(C = N) 1523s; υ(C = C) 1447m; υ(C=S) 797s. Magnetic moment μ_{eff}(BM)= 3.45. Mass spectra: m/z[Ni $(C_{13}H_{17}N_7S_2)]^+$: 394.04 amu (parent ion peak).

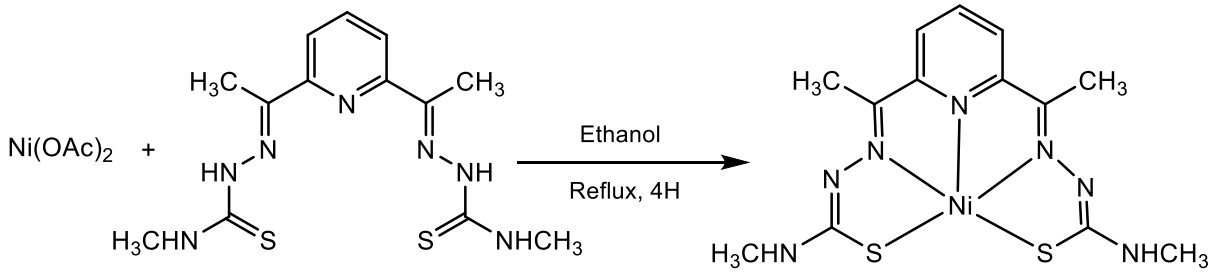

2,6 diacetylpyridine N-methyl bisthiosemicarbazone

[Ni(2,6-bdptsc,N-Me)]

3.6.12 [Ni(2,6 bdptsc N-Ph)] 24.

To a solution of 2,6 Diacetyl pyridine N-phenyl bisthiosemicarbazone (0.025g, 0.2mmol), was added $Ni(OAc)_2$ (0.0134g, 0.2mmol) in ethanol. The dark red coloured solution was refluxed for 4 hours. After two to three days dark brown coloured compound was obtained and dried in vaco. Yield: 89%, M.P. 239-241˚C. Main FTIR bands (neat, cm^{-1}); $\upsilon(NH_2)$ 3366m, 3272m; υ(C=N) 1615s; υ(C = C) 1528m; υ(C = S) 769s. Magnetic moment μ_{eff}(BM)= 2.8. Mass spectra: m/z$[Ni(C_{23}H_{21}N_7S_2)]^+$:518.07 amu (parent ion peak).

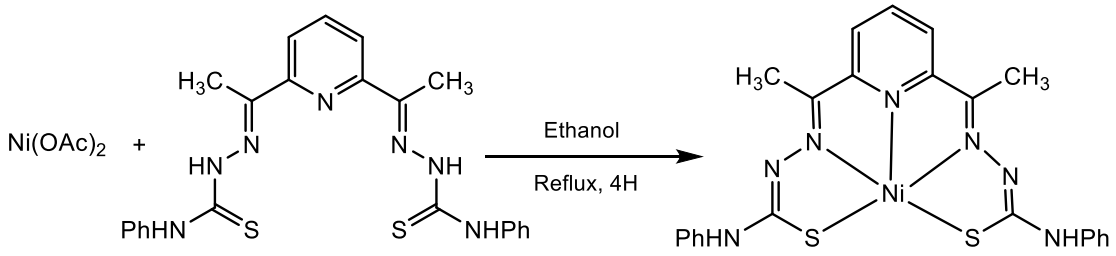

2,6 diacetylpyridine N-phenyl bisthiosemicarbazone

[Ni(2,6-bdptsc,N-Ph)]

3.7 Synthesis of Copper(II) complexes

3.7.1 [Cu(2,5 bttsc)] 25.

To a solution of 2,5 thiophene dicarboxaldehyde bisthiosemicarbazone (0.035g, 0.122 mmol), was added $Cu(OAc)_2$ (0.025g, 0.125mmol) in ethanol. The dark brown coloured solution was refluxed for 4 hours. After two to three days dark brown coloured compound was obtained and dried in vaco. Yield: 80%, M.P. 228-230°C. Main FTIR bands (neat, cm^{-1}); $\upsilon(NH_2)$ 3409, 3278m; υ(C = N) 1599s; υ(C = C) 1535m; $\delta(NH_2)$ 1451s; υ(C = S) 781s. ESR data (g, tensor, A, gauss): $g_{\parallel}$ 2.40; $g_{\perp}$, 2.08; $A_{\parallel}$, 174; $A_{\perp}$, 40. Mass spectra: m/z$[Cu(C_8H_{10}N_6S_3)]^+$: 343.12amu (Parent ion peak), 313amu(Loss of NH_2-C-N).

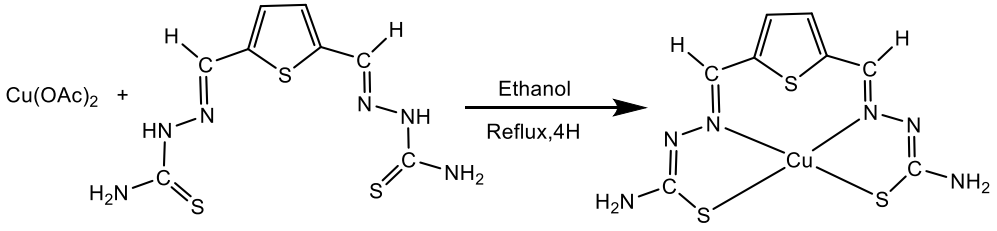

3.7.2 [Cu(2,5 bttsc-N-Me)] 26.

To a solution of 2,5thiophene dicarboxaldehyde-N-methyl bisthiosemicarbazone (0.039g, 0.12 mmol), was added $Cu(OAc)_2$ (0.025g, 0.12mmol) in ethanol. The dark red coloured solution was refluxed for 4 hours. After two to three days dark brown coloured compound was obtained and dried in vaco. Yield: 78%, M.P. 235-237°C. Main FTIR bands (neat, cm^{-1}); $\upsilon(NH_2)$ 3372; υ(C = N) 1537s; υ(C = C) 1508m; υ(C = S) 761s; υ(M–N) 485s. ESR data (g, tensor, A, gauss): $g_{\parallel}$ 2.15; $g_{\perp}$, 2.07; $A_{\parallel}$, 160; $A_{\perp}$, 45. Mass spectra: m/z$[Cu(C_{10}H_{14}N_6S_3)]^+$: 376.97 amu ($M^+$).

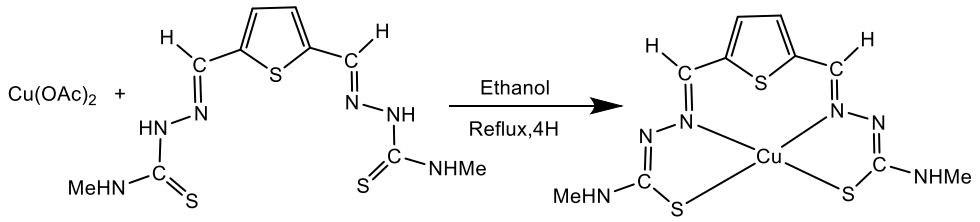

2,5 thiophene dicarboxaldehyde
N-methyl bisthiosemicarbazone

[Cu(2,5-bttsc-N-Me)]

3.7.3 [Cu(2,5 bttsc-N-Ph)] 27.

To a solution of 2,5 thiophene dicarboxaldehyde-N-phenyl bisthiosemicarbazone (0.011g, 0.12 mmol),

was added $Cu(OAc)_2$ (0.025g, 0.12mmol) in ethanol . The dark red coloured solution was refluxed for 4 hours. After two to three days dark brown coloured compound was obtained and dried in vaco. Yield: 80%, M.P. 230-232˚C. Main FTIR bands (neat, cm^{-1}); $\upsilon(NH_2)$ 3390; $\upsilon(C = N)$ 1679s; $\upsilon(C = C)$ 1595m; $\upsilon(C = S)$ 747s. ESR data (g, tensor, A, gauss): $g_{\parallel}$ 2.20; $g_{\perp}$, 2.12; $A_{\parallel}$, 148; $A_{\perp}$, 45. Mass spectra: m/z[$Cu(C_{20}H_{18}N_6S_3)$]: 500.08 (M^+).

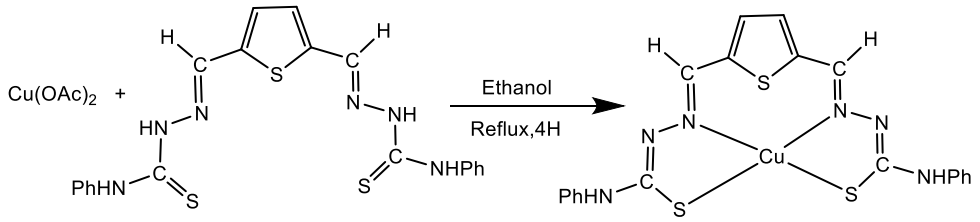

2,5 thiophene dicarboxaldehyde
N-phenyl bisthiosemicarbazone

[Cu(2,5-bttsc-N-Ph)]

3.7.4 [Cu(bitsc)] 28.

To a solution of isatin thiosemicarbazone (0.073g, 0.2mmol), was added $Cu(OAc)_2$ (0.050g, 0.2mmol) in ethanol. The dark red coloured solution was refluxed for 4 hours. After two to three days dark brown coloured compound was obtained and dried in vaco. Yield: 78%, M.P. 235-237˚C. Main FTIR peaks (neat, cm^{-1}); $\upsilon(NH_2)$ 3239m; $\upsilon(C=N)$ 1659s; $\upsilon(C=C)$ 1556m; $\delta(NH_2)$ 1511s; $\upsilon(C=S)$ 823s. ESR data (g, tensor, A, gauss): $g_{\parallel}$ 2.24; $g_{\perp}$, 2.09; $A_{\parallel}$, 170; $A_{\perp}$, 38. Mass spectra: m/z[$Cu(C_{10}H_9N_7S_2)$]$^+$: 355.06 (parent ion peak).

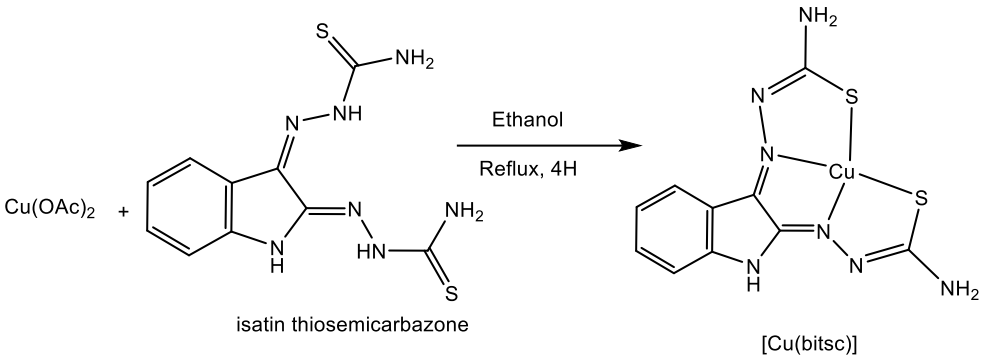

3.7.5 [Cu(bitsc-N-Me)] 29.

To a solution of isatin bis-N-methyl thiosemicarbazone (0.080g, 0.2 mmol) was added $Cu(OAc)_2$ (0.050g, 0.2mmol) in ethanol. The dark red coloured solution was refluxed for 4 hours. After two to three days dark brown coloured compound was obtained and dried in vaco. Yield: 80%, M.P. 230-232˚C. Main FTIR bands (neat, cm^{-1}); $\upsilon(NH_2)$ 3223m; υ(C = N) 1643s; υ(C = C)1525m; υ(C = S) 857s. ESR data (g, tensor, A, gauss): $g_{\parallel}$ 2.17; $g_{\perp}$, 2.11; $A_{\parallel}$, 145; $A_{\perp}$, 25. Mass spectra: m/z$[Cu(C_{12}H_{13}N_7S_2)]^+$: 381.29 (parent ion peak).

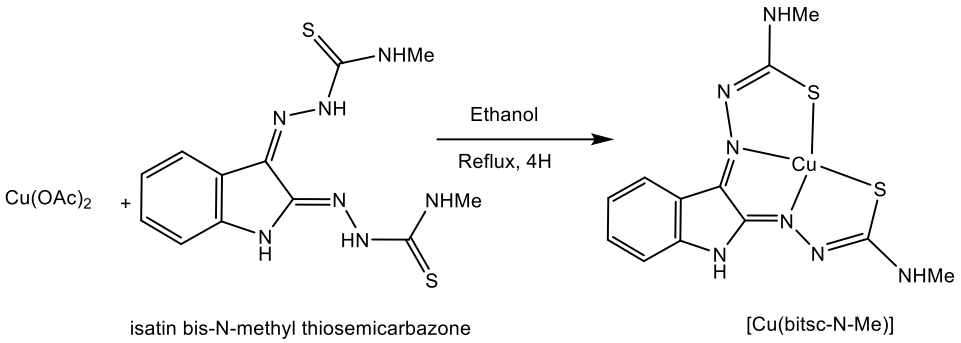

3.7.6 [Cu(bitsc-N-Ph)] 30.

To a solution of isatin bis-N-phenyl thiosemicarbazone (0.1g, 0.2mmol) was added $Cu(OAc)_2$ (0.050g, 0.2mmol) in ethanol. The dark red coloured solution was refluxed for 4 hours. After two to three days dark brown coloured compound was obtained and dried in vaco. Yield: 78%, M.P. 215-217˚C. Main FTIR bands (neat, cm^{-1}); $\upsilon(NH_2)$ 3205m; υ(C = N) 1654s; υ(C = C) 1596m; υ(C = S) 822s. ESR data (g, tensor, A, gauss): $g_{\parallel}$ 2.26; $g_{\perp}$, 2.08; $A_{\parallel}$, 165; $A_{\perp}$, 45. Mass spectra: m/z$[Cu(C_{22}H_{17}N_7S_2)]^+$: 505.22 (parent ion peak).

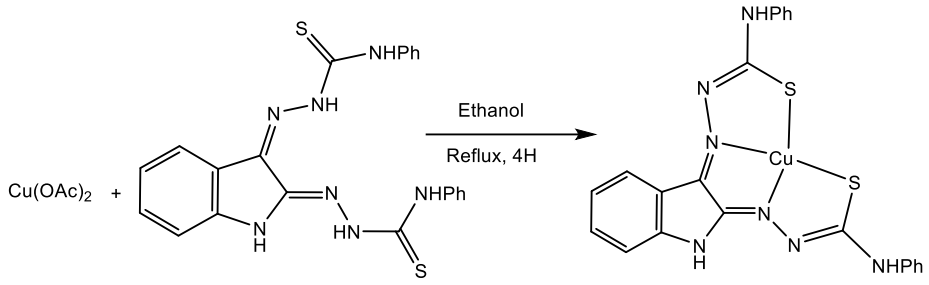

isatin bis-N-phenyl thiosemicarbazone [Cu(bitsc-N-Ph)]

3.7.7 [Cu(2,5 bptsc)] 31.

To a solution of 2,5 piperazinedione bisthiosemicarbazone (0.064g, 0.2mmol), was added $Cu(OAc)_2$ (0.050g, 0.2mmol) in ethanol. The dark red coloured solution was refluxed for 4 hours. After two to three days dark brown coloured compound was obtained and dried in vaco. Yield: 87%, M.P. 225-227°C. Main FTIR peaks (neat, cm^{-1}); $\upsilon(NH_2)$ 3407m; $\upsilon(C=N)$ 1598s; $\upsilon(C=C)$ 1487m; $\delta(NH_2)$ 1434s; $\upsilon(C=S)$ 763s. ESR data (g, tensor, A, gauss): $g_{\parallel}$ 2.465; $g_{\perp}$, 2.147; $A_{\parallel}$, 164; $A_{\perp}$, 42. Mass spectra: m/z$[Cu(C_6H_{12}N_8S_2)]^+$: 325.25 (parent ion peak).

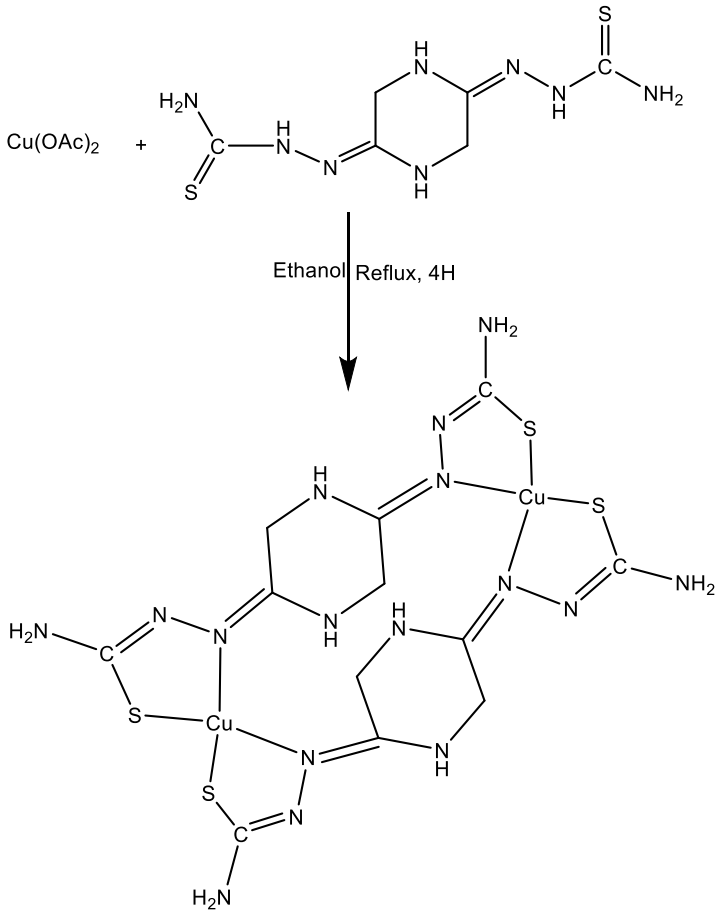

3.7.8 Cu(2,5 bptsc N-Me)] 32.

To a solution of 2,5 piperazinedione N-methyl bisthiosemicarbazone (0.119g, 0.2mmol), was added $Cu(OAc)_2$ (0.050g, 0.2mmol) in ethanol. The dark red coloured solution was refluxed for 4 hours. After two to three days dark brown coloured compound was obtained and dried in vaco. Yield: 88%, M.P. 220-222°C. Main IR bands (neat, cm^{-1}); υ (NH_2) 3290m, υ(C = N) 1550s, υ(C = C) 1487m, υ(C=S) 767s. ESR data (g, tensor, A, gauss): $g_{\parallel}$ 2.48; $g_{\perp}$, 2.14; $A_{\parallel}$, 168; $A_{\perp}$, 51. Mass spectra: m/z[$Cu(C_8H_{16}N_8S_2)]^+$: 349.11 (parent ion peak).

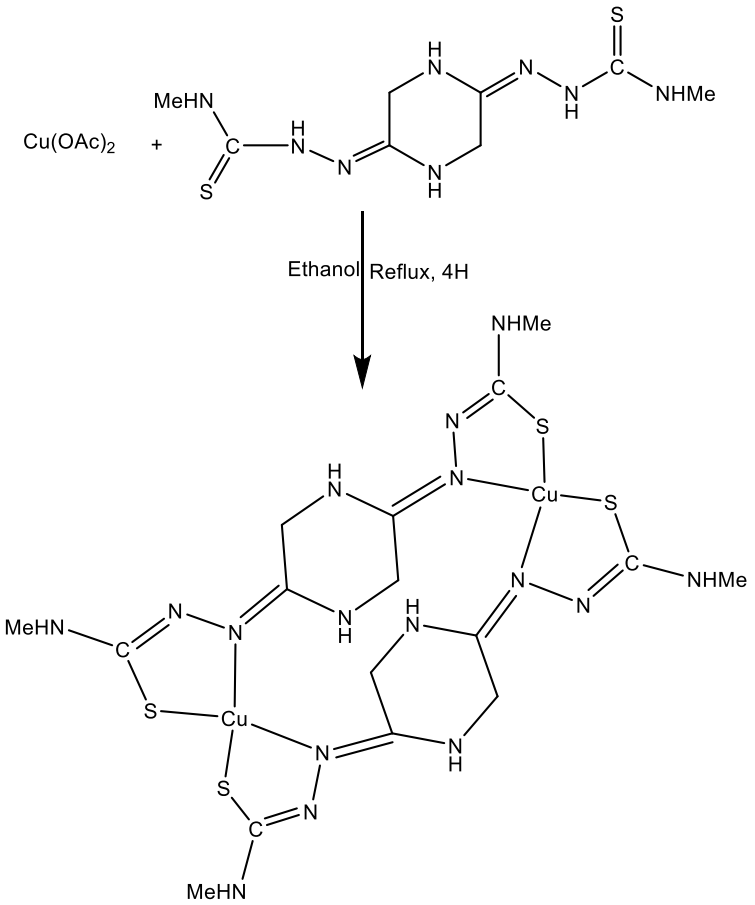

3.7.9 Cu(2,5 bptsc N-Ph)] 33.

To a solution of 2,5 piperazinedione N-phenyl bisthiosemicarbazone (0.102g, 0.2mmol), was added $Cu(OAc)_2$ (0.050g, 0.2mmol) in ethanol. The dark red coloured solution was refluxed for 4 hours. After two to three days dark brown coloured compound was obtained and dried in vaco. Yield: 88%, M.P. 234-236°C. Main FTIR peaks (neat, cm^{-1}); υ(NH_2) 3277m; υ(C=N) 1638s; υ(C=C) 1595m; υ(C=S) 807s. ESR data (g, tensor, A, gauss): $g_{\parallel}$ 2.48; $g_{\perp}$, 2.146; $A_{\parallel}$, 162; $A_{\perp}$, 40. Mass spectra: m/z[$Cu(C_{18}H_{22}N_8S_2)]^+$: 474.12 (parent ion peak).

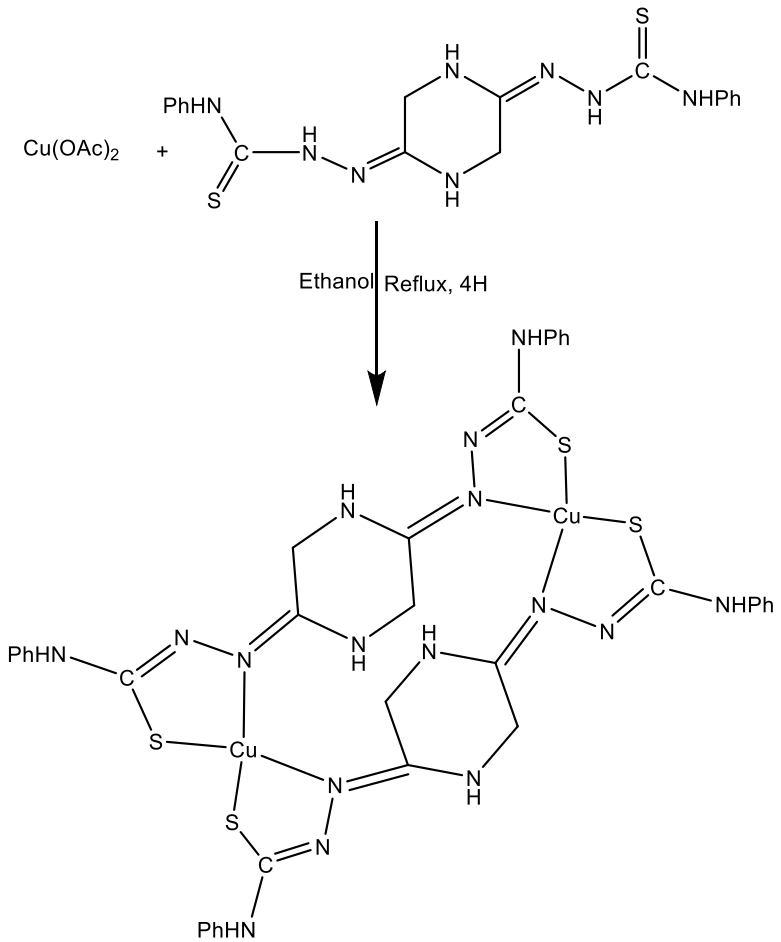

3.7.10 [Cu(2,6 bdptsc)] 34.

To a solution of 2,6 Diacetyl pyridine bisthiosemicarbazone (0.025g, 0.8mmol), was added $Cu(OAc)_2$ (0.016g, 0.8mmol) in ethanol. The dark red coloured solution was refluxed for 4 hours. After two to three days dark brown coloured compound was obtained and dried in vaco. Yield: 87%, M.P. 225-227°C. Main FTIR peaks (neat, cm^{-1}); $\upsilon(NH_2)$ 3311m, 3200, $\upsilon(C=N)$ 1627s, $\upsilon(C=C)$ 1588m, $\delta(NH_2)$ 1461s, $\upsilon(C=S)$ 806s. ESR data (g, tensor, A, gauss): $g_{\parallel}$ 2.2; $g_{\perp}$, 2.10; $A_{\parallel}$, 147; $A_{\perp}$, 44. Mass spectra: m/z$[Cu(C_{11}H_{13}N_7S_2)]^+$: 371.18 (parent ion peak).

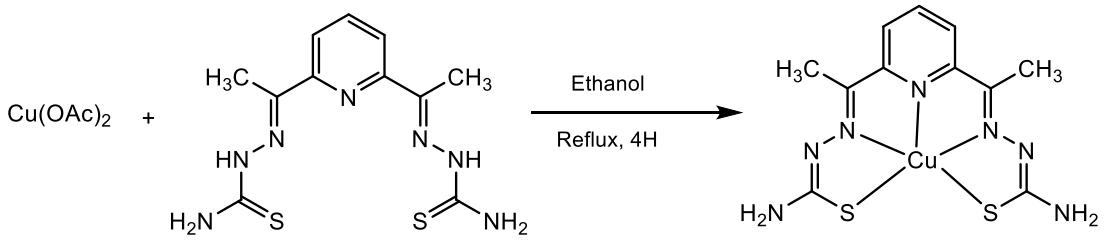

3.7.11 [Cu(2,6 bdptsc N-Me)] 35.

To a solution of 2,6 Diacetyl pyridine N-methyl bisthiosemicarbazone (0.025g, 0.7mmol), was added $Cu(OAc)_2$ (0.014g, 0.7mmol) in ethanol. The dark red coloured solution was refluxed for 4 hours. After two to three days dark brown coloured compound was obtained and dried in vaco. Yield: 89%, M.P. 232-234°C. Main FTIR peaks (neat, cm^{-1}); $\upsilon(NH_2)$ 3295m; υ(C=N) 1579s; υ(C=C) 1511m; υ(C=S) 787s. ESR data (g, tensor, A, gauss): $g_{\parallel}$ 2.45; $g_{\perp}$, 2.12; $A_{\parallel}$, 168; $A_{\perp}$, 49. Mass spectra: m/z$[Cu(C_{13}H_{17}N_7S_2)]^+$: 399.17(parent ion peak).

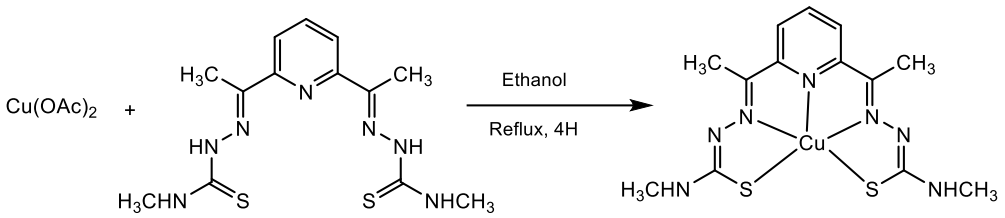

3.7.12 [Cu(2,6 bdptsc N-Ph)] 36.

To a solution of 2,6 Diacetyl pyridine N-phenyl bisthiosemicarbazone (0.025g, 0.5mmol), was added $Cu(OAc)_2$ (0.010g, 0.5mmol) in ethanol. The dark red coloured solution was refluxed for 4 hours. After two to three days dark brown coloured compound was obtained and dried in vaco. Yield: 86%, M.P. 237-239°C. Main FTIR peaks (neat, cm^{-1}); $\upsilon(NH_2)$ 3374m, 3246m; υ(C=N) 1591s; υ(C=C) 1527m; υ(C=S) 752s. ESR data (g, tensor, A, gauss): $g_{\parallel}$ 2.25; $g_{\perp}$, 2.10; $A_{\parallel}$, 164; $A_{\perp}$, 44. Mass spectra: m/z$[Cu(C_{23}H_{21}N_7S_2)]^+$: 524.15 (parent ion peak).

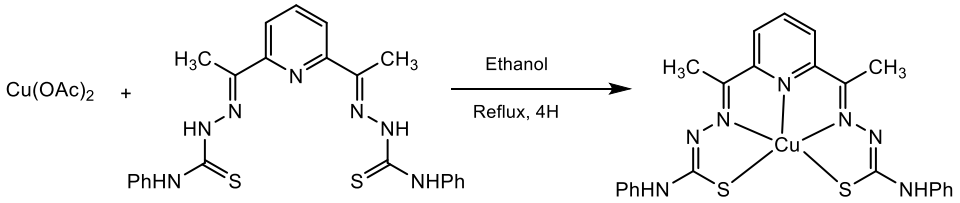

3.8.1 [Zn(2,5 bttsc)] 37.

To a solution of 2,5 thiophene dicarboxaldehyde bisthiosemicarbazone (0.026g, 0.11 mmol), was added $Zn(OAc)_2$ (0.025g, 0.11mmol) in ethanol. The dark orange coloured solution was refluxed for 4 hours. After two to three days orange coloured compound was obtained and dried in vaco. Yield: 81%, M.P. 224-226°C. Main FTIR peaks (neat, cm^{-1}); 3408m, 3277; υ(–NH–) 3154w; υ(C=N) 1598s; υ(C=C) 1534s; δ(NH_2) 1451s; υ(C=S) 805s. Mass spectra: m/z$[Zn(C_8H_8N_6S_3)]^+$: 393.29 amu (parent ion peak), 287 amu (Loss of Zn metal ion).

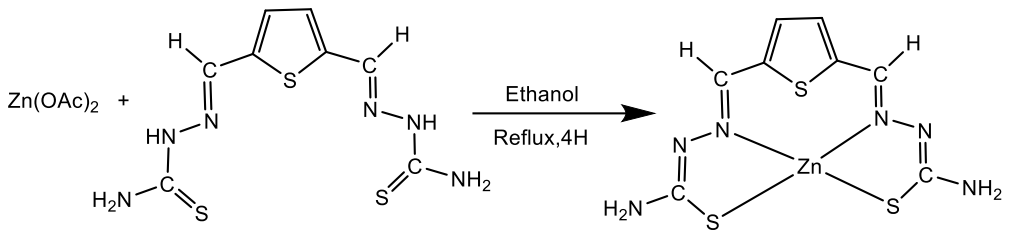

2,5 thiophene dicarboxaldehyde bisthiosemicarbazone [Zn(2,5-bttsc)]

3.8.2 [Zn(2,5bttsc N-Me)] 38.

To a solution of 2,5 thiophene dicarboxaldehyde N-methyl bisthiosemicarbazone (0.039g, 0.098 mmol), was added $Zn(OAc)_2$ (0.025g, 0.098mmol) in ethanol. The dark red coloured solution was refluxed for 4 hours. After two to three days dark brown coloured compound was obtained and dried in vaco. Yield: 87%, M.P. 232-234°C. Main FTIR peaks (neat, cm^{-1}); υ(NH_2) 3325; υ(C=N) 1576s; υ(C=C) 1475m; υ(C=S) 801s. Mass spectra: m/z$[Zn(C_{10}H_{12}N_6S_3)]^+$: 413.26 amu (parent ion peak).

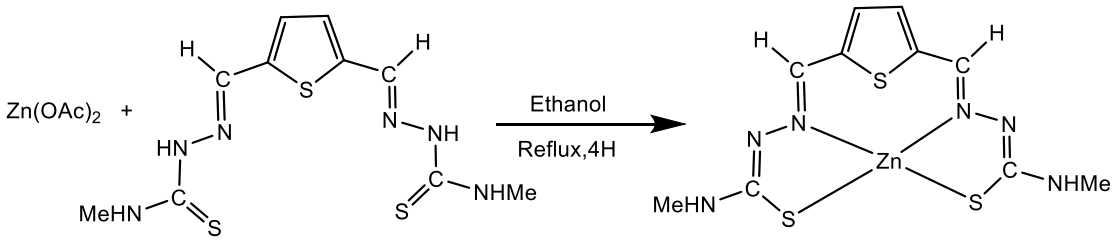

2,5 thiophene dicarboxaldehyde N-methyl bisthiosemicarbazone [Zn(2,5-bttsc,N-Me)]

3.8.3 [Zn(2,5bttsc,N-Ph)] 39.

To a solution of 2,5 thiophene dicarboxaldehyde N-phenyl bisthiosemicarbazone (0.025g, 0.057 mmol), was added $Zn(OAc)_2$ (0.014g, 0.057mmol) in ethanol. The dark red coloured solution was refluxed for 4 hours. After two to three days dark brown coloured compound was obtained and dried in vaco. Yield: 83%, M.P. 226-228˚C. Main FTIR peaks (neat, cm^{-1}); $\upsilon(NH_2)$ 3334m, 3200m; υ(C=N) 1598s; υ(C=C) 1436m; υ(C=S) 742s. Mass spectra: m/z$[Zn(C_{10}H_{12}N_6S_3)]^+$: 521.13 amu (parent ion peak).

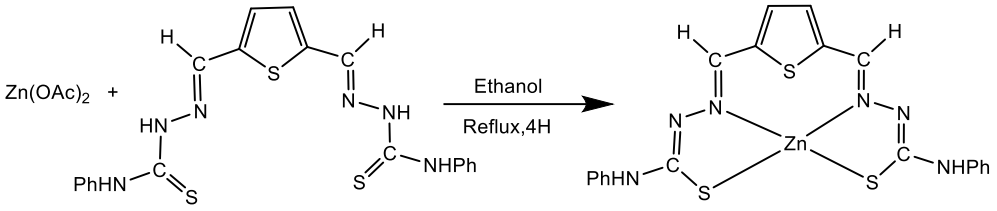

2,5 thiophene dicarboxaldehyde N-phenyl bisthiosemicarbazone

[Zn(2,5-bttsc,N-Ph)]

3.8.4 [Zn(bitsc)] 40.

To a solution of 2,3-isatin bisthiosemicarbazone (0.066g, 0.22mmol) was added $Zn(OAc)_2$ (0.050g, 0.22mmol) in ethanol. The dark red coloured solution was refluxed for 4 hours. After two to three days dark brown coloured compound was obtained and dried in vaco. Yield: 88%, M.P. 218-220˚C. Main FTIR bands (neat, cm^{-1}); υ (NH_2) 3226m; υ(C = N) 1540s; υ(C = C) 1440m; δ (NH_2) 1280s; υ(C=S) 749s. Mass spectra: m/z$[Zn(C_{10}H_9N_7S_2)]^+$: 365.02 amu (parent ion peak).

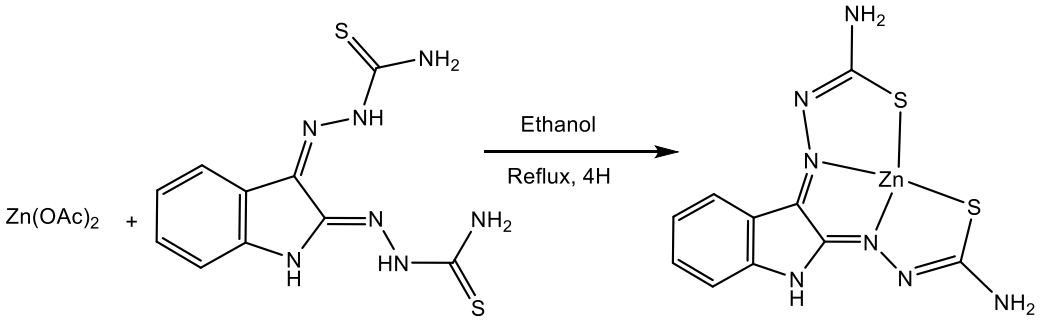

2,3-isatin bisthiosemicarbazone

[Zn(2,3-bitsc)]

3.8.5 [Zn(bitsc-N-Me)] 41.

To a solution of 2,3-isatin-N-methyl bisthiosemicarbazone (0.070g, 0.20mmol) was added $Zn(OAc)_2$ (0.050g, 0.20mmol) in ethanol. The dark red coloured solution was refluxed for 4 hours. After two to three days dark brown coloured compound was obtained and dried in vaco. Yield:

84%, M.P. 236-238°C, Main FTIR bands (neat, cm^{-1}); υ (NH_2) 3367m; υ(C = N) 1612s; υ(C = C) 1550m; υ (C = S) 745s. m/z: (M^+). 743s. Mass spectra: m/z[$Zn(C_{10}H_9N_7S_2)]^+$: 429 .03 amu (parent ion peak).

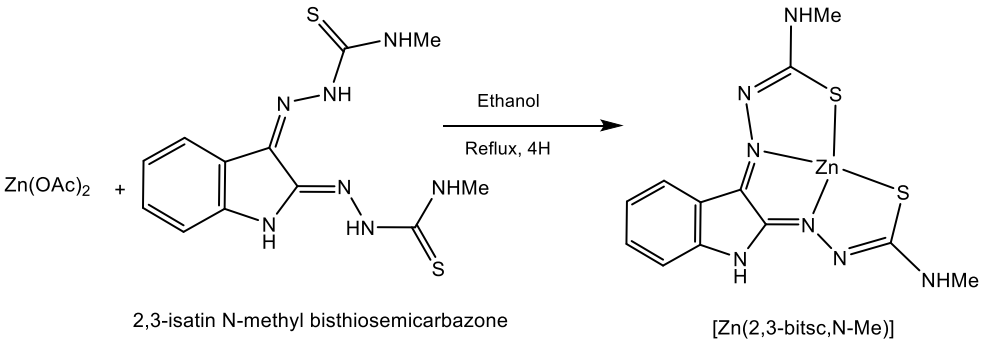

3.8.6 [Zn(bitsc-N-Ph)] 42.

To a solution of 2,3-isatin-N-phenylbisthiosemicarbazone (0.10g, 0.20mmol) was added $Zn(OAc)_2$ (0.050g, 0.20mmol) in ethanol. The dark red coloured solution was refluxed for 4 hours. After two to three days dark brown coloured compound was obtained and dried in vaco. Yield: 85%, M.P. 220-222°C. Main FTIR bands (neat, cm^{-1}); υ (NH_2) 3358m; υ(C =N) 1690s; υ(C = C) 1597m; υ(C=S) 782s. Mass spectra: m/z[$Zn(C_{22}H_{17}N_7S_2)]^+$: 528.04 amu (parent ion peak).

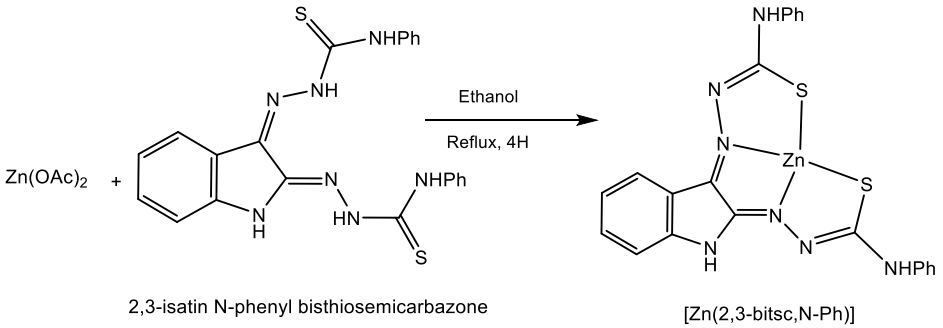

3.8.7 [Zn(2,5 bptsc)] 43.

To a solution of 2,5 piperazinedione bisthiosemicarbazone (0.058g, 0.2mmol), was added $Zn(OAc)_2$ (0.050g, 0.2mmol) in ethanol. The creamish coloured solution was refluxed for 4 hours. After two to three days dark cream coloured compound was obtained and dried in vaco. Yield: 88%, M.P. 225-227°C. Main FTIR peaks (neat, cm^{-1}); υ(NH_2) 3304m,3220; υ(C=N) 1582s; υ(C=C) 1521m; δ(NH_2) 1432s; υ(C=S) 753s. Mass spectra: m/z[$Zn(C_{22}H_{17}N_7S_2)]^+$: 329.20 amu (parent ion peak).

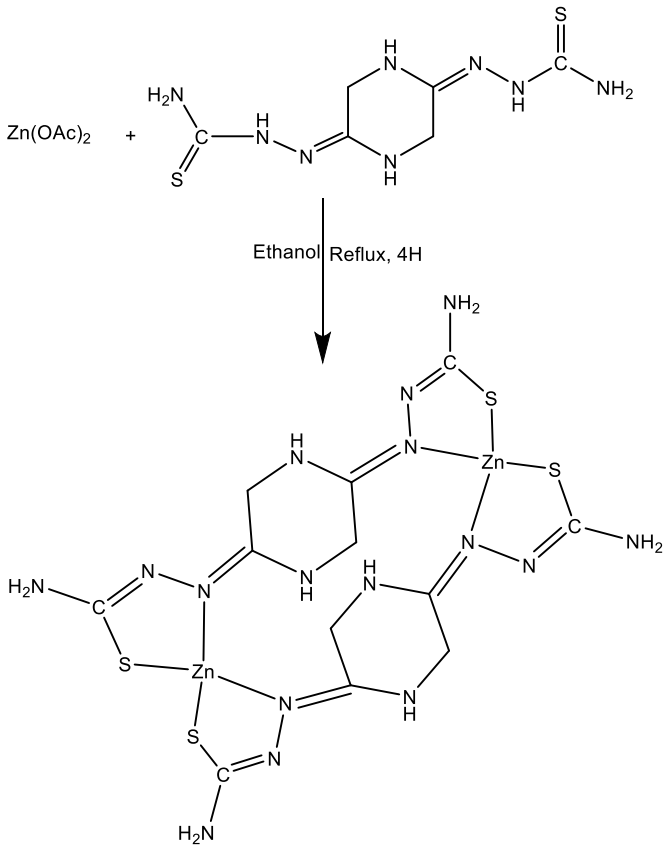

3.8.8 [Zn(2,5 bptsc,N-Me)] 44.

To a solution of 2,5 piperazinedione N-methyl bisthiosemicarbazone (0.056g, 0.2mmol), was added $Zn(OAc)_2$ (0.050g, 0.2mmol) in ethanol. The creamish coloured solution was refluxed for 4 hours. After two to three days brown coloured compound was obtained and dried in vaco. Yield: 90%, m.p. 228-230°C. Main FTIR peaks (neat, cm^{-1}); $\upsilon(NH_2)$ 3265; υ(C=N) 1553s; υ(C=C) 1427m; υ(C=S) 741s. Mass spectra: m/z $[Zn(C_8H_{16}N_8S_2)]^+$: 357.01 amu (parent ion peak).

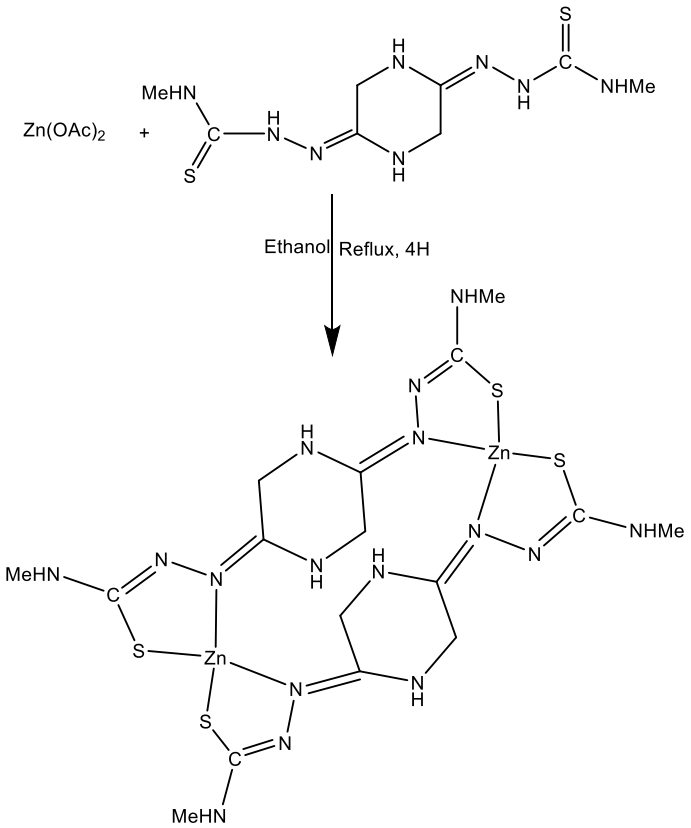

3.8.9 [Zn(2,5 bptsc N-Ph)] 45.

To a solution of 2,5 piperazinedione N-phenyl bisthiosemicarbazone (0.092g, 0.2mmol), was added $Zn(OAc)_2$ (0.050g, 0.2mmol) in ethanol. The creamish coloured solution was refluxed for 4 hours. After two to three days cream coloured compound was obtained and dried in vaco. Yield: 88%, m.p. 248-250˚C. Main IR bands (neat, cm^{-1}); $\upsilon(NH_2)$ 3395m, 3200m; υ (C = N) 1666s; υ(C = C) 1457m; υ (C = S) 737s. Mass spectra: m/z$[Zn(C_{22}H_{17}N_7S_2)]^+$: 477.08 amu (parent ion peak).

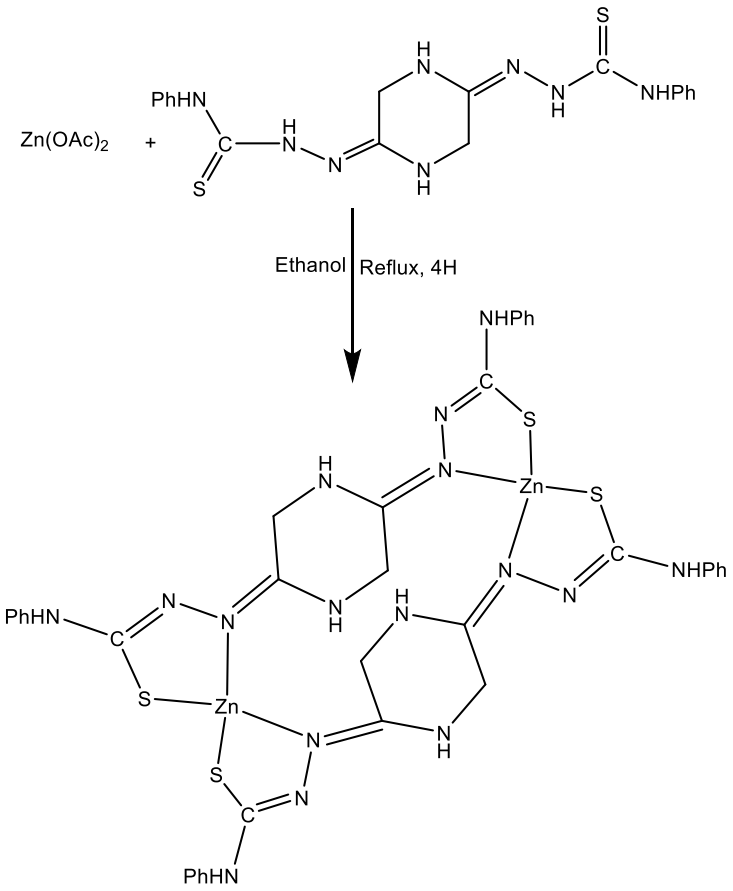

3.8.10 [Zn(2,6 bdptsc)] 46.

To a solution of 2,6 Diacetyl pyridine bisthiosemicarbazone (0.025g, 0.2mmol), was added $Zn(OAc)_2$ (0.017g, 0.2mmol) in ethanol. The dark red coloured solution was refluxed for 4 hours. After two to three days dark brown coloured compound was obtained and dried in vaco. Yield: 89%, m.p. 242-244°C. Main FTIR peaks (neat, cm^{-1}); $\upsilon(NH_2)$ 3437m,3310m; $\upsilon(C=N)$ 1587s, $\upsilon(C=C)$ 1487m, $\delta(NH_2)$ 1419s, $\upsilon(C=S)$ 717s. Mass spectra: m/z$[Zn(C_{11}H_{13}N_7S_2)]^+$: 372.00 amu (parent ion peak).

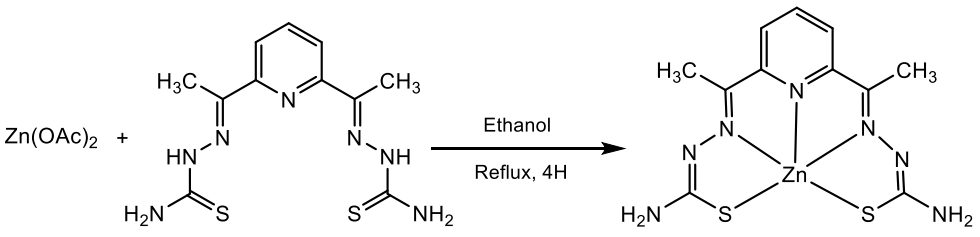

2,6 diacetylpyridine bisthiosemicarbazone [Zn(2,6-bdptsc)]

3.8.11 [Zn(2,6 bdptsc N-Me)] 47.

To a solution of 2,6 Diacetyl pyridine N-methyl bisthiosemicarbazone (0.025g, 0.2mmol), was added $Zn(OAc)_2$ (0.016g, 0.2mmol) in ethanol. The dark red coloured solution was refluxed for 4 hours. After two to three days dark brown coloured compound was obtained and dried in vaco. Yield: 84%, M.P. 235-237°C. Main FTIR peaks (neat, cm^{-1}); $\upsilon(NH_2)$ 3395m, 3259m; $\upsilon(C=N)$ 1590s; $\upsilon(C=C)$ 1528m; $\upsilon(C=S)$ 745s. Mass spectra: m/z$[Zn(C_{13}H_{17}N_7S_2)]^+$: 400.03 amu (parent ion peak).

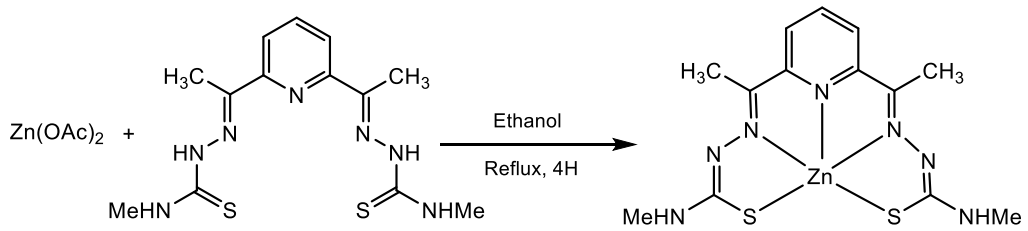

2,6 diacetylpyridine N-methyl bisthiosemicarbazone [Zn(2,6-bdptsc,N-Me)]

3.8.12 [Zn(2,6 bdptsc N-Ph)] 48.

To a solution of 2,6 Diacetyl pyridine N-phenyl bisthiosemicarbazone (0.025g, 0.2mmol), was added $Zn(OAc)_2$ (0.01g, 0.2mmol) in ethanol. The dark red coloured solution was refluxed for 4 hours. After two to three days dark brown coloured compound was obtained and dried in vaco. Yield: 90%, M.P. 240-242°C. Main FTIR peaks (neat, cm^{-1}); $\upsilon(NH_2)$ 3269m; $\upsilon(C=N)$ 1598s; $\upsilon(C=C)$ 1489m; $\upsilon(C=S)$ 751s. Mass spectra: m/z$[Zn(C_{23}H_{21}N_7S_2)]^+$: 524.06 amu (parent ion peak).

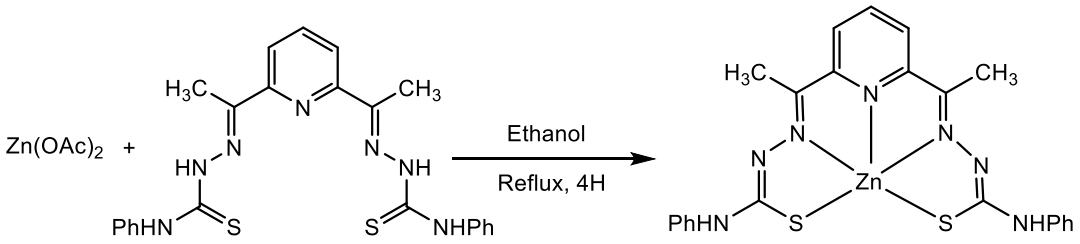

2,6 diacetylpyridine N-phenyl bisthiosemicarbazone [Zn(2,6-bdptsc,N-Ph)]

CHAPTER-4

RESULT AND DISCUSSION (Ligands)

4.1 Discussion on Synthesis of Ligands

Thiosemicarbazide is reacted with different aldehydes or ketones in 2:1 molar ratio to form bisthiosemicarbazones. The synthesized bisthiosemicarbazones along with their structures are given in Table **4.1**. The scheme (V) to (VIII) below represents the formation of different heterocyclic bisthiosemicarbazones.

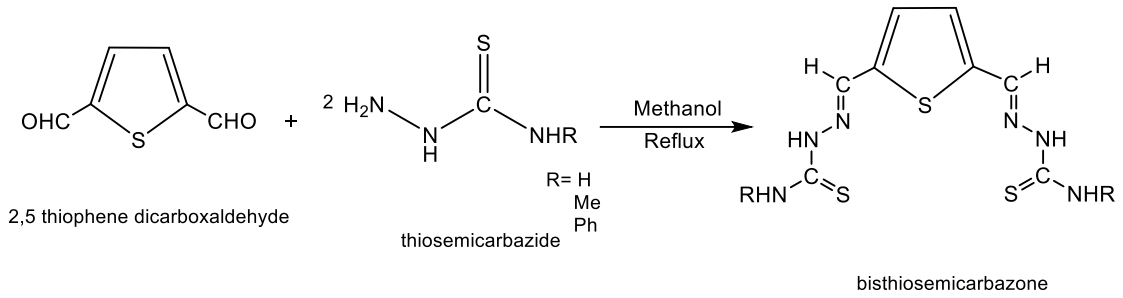

(V)

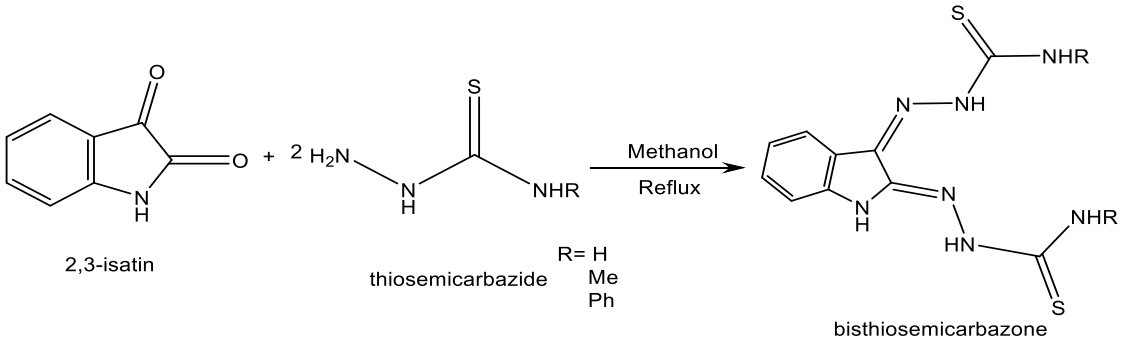

(VI)

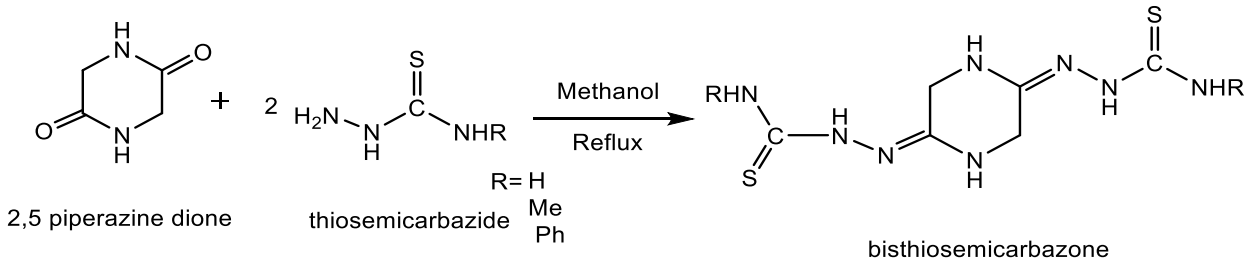

(VII)

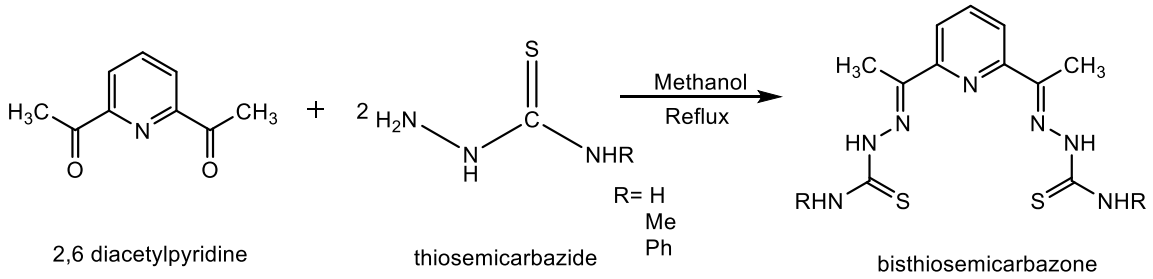

(VIII)

Table 4.1 Synthesized bisthiosemicarbazones (**H^1L - $H^{12}L$**)

Sr. No.	**Name of synthesized bisthiosemicarbazone ligands**	**Structure of Synthesized bisthiosemicarbazone ligands**
1.	2,5 thiophene dicarboxaldehyde Bisthiosemicarbazone **(2,5 H_2bttsc, ^1H_2L)**	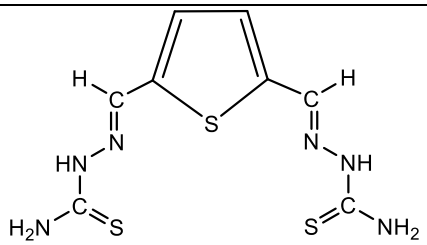
2.	2,5 thiophene dicarboxaldehyde-N-methyl bisthiosemicarbazone **(2,5 H_2bttsc N-Me, ^2H_2L)**	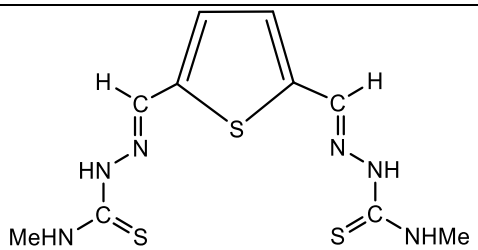

3.	2,5 thiophene dicarboxaldehyde-N-phenyl bisthiosemicarbazone **(2,5 H_2bttsc N-Ph, ^3H_2L)**	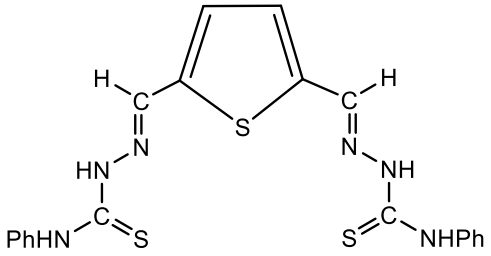
4.	2,3-isatin bisthiosemicarbazone **(2,3 H_2bitsc, ^4H_2L)**	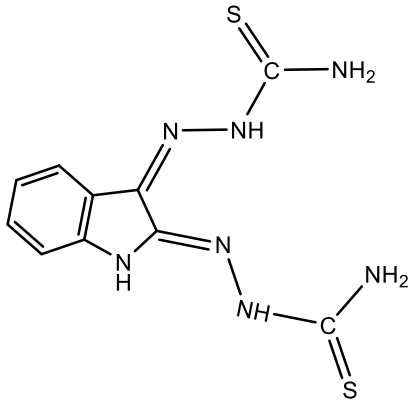
5.	2,3-isatin-N-methyl bisthiosemicarbazone **(2,3 H_2bitsc-N-Me, ^5H_2L)**	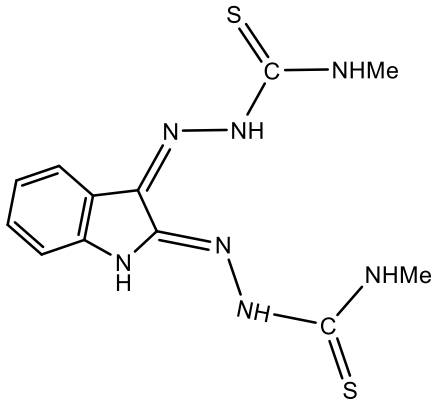
6.	2,3-isatin-N-phenyl bisthiosemicarbazone **(2,3 H_2bitsc-N-Ph, ^6H_2L)**	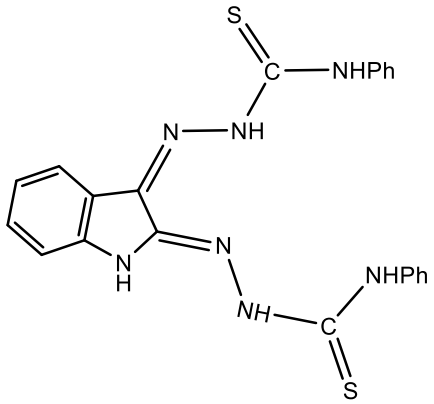

7.	2,5-Piperazine bisthiosemicarbazone **(2,5 H_2bptsc, ^7H_2L)**	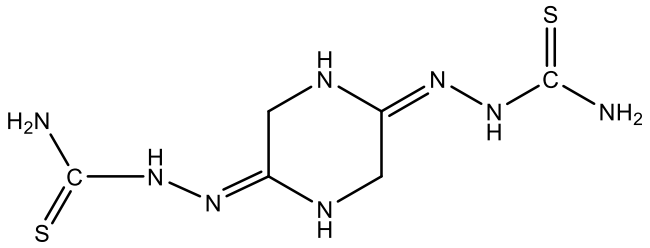
8.	2,5-Piperazine bis N-methyl thiosemicarbazone **(2,5 H_2bptsc N-Me, ^8H_2L)**	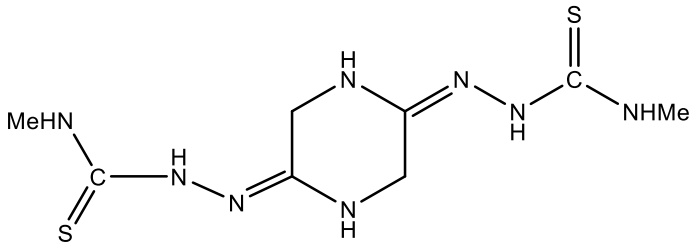
9.	2,5-Piperazine bis N-phenyl thiosemicarbazone **(2,5 H_2bptsc N-Ph, ^9H_2L)**	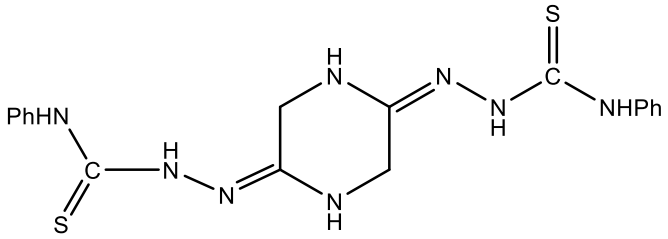
10.	2,6 Diacetyl pyridine bisthiosemicarbazone **(2,6 H_2bdptsc, $^{10}H_2L$)**	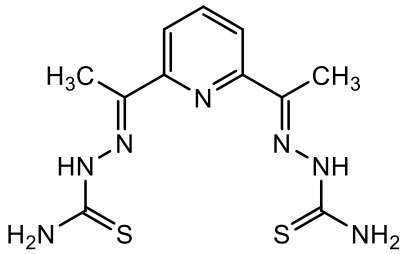
11.	2,6 Diacetyl pyridine bis N-methyl thiosemicarbazone **(2,6 H_2bdptsc N-Me, $^{11}H_2L$)**	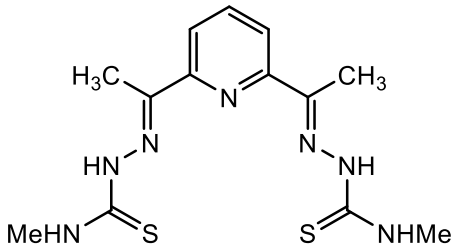
12.	2,6 Diacetyl pyridine bis N-phenyl thiosemicarbazone **(2,6 H_2bdptsc N-Ph, $^{12}H_2L$)**	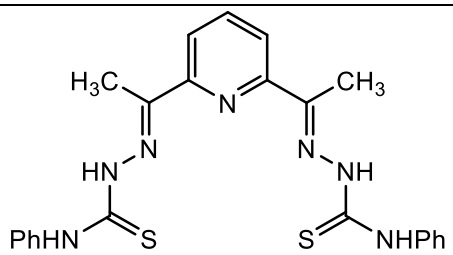

4.2 IR Spectroscopy:

Important IR peaks of bisthiosemicarbazones are mentioned in table **4.2** and spectra are presented in Figures 4.2-4.2.19.

In thiosemicarbazide, amine nitrogen peak υ(N-H) appeared at 3352 and 3252 $cm^{-1}$and amide nitrogen peak υ(-NH-) appeared at 3159 $cm-^{1}$. The υ(-NH-) band can be divided broadly in two categories (i) bands in the range 3461-3207cm^{-1} for symmetric and asymmetric stretching, (ii) bands due to amide group υ(-NH-) of bisthiosemicarbazones observed in the range 3190-3156 cm^{-1} indicates the attachment of thio- moieties to the rings of ligands **($^{1}H_2L$-$^{12}H_2L$)**. While the $–NH_{(isatin)}$ stretching vibration observed in the range 3097-3069 cm^{-1} [170]. The vibrational mode υ(C=O) observed in the range, 1722-1657 cm^{-1} in **$^{1}H_2L$-$^{12}H_2L$**. Disappearance of υ(C=O) band and appearance of υ(C=N) band in the range, 1698-1594 $cm-^{1}$ in **$^{1}H_2L$-$^{12}H_2L$** indicate the condensation of free ligands with thiosemicarbazide. The specific C=S band in ligands **$^{1}H_2L$-$^{12}H_2L$** observed in the range, 896-827 cm^{-1}.

Table 4.2 Significant IR peaks of bisthiosemicarbazones ($^{1}H_2L$-$^{12}H_2L$)

Ligands	$\upsilon(NH_2)$	υ(-NH-)	υ(C=N), υ(C=C) ,δ (NH_2)	υ(C=S)
2,5 H_2bttsc, ($^{1}H_2L$)	3409m 3277m	3155w	1600s,1583m,1535s	836s
2,5 H_2bttscN-Me, ($^{2}H_2L$)	3373m	3155w	1594s,1462m,1428s	812s
2,5 H_2bttsc N-Ph, ($^{3}H_2L$)	3303m	3156w	1636s,1594w,1524s	895s
2,3 H_2bitsc, ($^{4}H_2L$)	3332m 3259m	3156w	1698s,1618w,158s	851s
2,3 H_2bitsc-N^1-Me, ($^{5}H_2L$)	3461m, 3207m	3100w	1683s,1616m,1546s	831s
2,3 H_2bitsc-N^1-Ph, ($^{6}H_2L$)	3290m	3173w	1685s,1591m,1533s	827s
2,5 H_2bptsc, ($^{7}H_2L$)	3356m, 3253m	3166mw	1640s,1512m,1526s	895s
2,5 H_2bptsc N-Me, ($^{8}H_2L$)	3282	3198	1639,1549s	807
2,5 H_2bptsc N-Ph, ($^{9}H_2L$)	3301m	3158w	1639s, 1466m	829s
2,6 H_2bdptsc, ($^{10}H_2L$)	3423m, 3209m	3158m w	1606 s, 1513 m	827s
2,6 H_2bdptsc N-Me, ($^{11}H_2L$)	3450m, 3329m	3190 w	1634s, 1555m	836s
2,6 H_2bdptsc N-Ph, ($^{12}H_2L$)	3303m	3156 w	1636 s, 1594m	836s

4.3. NMR Spectroscopy:

4.3.1. ^{1}H NMR Spectroscopy:

Important ^{1}HNMR signals of ligands are given in **Table 4.3** and spectra are presented in Figures 4.3.1.1-4.3.1.11.

In ^{1}H NMR spectra, amide proton ($N^{2,2'}H$) in **$^{1}H_2L$-$^{12}H_2L$** appeared in the range δ12.85-8.65 ppm. Two broad singlets appeared in the range δ 9.04-7.21ppm in **$^{1}H_2L$, $^{4}H_2L$, $^{7}H_2L$, $^{10}H_2L$** due to non-equivalent $N^{1,1'}H_2$ proton. The amino proton in **$^{2}H_2L$ -$^{6}H_2L$** and **$^{11}H_2L$ -$^{12}H_2L$** appeared in the range δ10.84-8.03ppm respectively. Signal of $N^{4}H$ proton observed in the range, 11.80-4.75ppm in ligands **$^{4}H_2L$ -$^{7}H_2L$** and **$^{9}H_2L$**. Signal of ($C^{2,2'}H$) in ligands **$^{1}H_2L$ -$^{4}H_2L$** and **$^{10}H_2L$ -$^{11}H_2L$** appeared in the range δ9.16-6.20ppm. The signal due to methyl group in ligands **$^{2}H_2L$, $^{5}H_2L$, $^{8}H_2L$** and **$^{11}H_2L$** appeared in the range δ3.12-2.43 ppm. Ring protons in **$^{1}H_2L$-$^{12}H_2L$** appeared in the range δ8.55-4.57ppm. The signal at δ3.35 ppm is due to water peak in deuterated dimethylsulfoxide (d-DMSO). Presence of all these signals ensures the formation of bisthiosemicarbazones (**$^{1}H_2L$-$^{12}H_2L$**).

Table 4.3 ^{1}H NMR signals of synthesized bisthiosemicarbazone ligands

Synthesized Ligands	($N^{2,2'}H$)	($N^{1'1'}H_2$)	($C^{2'2'}H$)	($N^{4}H$)	(CH_3)	(ring protons)
2,5 H_2bttsc, ($^{1}H_2L$)	11.60 s	8.32s	8.19s	-	-	7.41s
2,5 H_2bttscN-Me, ($^{2}H_2L$)	11.62s	8.20s	8.14s	-	3.02s	7.41s
2,5 H_2bttsc N-Ph, ($^{3}H_2L$)	10.36s	9.83s	9.16s	-	-	7.66 -7.14 m (10H)
2,3 H_2bitsc, ($^{4}H_2L$)	12.47s	9.04s 8.68s	6.21 s, 6.20 s	11.20s	-	7.64 -6.94
2,3H_2bitsc-N^{1}-Me, ($^{5}H_2L$)	12.60s	9.25s	c	11.21s	3.12s	7.66 -6.93
2,3 H_2bitsc-N^{1}-Ph, ($^{6}H_2L$)	12.80s	11.28s	-	10.84s	-	7.790-6.95
2,5 H_2bptsc, ($^{7}H_2L$)	8.65s	7.57, 7.21s	-	8.04s	-	4.57(4H, $C^{3,3'}H$).
2,5 H_2bptsc N-Ph, ($^{9}H_2L$)	9.10s	9.61, 8.03s	-	4.75s	-	7.63-7.10 (10H)

2,6 H_2bdptsc, ($^{10}H_2L$)	10.32s	8.42s	7.76s , 7.56s	-	2.43	8.16s(2H, $C^{4,4'}$H); 7.83s(1H, C^5H)
2,6 H_2bdptsc N-Me, ($^{11}H_2L$)	10.34s	8.70s	7.65 s, 6.63 s	-	3.05 (N^1HMe); 2.43 (6HMe).	8.55s(2H, $C^{4,4'}$H); 7.85s(1H, C^5H);
2,6 H_2bdptsc N-Ph, ($^{12}H_2L$)	10.69s	10.23s	-	-	2.51	8.55s(2H, $C^{4,4'}$H); 7.84s(1H, C^5H); 7.49-7.26(Ring protons of phenyl ring);

4.3.2. ^{13}C NMR Spectroscopy:

Important ^{13}CNMR signals of ligands are given in Table 4.3.2. and their spectra are given in figure 4.3.2.1-4.3.2.9.

In ^{13}CNMR spectra, $C^{1,1'}$ in **^1H_2L-$^{12}H_2L$** observed in the range δ(181.42 -176.49)ppm. $C^{2,2'}$signal in **^1H_2L-$^{12}H_2L$** appeared in the range δ(166.78 -139.43) ppm. The signal due to $C^{3,3'}$ in **^1H_2L-$^{12}H_2L$** appeared in the range δ(154.37-45.09) ppm. The signal due to methyl group in ligand **^2H_2L** appeared at δ31.37 ppm, in ligands **^2H_2L, ^5H_2L, ^8H_2L** and **$^{11}H_2L$** the signal of methyl group appeared in the range δ (39.53-31.59) ppm. Ring carbons in **^1H_2L-^4H_2L** appeared in the range δ(139.69-111.03) ppm. Presence of all these signals ensures the formation of bisthiosemicarbazones **(^1H_2L-$^{12}H_2L$)**.

Table 4.3.2 ^{13}C signals of bisthiosemicarbazones **(^1H_2L-$^{12}H_2L$)**

Synthesised Ligands	**($C^{1,1'}$)**	**($C^{2,2'}$)**	**($C^{3,3'}$)**	**CH_3**	**Ring carbon**
2,5 H_2bttsc, (^1H_2L)	178.43	140.67	137.2	-	131.17-114.80
2,5 H_2bttscN-Me, (^2H_2L)	177.75	140.70	137.01	31.37	131.0
2,5 H_2bttsc N-Ph, (^3H_2L)	179.89	139.43	-	-	128.69-123.30
2,3 H_2bitsc, (^4H_2L)	179.16	163.19	142.82	-	132.65-111.50
2,3H_2bitsc-N^1-Me, (^5H_2L)	179.58	162.78	143.21	39.53	132.97-111.19

2,3 H_2bitsc-N^1-Ph, (^6H_2L)	176.49	162.64	142.27	-	138.25-111.03
2,5 H_2bptsc, (^7H_2L)	181.42	166.54	45.12	-	-
2,5 H_2bptsc N-Ph, (^9H_2L)	180.30	166.82	45.09	-	139.48-123.78
2,6 H_2bdptsc, ($^{10}H_2L$)	179.09	154.09	148.60	-	139.69 (C^5); 122.15($C^{4,4'}$)
2,6 H_2bdptsc N-Me, ($^{11}H_2L$)	179.47	148.0	154.37	31.59 (N^1HMe); 12.27(Me)	121.53($C^{4,4'}$)
2,6 H_2bdptsc N-Ph, ($^{12}H_2L$)	-	-	-	-	-

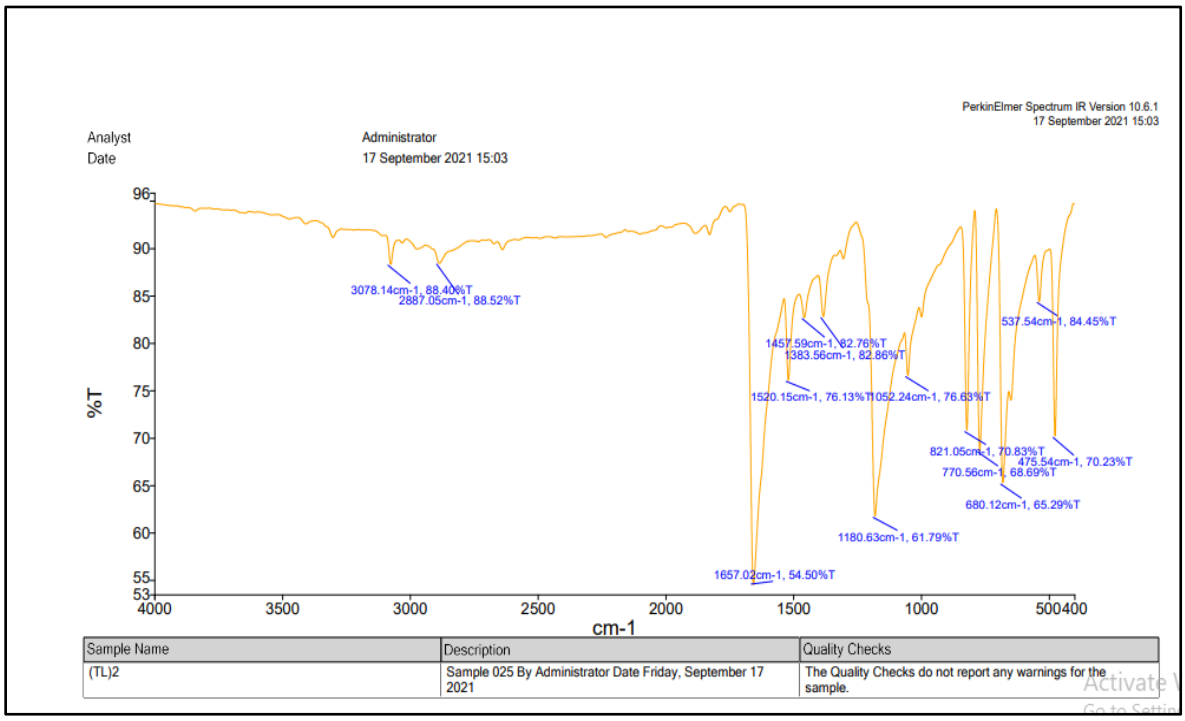

Figure 4.2.1: IR Spectra of 2,5 thiophene

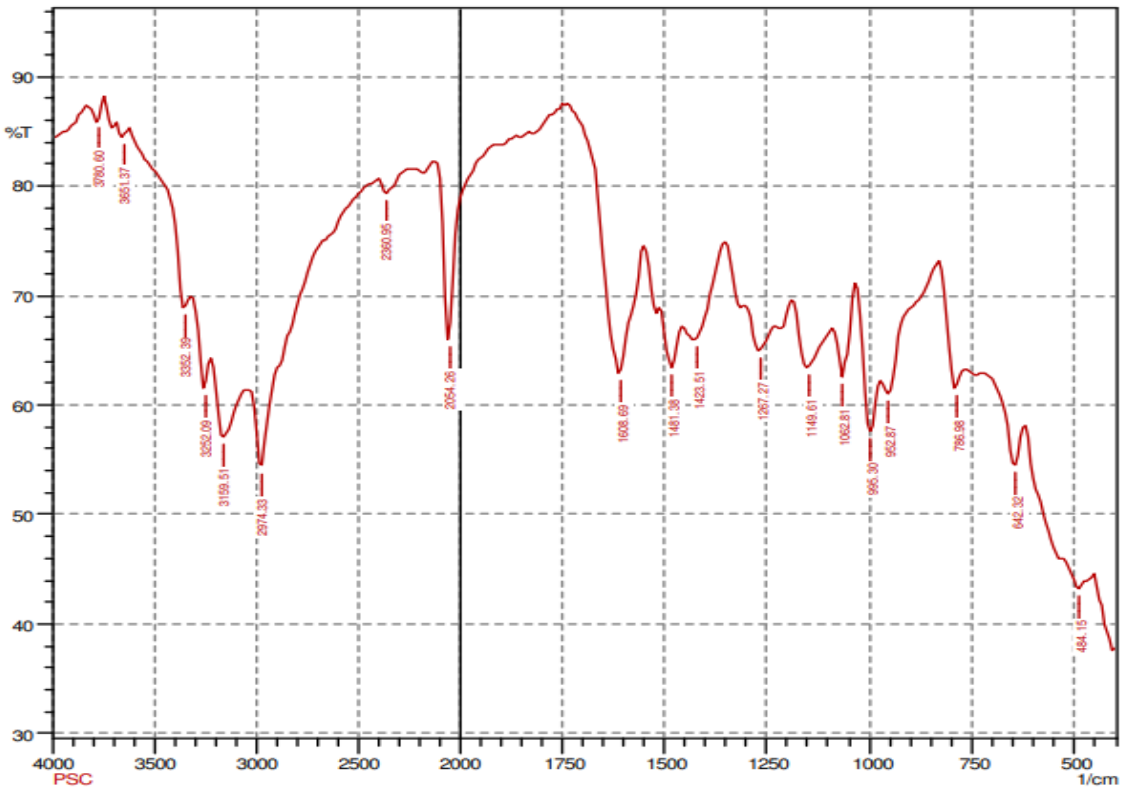

Figure 4.2.2: IR Spectra of thiosemicarbazide

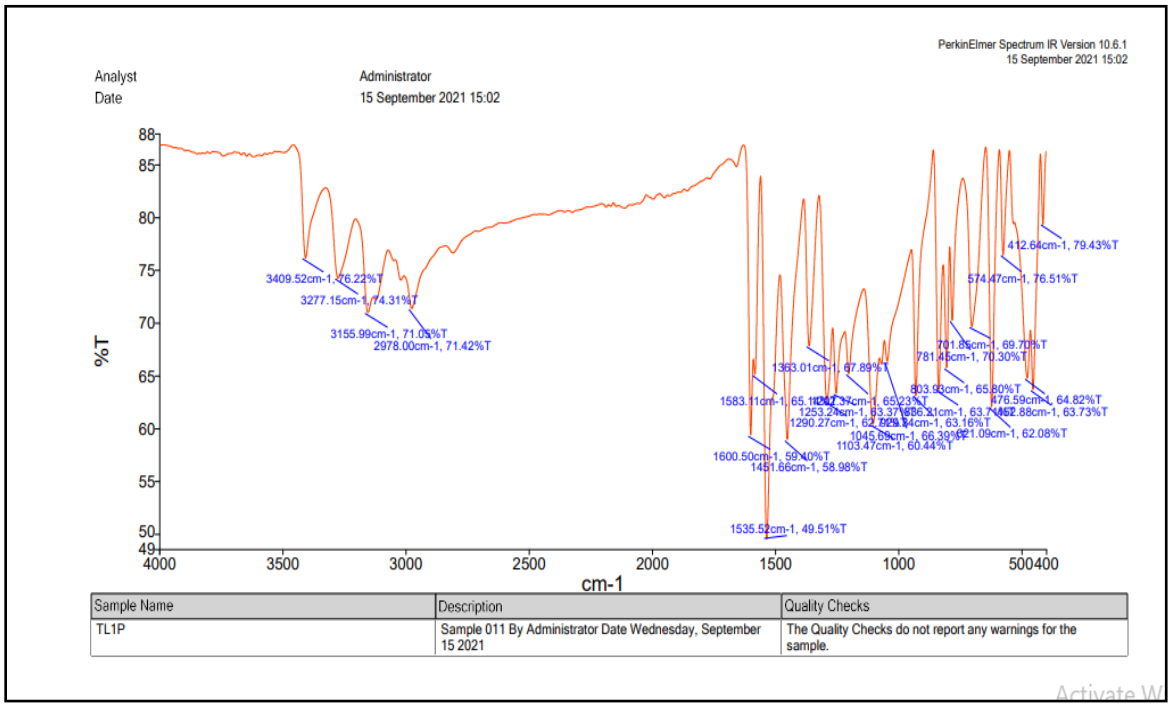

Figure 4.2.3: IR spectra of 2,5 thiophene dicarboxaldehyde bisthiosemicarbazone (^1H_2L)

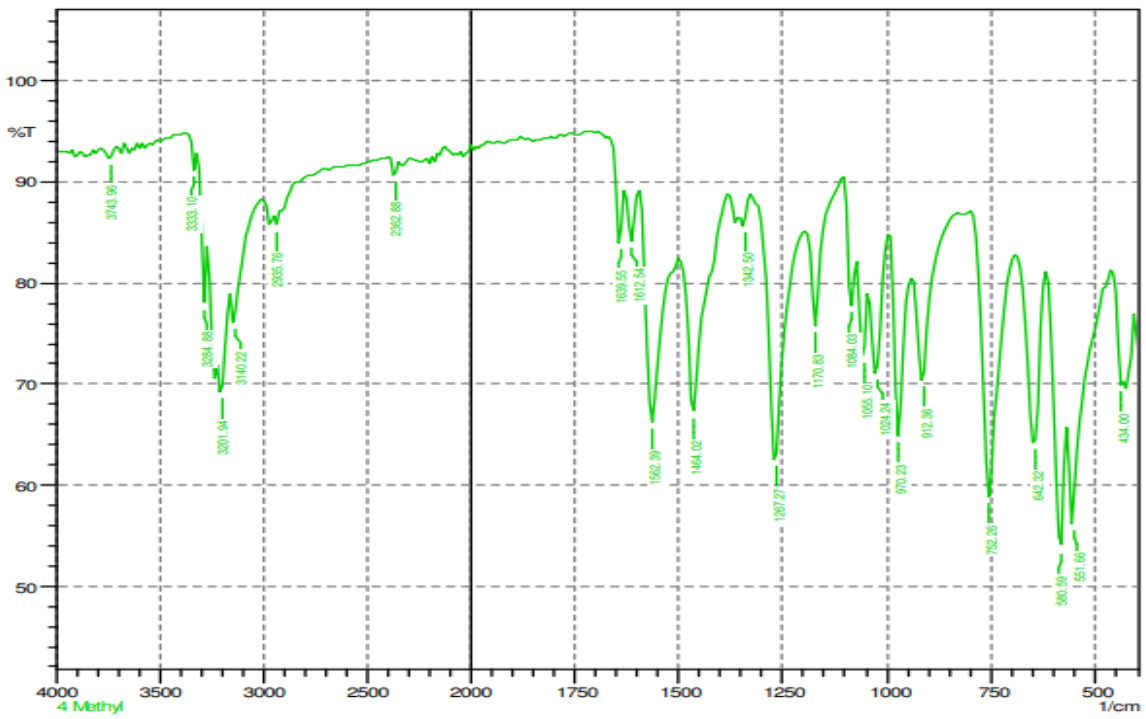

Figure 4.2.4: IR spectra of N-methyl thiosemicarbazide

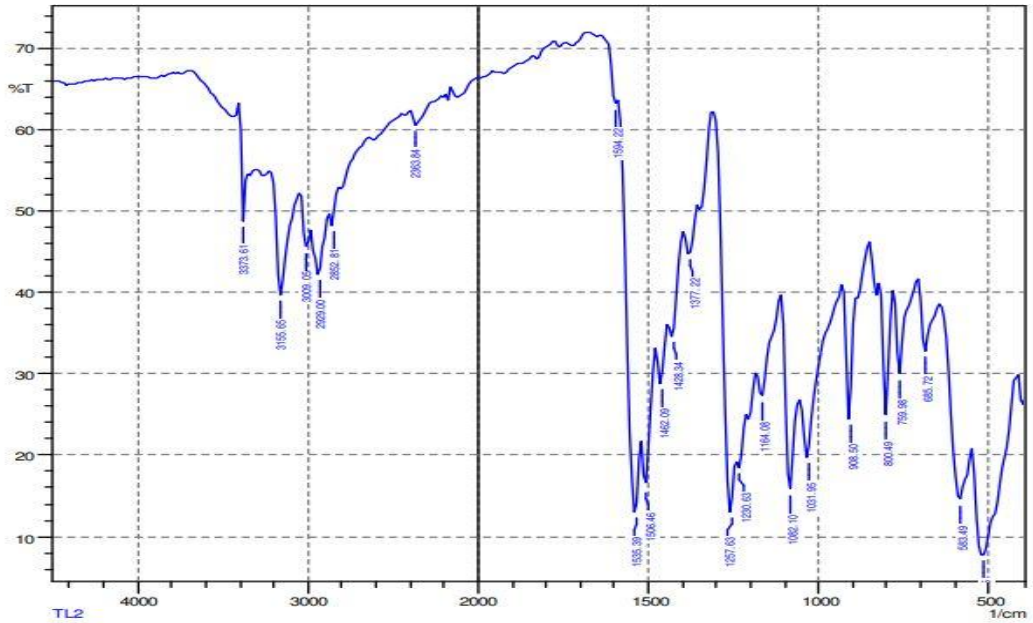

Figure 4.2.5: IR Spectra of 2,5 thiophene dicarboxaldehyde N-methyl bisthiosemicarbazone (2,5 H_2bttscN-Me, ^2H_2L)

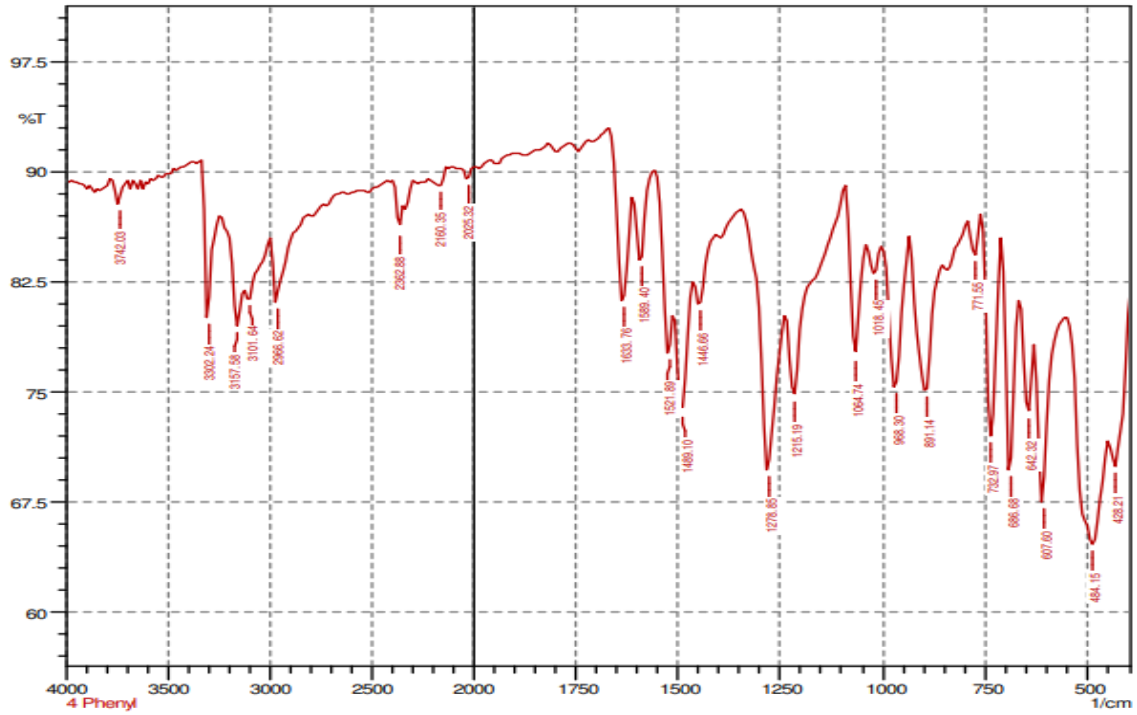

Figure 4.2.6: IR Spectra of N-phenyl thiosemicarbazide

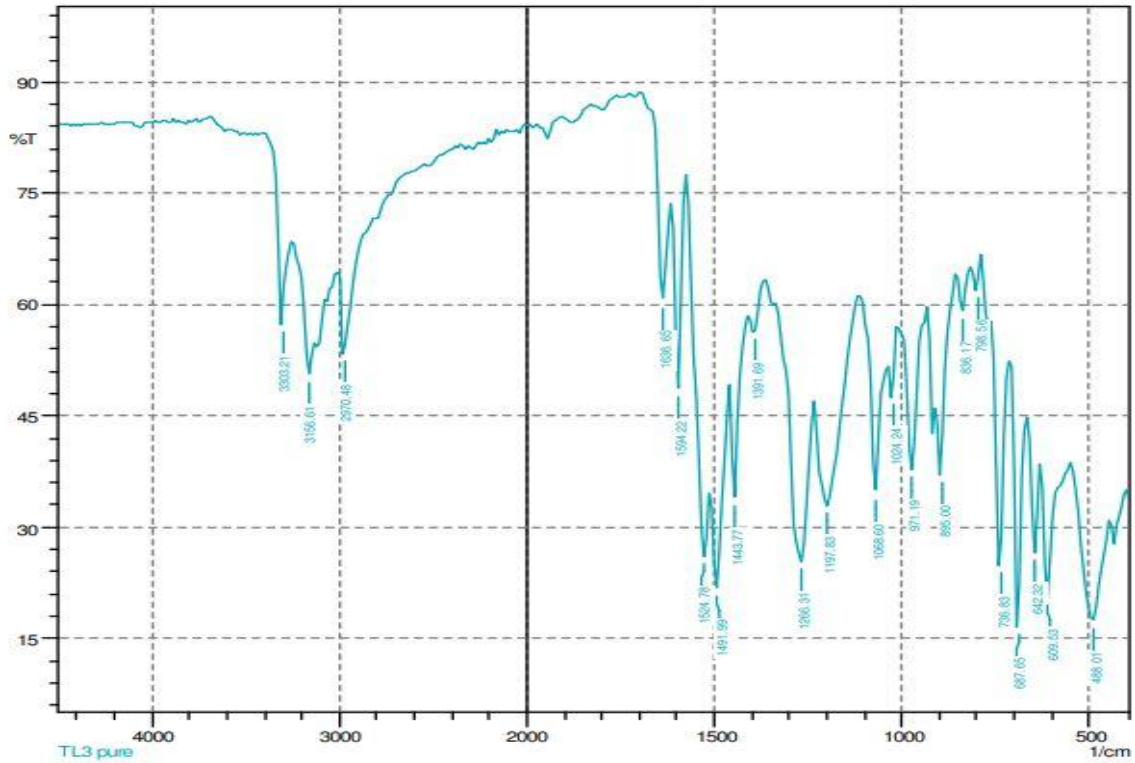

Figure 4.2.7: IR Spectra of 2,5 thiophene dicarboxaldehyde N-phenyl bisthiosemicarbazone (2,5 H_2bttsc N-Ph, ^3H_3L)

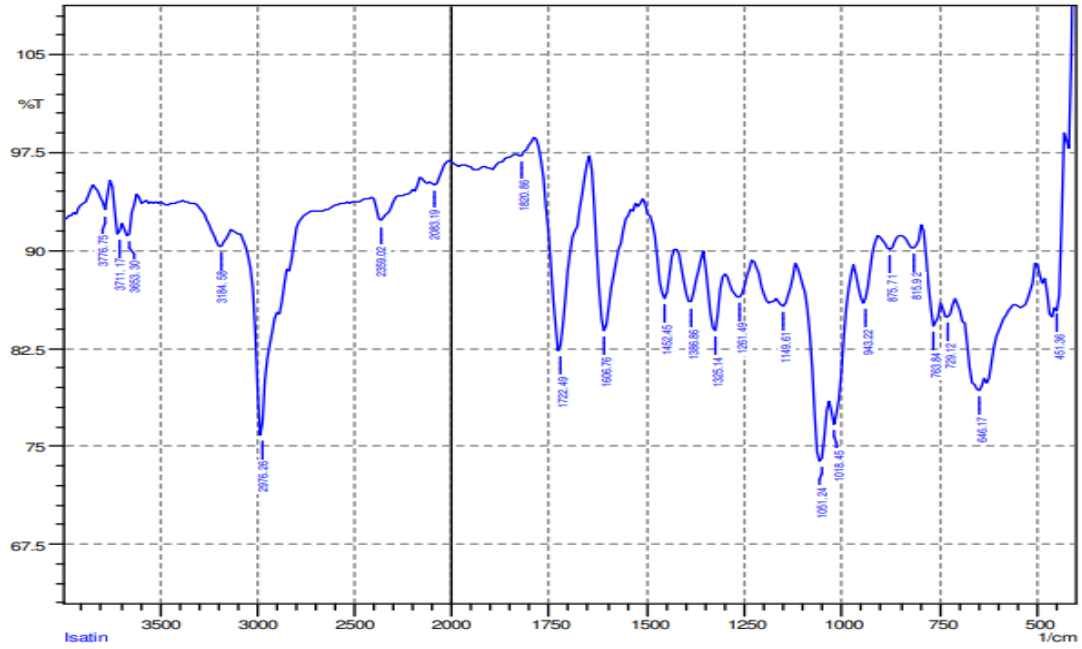

Figure 4.2.8: IR Spectra of 2,3- isatin

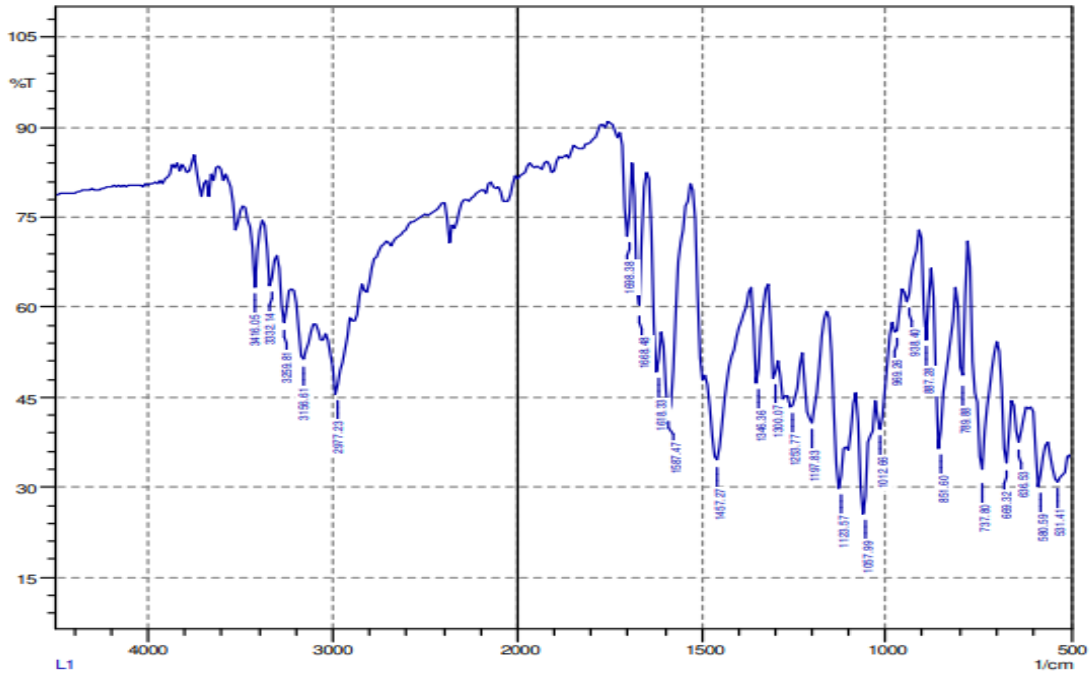

Figure 4.2.9: IR Spectra of 2,3-isatin bisthiosemicarbazone (2,3bitsc, $^{4}H_2L$)

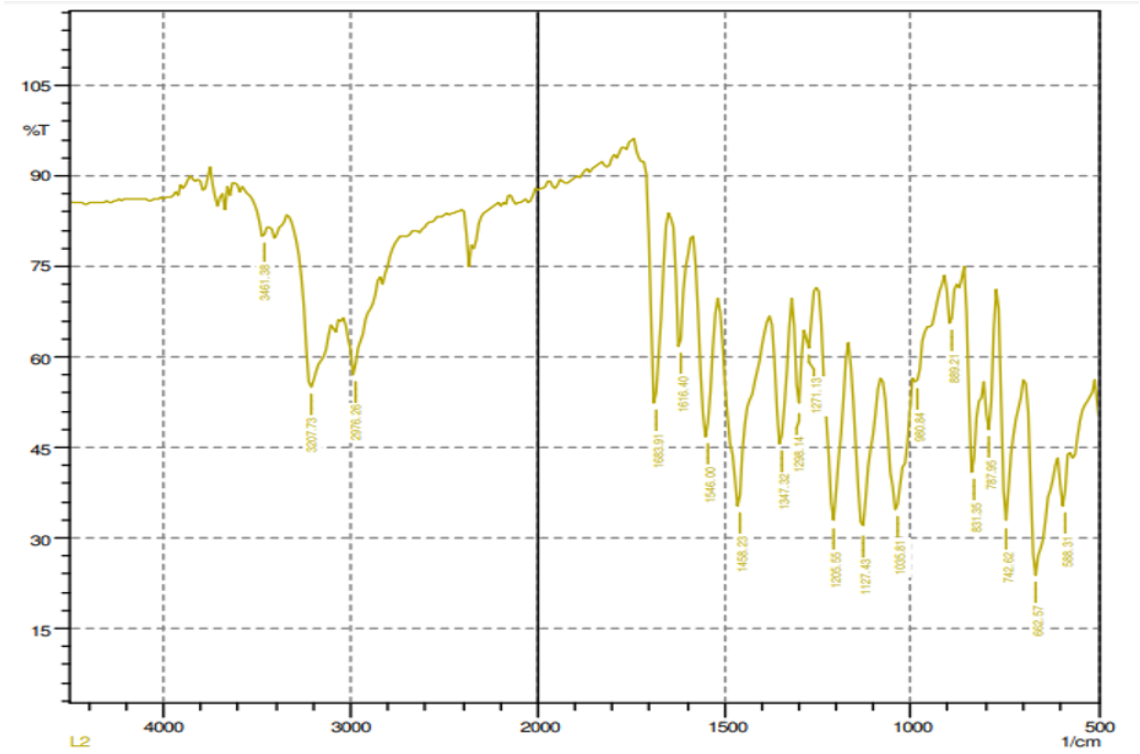

Figure 4.2.10: IR spectra of 2,3-isatin bis N-methyl thiosemicarbazone ($^{5}H_2L$)

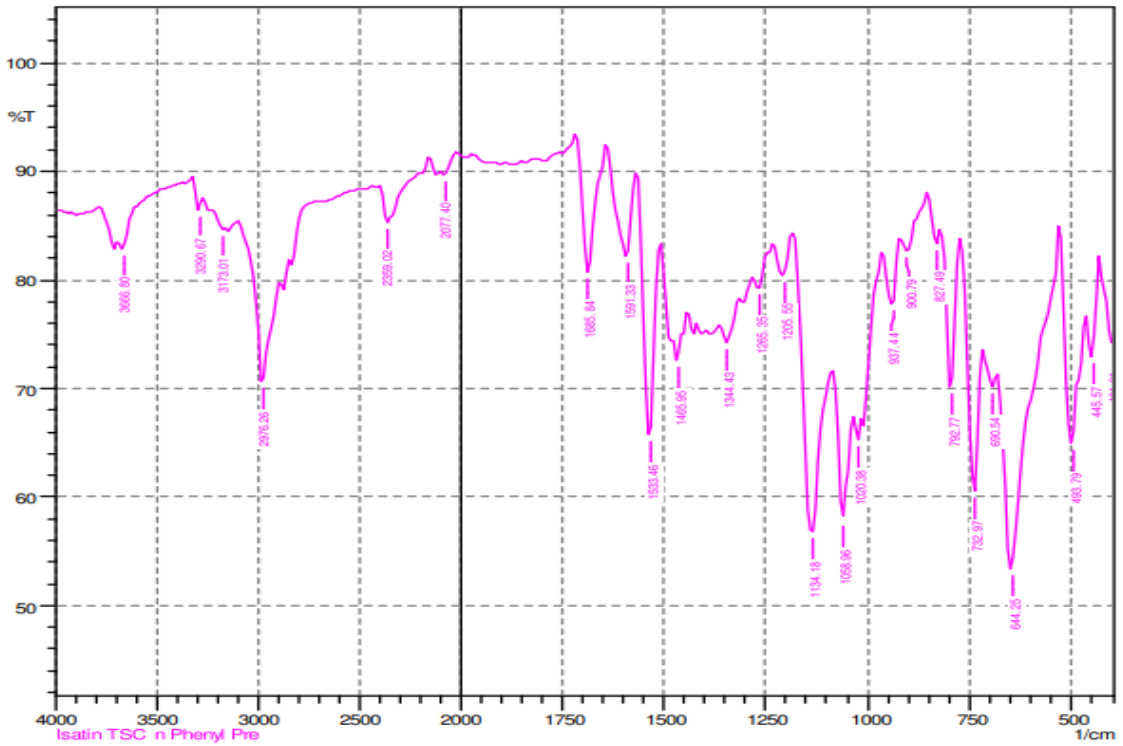

Figure 4.2.11: IR Spectra of 2,3-isatin bis N-phenylthiosemicarbazone ($^{6}H_2L$)

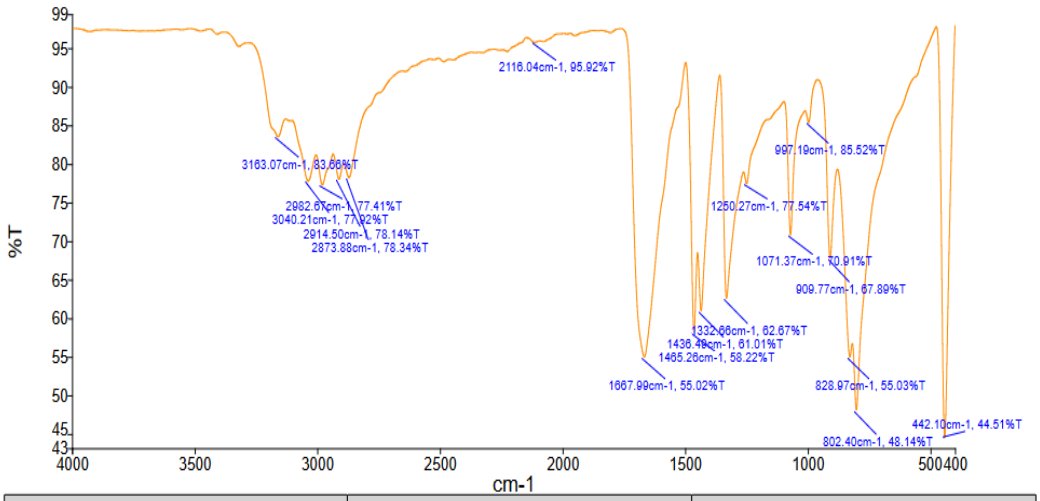

Sample Name	Description	Quality Checks
PL	Sample 015 By PEService Date Wednesday, March 30 2022	The Quality Checks do not report any warnings for the sample.

Figure 4.2.12: IR Spectra of 2,5-Piperazinedione

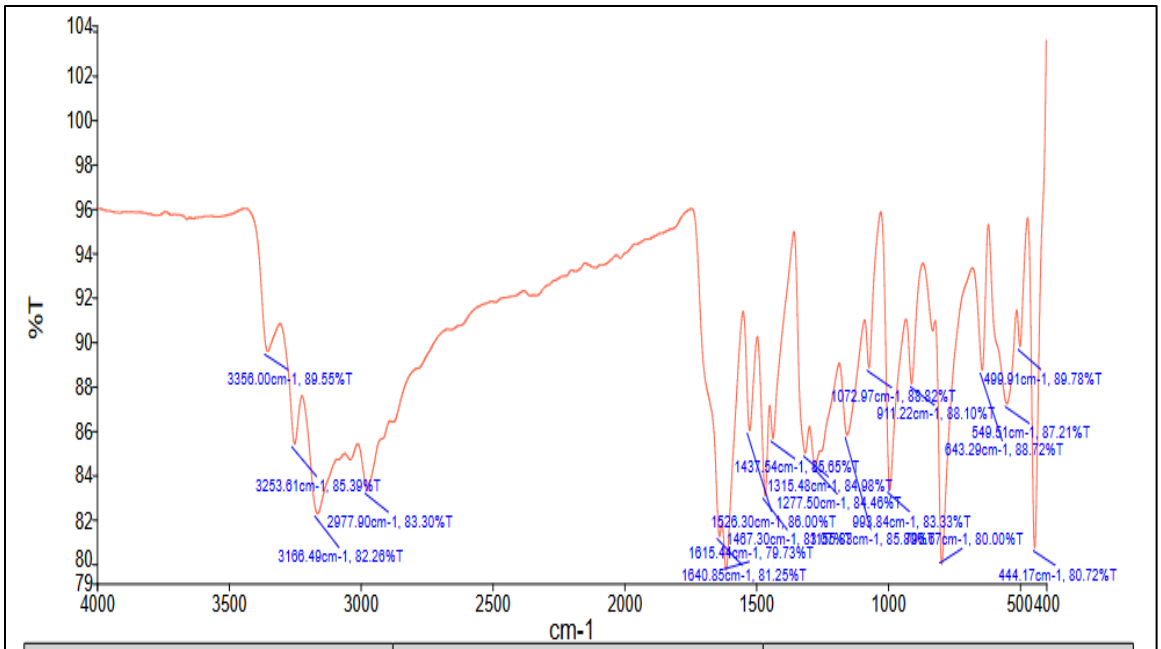

Sample Name	Description	Quality Checks
PIP. L1	Sample 021 By PEService Date Tuesday, March 22 2022	The Quality Checks do not report any warnings for the sample.

Figure 4.2.13: IR Spectra of 2,5-Piperazine bisthiosemicarbazone (2,5 H_2bptsc, ^7H_2L)

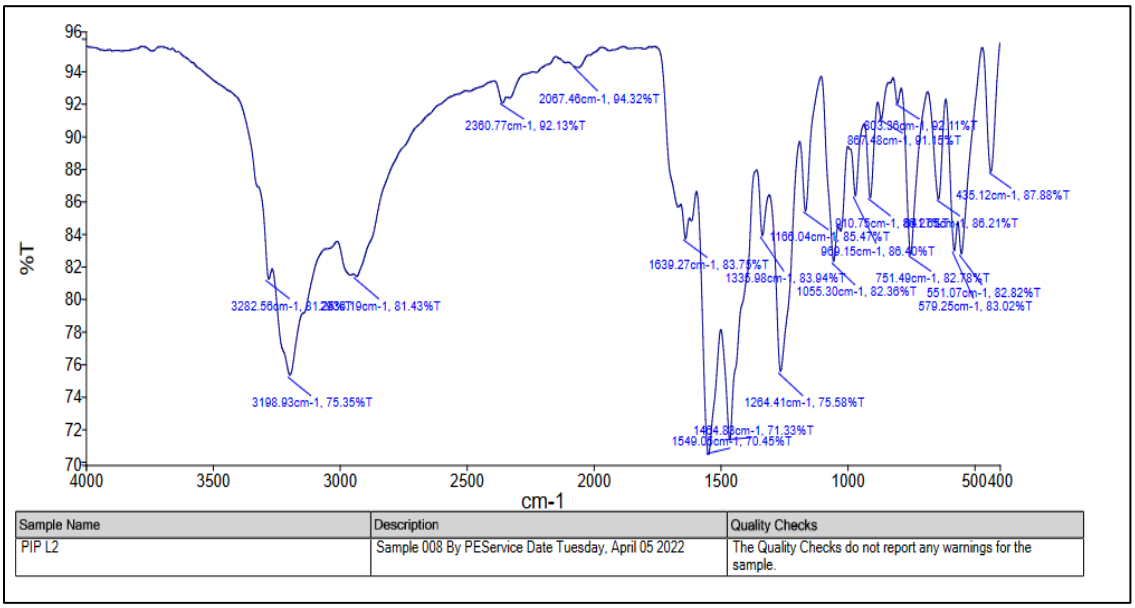

Figure 4.2.14: IR Spectra of 2,5-Piperazine bis N-methyl thiosemicarbazone (2,5 H_2bptsc, ^8H_2L)

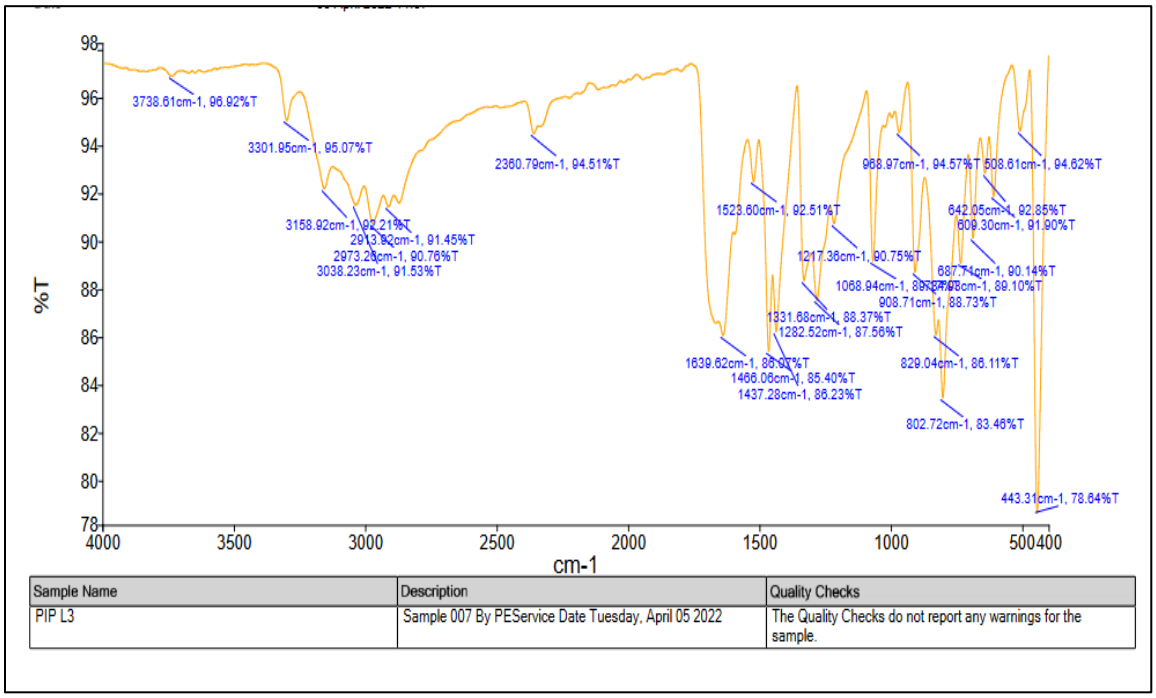

Figure 4.2.15: IR Spectra of 2,5-Piperazine bis N-phenyl thiosemicarbazone (2,5 H_2bptsc, ^9H_2L)

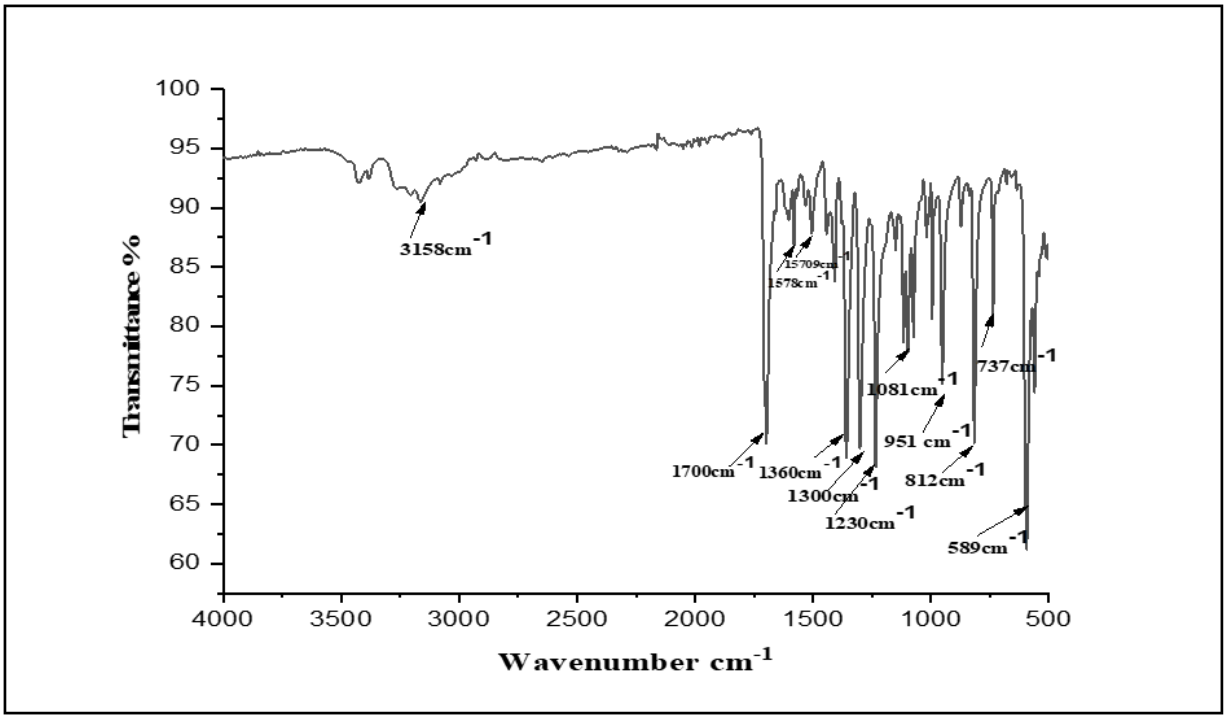

Figure 4.2.16: IR Spectra 2,6 Diacetyl pyridine

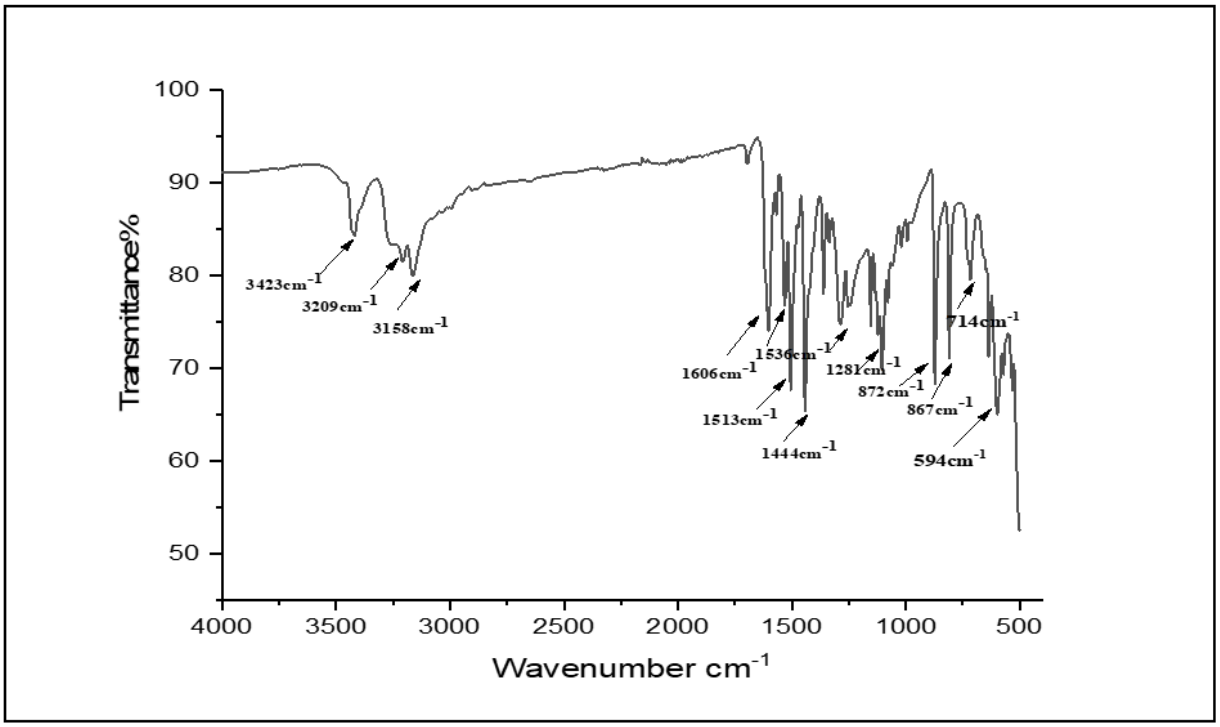

Figure 4.2.17: IR Spectra 2,6 Diacetyl pyridine bisthiosemicarbazone (2,6 H_2bdptsc, $^{10}H_2L$)

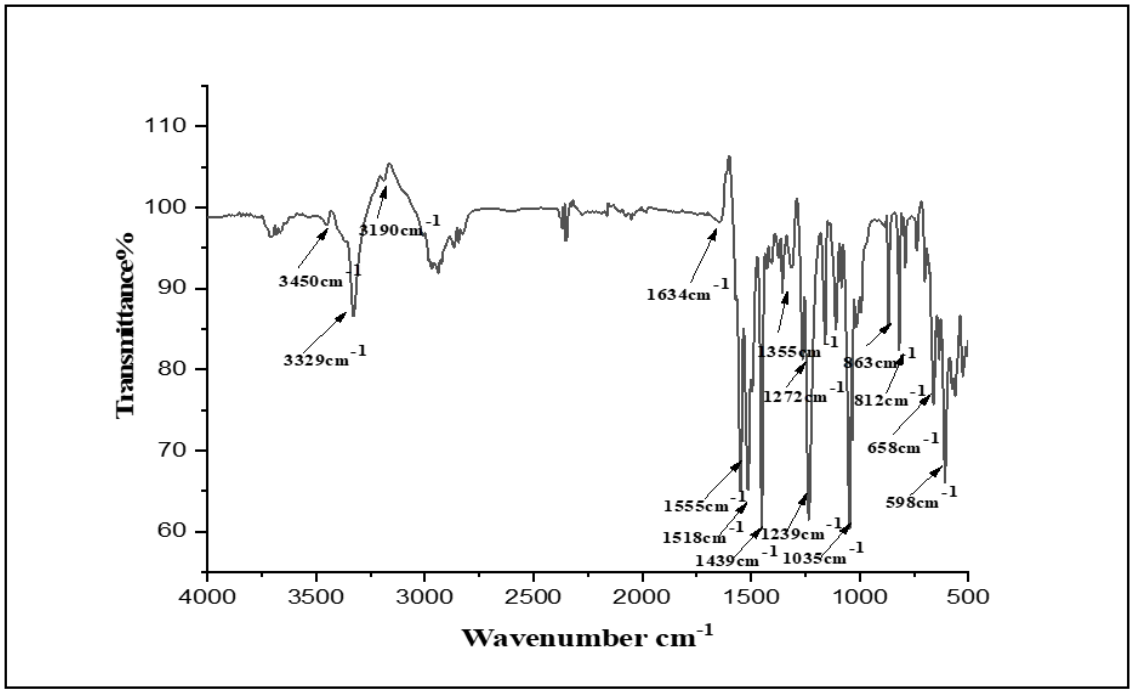

Figure 4.2.18: IR Spectra 2,6 Diacetyl pyridine bis N-methyl thiosemicarbazone (2,6 H_2bdptsc N-Me, $^{11}H_2L$)

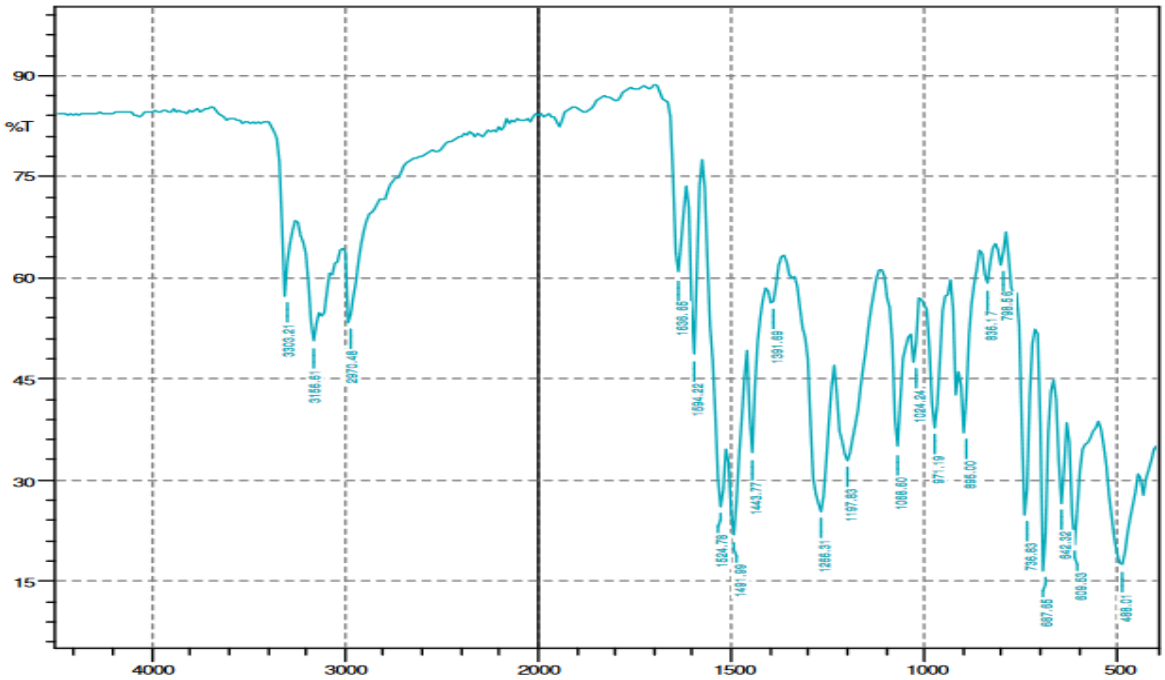

Figure 4.2.19. IR Spectra of 2,6 Diacetyl pyridine bis N-phenyl thiosemicarbazone (2,6 H_2bdptsc N-Ph, $^{12}H_2L$)

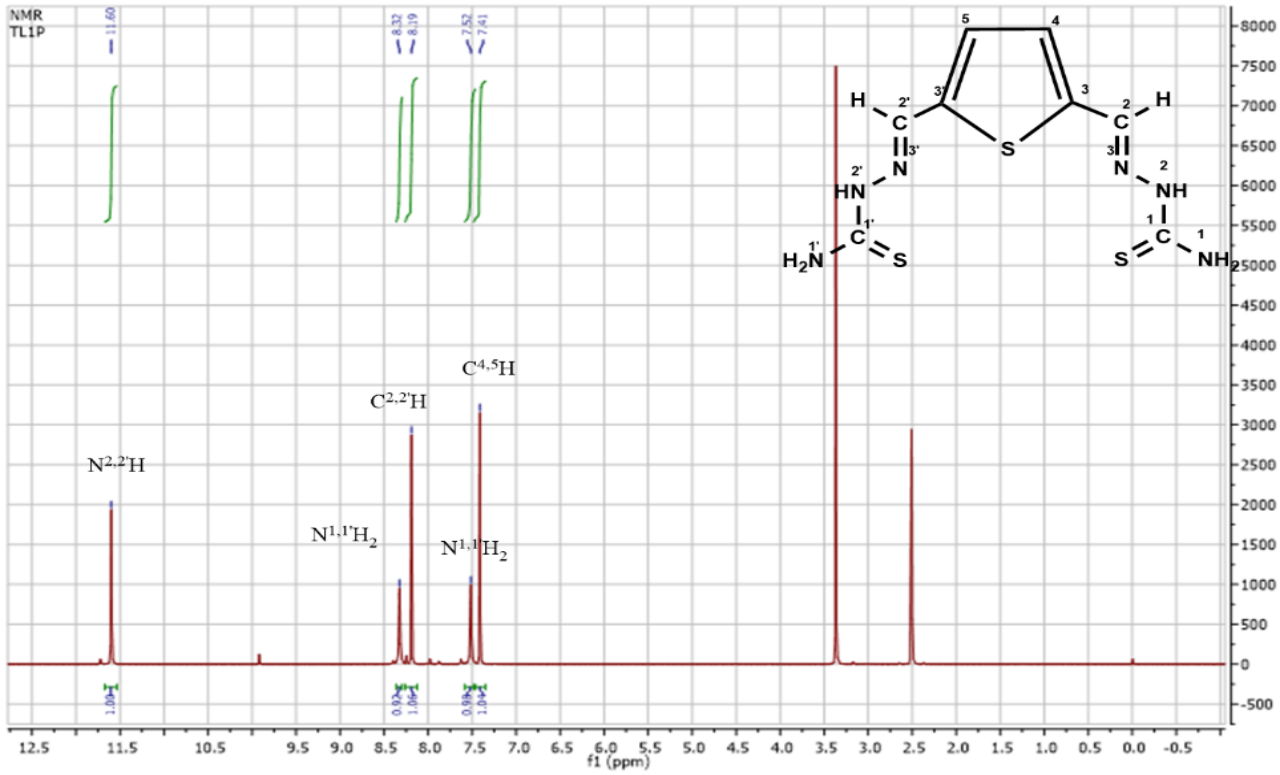

Figure 4.3.1.1: ^{1}HNMR spectra of 2,5 thiophene dicarboxaldehyde bisthiosemicarbazone ($^{1}H_2L$)

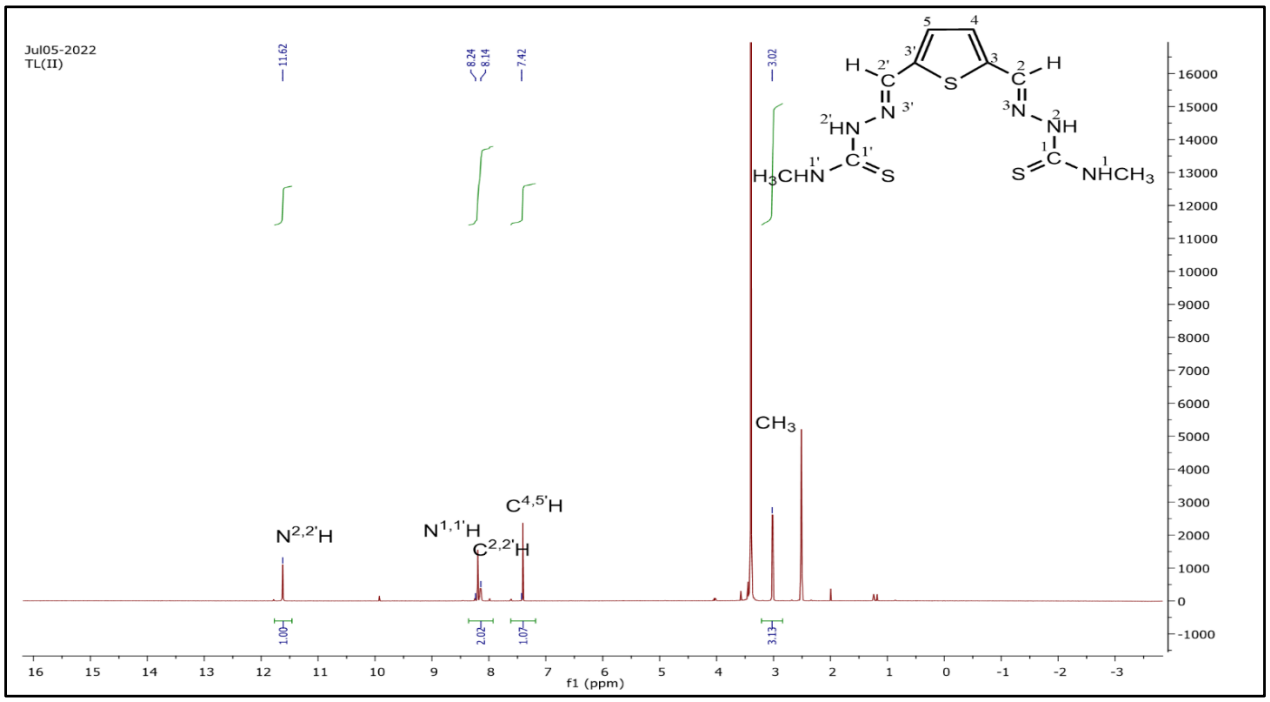

Figure 4.3.1.2: ^{1}HNMR spectra of 2,5 thiophene dicarboxaldehyde, N-methyl bisthiosemicarbazone ($^{2}H_2L$)

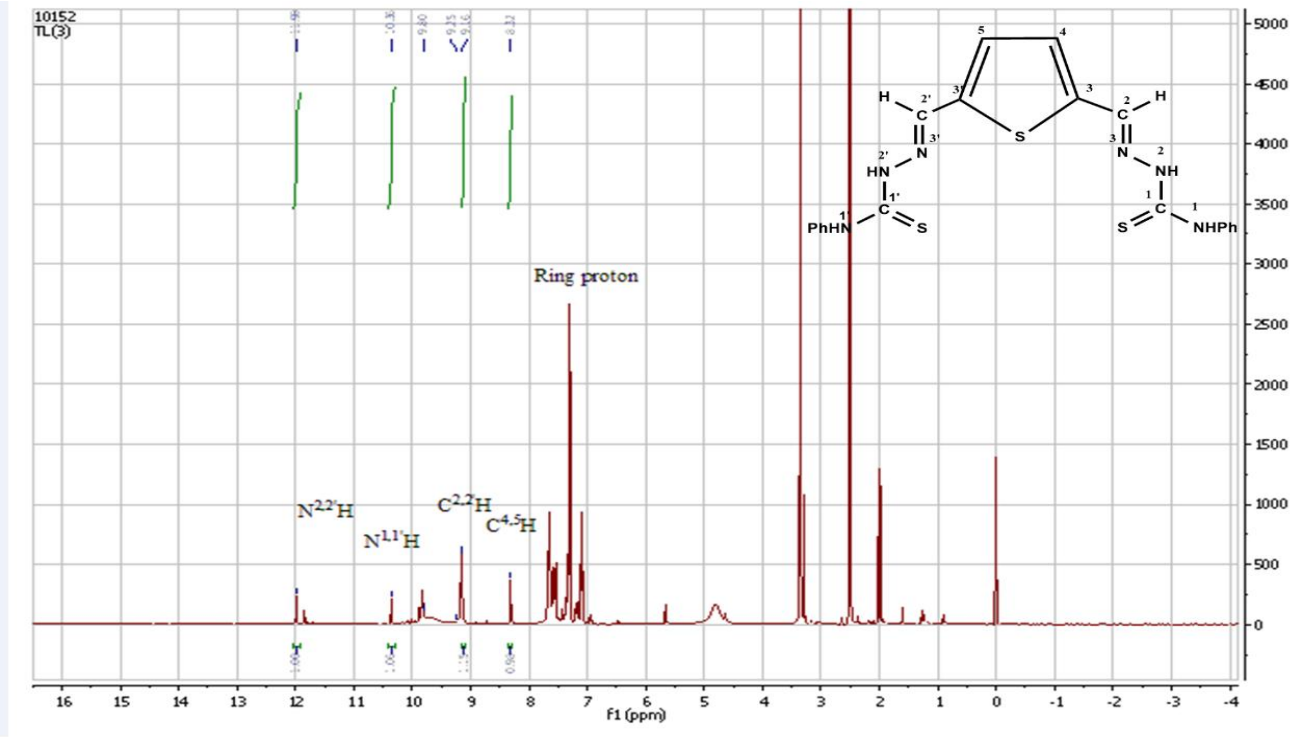

Figure 4.3.1.3: ^{1}HNMR spectra of 2,5 thiophene dicarboxaldehyde N-phenyl bisthiosemicarbazone ($^{3}H_2L$)

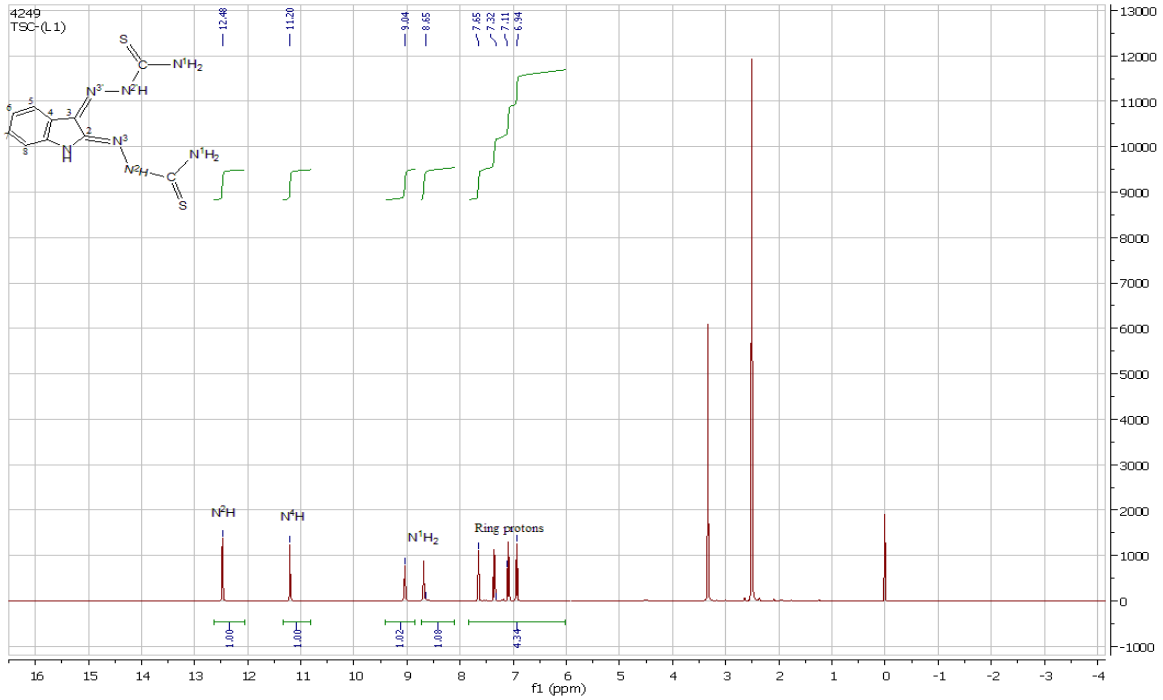

Figure 4.3.1.4a: ^{1}HNMR spectra of 2,3-isatin bisthiosemicarbazone ($^{4}H_2L$)

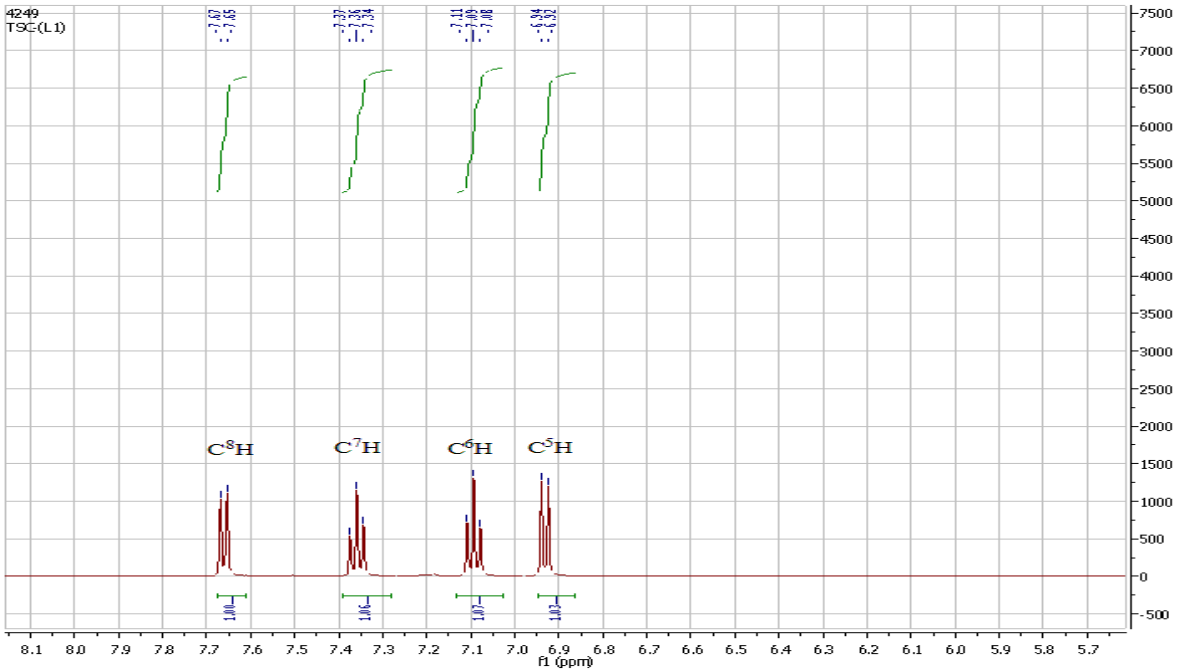

Figure 4.3.1.4b: Expanded ^{1}HNMR spectra of 2,3-isatin bisthiosemicarbazone ($^{4}H_2L$)

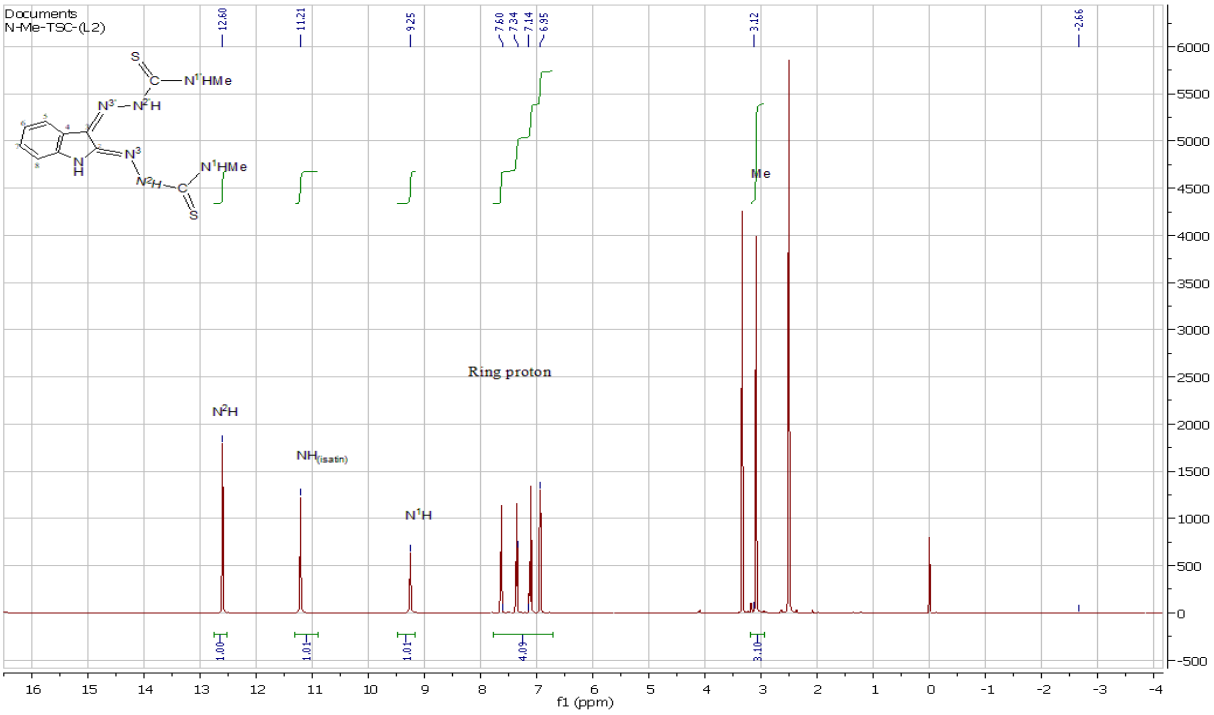

Figure 4.3.1.5a: ^{1}HNMR spectra of 2,3-isatin bis N-methyl thiosemicarbazone ($^{5}H_2L$)

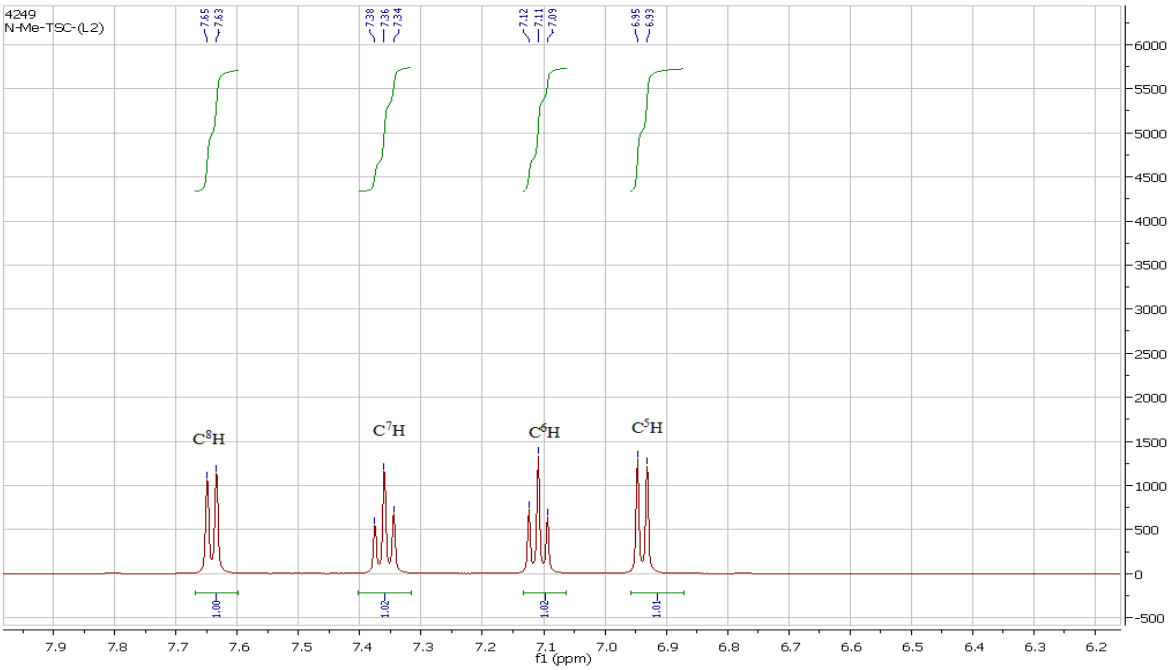

Figure 4.3.1.5b: Expanded ^{1}HNMR spectra of 2,3-isatin bis N- methyl thiosemicarbazone ($^{5}H_2L$)

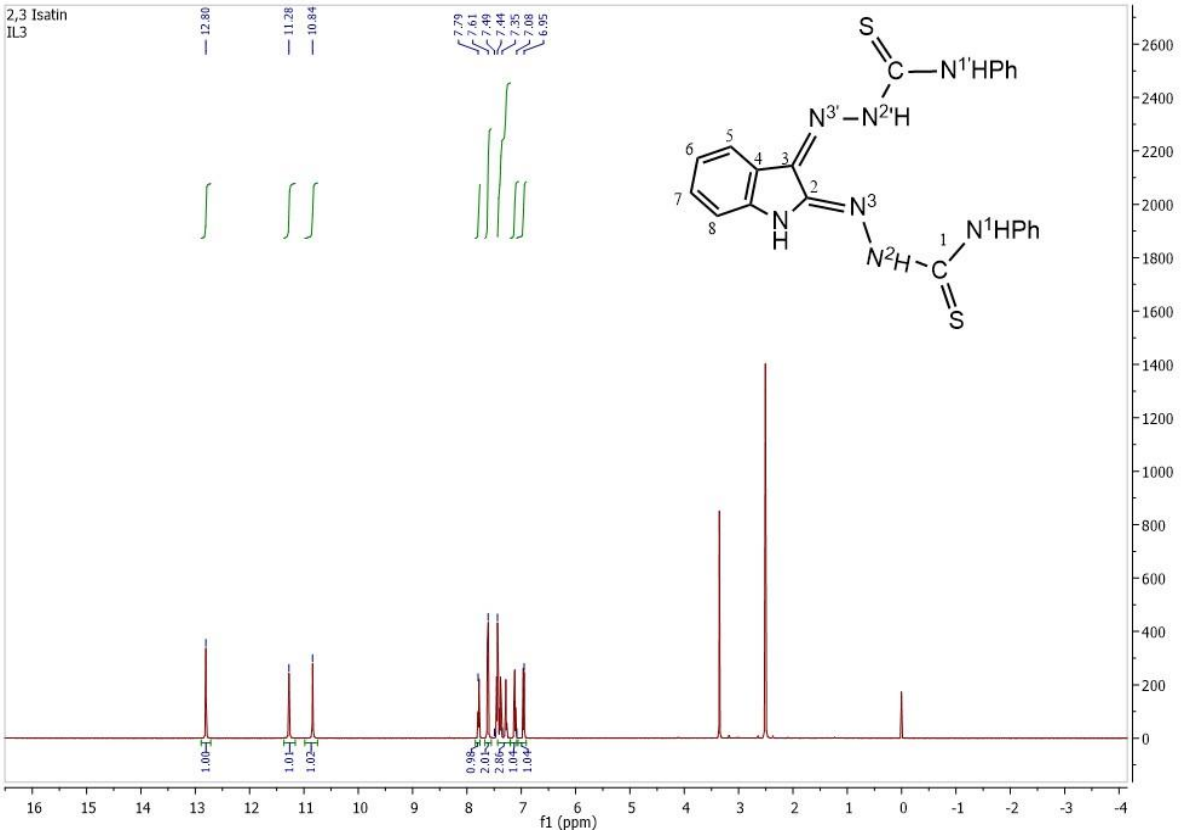

Figure 4.3.1.6: ^{1}HNMR of 2,3-isatin bis N-phenylthiosemicarbazone ($^{6}H_2L$)

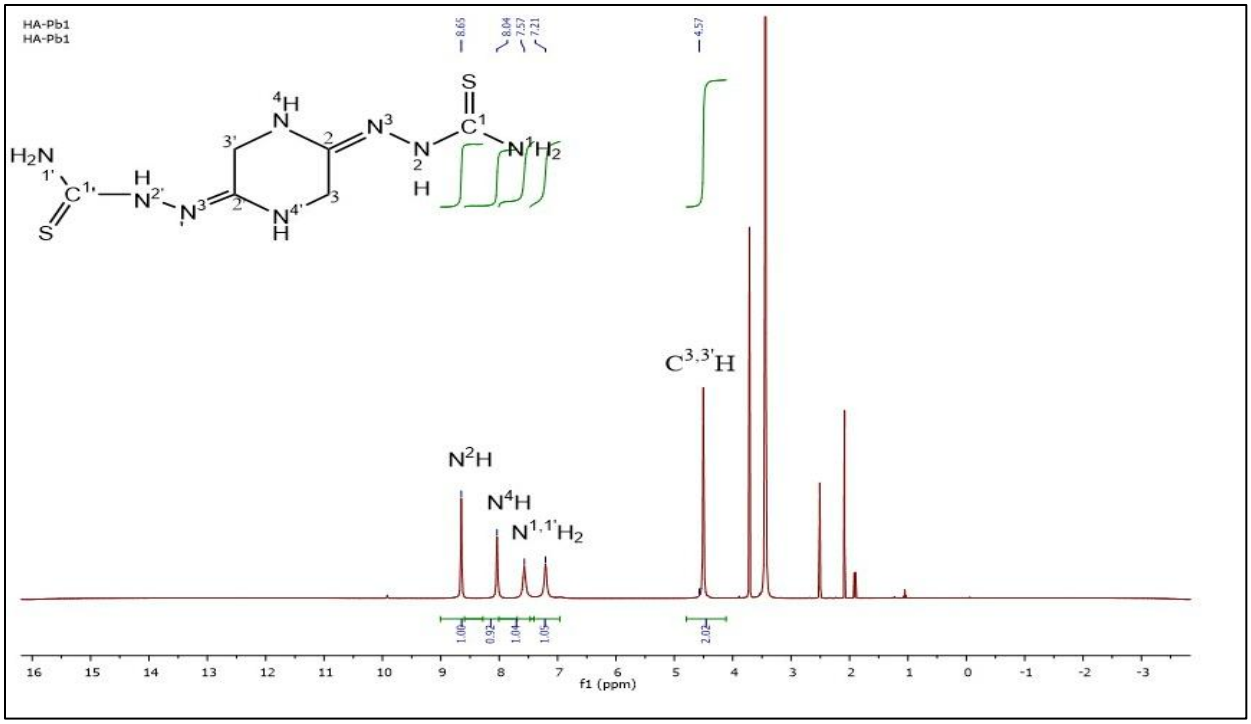

Figure 4.3.1.7. ^{1}HNMR spectra of 2,5-Piperazine bisthiosemicarbazone, (2,5 H_2bptsc, [7]H_2L)

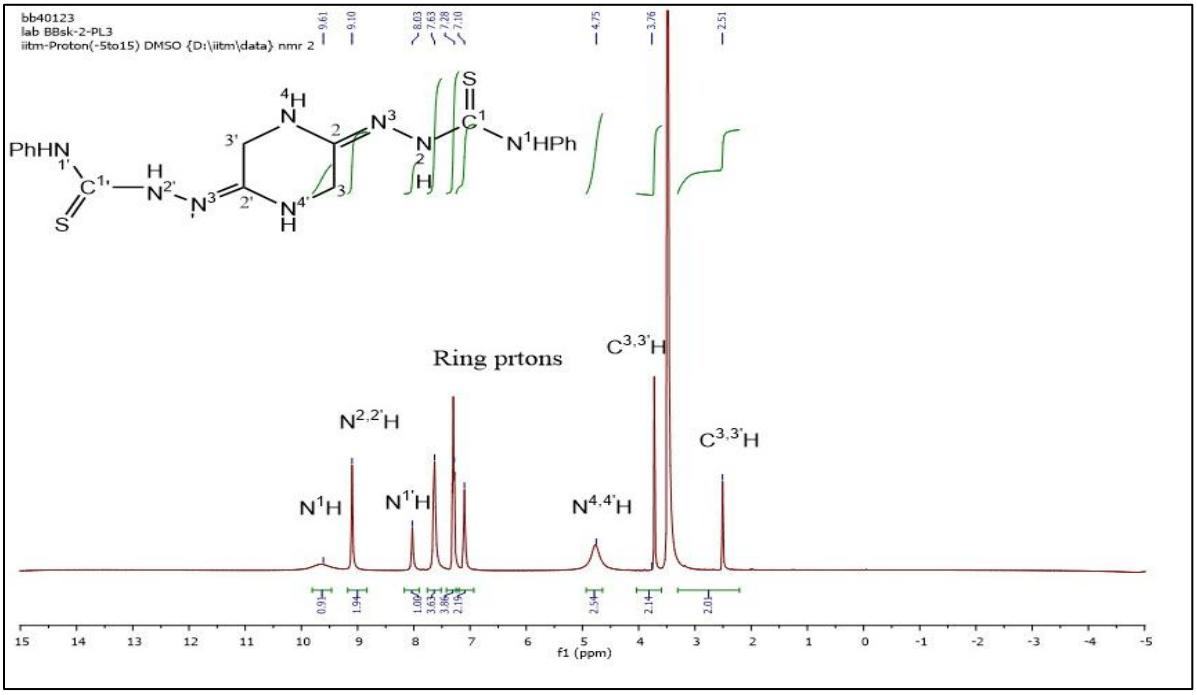

Figure 4.3.1.8: ^{1}H NMR spectra of 2,5-Piperazine bis N-phenyl thiosemicarbazone (2,5 H_2bptsc, [9]H_2L)

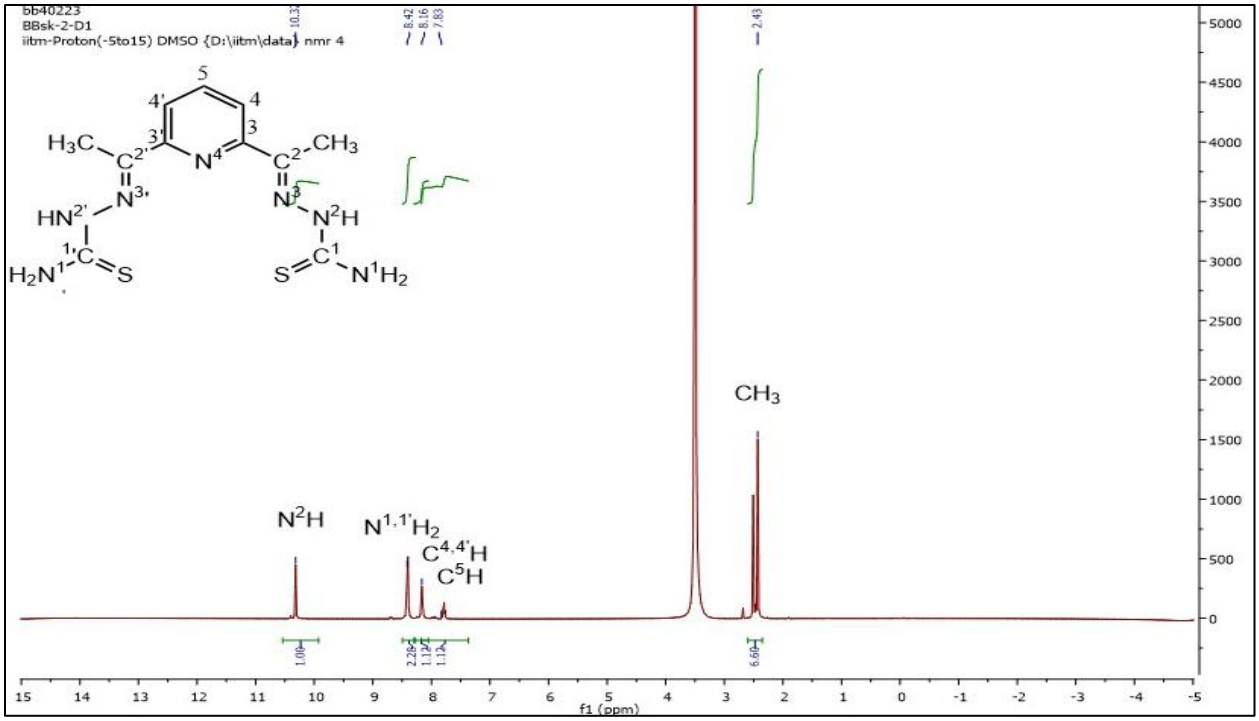

Figure 4.3.1.9: ^{1}H NMR spectra of 2,6 Diacetyl pyridine bisthiosemicarbazone (2,6 H_2bdptsc, $^{10}H_2L$)

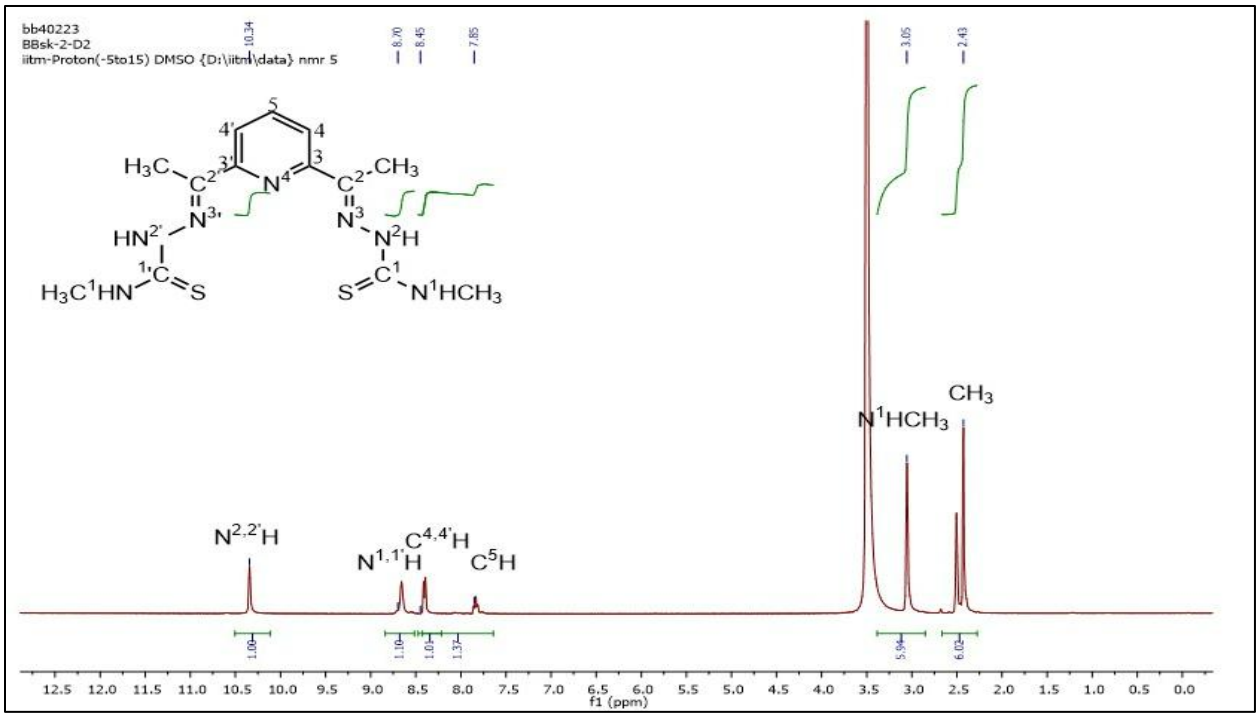

Figure 4.3.1.10: ^{1}HNMR Spectra 2,6 Diacetyl pyridine bis N-methyl thiosemicarbazone (2,6 H_2bdptsc N-Me, $^{11}H_2L$)

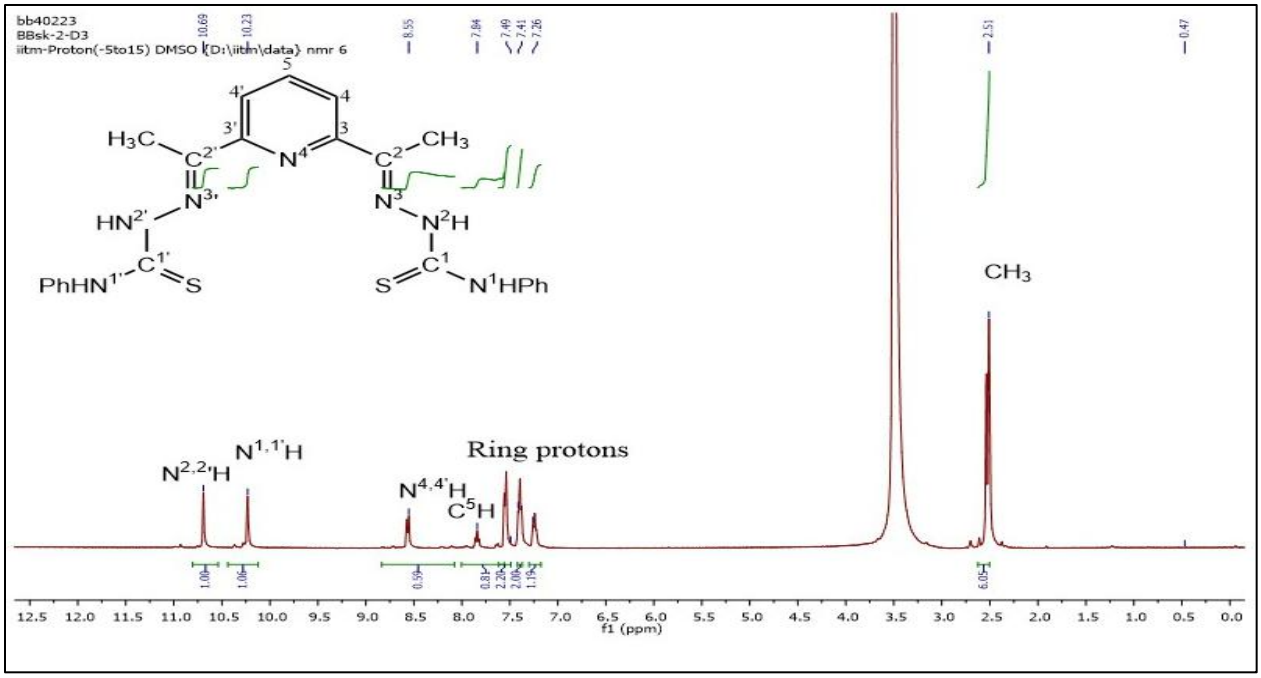

Figure 4.3.1.11: ^{1}H NMR Spectra of 2,6 Diacetyl pyridine bis N-phenyl thiosemicarbazone (2,6 H_2bdptsc N-Ph, $^{12}H_2L$)

In an NMR spectrum, the hygroscopic nature of DMSO often leads to a substantial water signal at 3.35 ppm [171,172].

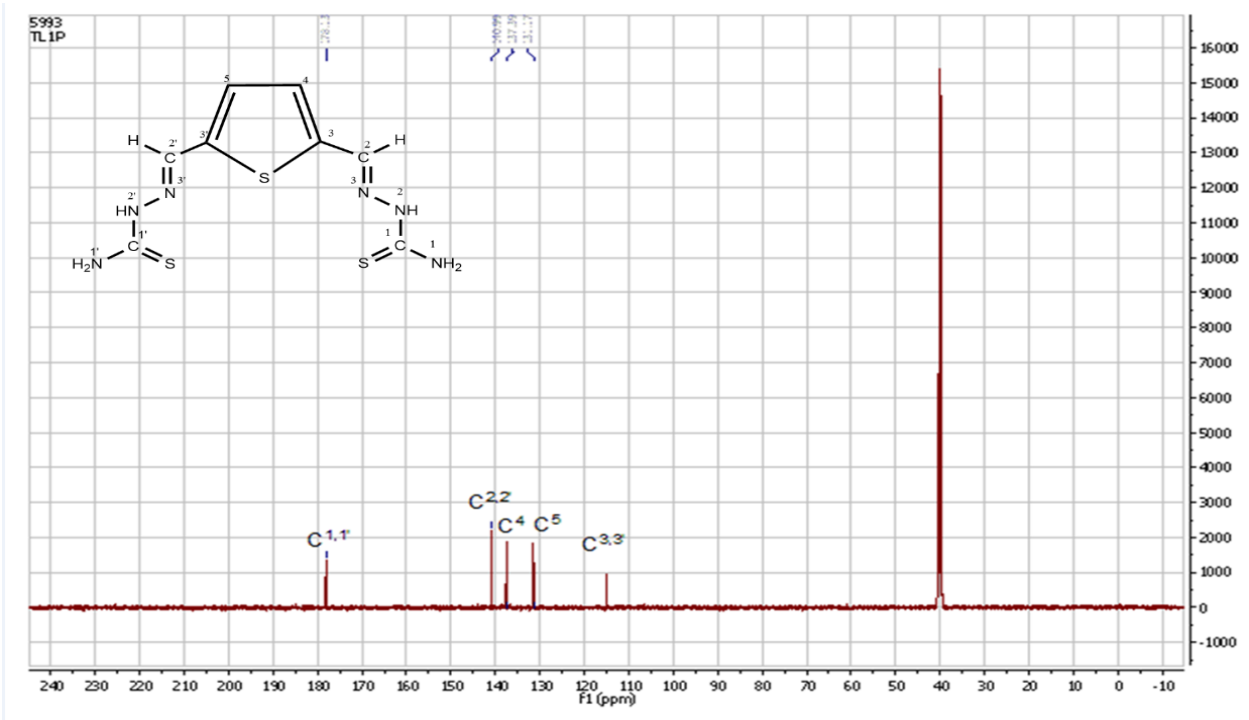

Figure 4.3.2.1: ^{13}CNMR spectra of 2,5 thiophene dicarboxaldehyde bisthiosemicarbazone ($^{1}H_2L$)

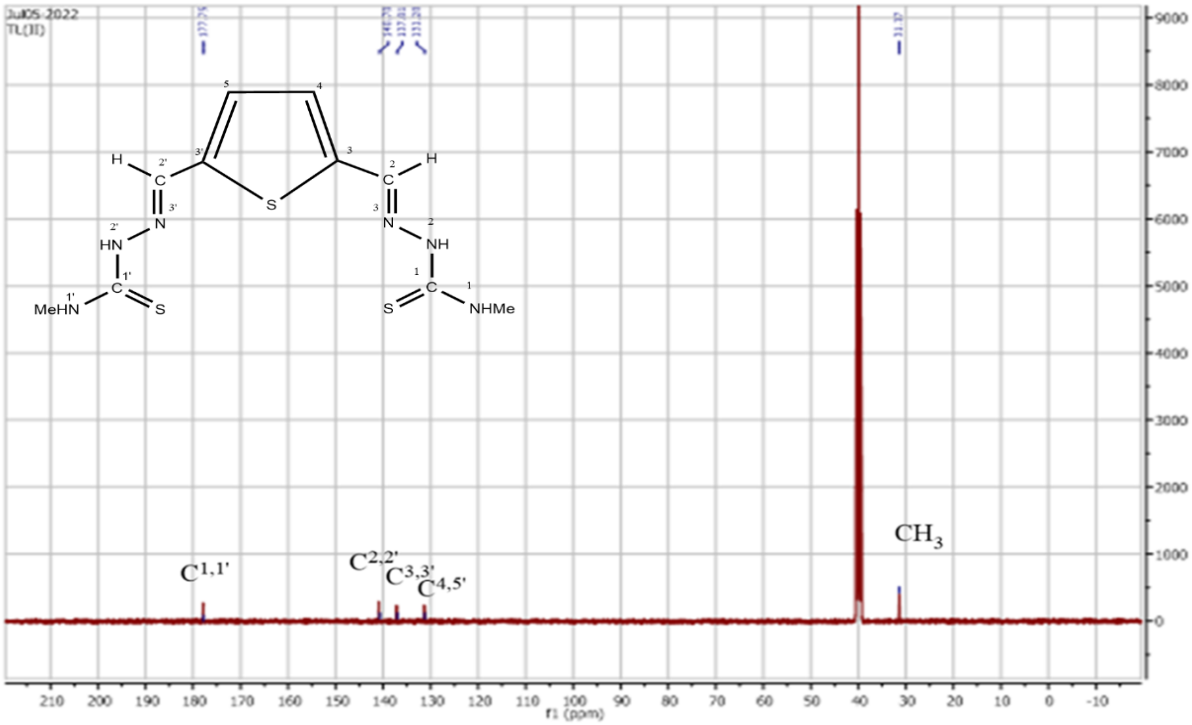

Figure 4.3.2.2: ^{13}CNMR spectra of 2,5 thiophene dicarboxaldehyde N-Me bisthiosemicarbazone ($^{2}H_2L$)

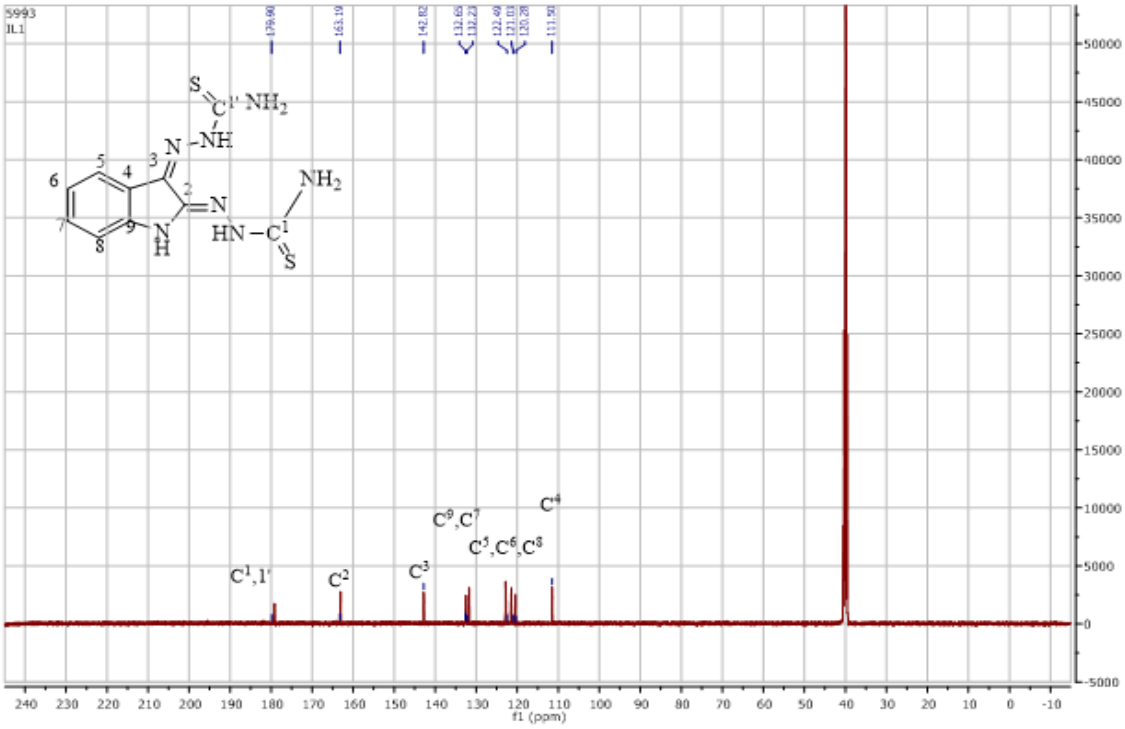

Figure 4.3.2.3: ^{13}CNMR spectra of 2,3-isatin bisthiosemicarbazone ($^{4}H_2L$)

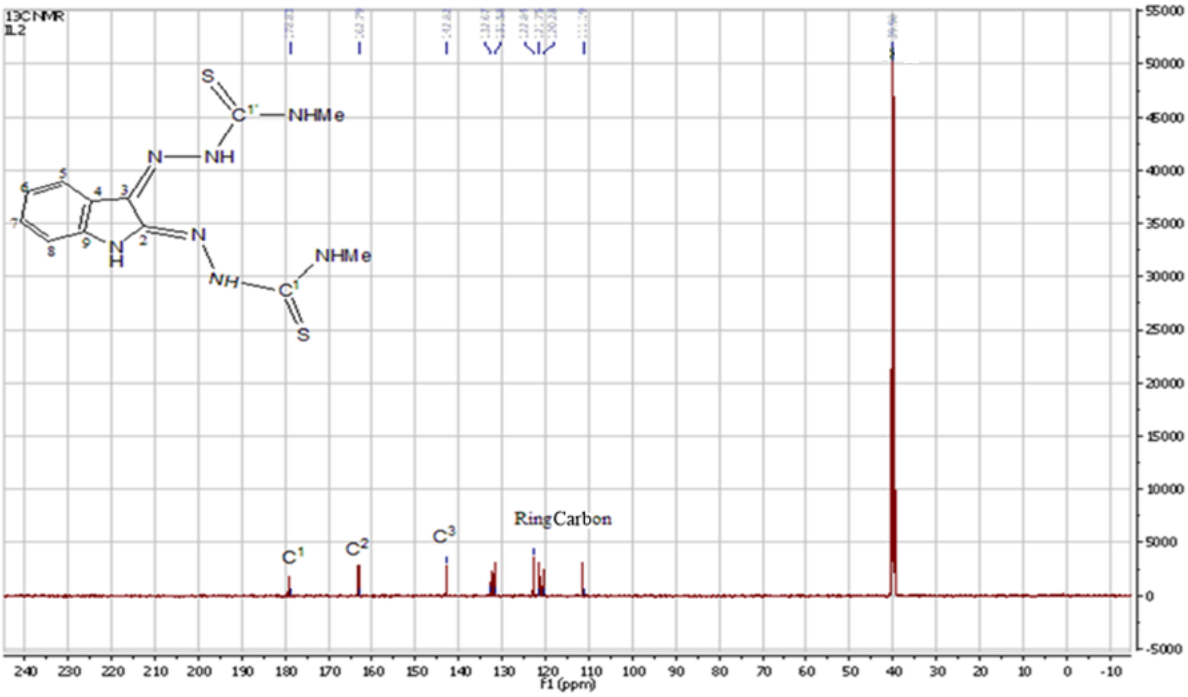

Figure 4.3.2.4: ^{13}CNMR spectra of 2,3-isatin bis N-methyl thiosemicarbazone ($^{5}H_2L$)

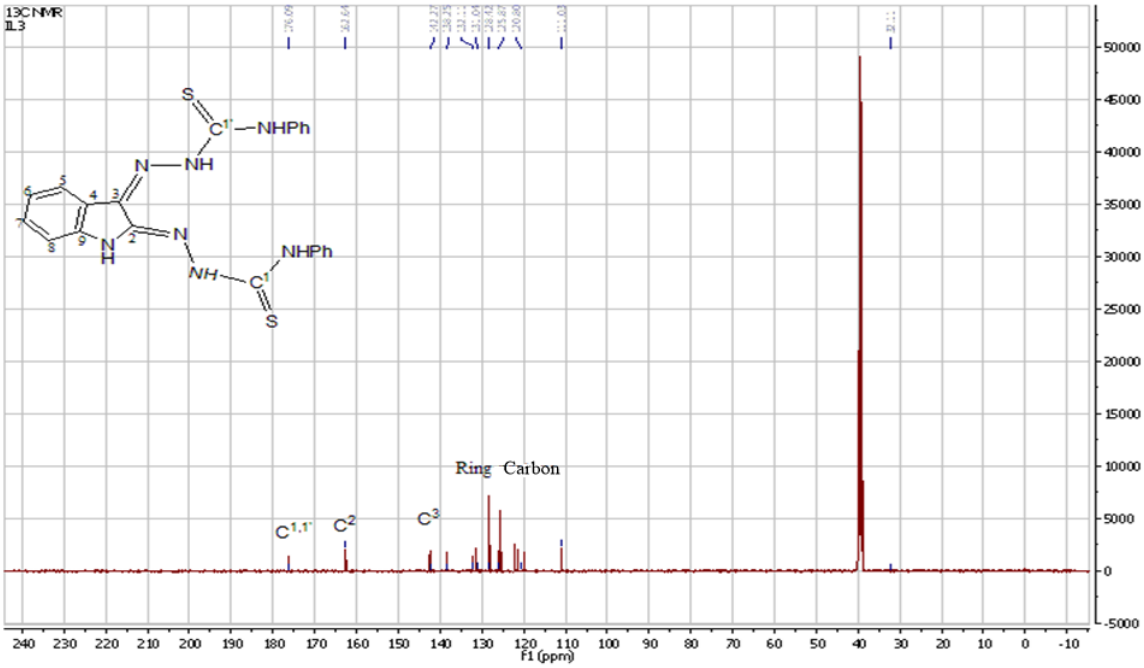

Figure 4.3.2.5: ^{13}CNMR of 2,3-isatin bis N-phenyl thiosemicarbazone ($^{6}H_2L$)

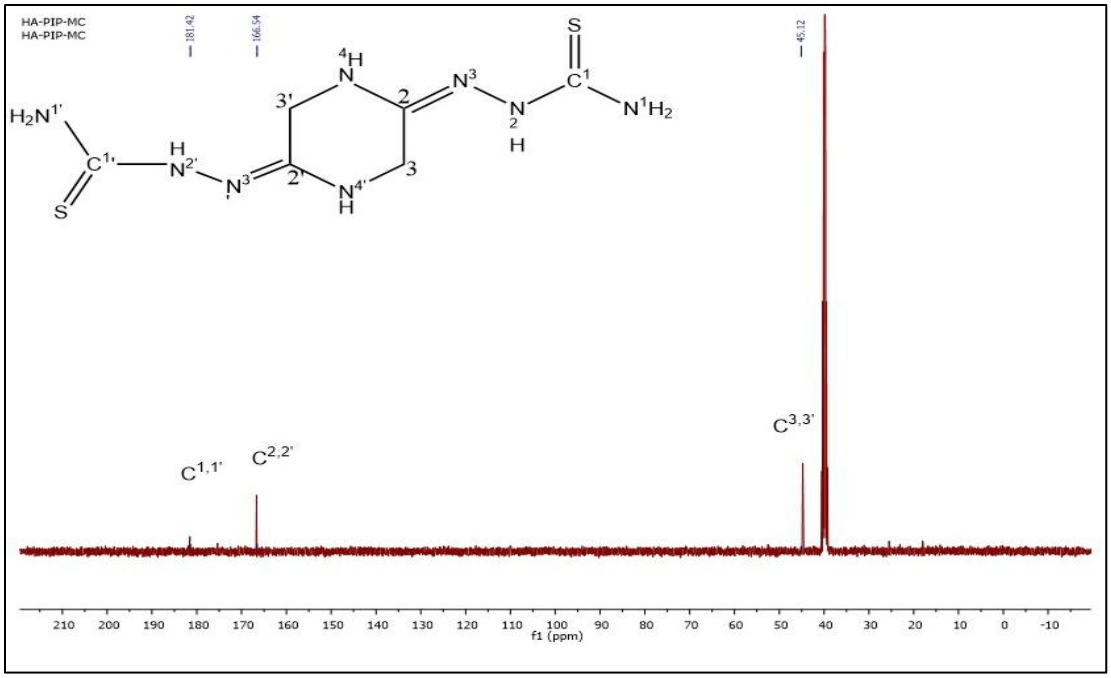

Figure 4.3.2.6: ^{13}C NMR spectra of 2,5-Piperazine bisthiosemicarbazone, (2,5 H_2bptsc, $^{7}H_2L$)

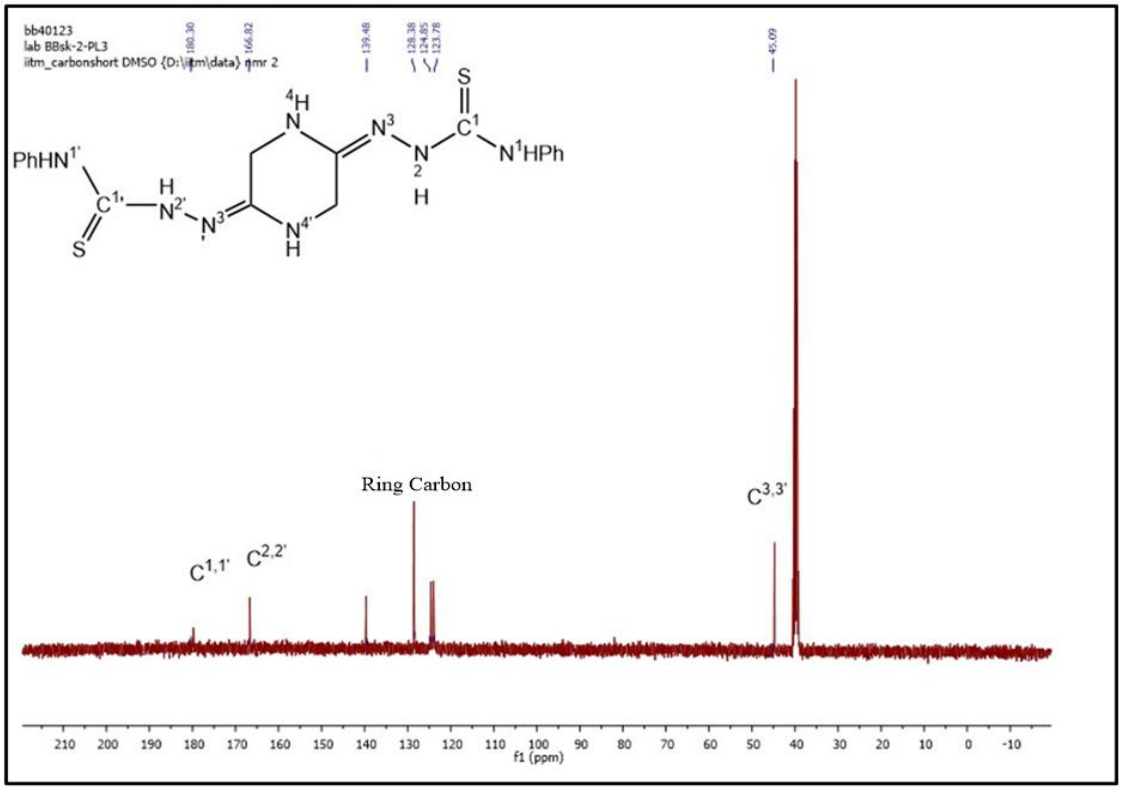

Figure 4.3.2.6: ^{13}C NMR spectra of 2,5-Piperazine N-Phenyl bisthiosemicarbazone, (2,5 H_2bptsc, N-Ph $^{9}H_2L$)

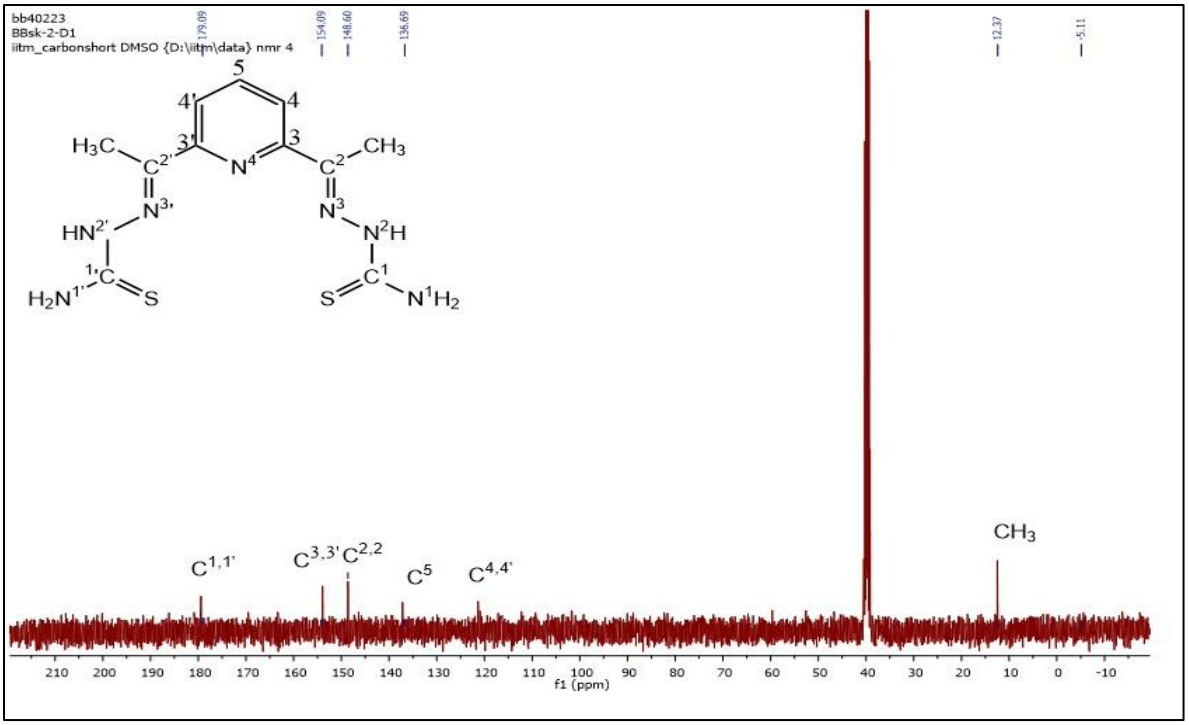

Figure 4.3.2.8: ^{13}C NMR spectra of 2,6 Diacetyl pyridine bisthiosemicarbazone (2,6 H_2bdptsc, $^{10}H_2L$).

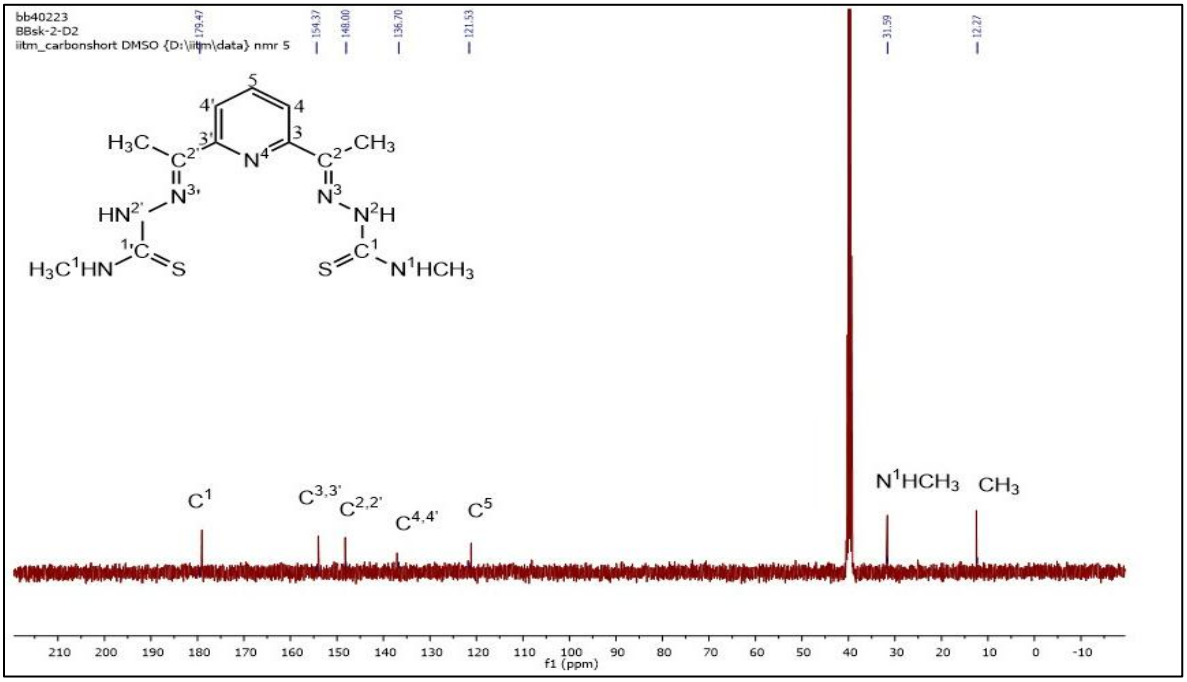

Figure 4.3.2.9: ^{13}C NMR Spectra 2,6 Diacetyl pyridine bis N-methyl thiosemicarbazone (2,6 H_2bdptsc N-Me, $^{11}H_2L$)

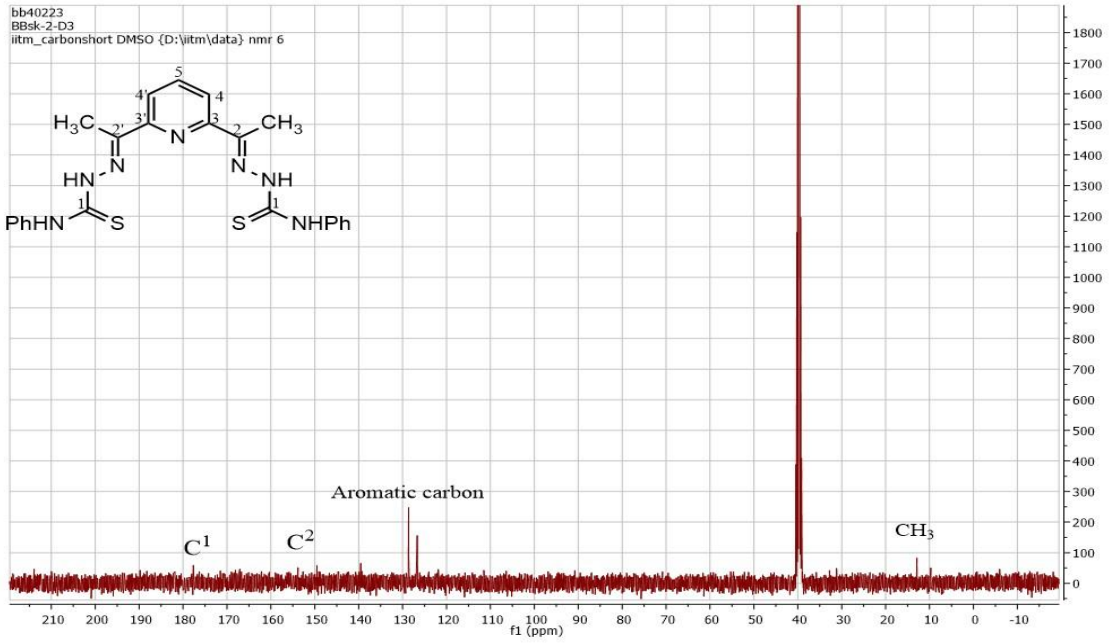

Figure 4.3.2.10: ^{13}C NMR Spectra 2,6 Diacetyl pyridine bis N-phenyl thiosemicarbazone (2,6 H_2bdptsc N-Ph, $^{12}H_2L$)

CHAPTER 5

COBALT(II) COMPLEXES

5.1 Discussion on Complexes of Cobalt (II)

Reaction of Cobalt acetate with ligands **$^{1}H_2L$-$^{12}H_2L$** in molar ratio 1:1 resulted in the formation of complexes of stoichiometry, [Co(L)] (L=^{1}L-^{6}L, ^{10}L-^{12}L; **1-6**, **10-12**) and the complexes (**7-9**) with substituted 2,5 piperazine bisthiosemicarbazone (**$^{7}H_2L$-$^{9}H_2L$)** of formula [$Ni_2(L)_2$] give the formation of dimer. The stoichiometry of complexes was confirmed by the binding ratio study using job plot method. The binding ratio of representative ligand with cobalt(II) **$^{4}H_2L$:Co(II)** came out as 1:1. The list of complexes formed is given in Table 5.1

Table 5.1: Bisthiosemicarbazone complexes of cobalt(II) **1-12**

Sr. No.	**Ligands**	**Complexes**
1.	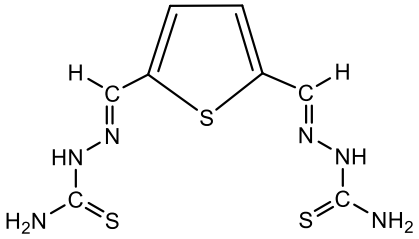 2,5 thiophene dicarboxaldehyde Bisthiosemicarbazone **(2,5 H_2bttsc, $^{1}H_2L$)**	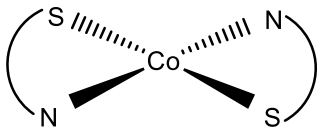 **[Co(2,5 bttsc)]1**
2.	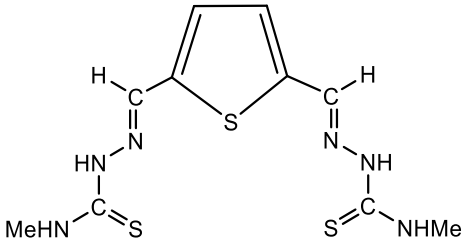 2,5thiophene dicarboxaldehyde-N-methyl bisthiosemicarbazone **(2,5 H_2bttsc -N-Me, $^{2}H_2L$)**	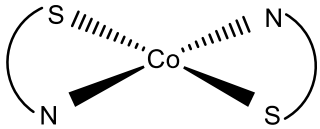 **[Co(2,5 bttsc,N-Me)]2**

3.	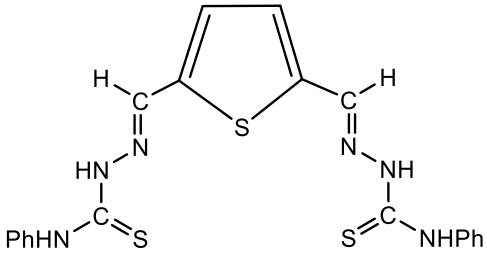 2,5thiophene dicarboxaldehyde-N-phenyl bisthiosemicarbazone **(2,5 H_2bttsc- N-Ph, ^3H_2L)**	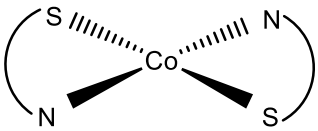 **[Co(2,5 bttsc,N-Ph)]3**
4.	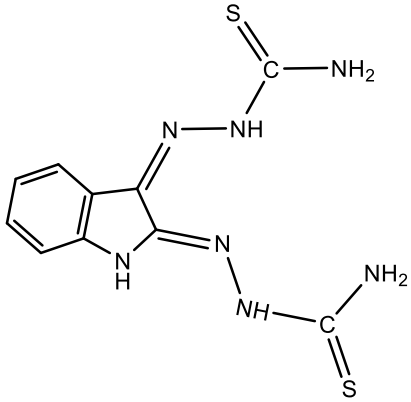 2,3-isatin bisthiosemicarbazone **(2,3 H_2bitsc, ^4H_2L)**	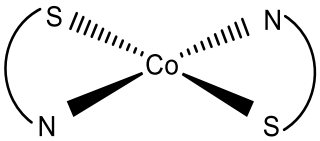 **[Co(2,3 bitsc)]4**
5.	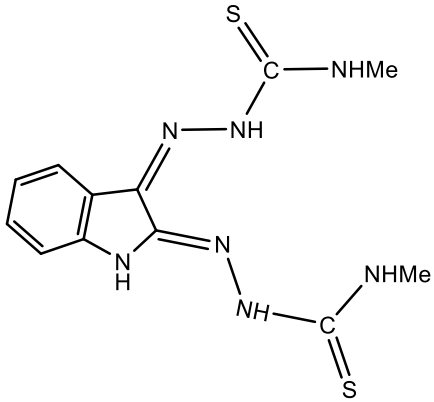 2,3-isatin-N-methyl bisthiosemicarbazone **(2,3 H_2bitsc-N-Me, ^5H_2L)**	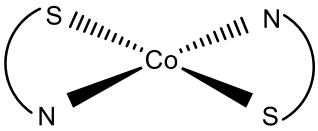 **[Co(2,3 bitsc-N-Me)]5**

6.	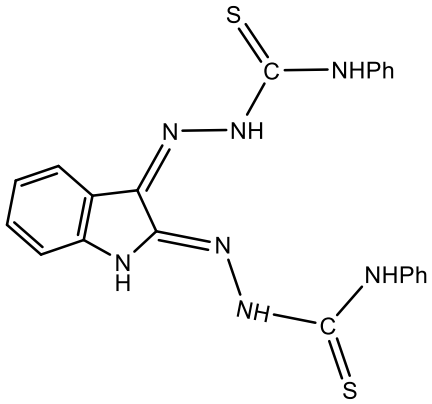 2,3-isatin-N-phenyl bisthiosemicarbazone **(2,3 H_2bitsc-N-Ph, ^6H_2L)**	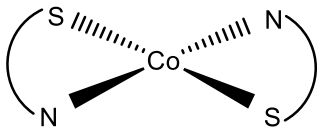 **[Co(2,3 bitsc-N-Ph)]6**
7.	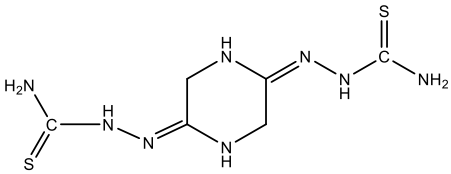 2,5-Piperazine bisthiosemicarbazone **(2,5 H_2bptsc, ^7H_2L)**	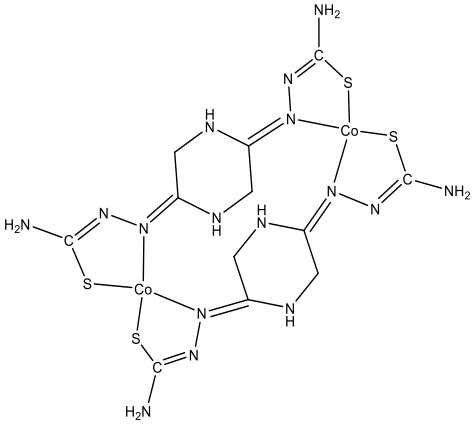 **[Co(2,5 bptsc)]7**
8.	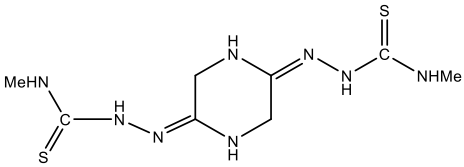 2,5-Piperazine bis N-methyl thiosemicarbazone **(2,5 H_2bptsc N-Me, ^8H_2L)**	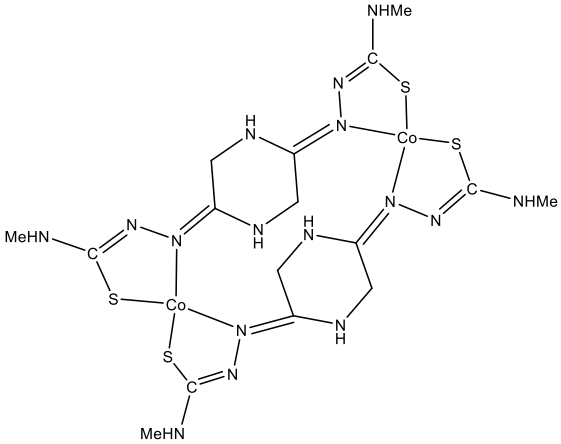 **[Co(2,5 bptsc N-Me]8**

9.	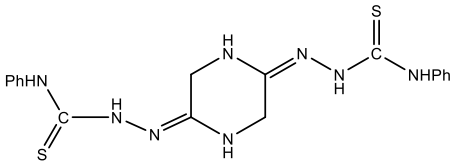 2,5-Piperazine bis N-phenyl thiosemicarbazone **(2,5 H_2bptsc N-Ph, $^{9}H_2L$)**	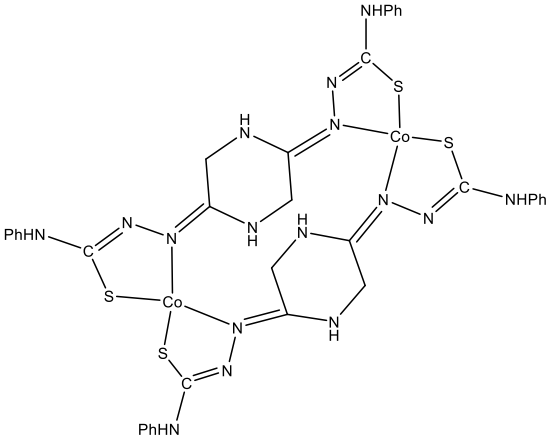 **[Co(2,5 bptsc N-Ph]9**
10.	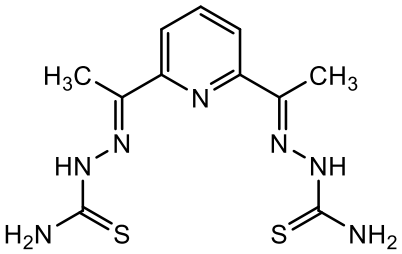 2,6 Diacetyl pyridine bisthiosemicarbazone **(2,6 H_2bdptsc, $^{10}H_2L$)**	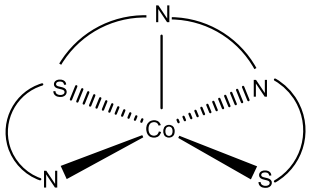 **[Co(2,6 bdptsc]10**
11.	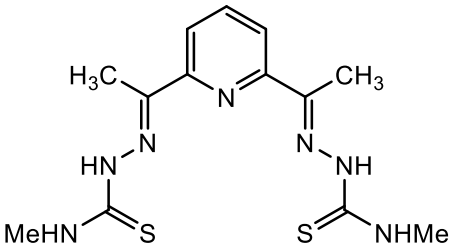 2,6 Diacetyl pyridine bis N-methyl thiosemicarbazone **(2,6 H_2bdptsc N-Me, $^{11}H_2L$)**	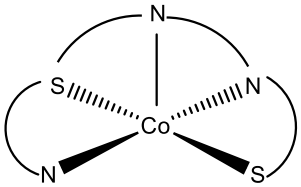 **[Co(2,6 bdptsc,N-Me] 11**

12.	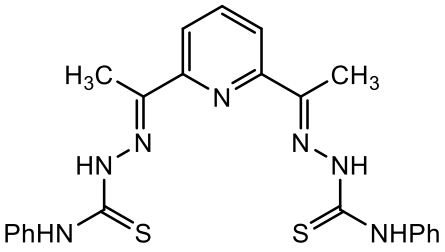 2,6 Diacetyl pyridine bis N-phenyl thiosemicarbazone **(2,6 H_2bdptsc N-Ph, $^{12}H_2L$)**	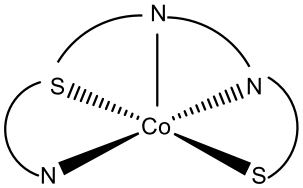 **[Co(2,6 bdptsc,N-Ph] 12**

5.2 Binding studies: By Job Plot method

To confirm the structure of the complex (No. of binding sites) the representative ligand **2,3 H_2bitsc (^4H_2L)** was selected for binding study with cobalt (II) using UV-visible spectroscopy.

Solvents like methanol, acetonitrile, ethanol, and DMSO were used in the UV-visible studies. Due to better sample solubility and finer absorption bands, it has been found that DMSO is the best solvent among the alternatives. Using the same solvent, 1 mM metal salt solutions were made and 20 equivalents of 1 mM Cobalt(II) solution were incrementally added to 0.3 mM of ligand to conduct the UV-visible titrations for the ion analysis, 20 equivalents of 1mM of metal solution were successively added to 0.3 mM of ligand solution **^4H_2L**. The results for the sample with 20 equivalents of each metal ion in the compound **^4H_2L** solution are depicted in Figure 5.2.1. The corresponding shift in absorbance maxima (A_n/A_o) after 20 equivalents of Co(II) ions are added at a time is illustrated in Figure 5.2.2 (a). A_n represents the absorbance maxima with the subsequent Co(II) ions addition, while A_o represents the absorbance maxima of **^4H_2L**. (b) To determine the detection limit for Co(II), correlate [A_o-A_n/A_o] vs. Co(II) Concentration. Based on Linear calibration curve, detection limit for Co(II) was came out to be 8.5 µM, displayed in Figure 2(b), and the binding ratio was calculated as 1:1 for (**^4H_2L**): Co(II)[173].

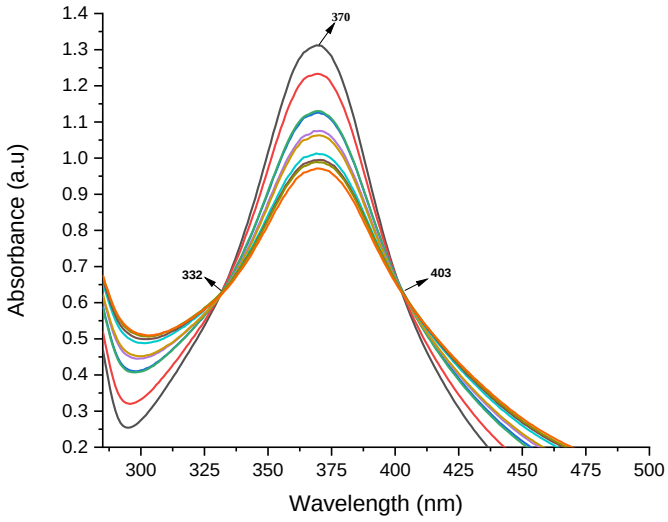

Figure 5.2.1: Absorbance responses measured after adding 20 equivalents of 1 mM Co(II) solution to the solution of **^4H_2L** (0.3 mM).

The difference between absorbance values before and after isosbestic points (Where the overall absorbance of sample remains constant) can be seen at wavelength 332nm and 403nm, as well as hypsochromic shifting (shift to a shorter wavelength in the spectral band) of maxima between both wavelengths with a notable decrease in intensity[174], which confirm the binding of ligand with metal ion.

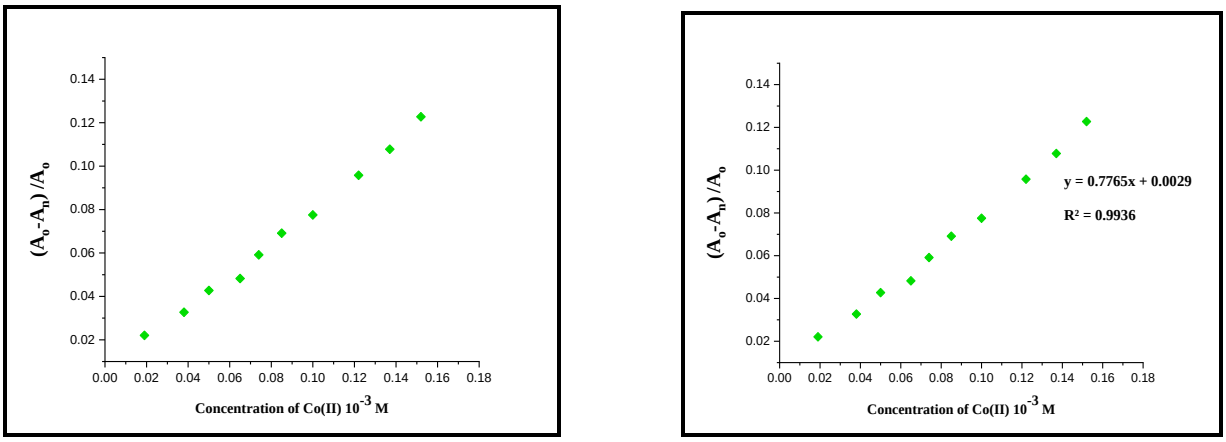

(a) **(b)**

Figure 5.2.2: a) Relative shift in absorbance maxima; **b)** Linear calibration curve [A_o-A_n/A_oVs.(A_n/A_o) after 20 equivalent of Co(II) addition.

b) A_n = Absorbance maxima for detection of Co (II) with addition, and A_o = Absorbance maxima of (**^4H_2L**)

5.3 IR Spectroscopy:

The important IR peaks of bisthiosemicarbazones and their Co(II) complexes are mentioned in Table 5.3.1 and spectra are given in Figures 5.3.1-5.3.12. The ν(N-H) bands in ligands **^1H_2L-$^{12}H_2L$** appeared in the range 3461-3204 cm^{-1} which showed a slight high energy shift in complexes (3491-3200 cm^{-1}). The bands due to $–N^2H$ – group in the range, 3190-3126 cm^{-1} appeared in ligands. But on complexation this band gets disappeared in all the complexes (**1-12**) suggesting deprotonation on complexation and coordination of bisthiosemicarbazone to metal centre in dianionic form [175]. The bands of υ(C=N) in the range, 1698-1594 cm^{-1} in the ligands is shifted to lower frequency in complexes **1-12** and appeared in the range 1654-1500 cm^{-1}. The specific ν(C=S) band observed in the range, 896-812 cm^{-1} in free ligands which get shifted to lower energy in Co(II) complexes (**1-12)** and observed in the range, 793-687 cm^{-1}. The significant low energy shift of this band indicates binding of bis- ligand in thiolate form [176]

Table 5.3.1: IR peaks of bisthiosemicarbazones (**^1H_2L–$^{12}H_2L$**) and their cobalt (II) complexes (**1-12**)

Synthesized Ligands and Metal complexes	$\upsilon(NH_2)$	υ(-NH-)	υ(C=N)	υ(C=C)	δ (NH_2)	υ(C=S)
(2,5 H_2bttsc, ^1H_2L)	3409m, 3277m	3155s	1600s	1583m	1535s	836s
[Co(bttsc)] **1**	3301m	-	1609s	1478m	1334s	656s
(2,5 H_2bttscN-Me, ^2H_2L)	3373m	3155s	1594s	1462m	-	812s
[Co(bttsc,N-Me)] **2**	3339m	-	1500s	1403m	-	766s
(2,5 H_2bttsc N-Ph, ^3H_2L)	3303m	3156s	1636s	1594w	-	895s
[Co(bttsc,N-Ph)] **3**	3251m	-	1592s	1534m	-	748
(2,3 H_2bitsc, ^4H_2L)	3332m, 3259m	3156m	1698s	1618w	1584s	851s
[Co(bitsc)] **4**	3276m	-	1640s	1589m	1540m	773s
(2,3 H_2bitsc-N^1-Me, ^5H_2L)	3461m, 3207m	3190m	1683s	1616m	-	831s
[Co(bitsc,N-Me)] **5**	3220m	-	1643s	1593m	1532	743s
(2,3 H_2bitsc-N^1-Ph, ^6H_2L)	3290m	3173m	1685s	1591m	-	827s
[Co(bitsc,N-Ph)] **6**	3217m	-	1654s	1513m	1450	744s
(2,5 H_2bptsc, ^7H_2L)	3356m, 3253m	3166s	1640s	1526s	1512m	895s

[Co(bptsc)] **7**	3491m, 3262m	-	1643s	1533m	1438m	733s
(2,5 H_2bptsc N-Me, ^8H_2L)	3335m, 3287m	3197m	1642s	1558s	-	804s
[Co(bptsc,N-Me)] **8**	3290m, 3202	-	1545s	1424m	-	743s
(2,5 H_2bptsc N-Ph, ^9H_2L)	3301m	3158m	1639s,	1466m	-	829s
[Co(bptsc,N-Ph)] **9**	3479	-	1577s	1488m	-	753
(2,6 H_2bdptsc, $^{10}H_2L$)	3423m, 3209m	3158m	1606 s	1513 m		827s
[Co(dptsc)] **10**	3285m	-	1590s	1487m	1447	793s
(2,6 H_2bdptsc N-Me, $^{11}H_2L$)	3450m, 3329m	3190m	1634s,	1555m	-	836s
[Co(dptsc,N-Me)] **11**	3265m	-	1619s	1508m		687s
(2,6H_2bdptscN-Ph,$^{12}H_2L$)	3303m	3156 s	1636 s,	1594m	-	896s
[Co(dptsc,N-Ph)] **12**	3385m, 3200	-	1604s	1477m	-	749s

***s= strong; m= medium and w= weak**

5.4 Mass Spectrometry:

The molecular ion peak $[M]^+$ observed are listed in Table 5.3 and spectra are given in Figures 5.4.1-5.4.12. All the complexes have m/z values in well agreement with proposed stoichiometry. The parental ion peak in $(m/z)^+$ found at 340.28 amu (**1**), 373.16 amu (**2**), 492.07 amu (**3**), 355.06 amu (**4**), 382.07 amu (**5**), 519.07 amu (**6**), 318.34 amu (**7**), 347.21 amu (**8**), 471.28 amu (**9**), 367.08 amu (**10**), 394.29 amu (**11**), 518.13 amu (**12**) confirms the formation of bisthiosemicarbazones.

Table 5.4.1: The m/z values (amu) derived from mass spectra and expected formula of complexes **1-12.**

Sr. No.	Parent peak (experimental mass)	Expected formula for parent ion $(m/z)^+$
1	340.28	$[Co(C_8H_8N_6S_3)]$ **1**
2	373.16	$[Co(C_{10}H_{12}N_6S_3)]$ **2**
3	492.07	$[Co(C_{20}H_{16}N_6S_3)]$ **3**
4	355.06	$[Co(C_{10}H_9N_7S_2)]$ **4**
5	382.07	$[Co(C_{12}H_{13}N_7S_2)]$ **5**
6	519.07	$[Co(C_{22}H_{17}N_7S_2)]$ **6**
7	318.34	$[Co(C_6H_{12}N_8S_2)]$ **7**
8	347.21	$[Co(C_8H_{16}N_8S_2)]$ **8**
9	471.28	$[Co(C_{18}H_{20}N_8S_2)]$ **9**
10	367.08	$[Co(C_{11}H_{13}N_7S_2)]$**10**
11	394.29	$[Co(C_{13}H_{17}N_7S_2)]$**11**
12	518.13	$[Co(C_{23}H_{21}N_7S_2)]$**12**

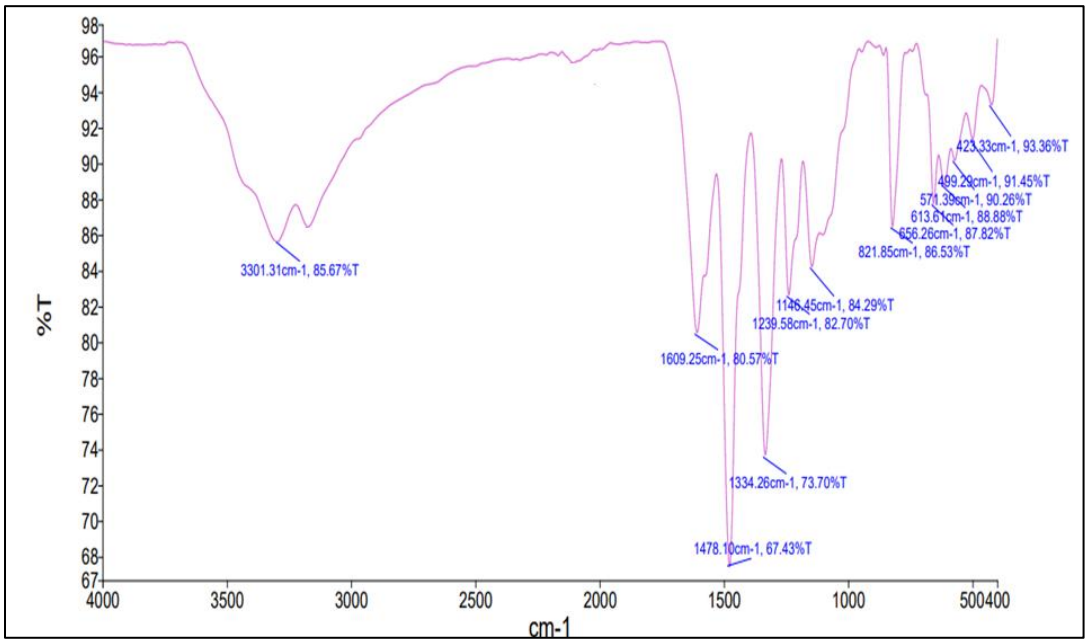

Figure 5.3.1: IR Spectra of [Co(bttsc)] **1**

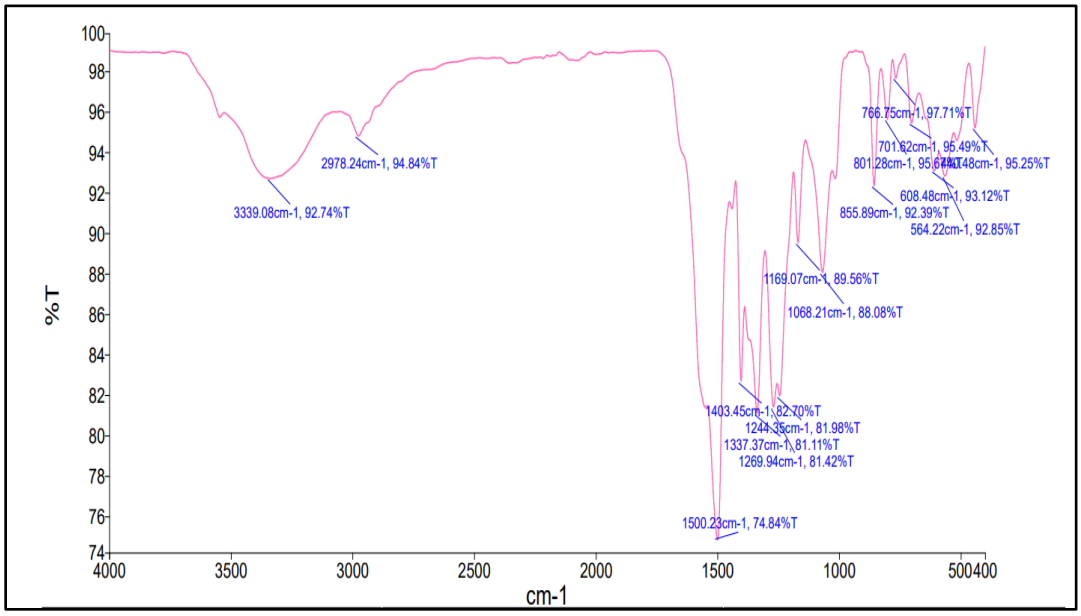

Figure 5.3.2: IR Spectra of [Co(bttsc,N-Me)] **2**

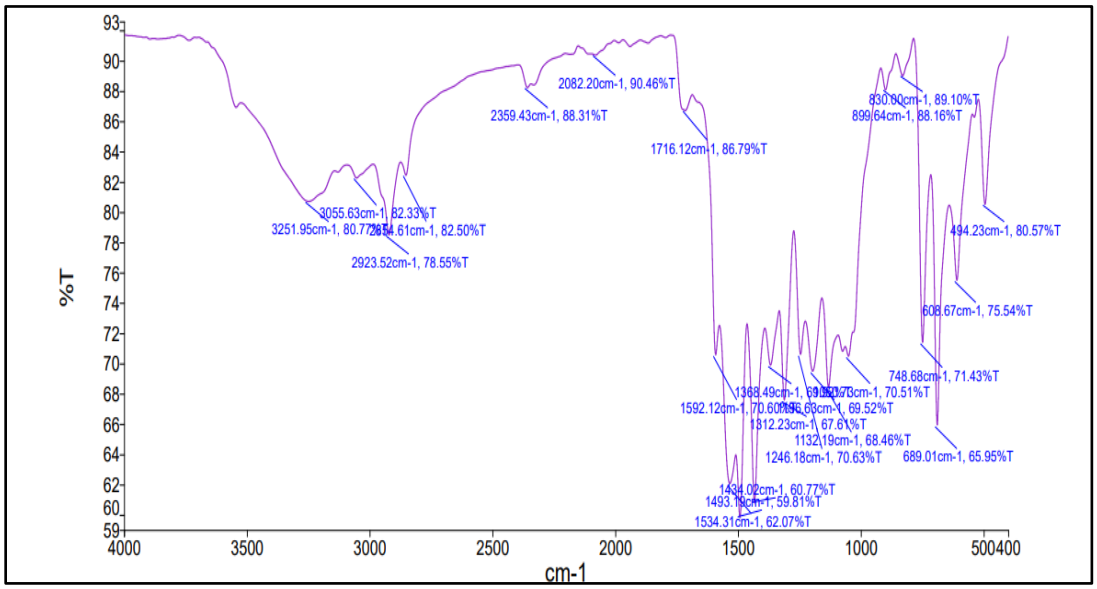

Figure 5.3.3: IR Spectra of [Co(bttsc,N-Ph)] **3**

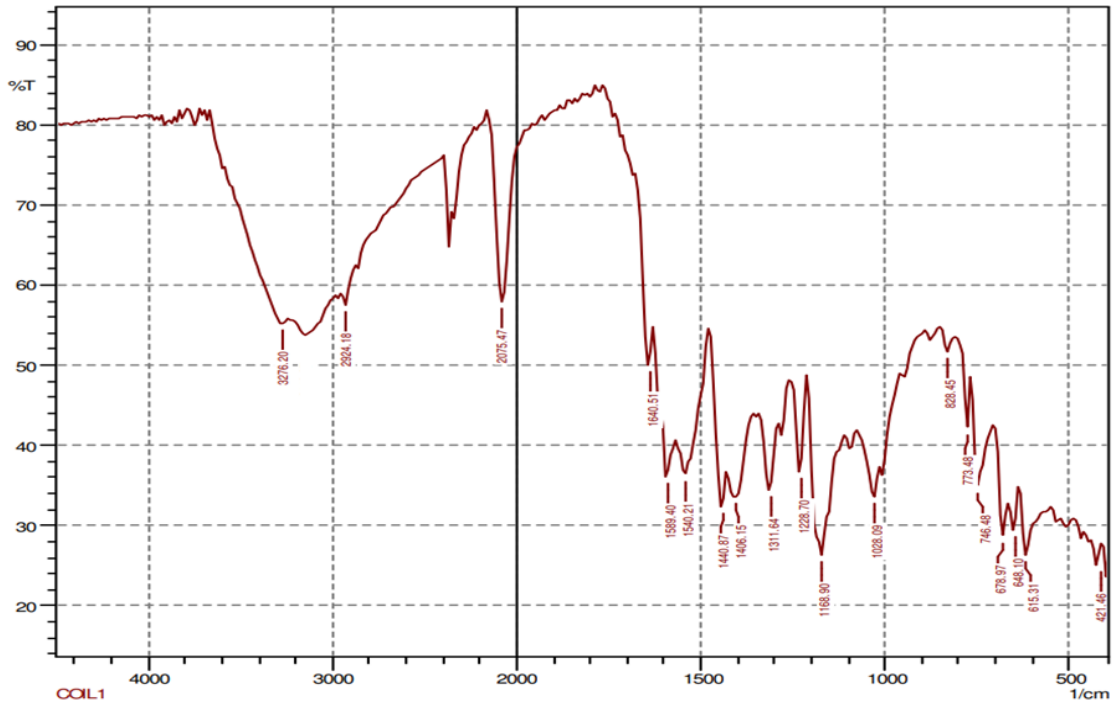

Figure 5.3.4: IR Spectra of [Co(bitsc)] **4**

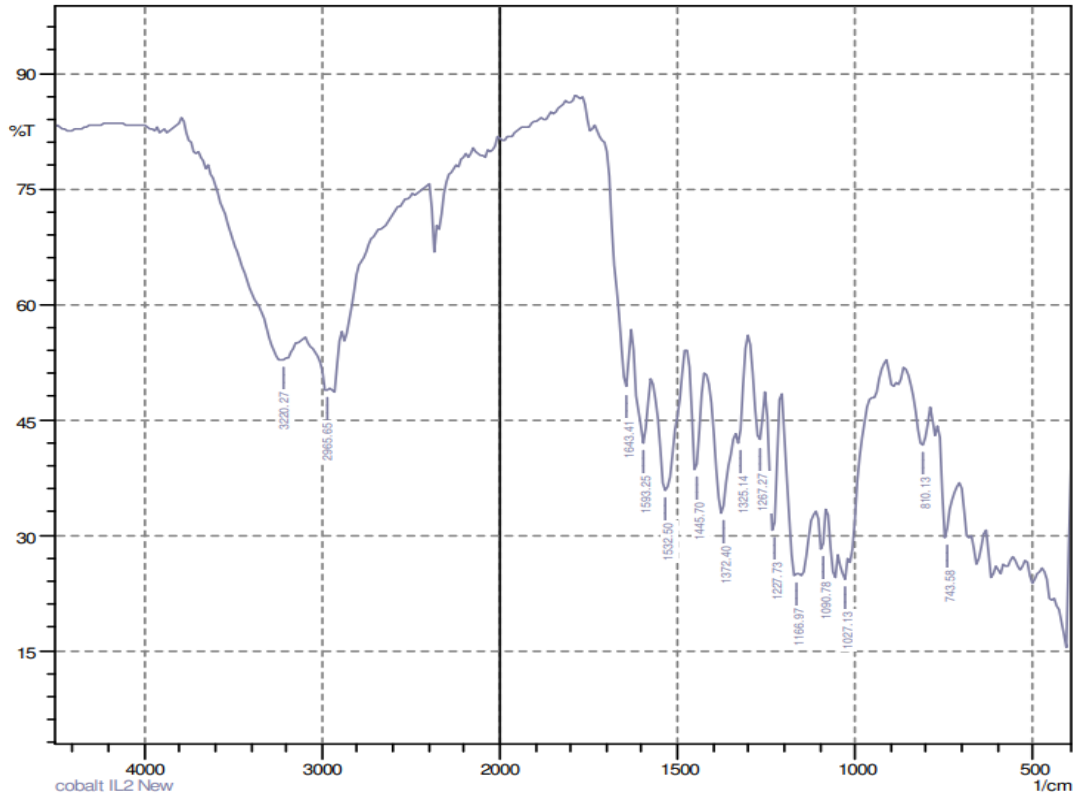

Figure 5.3.5: IR Spectra of [Co(btisc,N-Me)] **5**

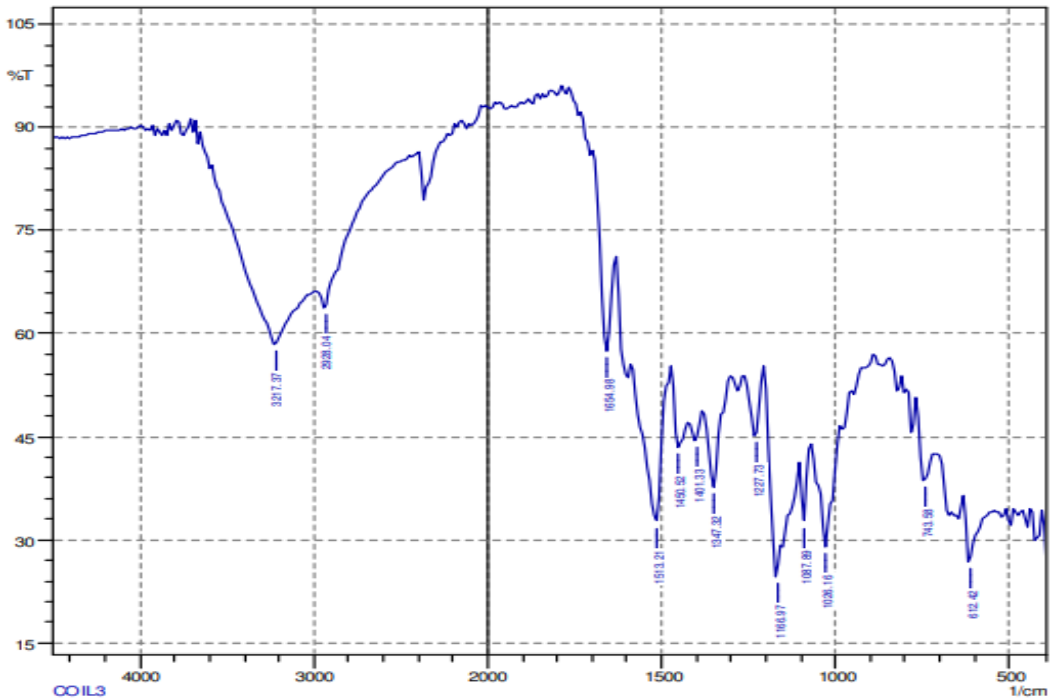

Figure 5.3.6: IR Spectra of [Co(bitsc,N-Ph)] **6**

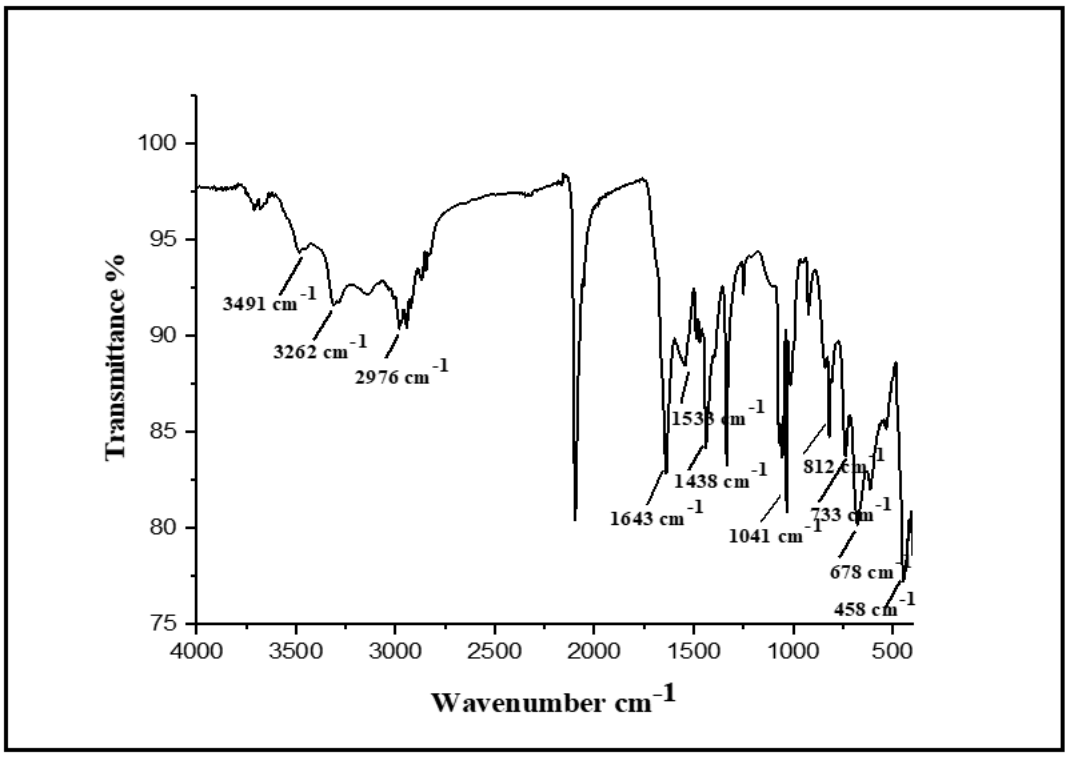

Figure 5.3.7: IR Spectra of [Co(bptsc)] **7**

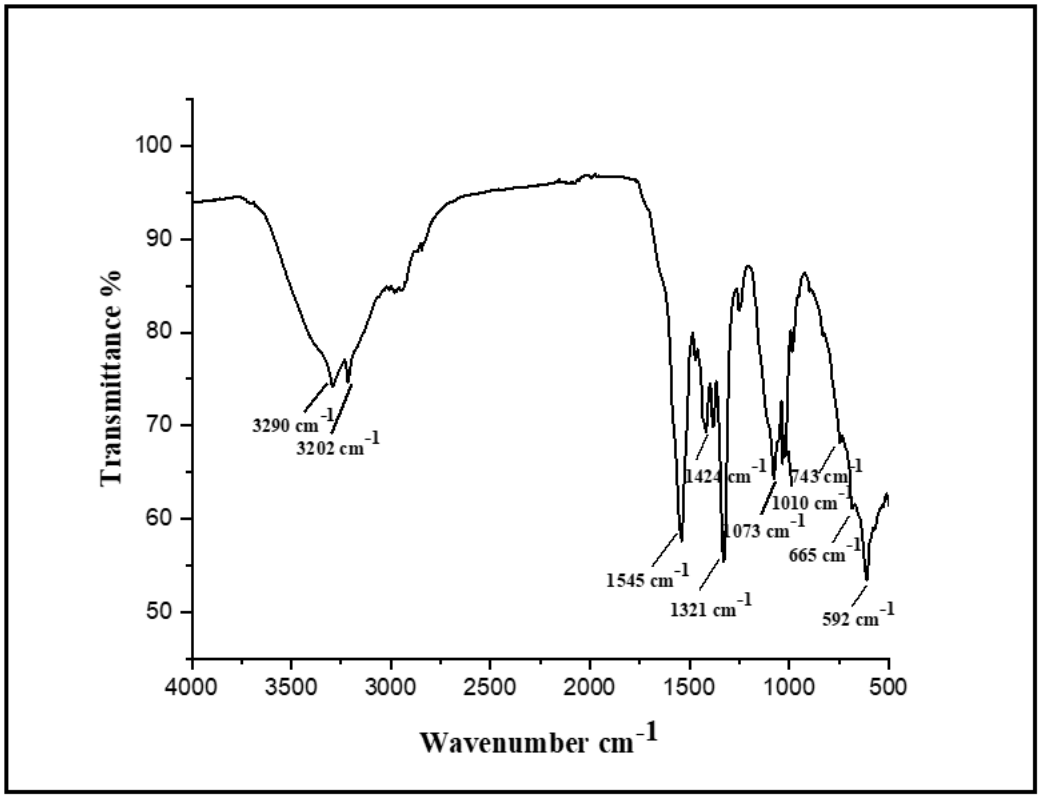

Figure 5.3.8: IR Spectra of [Co(bptsc,N-Me)] **8**

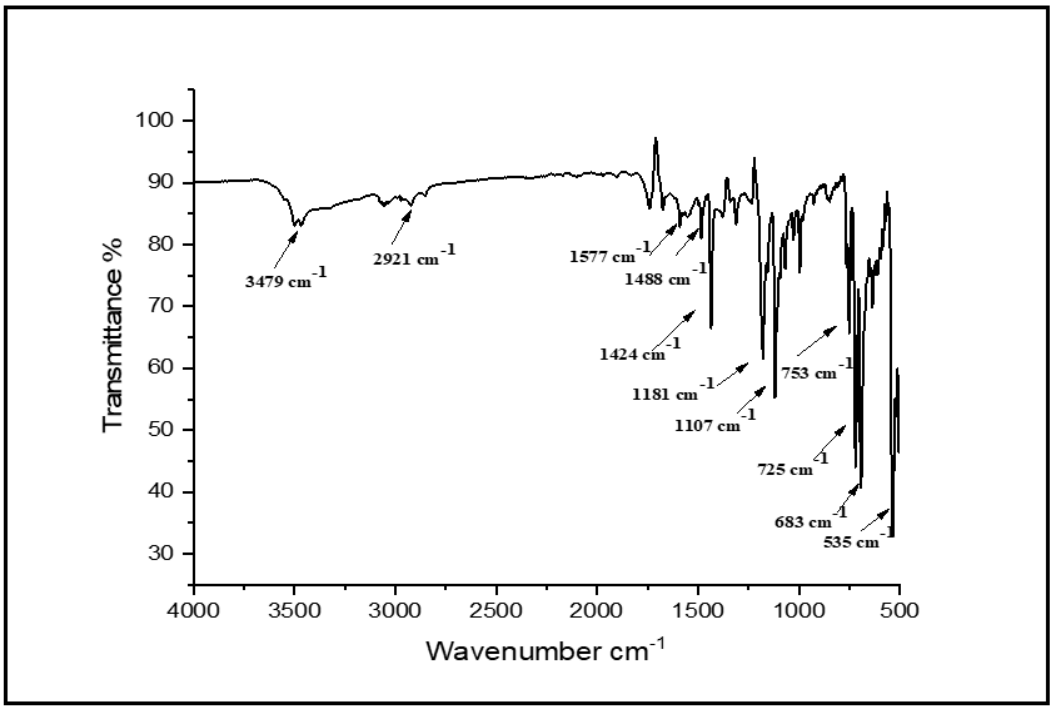

Figure 5.3.9: IR Spectra of [Co(bptsc,N-Ph)] **9**

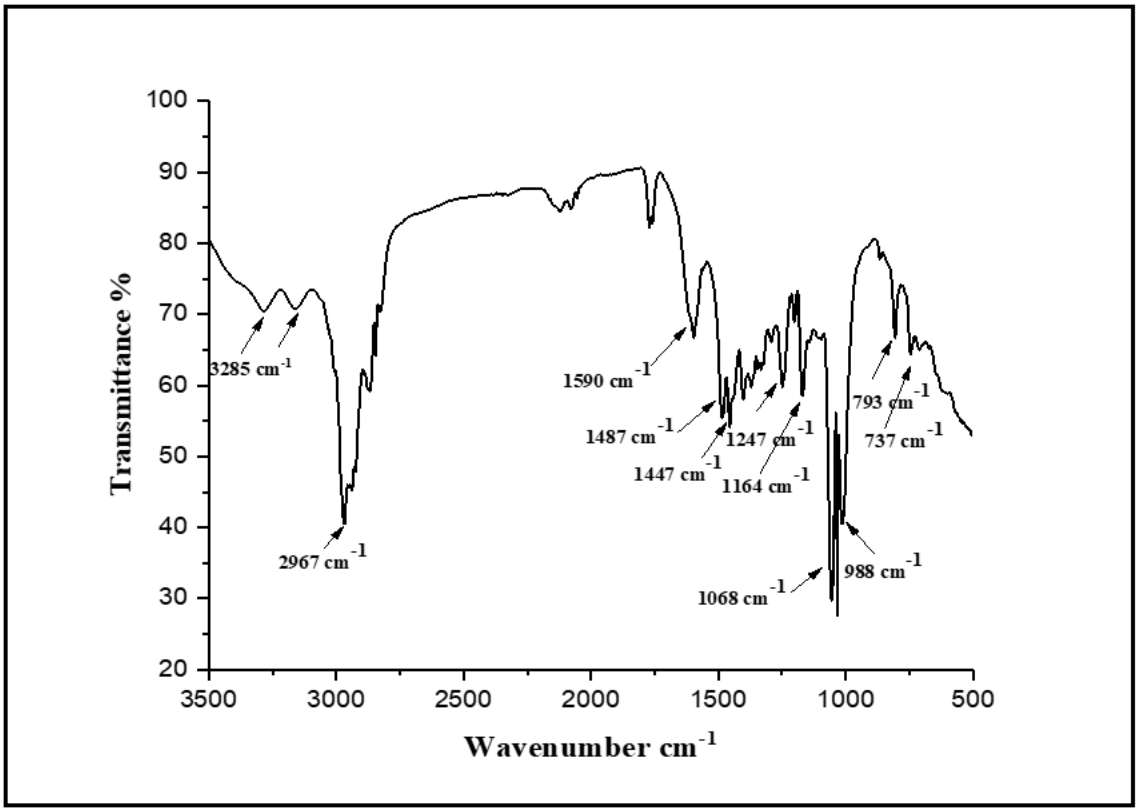

Figure 5.3.10: IR Spectra of [Co(bdptsc)] **10**

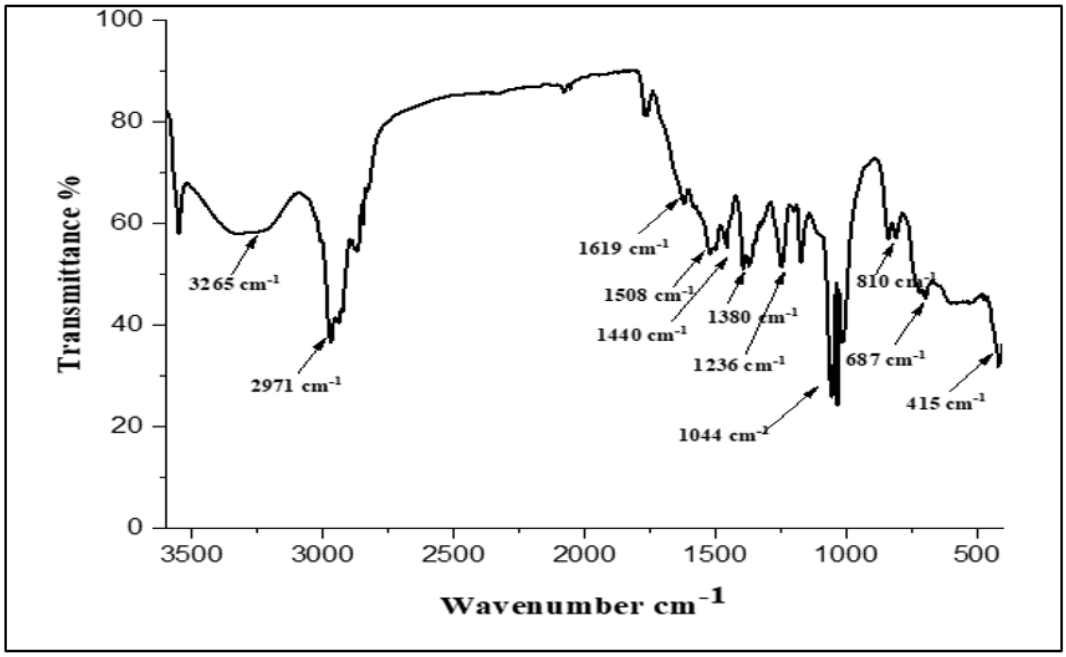

Figure 5.3.11: IR Spectra of [Co(bdptsc,N-Me)] **11**

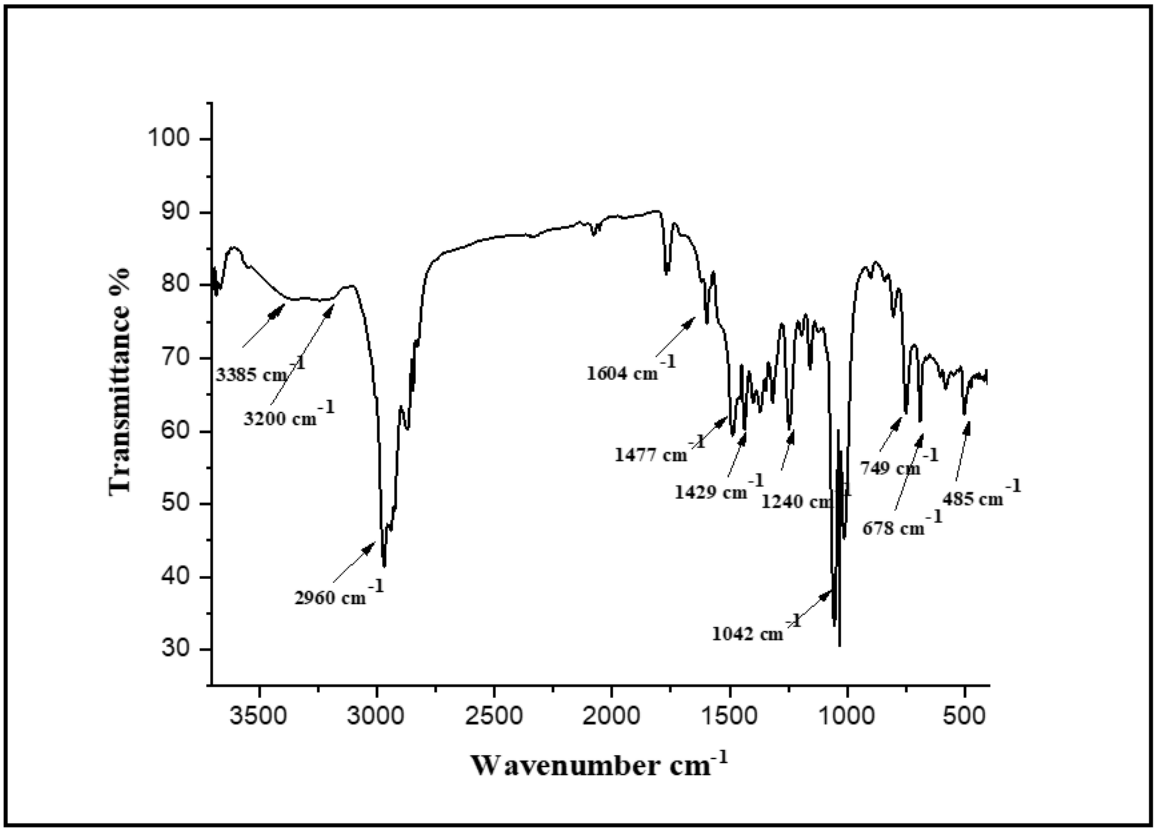

Figure 5.3.12: IR Spectra of [Co(bdptsc,N-Ph)] **12**

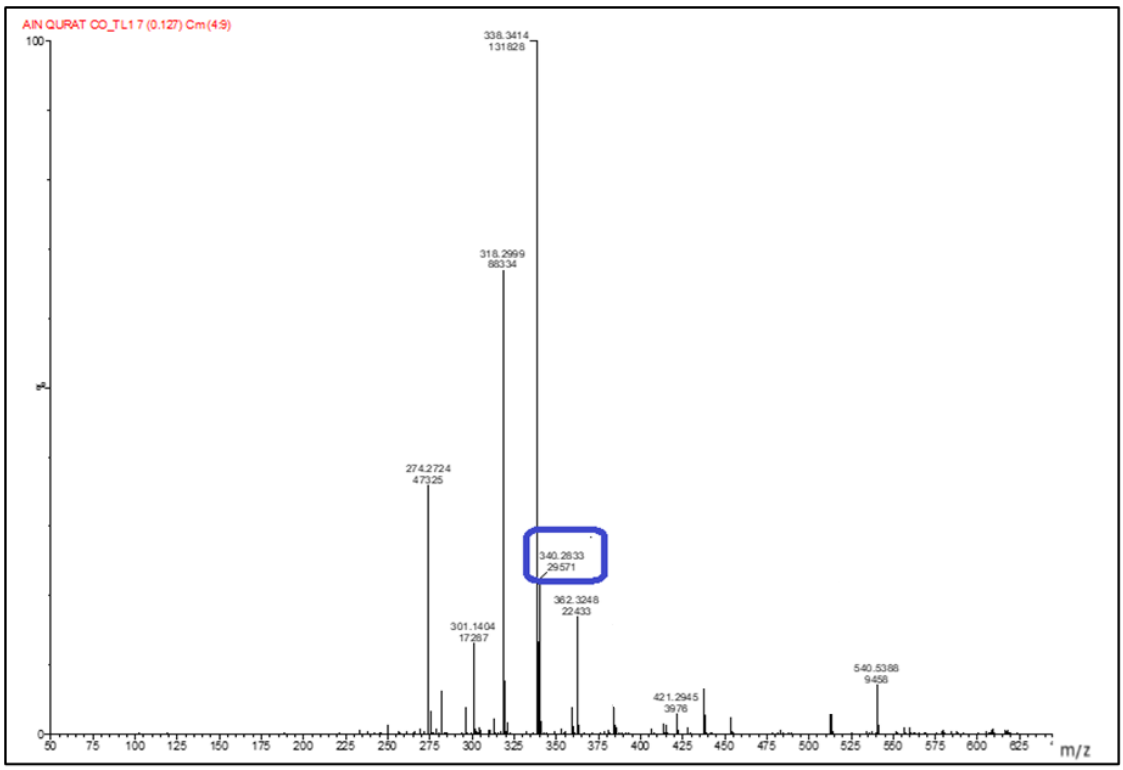

Figure 5.4.1: Mass spectrometry of complex [Co(bttsc)]**1**

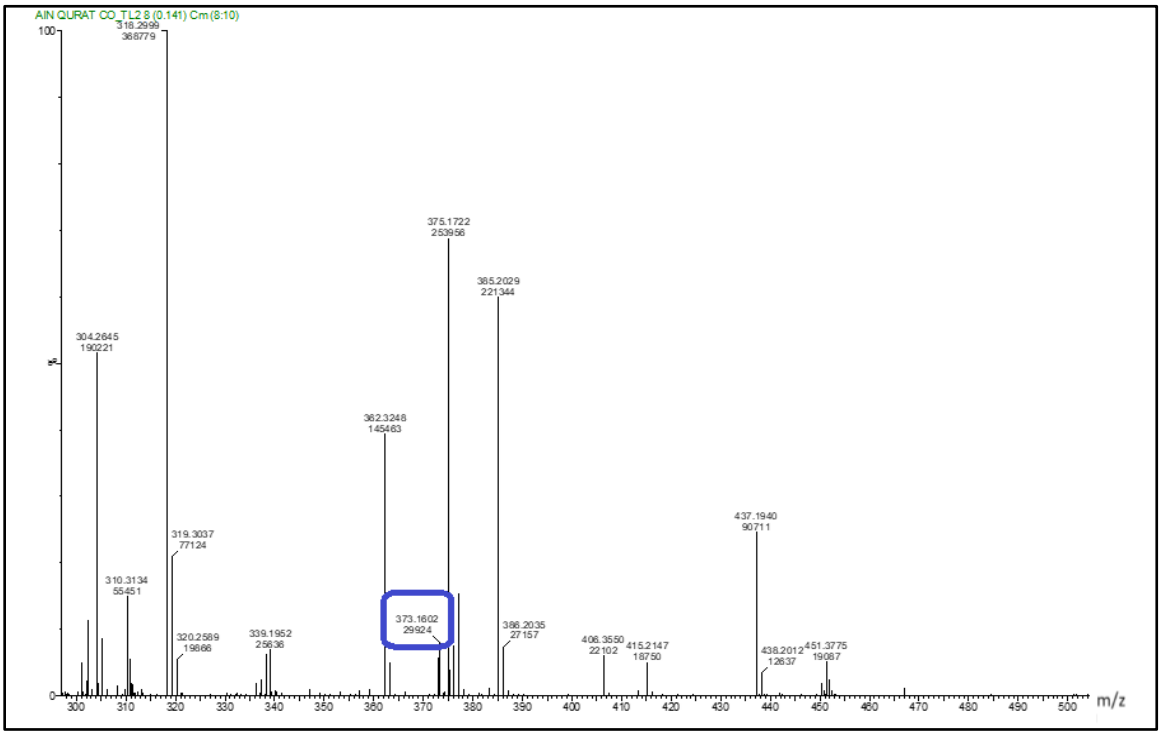

Figure 5.4.2: Mass spectrometry of complex [Co(bttsc,N-Me)]**2**

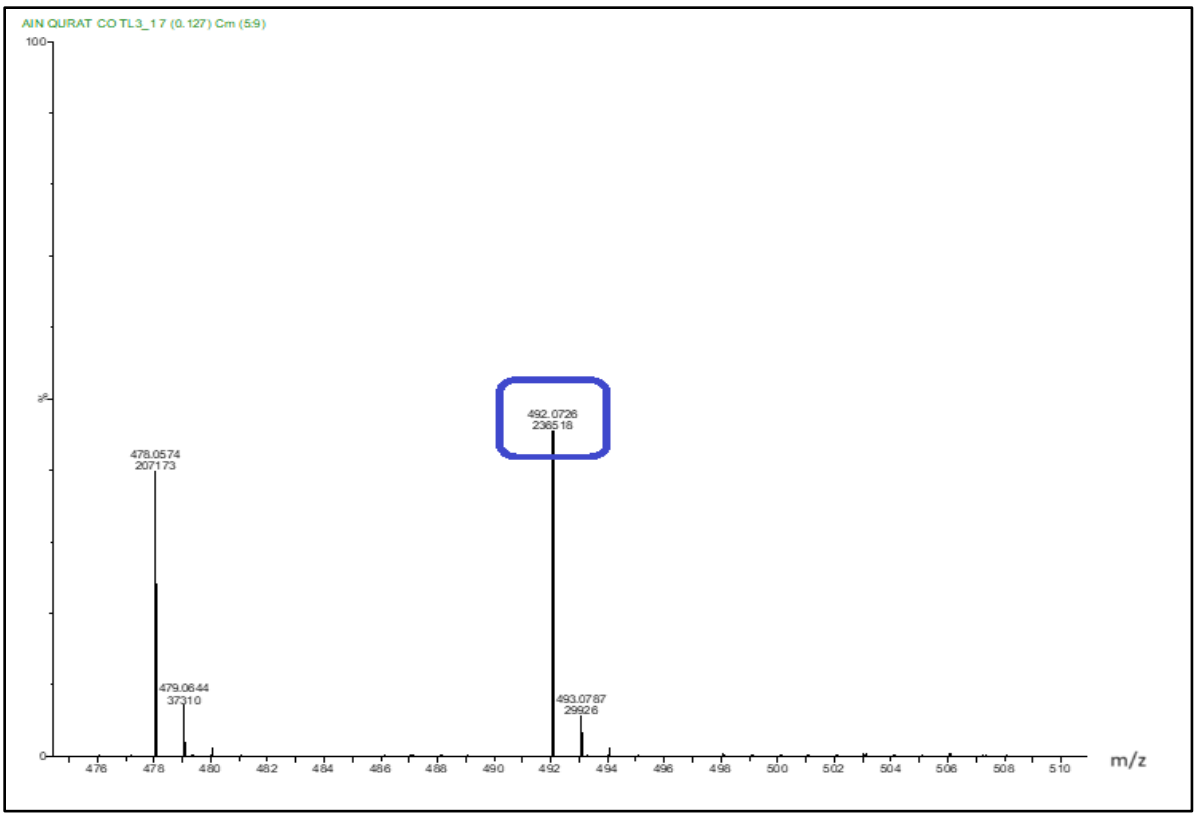

Figure 5.4.3: Mass spectrometry of complex [Co(bttsc,N-Ph)]**3**

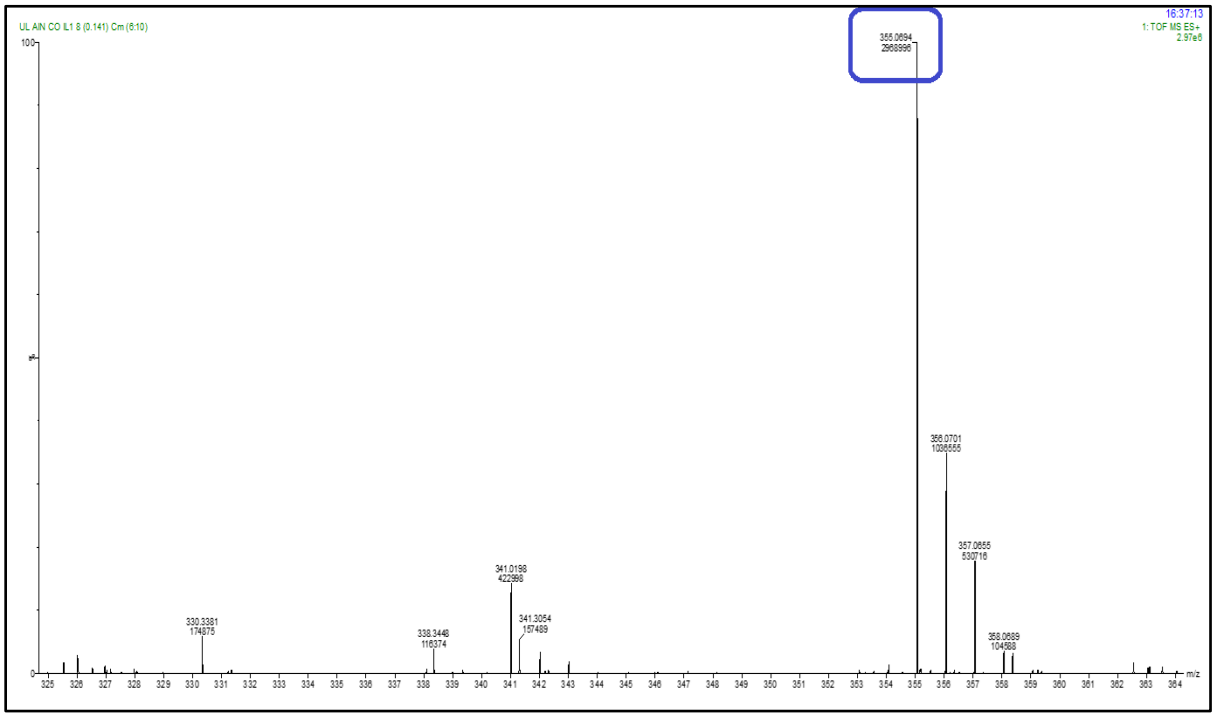

Figure 5.4.4: Mass spectrometry of complex [Co(bitsc)]**4**

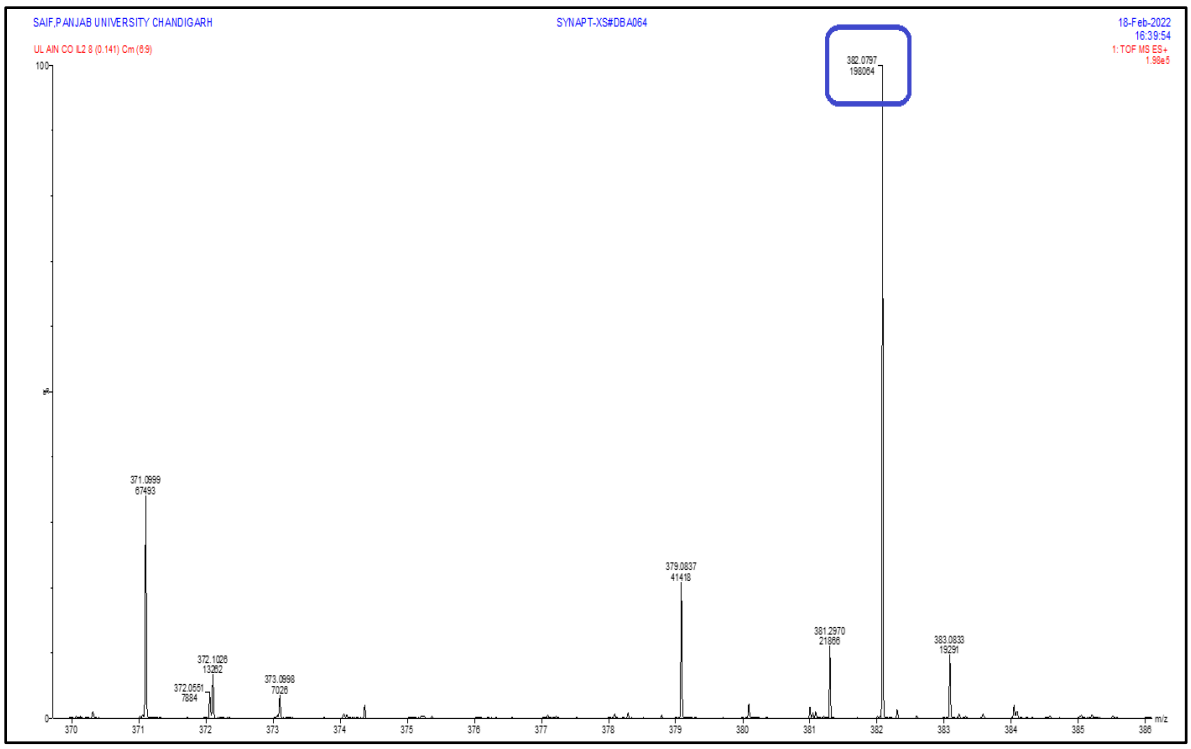

Figure 5.4.5: Mass spectrometry of complex [Co(bitsc, N-Me)]**5**

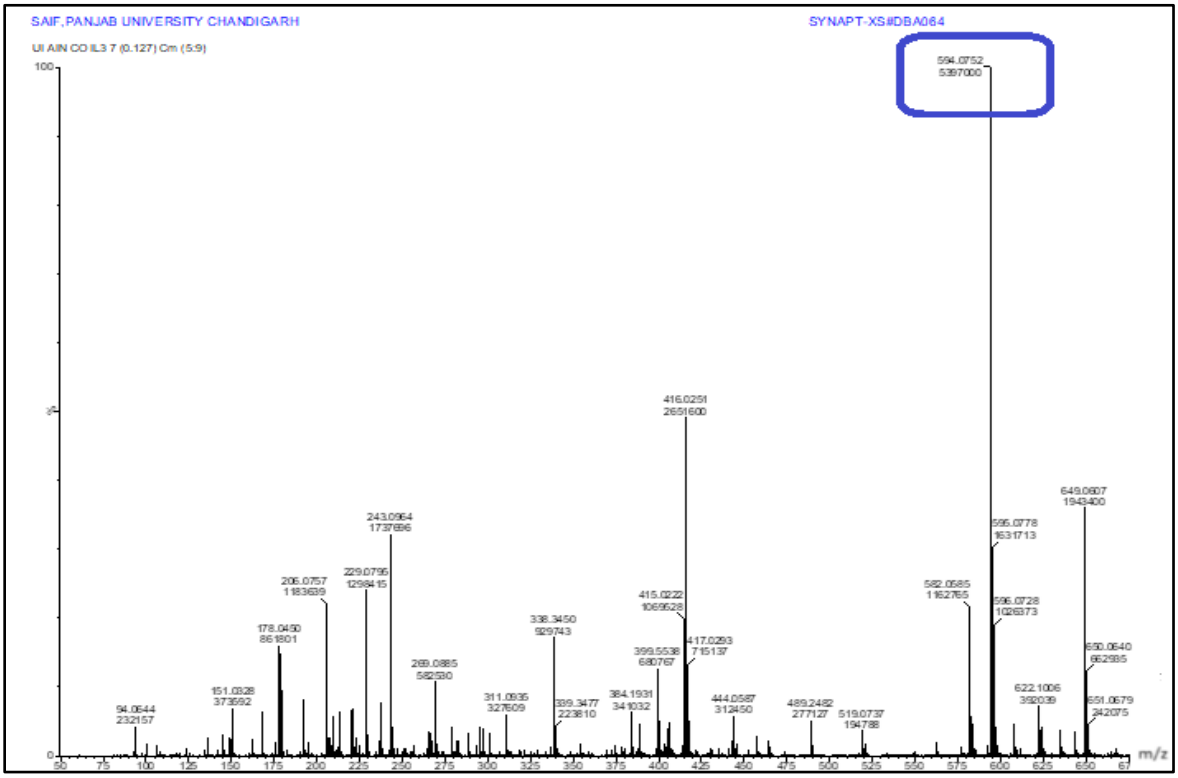

Figure 5.4.6: Mass spectrometry of complex [Co(bitsc, N-Ph)]**6**

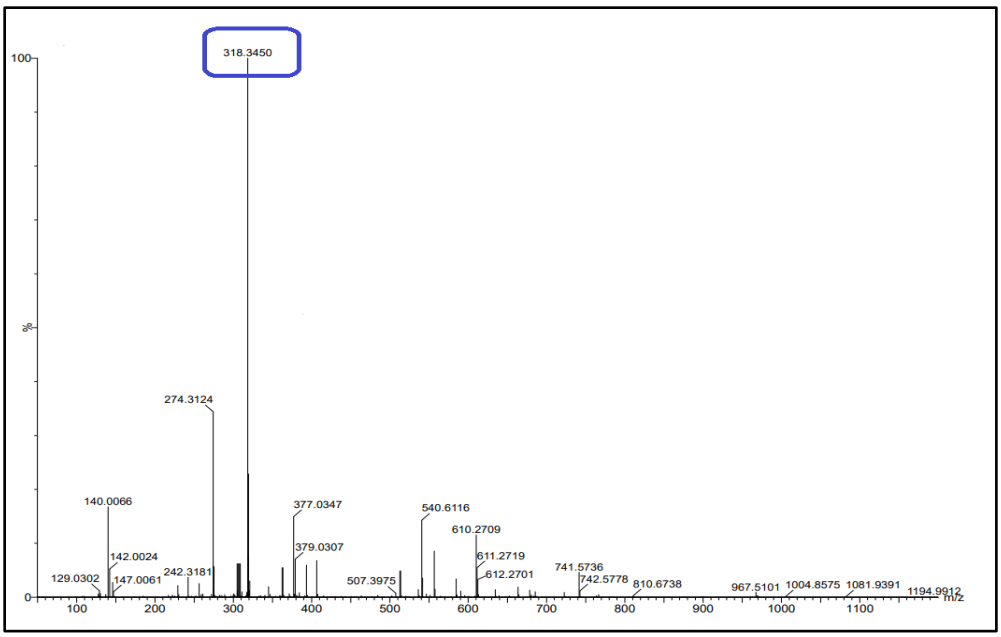

Figure 5.4.7: Mass spectrometry of complex [Co(bptsc)] **7**

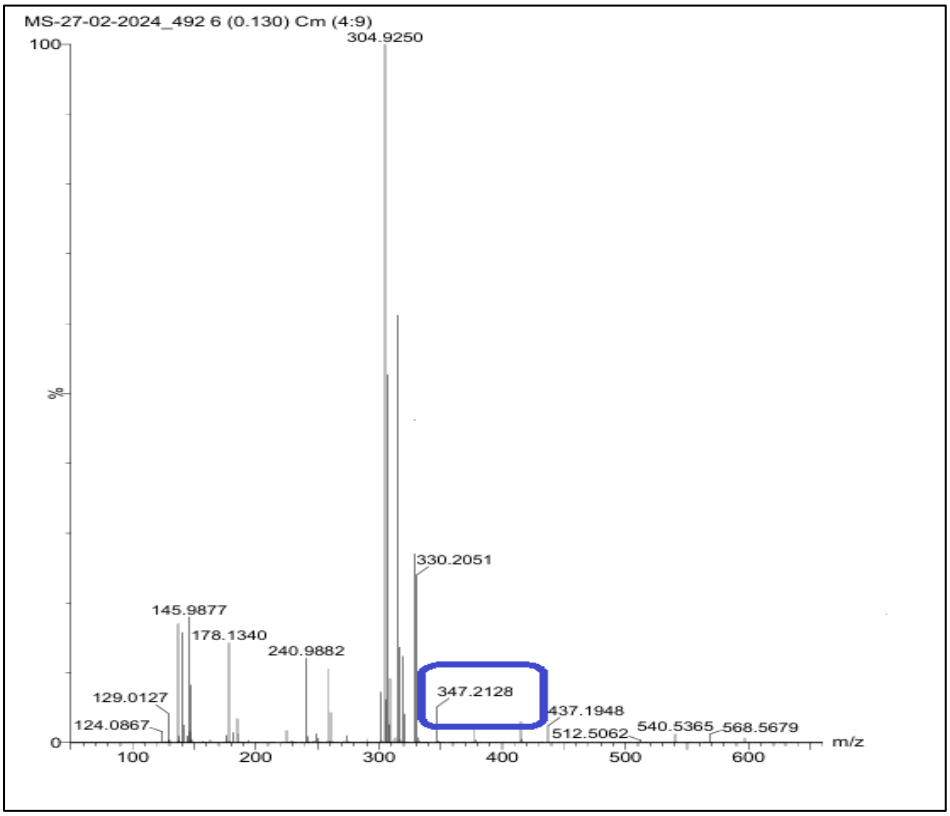

Figure 5.4.8: Mass spectrometry of complex [Co(bptsc,N-Me)] **8**

Figure 5.4.9: Mass spectrometry of complex [Co(bptsc,N-Ph)] **9**

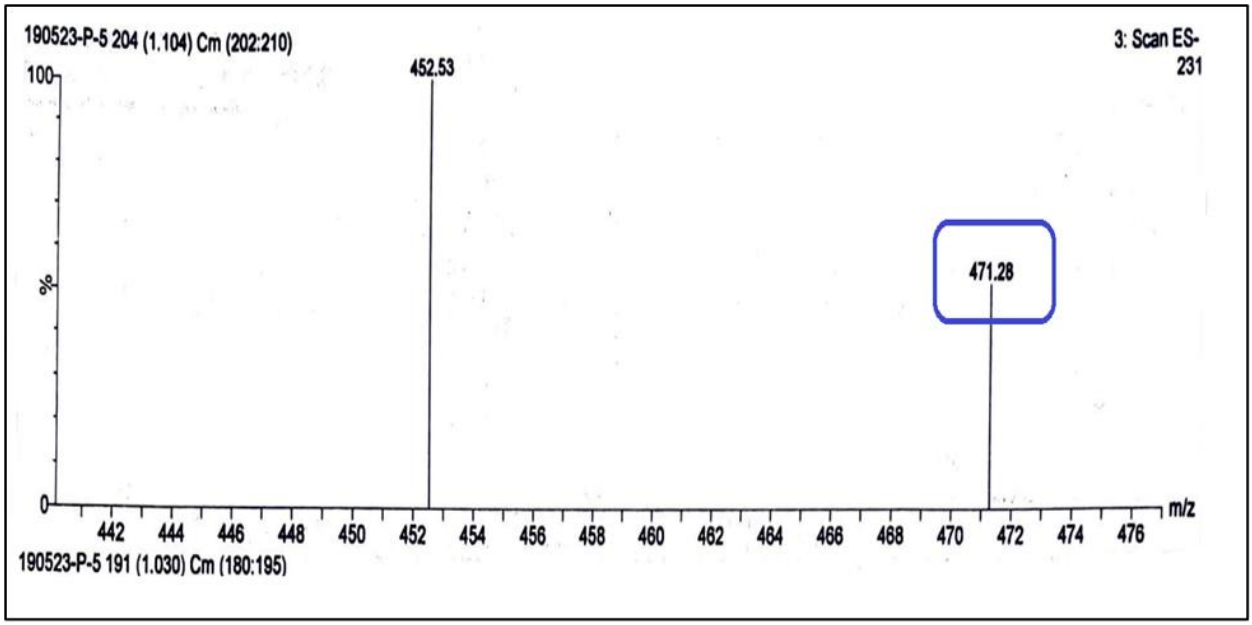

Figure 5.4.10: Mass spectrometry of complex [Co(dptsc)] **10**

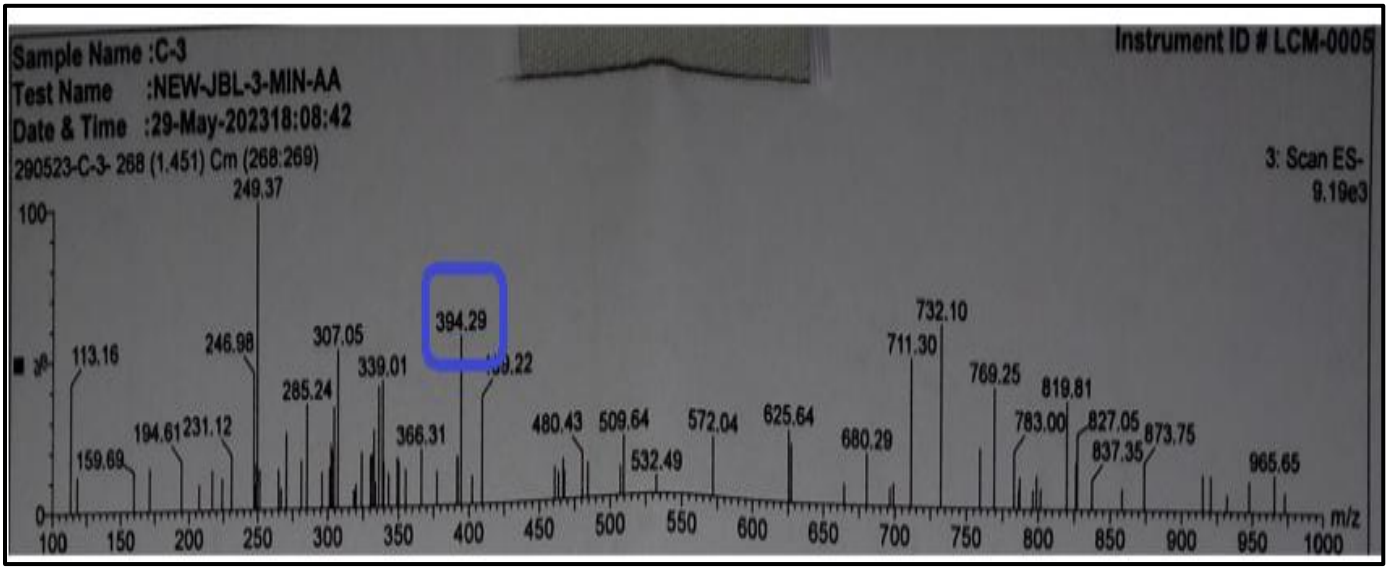

Figure 5.4.11: Mass spectrometry of complex [Co(dptsc,N-Me)] **11**

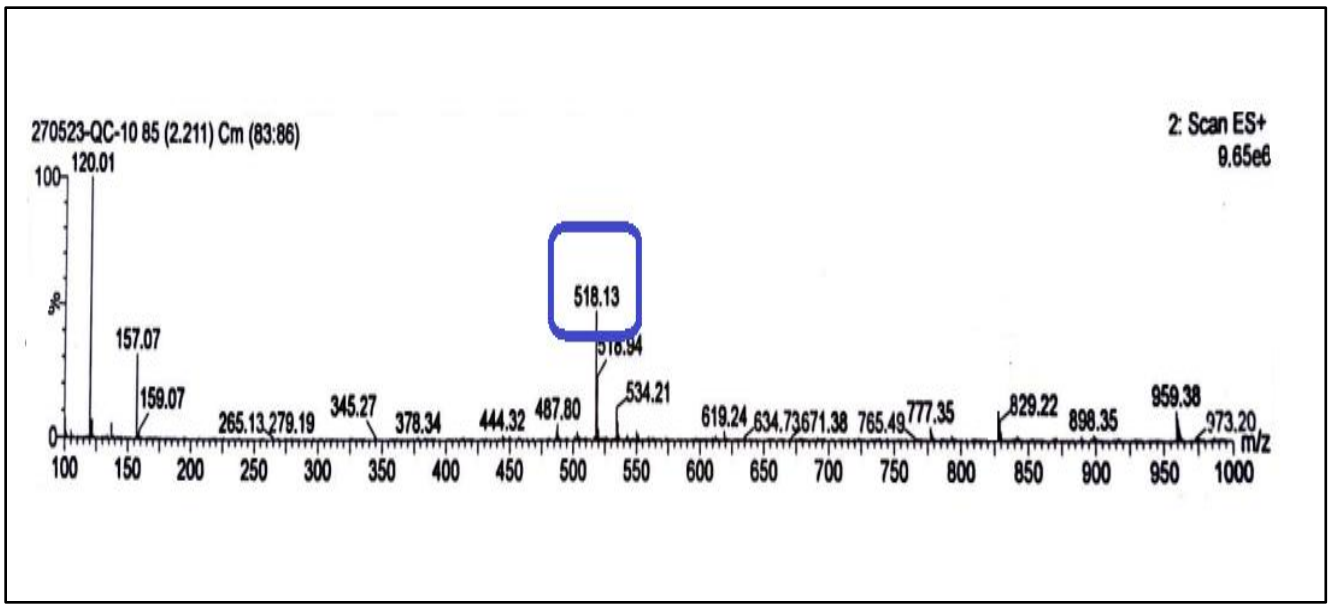

Figure 5.4.12: Mass spectrometry of complex [Co(dptsc,N-Ph)] **12**

5.5 ESR spectroscopy:

The ESR spectra of cobalt(II) complexes **1-12** was done at temperature 125k. The spectra are given in Figures 5.5.1-5.5.12 and experimental data are given in Table **5.5.1**. The two different g values ($g_{\parallel}$ and $g_{\perp}$) of complexes **1-12** represent axial symmetry for the complexes. The experimentally calculated $g_{\parallel}$ values of complexes are higher than $g_{\perp}$, which are further higher than g value of free electron supports ground term, $d_{x^2-y^2}$ in tetrahedral structure [177].

Geometric parameter *G* was calculated using (Equation -5) to measure the exchange interaction between cobalt centre.

$$G_{(axial)} = \frac{g_{\parallel} - 2.0023}{g_{\perp} - 2.0023} \qquad \ldots\ldots\ldots\ldots (5)$$

The G value obtained for complexes **(1-12)** was found to be less than 4. According to Hathaway and Tomlinson, negligible exchange was observed between two cobalt centre ($G < 4$).

Table 5.5.1: ESR calculation of complexes **1-12** at 125k temperature

Complexes	**Polycrystalline state (at RT)**	**$g_{\perp}$**	**$g_{\parallel}$**	**g_{iso}**	**G(at RT)**
[Co(2,5 bttsc)] **1**	2.27 / 2.07 ($g_{\parallel}$ / $g_{\perp}$)	2.07	2.27	2.13	3.95
[Co(2,5bttsc-N-Me)] **2**	2.22 / 2.12($g_{\parallel}$ / $g_{\perp}$)	2.12	2.22	2.15	1.84

[Co(2,5bttsc-N-Ph)] **3**	2.25/ 2.08 ($g_{\parallel}$ / $g_{\perp}$)	2.08	2.25	2.13	3.21
[Co(2,3H_2bitsc)] **4**	2.18/2.11 ($g_{\parallel}$ / $g_{\perp}$)	2.11	2.18	2.12	1.64
[Co(2,3H_2bitsc-N^1-Me)] **5**	2.31/2.09($g_{\parallel}$ /$g_{\perp}$)	2.09	2.31	2.16	3.50
[Co(2,3H_2bitsc-N^1-Ph)] **6**	2.20/2.12($g_{\parallel}$ /$g_{\perp}$)	2.12	2.20	2.17	1.67
[Co(2,5H_2bptsc)]**7**	2.35/2.17($g_{\parallel}$ /$g_{\perp}$)	2.17	2.35	2.62	2.07
[Co(2,5H_2bptsc-N^1-Me)] **8**	2.58/2.06($g_{\parallel}$ /$g_{\perp}$)	2.06	2.58	2.40	1.73
[Co(2,5H_2bptsc-N^1-Ph)] **9**	2.34/2.14($g_{\parallel}$ /$g_{\perp}$)	2.14	2.34	2.21	2.52
[Co(2,6H_2bdptsc)] **10**	2.22/ 2.05($g_{\parallel}$ / $g_{\perp}$)	2.05	2.22	2.16	4.5
[Co(2,6H_2bdptsc-N^1Me)] **11**	2.28/2.22($g_{\parallel}$ /$g_{\perp}$)	2.22	2.28	2.25	1.27
[Co(2,6H_2bdptsc-N^1-Ph)] **12**	2.45/2.31($g_{\parallel}$ /$g_{\perp}$)	2.31	2.45	2.39	1.45

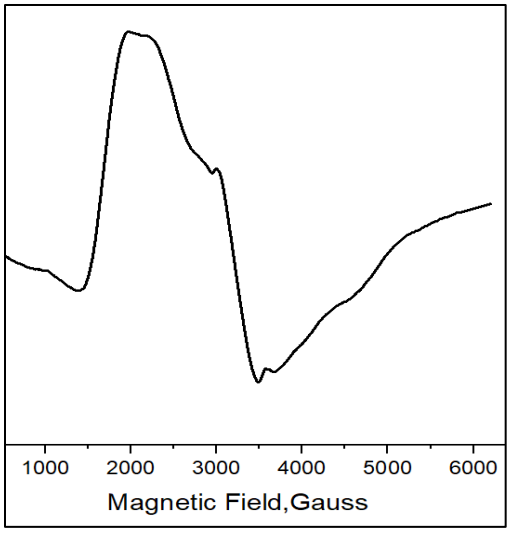

Figure 5.5.1: ESR Spectrum of complex **1**

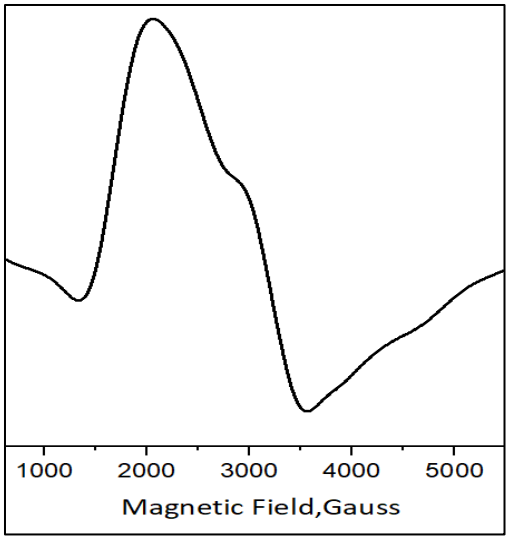

Figure 5.5.2: ESR Spectrum of complex **2**

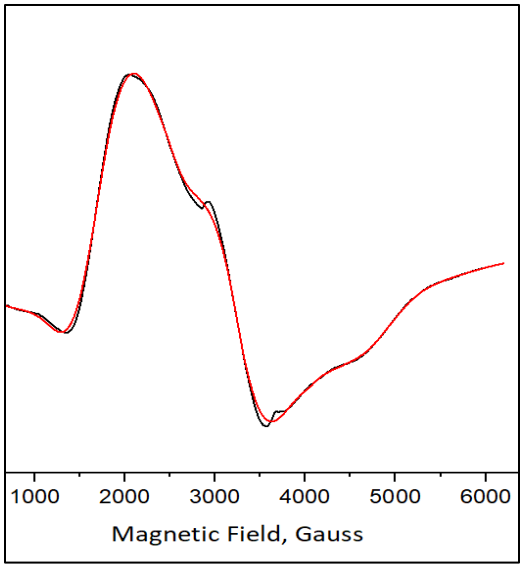

Figure 5.5.3: Spectrum of complex **3** ESR best fit simulated (red) and Experimental (black)

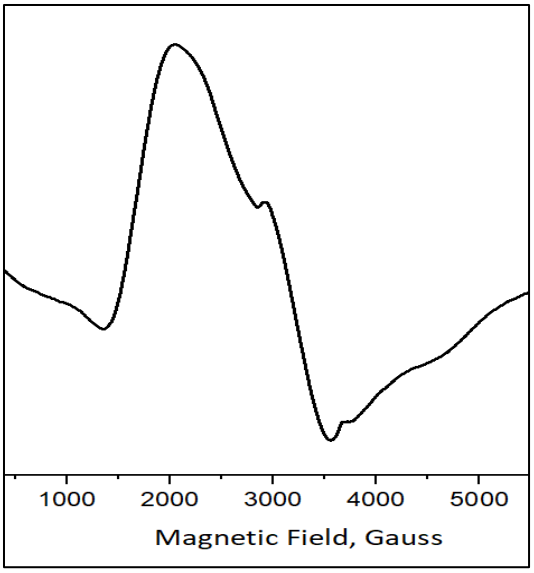

Figure 5.5.4: Spectrum of complex **4**

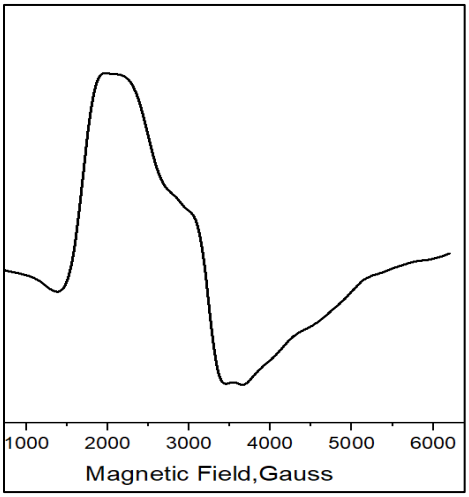

Figure 5.5.5: Spectrum of complex **5**

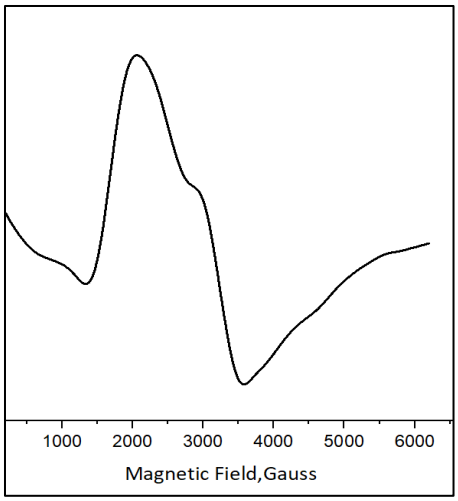

Figure 5.5.6: Spectrum of complex **6**

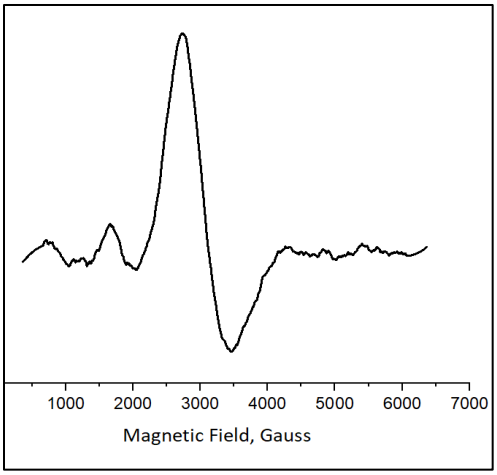

Figure 5.5.7: Spectrum of complex **7**

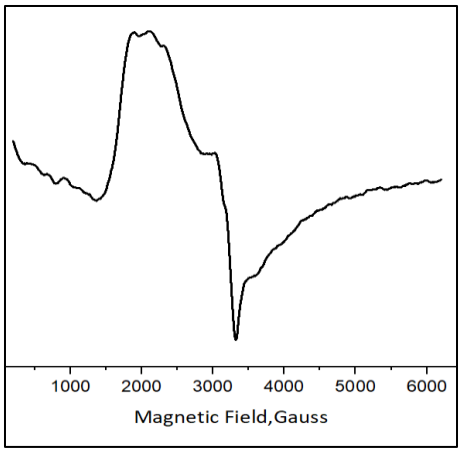

Figure 5.5.8: Spectrum of complex **8**

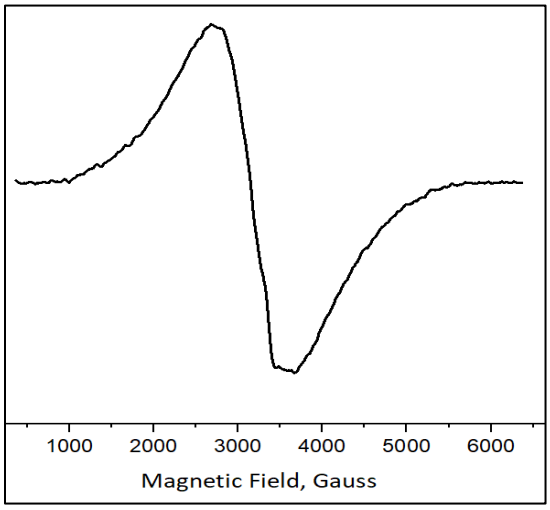

Figure 5.5.9: Spectrum of complex **9**

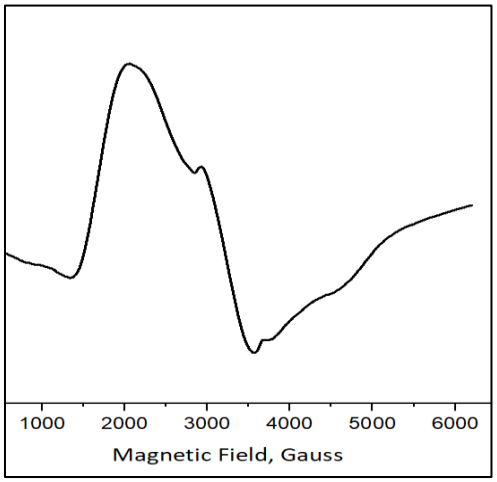

Figure 5.5.10: Spectrum of complex **10**

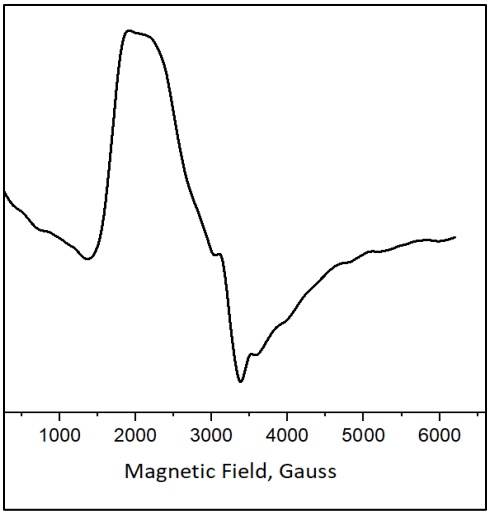

Figure 5.5.11: Spectrum of complex **11**

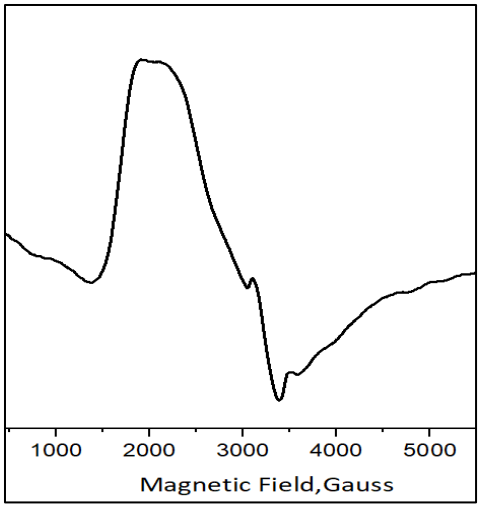

Figure 5.5.12: Spectrum of complex **12**

5.6 Electronic spectra:

The electronic spectra of ligands (**^{4}H$_2$L-^{6}H$_2$L)** and their cobalt complexes (**4-6**) were recorded at wavelength 400-800nm at room temperature. A strong band in the range, 41,666 cm^{-1}-37,593 cm^{-1} in **^{4}H$_2$L-^{6}H$_2$L** corresponds to $\pi \rightarrow \pi^*$ transition, additional band at 36,363cm^{-1} in **^{6}H$_2$L** appeared due to $n \rightarrow \pi^*$ transition[139]. Apart from the bands appeared in ligands, some additional bands also appeared in electronic spectra of complexes. The bands at 25,000cm^{-1} (**4**), 24,330cm^{-1} (**5**) and 22,321cm^{-1} (**6**) are due to the d-d transition in the visible region transition from electronic level $^2b_{1g} \rightarrow {}^2A_{1g}$ of Co(II) atom and have been assigned to LCMT transitions[178]. The presence of these bands ensure tetrahedral geometry around the Co(II) atom.

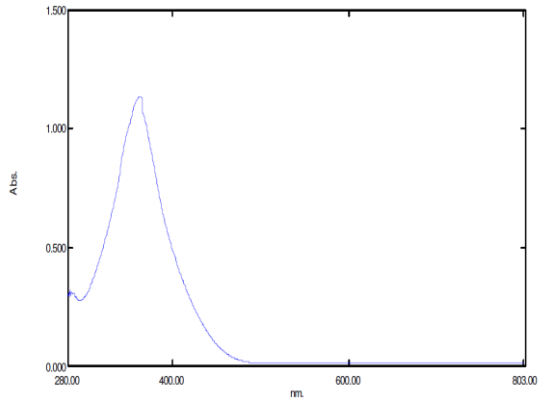

^{4}H$_2$L

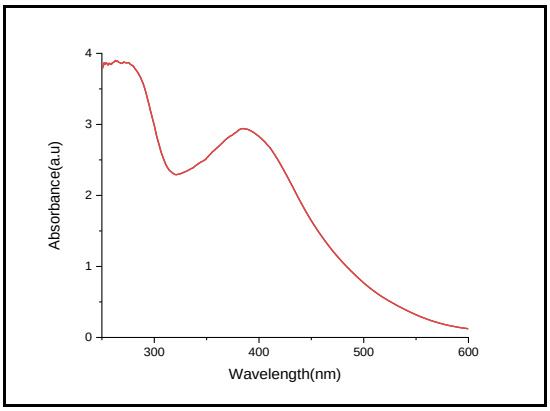

4

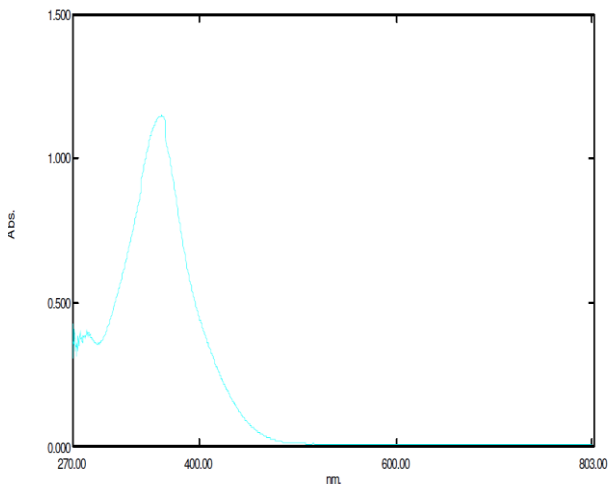

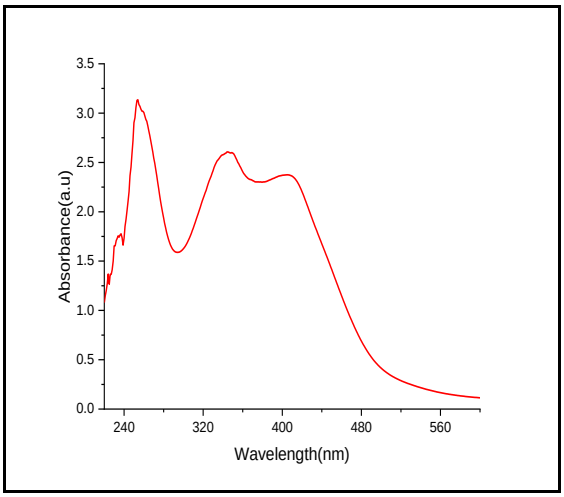

$^{5}H_2L$ **5**

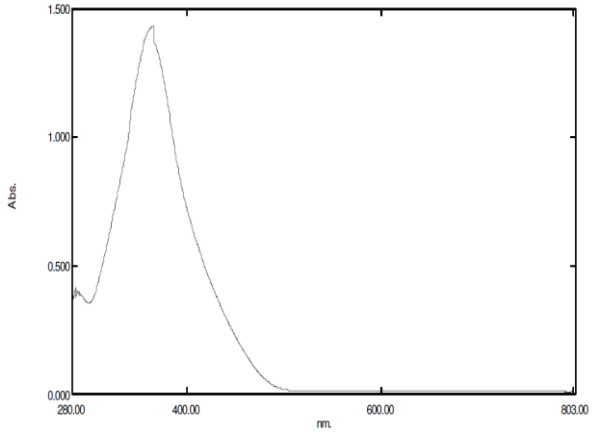

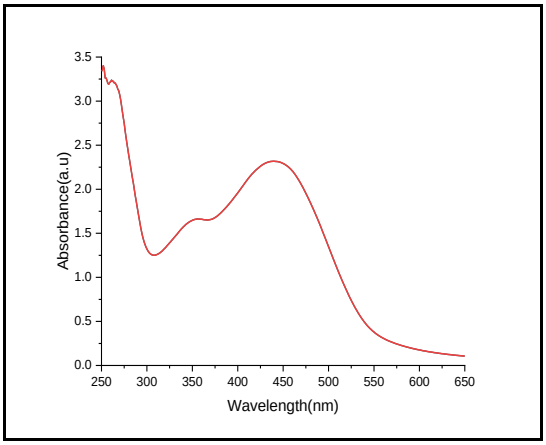

$^{6}H_2L$ **6**

Figure 5.6: Electronic spectra of Ligands(**$^{4}H_2L$-$^{6}H_2L$**) and their metal complexes (**4-6**).

5.7 Anti-tuberculosis activity:

Ligands **($^{1}H_2L$-$^{12}H_2L$)** and their corresponding cobalt(II) complexes **(1-12)** were evaluated and given in Table 5.7.1 [179]. No particular structure-activity relationship has been observed. The anti-T.B activity of ligands generally gets enhanced upon complexation. It was found from the experimental data that the activity of ligand **2,5 H_2bttsc N-Ph ($^{3}H_2L$), 2,3 H_2bitsc ($^{4}H_2L$) and 2,5 H_2bptsc ($^{7}H_2L$**) showed no change upon complexation, maintaining its maximum anti-TB activity with an MIC of 1.6 µg/ml, equivalent to the standard drugs Rifampicin and Streptomycin (MIC = 1.6 µg/ml). It has been observed that increasing the hydrophobicity of a ligand, due to substitutions

at the N1 atom, enhances anti-TB activity. The increased hydrophobicity likely facilitates transport through the cell membrane, thereby boosting activity. Whereas, the activity of ligand **(2,5 H_2bptsc, N-Me) and (2,5 H_2bptsc)** (MIC = 3.12 and 1.6µg/ml) was also high but the activity gets low in its complex **8** and **10** as compared to its ligands. The anti-TB activity of ligands ^{1}**H_2L,** ^{2}**H_2L**, ^{5}**H_2L**, ^{6}**H_2L**, ^{9}**H_2L,** ^{10}**H_2L and** ^{12}**H_2L (**MIC = 6.25 ^{1}**H_2L;** 3.12 ^{2}**H_2L,** ^{9}**H_2L**; 100 ^{5}**H_2L,** ^{6}**H_2L**; 50 ^{10}**H_2L,**^{12}**H_2L** µg/ml) get enhanced on complexation with cobalt(II) (MIC = 1.6 **1,2,9**; 25 **5,12**; 50 **6,10** µg/ml). Chelation of ligand with cobalt (II) may have resulted in increase of its retention time on bio-membrane to allow longer interaction at target site. The possible interactions of ligand as well as complexes have been studied using molecular docking for most potent ligand **2,5 H_2bttsc (^{1}H_2L)** and its **[Co(2,5bttsc)]** complex.

Table 5.7.1: Anti-T.B activity of bisthiosemicarbazones (**H^{1}L-H^{12}L**) and complexes **(1-12)**

		MIC (µg /mL)							
S. No	**Compound**	***100***	***50***	***25***	***12.5***	***6.25***	***3.12***	***1.6***	***0.8***
1.	**2,5 H_2bttsc (^1H_2L)**	S	S	S	S	S	R	R	R
2.	**[Co(2,5 bttsc)] 1**	S	S	S	S	S	S	S	R
3.	**2,5H_2bttsc N-Me(^2H_2L)**	S	S	S	S	S	S	R	R
4.	**[Co(2,5 bttsc N-Me)] 2**	S	S	S	S	S	S	S	R
5.	**2,5 H_2bttsc N-Ph (^3H_2L)**	S	S	S	S	S	S	S	R
6.	**[Co(2,5 bttsc N-Ph)] 3**	S	S	S	S	S	S	S	R
7.	**2,3 H_2bitsc (^4H_2L)**	S	S	R	R	R	R	R	R
8.	**[Co(2,3 bitsc)] 4**	S	S	R	R	R	R	R	R
9.	**2,3 H_2bitsc-N^1-Me (^5H_2L)**	S	R	R	R	R	R	R	R
10.	**[Co(2,3 bitsc-N^1-Me)] 5**	S	S	S	R	R	R	R	R
11.	**2,3 H_2bitsc-N^1-Ph (^6H_2L)**	S	R	R	R	R	R	R	R
12.	**[Co(2,3 bitsc-N^1-Ph Me)] 6**	S	S	R	R	R	R	R	R
13.	**2,5 H_2bptsc (^7H_2L)**	S	S	S	S	S	S	S	R
14.	**[Co(2,5 bptsc)] 7**	S	S	S	S	S	S	S	R
15.	**2,5 H_2bptsc, N-Me (^8H_2L)**	S	S	S	S	S	S	R	R
16.	**[Co(2,5 bptsc, N-Me)] 8**	S	S	S	S	S	R	R	R

17.	**2,5 H_2bptsc, N-Ph ($^{9}H_2L$)**	S	S	S	S	S	S	R	R
18.	**[Co(2,5 bptsc, N-Ph)] 9**	S	S	S	S	S	S	S	R
19.	**2,5 H_2bdptsc ($^{10}H_2L$)**	S	S	S	S	R	R	R	R
20.	**[Co(2,5 bptsc)] 10**	S	S	S	R	R	R	R	R
21.	**2,5 H_2bdptsc, N-Me ($^{11}H_2L$)**	S	S	R	R	R	R	R	R
22.	**[Co(2,5 bdptsc, N-Me)] 11**	S	S	S	R	R	R	R	R
23.	**2,5 H_2bdptsc, N-Ph ($^{12}H_2L$)**	S	S	R	R	R	R	R	R
24.	**[Co(2,5 bdptsc, N-Ph)] 12**	S	S	S	R	R	R	R	R

5.8 Human Serum Albumin binding studies of 2,5 H_2bttsc ($^{1}H_2L$) and [Co(2,5bttsc)]

Interaction of human serum albumin (HSA) with amphiphilic compound is due to hydrophobic and hydrophilic characters of its amino acid residues. Its reversible binding to numerous drugs molecules, enhances the solubility, reduces the toxicity and guarded the bounded molecules from oxidation in plasma. It has been chosen as a key target in drug-protein binding to comprehend the pharmacokinetics and pharmacological effects of drug molecules because of these exceptional potentials. Interactions of HSA with most potent ligand **$^{1}H_2L$** and its complex **1** has been studied through UV-visible and fluorescence spectroscopy.

5.8.1 UV-visible spectroscopic study

HSA (7 µM) shows an absorption band at 280 nm in its UV-visible absorption spectrum. On incremental additions of ligand 2,5 H_2bttsc (0-5 µM) and [Co(2,5bttsc)] (0-8µM) remarkable increase in absorbance of (HSA) at 280 nm (41% for ligand 2,5H_2bttsc and 31% for [Co(2,5bttsc)] was observed. The enhanced intensity of absorption peak can be due to change in concentrations of ligand 2,5H_2bttsc and complex [Co(2,5bttsc)] showed agitations in the microenvironment of protein's chromophores due to the interaction of HSA with ligand and its complex. On addition a

new peak at 385 nm was observed due to the electronic transition between metal orbitals. The binding constants for interactions of 2,5H_2bttsc-HSA and [Co(2,5bttsc)]-HSA systems were determined with the Equation-2 (Benesi-Hildebrand equation), and initiate to be (7.14×10^5)M^{-1} and (15.07×10^5) M^{-1}(Figure 5.8.1.2). The high binding constant obtained confirmed the strong binding affinities for effective delivery to their targeted sites.

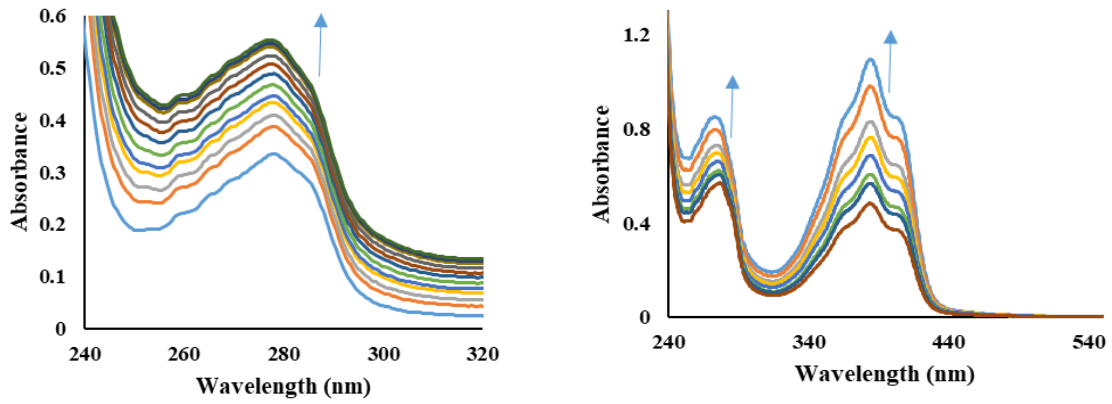

Figure 5.8.1.1: UV-visible absorption of HSA with incremental additions of ligand 2,5H_2bttsc (a) and [Co(2,5bttsc)] (b)

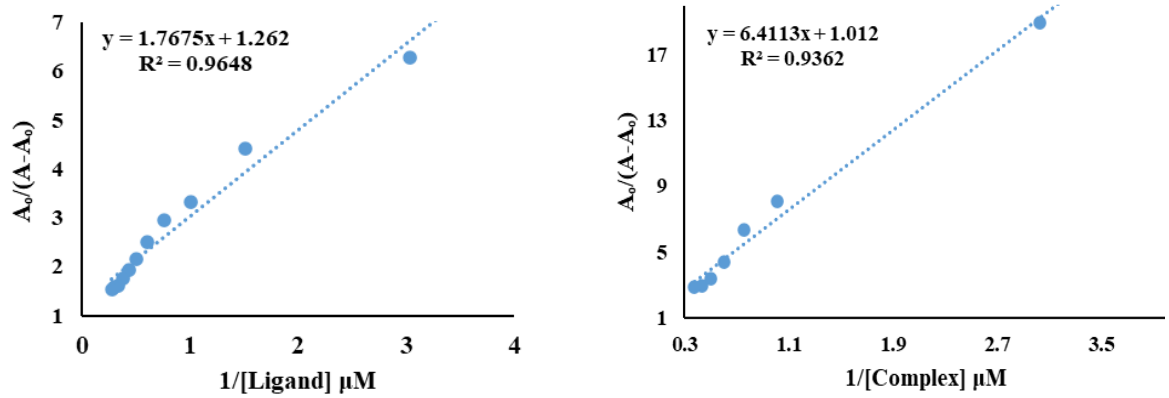

Figure 5.8.1.2: Benesi-Hildebrand plot {$A_o/(A-A_o)$ vs. 1/[ligand or complex]} for binding studies of HSA with ligand 2,5H_2bttsc (a) and complex [Co(2,5bttsc)] (b).

5.8.2 Fluorescence studies

Fluorescence titrations were performed using HSA (7 µM) with progressive additions of 2,5H_2bttsc (0-7 µM) and complex [Co(2,5bttsc)] (0-8 µM). Binding of ligand and complex was also confirmed by Fluorescence studies. Aromatic fluorophores of HSA, such as (TRP) and (TYR)

amino acid residues, exhibit intrinsic fluorescence[180]. The interaction of ligand 2,5H_2bttsc and complex [Co(2,5bttsc)] with HSA may influence the fluorescence produced by these fluorophores [181–183]. When (TRP-214) amino acid residue was positioned in subdomain IIA of HSA, an emission band at 353 nm was exposed in the emission spectrum of HSA (7 μM) when 280 nm was used as the excitation wavelength[184]. Increasing the amounts of ligand 2,5H_2bttsc (0-7 μM) and complex [Co(2,5bttsc)] (0-8 μM) resulted in favourable quenching (92-94%) of HSA emission at 353nm (Figure 5.8.2.1), indicating the binding of ligand 2,5H_2bttsc and complex [Co(2,5bttsc)] to HSA.

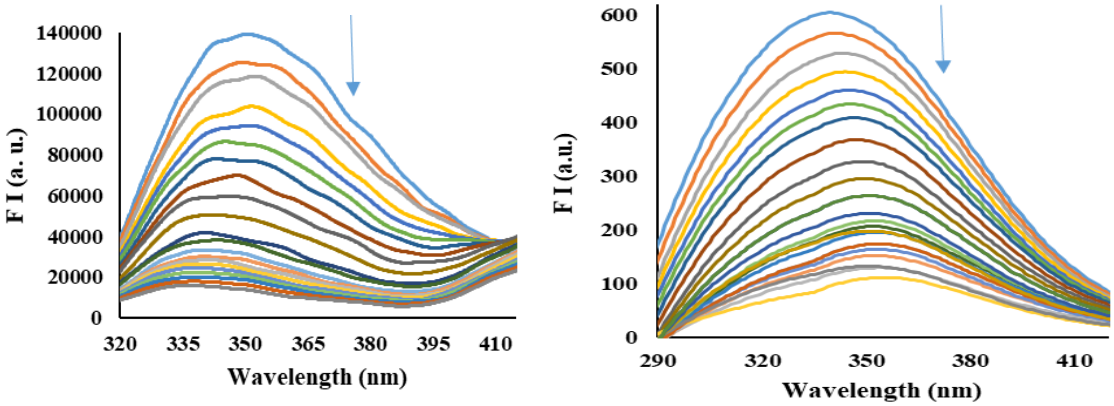

Figure 5.8.2.1: Emission spectra of HSA (λ_{ex} = 280 nm) in incremental additions of ligand 2,5H_2bttsc (a) and complex [Co(2,5bttsc)] (b)

The Equation-3 (Stern-Volmer equation) was employed to analyse quenching in fluorescence, and Stern-Volmer graphs [185] (Figure 5.8.2.2) have been created. Throughout the studies, good linearity of plots was seen, with correlation coefficients (R) of 0.9737 for the ligand 2,5H_2bttsc and 0.9188 for complex [Co(2,5bttsc)]. The ligand 2,5H_2bttsc and complex [Co(2,5bttsc)] were found to have fluorescence quenching efficiency values of 1.52×10^6 M^{-1} and 2.74 $\times10^6$ M^{-1}, respectively, as a result, the complex formation of ligand 2,5H_2bttsc and complex [Co(2,5bttsc)] with HSA may be the cause of the speckled quenching in HSA fluorescence upon the addition of these molecules.

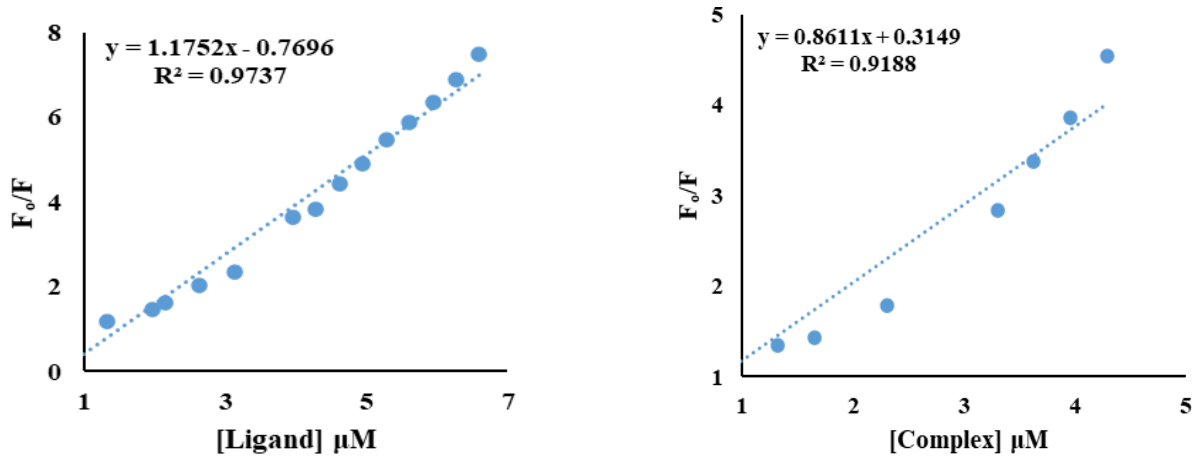

Figure 5.8.2.2: Stern-Volmer graphs (F_0/F versus [ligand or complex]) for HSA binding to ligand 2,5H_2bttsc (a) and complex [Co(2,5bttsc)](b).

Using a modified Stern-Volmer (Equation-4), double logarithmic graphs were formed to examine the interaction between ligand 2,5H_2bttsc and its complex [Co(2,5bttsc)] with HAS [186,187], (Figure 5.8.2.3). The binding constants (Kb) were found for 2,5H_2bttsc and [Co(2,5bttsc)] as 2.691×10^6 M^{-1} and 5.623×10^6 M^{-1}. The significant binding affinity of ligand 2,5H_2bttsc and complex [Co(2,5bttsc)] with HSA is confirmed by the binding constant values, which were found to be in the 5.623-2.691×10^6 M^{-1} range for both the ligand-HSA and complex-HSA. Based on the modified Stern-Volmer equation, binding sites (n) for the binding of ligand 2,5H_2bttsc and complex [Co(2,5bttsc)] with HSA was determined to be 1.21 and 1.37 respectively.

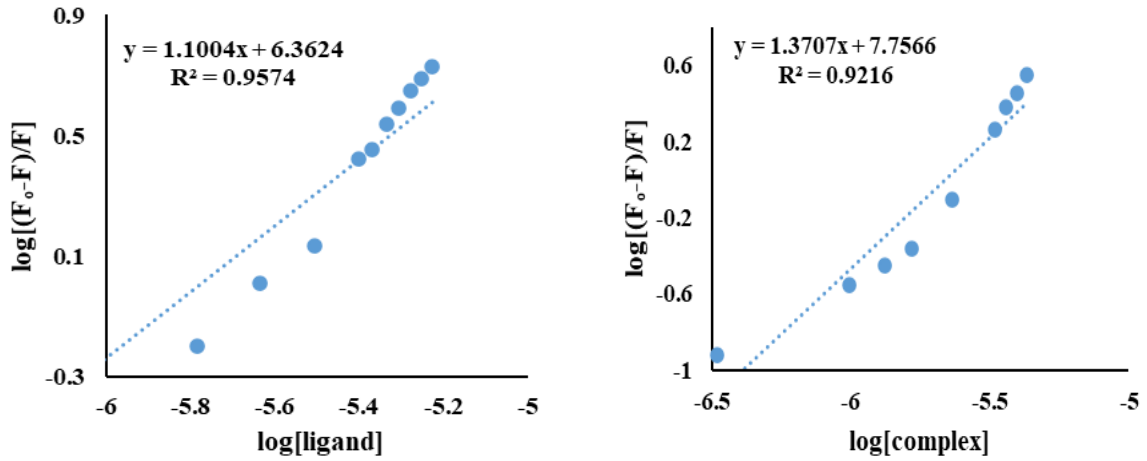

Figure 5.8.2.3: Modified Stern-Volmer plots {log(F_0-F)/F vs log [ligand or complex]} for HSA interaction with ligand 2,5H_2bttsc (a) and complex [Co(2,5bttsc)] (b)

5.9 Docking study

Docking of ligand 2,5bttsc **(^1H_2L)** its cobalt (II) complex [Co(2,5bttsc)] **1** with mycobacterium tuberculosis enoyl reductase showed -5.8 and -6.8 Kcal/mol, minimum binding energy respectively. The detailed modelling study of interactions between ligand **(^1H_2L)** and its complex **1** with target mycobacterium tuberculosis enoyl reductase revealed that the ligand **(^1H_2L)** exhibited hydrogen bonding interactions with oxygen atom of (ASP 148) (*d* = 2.68 Å) and (PRO156) (*d* = 2.61 Å) amino acid residues of chain A. Nitrogen atom of ligand exhibited hydrogen bonding with (TYR158) (*d* = 2.60 Å) amino acid residue. Ligand **(^1H_2L)** interacted with (PHE149), (TYR158), (PRO193), and (MET199) amino acid residues, of chain A through hydrophobic and other interactions. The cobalt complex **1** exhibited hydrogen bonding interactions with (GLY192) (*d* = 2.80 Å), (ILE194) (*d* = 1.96 Å), and (MET199) (*d* = 3.69 Å) amino acid residues, of chain A. Additionally, it interacted with (PHE149) amino acid residues, of chain A through sulfur-π type interactions (Figure 5.9.1).

.

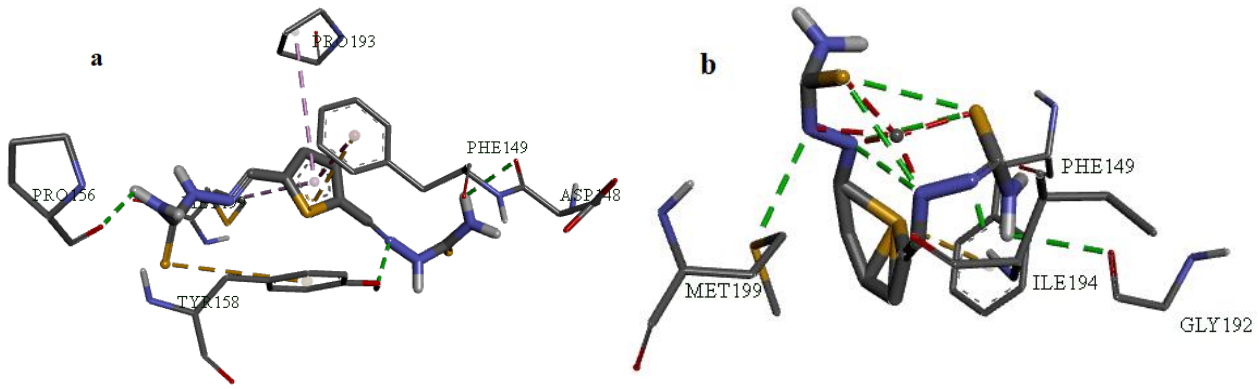

Figure 5.9.1: 3D representation of interactions of ligand **(^1H_2L)** (a), its complexes with cobalt(II) **1** (b) with mycobacterium tuberculosis enoyl reductase

5.10 <u>Conclusion:</u> Reaction of cobalt (II) acetate with ^{1}**H$_2$L-**^{12}**H$_2$L** yielded complexes of stoichiometry, [Co(L)] **1-12** in molar ratio 1:1. The complexes were characterized using FTIR, mass spectrometry, UV-visible spectroscopy, and ESR spectroscopy. The ligands (^{1}**H$_2$L-**^{12}**H$_2$L**) and their cobalt(II) complexes (**1-12**) were tested for anti-tuberculosis activity. The following conclusion has been drawn from the results obtained:

1. All the complexes have m/z values in well agreement with proposed stoichiometry.
2. In ESR spectroscopy, the $g_{\parallel}$ value is higher than $g_{\perp}$, it indicates the existence of unpaired electrons in the ground state term $d_{x^2-y^2}$ within the tetrahedral structure.
3. Anti-T.B activity of ligands generally get enhanced upon complexation. The anti-TB activity of ^{1}**H$_2$L** (MIC = 6.25µg/ml) get more enhanced on complexation with Co(II) **1** (MIC=1.6µg/ml).
4. Low binding energy obtained from molecular modelling (-5.8) ^{1}**H$_2$L**, (-6.68) **1** Kcal/ mol, indicate strong interaction, which also supports the experimental data.
5. The ligand ^{1}**H$_2$L** and complex (**1**) exhibited highest binding affinities with HSA, exhibiting binding constant 7.14×10^{5} M^{-1} and 15.07×10^{5} M^{-1}. The binding sites (n) for the binding of ligand (^{1}**H$_2$L**) and complex **(1)** with HSA obtained from modified Stern-Volmer equation were found to be 1.10 and 1.37.

CHAPTER 6

NICKEL(II) COMPLEXES

6.1 Discussion on Complexes of Nickel (II):

Reaction of nickel acetate with ligands **$^{1}H_2L$-$^{12}H_2L$** form complexes of stoichiometry, [Ni(L)] in 1:1 (M:L) molar ratio (L=^{1}L-^{12}L; **13 -18**, **22-24**) and the complexes (**19-21**) with substituted 2,5 piperazine bisthiosemicarbazone (**$^{7}H_2L$-$^{9}H_2L$)** of formula $[Ni_2(L)_2]$ give the formation of dimer. The stoichiometry of complexes was confirmed by the binding ratio study using job plot method. The binding ratio of representative ligand with Nickel(II) **$^{10}H_2L$:Ni(II)** came out as 1:1. The list of complexes formed is given in Table 6.1.1.

Table 6.1.1: Bisthiosemicarbazone complexes of Nickel(II) **1-12**

Sr. No.	**Ligands**	**Complexes**
1.	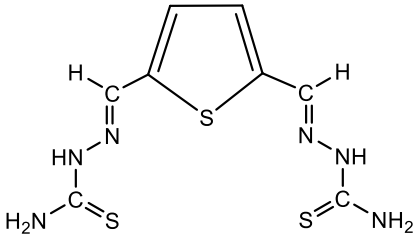 2,5thiophene dicarboxaldehyde bisthiosemicarbazone **(2,5 H_2bttsc, $^{1}H_2L$)**	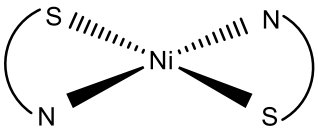 **[Ni(2,5 bttsc)]1**
2.	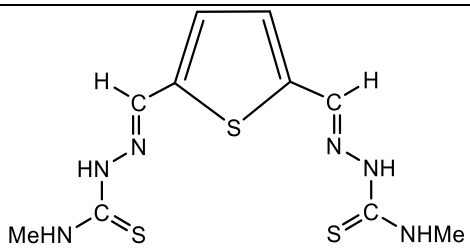 2,5thiophene dicarboxaldehyde-N-methyl bisthiosemicarbazone **(2,5 H_2bttsc -N-Me, $^{2}H_2L$)**	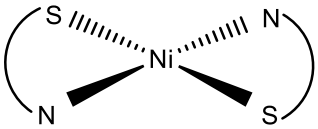 **[Ni(2,5 bttsc,N-Me)]2**

3.	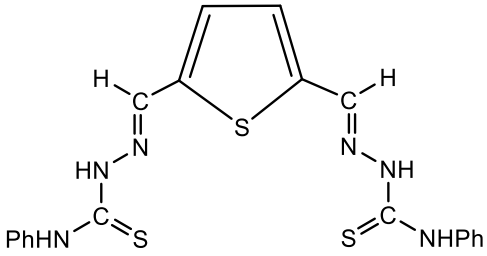 2,5thiophene dicarboxaldehyde-N-phenyl bisthiosemicarbazone **(2,5 H_2bttsc- N-Ph, ^3H_2L)**	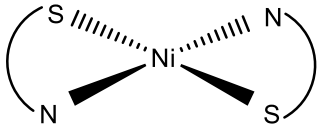 **[Ni(2,5 bttsc,N-Ph)]3**
4.	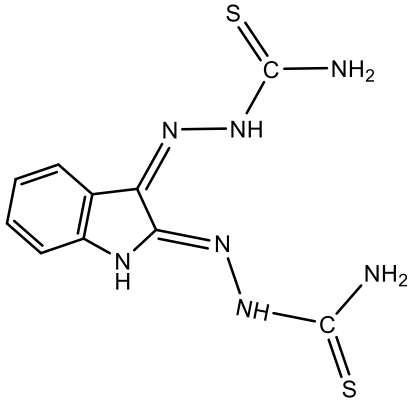 2,3-isatin bisthiosemicarbazone **(2,3 H_2bitsc, ^4H_2L)**	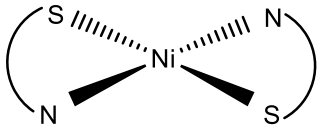 **[Ni(2,3 bitsc)]4**
5.	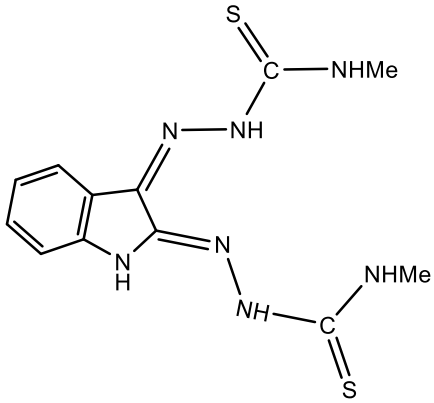 2,3-isatin-N-methyl bisthiosemicarbazone **(2,3 H_2bitsc-N-Me, ^5H_2L)**	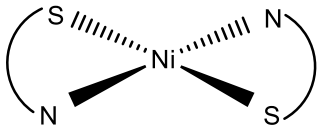 **[Ni(2,3 bitsc-N-Me)]5**

6.	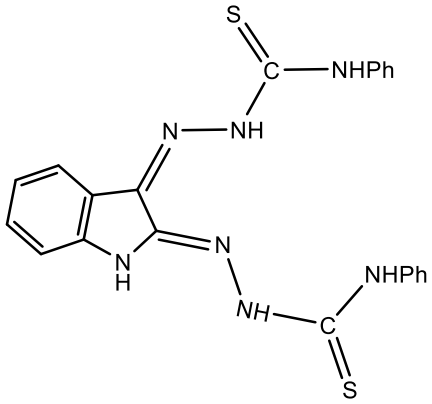 2,3-isatin-N-phenyl bisthiosemicarbazone **(2,3 H_2bitsc-N-Ph)**	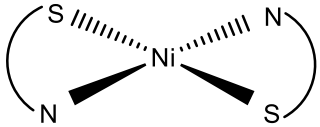 **[Ni(2,3 bitsc-N-Ph)]6**
7.	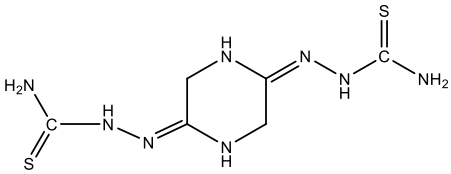 2,5-Piperazine bisthiosemicarbazone **(2,5 H_2bptsc, ^7H_2L)**	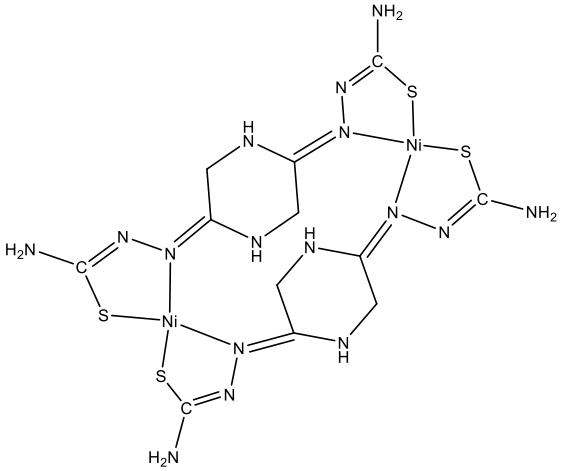 **[Ni(2,5 bptsc)]7**
8.	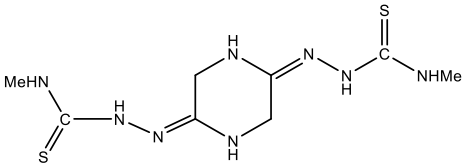 2,5-Piperazine bis N-methyl thiosemicarbazone **(2,5 H_2bptsc N-Me, ^8H_2L)**	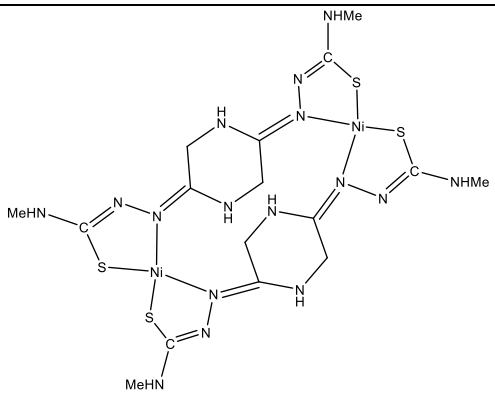 **[Ni(2,5 bptsc N-Me]8**

9.	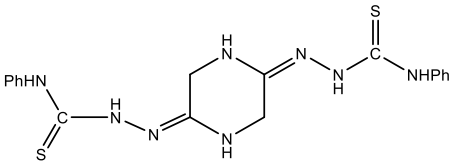 2,5-Piperazine bis N-phenyl thiosemicarbazone **(2,5 H_2bptsc N-Ph, $^{9}H_2L$)**	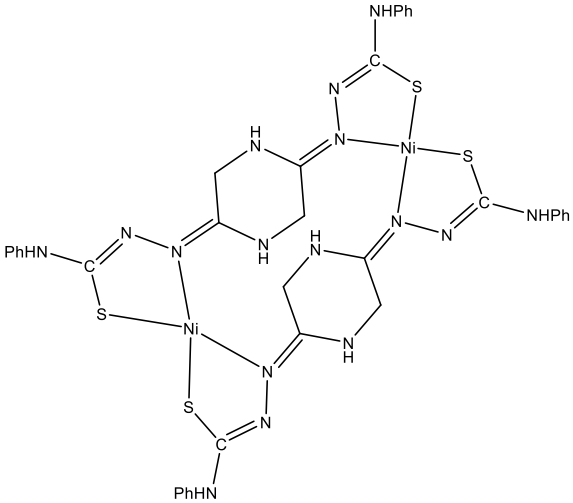 **[Ni(2,5 bptsc N-Ph]9**
10.	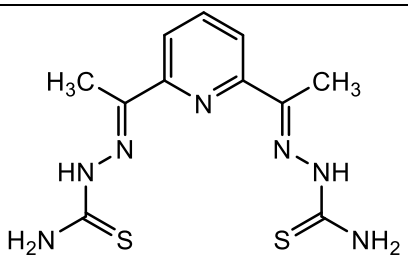 2,6 Diacetyl pyridine bisthiosemicarbazone **(2,6 H_2bdptsc, $^{10}H_2L$)**	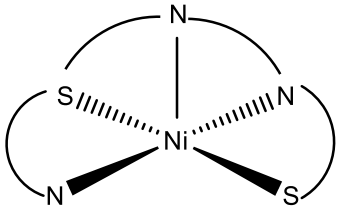 **[Ni(2,6 bdptsc]10**
11.	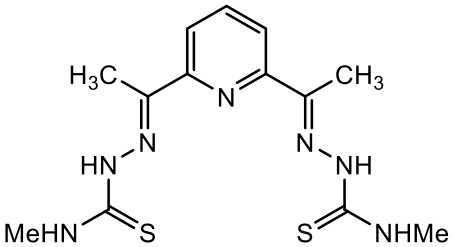 2,6 Diacetyl pyridine bis N-methyl thiosemicarbazone **(2,6 H_2bdptsc N-Me, $^{11}H_2L$)**	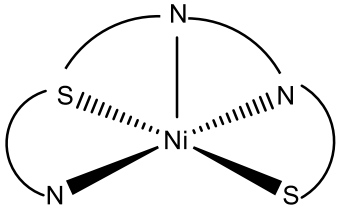 **[Ni(2,6 bdptsc,N-Me] 11**

12.	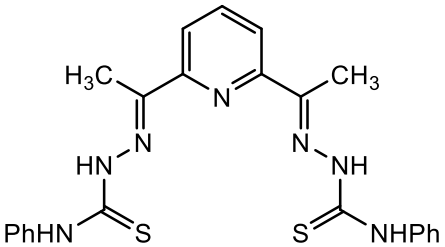 2,6 Diacetyl pyridine bis N-phenyl thiosemicarbazone **(2,6 H_2bdptsc N-Ph, $^{12}H_2L$)**	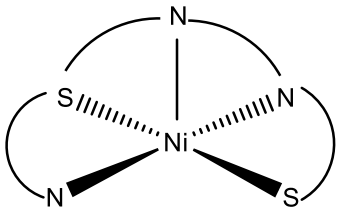 **[Ni(2,6 bdptsc,N-Ph] 12**

6.2 Binding studies: By Job Plot method

To confirm the structure of the complex (No. of binding sites) the representative ligand **2,6 H_2dptsc ($^{10}H_2L$)** was selected for binding study with nickel(II) using Uv-visible spectroscopy. Based on the fine spectrum and solubility found in a variety of solvents, including methanol, ethanol, acetonitrile, and DMSO. The DMSO as the solvent system was made possible by the probe's solubility in DMSO solvent. To optimise the concentration level and ascertain the detection mechanism, a 0.5 mM **$^{10}H_2L$** solution was prepared using DMSO as the solvent. Metal salt solutions containing 1 mM were prepared using the same solvent. To perform the UV-visible titrations for the ion analysis, 0.5 mM of ligand was gradually supplemented with 28 equivalents of 1 mM metal ion solution. For the **$^{10}H_2L$**, 0.3 mM of receptor solution was gradually supplemented with 24 equivalents of 1 mM Ni(II) ion solution. The results for the sample 2,6 H_2dptsc **$^{10}H_2L$** solution that contained 24 equivalents of each metal ion shows a notable absorption peak at 361,400nm with a shoulder peak at 377nm. (Figure 6.2.2)

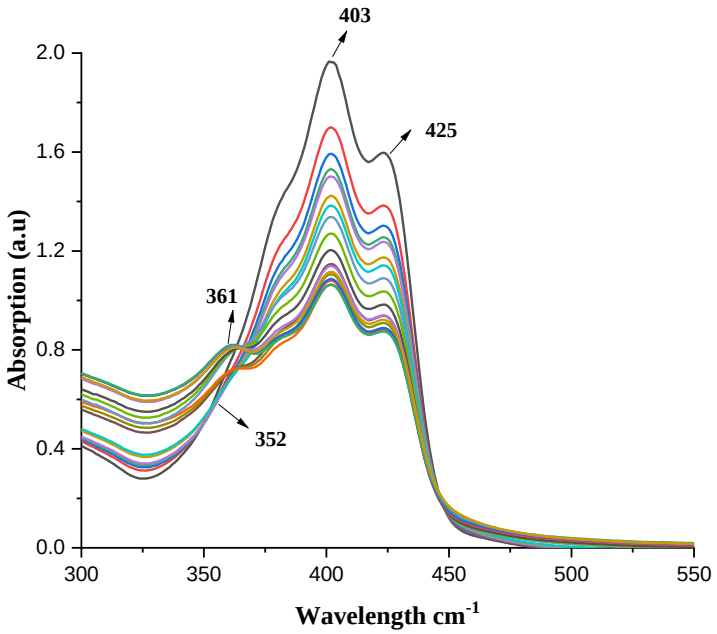

Figure 6.2.2: Absorbance responses measured after adding 24 equivalents of 1mM Ni(II) solution to solution of 0.5 mM ^{4}**H$_2$L**.

The absorption peak at 361 nm decrease to a wavelength value of 352 nm when the Ni(II) ion concentration is increased. This causes a noticeable hypsochromic shift (blue shift) [188,189] along with a distinct isobastic point at 352 nm, and the development of a robust complexation between the ligand ^{10}**H$_2$L** and **Ni(II)** [190].

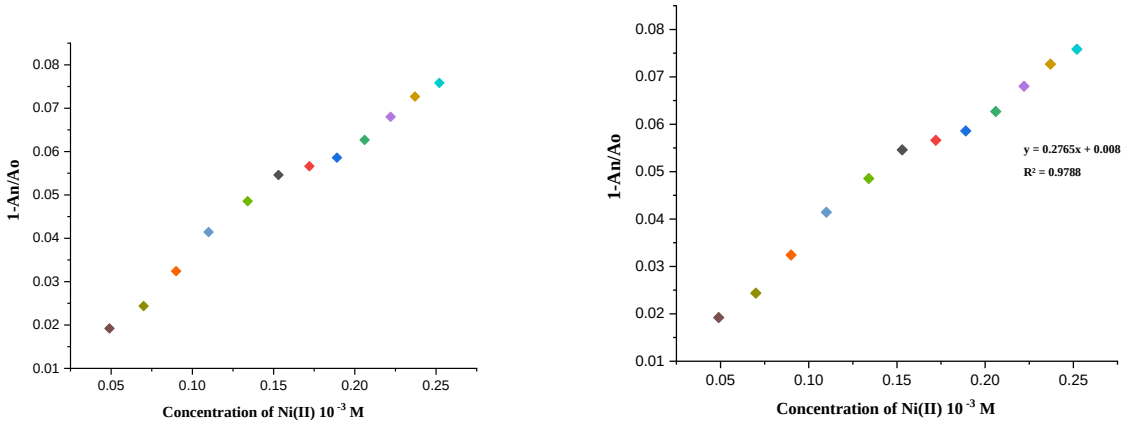

Figure 6.2.3:a) Relative shift in absorbance maxima; **b)** Linear calibration curve [A_o-A_n/A_oVs.(A_n/A_o) after addition of 24 equivalent of Ni(II) .

A_n = Sequential addition of Ni(II) ions for detection of absorbance maxima and A_o = Peak absorbance maxima of (**$^{10}H_2L$**).

6.3 IR Spectroscopy:

The important IR peaks of bisthiosemicarbazones and their (II) complexes are mentioned in Table 6.3.1 and spectra are given in Figures 6.3.1-6.3.12. The ν(N-H) bands in ligands **$^{1}H_2L$-$^{12}H_2L$** appeared in the range 3461-3204 cm^{-1} which showed a slight low energy shift in complexes 3419-3204 cm^{-1}. The bands in free ligands due to $–N^2H$ – group appeared in the range 3190-3126cm^{-1}. But on complexation this band gets disappeared in all the complexes (**13-24**) suggesting deprotonation on complexation and coordination of bisthiosemicarbazone to metal centre in dianionic form[175]. The bands of υ(C=N) in the range, 1698-1594 cm^{-1} in the ligands is shifted to lower frequency in complexes **13-24** and appeared in the range 1666-1523 cm^{-1}. The specific ν(C=S) band observed in the range 896-812 cm^{-1} in **$^{1}H_2L$-$^{12}H_2L$**, which get shifted to lower energy in complexes **(13-24)** and observed in the range, 797-698 cm^{-1}. Significant low energy shift of this band indicates binding of bis- ligand in thiolate form [176].

Table 6.3.1: Significant IR peaks of bisthiosemicarbazones (**$^{1}H_2L$–$^{12}H_2L$**) and Nickel(II) complexes (**13-24**)

Synthesized bisthiosemicarbazones Ligands and Metal complexes	**$\upsilon(NH_2)$**	**υ(-NH-)**	**υ(C=N)**	**υ(C=C)**	**δ (NH_2)**	**υ(C=S)**
(2,5 H_2bttsc, $^{1}H_2L$)	3409m, 3277m	3155m	1600s	1583m	1535s	836s
[Ni(bttsc)] **13**	3419m, 3302m	-	1598s	1495m	1436s	698s
(2,5 H_2bttscN-Me, $^{2}H_2L$)	3373m	3155w	1594s	1462m	-	812s
[Ni(bttsc,N-Me)] **14**	3314m	-	1647s	1564m	-	797s
(2,5 H_2bttsc N-Ph, $^{3}H_2L$)	3303m	3156w	1636s	1594w	-	895s
[Ni(bttsc,N-Ph)] **15**	3297m, 3217s	-	1590s	1509	-	751s
(2,3 H_2bitsc, $^{4}H_2L$)	3332m, 3259m	3156w	1698s	1618w	1584s	851s
[Ni(bitsc)] **16**	3267m	-	1659s	1571m	1452m	776s
(2,3 H_2bitsc-N^1-Me, $^{5}H_2L$)	3461m, 3207m	-	1683s	1616m	-	831s
[Ni(bitsc,N-Me)] **17**	3220m	-	1655s	1515m	-	776s
(2,3 H_2bitsc-N^1-Ph)	3290m	3173w	1685s	1591m	-	827s

[Ni(bitsc,N-Ph)] **18**	3229m	-	1670s	1595m	-	746s
(2,5 H_2bptsc, ^7H_2L)	3356m, 3253m	3166m	1640s	1526s	1512m	895s
[Ni(bptsc)] **19**	3328m 3204m,	-	1659s	1458m	1329m	772s
(2,5 H_2bptsc N-Me, ^8H_2L)	3335m, 3287m	3197m	1642s	1558s	-	804s
[Ni(bptsc,N-Me)] **20**	3272s	-	1562	1410	-	725
(2,5 H_2bptsc N-Ph, ^9H_2L)	3301m	3158w	1639s,	1466m	-	829s
[Ni(bptsc, N-Ph)] **21**	3292m, 3204m	-	1666s	1467m	-	798s
(2,6 H_2bdptsc, $^{10}H_2L$)	3423m, 3209m	3158m	1606 s	1513 m		827s
[Ni(dptsc)] **22**	3296m	-	1602s	1524m	1495m	786s
(2,6 H_2bdptsc N-Me, $^{11}H_2L$)	3450m, 3329m	3190w	1634s,	1555m	-	836s
[Ni(dptsc,N-Me)] **23**	3290m	-	1523s	1447m	-	797s
(2,6H_2bdptsc N-Ph, $^{12}H_2L$)	3303m	3156 w	1636 s,	1594m	-	896s
[Ni(dptsc,N-Ph)] **24**	3366m, 3272m	-	1615s	1528m	-	733s

***s= strong; m= medium and w= weak**

6.4 Mass Spectrometry:

The molecular ion peak $[M]^+$ observed are listed in Table 6.4.1 and spectra are given in Figures 6.4.1-6.4.12. All the complexes have m/z values in well agreement with proposed stoichiometry. The parental ion peak in $(m/z)^+$ found at 342.94amu (**1**), 370.97amu (**2**), 502.37amu (**3**), 355.03 amu (**4**), 393.36 amu (**5**), 500.08 (**6**), 318.34 amu (**7**), 347.21amu (**8**), 545.48amu (**9**), 365.99 amu (**10**), 394.04 amu (**11**), 518.07 amu (**12**) confirms the formation of bisthiosemicarbazones.

Table 6.4.1: The m/z values (amu) derived from mass spectra and expected formula of complexes **13-24.**

Sr. No.	**Parent peak (experimental mass)**	**Expected formula for parent ion $(m/z)^+$**
1	342.94	$[Ni(C_8H_{10}N_6S_3)]$ **13**
2	370.97	$[Ni(C_{10}H_{12}N_6S_3)]$ **14**
3	502.37	$[Ni(C_{20}H_{16}N_6S_3)]$ **15**
4	355.03	$[Ni(C_{10}H_9N_7S_2)]$ **16**
5	393.36	$[Ni(C_{12}H_{13}N_7S_2)]$ **17**
6	500.08	$[Ni(C_{22}H_{17}N_7S_2)]$ **18**
7	318.34	$[Ni(C_6H_{12}N_8S_2)]$ **19**
8	347.21	$[Ni(C_8H_{16}N_8S_2)]$ **20**
9	545.48	$Ni(C_{18}H_{22}N_8S_2)]$ **21**
10	365.99	$[Ni(C_{11}H_{13}N_7S_2)]$ **22**
11	394.04	$[Ni\ (C_{13}H_{17}N_7S_2)]$ **23**
12	518.07	$[Ni(C_{23}H_{21}N_7S_2)]$ **24**

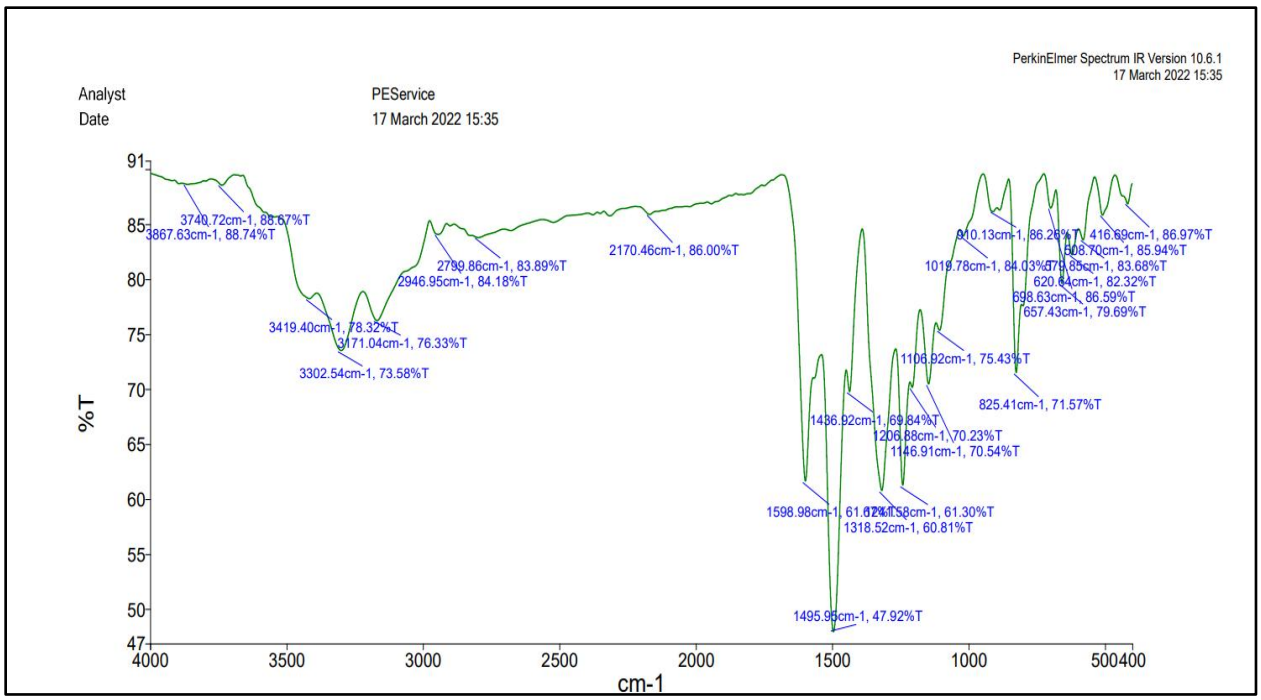

Figure 6.3.1: IR Spectra of [Ni(bttsc)] **13**

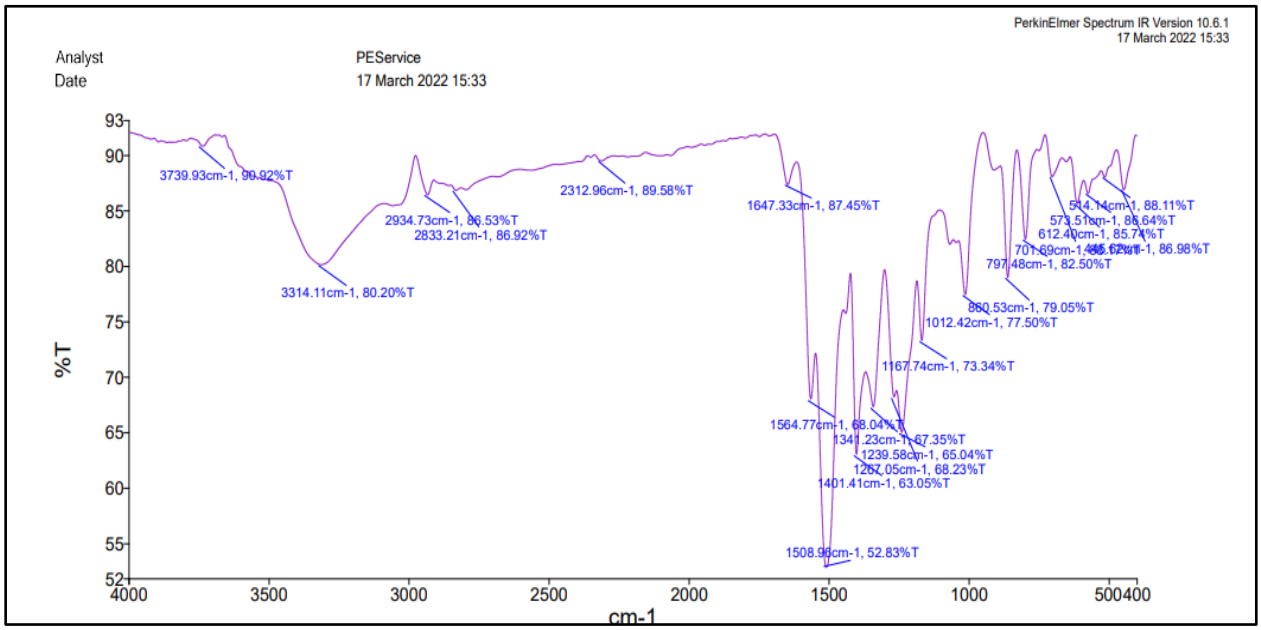

Figure 6.3.2: IR Spectra of [Ni(bttsc,N-Me)] **14**

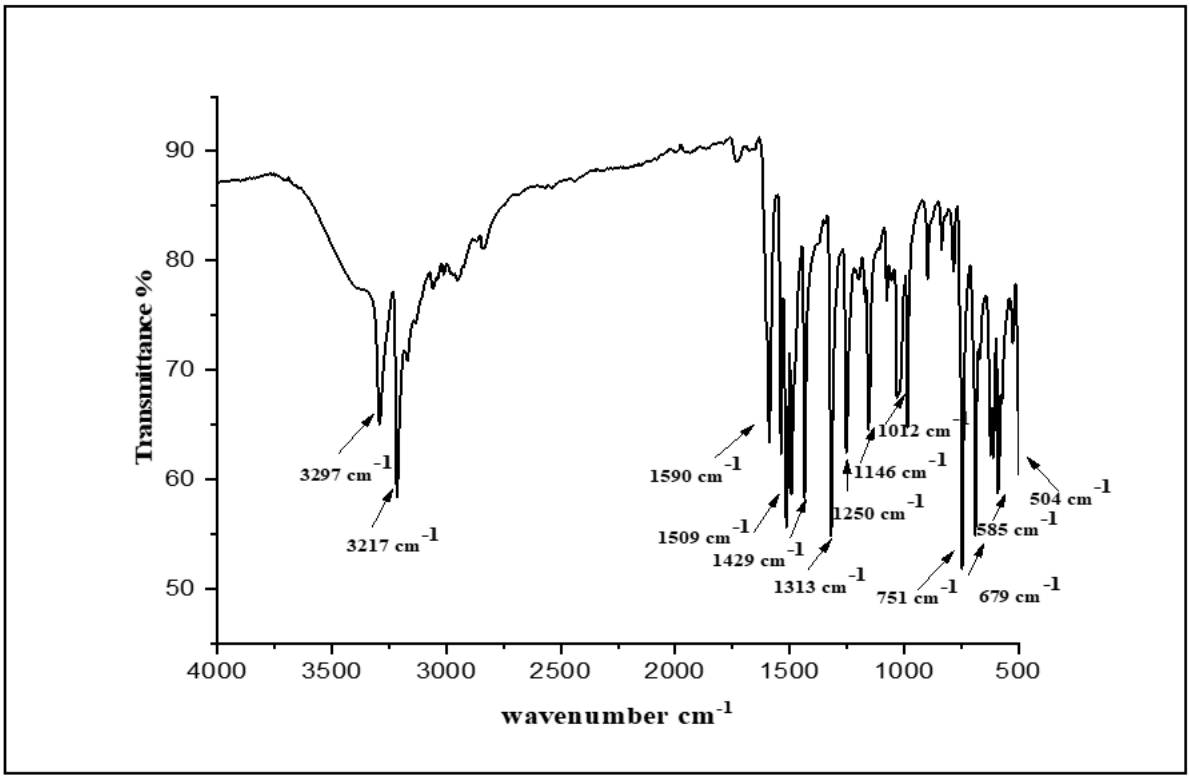

Figure 6.3.3: IR Spectra of [Ni(bttsc,N-Ph] **15**

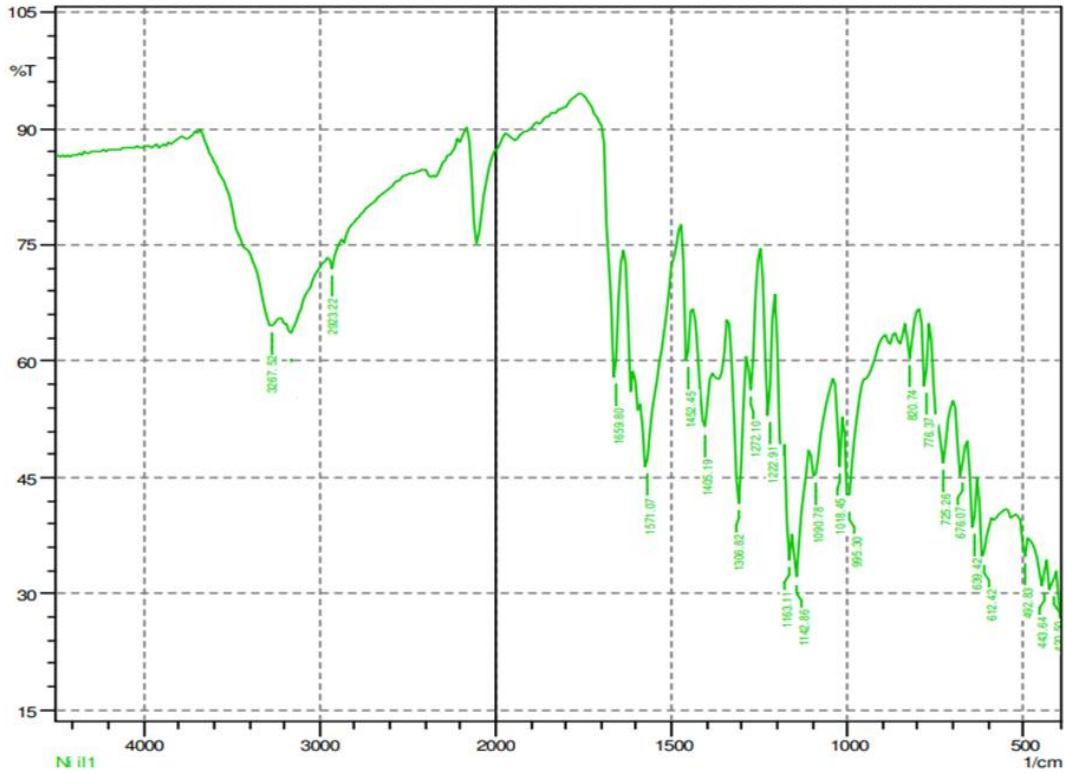

Figure 6.3.4: IR Spectra of [Ni(bitsc)] **16**

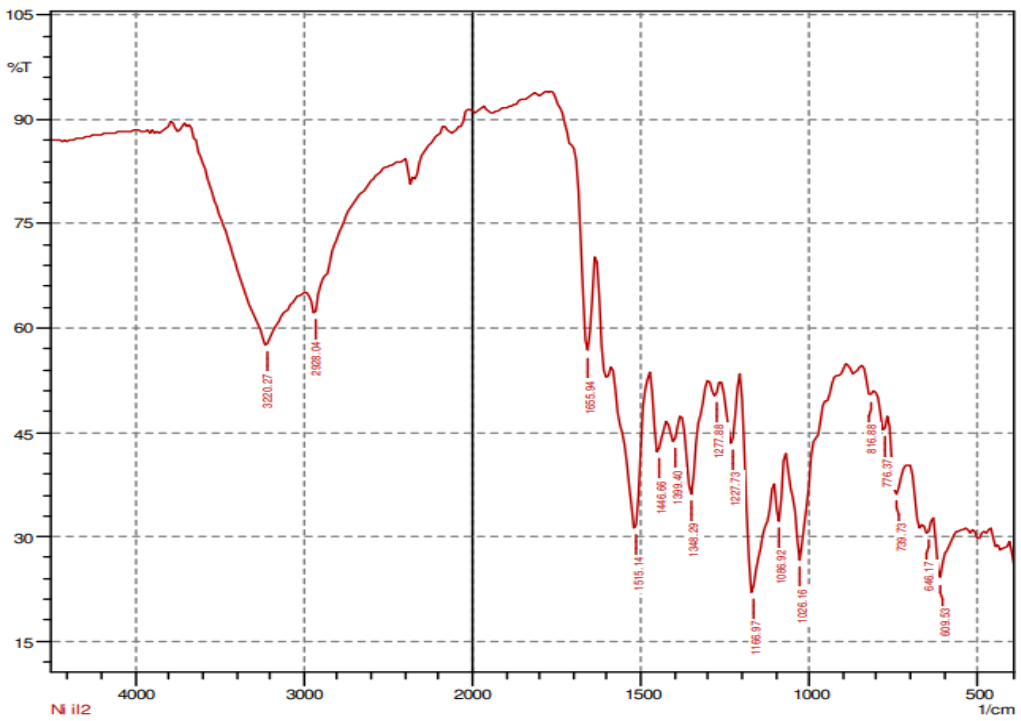

Figure 6.3.5: IR Spectra of [Ni(bitsc,N-Me)] **17**

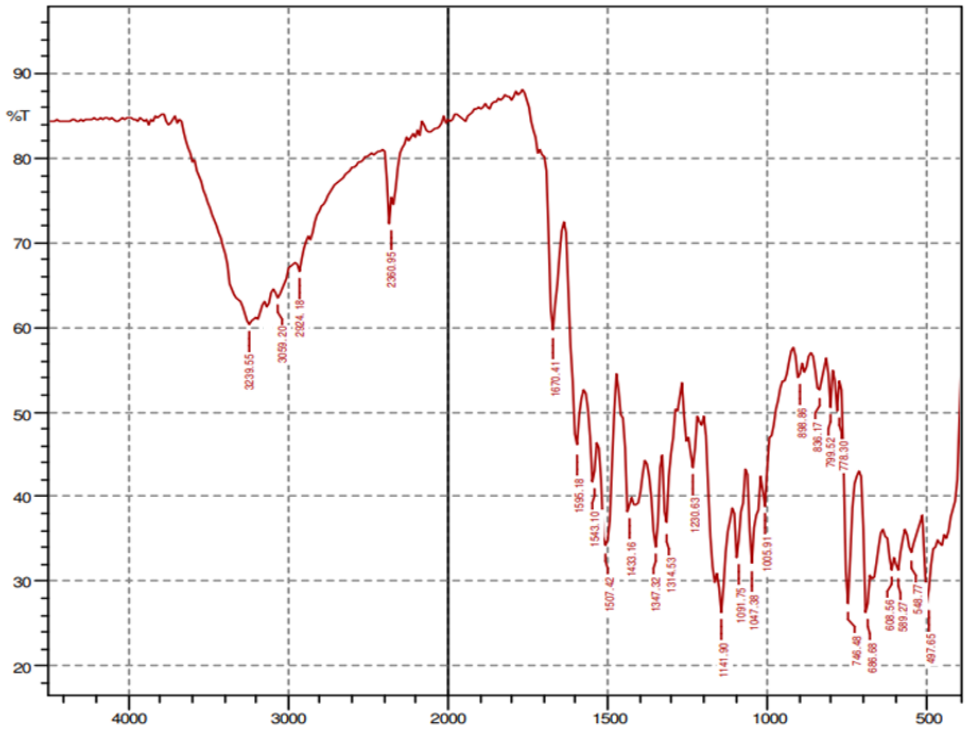

Figure 6.3.6: IR Spectra of [Ni(bitsc,N-Ph)] **18**

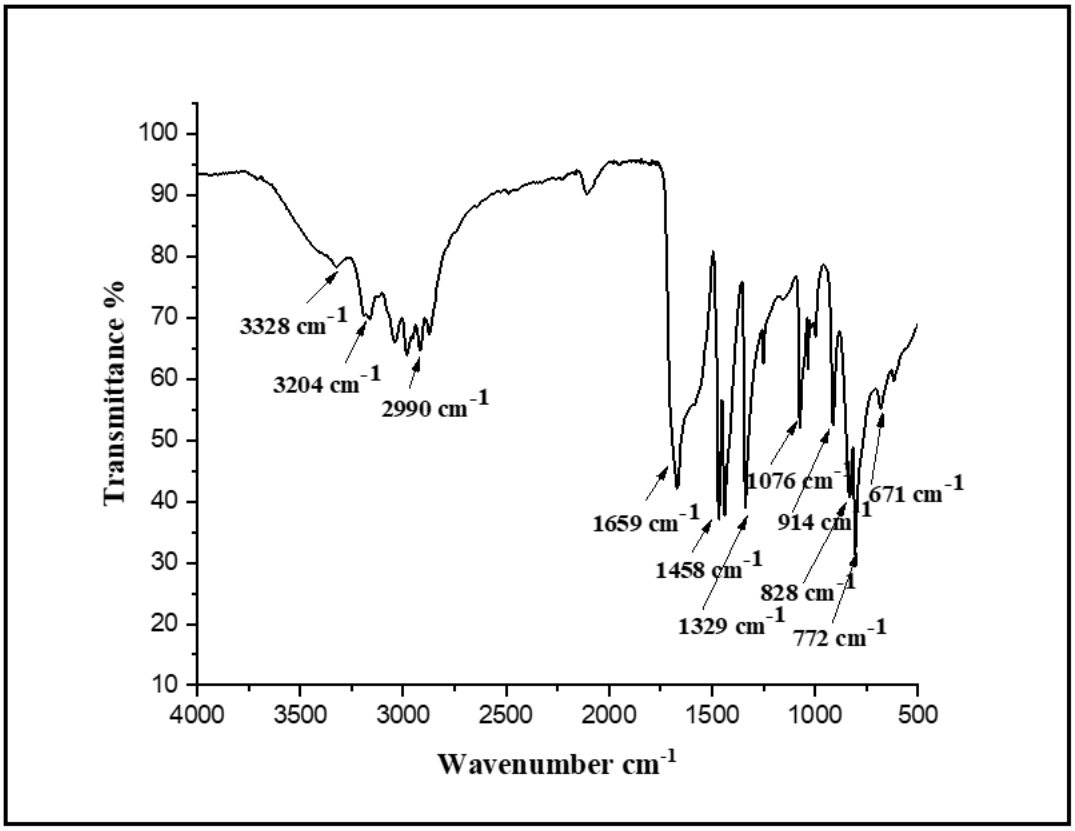

Figure 6.3.7: IR Spectra of [Ni(bptsc)] **19**

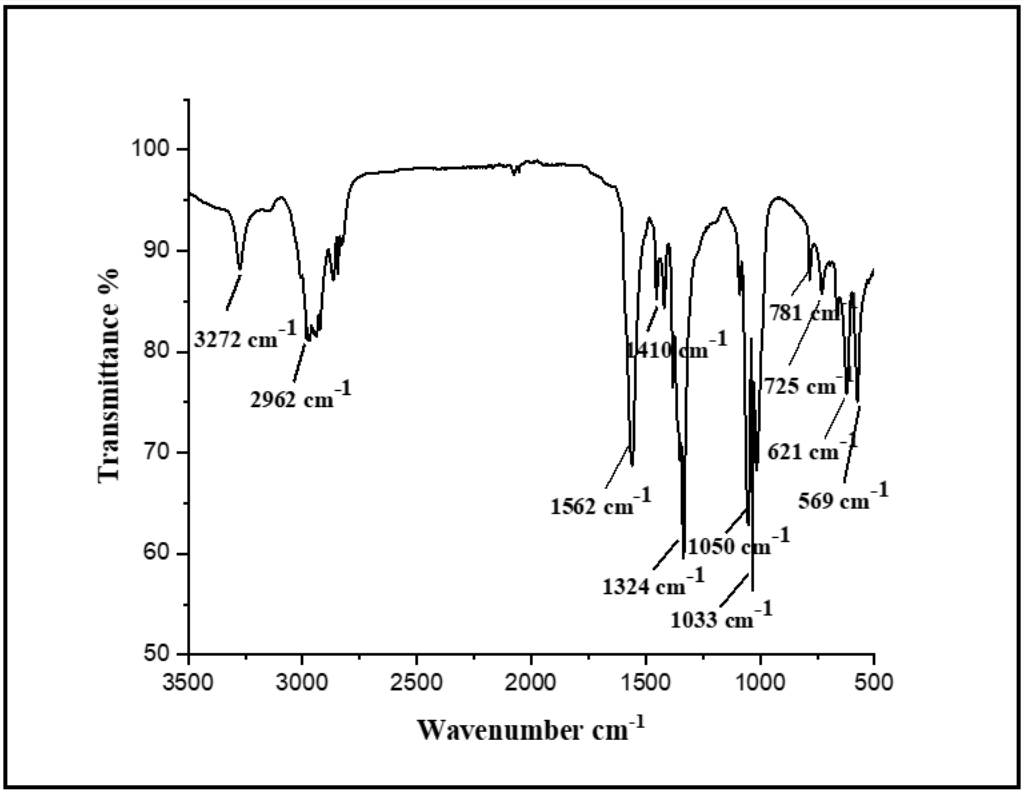

Figure 6.3.8: IR Spectra of [Ni(bptsc, N-Me)] **20**

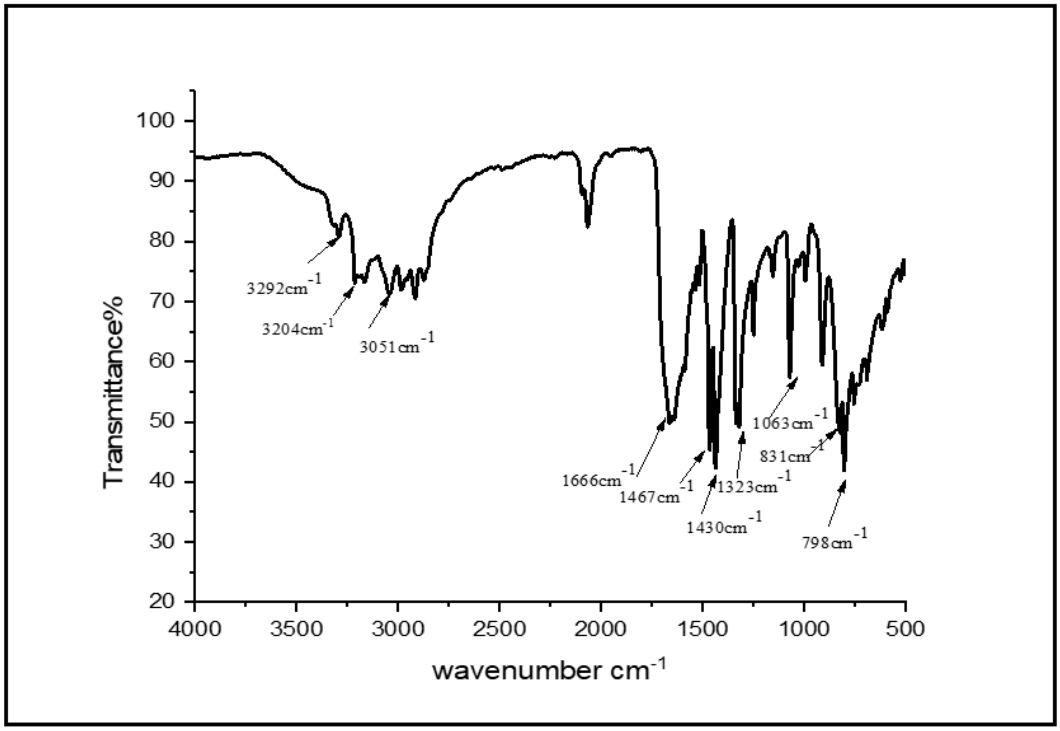

Figure 6.3.9: IR Spectra of [Ni(bptsc,N-Ph)] **21**

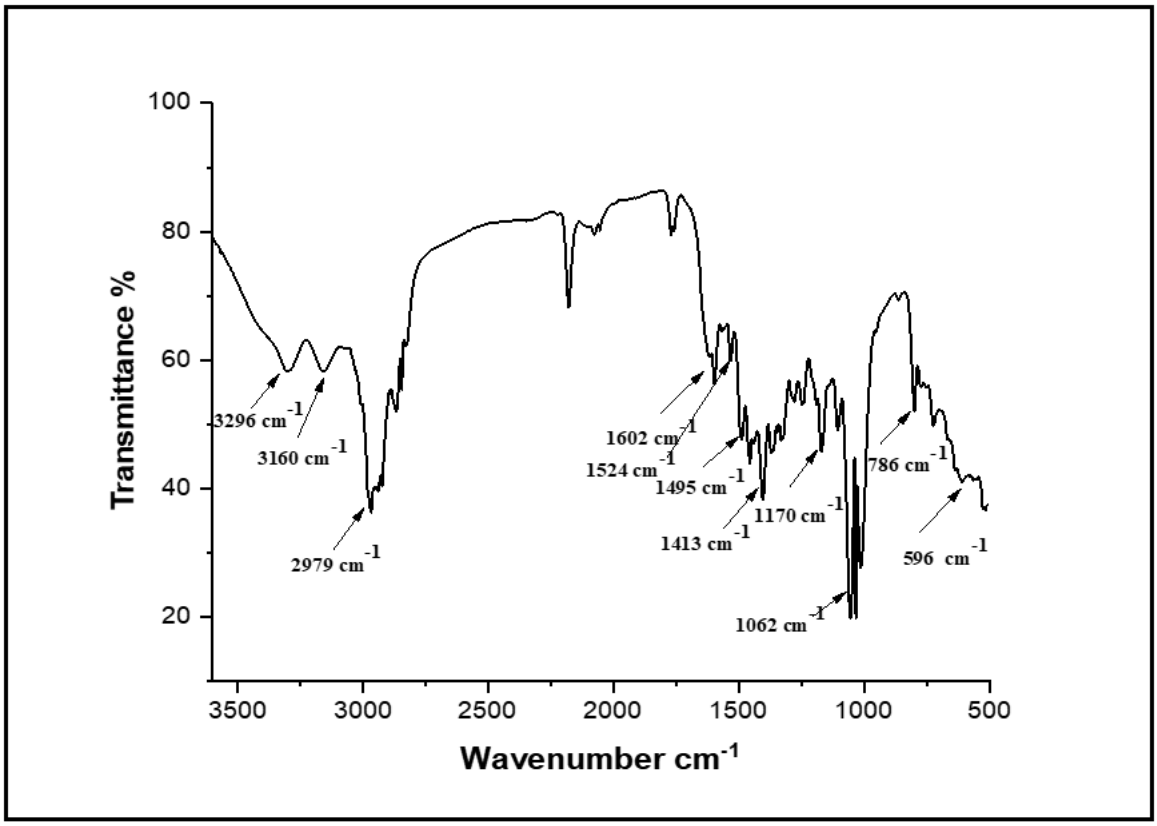

Figure 6.3.10: IR Spectra of [Ni(bdptsc)] **22**

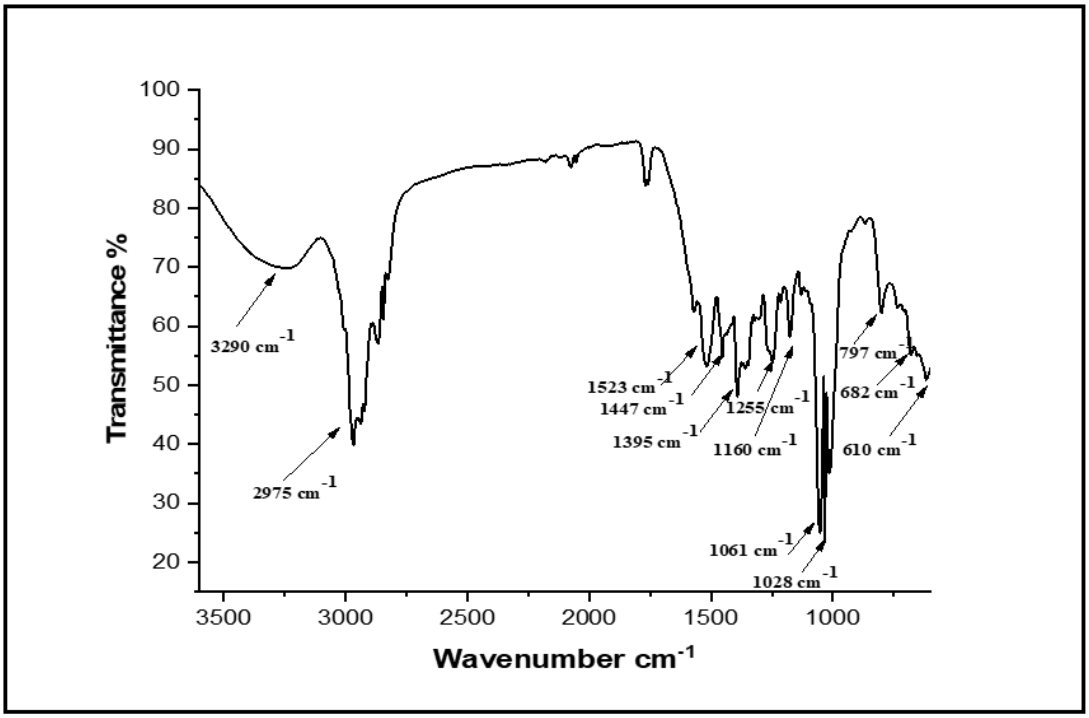

Figure 6.3.11: IR Spectra of [Ni(bdptsc,N-Me)] **23**

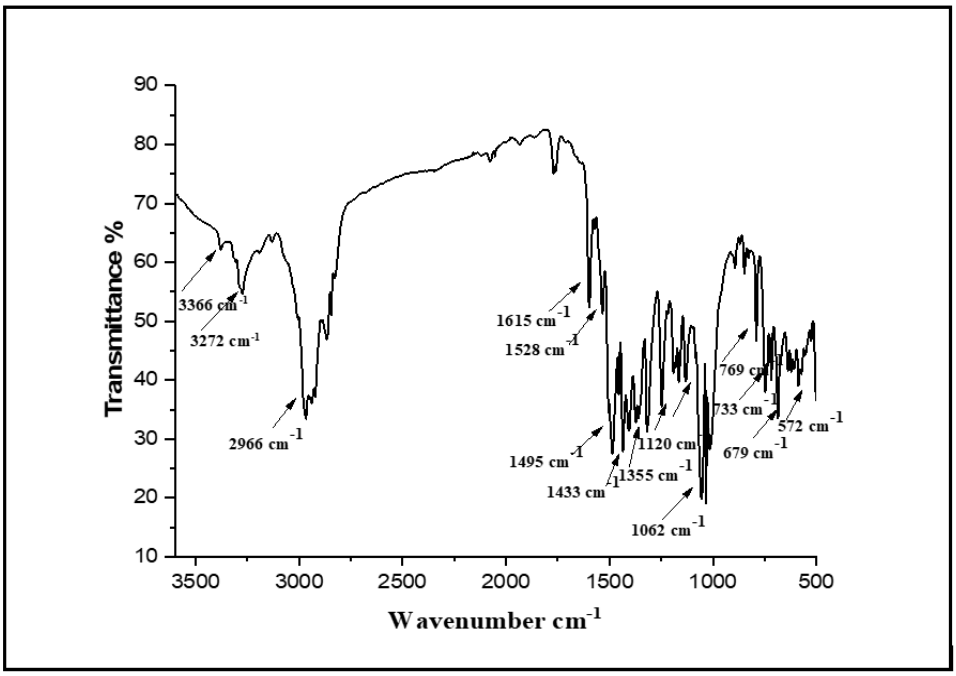

Figure 6.3.12: IR Spectra of [Ni(bdptsc,N-Ph)] **24**

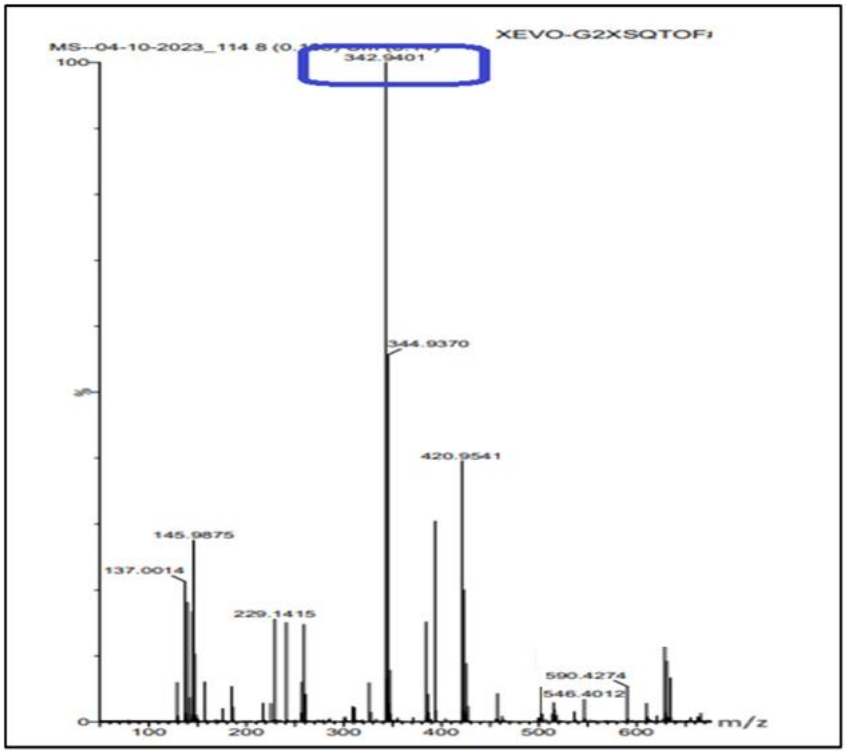

Figure 6.4.1: Mass spectrometry of complex [Ni(bttsc)]**13**

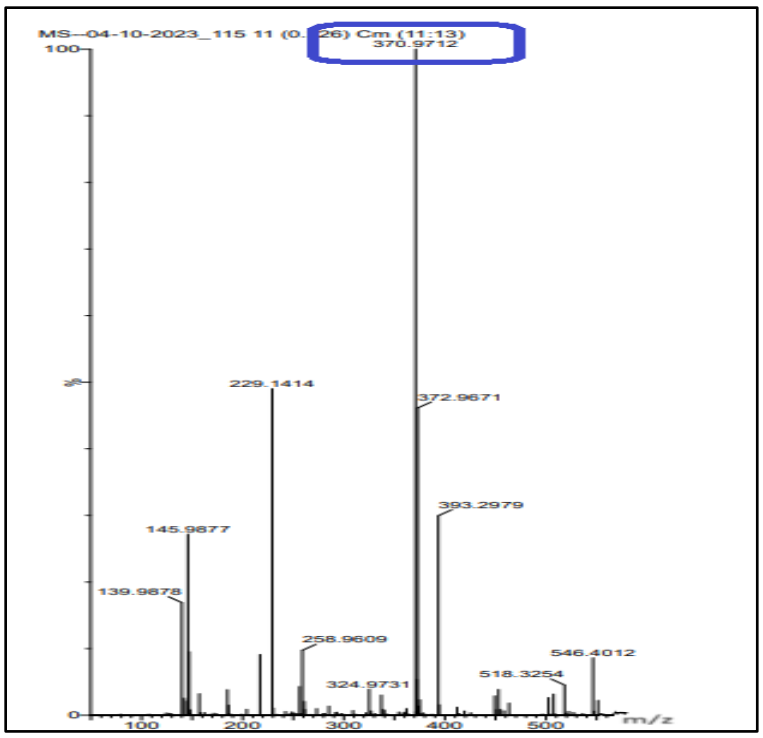

Figure 6.4.2: Mass spectrometry of complex [Ni(bttsc,N-Me)]**14**

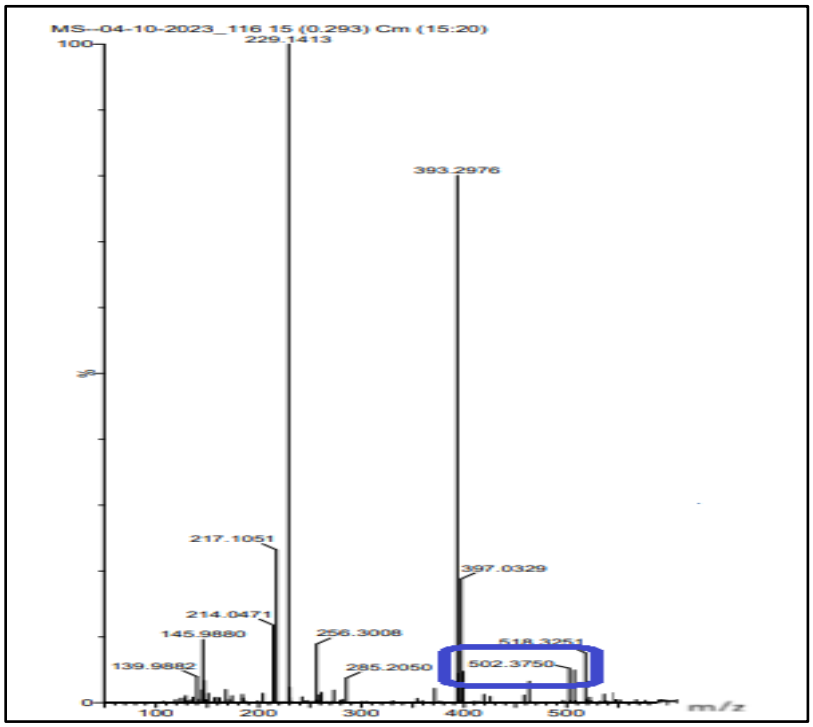

Figure 6.4.3: Mass spectrometry of complex [Ni(bttsc,N-Ph)]**15**

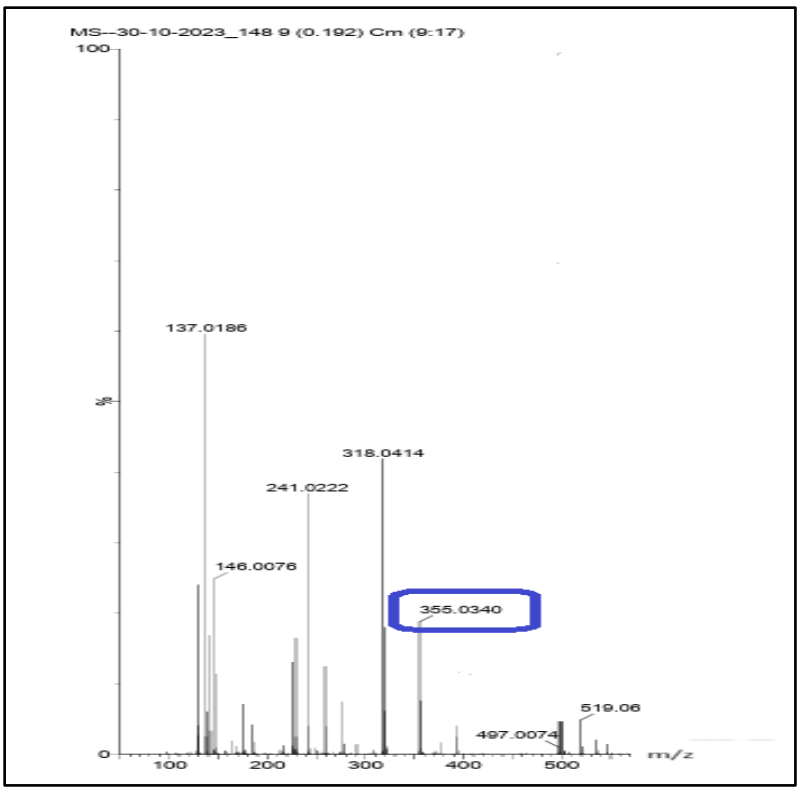

Figure 6.4.4: Mass spectrometry of complex [Ni(bitsc)]**1**

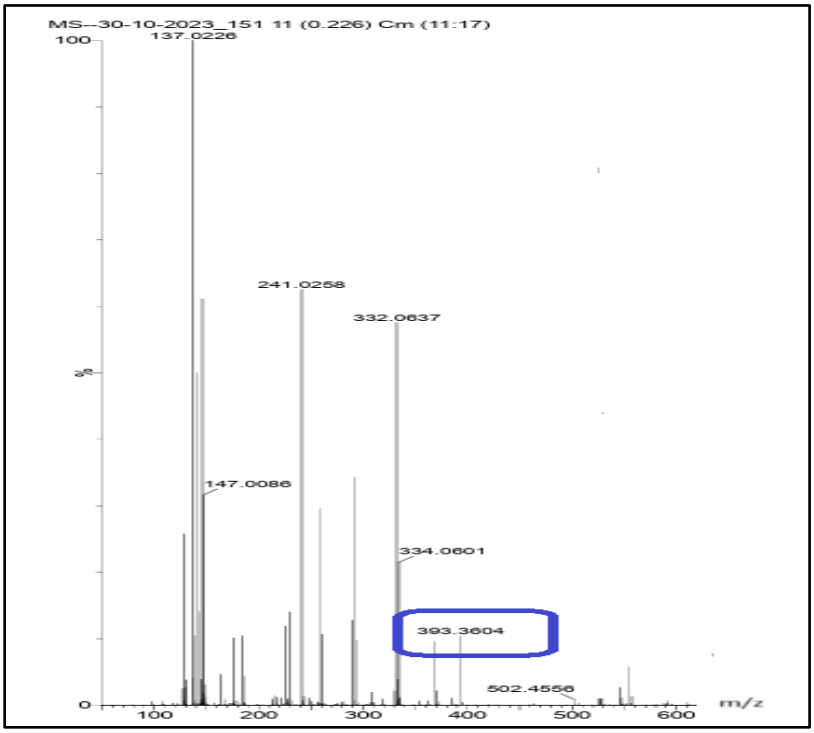

Figure 6.4.5: Mass spectrometry of complex [Ni(bitsc,N-Me)]**17**

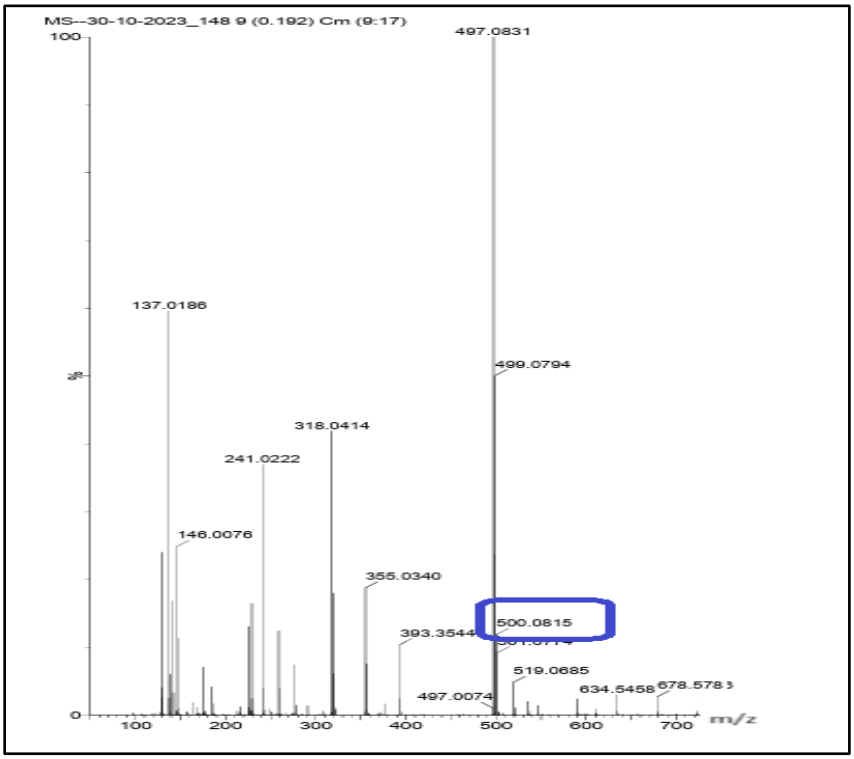

Figure 6.4.6: Mass spectrometry of complex [Ni(bitsc,N-Ph)]**18**

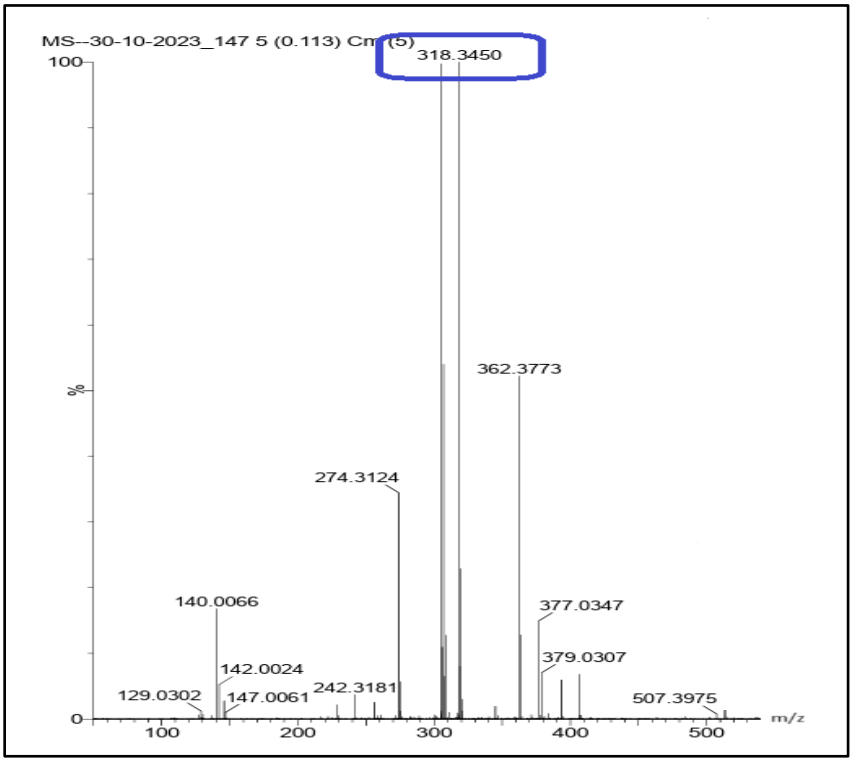

Figure 6.4.7: Mass spectrometry of complex [Ni(bptsc)]**19**

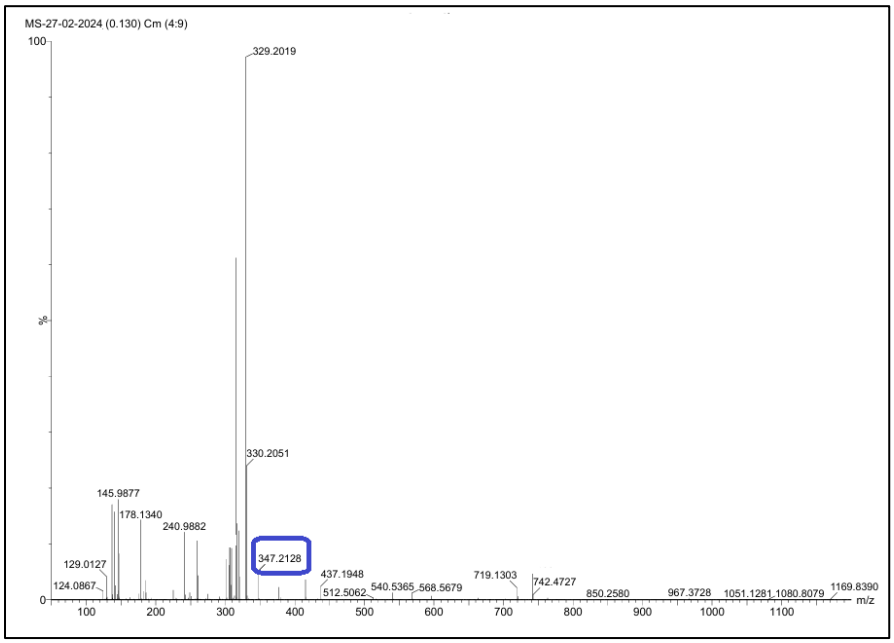

Figure 6.4.8: Mass spectrometry of complex [Ni(bptsc,N-Me)]**20**

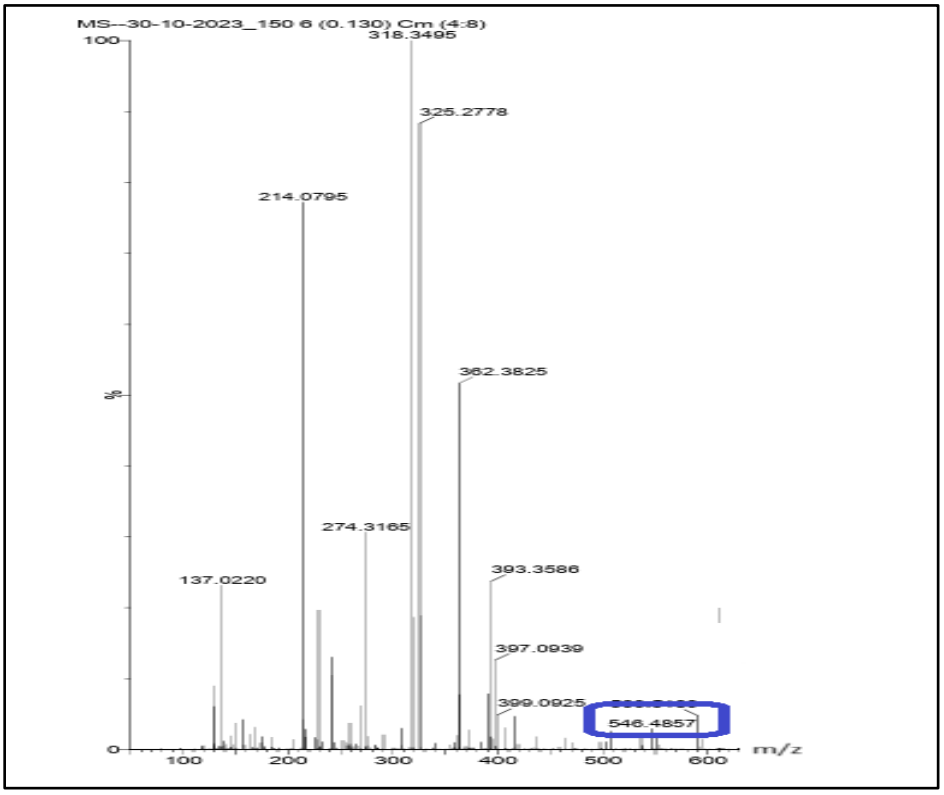

Figure 6.4.9: Mass spectrometry of complex [Ni(bptsc,N-Ph]**21**

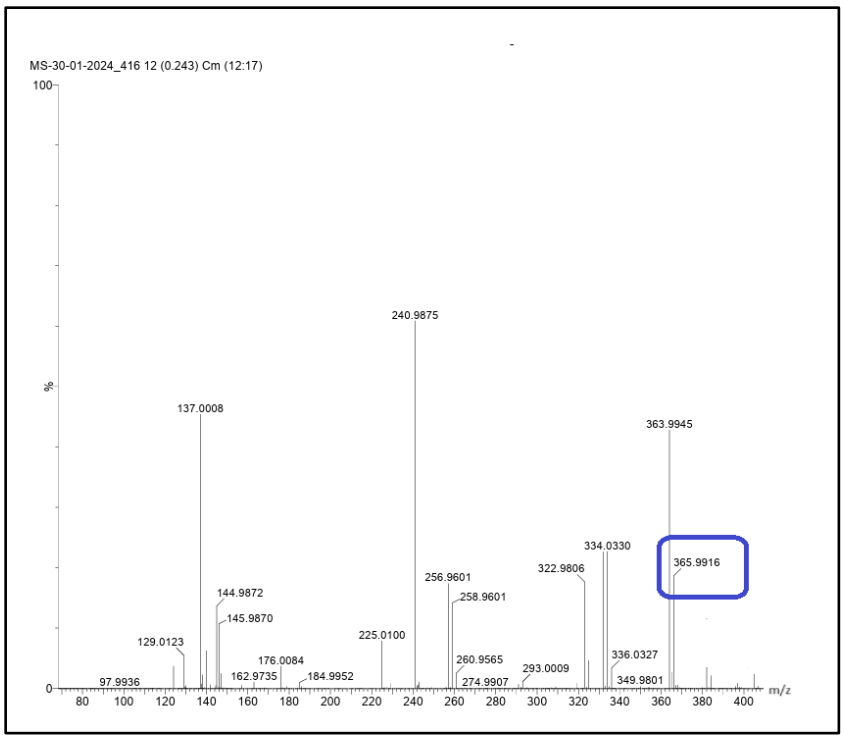

Figure 6.4.10: Mass spectrometry of complex [Ni(dpbtsc]**22**

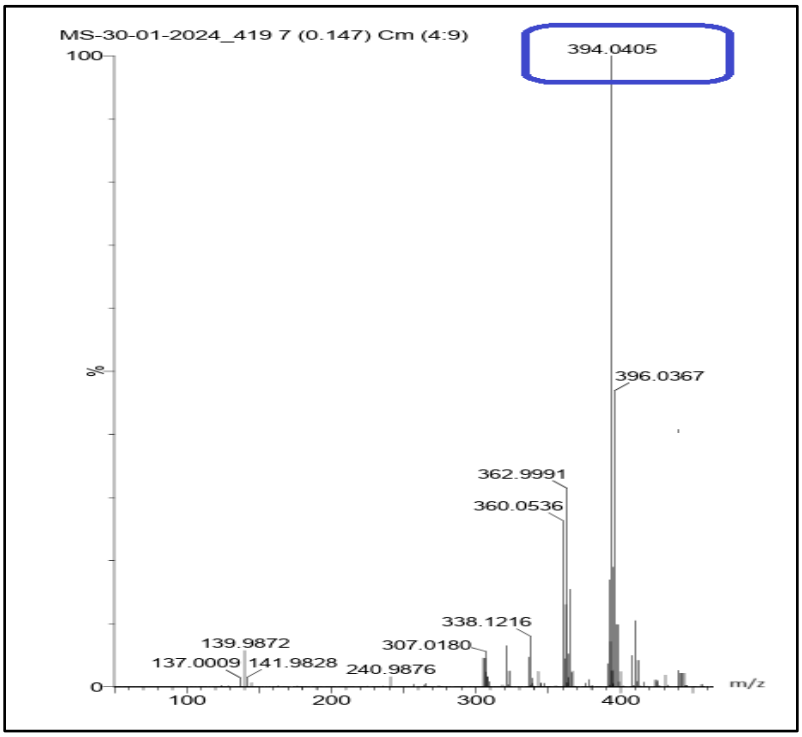

Figure 6.4.11: Mass spectrometry of complex [Ni(dpbtsc,N-Me]**23**

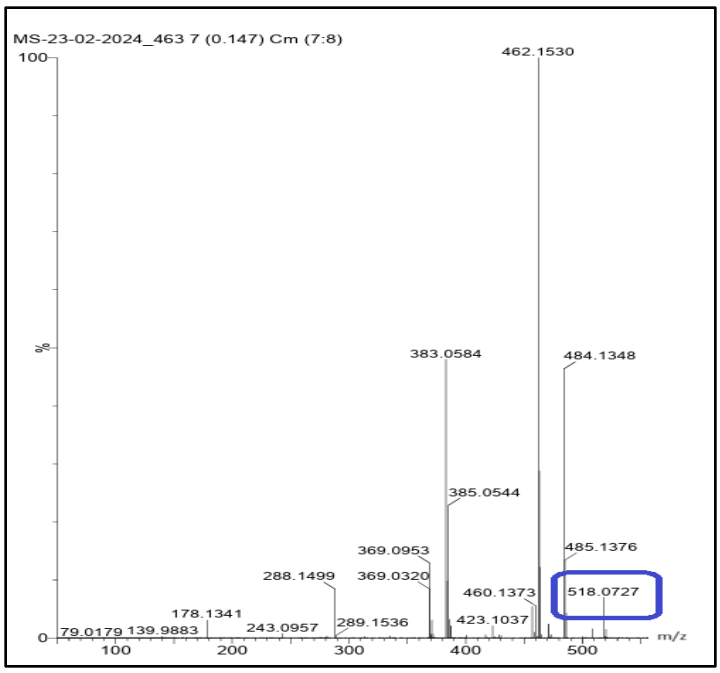

Figure 6.4.12: Mass spectrometry of complex [Ni(dpbtsc,N-Ph]**24**

The Electron spin resonance (ESR) for Ni(II) complexes was difficult to get because of their large D value and peculiar relaxation properties. Therefore, Vibrational spectroscopy with magnetic field (VSM) was possible for Ni(II) complexes.

6.5 Vibrational spectroscopy with magnetic field (VSM)

VSM can be used to determine the material's magnetic properties. The main premise is based on Faraday's law of electromagnetic induction. According to law, a change in magnetic field produces an electric field. This technique is used for the calculation of magnetic properties such as coercivity (Hc), remanence (Mr), and saturation magnetization (Ms).

VSM analysis was performed to measure the magnetic properties of the synthesized complexes. Complexes **(13-24)** were taken for VSM analysis. Magnetic hysteresis loops obtained experimentally are given in Figures 6.5.1-6.5.12. In the magnetic field range of +12 to -12 KOe, the M-H hysteresis pattern for the synthesised nickel(II) complexes at ambient temperature are displayed in Figure 6. The magnetic characteristic saturation magnetization (Ms): A point at which no further increase in magnetization is feasible with increasing the external magnetic field. Remanence (Mr): magnetization left behind after removing the external magnetic field. Coercivity (Hc): It is the measure of reverse field needed to bring the magnetization to zero after saturation,

are shown in Table 6.5.1. To calculate the experimental magnetic moment, (Equation-6) was used [191,192].

$$nB = \frac{Ms*Mw}{5585} \qquad \ldots\ldots\ldots\ldots(6)$$

Where, Ms is the saturation magnetization and Mw is the molecular weight of compound. The magnetic moment found experimentally was in the range of 2.8-4.62 B.M for complexes (**13-24)**. The magnetic moment depends on both spin and orbital angular momentum contributions. The spin-only formula is given below in (Equation -7):

$$\mu_{S.O.} = \sqrt{4S(S+1)} \qquad \ldots\ldots\ldots\ldots (7)$$

Orbital angular momentum can be added to this by the (Equation-8).

$$\mu_{S+L} = 4S(S+1) + L(L+1) \qquad \ldots\ldots\ldots\ldots\ldots (8)$$

It is anticipated that an orbital angular momentum contribution will occur when the ground term exhibits triply degeneracy, or a triplet state.

Four coordinate Nickel(II) system has possibility to form square planar geometry and tetrahedral geometry. In square planar geometry all the electrons are paired up so there is no unpaired electron and thus no magnetization is possible. But in tetrahedral geometry two electrons remain unpaired due to which magnetization occurs in this case and the lowest energy term will be $^4T_{1g}$. Nickel (II) has an effective electronic configuration of $3d^8$, the complexes are tetrahedral with a d electron configuration of $e^4\,t2^4$, and the spin-only magnetic moment can be estimated as 2.83 BM. It was observed that the complexes shows a magnetic moment that is greater than what would be predicted for two unpaired electrons in tetrahedral environment due to the orbital angular momentum of the tetrahedral Ni(II) complex significantly contributes to the magnetic moment, resulting in magnetic moment values as high as 4.0 BM [193,194].

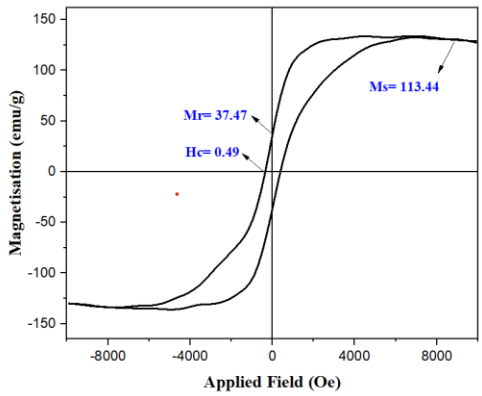

Figure 6.5.1: VSM plot of complex **13**

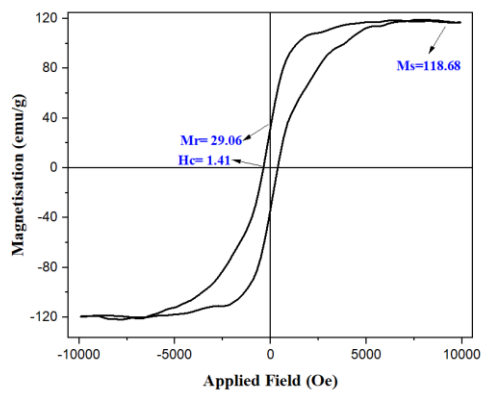

Figure 6.5.2: VSM plot of complex **14**

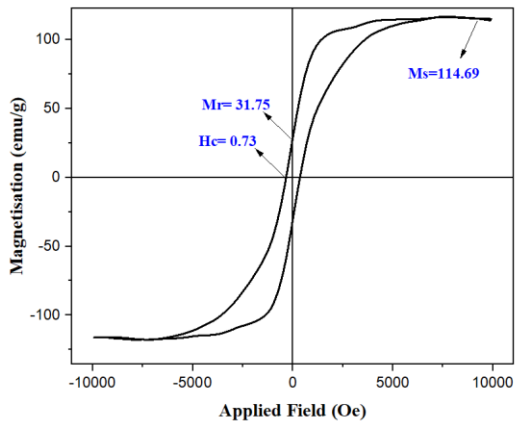

Figure 6.5.3: VSM plot of complex **15**

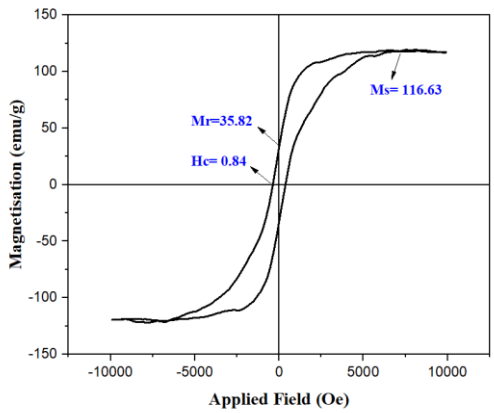

Figure 6.5.4: VSM plot of complex **16**

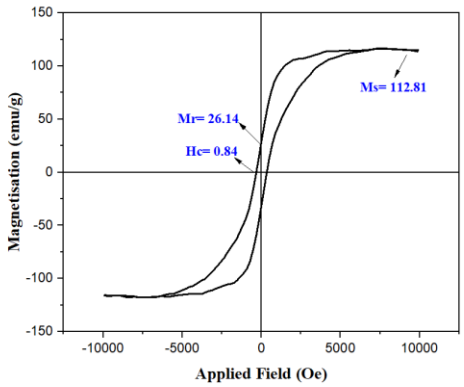

Figure 6.5.5: VSM plot of complex **17**

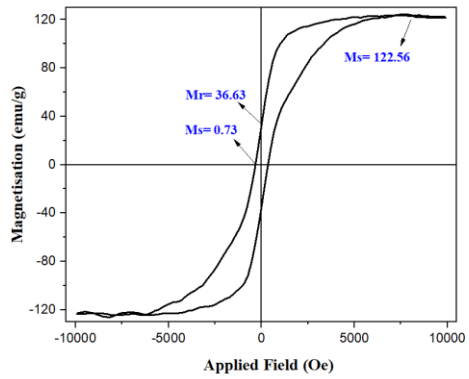

Figure 6.5.6: VSM plot of complex **18**

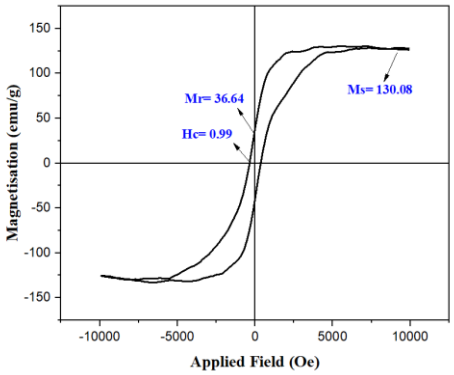

Figure 6.5.7: VSM plot of complex **19**

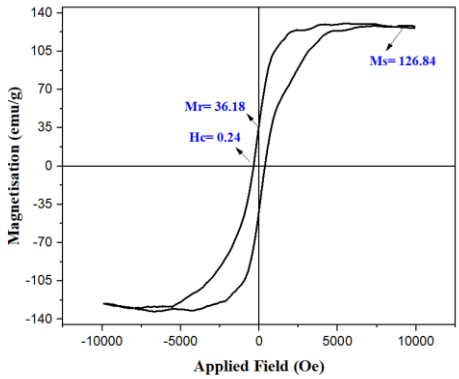

Figure 6.5.8: VSM plot of complex **20**

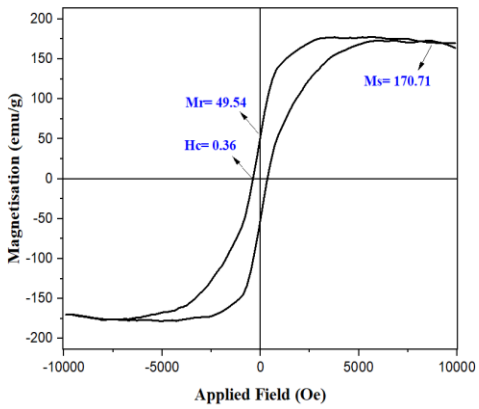

Figure 6.5.9: VSM plot of complex **21**

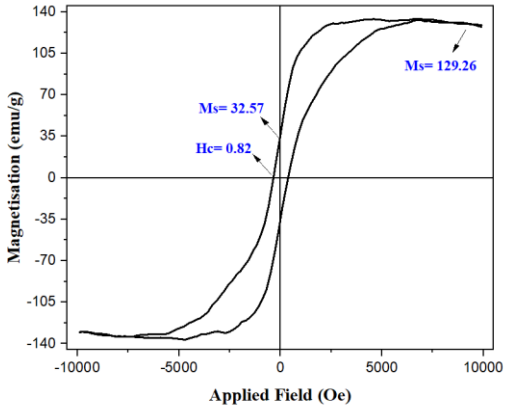

Figure 6.5.10: VSM plot of complex **22**

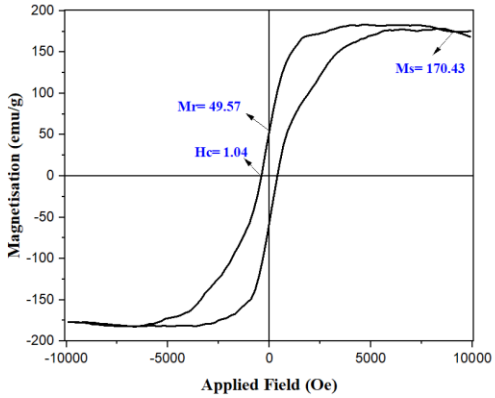

Figure 6.5.11: VSM plot of complex **23**

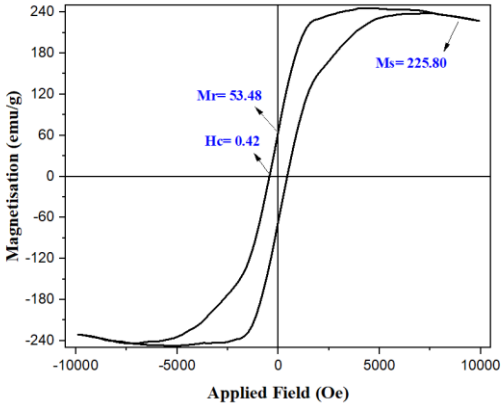

Figure 6.5.12: VSM plot of complex **24**

Table 6.5.1: VSM parameters of nickel(II) complexes **(13-24)**

Metal Complexes	Saturation magnetization (emu/g)	Coercivity magnetization (emu/g)	Remanence magnetization (emu/g)	Magnetic moment (B.M)
[Ni(2,5 bttsc)]13	113.34	0.49	37.47	3.22
[Ni(2,5 bttsc N-Me)]14	118.68	1.41	29.06	3.63
[Ni(2,5 bttsc N-Ph)]15	114.69	0.73	31.75	3.10
[Ni(2,3 H_2bitsc)]16	116.63	0.84	35.82	3.17
[Ni(2,3 H_2bitsc-N^1-Me)]17	112.81	0.84	26.14	3.07
[Ni(2,3 H_2bitsc-N^1-Ph)]18	122.56	0.73	36.63	3.32
[Ni(2,5 H_2bptsc)]19	130.08	0.99	36.64	3.53
[Ni(2,5 H_2bptsc-N-Me)]20	126.84	0.24	36.18	3.45
[Ni(2,5 H_2bptsc-N-Ph)] 21	170.71	0.36	49.54	4.62
[Ni(2,5 H_2bdptsc)]22	129.26	0.82	32.57	3.53
[Ni(2,5 H_2bdptsc-N-Me)]23	170.43	1.04	49.57	3.45
[Ni(2,5 H_2bdptsc-N-Ph)]24	225.80	0.42	53.48	3.00

From the above table it is clear that the **13-24** possess high magnetic moment than spin only moment because of orbital contribution.

6.6 Anti-tuberculosis activity:

All the ligands **(^1H_2L-$^{12}H_2L$)** and their nickel(II) complexes **(13-24)** were evaluated and are given in Table 6.5 [179]. No particular structure-activity relationship has been observed. The anti-T.B activity of ligands generally gets enhanced upon complexation, but it was found from the experimental data that the activity of ligand **2,5 H_2bptsc (^7H_2L)** has no change on complexation and exhibited maximum anti-T.B activity (MIC = 1.6µg/ml), even same to standard drugs Rifampicin or Streptomycin (MIC = 1.6µg/ml). The activity of ligand **(^1H_2L- ^3H_2L) and ($^{12}H_2L$)** (MIC = 6.25 **(^1H_2L)**; 1.6 **(^2H_2L), (^3H_2L)** and 12.5 µg/ml **($^{12}H_2L$)**) was also high but the activity gets low in its complex **13 -15** and **24** (MIC = 12.5 **13,14**; 3.12 **15** and 50 **24** µg/ml) as compared to its ligands. The anti-TB activity of ligands **^4H_2L- ^6H_2L**, **^9H_2L- $^{11}H_2L$ (**MIC **=** 50 **^4H_2L;** 100 **^3H_2L, ^6H_2L**; 3.12 **^9H_2L**; 50 **$^{10}H_2L$,$^{11}H_2L$** µg/ml) get enhanced on complexation with nicke(II) (MIC = 25 **4-6**; 1.6 **9**; 12.5 **10,11** µg/ml). Chelation of ligand with nickel(II) may have resulted in increase of its retention time on bio-membrane to allow longer interaction at target site. The

possible interactions of ligand as well as complexes have been studied using molecular docking for most potent ligand **2,5 H_2bttsc ($^{10}H_2L$)** and its **[Ni(2,6 bdptsc)] 22** complex.

Table 6.5: Anti-T.B activity of bisthiosemicarbazones (**H^1L-$H^{12}L$**) and complexes **(13-24)**

		Mycobacterium tuberculosis H37RV strain							
		MIC (µg /mL)							
S. No	**Compound**	***100***	***50***	***25***	***12.5***	***6.25***	***3.12***	***1.6***	***0.8***
1.	**2,5 H_2bttsc (^1H_2L)**	S	S	S	S	S	R	R	R
2.	**[Ni(2,5 bttsc)] 13**	S	S	S	S	R	R	R	R
3.	**2,5H_2bttsc N-Me (^2H_2L)**	S	S	S	S	S	S	S	R
4.	**[Ni(2,5 bttsc N-Me)] 14**	S	S	S	S	R	R	R	R
5.	**2,5 H_2bttsc N-Ph (^3H_2L)**	S	S	S	S	S	S	S	R
6.	**[Ni(2,5 bttsc N-Ph)] 15**	S	S	S	R	R	R	R	R
7.	**2,3 H_2bitsc (^4H_2L)**	S	S	R	R	R	R	R	R
8.	**[Ni(2,3 bitsc)] 16**	S	S	S	R	R	R	R	R
9.	**2,3 H_2bitsc-N^1-Me (^5H_2L)**	S	R	R	R	R	R	R	R
10.	**[Ni(2,3 bitsc-N^1-Me)] 17**	S	S	S	R	R	R	R	R
11.	**2,3 H_2bitsc-N^1-Ph (^6H_2L)**	S	R	R	R	R	R	R	R
12.	**[Ni(2,3 bitsc-N^1-Ph)] 18**	S	S	S	R	R	R	R	R
13.	**2,5 H_2bptsc (^7H_2L)**	S	S	S	S	S	S	S	R
14.	**[Ni(2,5 bptsc)] 19**	S	S	S	S	S	S	S	R
15.	**2,5 H_2bptsc, N-Me (^8H_2L)**	S	S	S	S	S	S	R	R
16.	**[Ni(2,5 bptsc, N-Me)] 20**	S	S	S	S	S	R	R	R

17.	**2,5 H_2bptsc, N-Ph ($^{9}H_2L$)**	S	S	S	S	S	S	R	R
18.	**[Ni(2,5 bptsc, N-Ph)] 21**	S	S	S	S	S	S	S	R
19.	**2,5 H_2bdptsc ($^{10}H_2L$)**	S	S	R	R	R	R	R	R
20.	**[Ni(2,5 bdptsc)] 22**	S	S	S	S	R	R	R	R
21.	**2,5 H_2bdptsc, N-Me ($^{11}H_2L$)**	S	S	R	R	R	R	R	R
22.	**[Ni(2,5 bdptsc, N-Me)] 23**	S	S	S	S	R	R	R	R
23.	**2,5 H_2bdptsc, N-Ph ($^{12}H_2L$)**	S	S	S	S	R	R	R	R
24.	**[Ni(2,5 bdptsc, N-Ph)] 24**	S	S	R	R	R	R	R	R

6.7 Human Serum Albumin binding studies:

Interactions of HSA with most potent ligand **2,6 H_2bdptsc ($^{10}H_2L$)** and its complex **[Ni(2,6 bdptsc)] 34** has been studied through UV-visible spectroscopy.

6.7.1 UV-visible spectroscopic study

Interactions of HSA with ligand **2,6 H_2bdptsc** and its complex **[Ni(2,6 bdptsc)]** has been studied using UV-visible absorption of HSA (7μM) in the non-appearance and incremental additions of **2,6 H_2bdptsc** (0-5 μM) and **[Ni(2,6 bdptsc)]** (0-6 μM). The HSA's UV-visible spectrum shows an absorption peak at 280 nm. Significant, increase in absorbance of HSA at 280 nm (58% for ligand **2,6 H_2bdptsc** and 47% for **[Ni (2,6 bdptsc)]** on increasing concentrations of ligand **2,6 H_2bdptsc** and complex **[Ni(2,6 bdptsc)]** showed agitations in the microenvironment of protein's chromophores due to the interaction of HSA with ligand and its complex. With the increase in concentration of ligand and its complex, a new peak at 320 nm appeared due to electronic transition of ligand and its Ni(II) complex. Using the Benesi-Hildebrand equation, the binding constants for

the ligand-HSA and complex-HSA system interactions were determined by (Equation-2) [195] and initiate to be (5.2×10^5) M^{-1} and (6.4×10^5) M^{-1}, respectively (Figure 6.7.1.2). The strong binding affinities (high binding constant) indicate the effective transport of ligand **2,6 H_2bdptsc** and complex **[Ni(2,6 bdptsc)]** to their target sites.

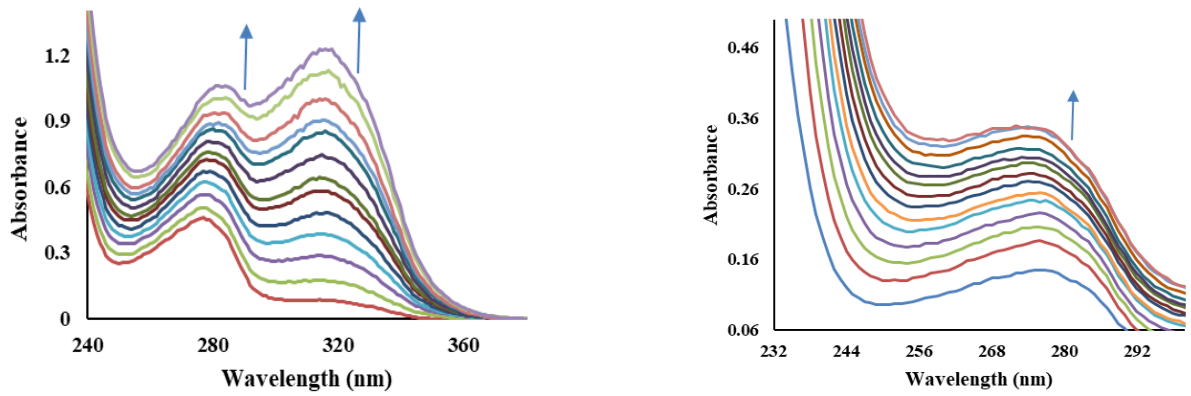

Figure 6.7.1.1: UV-visible absorption of HSA with incremental additions of ligand **2,6 H_2bdptsc** (a) and **[Ni(2,6 bdptsc)]** (b)

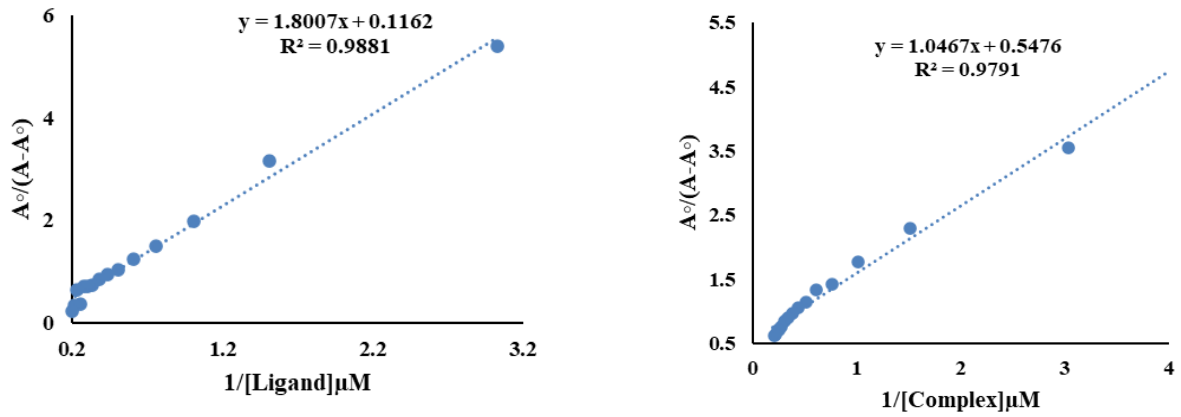

Figure 6.7.1.2: Benesi-Hildebrand plot {$A_o/(A-A_o)$ vs. 1/[ligand or complex]} for binding studies of HSA with ligand **2,6 H_2bdptsc** (a) and complex **[Ni(2,6 bdptsc)]** (b)

6.8 Docking studies:

The interactions of the potent ligand 2,6 H_2bdptsc (**$^{10}H_2L$**) and their nickel complex [Ni(2,6 bdptsc)] **34** have been studied by molecular docking using Autodock 4.0 in order to corroborate and explain the experimental results [46]. Docking of ligand **2,6 H_2bdptsc** and their nickel complex **[Ni(2,6 bdptsc)]** with mycobacterium tuberculosis enoyl reductase yielded minimal binding energies of -6.4 and -7.0 Kcal/mol, respectively. The results show that the strongest

binding with the target was exhibited by $^{10}H_2L$ and its complex **34**. It is evident from the binding energy statistics that complexes **34** gets more firmly bound in comparison to free ligands with mycobacterium tuberculosis enoyl reductase. For complex **34** a higher binding energy (negative) denotes an extra stable structure in docked state. This corresponds to the same order as the experimental data showed.

The docking analysis of interactions between ligand $^{10}H_2L$ and its complex **34** with mycobacterium tuberculosis enoyl reductase revealed that the ligand $^{10}H_2L$ had interaction (hydrogen bonding) with oxygen atom of amino acid residue lysine (LYS 164) (d = 2.81 Å), and proline (PRO 155) (d = 2.39 Å) of chain A. The ligand $^{10}H_2L$ interacts with amino acid residues methionine (MET198), tyrosine (TYR157), phenylalanine (PHE148), isoleucine (ILE 214) and leucine (LEU 217) of chain A via hydrophobic and other interactions. The complex **34** interacts with the target by hydrogen bonding with isoleucine (ILE 193) (d = 3.64 Å), tyrosine (TYR 157) (d = 5.09 Å) amino acid residues of the chain (Figure 6.8.1)

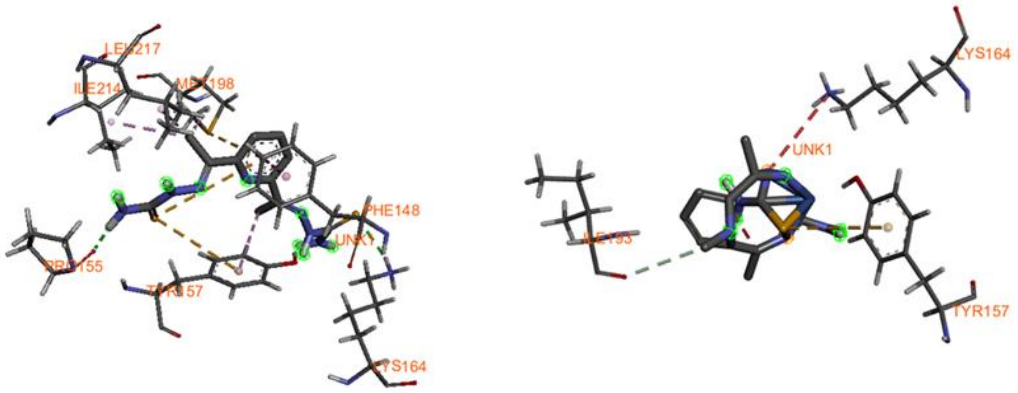

(a) (b)

Figure 6.8.1: 3D representation of interactions of ligand $^{10}H_2L$ (a) and its complex **22** (b) with mycobacterium tuberculosis enoyl reductase

6.9 <u>Conclusion:</u> Reaction of Nickel (II) acetate with $^{1}\mathbf{H_2L}$-$^{12}\mathbf{H_2L}$ yielded complexes of stoichiometry, [Ni(L)] **13-24** molar ratio in 1:1. All complexes were meticulously characterized using FTIR, Mass, UV-visible, and V.SM. Ligands ranging from $^{1}\mathbf{H_2L}$-$^{12}\mathbf{H_2L}$, together with their respective complexes (**13-24**), and were subjected to evaluation for anti-tuberculosis efficacy. The following conclusion has been drawn from the results obtained:

1. All the complexes have m/z values in well agreement with proposed stoichiometry.
2. The magnetic moment found experimentally was in the range of 3.0-4.62 B.Mn for complexes (**13-24)** confirms the tetrahedral geometry.
3. The anti-T.B activity of ligands generally get enhanced upon complexation. It has been observed that with the increase of hydrophobicity of ligand due to substituent present at N^1 atom, mostly the anti-TB activity gets increased. Also, the anti-TB activity of $^{10}\mathbf{H_2L}$ (MIC = 50µg/ml) get more enhanced on complexation with Ni(II) **22** (MIC=12.5µg/ml).
4. Low binding energy obtained from molecular modelling (-6.4) $^{10}\mathbf{H_2L}$, (-7.0) **22** Kcal/ mol, indicate strong interaction, which also supports the experimental data.
5. The ligand $^{10}\mathbf{H_2L}$ and complex (**22)** exhibited highest binding interactions, featuring binding constant of 6.4×10^5 M^{-1} and 5.2×10^5 M^{-1} with HSA.

CHAPTER 7

COPPER(II) COMPLEXES

7.1 Discussion on Complexes of Copper (II):

Reaction of Copper acetate with ligands **$^{1}H_2L$-$^{12}H_2L$** form complexes of stoichiometry, [Cu(L)] (L=^{1}L, **25**-^{12}L, **36**) and and the complexes (**31-33**) with substituted 2,5 piperazine bisthiosemicarbazone (**$^{7}H_2L$-$^{9}H_2L$)** of formula $[Cu_2(L)_2]$ give the formation of dimer in 1:1 (M:L) molar ratio. The formula [Cu(L)] for complexes is also confirmed by finding the binding ratio of ligand with copper metal. The binding ratio of representative ligand with copper (II) **$^{1}H_2L$:Cu(II)** came out as 1:1. The list of complexes formed is given in Table 7.1.1.

Table 7.1.1: Bisthiosemicarbazone complexes of Copper(II) **25-36**

Sr. No.	**Ligands**	**Complexes**
1.	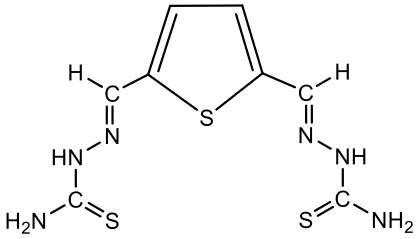 2,5thiophene dicarboxaldehyde Bisthiosemicarbazone **(2,5 H_2bttsc, $^{1}H_2L$)**	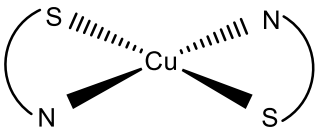 **[Cu(2,5 bttsc)]1**
2.	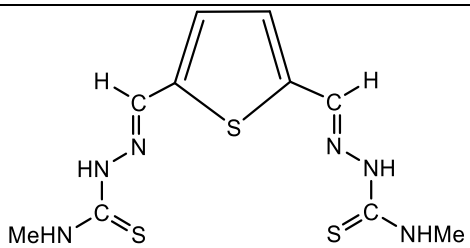 2,5thiophene dicarboxaldehyde-N-methyl bisthiosemicarbazone **(2,5 H_2bttsc -N-Me, $^{2}H_2L$)**	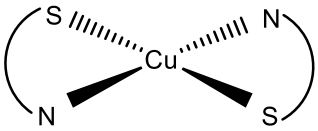 **[Cu(2,5 bttsc,N-Me)]2**

3.	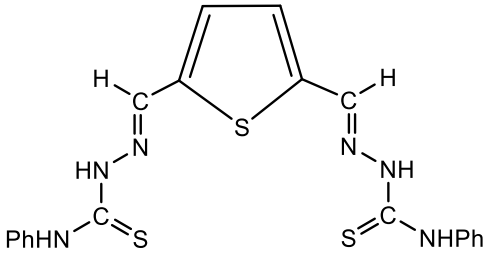 2,5thiophene dicarboxaldehyde-N-phenyl bisthiosemicarbazone **(2,5 H_2bttsc- N-Ph, ^3H_2L)**	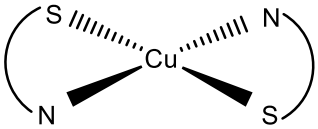 **[Cu(2,5 bttsc,N-Ph)]3**
4.	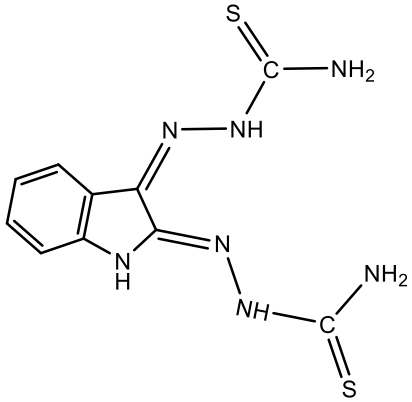 2,3-isatin bisthiosemicarbazone **(2,3 H_2bitsc, ^4H_2L)**	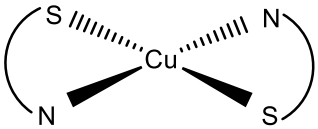 **[Cu(2,3 bitsc)]4**
5.	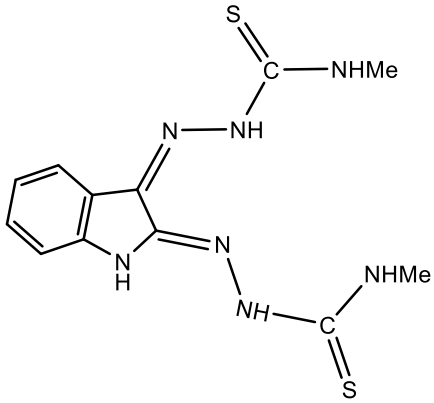 2,3-isatin-N-methyl bisthiosemicarbazone **(2,3 H_2bitsc-N-Me, ^5H_2L)**	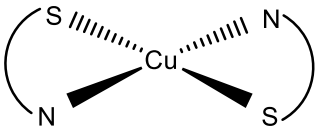 **[Cu(2,3 bitsc-N-Me)]5**

6.	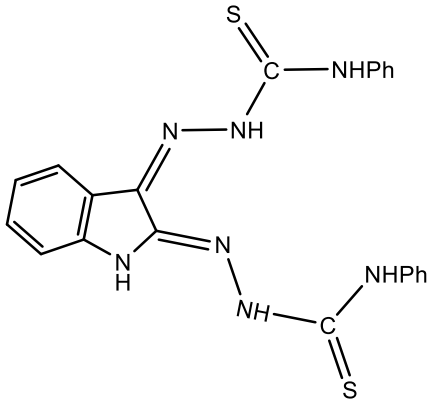 2,3-isatin-N-phenyl bisthiosemicarbazone **(2,3 H_2bitsc-N-Ph)**	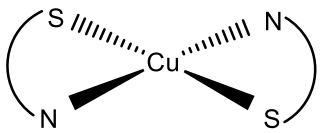 **[Cu(2,3 bitsc-N-Ph)]6**
7.	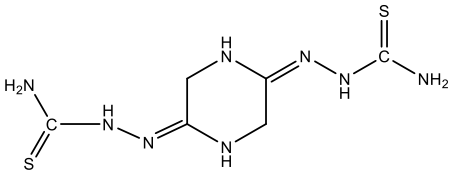 2,5-Piperazine bisthiosemicarbazone **(2,5 H_2bptsc, ^7H_2L)**	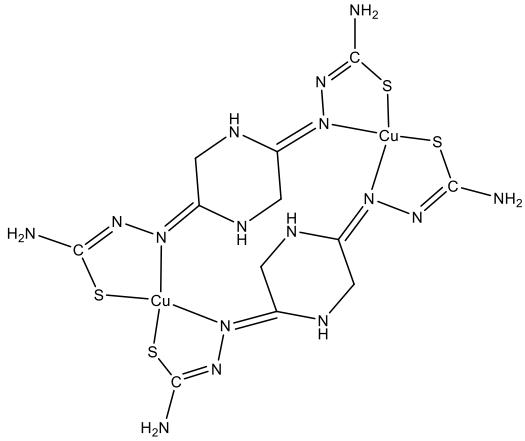 **[Cu(2,5 bptsc)]7**
8.	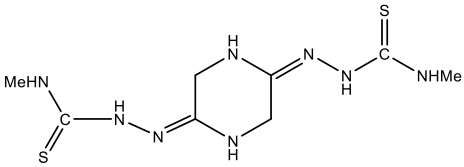 2,5-Piperazine bis N-methyl thiosemicarbazone **(2,5 H_2bptsc N-Me, ^8H_2L)**	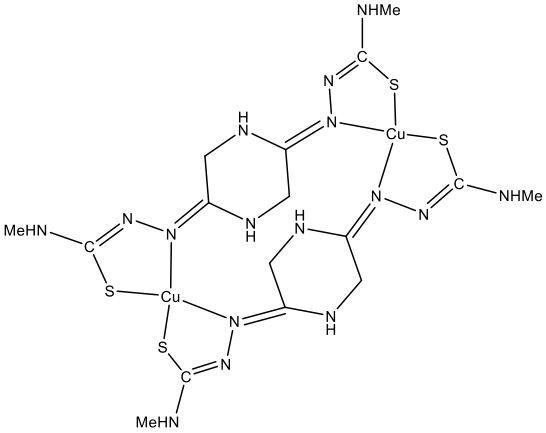

		[Cu(2,5 bptsc N-Me]8
9.	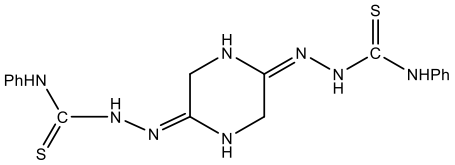 2,5-Piperazine bis N-phenyl thiosemicarbazone **(2,5 H_2bptsc N-Ph, $^{9}H_2L$)**	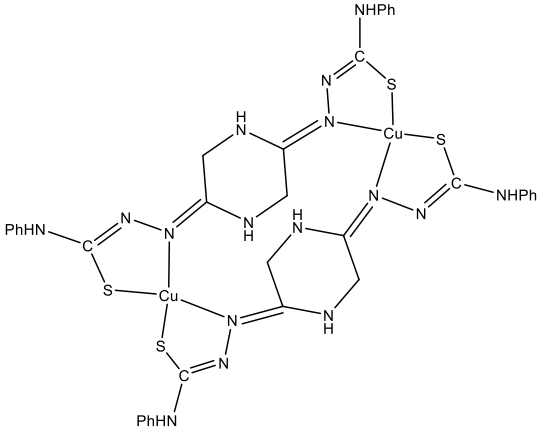 **[Cu(2,5 bptsc N-Ph]9**
10.	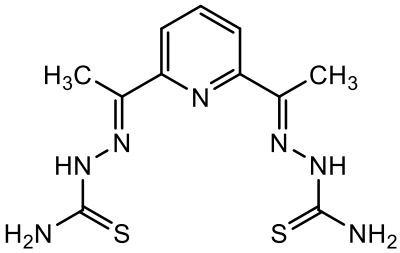 2,6 Diacetyl pyridine bisthiosemicarbazone **(2,6 H_2bdptsc, $^{10}H_2L$)**	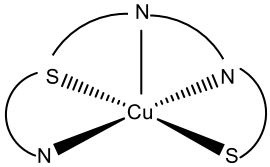 **[Cu(2,6 bdptsc]10**
11.	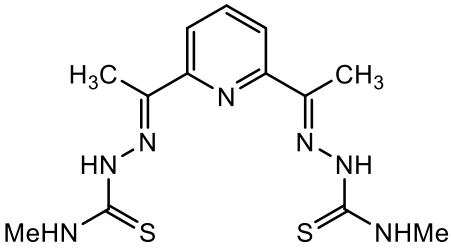 2,6 Diacetyl pyridine bis N-methyl thiosemicarbazone **(2,6 H_2bdptsc N-Me, $^{11}H_2L$)**	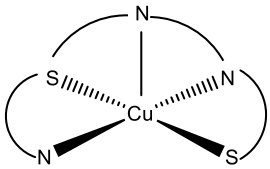 **[Cu(2,6 bdptsc,N-Me] 11**

12.	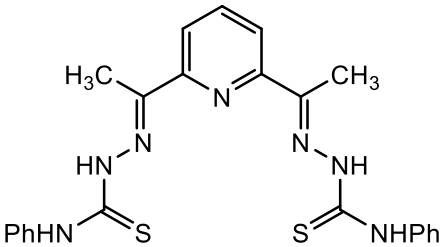 2,6 Diacetyl pyridine bis N-phenyl thiosemicarbazone **(2,6 H_2bdptsc N-Ph, $^{12}H_2L$)**	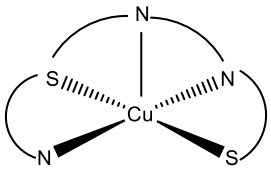 **[Cu(2,6 bdptsc,N-Ph] 12**

7.2 Binding studies: By Job Plot method

To confirm the structure of the complex (No. of binding sites) the representative ligand ligands **2,5 H_2bttsc** and **2,3 H_2bitsc** with **copper(II)** was selected for binding study using Uv-visible spectroscopy.

7.2.1 Binding ratio of 2,5 H_2bttsc with Copper(II)

UV-visible spectroscopy studies were carried out using methanol, acetonitrile, ethanol, and DMSO as solvents. However, DMSO was chosen as the preferred solvent due to its superior solubility and the distinct, well-defined absorption peaks observed. The concentration optimization is done with 0.3 mM solution of 2,5 H_2bttsc in DMSO. 1mM solution of copper(II) acetate was prepared in DMSO and 24 equivalents of this solution was added to 0.3mM solution of 2,5 H_2bttsc successively [196–198].

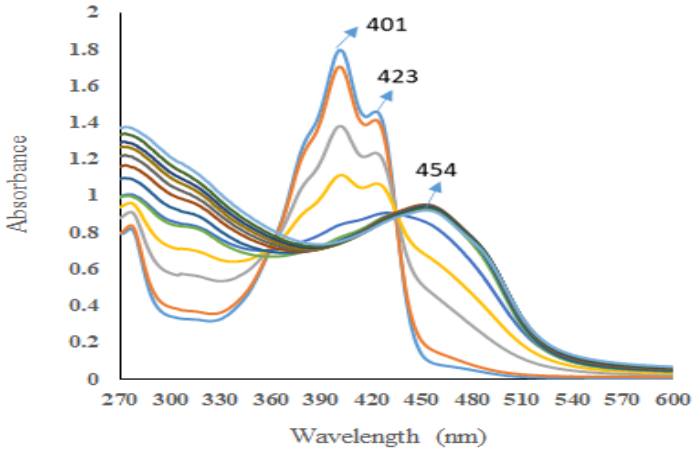

Figure 7.2.1: Absorbance recorded with sequential accumulation of 24 equivalent 1 mM Cu(II) solution in the solution of 0.3 mM 2,5 H_2bttsc.

The solution of 2,5 H_2bttsc give absorption peak at 401 nm along with a small shoulder peak at 423 nm with absorption intensities 1.793 and 1.457 respectively. Incremental addition of metal solution to the ligand resulted in a hypochromic shift accompanied by a bathochromic shift exhibiting the merging and shifting of the two peaks at 401 nm and 423 nm into a new peak at 454 nm are shown in Figure 7.2.1. This significant shift can be attributed to the redistribution of electrons between the metal and the ligand., which confirms the binding of ligand to metal [199,200]. The relative change in absorbance maxima (An/Ao) upon the sequential addition of 24 equivalents of Cu(II) ions is illustrated in Figure 7.2.2 (a)

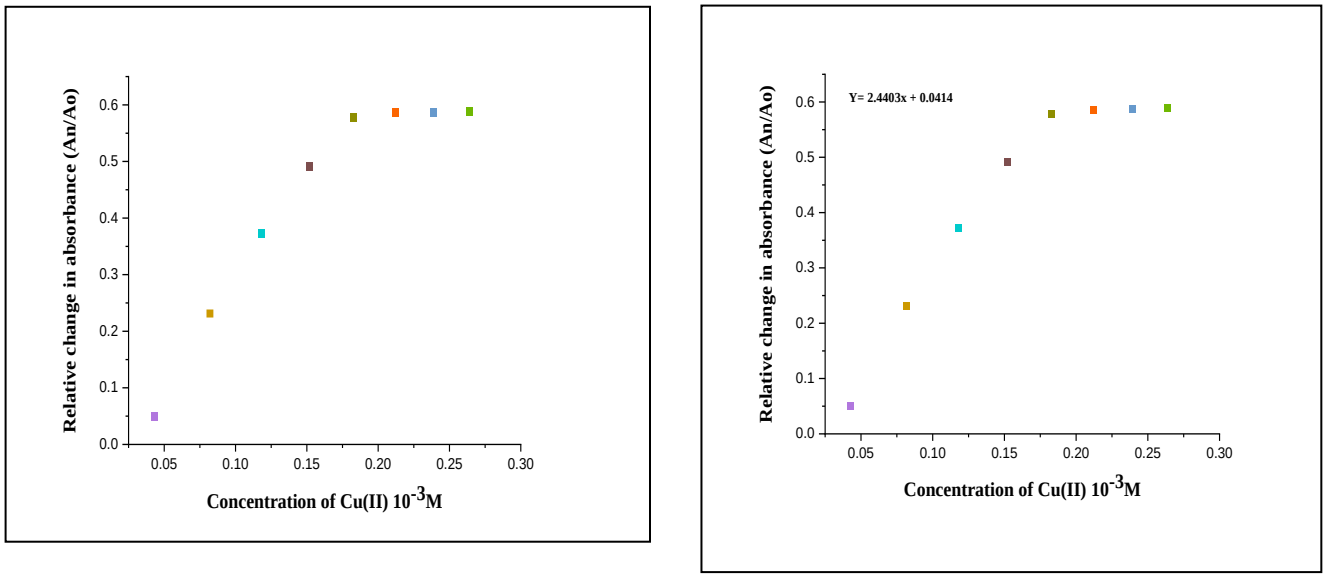

(a) **(b)**

Figure: 7.2.2: a) Comparative change in peak absorbance; **b)** Linear calibration curve [A_o- A_n/A_o Vs. (A_n/A_o) on sequential accumulation of 24 equivalent of Cu(II)]

The detection limit of Cu(II) has been calculated using Linear calibration curve [A_o-A_n/A_o] Vs. concentration of Cu(II) (Figure 7.2.2) and calculated to be 0.447 µM, and with the binding ratio of 2,5 H_2bttsc : Cu(II) as 1 : 1 suggest the strong chelation of 2,5 H_2bttsc with copper [173].

7.3 Binding ratio of 2,3 H_2bitsc with Copper(II)

After optimising the concentration value using absorption studies, 0.2 mM solution of 2,3 H_2bitsc was prepared. Metal salt solutions at a concentration of 1 mM using the same solvent, were prepared. The UV-visible titrations for the ion analysis were carried out by adding 30 equivalents of 1 mM of metal solution into 0.2 mM of ligand solution of 2,3 H_2bitsc [201–205].

The UV-visible titrations for the ion analysis were carried out by adding 30 equivalents of 1 mM of metal solution into 0.2 mM of ligand solution of **2,3 H_2bitsc.** Upon adding Cu(II) ions successively, the intensity of absorption was noticeably reduced between 353nm and 391nm (Figure 7.3.1), whereas the intensity of absorption increased below 353nm and above 391nm, leading to isosbestic points at these specific wavelengths. At the same time the concentration of Cu(II) increased, a 2 nm hypsochromic shift was observed, which confirms the binding of the metal ions by the ligand [206].

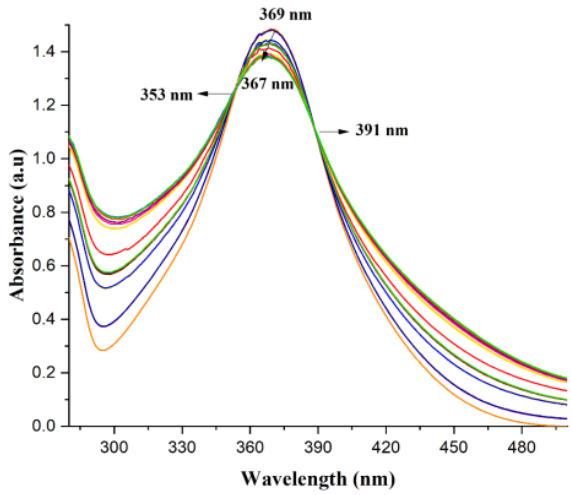

Figure 7.3.1: Uv visible responses to the addition of 30 equivalents of 1 mM Cu(II) solution to 0.2mM solution of 2,3 H_2bitsc

The detection limit of Cu(II) was obtained using a correlation plot of A_o-A_n/A_o against conc. of Cu(II) ions (Figure 7.3.2), where absorbance maxima with subsequent addition of Copper(II) ions is A_n, and of 2,3 H_2bitsc is A_o at 0.2mM [207]. Detection limit of Cu(II) was found to be 0.438 µM. The binding ratio obtained is 1:1 (2,3 H_2bitsc: Cu(II)) which indicates strong binding of 2,3 H_2bitsc with copper [206].

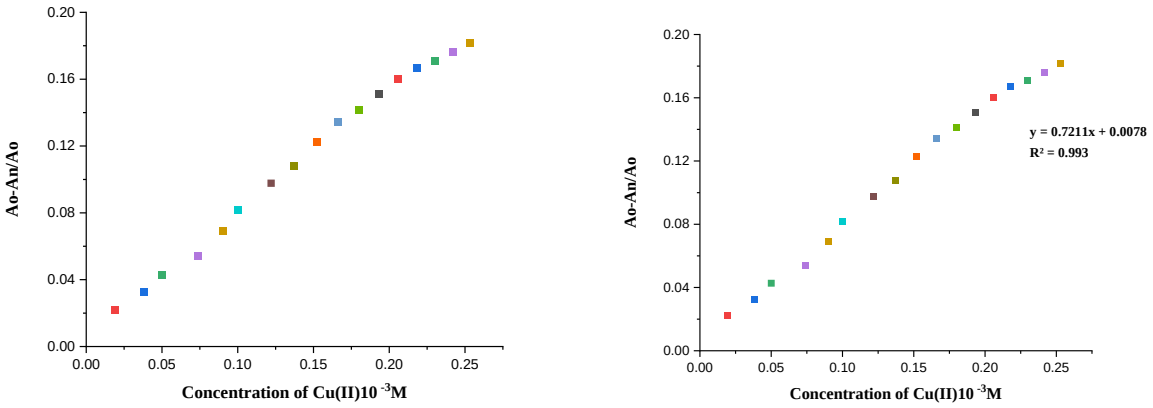

Figure 7.3.2: a) Comparative change in peak absorbance; b) [A_o-A_n/A_o] vs concentration of Cu(II) correlation plot.

7.4 IR Spectroscopy:

The important IR peaks of bisthiosemicarbazones and their Cu(II) complexes are mentioned in Table 7.5.1 and spectra are given in Figures 7.4.1-7.4.12. The ν(N-H) bands in ligands **$^{1}H_2L$-$^{12}H_2L$** appeared in the range 3461-3204 cm^{-1} which showed a slight high energy shift in complexes(3409-3200 cm^{-1}). The bands due to –N^2H – group appeared in the range 3190-3126 cm^{-1}. But on complexation this band gets disappeared in all the complexes (**25-36)** which suggested deprotonation during complexation and coordination of bisthiosemicarbazone to metal centre in dianionic form [175]. The bands of υ(C=N) in the range, 1698-1594 cm^{-1} in the ligands is shifted to lower frequency in complexes **25-36** and appeared in the range 1679-1537 cm^{-1}The specific ν(C=S) band observed in the range, 896-812 cm^{-1} in **$^{1}H_2L$-$^{12}H_2L$** which get shifted to lower energy in complexes (**25-36)** and observed in the range, 787-746 cm^{-1}. Significant low energy shift of this band indicates binding of bis- ligand in thiolate form [176].

Table 7.4.1: Significant IR peaks of bisthiosemicarbazones (**$^{1}H_2L$–$^{12}H_2L$**) and their Copper(II) complexes (**25-36**)

Synthesized Ligands and Metal complexes	**υ(NH_2)**	**υ(-NH-)**	**υ(C=N)**	**υ(C=C)**	**δ (NH_2)**	**υ(C=S)**
(2,5 H_2bttsc, $^{1}H_2L$)	3409m, 3277m	3155m	1600s	1583m	1535s	836s
[Cu(bttsc)] **25**	3409m, 3278m	-	1599s	1535m	1451s	781s
(2,5 H_2bttscN-Me, $^{2}H_2L$)	3373m	3155w	1594s	1462m	-	812s
[Cu(bttsc,N-Me)] **26**	3372m	-	1537s	1508m	-	761s
(2,5 H_2bttsc N-Ph, $^{3}H_2L$)	3303m	3156w	1636s	1594w	-	895s
[Cu(bttsc,N-Ph)] **27**	3390m, 3204m	-	1679s	1595	-	747s
(2,3 H_2bitsc, $^{4}H_2L$)	3332m, 3259m	3156w	1698s	1618w	1584s	851s
[Cu(bitsc)] **28**	3239m	-	1679s	1609m	1556m	785s
(2,3H_2bitsc-N^1-Me,$^{5}H_2L$)	3461m, 3207m	3100w	1683s	1616m	-	831s
[Cu(bitsc,N-Me)] **29**	3223m	-	1643s	1607m	-	780s
(2,3 H_2bitsc-N^1-Ph)	3290m	3173w	1685s	1591m	-	827s
[Cu(bitsc,N-Ph)] **30**	3205m	-	1654s	1596m	-	778s

(2,5 H_2bptsc, ^7H_2L)	3356m, 3253m	3166m	1640s	1526s	1512m	895s
[Cu(bptsc)] **31**	3407m	-	1598s	1487m	1428m	763s
(2,5H_2bptsc N-Me, ^8H_2L)	3335m, 3287m	3197m	1642s	1558s	-	804s
[Cu(bptsc, N-Me)] **32**	3290m	-	1550s	1424m	-	767
(2,5 H_2bptsc N-Ph, ^9H_2L)	3301m	3158m	1639s	1466m	-	829s
[Cu(bptsc,N-Ph)] **33**	3277m	-	1638s	1595m	-	749s
(2,6 H_2bdptsc, $^{10}H_2L$)	3423m, 3209m	3158m	1606 s	1513 m		827s
[Cu(dptsc)] **34**	3311m, 3200m	-	1627s	1588m	1461m	746s
(2,6 H_2bdptsc N-Me, $^{11}H_2L$)	3450m, 3329m	3190m	1634s,	1555m	-	836s
[Cu(dptsc,N-Me)] **35**	3295m	-	1579s	1501m	-	787s
(2,6 H_2bdptsc N-Ph, $^{12}H_2L$)	3303m	3156m	1636 s,	1594m	-	836s
[Cu(dptsc,N-Ph)] **36**	3374m, 3246m	-	1591s	1527m	-	752s

7.5 Mass Spectrometry:

The mass spectra of compounds (**25-36)** are given in Figures **7.6.1– 7.6.12**. The molecular ion peak $[M]^+$ was found and listed in Table 7.5.1. All the complexes have m/z values in well agreement with proposed stoichiometry. The parental ion peak in $(m/z)^+$ found at 345.01 amu (**25**), 376.97 amu (**26**), 500.08 amu (**27**), 355.06 amu (**28**), 381.29 amu (**29**), 505.22 amu (**30**), 325.25 amu (**31**), 349.11 amu (**32**), 474.12 amu (**33**), 372.17 amu (**34**), 399.17 amu (**35**), 524.15 amu (**36**) confirms the formation of bisthiosemicarbazones.

Table 7.5.1: The m/z values (amu) derived from mass spectra and expected formula of complexes **(25-36).**

Sr. No.	Parent peak (experimental mass)	Expected formula for parent ion $(m/z)^+$
1.	343.12	$[Cu(C_8H_{10}N_6S_3)]$ **25**
2.	376.97	$[Cu(C_{10}H_{14}N_6S_3)]$ **26**
3.	500.08	$[Cu(C_{20}H_{16}N_6S_3)]$ **27**
4.	355.06	$[Cu(C_{10}H_9N_7S_2)]$ **28**
5.	381.29	$[Cu(C_{12}H_{13}N_7S_2)]$ **29**
6.	505.22	$[Cu(C_{22}H_{17}N_7S_2)]$ **30**
7.	325.25	$[Cu(C_6H_{12}N_8S_2)]$ **31**
8.	349.11	$[Cu(C_8H_{16}N_8S_2)]$ **32**
9.	474.12	$[Cu(C_{18}H_{20}N_8S_2)]$ **33**
10.	371.18	$[Cu(C_{11}H_{13}N_7S_2)]$ **34**
11.	399.17	$[Cu\ (C_{13}H_{17}N_7S_2)]$ **35**
12.	524.15	$[Cu(C_{23}H_{21}N_7S_2)]$ **36**

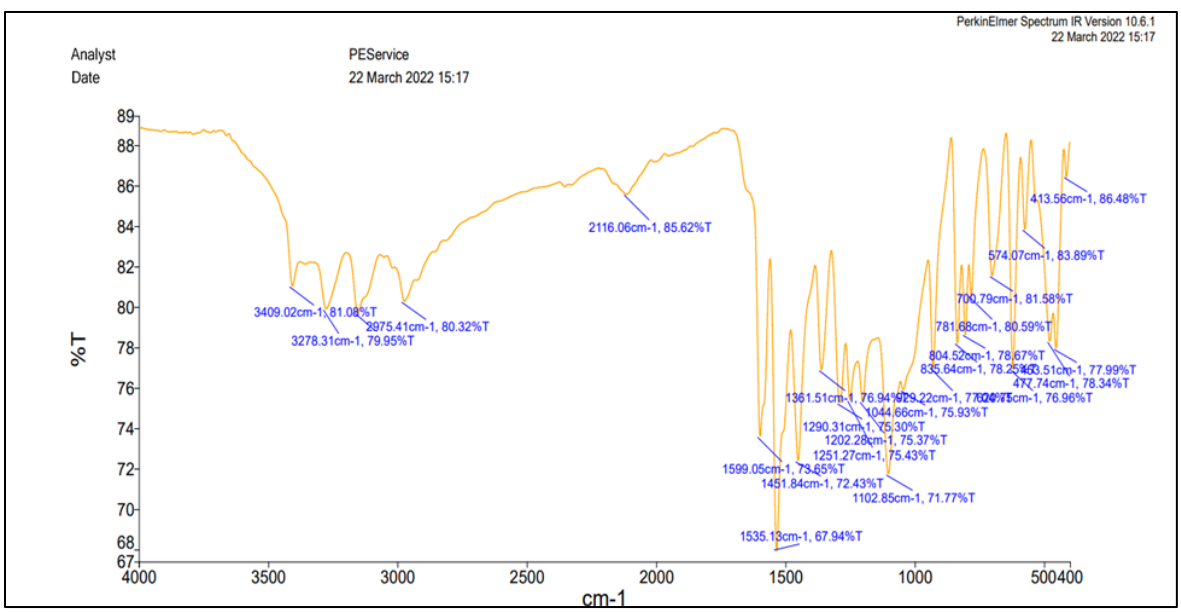

Figure 7.4.1: IR Spectra of [Cu(bttsc)] **25**

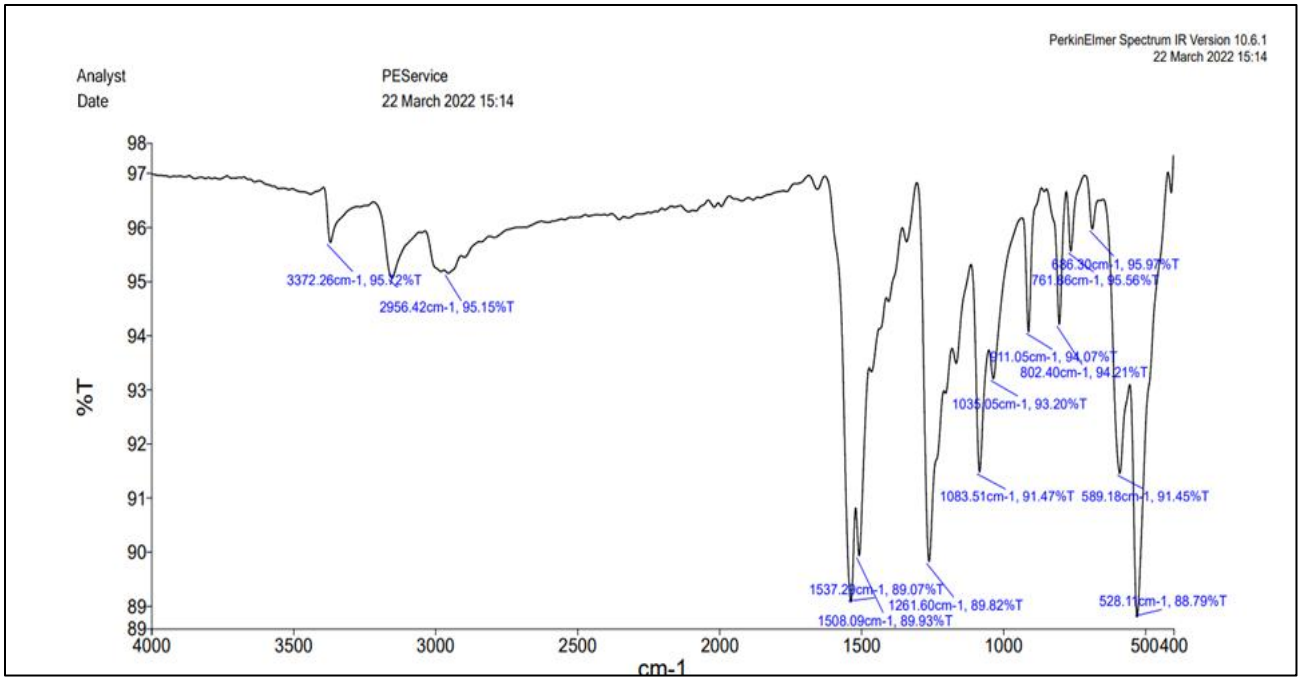

Figure 7.4.2: IR Spectra of [Cu(bttsc,N-Me)] **26**

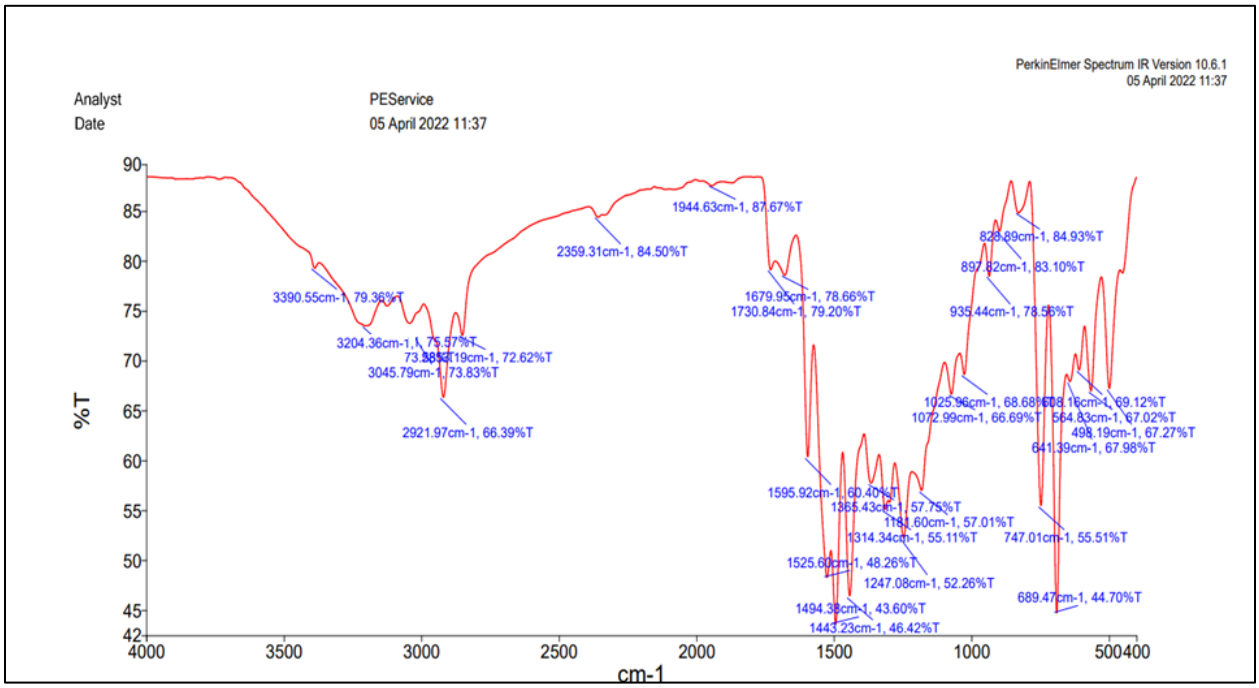

Figure 7.4.3: IR Spectra of [Cu(bttsc,N-Ph)] **27**

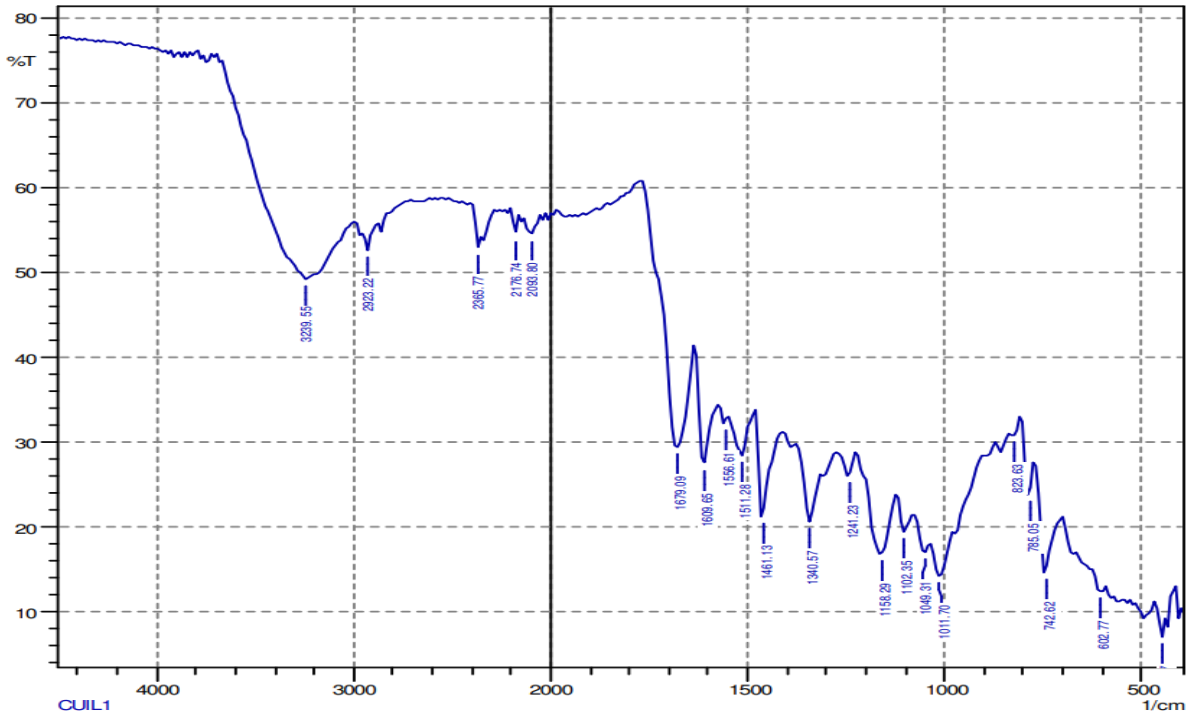

Figure 7.4.4: IR Spectra of [Cu(bitsc)] **28**

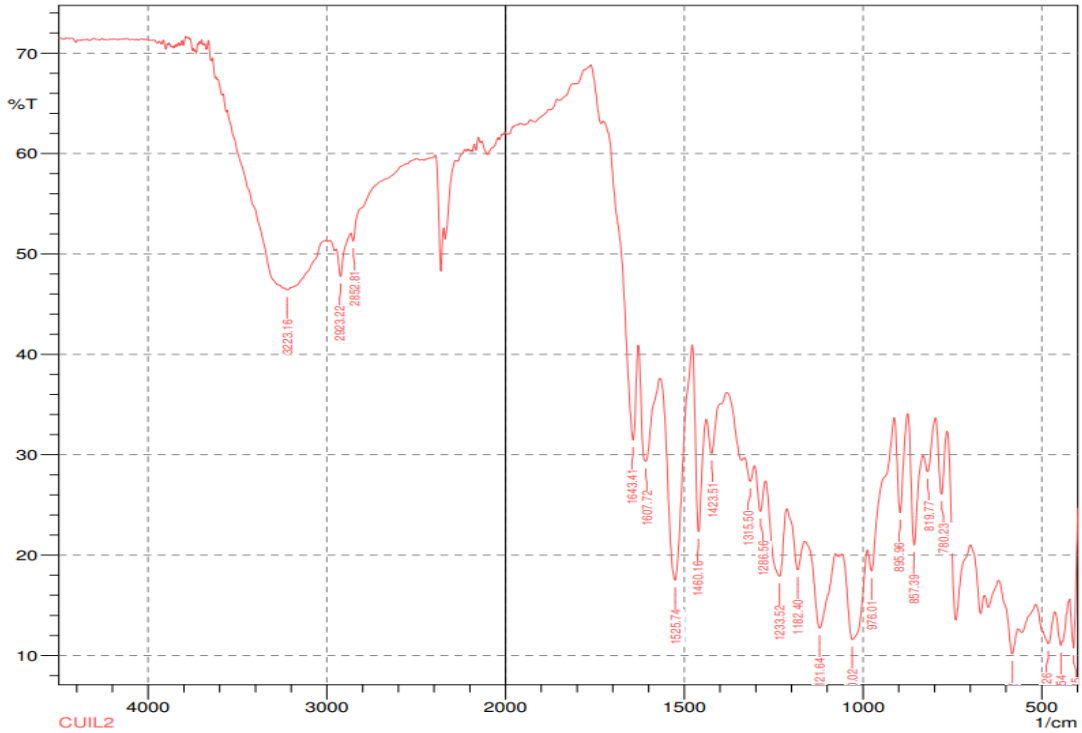

Figure 7.4.5: IR Spectra of [Cu(bitsc,N-Me)] **29**

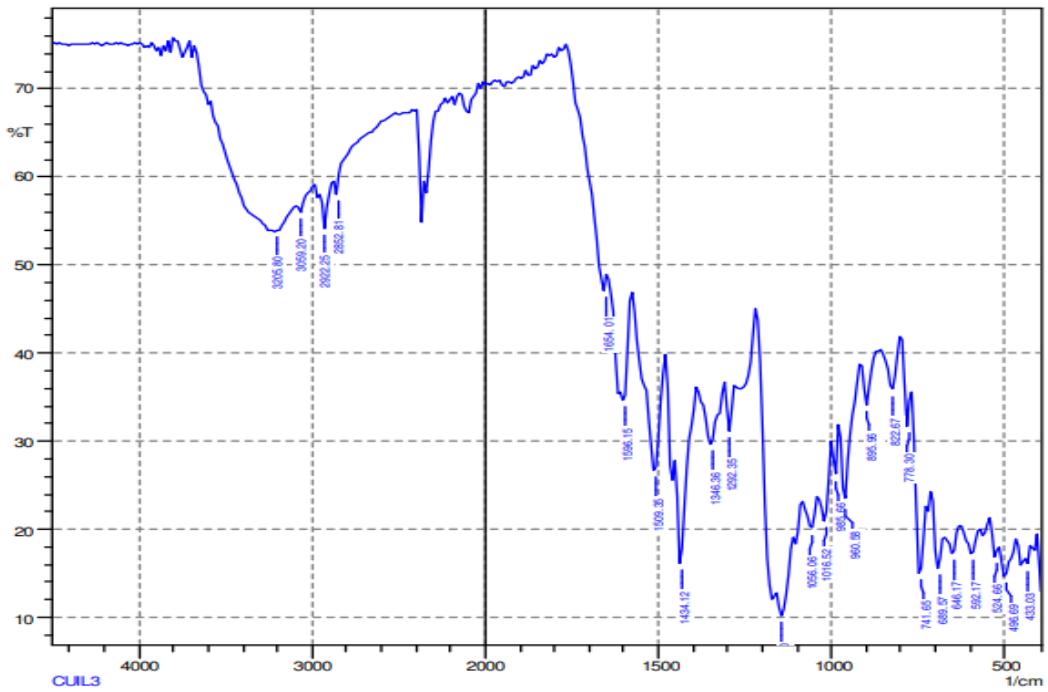

Figure 7.4.6: IR Spectra of [Cu(bitsc,N-Ph)] **30**

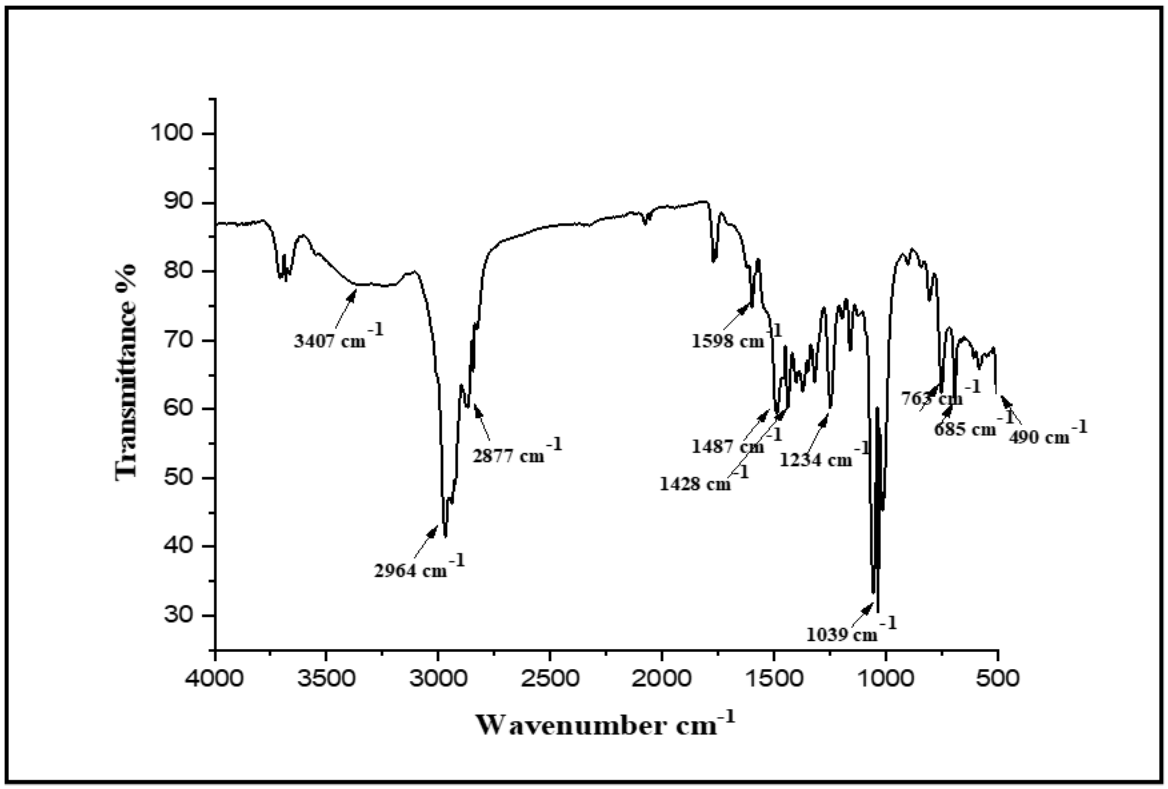

Figure 7.4.7: IR Spectra of [Cu(bptsc)] **31**

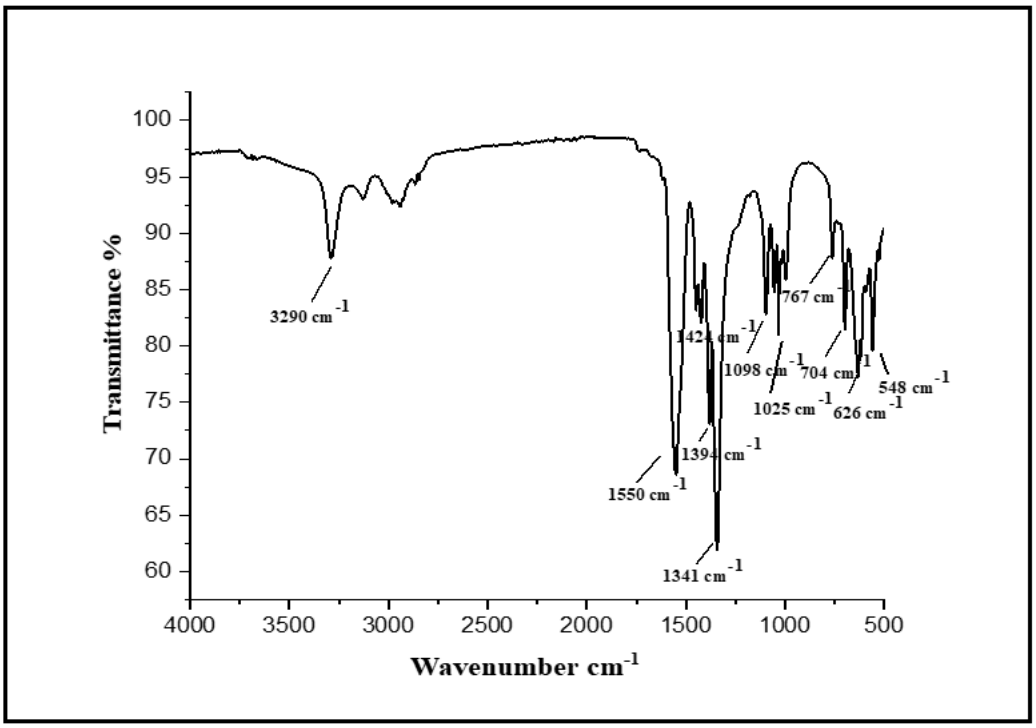

Figure 7.4.8: IR Spectra of [Cu(bptsc,N-Me)] **32**

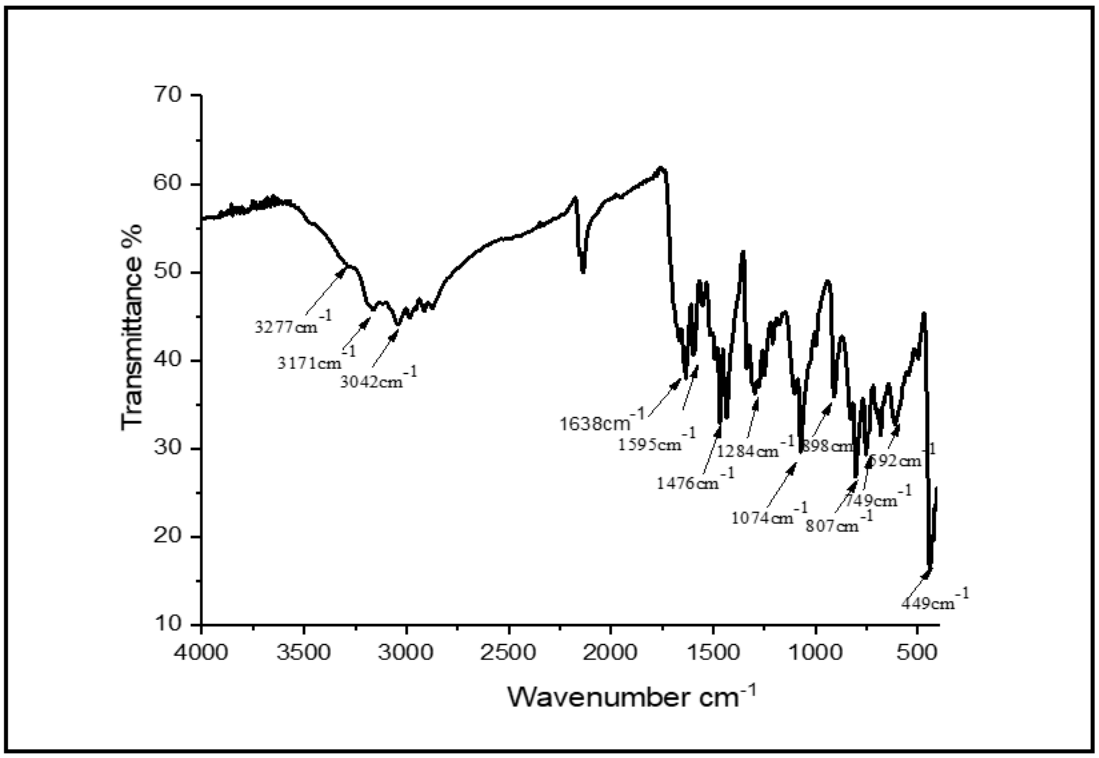

Figure 7.4.9: IR Spectra of [Cu(bptsc,N-Ph)] **33**

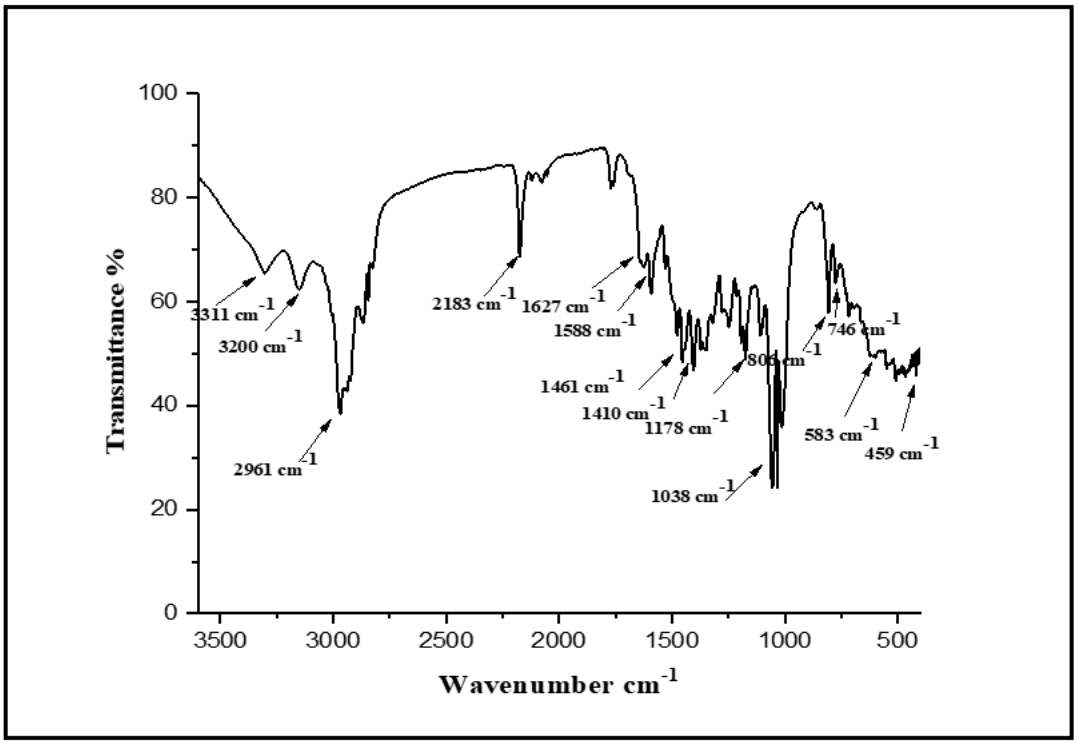

Figure 7.4.10: IR Spectra of [Cu(bdptsc)] **34**

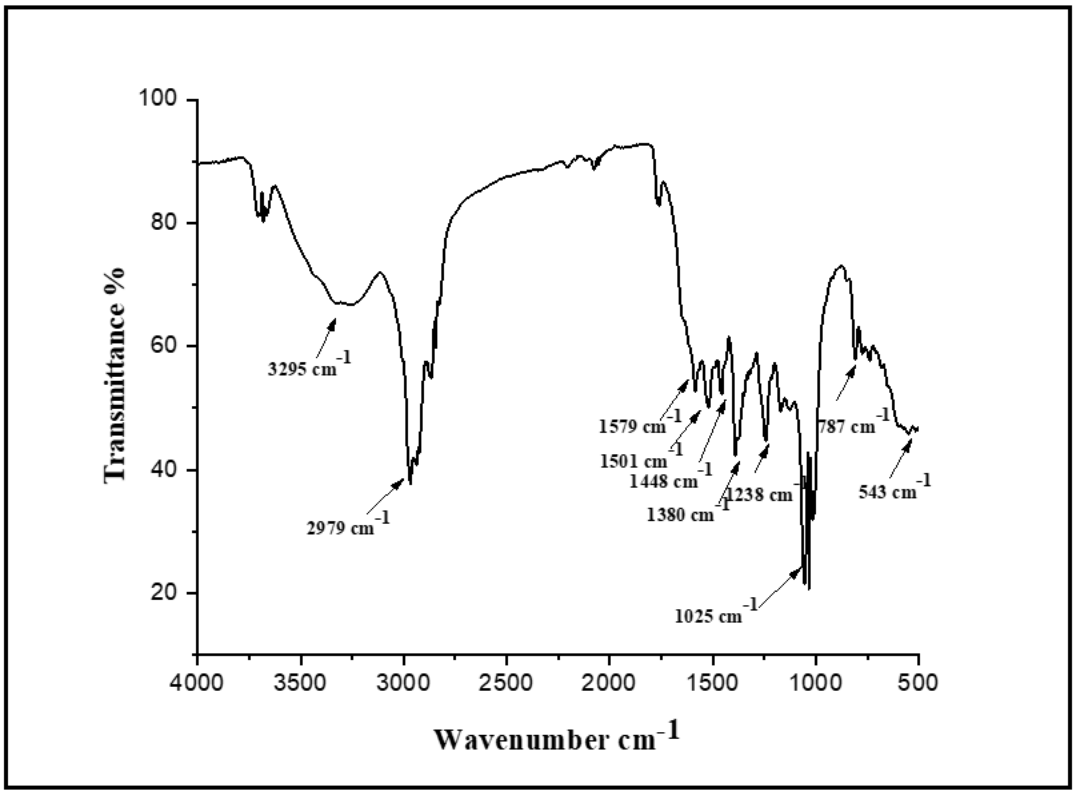

Figure 7.4.11: IR Spectra of [Cu(bdptsc,N-Me)] **35**

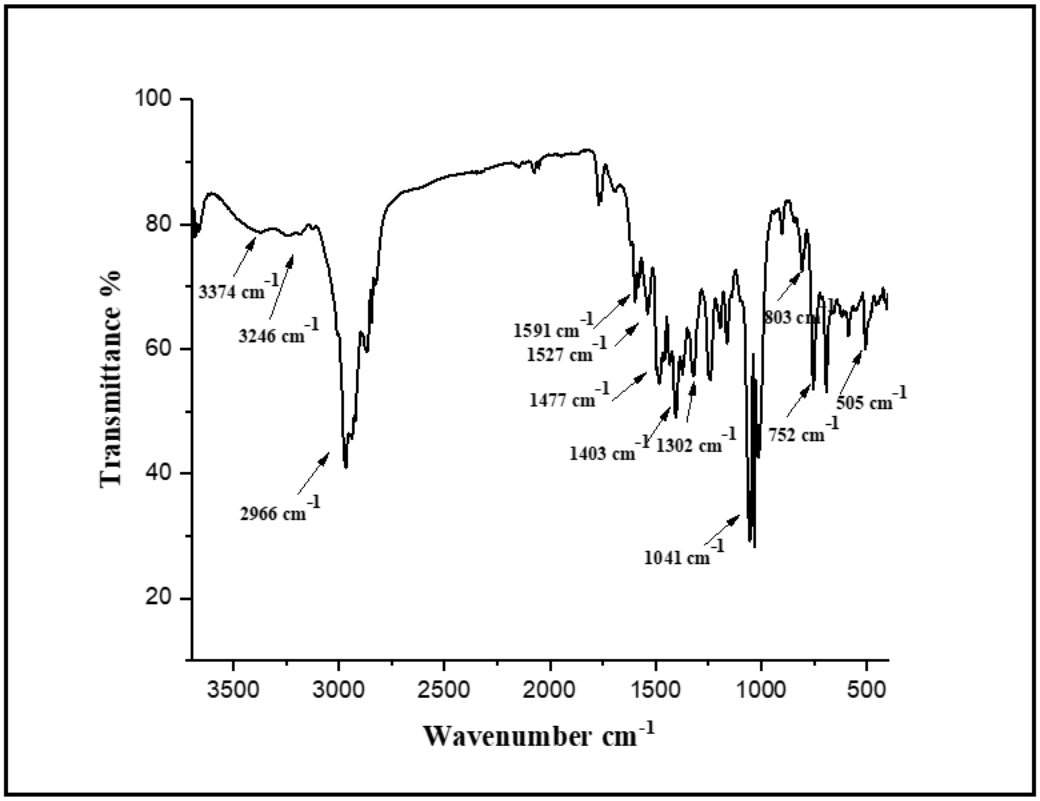

Figure 7.4.12: IR Spectra of [Cu(bdptsc,N-Ph)] **36**

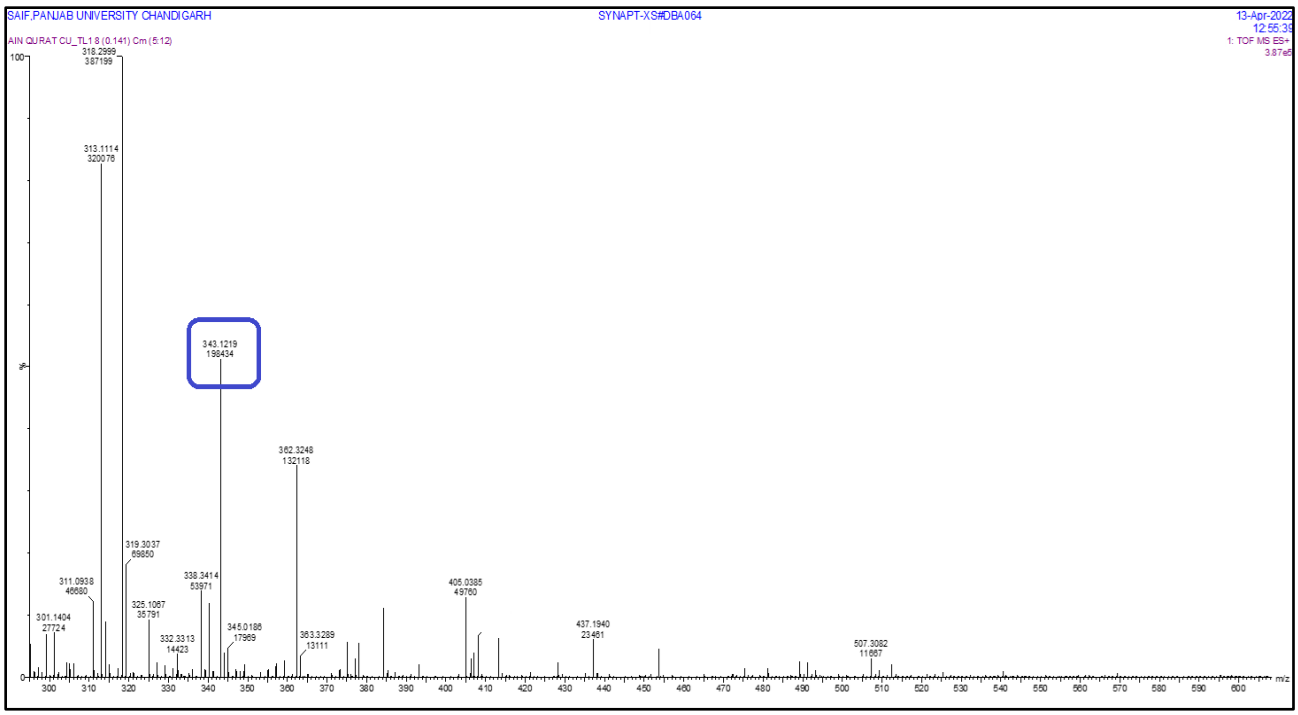

Figure 7.5.1: Mass spectrometry of complex [Cu(bttsc)] **25**

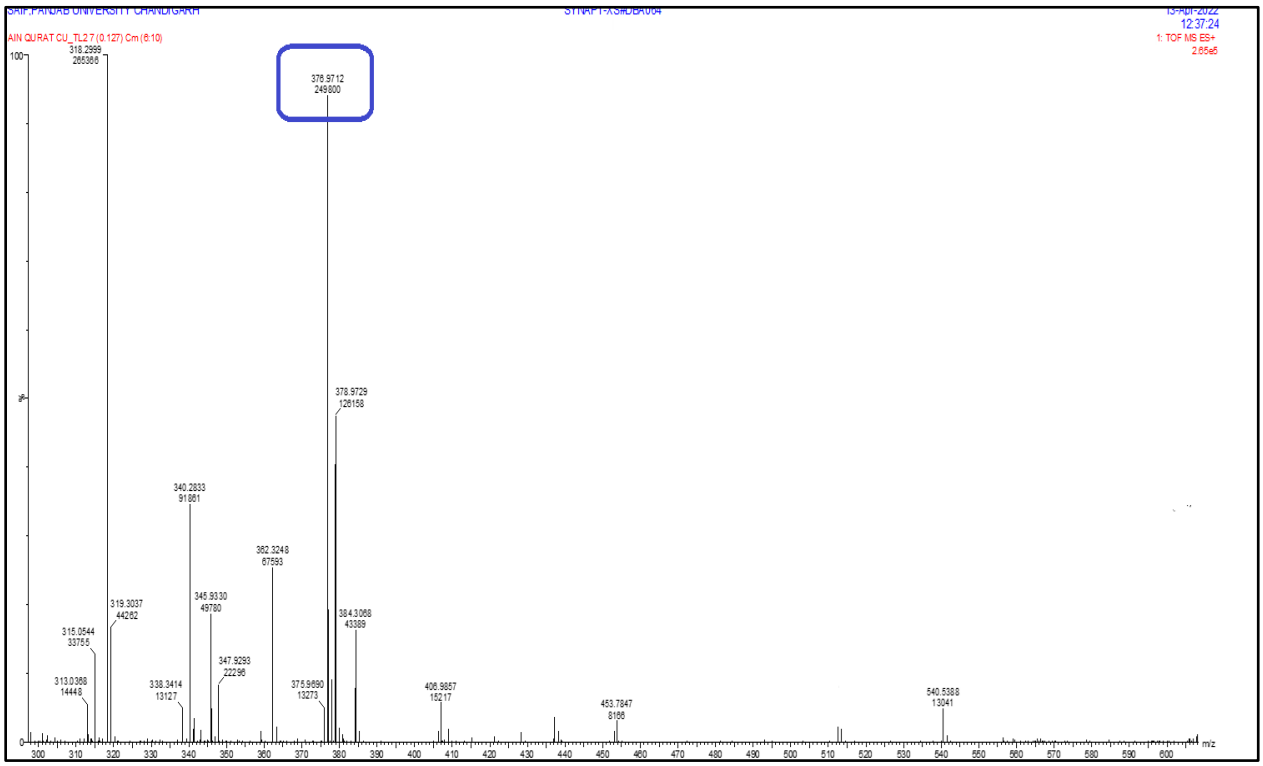

Figure 7.5.2: Mass spectrometry of complex [Cu(bttsc,N-Me)] **26**

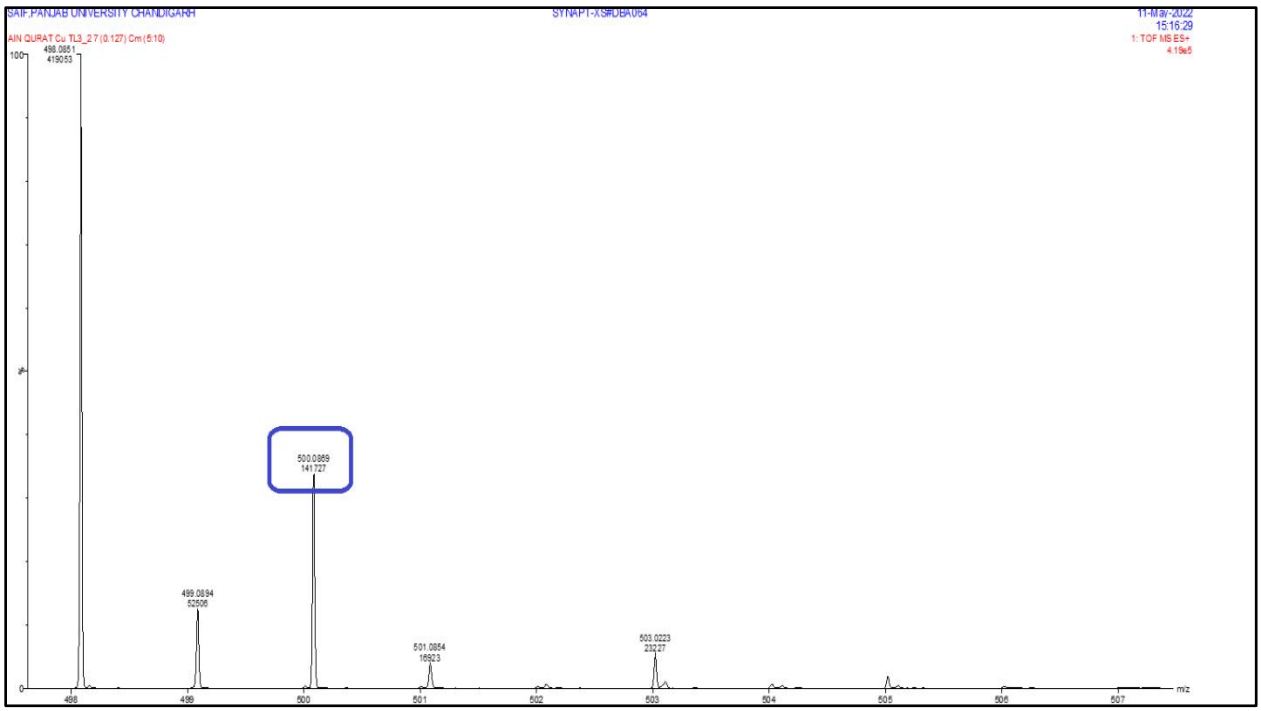

Figure 7.5.3: Mass spectrometry of complex [Cu(bttsc,N-Ph)] **27**

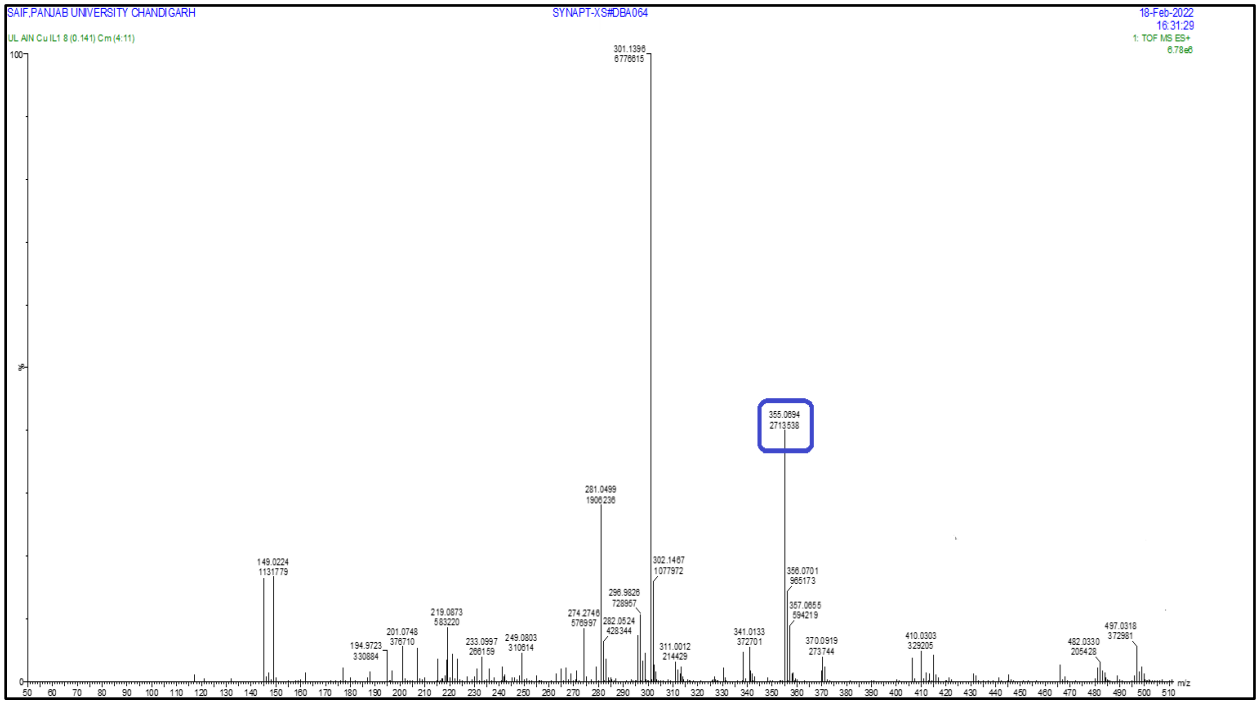

Figure 7.5.4: Mass spectrometry of complex [Cu(bitsc)] **28**

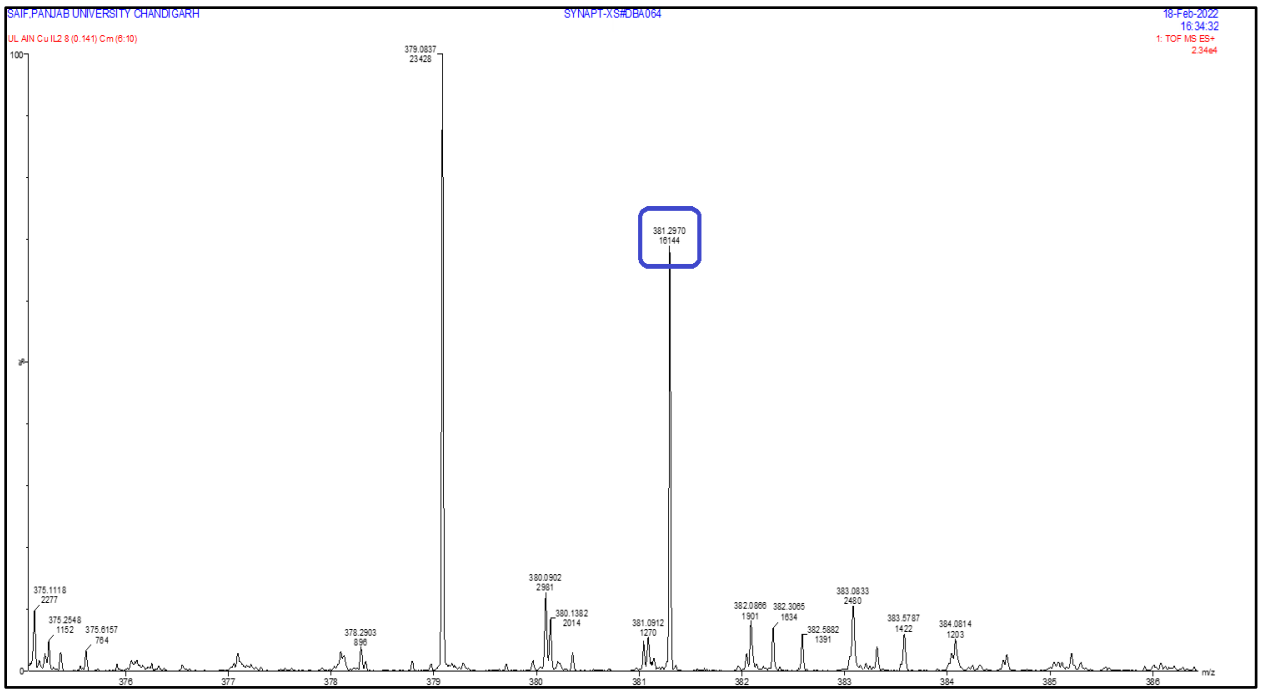

Figure 7.5.5: Mass spectrometry of complex [Cu(bitsc,N-Me)] **29**

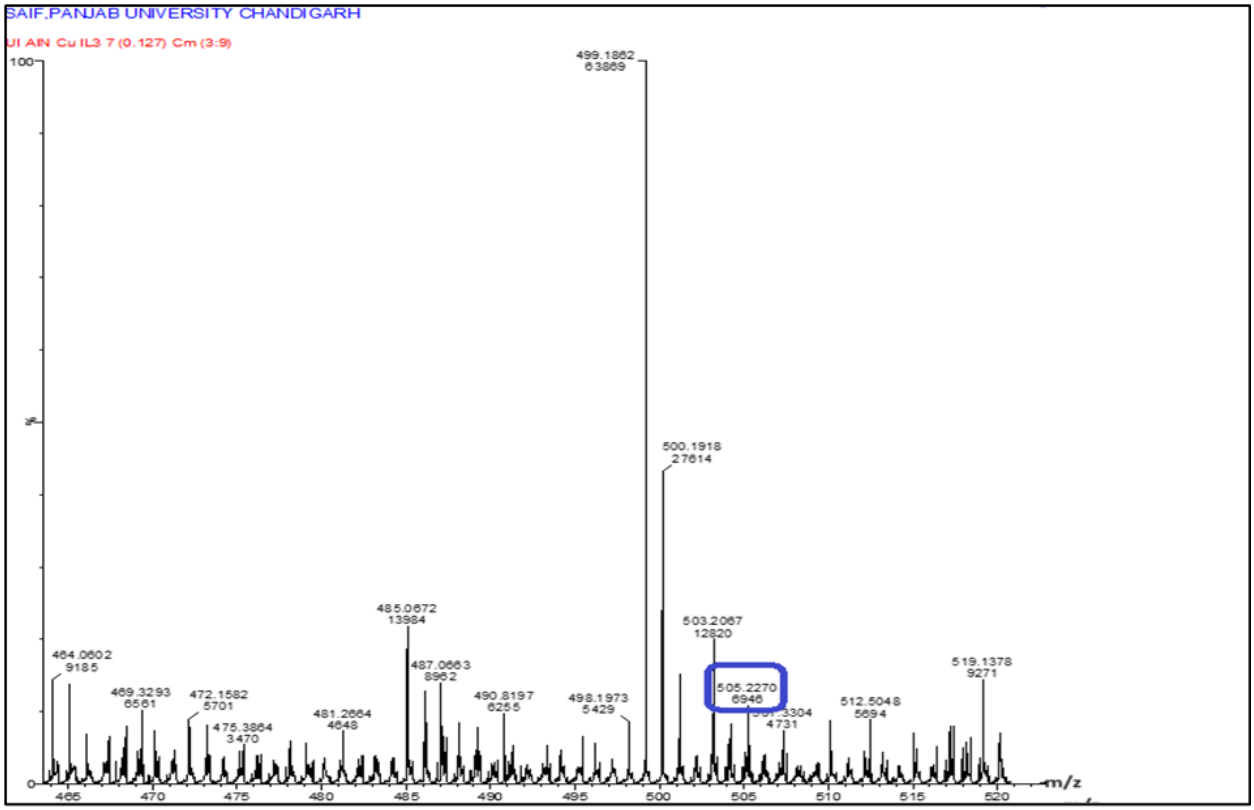

Figure 7.5.6: Mass spectrometry of complex [Cu(bitsc,N-Ph)] **30**

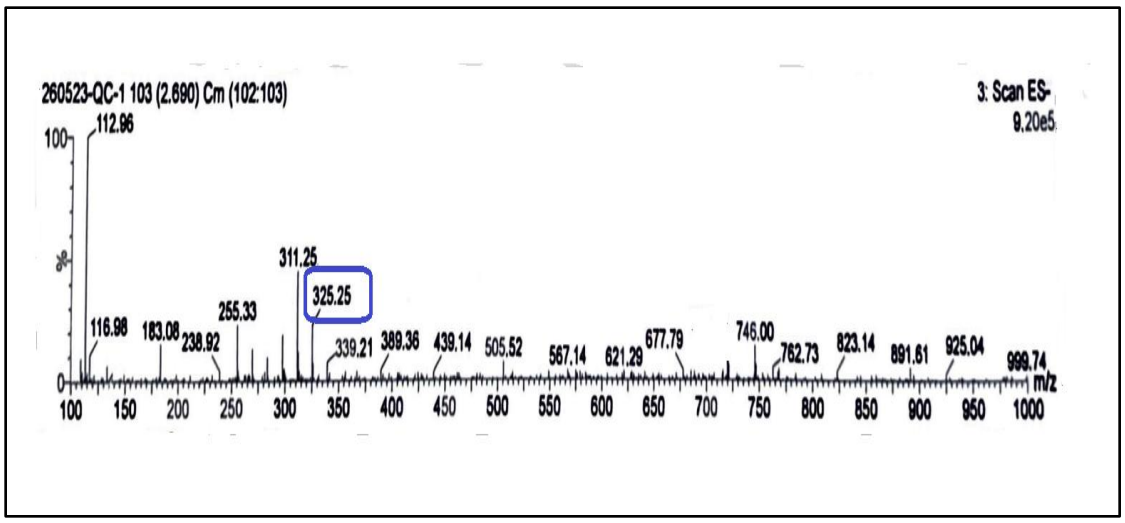

Figure 7.5.7: Mass spectrometry of complex [Cu(bptsc)] **31**

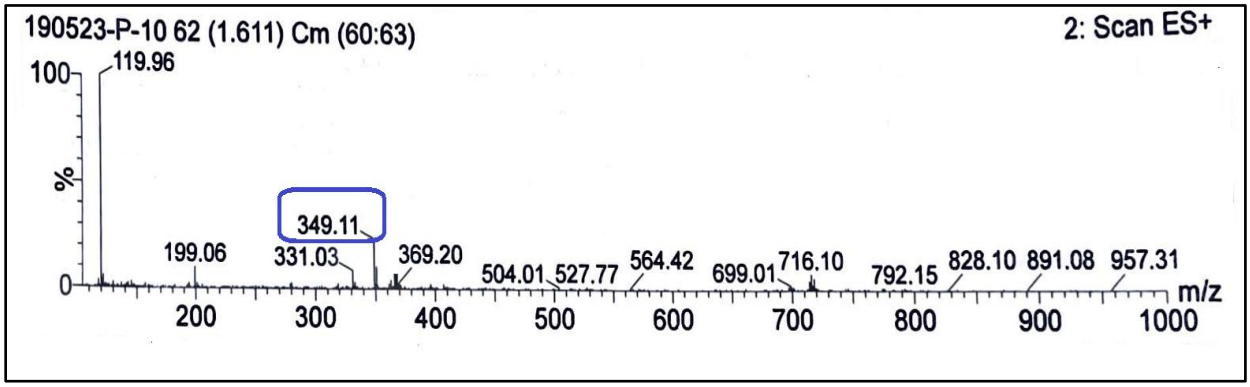

Figure 7.5.8: Mass spectrometry of complex [Cu(bptsc,N-Me)] **32**

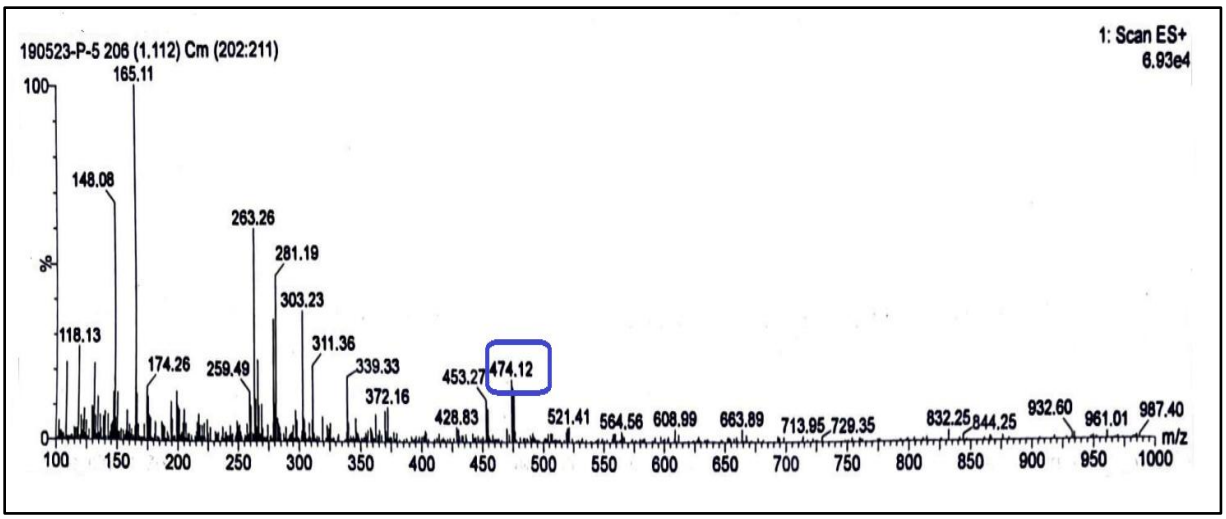

Figure 7.5.9: Mass spectrometry of complex [Cu(bptsc,N-Ph)] **33**

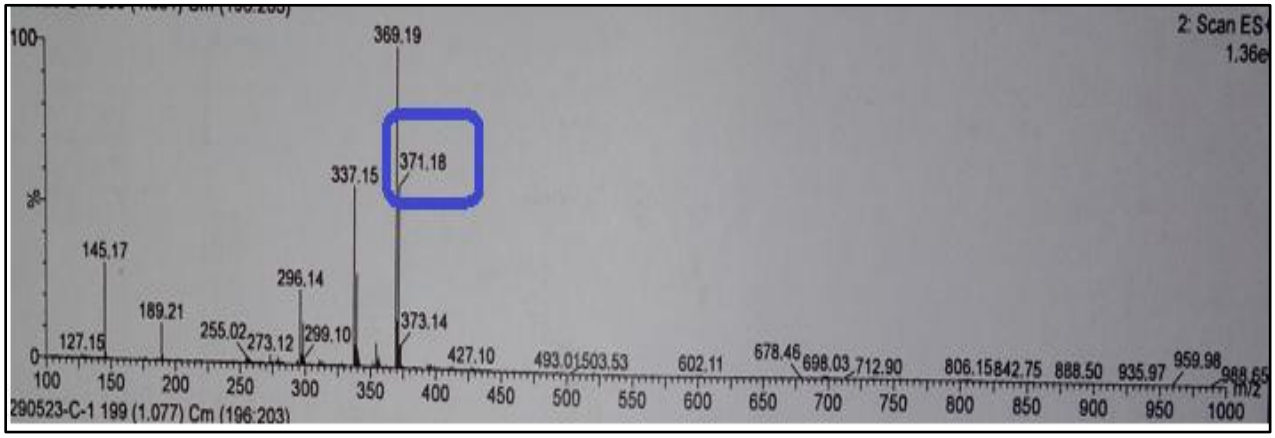

Figure 7.5.10. Mass spectrometry of complex [Cu(dptsc)] **34**

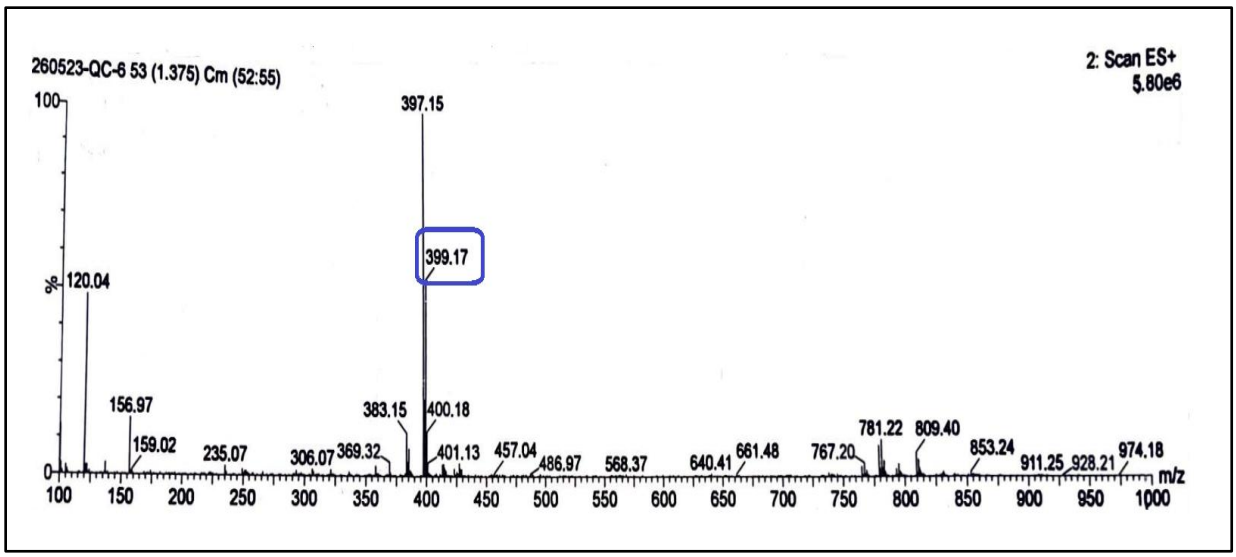

Figure 7.5.11. Mass spectrometry of complex [Cu(dptsc,N-Me)] **35**

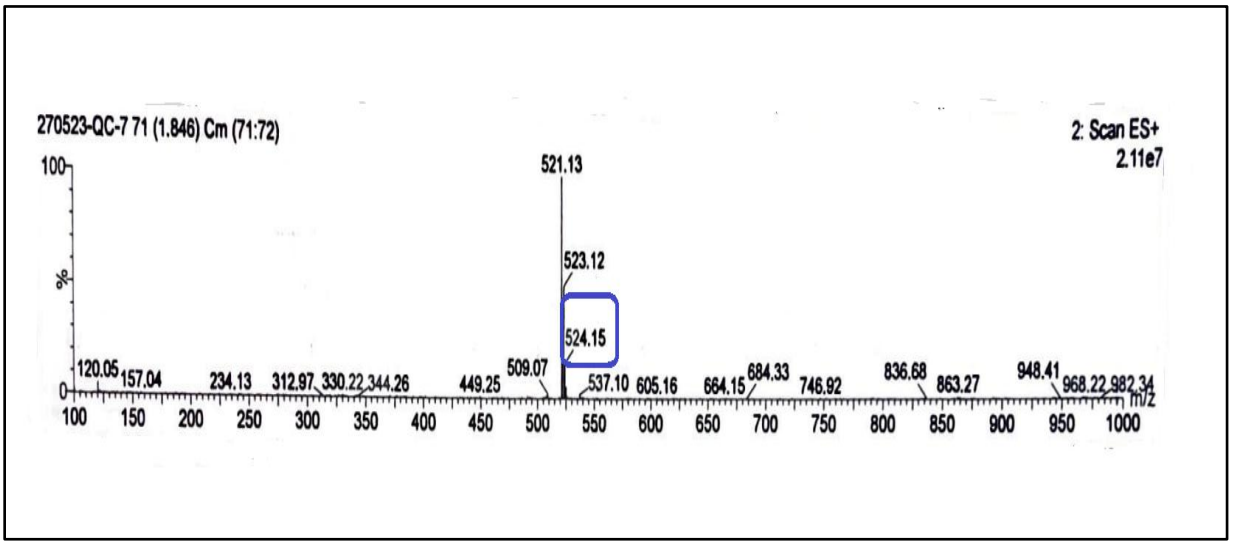

Figure 7.5.12: Mass spectrometry of complex [Cu(dptsc,N-Ph)] **36**

7.6 ESR spectroscopy:

The ESR spectra of copper (II) complexes **25-36** was done at room temperature as well as at 125k. The experimental calculations are given in Table 7.6.1 and 7.6.2. All the spectra are presented in Figures 7.6.1-7.6.12. The presence of two different g values ($g_{\parallel}$ and $g_{\perp}$) suggests axial symmetry of the complexes (**25-36)**. Experimentally found $g_{\parallel}$ values of complexes are greater than $g_{\perp}$, which further are more than g value of free electron supports ground term $d_{x^2-y^2}$ in square planar structure [208]. Geometric parameter *G* was calculated using (Equation-5) to measure the exchange interaction between copper centre.

$$G_{(axial)} = \frac{g_{\parallel} - 2.0023}{g_{\perp} - 2.0023} \qquad \ldots\ldots\ldots\ldots\ldots(5)$$

According to Hathaway and Tomlinson, exchange interaction will be negligible if the alignment of tetragonal axis is parallel ($G > 4$), otherwise significant exchange interaction with considerable misalignment ($G < 4$) will be observed [209,210]. The G value of 2.19 **(26)**, 1.62 **(27)**, 2.71 **(28)**, 1.55 **(29)**, and 3.34 **(30)** respectively indicate a significant exchange interaction between copper center, whereas exchange interaction is negligible in complexes **25** (G = 5.15). The structure of complexes and encompass of distortion from regular geometry can determined from (empirical factor), $f = g_{\parallel} / A_{\parallel}$ (cm^{-1}) [211–213]. From the literature, it has been observed that square planar complexes have empirical factor in the range, 105-146 cm^{-1} [210]. The observed value of f for **25-36,** lies in the range, 134-148 cm^{-1} for complexes **25-36** indicating a square planar geometry with slight distortion for these complexes.

The g_{iso} and A_{iso} has been calculated using (Equation 9 and 10) respectively [214].

$$g_{iso} = g_{\parallel} + 2g_{\perp} / 3 \qquad \ldots\ldots\ldots..(9)$$

$$A_{iso} = A_{\parallel} + 2A_{\perp} / 3 \qquad \ldots\ldots\ldots(10)$$

From g_{iso} and A_{iso} values, sigma bonding parameter (α^2) can be calculated using (Equation-11) [213].

$$\alpha^2 = \frac{A_{iso}}{PK} + \frac{g_{iso} - 2.0023}{K} \qquad \ldots\ldots\ldots(11)$$

In this case, (K) stands for Fermi contact (K = 0.43), and (P) stands for free ion dipole term (P = 0.036 cm^{-1}) [201]. Pure ionic bonding is supported by a value of $\alpha^2 = 1$, whereas pure covalent bonding is supported by a value of 0.5. The α^2 value of complexes **25-36** falls in the range, 0.65 – 0.87 thus confirms a mixture of ionic and covalent bonding.

Table 7.6.1: ESR calculations for complexes **25-36**

Compound	Polycrystalline state (at RT)	$g_\perp$	$g_\parallel$	g_{iso}	$^*A_\parallel$	$^*A_\perp$	$^*A_{iso}$
[Cu(2,5 bttsc)] **25**	2.40 / 2.08 ($g_\parallel$ / $g_\perp$)	2.08	2.40	2.18	174	40	66.6
[Cu(2,5bttsc-N-Me)] **26**	2.15 / 2.07 ($g_\parallel$ / $g_\perp$)	2.07	2.15	2.18	160	45	70.3
[Cu(2,5bttsc-N-Ph)] **27**	2.20/ 2.12 ($g_\parallel$ / $g_\perp$)	2.12	2.20	2.14	148	45	79.3
[Cu(2,3H_2bitsc)] **28**	2.24/2.09 ($g_\parallel$ / $g_\perp$)	2.09	2.24	2.12	170	38	65.1
[Cu(2,3H_2bitsc-N^1-Me)] **29**	2.17/2.11($g_\parallel$ /$g_\perp$)	2.11	2.17	2.13	145	25	65.0
[Cu(2,3H_2bitsc-N^1-Ph)] **30**	2.26/2.08($g_\parallel$ /$g_\perp$)	2.08	2.26	2.14	165	45	85.2
[Cu(2,5H_2bptsc)]**31**	2.46/2.147($g_\parallel$ /$g_\perp$)	2.147	2.46	2.24	169	50	57.1
[Cu(2,5H_2bptsc-N^1-Me)] **32**	2.18/2.146($g_\parallel$ /$g_\perp$)	2.146	2.48	2.25	168	51	58.2
[Cu(2,5H_2bptsc-N^1-Ph)] **33**	2.48/2.143($g_\parallel$ /$g_\perp$)	2.143	2.48	2.26	170	52	91.3
[Cu (2,6 H_2bdptsc)] **34**	2.2/ 2.10 ($g_\parallel$ / $g_\perp$)	2.10	2.2	2.12	147	44	79.1
[Cu (2,6 H_2bdptsc - N^1-Me)] **35**	2.45/2.12($g_\parallel$ /$g_\perp$)	2.12	2.45	2.22	168	49	56.9
[Cu (2,6 H_2bdptsc - N^1-Ph)] **36**	2.25/2.10($g_\parallel$ /$g_\perp$)	2.10	2.25	2.15	164	44	85

* Expressed in units of cm^{-1} multiplied by a factor of 10^{-4}

Table 7.6.2: ESR bonding parameters for complexes **25-36**

Compound	**G** (at RT)	α^2	f^a
[Cu(2,5 bttsc)] **25**	5.15	0.83	137
[Cu(2,5 bttsc-N-Me)] **26**	2.19	0.65	134
[Cu(2,5 bttsc-N-Ph)] **27**	1.62	0.83	148
[Cu(2,3 H_2bitsc)] **28**	2.71	0.69	131
[Cu(2,3 H_2bitsc-N^1-Me)] **29**	1.55	0.71	146
[Cu(2,3 H_2bitsc-N^1-Ph)] **30**	3.34	0.87	129
[Cu(2,5 H_2bptsc)] **31**	3.34	0.93	144
[Cu(2,5H_2bptsc-N^1-Me)] **32**	3.35	0.94	144
[Cu(2,5H_2bptsc-N^1-Ph)] **33**	3.48	0.84	145
[Cu (2,6 H_2bdptsc)] **34**	1.60	0.82	147
[Cu (2,6 H_2bdptsc -N^1-Me)] **35**	3.32	0.91	143
[Cu (2,6 H_2bdptsc -N^1-Ph)] **36**	3.33	0.87	128

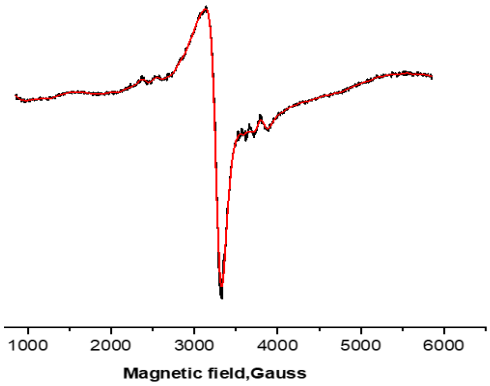

Figure 7.6.1. Spectrum of complex **25**
ESR best fit simulated (red) and Experimental (black)

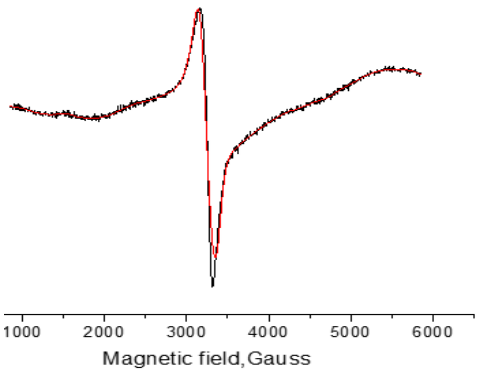

Figure 7.6.2. Spectrum of Complex **26**
ESR best fit simulated (red) and Experimental (black)

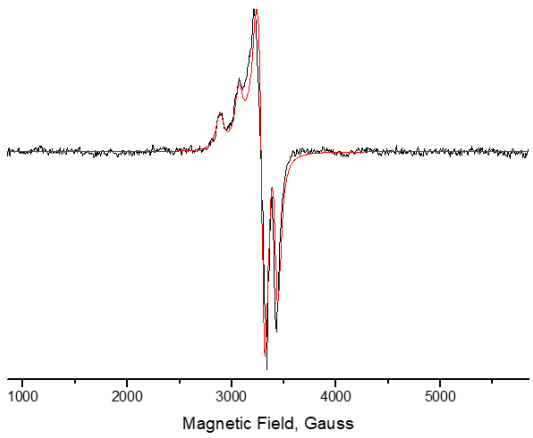

Figure 7.6.3: Spectrum of complex **27**
ESR best fit simulated (red) and
Experimental (black)

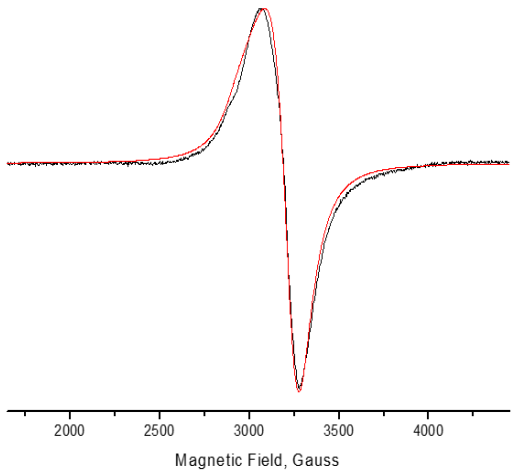

Figure 7.6.4: Spectrum of complex **28**
ESR best fit simulated (red) and
Experimental (black)

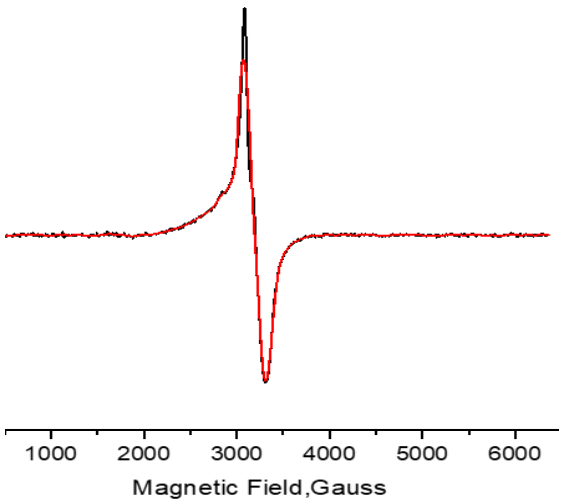

Figure 7.6.5: Spectrum of complex **29**
ESR best fit simulated (red) and
Experimental (black)

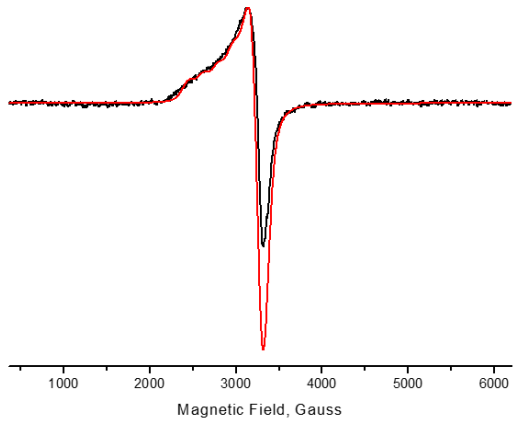

Figure 7.6.6: Spectrum of complex **30** ESR best fit simulated (red) and Experimental (black)

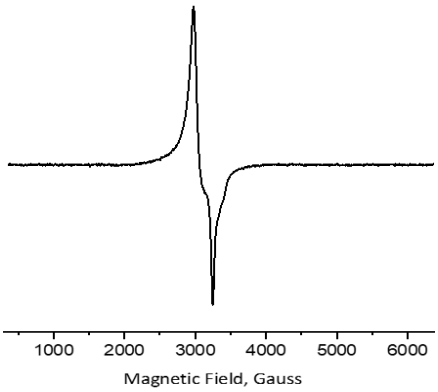

Figure 7.6.7: Spectrum of complex **31** at room temp.

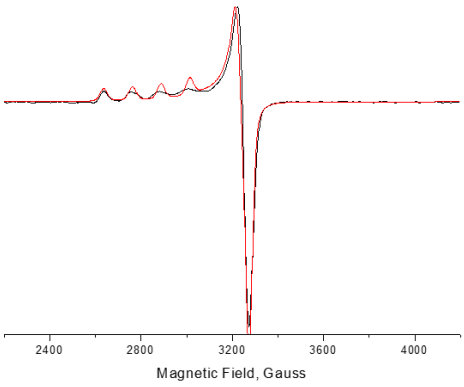

Figure 7.6.8: Spectrum of complex **31** a at low temp. ESR best fit simulated (red) Experimental (black)

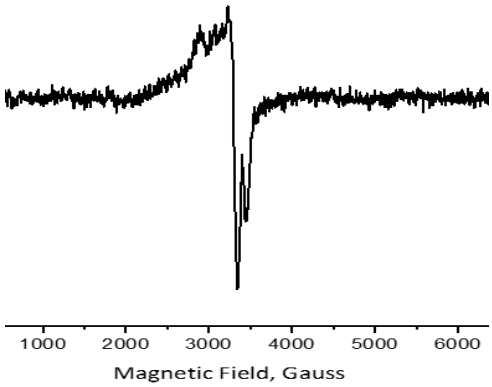

Fig. 7.6.9. Spectrum of complex **32** at Room temp.

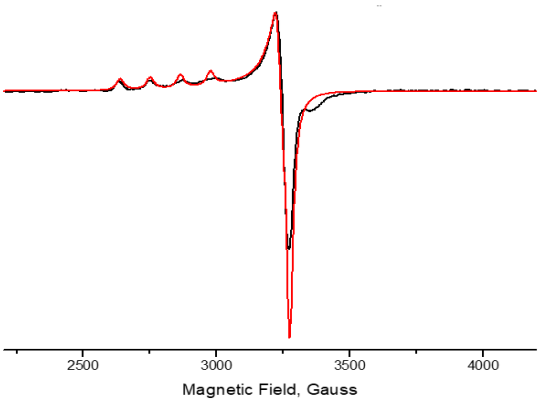

Figure 7.6.10. Spectrum of complex **32** at low temp. ESR best fit simulated (red) and Experimental (black)

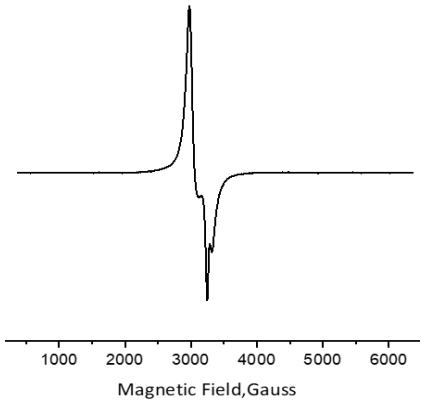

Figure 7.6.11. Spectrum of complex **33** at room temp.

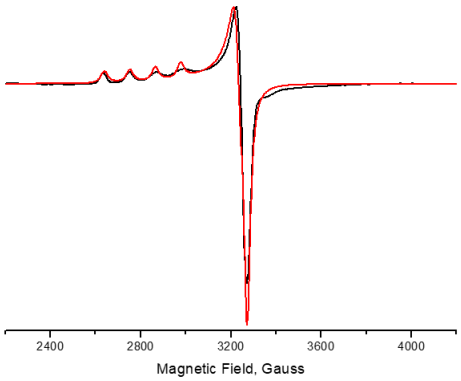

Figure 7.6.12: Spectrum of complex **33** at low temp. ESR best fit simulated (red) and Experimental (black)

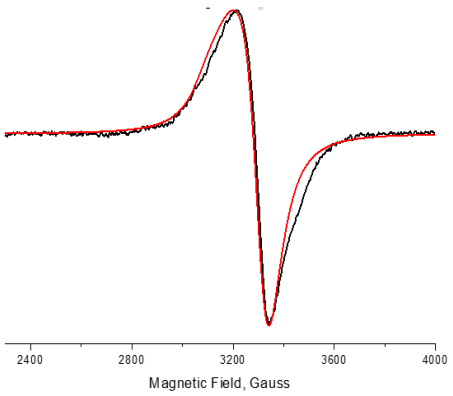

Figure 7.6.13: Spectrum of complex **34** at low temp. ESR best fit simulated (red) and Experimental (black)

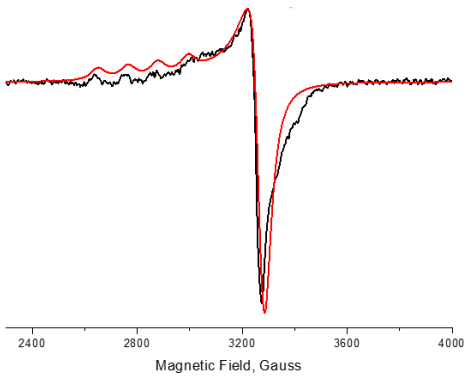

Figure 7.6.14: Spectrum of complex **35** at low temp. ESR best fit simulated (red) and Experimental (black)

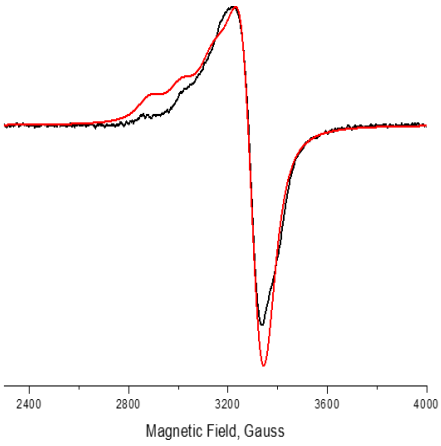

Figure 7.6.15. Spectrum of complex **36** at low temp. ESR best fit simulated (red) and Experimental (black)

7.7 Anti-tuberculosis activity:

All the ligands **($^{1}H_2L$-$^{12}H_2L$)** and their copper complexes **(25-36)** were evaluated and is given in Table 7.7.1 [179]. The anti-T.B activity of ligands generally gets enhanced upon complexation. It was found from the experimental data that the activity of ligand **2,5H_2bttsc N-Me ($^{2}H_2L$) and 2,5 H_2bptsc ($^{7}H_2L$)** has no change on complexation and exhibited maximum anti-TB activity (MIC = 1.6µg/ml), even same to standard drugs Rifampicin or Streptomycin (MIC = 1.6µg/ml). The activity of ligands 2,5 H_2bttsc N-Ph, 2,5 H_2bptsc, N-Me and 2,5 H_2bdptsc, N-Ph (MIC = 1.6, 3.12

and 12.5 µg/ml) was also high but the activity gets low in its complex **27**, **32** and **36** (MIC = 1.6 **27,36;** 25 **32** µg/ml) as compared to its ligands. The anti-TB activity of ^{1}**H_2L**, ^{4}**H_2L**,^{5}**H_2L**, ^{6}**H_2L**, ^{9}**H_2L,** ^{10}**H_2L and** ^{12}**H_2L (**MIC **=** 6.25 ^{1}**H_2L;** 3.12 ^{2}**H_2L,** ^{9}**H_2L**; 100 ^{5}**H_2L,** ^{6}**H_2L**; 50 ^{10}**H_2L,**^{11}**H_2L** µg/ml) get enhanced on complexation with copper(II) (MIC = 3.12 **25;** 25 **28**; 50 **29,30**; 1.6 **33**; 12.5 **34** and 6.25 **35** µg/ml). Chelation of ligand with copper(II) may have resulted in increase of its retention time on bio-membrane to allow longer interaction at target site. The possible interactions of ligand as well as complexes have been studied using molecular docking for most potent ligands 2,5 H_2bttsc N-Me (**^{2}H_2L**) ,2,3 H_2bitsc **(^{1}H_2L)** and its complexes [Cu(2,5bttsc N-Me)] **26** and [Cu(2,3bitsc)] **28**.

Table 7.7.1: Anti-T.B activity of Bisthiosemicarbazones (^{1}**H$_2$L** -^{12}**H$_2$L**) and complexes **(25-36)**

		MIC (µg /mL)							
S. No	**Compound**	***100***	***50***	***25***	***12.5***	***6.25***	***3.12***	***1.6***	***0.8***
1.	**2,5 H$_2$bttsc (^{1}H$_2$L)**	S	S	S	S	S	R	R	R
2.	**[Cu(2,5 bttsc)] 25**	S	S	S	S	S	S	R	R
3.	**2,5H$_2$bttsc N-Me (^{2}H$_2$L)**	S	S	S	S	S	S	S	R
4.	**[Cu(2,5 bttsc N-Me)] 26**	S	S	S	S	S	S	S	R
5.	**2,5 H$_2$bttsc N-Ph (^{3}H$_2$L)**	S	S	S	S	S	S	S	R
6.	**[Cu(2,5 bttsc N-Ph)] 27**	S	S	S	R	R	R	R	R
7.	**2,3 H$_2$bitsc (^{4}H$_2$L)**	S	S	R	R	R	R	R	R
8.	**[Cu(2,3 bitsc)] 28**	S	S	S	R	R	R	R	R
9.	**2,3 H$_2$bitsc-N^{1}-Me (^{5}H$_2$L)**	S	R	R	R	R	R	R	R
10.	**[Cu(2,3 bitsc-N^{1}-Me)] 29**	S	S	R	R	R	R	R	R
11.	**2,3 H$_2$bitsc-N^{1}-Ph (^{6}H$_2$L)**	S	R	R	R	R	R	R	R
12.	**[Cu(2,3 bitsc-N^{1}-Ph)] 30**	S	S	R	R	R	R	R	R
13.	**2,5 H$_2$bptsc (^{7}H$_2$L)**	S	S	S	S	S	S	S	R
14.	**[Cu(2,5 bptsc)] 31**	S	S	S	S	S	S	S	R
15.	**2,5 H$_2$bptsc, N-Me (^{8}H$_2$L)**	S	S	S	S	S	S	R	R
16.	**[Cu(2,5 bptsc, N-Me)] 32**	S	S	S	S	S	R	R	R
17.	**2,5 H$_2$bptsc, N-Ph (^{9}H$_2$L)**	S	S	S	S	S	S	R	R
18.	**[Cu(2,5 bptsc, N-Ph)] 33**	S	S	S	S	S	S	S	R

19.	**2,5 H_2bdptsc ($^{10}H_2L$)**	S	S	R	R	R	R	R	R
20.	**[Cu(2,5 bptsc)] 34**	S	S	S	S	R	R	R	R
21.	**2,5 H_2bdptsc, N-Me ($^{11}H_2L$)**	S	S	R	R	R	R	R	R
22.	**[Cu(2,5 bdptsc, N-Me)] 35**	S	S	S	S	S	R	R	R
23.	**2,5 H_2bdptsc, N-Ph ($^{12}H_2L$)**	S	S	S	S	R	R	R	R
24.	**[Cu(2,5 bdptsc, N-Ph)] 36**	S	S	S	R	R	R	R	R

7.8 Human Serum Albumin binding studies

Interactions of HSA with most potent ligand 2,5 H_2bttsc N-Me **(^2H_2L)**, 2,3 H_2bitsc **(^4H_2L)** and its complex [Cu(2,5bttsc N-Me)] **26**, [Cu(2,3bitsc)] **28** has been studied through UV-visible and fluorescence spectroscopy.

7.8.1 UV-visible spectroscopic study

HSA (7 µM) shows an absorption band at 280 nm in its UV-visible absorption spectrum. On incremental additions of 2,5 H_2bttsc N-Me and its complex [Cu(2,5bttsc N-Me)] (0-9µM) the absorbance of HSA at 280nm was significantly increased (56% for ligand 2,5H_2bttsc N-Me and 45% for [Cu(2,5bttsc N-Me)]. The enhanced intensity of absorption peak can be due to change in concentrations of ligand 2,5H_2bttsc N-Me and complex [Cu(2,5bttsc N-Me)] showed agitations in the microenvironment of protein's chromophores due to the interaction of HSA with ligand and its complex (Figure 7.8.1.1). On addition a new peak at 389 nm was observed due to the electronic transition between metal orbitals. Using the Benesi-Hildebrand equation, the binding constants for the interactions of the ligand-HSA and complex-HSA system were determined. (Equation-2) [195] and initiate to be (4.24×10^5) M^{-1} and (4.92×10^5) M^{-1}, respectively (Figure 7.8.1.1). The strong binding affinities (high binding constant) indicate the effective transport of ligand 2,5H_2bttsc N-Me and complex [Cu(2,5bttsc N-Me)] to their target sites.

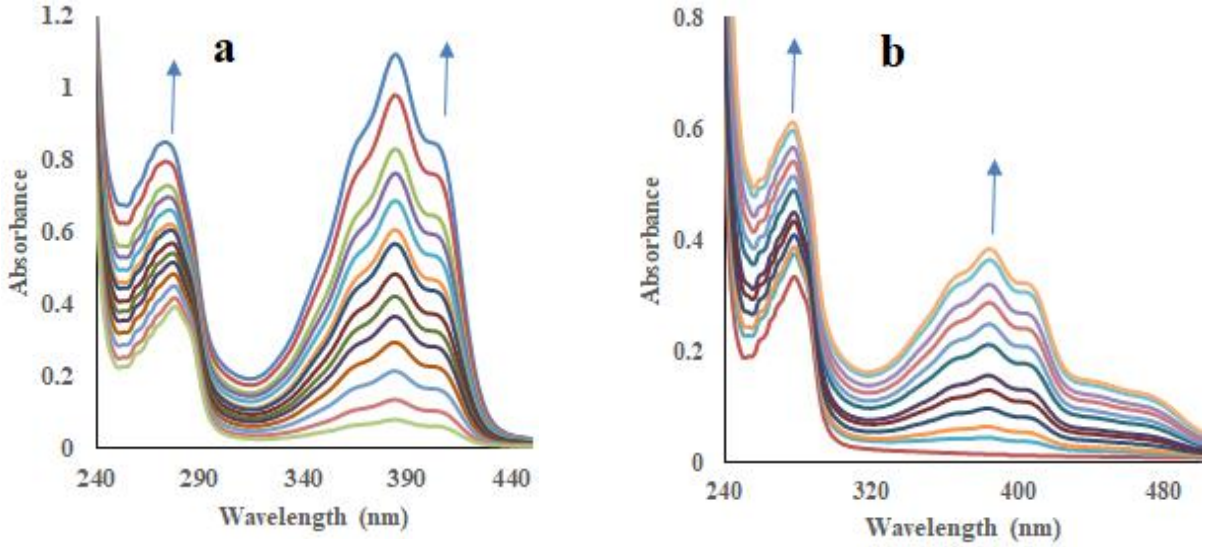

Figure 7.8.1.1: UV-visible absorption of HSA with incremental additions of ligand 2,5H_2bttsc N-Me (a) and complex [Cu(2,5bttsc N-Me)] (b)

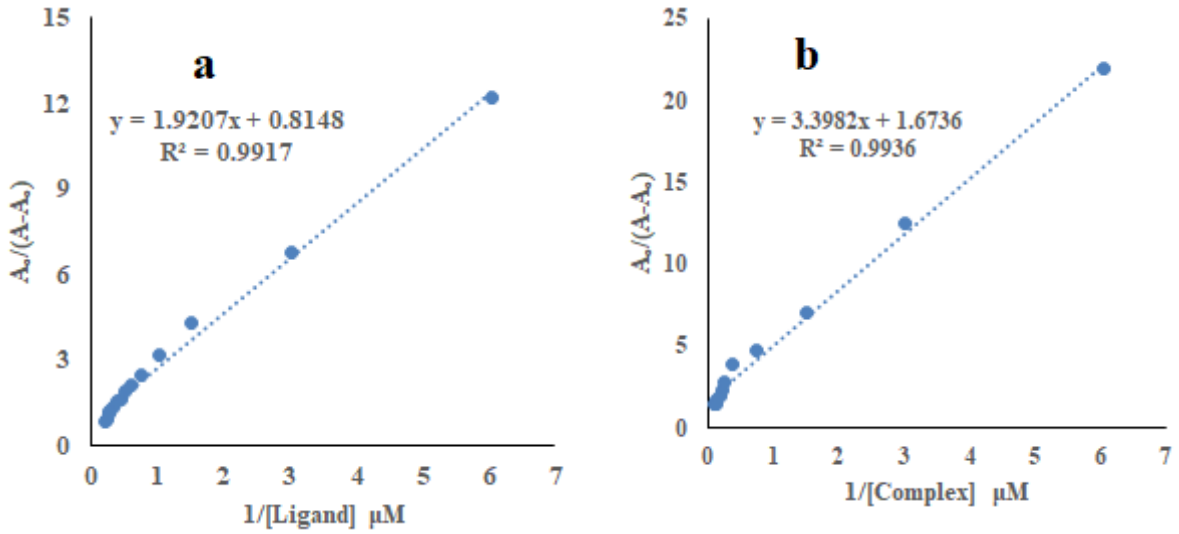

Figure 7.8.1.2: Benesi-Hildebrand plot {$A_o/(A-A_o)$ vs. 1/[ligand or complex]} for binding studies of HSA with ligand 2,5H_2bttsc N-Me (a) and complex [Cu(2,5bttsc N-Me)] (b)

7.8.2 Fluorescence study

Fluorescence titrations have been carried out using HSA (7 μM) with incremental additions of 2,5H_2bttsc N-Me (0-8 μM) and complex [Cu(2,5bttsc N-Me)] (0-16 μM). Binding of ligand and complex was also confirmed by Fluorescence studies. Aromatic fluorophores of HSA such as (TRP) and (TYR) amino acid residues displays intrinsic fluorescence [180]. The fluorophores

produced by fluorescence, could affect the interaction of ligand 2,5H_2bttsc N-Me and complex [Cu(2,5bttsc N-Me)] to HSA [181–183]. Tryptophan (Trp-214), an amino acid residue located in subdomain IIA of HSA, caused an emission band to appear in the emission spectrum of HSA (7 μM) at 349 nm when excitation wavelength was set at 280 nm [184]. Increasing concentrations of ligand 2,5H_2bttsc N-Me (0-8 μM) and complex [Cu(2,5bttsc N-Me)] (0-16 μM) directed to satisfactory quenching (91-94%) of emission of HSA at 349 nm (Figure 7.8.2.1) which confidently directed the binding of ligand 2,5H_2bttsc N-Me and complex [Cu(2,5bttsc N-Me)] to HSA.

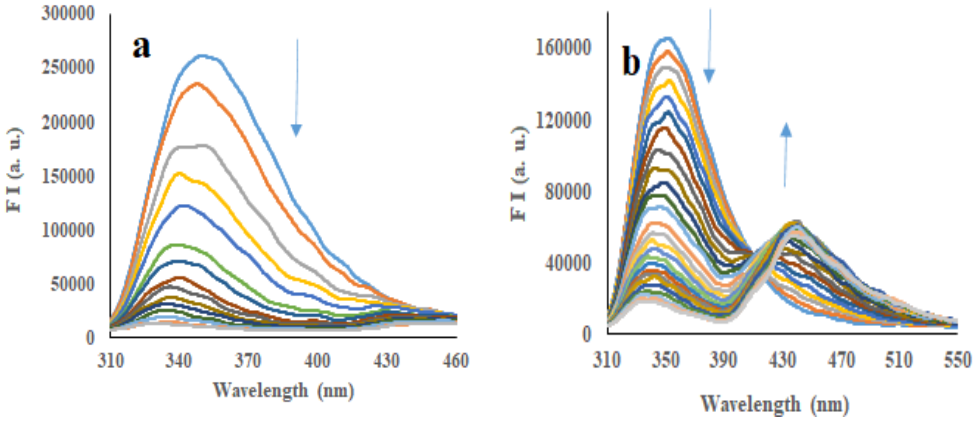

Figure 7.8.2.1: Emission spectra of HSA (λ_{ex} = 280 nm) in incremental additions of ligand 2,5H_2bttsc N-Me (a) and complex [Cu(2,5bttsc N-Me)] (b)

Quenching in fluorescence have been evaluated with the help of the Stern-Volmer equation eqnuation (Equation-3)[215] and Stern-Volmer plots were formed (Figure 7.8.2.2). The graphs' good linearity was found using the correlation coefficient (R) 0.9858 for ligand 2,5H_2bttsc N-Me and 0.9543 for complex [Cu(2,5bttsc N-Me)] during the experiments. Stern-Volmer quenching constant (K_{sv}) a parameter for fluorescence quenching efficiency of the ligand 2,5H_2bttsc N-Me and complex [Cu(2,5bttsc N-Me)], were determined and calculated to be 2.03×10^6 M^{-1} for ligand 2,5H_2bttsc N-Me and 22.51×10^6 M^{-1} for complex [Cu(2,5bttsc N-Me)] (Table 7.7). Therefore, the spotted quenching in HSA fluorescence on the additions of ligand 2,5H_2bttsc N-Me and complex [Cu(2,5bttsc N-Me)] may be due to the complex formation of ligand 2,5H_2bttsc N-Me and complex [Cu(2,5bttsc N-Me)] with HSA.

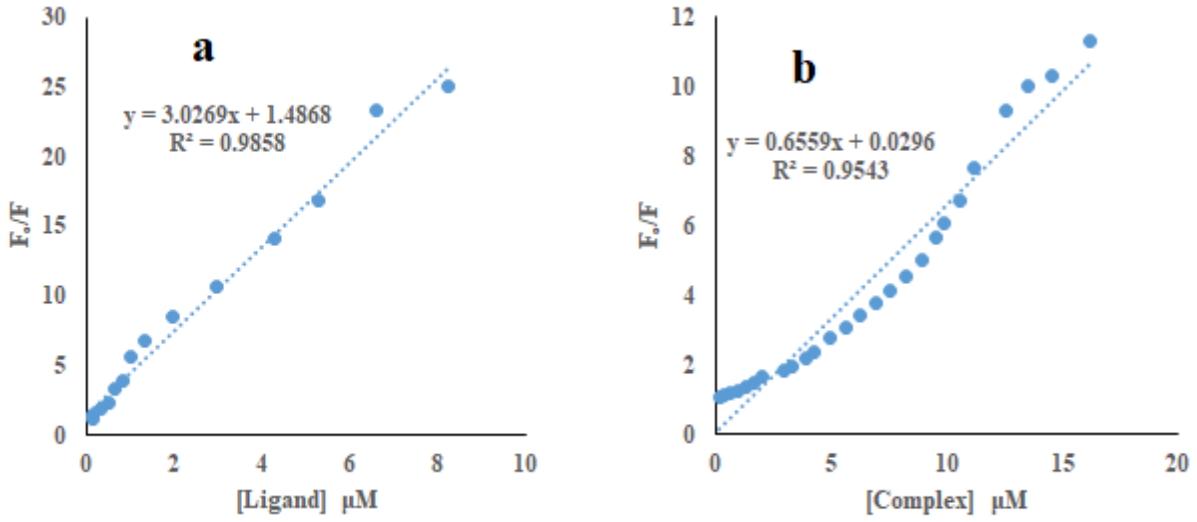

Figure 7.8.2.2: Stern-Volmer plots (F_0/F vs [ligand or complex]) for binding of HSA with ligand 2,5H_2bttsc N-Me (a) and complex [Cu(2,5bttsc N-Me)] (b)

Double logarithmic plots were achieved using modified Stern-Volmer (Equation-4) [186,216] for checking interaction of ligand 2,5H_2bttsc N-Me and complex [Cu(2,5bttsc N-Me)]with HSA. The values of binding constants (K_b) were found to be (4.55×10^6) M^{-1}, 2,5H_2bttsc N-Me and (5.52×10^6) M^{-1} [Cu(2,5bttsc N-Me)] (Table 4). The value of binding constant for the ligand-HSA and complex-HSA were found in the range of 4.55-5.52 $\times 10^6$ M^{-1} which confirms the strong binding affinity of 2,5H_2bttsc N-Me and complex [Cu(2,5bttsc N-Me)] with HSA. The binding sites (n) for the binding of ligand 2,5H_2bttsc N-Me and complex [Cu(2,5bttsc N-Me)] with HSA have been gained from the modified Stern-Volmer equation and were initiate to be 1.02 and 1.21, respectively (Table 7.8.2.1) (Figure 7.8.2.2).

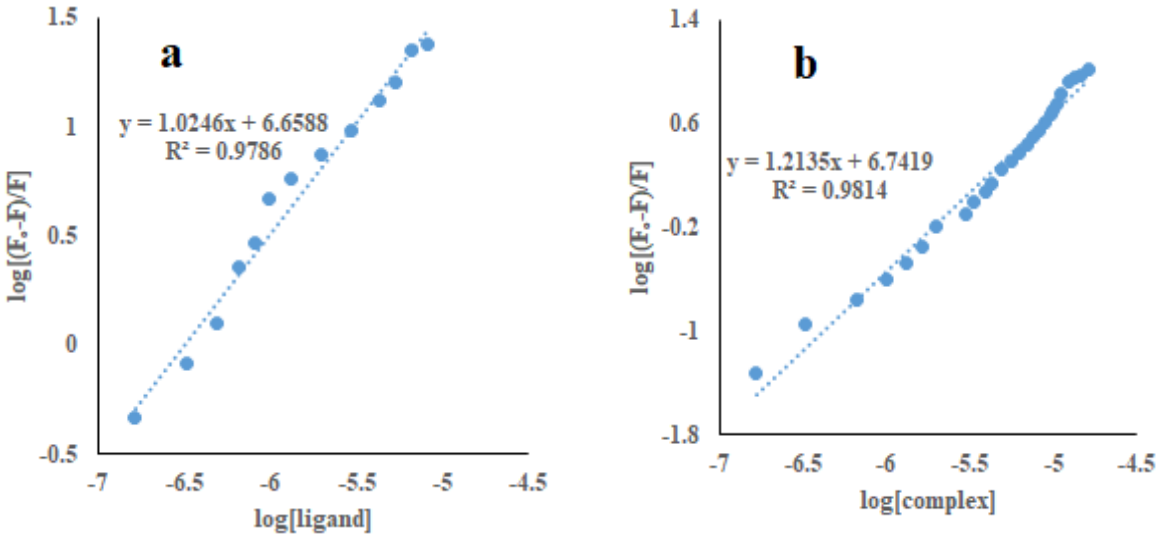

Figure 7.8.2.3: Modified stern-volmer plots {log(F_o-F)/F vs log [ligand or complex]} for binding of HSA with ligand 2,5H_2bttsc N-Me (a) and complex [Cu(2,5bttsc N-Me)] (b)

Table 7.8.2.1: Interaction parameters for binding of ^2H_2L and 26 with HSA

Compound	**K_{sv} (10^6 M^{-1})**	**[a]R**	**K_b (10^6 M^{-1})**	**n**	**[a]R**
^1H_2L	2.03	0.9858	4.55	1.02	0.9786
[Cu(2,5bttsc N-Me)]	22.51	0.9543	5.52	1.21	0.9814

[a]R is the correlation coefficient

7.8.3 HSA Binding Studies of 2,3 H_2bitsc (^1H_2L) and [Cu(2,3bitsc)]

Studies on UV-vis absorption

The absorption spectra (UV-visible) of HSA (7μM) were measured in without or with incremental additions of 2,3 H_2bitsc (0-6 μM) and complex [Cu(2,3bitsc)] (0-8 μM) to determine the interactions between HSA and H_2bitsc or complex [Cu(2,3bitsc)]. An increase in HSA absorbance at 280 nm (67% for 2,3 H_2bitsc and 83% for [Cu(2,3bitsc)]) by increasing the amount of 2,3 H_2bitsc or complex [Cu(2,3bitsc)] indicates changes in the microenvironment of protein chromophores due to its interaction 2,3 H_2bitsc and complex [Cu(2,3bitsc)] (Figure 7.8.3.1).With increased concentration of H_2bits can additional peak at 356 nm and of complex [Cu(2,3bitsc)] peak at 406 nm appeared indicating electronic transition in ligand orbitals and metal orbitals, respectively. Benesi-Hildebrand equation (Equation- 2) was employed to calculate binding constants for interactions in the H_2bitsc-HSA and [Cu(2,3bitsc)]-HSA systems and found to be 4.90×10^5 M^{-1}

and 6.09×10^5 M^{-1}, respectively (Figure 7.8.3.2). Results demonstrated that 2,3 H_2bitsc and [Cu(2,3bitsc)] had high binding affinities for successful transport to their target locations.

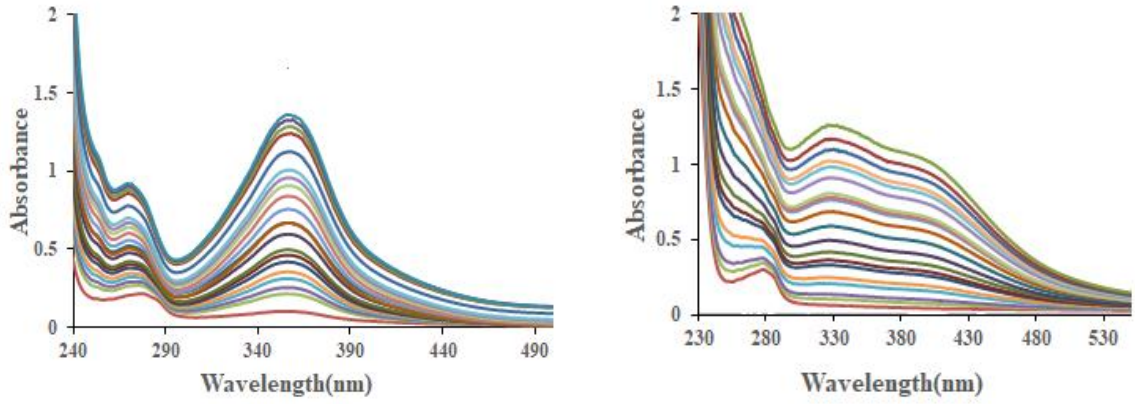

(a) **(b)**

Figure 7.8.3.1: UV-visible absorption of HSA with incremental additions of ligand 2,3 H_2bitsc (a) and [Cu(2,3bitsc)] (b)

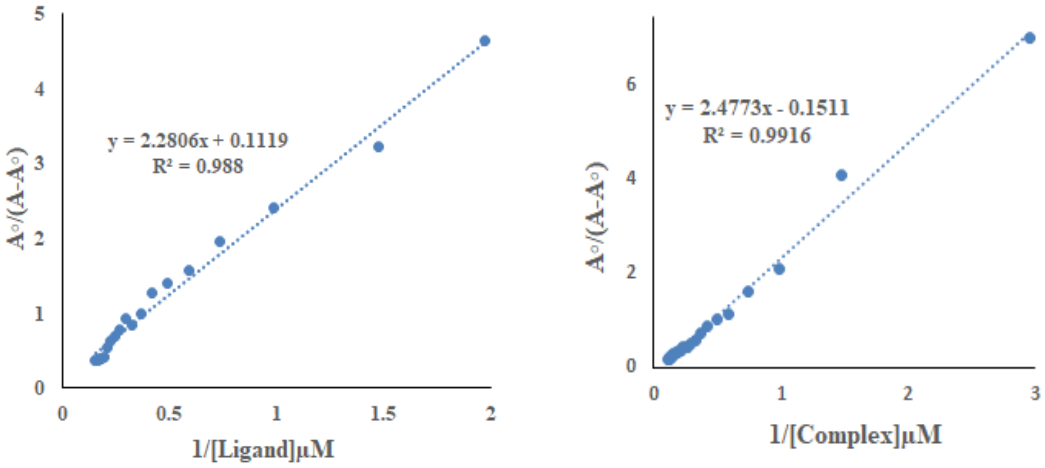

(a) (b)

Figure 7.8.3.2: Benesi-Hildebrand plot {$A_o/(A-A_o)$ vs. 1/[ligand or complex]} for binding studies of HSA with ligand 2,3 H_2bitsc (a), and complex [Cu(2,3bitsc)] (b)

7.8.4. Fluorescence studies

The interaction of 2,3 H_2bitsc and [Cu(2,3bitsc)] with HSA may influence the fluorescence produced aromatic fluorophores of HSA[217]. Amino acid tryptophan (Trp-214) located at sub domain IIA of HSA is responsible for emission band at 350 nm of HSA (7 μM). The intensity of this band decreases with increasing concentration (0-8 μM) of 2,3 H_2bitsc and [Cu(2,3bitsc)]

indicates high quenching (91-94%) of HSA emission confirming binding of 2,3 H_2bitsc and [Cu(2,3bitsc)] to HSA [218] (Figure **7**.8.4.1).

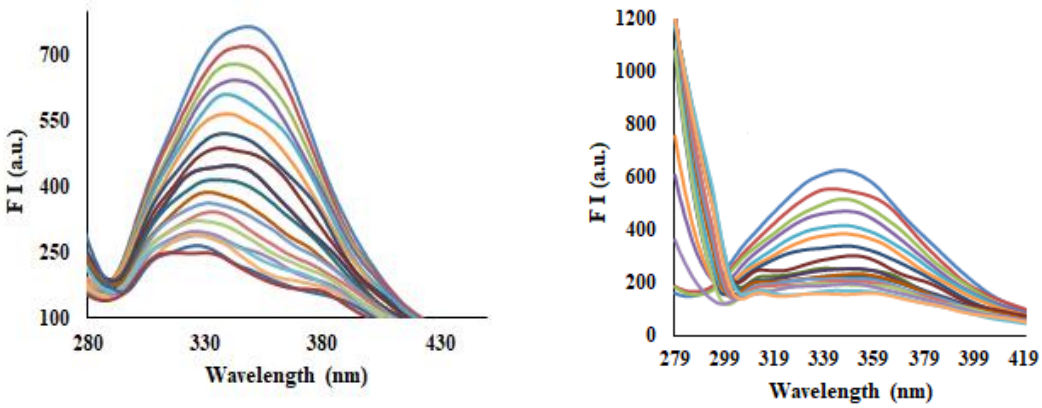

(a) (b)

Figure 7.8.4.1: Emission spectra of HSA (λ_{ex} = 280 nm) in incremental additions of ligand 2,3 H_2bitsc (a) and complex [Cu(2,3bitsc)] (b)

Stern-Volmer equation (Equation- 3) was employed to estimate quenching in fluorescence and Stern-Volmer graphs (Figure **7**.8.4.2) were plotted [218]. During the experiments, the graphs' good linearity was found using the correlation coefficient (R) of 0.9744 for H_2bitsc and 0.9515 for [Cu(2,3bitsc)]. The Stern-Volmer quenching constant (Ksv) of 2,3 H_2bitsc and [Cu(2,3bitsc)] was calculated and found to be $9.6\times10^4 M^{-1}$ and 4.5×10^5 M^{-1}, respectively (Table 4). As a result, the speckled quenching in HSA fluorescence with addition of 2,3 H_2bitsc and [Cu(2,3bitsc)] may be attributed to complex formation of 2,3 H_2bitsc and [Cu(2,3bitsc)] with HSA.

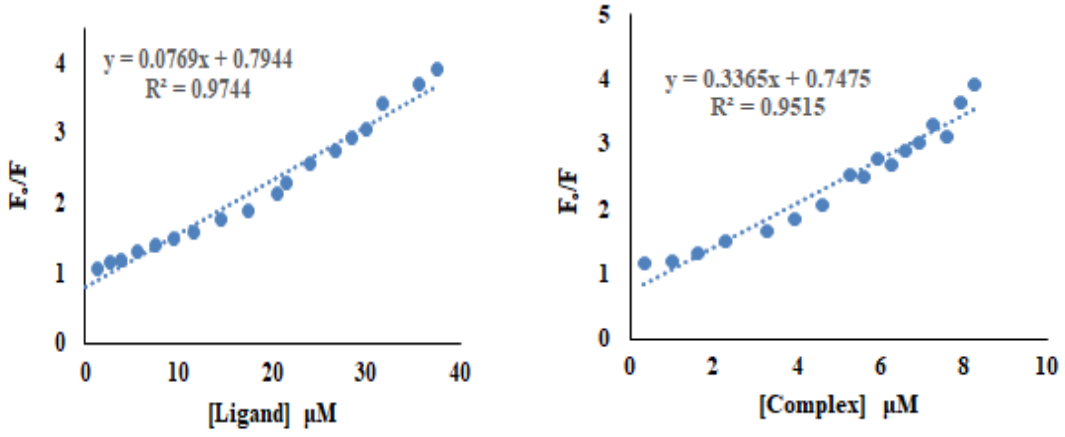

(a) (b)

Figure 7.8.4.2: Stern-Volmer plots (F_o/F vs [ligand or complex]) for binding of HSA with ligand 2,3 H_2bitsc (a) and complex [Cu(2,3bitsc)] (b)

Using modified Stern-Volmer (Equation-4), double logarithmic graphs were plotted to find interaction of 2,3 **H_2bitsc** and [Cu(2,3bitsc)] with HSA (Figure 8) [187]. High affinity of H_2bitsc and [Cu(2,3bitsc)] for HSA with binding constants (K_b) 2.59×10^5 M^{-1} and 5.77×10 M^{-1}, respectively was observed (Table 4). The number of binding sites (n) for 2,3 **H_2bitsc** and [Cu(2,3bitsc)] with HSA were confirmed by modified Stern-Volmer equation and found to be 1.10 and 1.25, respectively (Table 7.8.4.3, Figure 7.8.4.3).

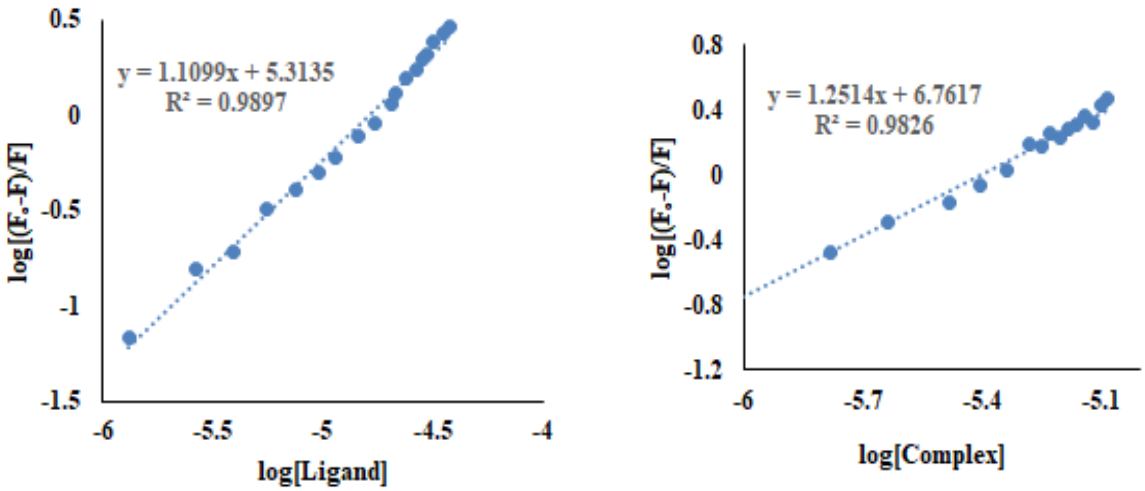

(a) (b)

Figure 7.8.4.3: Modified stern-volmer plots {log(F_o-F)/F vs log [ligand or complex]} for binding of HSA with ligand 2,3 H_2bitsc (a) and complex [Cu(2,3bitsc)] (b)

Table 7.8.4.3: Interaction of 2,3 H_2bitsc and **[Cu(2,3bitsc)]** parameters for binding with HSA

Ligand or complex	**K_{sv} (M^{-1})**	**[a]R**	**K_b (10^5 M^{-1})**	**n**	**[a]R**
2,3 H_2bitsc	9.6×10^4	0.9744	2.59	1.10	0.9897
[Cu(2,3bitsc)]	4.5×10^5	0.9515	5.77	1.25	0.9826

[a]R is the correlation coefficient

7.9 Docking studies

In order to validate and explain the experimental findings, interactions of potent ligands 2,5bttsc-N-Me (^{2}**H_2L)** with their copper complex [Cu(2,5bttsc-N-Me)] **26,** and 2,3 H_2bitsc (^{4}**H_2L)** with **[Cu(2,3bitsc)] 28** has been examined by molecular modeling using Autodock 4.0. [46]. The minimum binding energy obtained from docking of ^{2}**H_2L ,^{4}H_2L** and their copper complexes **26,**

28 with mycobacterium tuberculosis enoyl reductase is -5.8, -6.6, -7.6 and -8.7 and Kcal/mol respectively. Results indicate that ^{4}**H$_2$L** and its complex **28** displayed strongest binding with target. From the binding energy data, it is clear that compounds **26** and **28** are strongly bound with M. tuberculosis enoyl reductase vis-à-vis free ligands. A greater negative binding energy signifies a more stabilized structure in the docked state for **26** and **28**. This is in agreement with the same order as found from the experimental results.

The detailed docking study of interactions between ligand ^{2}**H$_2$L** and its complex **26** with mycobacterium tuberculosis enoyl reductase showed that the ligand ^{2}**H$_2$L** displayed interactions (hydrogen bonding) with amino acid residue of oxygen atom (PRO156) (*d* = 2.00 Å) of chain A. Ligand ^{2}**H$_2$L** interacted with (PHE 149), (TYR158), (PRO193), and (MET199) amino acid residues of chain A through hydrophobic and other interactions. The complex **26** unveiled interactions with target through hydrogen bonding with amino acid residues of serine (SER 94) (*d* = 3.54 Å), tyrosine (TYR 158) (*d* = 2.05 Å), and (LYS 165) (*d* = 2.62 Å) of chain (Figure 7.10.1).

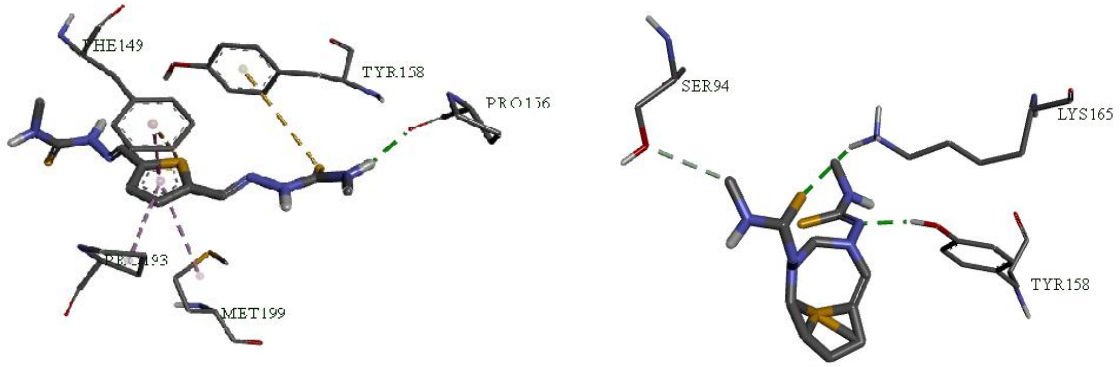

(a) (b)

Figure 7.10.1: 3D representation of interactions of ligand ^{2}**H$_2$L** (a), and its complex **26** (b)

During the docking studies of ^{4}**H$_2$L** with complex **28** the H-bonding interactions between oxygen atoms of amino acid residues of (GLY 14 and GLY 96) (d = 2.59 Å), (ILE15) (d = 2.49 Å), and (SER 94) (d = 2.39Å) of chain A of mycobacterium tuberculosis enoyl reductase with ^{4}**H$_2$L** were observed. Apart from that, amino acid residues of (PHE 41), (VAL 65), and (ILE 95 and ILE122) of amino acid residues of chain A also showed the hydrophobic interactions with of ^{4}**H$_2$L**. Complex **28** indicated hydrogen bonding interactions with the oxygen atoms of the chain A of amino acid residues (GLY14 and GLY 96) (d = 2.29 and 3.48 Å) and (SER 94) (d = 2.27Å) along

with other interactions with the amino acids (PHE 41), (VAL 65), and (ILE 95 and ILE 122). (Figure 7.10.2).

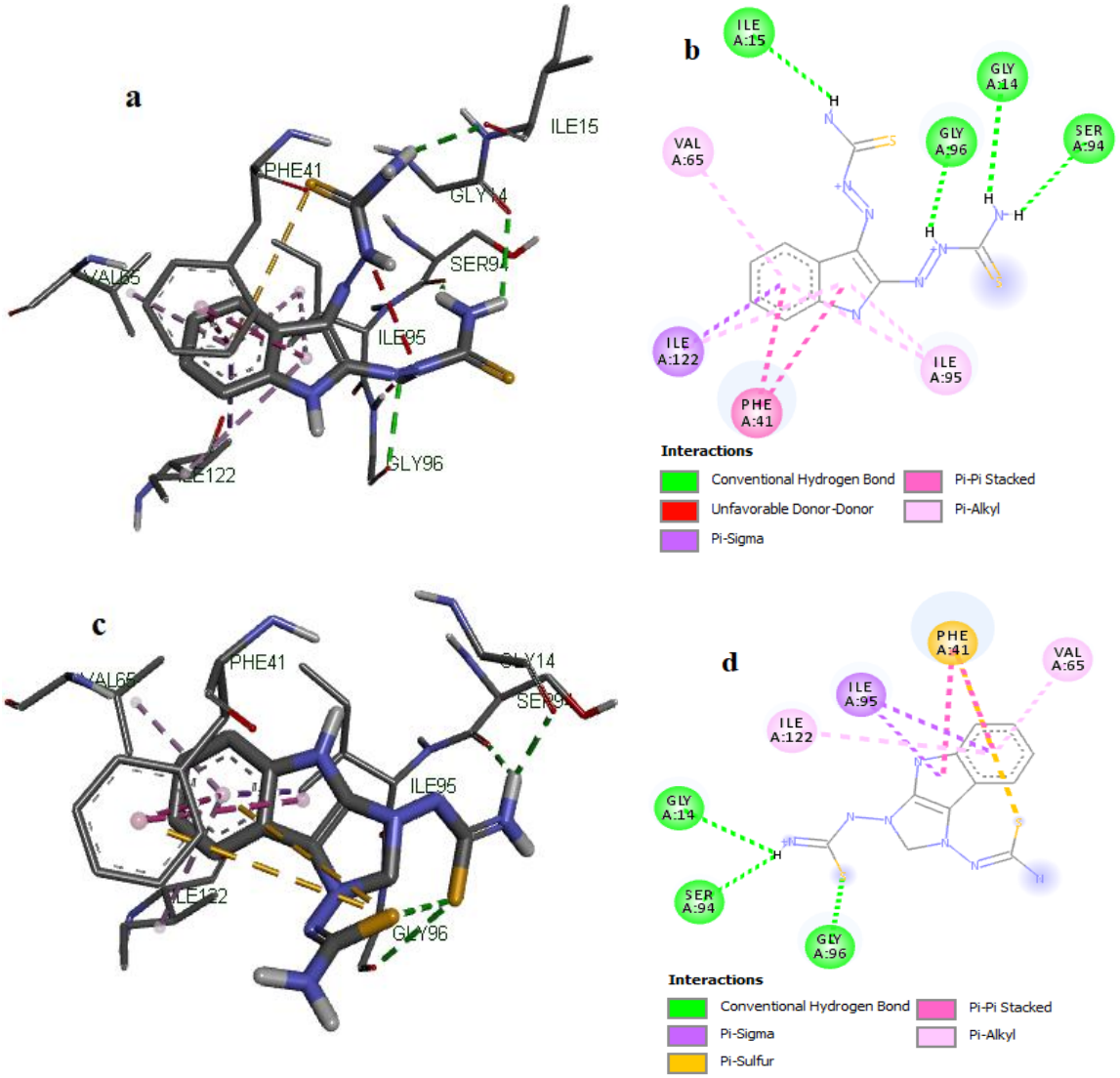

Figure 7.10.2: The interactions of the ligand $^{4}H_2L$ (a and b) and its copper complex **28** (c and d) with the enoyl reductase of Mycobacterium tuberculosis are shown in 3D and 2D, respectively.

7.10 <u>Conclusion:</u> Reaction of Cu(II) acetate with ^{1}**H$_2$L-**^{12}**H$_2$L** yielded complexes of stoichiometry, [Cu(L)] **25-36** in molar ratio1:1. All compounds were characterized through FTIR, Mass, UV-visible, and ESR spectroscopy. Ligands (^{1}**H$_2$L-**^{12}**H$_2$L**), along with their corresponding complexes (**25-36**), were scrutinized for anti-tuberculosis activity. The following conclusion has been drawn from the results obtained:

1. All the complexes have m/z values in well agreement with proposed stoichiometry.
2. The presence of two different g values, $g_{\parallel}$ and $g_{\perp}$, suggests axial symmetry for the complexes. Furthermore, a higher $g_{\parallel}$ value compared to $g_{\perp}$ confirms the existence of free electrons in the ground term $d_{x^2-y^2}$ within the square planar structure.
3. Empirical parameter (f) for complexes **25-36** ranges from **134 to 148** cm^{-1}, indicating a square planar structure with slight distortion.
4. Anti-T.B activity of ^{2}**H$_2$L** and ^{4}**H$_2$L** (MIC = 3.12, 50µg/ml) get enhanced on complexation with Cu(II) (MIC=1.6, 25µg/ml).
5. Molecular modelling studies with minimal binding energies -5.8 (^{2}**H$_2$L**), -7.6(^{4}**H$_2$L**), -6.6 (**26**) and -8.7 (**28**) Kcal/ mol, confirmed significant intermolecular interaction of these compounds which also supports the experimental data.
6. Strong binding interactions with HSA was shown by ligand ^{2}**H$_2$L,** ^{4}**H$_2$L** and complex **26,28** with binding constant (4.24 ×10^{5}) M^{-1} and (4.92 ×10^{5}) M^{-1} and (4.90×10$^{5)}$ M^{-1} and (6.09×10^{5}) M^{-1} indicates significant binding interaction with HSA, respectively.
7. The binding sites (n) for binding of ligand (**^{2}H$_2$L)** and complex **(26)** with HSA was found to be 1.02 and 1.21, and for ligand (**^{4}H$_2$L)** and complex **(28)** with HSA was 1.10 and 1.25 respectively.

CHAPTER 8

ZINC(II) COMPLEXES

8.1 Discussion on Complexes of Zinc (II):

Reaction of Zinc acetate with ligands **$^{1}H_2L$-$^{12}H_2L$** molar ratio in 1:1 resulted in the formation of complexes of stoichiometry, [Zn(L)] (L=^{1}L-^{6}L, ^{10}L-^{12}L; **37-42**, **46-48**) and the complexes (**43-45**) with substituted 2,5 piperazine bisthiosemicarbazone (**$^{7}H_2L$-$^{9}H_2L$)** of formula $[Ni_2(L)_2]$ give the formation of dimer. The stoichiometry of complexes was confirmed by the binding ratio study using job plot method. The binding ratio of representative ligand with **$^{1}H_2L$:Zn(II)** came out as 1:1 by using the job plot method. The list of complexes formed is given in Table 8.1.1:

Table 8.1.1: Bisthiosemicarbazone complexes of Zinc(II) **37-48**

Sr. No.	Ligands	Complexes
1.	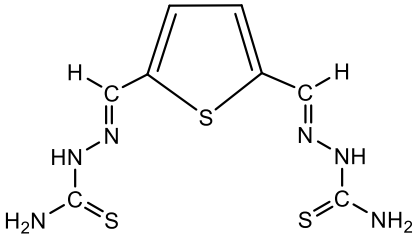 2,5thiophene dicarboxaldehyde Bisthiosemicarbazone **(2,5 H_2bttsc, $^{1}H_2L$)**	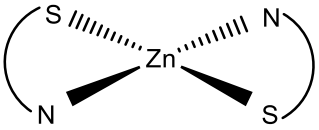 **[Zn(2,5 bttsc)] 37**
2.	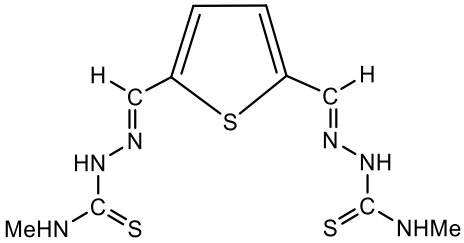 2,5thiophene dicarboxaldehyde-N-methyl bisthiosemicarbazone **(2,5 H_2bttsc -N-Me, $^{2}H_2L$)**	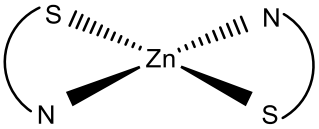 **[Zn(2,5 bttsc,N-Me)] 38**
3.	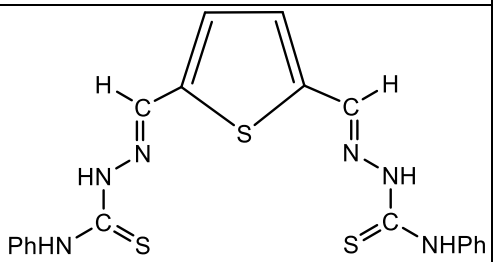	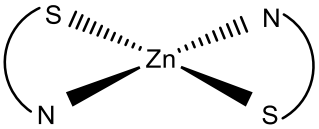 **[Zn(2,5 bttsc,N-Ph)] 39**

	2,5thiophene dicarboxaldehyde-N-phenyl bisthiosemicarbazone **(2,5 H_2bttsc- N-Ph, ^3H_2L)**	
4.	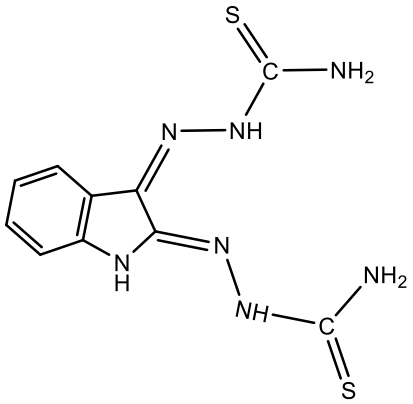 2,3-isatin bisthiosemicarbazone **(2,3 H_2bitsc, ^4H_2L)**	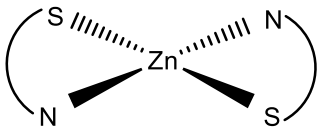 **[Zn (2,3 bitsc)] 40**
5.	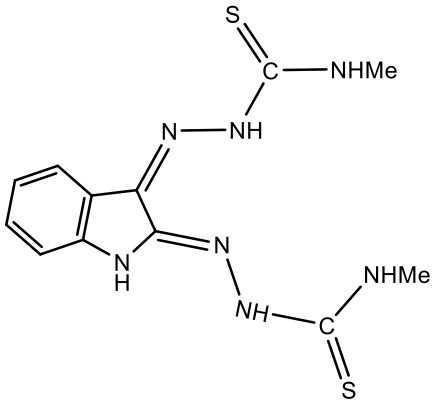 2,3-isatin-N-methyl bisthiosemicarbazone **(2,3 H_2bitsc-N-Me, ^5H_2L)**	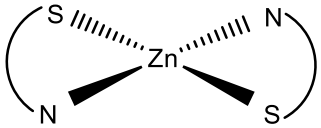 **[Zn (2,3 bitsc-N-Me)] 41**

6.	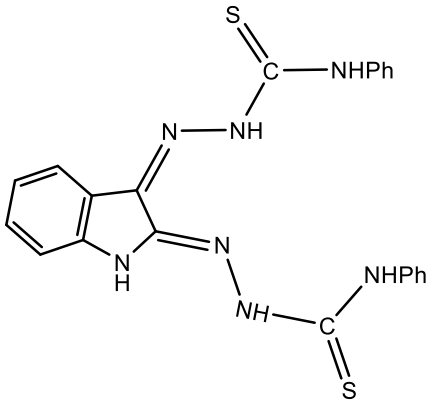 2,3-isatin-N-phenyl bisthiosemicarbazone **(2,3 H_2bitsc-N-Ph)**	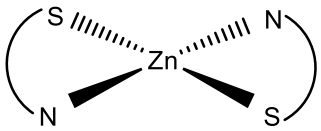 **[Zn(2,3 bitsc-N-Ph)] 42**
7.	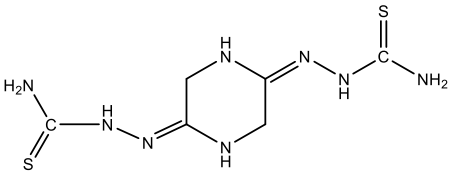 2,5-Piperazine bisthiosemicarbazone **(2,5 H_2bptsc, ^7H_2L)**	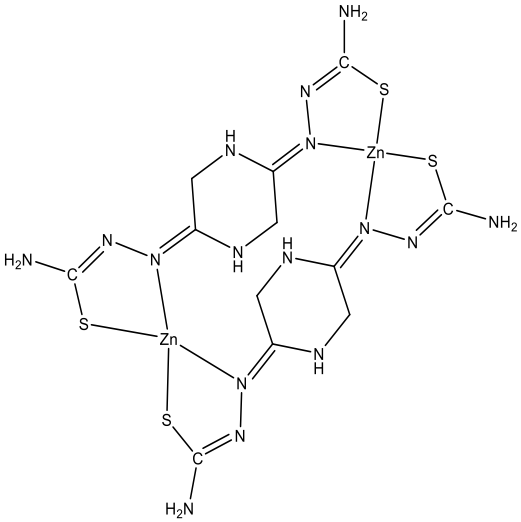 **[Zn(2,5 bptsc)] 43**
8.	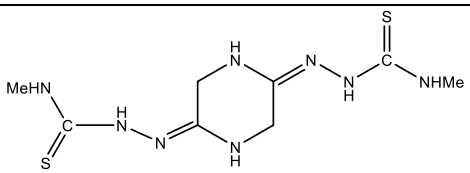 2,5-Piperazine bis N-methyl thiosemicarbazone **(2,5 H_2bptsc N-Me, ^8H_2L)**	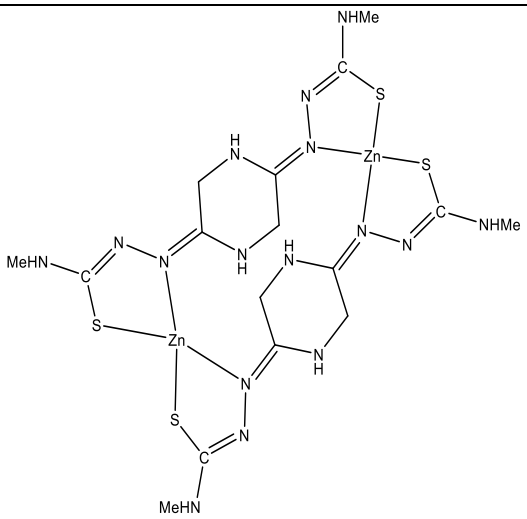

		[Zn(2,5 bptsc N-Me] 44
9.	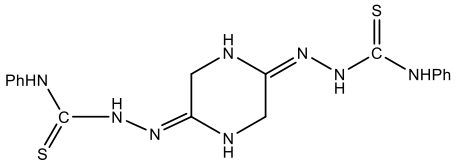 2,5-Piperazine bis N-phenyl thiosemicarbazone **(2,5 H_2bptsc N-Ph, $^{9}H_2L$)**	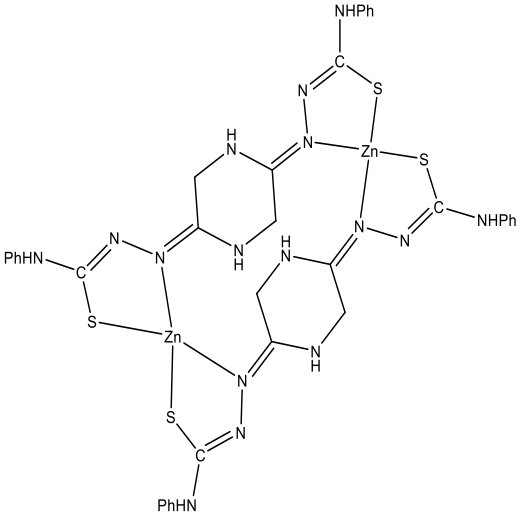 **[Zn(2,5 bptsc N-Ph] 45**
10.	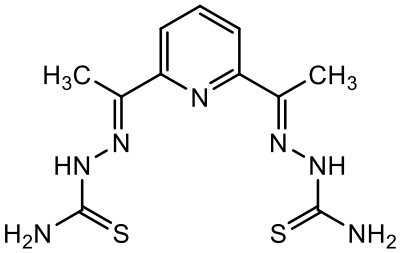 2,6 Diacetyl pyridine bisthiosemicarbazone **(2,6 H_2bdptsc, $^{10}H_2L$)**	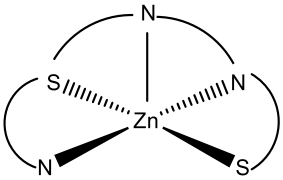 **[Zn(2,6 bdptsc] 46**
11.	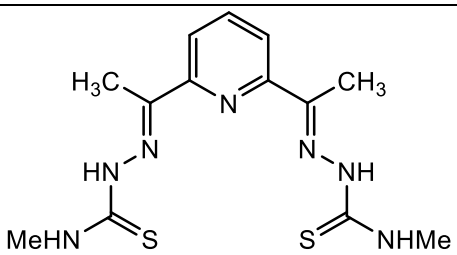 2,6 Diacetyl pyridine bis N-methyl thiosemicarbazone **(2,6 H_2bdptsc N-Me, $^{11}H_2L$)**	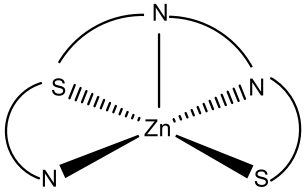 **[Zn(2,6 bdptsc,N-Me] 47**

12.	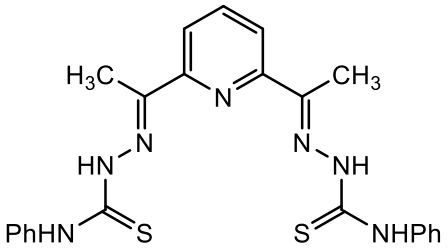 2,6 Diacetyl pyridine bis N-phenyl thiosemicarbazone **(2,6 H_2bdptsc N-Ph, $^{12}H_2L$)**	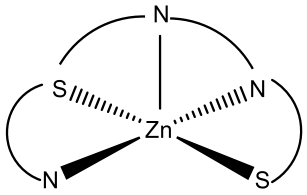 **[Zn(2,6 bdptsc,N-Ph] 48**

8.2 Binding studies: By Job Plot method

To confirm the structure of the complex (No. of binding sites) the representative ligand **(2,5 bptsc,N-Ph) ($^{9}H_2L$)** was selected for binding study with Zinc(II) using UV-visible spectroscopy. Synthesised (**$^{9}H_2L$**) has been explored for studies with the Zinc(II) metal in order to find out the binding ratio. The solution 0.4 mM of the probe (**$^{9}H_2L$**) was prepared in solvent DMSO, with the goal of optimising the concentration level and see out how it senses. Metal salt solutions were prepared with a concentration of 1 mM using the same solvent. To execute the UV-visible titrations for the ion analysis, 32 equivalents of 1mM of zinc(II) solution were successively added into 0.4mM of ligand (**$^{9}H_2L$**) solution. The results for the sample with 32 equivalents of each metal ion in the compound solution are depicted in Figure 8.2.1. The comparative alteration in absorbance maxima (An/Ao) upon sequential addition of 34 equivalents of Zinc(II) ions is shown in Figure 8.2.2 (a).

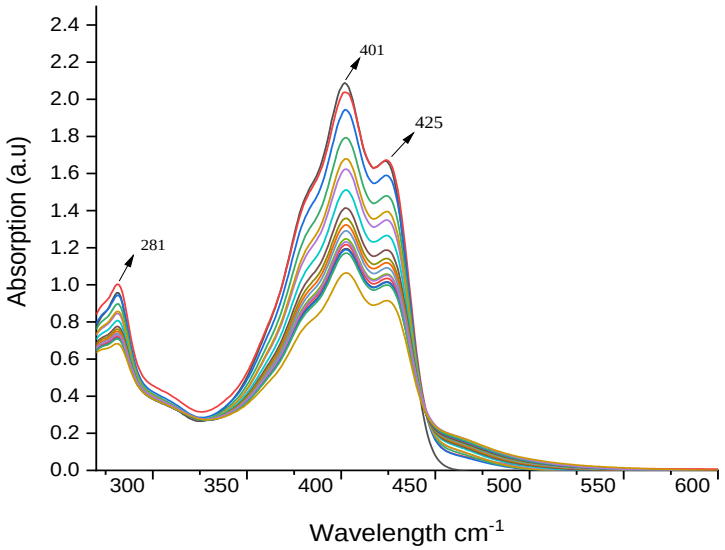

Figure 8.2.1: Absorbance noted with succeeding addition of 32 equivalents of 1mM Zinc(II) solution in the solution 0.4 mM of $^{9}H_2L$.

The ligand solution displayed absorption peak at 401nm along with a small shoulder peak at 425nm, corresponding to absorption intensities 1.06 and 0.91 respectively. Incremental addition of metal solution to the ligand resulted in a hyperchromic shift [190, 206].There by confirming the binding of the metal ions by the ligand.

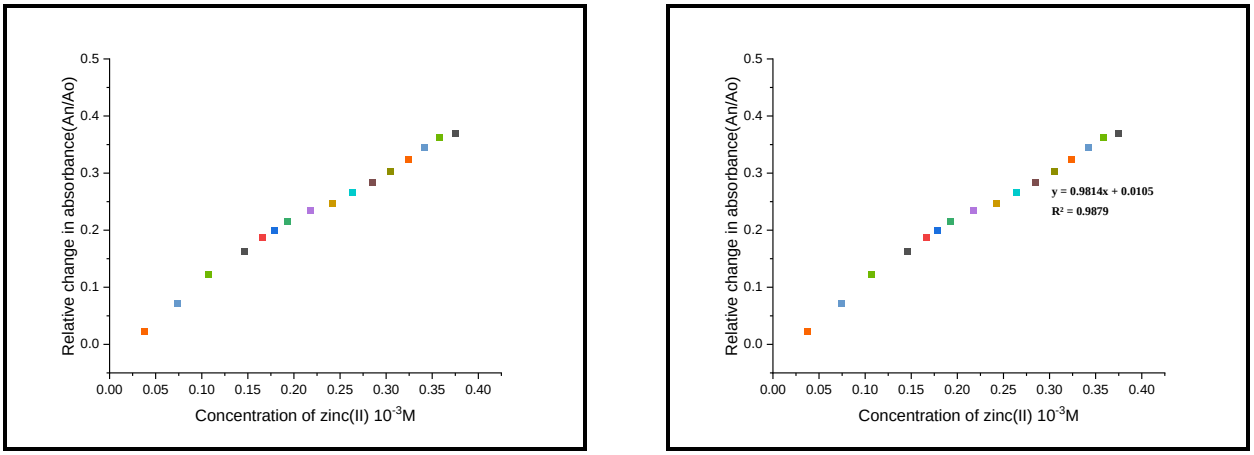

(a) **(b)**

Figure 8.2.2: a) The Virtual change in absorbance peak; **b)** Linear calibration curve [A_o- A_n/A_o Vs. (A_n/A_o) upon succeeding addition of 32 equivalent of concentration of Zn(II)]

The detection limit of Zn(II) has been calculated using Linear calibration curve of A_o-A_n/A_o Vs. the concentration of Zn(II) (Figure 8.2.2) and came out to be 0.447 µM, the binding ratio of $^{9}H_2L$:Zn(II) is 1 : 1 suggest the strong chelation of $^{9}H_2L$ with Zinc(II) [199].

8.3 IR Spectroscopy:

The important IR peaks of bisthiosemicarbazones and their Zinc(II) complexes are mentioned in Table 8.3.1 and spectra are given in Figures 8.3.1-8.3.12. The ν(N-H) bands in ligands **$^{1}H_2L$-$^{12}H_2L$** appeared in the range 3461-3204 cm^{-1} which showed a slight low energy shift in complexes (3408-3200 cm^{-1}). The bands due to –$N^{2}H$ – group observed in the range, 3190-3126 cm^{-1} in free ligands. But on complexation this band gets disappeared in all the complexes (**37-48**) suggesting deprotonation on complexation and coordination of bisthiosemicarbazone to metal centre in dianionic form [175]. The bands of υ(C=N) in the range, 1698-1594 cm^{-1} in the ligands is shifted to lower frequency in complexes **13-24** and appeared in the range 1666-1537 cm^{-1}. The specific ν(C=S) band observed in the range, 896-812 cm^{-1} in **$^{1}H_2L$-$^{12}H_2L$** which get shifted to lower energy in complexes (**37-48)** and observed in the range, 781-714 cm^{-1}. Significant low energy shift of this band indicates binding of bis- ligand in thiolate form [176].

Table 8.3.1: Significant IR peaks of bisthiosemicarbazones (**$^{1}H_2L$–$^{12}H_2L$**) and Zinc(II) complexes (**37-48**)

Ligands and Metal complexes	$\upsilon(NH_2)$	υ(-NH-)	υ(C=N)	υ(C=C)	$\delta(NH_2)$	υ(C=S)
(2,5 H_2bttsc, $^{1}H_2L$)	3409m, 3277m	3155m	1600s	1583m	1535s	836s
[Zn(bttsc)] **37**	3408m, 3277m	-	1576s	1475m	1396s	781s
(2,5 H_2bttscN-Me, $^{2}H_2L$)	3373m	3155w	1594s	1462m	-	812s
[Zn(bttsc,N-Me)] **38**	3325m	-	1537s	1508m	-	741s
(2,5 H_2bttsc N-Ph, $^{3}H_2L$)	3303m	3156w	1636s	1594w	-	895s
[Zn(bttsc,N-Ph)] **39**	3334m, 3200m	-	1598s	1436m	-	742s
(2,3 H_2bitsc, $^{4}H_2L$)	3332m, 3259m	3156w	1698s	1618w	1584s	851s
[Zn(bitsc)] **40**	3226m	-	1540s	1440m	1280m	749s
(2,3 H_2bitsc-N^1-Me, $^{5}H_2L$)	3461m, 3207m	-	1683s	1616m	-	831s
[Zn(bitsc,N-Me)] **41**	3367m	-	1612s	1550m	-	745s
(2,3 H_2bitsc-N^1-Ph)	3290m	3173w	1685s	1591m	-	827s

[Zn(bitsc,N-Ph)] **42**	3381m	-	1597s	1534m	-	752s
(2,5 H_2bptsc, ^7H_2L)	3356m, 3253m	3166m	1640s	1526s	1512m	895s
[Zn(bptsc)] **43**	3304m, 3220	-	1582s	1521m	1432m	753s
(2,5 H_2bptsc N-Me, ^8H_2L)	3335m, 3287m	3197m	1642s	1558s	-	804s
[Zn(bptsc,N-Me)] **44**	3265m	-	1553s	1427m	-	714s
(2,5 H_2bptsc N-Ph, ^9H_2L)	3301m	3158w	1639s,	1466m	-	829s
[Zn(bptsc,N-Ph)] **45**	3395m, 3200m	-	1666s	1457m	-	737
(2,6 H_2bdptsc, $^{10}H_2L$)	3423m, 3209m	3158m w	1606 s	1513m		827s
[Zn(dptsc)] **46**	3437m, 3310m	-	1587s	1471m	1419m	717s
(2,6H_2bdptsc N-Me,$^{11}H_2L$)	3450m, 3329m	3190 w	1634s,	1555m	-	836s
[Zn(dptsc,N-Me)] **47**	3395m, 3259m	-	1590s	1528m	-	745s
(2,6H_2bdptsc N-Ph, $^{12}H_2L$)	3303m	3156 w	1636s	1594m	-	896s
[Zn(dptsc,N-Ph)] **48**	3269m	-	1598m	1489s	-	751s

***s= strong; m= medium and w= weak**

8.4 Mass Spectrometry:

The molecular ion peak $[M]^+$ observed are listed in Table 8.4.1 and spectra are given in Figures 8.4.1-8.4.12. All the complexes have m/z values in well agreement with proposed stoichiometry. The parental ion peak in $(m/z)^+$ found at 393.29 amu (**37**), 413.26 amu (**38**), 521.13 amu (**39**), 365.02 amu (**40**), 429.03 amu (**41**), 528.04 amu (**42**), 329.20 amu (**43**), 357.01 amu (**44**), 477.08 amu (**45**), 372.00 amu (**46**), 400.03 amu (**47**), 524.06 amu (**48**) confirms the formation of bisthiosemicarbazones.

Table 8.4.1: The m/z values (amu) derived from mass spectra and expected formula of complexes **37-48.**

Sr. No.	**Parent peak (experimental mass)**	**Expected formula for parent ion $(m/z)^+$**
1	393.29	$[Zn(C_8H_{10}N_6S_3)]$ **37**
2	413.26	$[Zn(C_{10}H_{14}N_6S_3)]$ **38**
3	521.13	$[Zn(C_{20}H_{16}N_6S_3)]$ **39**
4	365.02	$[Zn(C_{10}H_9N_7S_2)]$ **40**
5	429.03	$[Zn(C_{12}H_{13}N_7S_2)]$ **41**
6	528.04	$[Zn(C_{22}H_{17}N_7S_2)]$ **42**
7	329.20	$[Zn(C_6H_{12}N_8S_2)]$ **43**
8	357.01	$[Zn(C_8H_{16}N_8S_2)]$ **44**
9	477.08	$[Zn(C_{18}H_{20}N_8S_2)]$ **45**
10	372.00	$[Zn(C_{11}H_{13}N_7S_2)]$ **46**
11	400.03	$[Zn(C_{13}H_{17}N_7S_2)]$ **47**
12	524.06	$[Zn(C_{23}H_{21}N_7S_2)]$ **48**

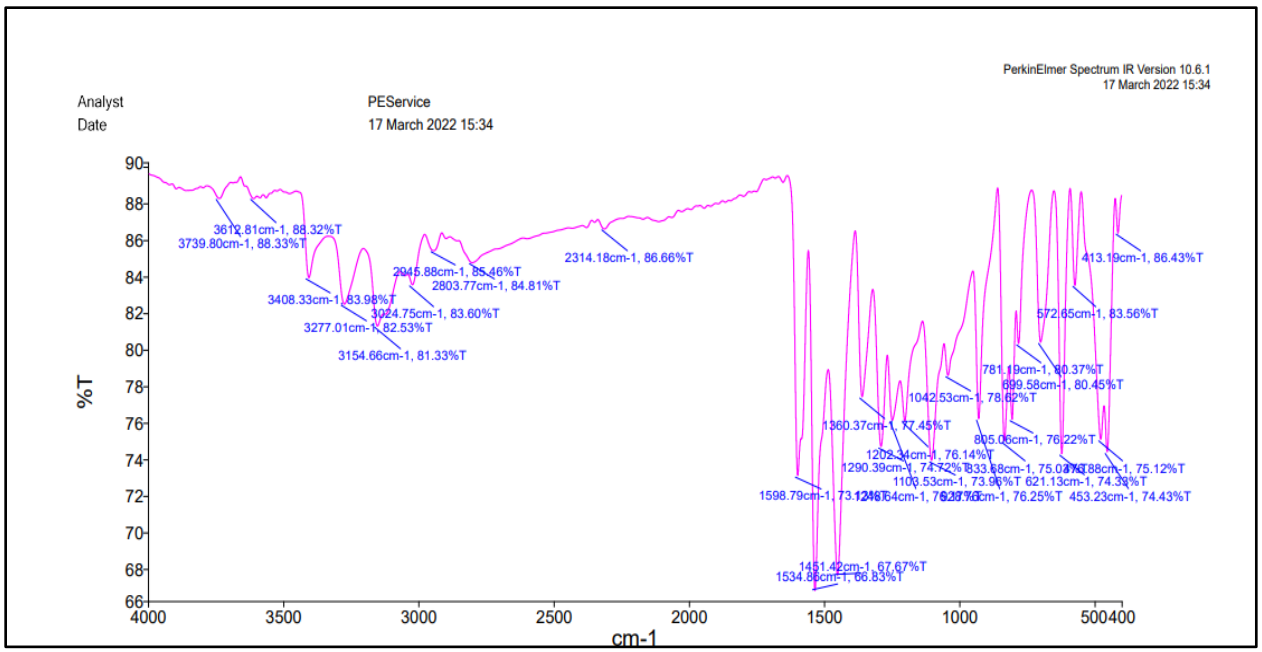

Figure 8.3.1: IR Spectra of [Zn(bttsc)] **37**

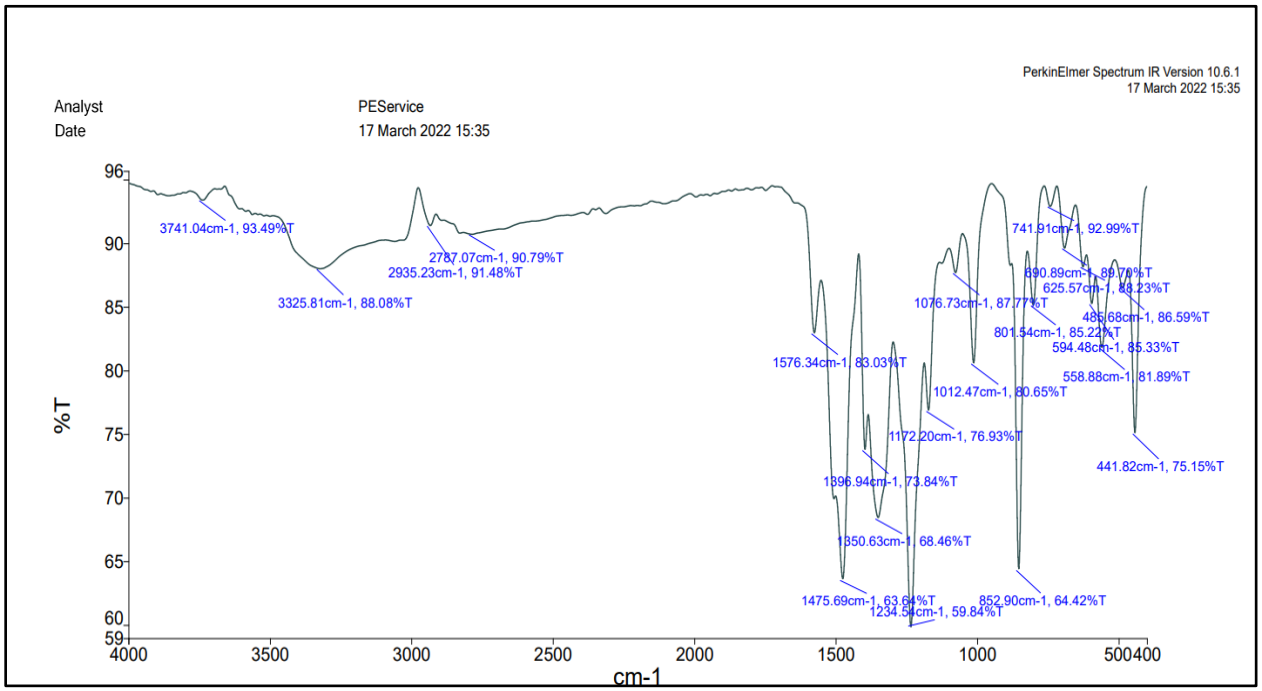

Figure 8.3.2: IR Spectra of [Zn(bttsc,N-Me)] **38**

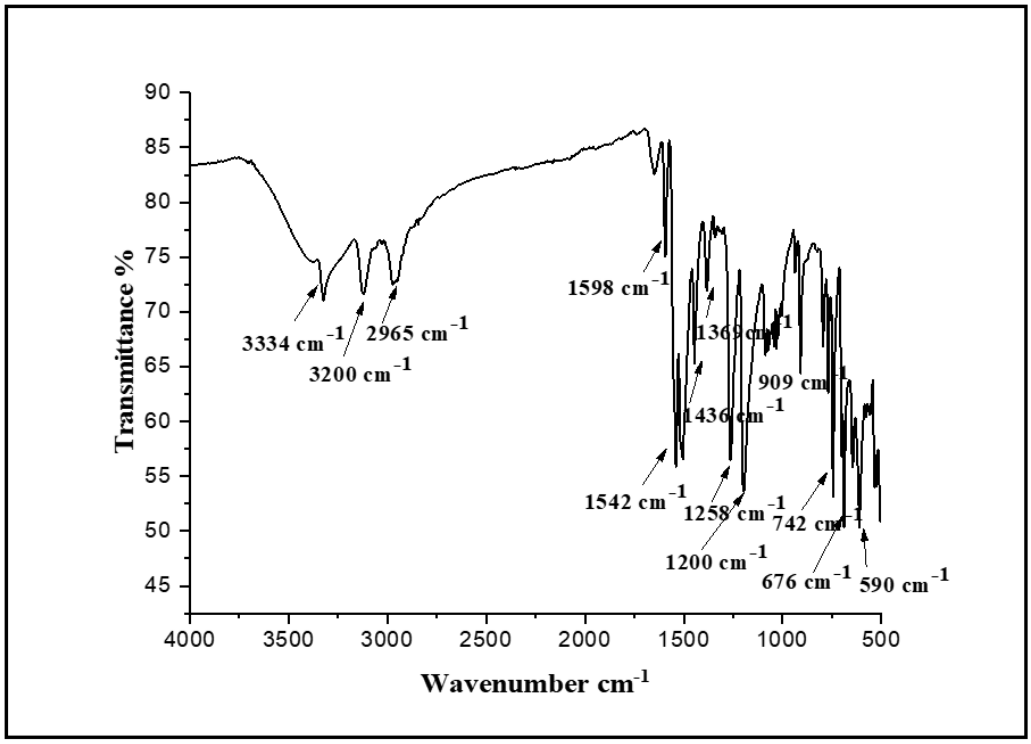

Figure 8.3.3: IR Spectra of [Zn(bttsc,N-Ph)] **39**

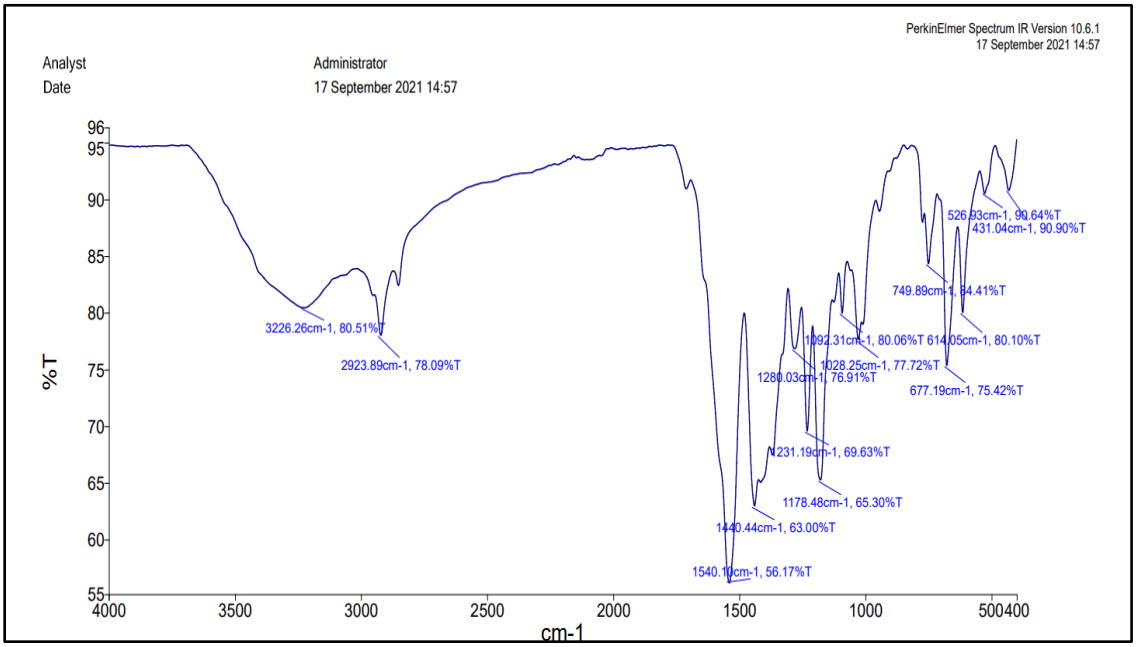

Figure 8.3.4: IR Spectra of [Zn(bitsc)] **40**

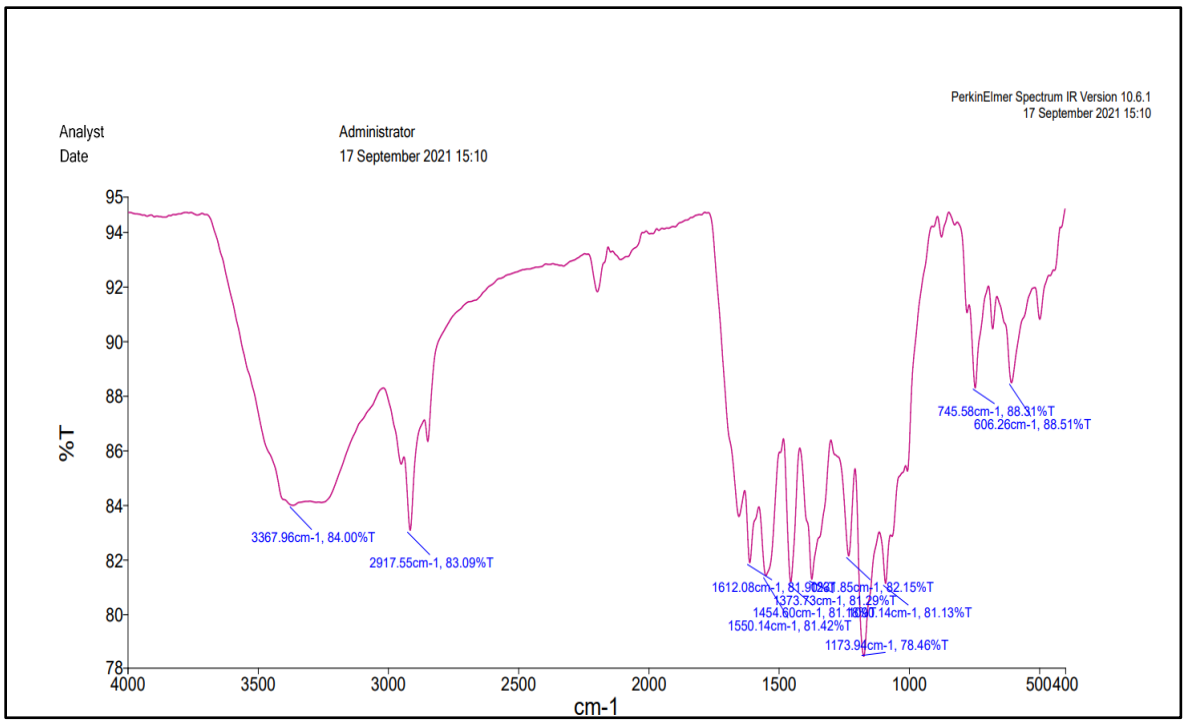

Figure 8.3.5: IR Spectra of [Zn(bitsc,N-Me)] **41**

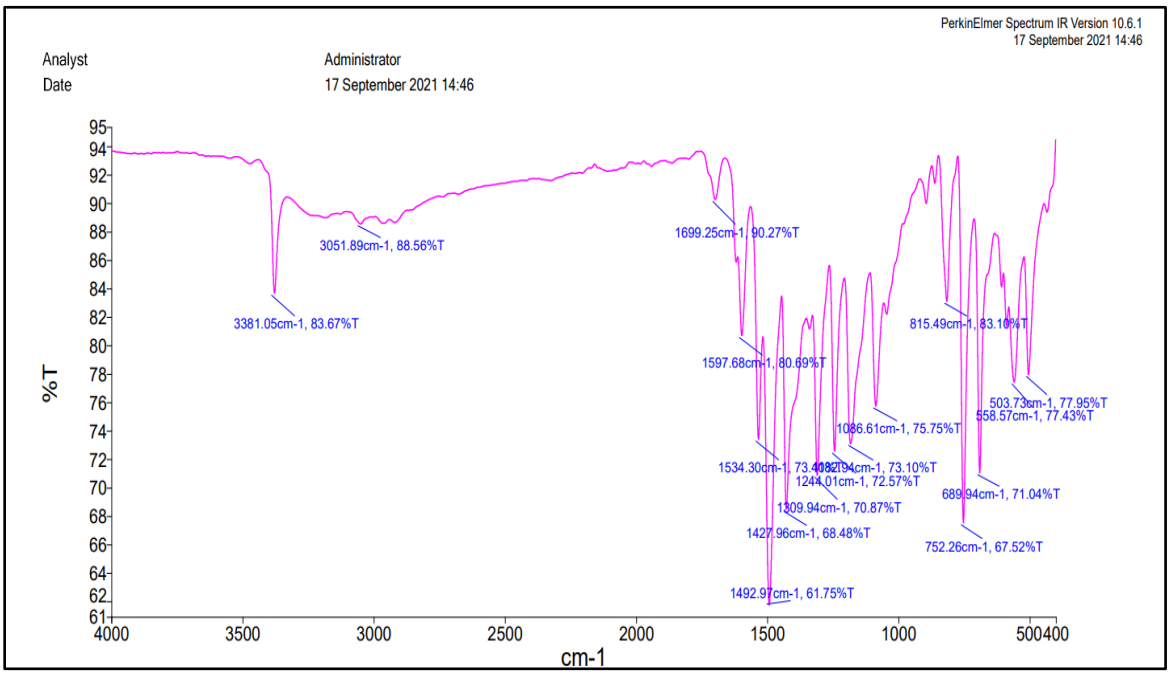

Figure 8.3.6: IR Spectra of [Zn(bitsc,N-Ph)] **42**

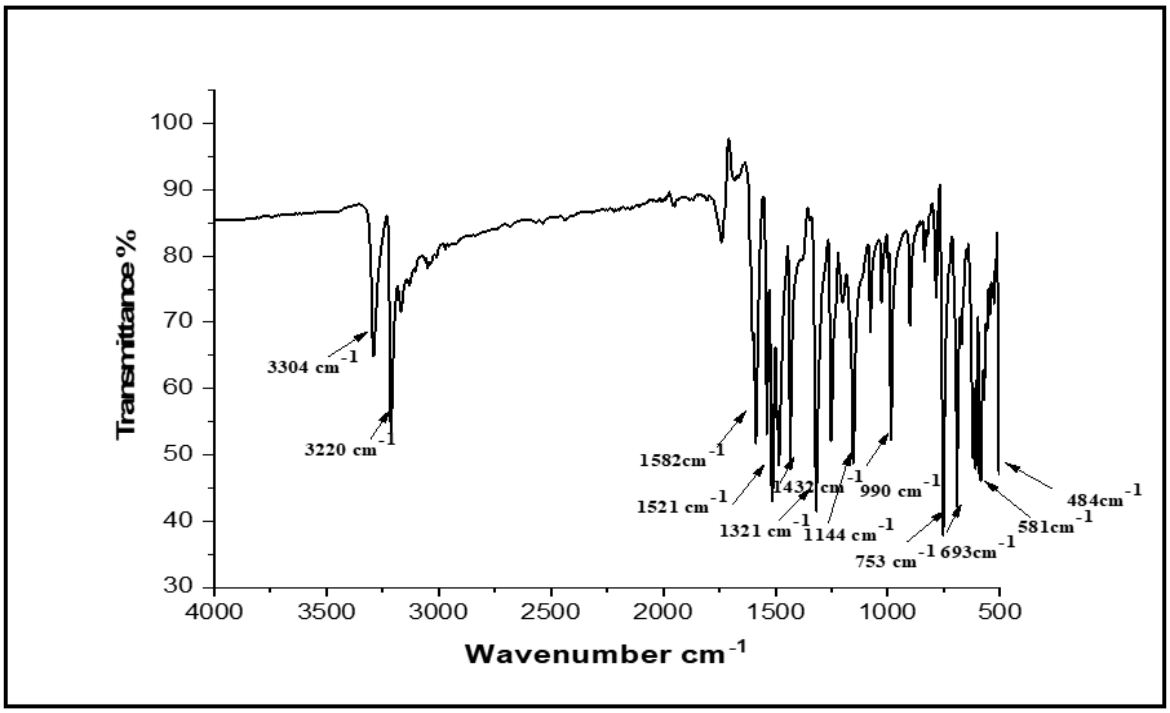

Figure 8.3.7: IR Spectra of [Zn(bptsc)] **43**

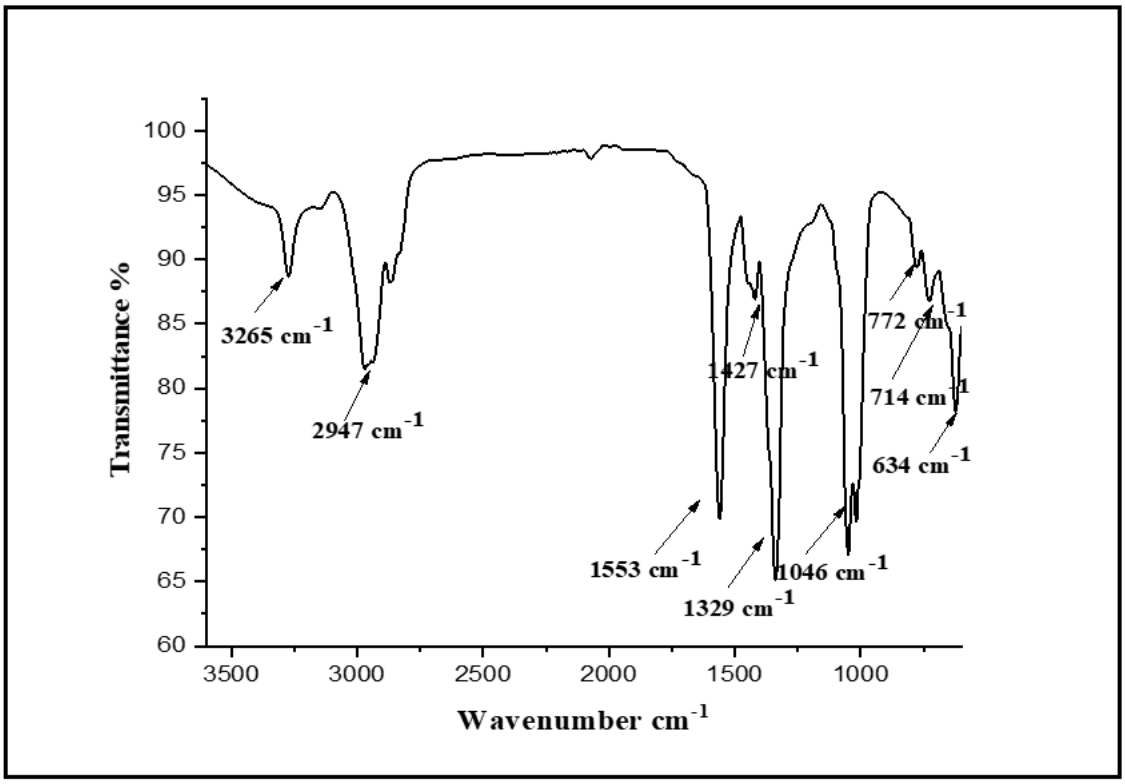

Figure 8.3.8: IR Spectra of [Zn(bptsc,N-Me)] **44**

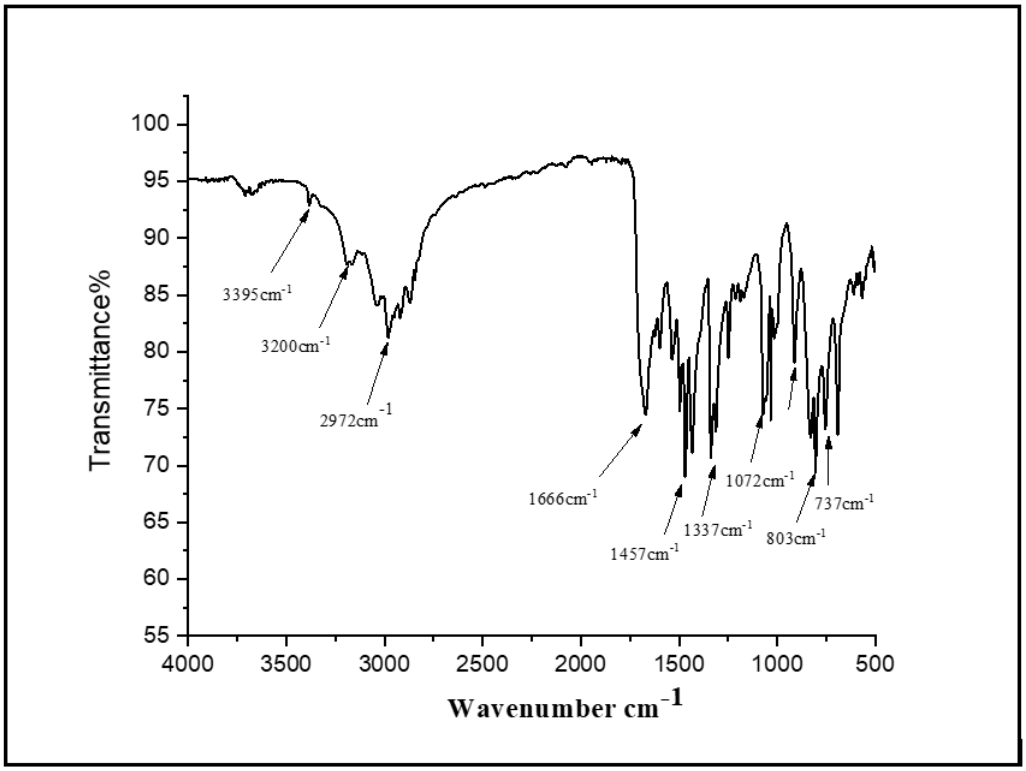

Figure 8.3.9: IR Spectra of [Zn(bptsc,N-Ph)] **45**

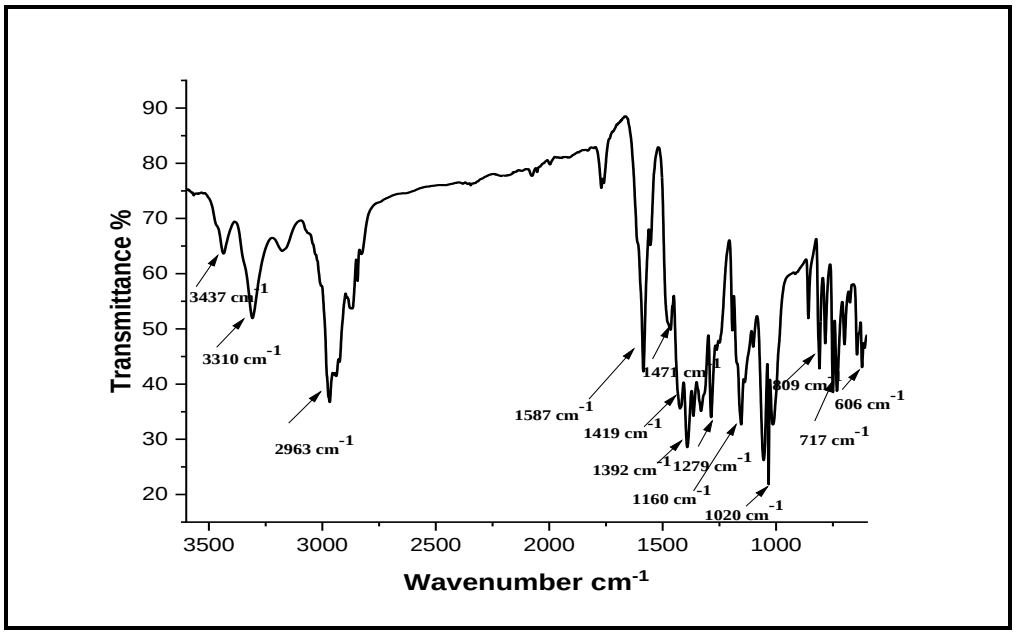

Figure 8.3.10: IR Spectra of [Zn(dptsc)] **46**

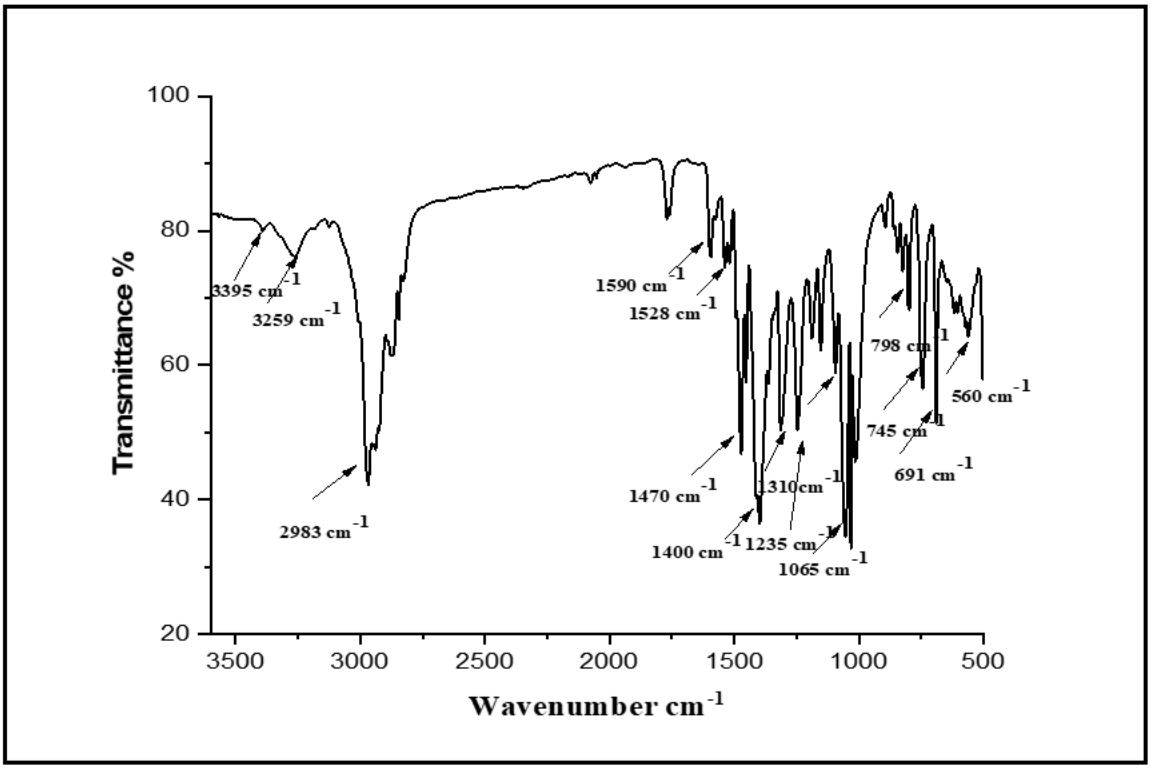

Figure 8.3.11: IR Spectra of [Zn(dptsc,N-Me)] **47**

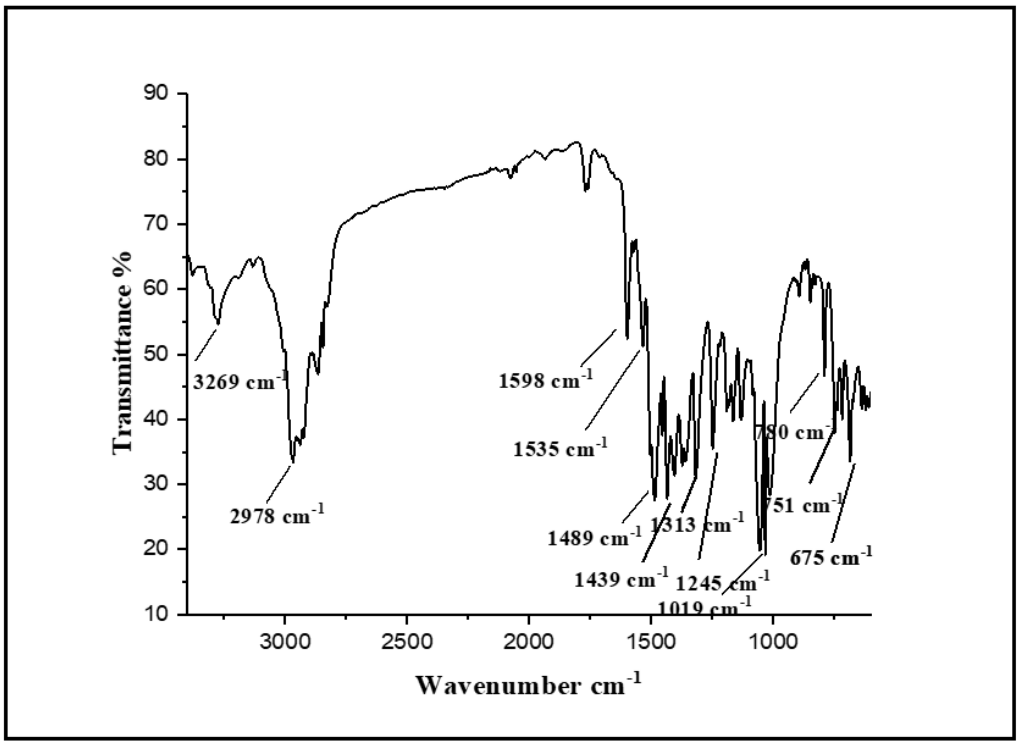

Figure 8.3.12: IR Spectra of [Zn(dptsc,N-Ph)] **48**

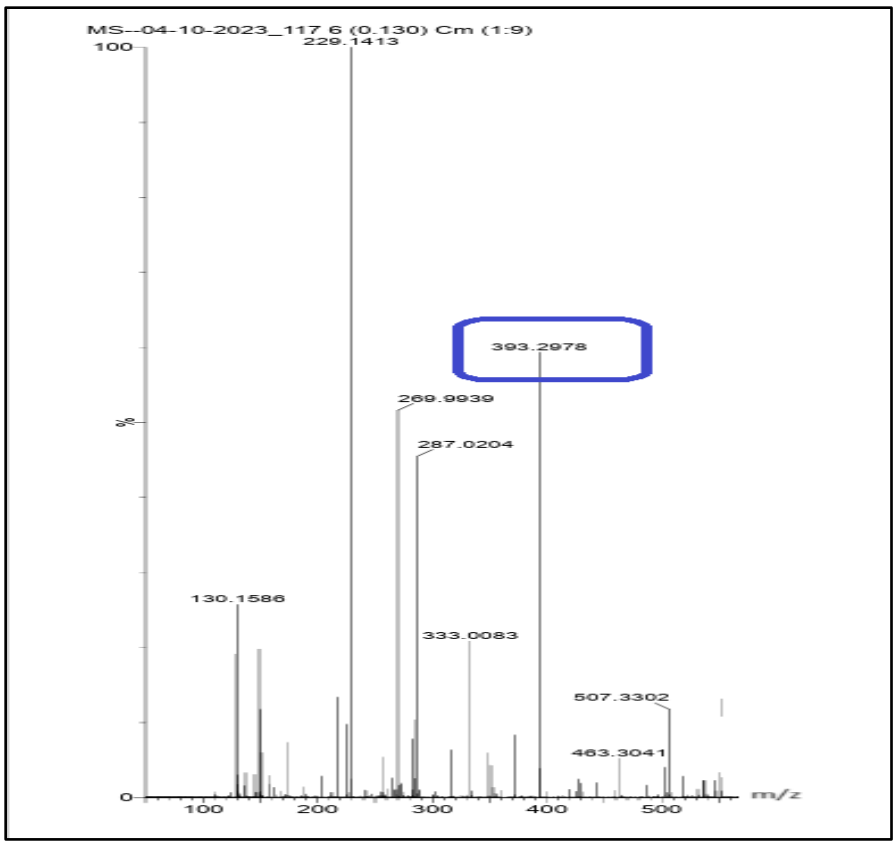

Figure 8.4.1: Mass spectrometry of complex [Zn(bttsc)] **37**

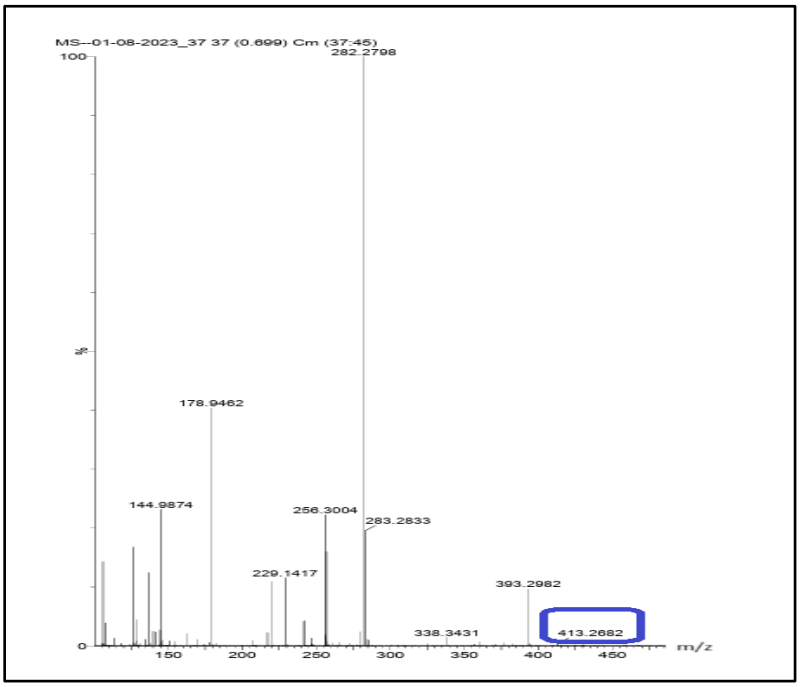

Figure 8.4.2: Mass spectrometry of complex [Zn(bttsc,N-Me)] **38**

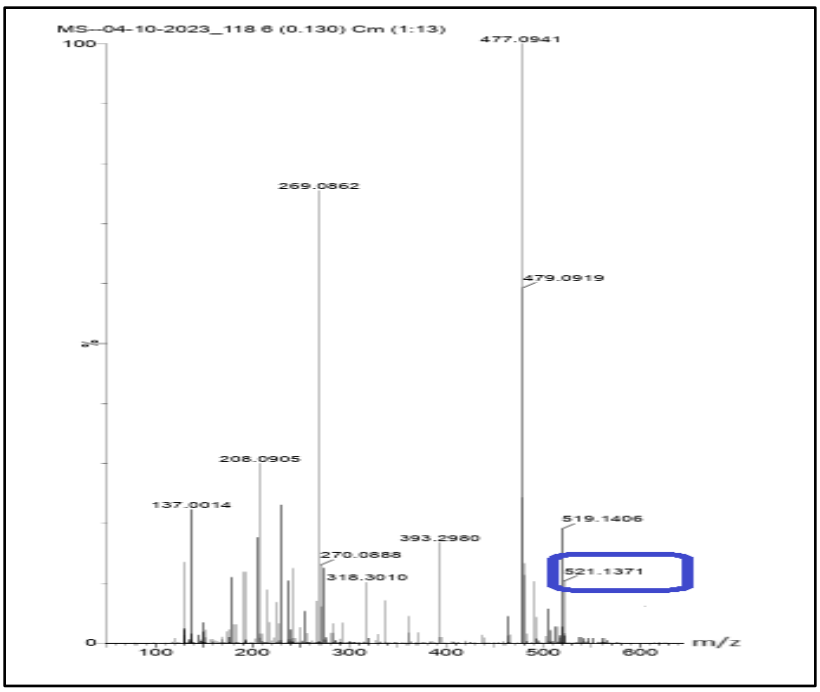

Figure 8.4.3: Mass spectrometry of complex [Zn(bttsc,N-Ph)] **39**

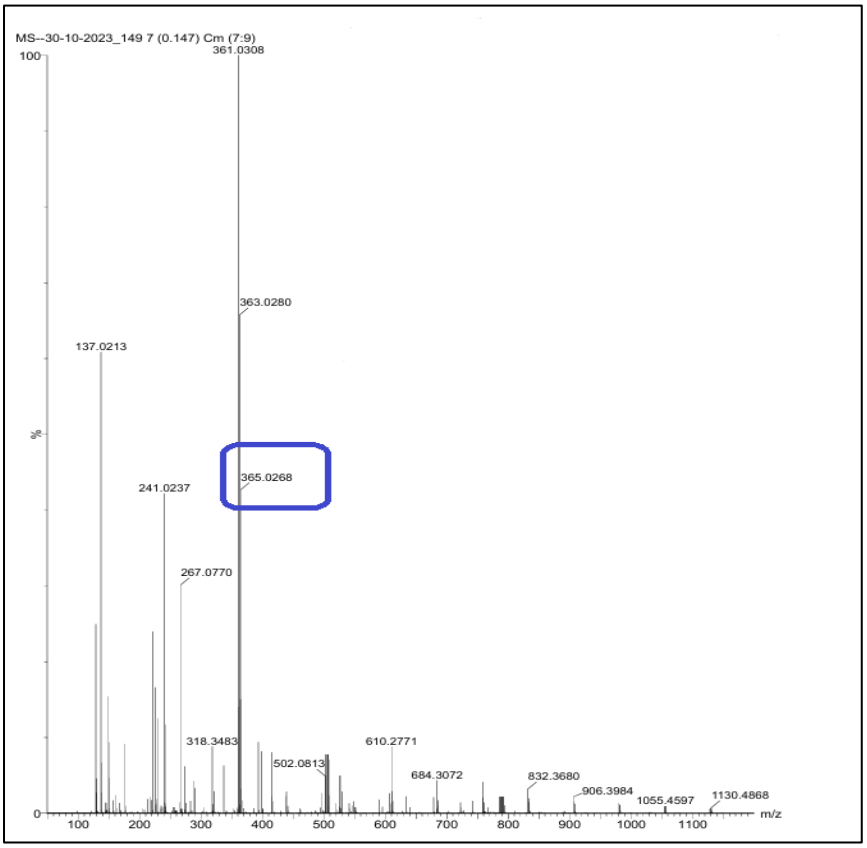

Figure 8.4.4: Mass spectrometry of complex [Zn(bitsc)] **40**

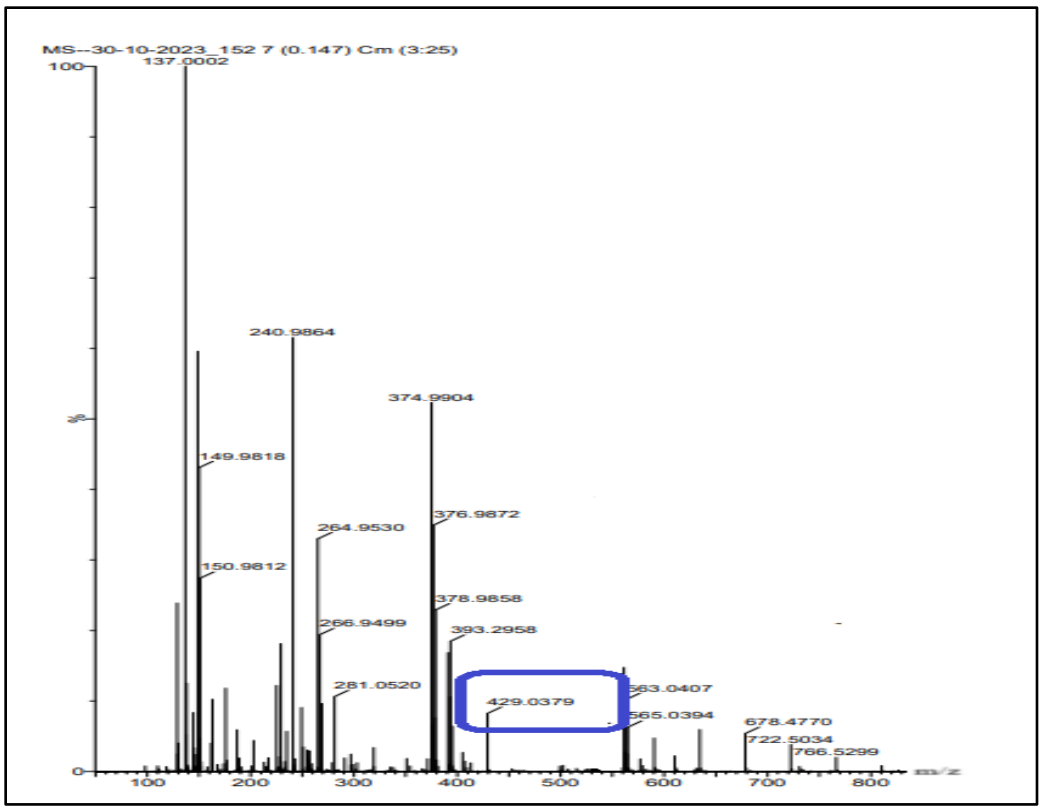

Figure 8.4.5: Mass spectrometry of complex [Zn(bitsc,N-Me)] **41**

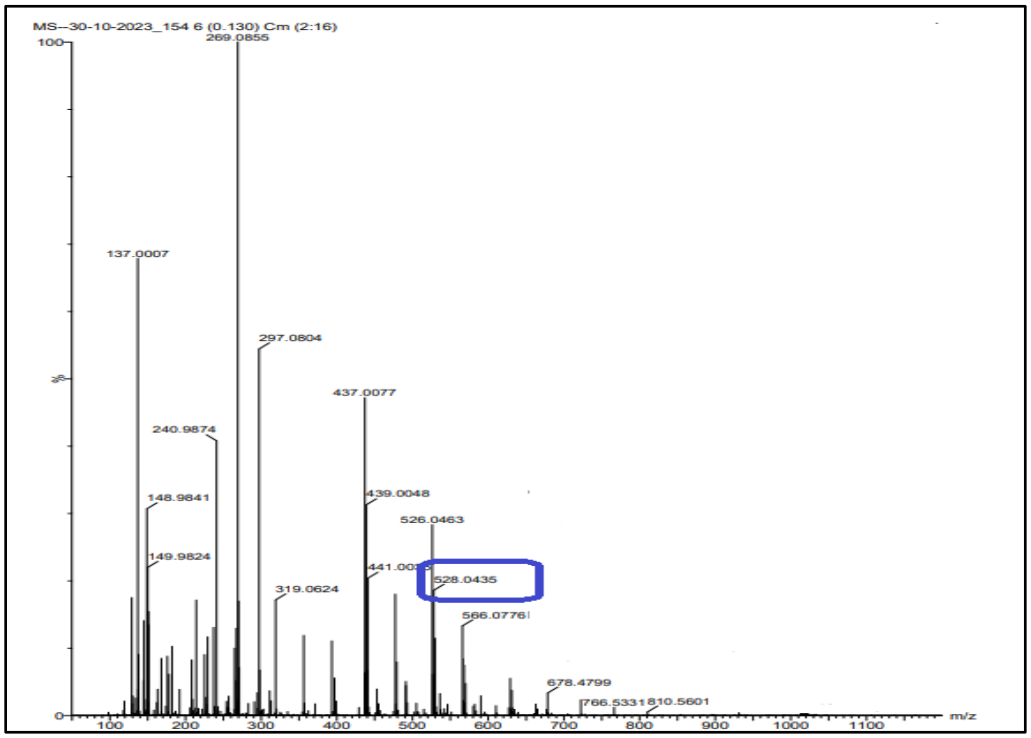

Figure 8.4.6: Mass spectrometry of complex [Zn(bitsc,N-Ph)] **42**

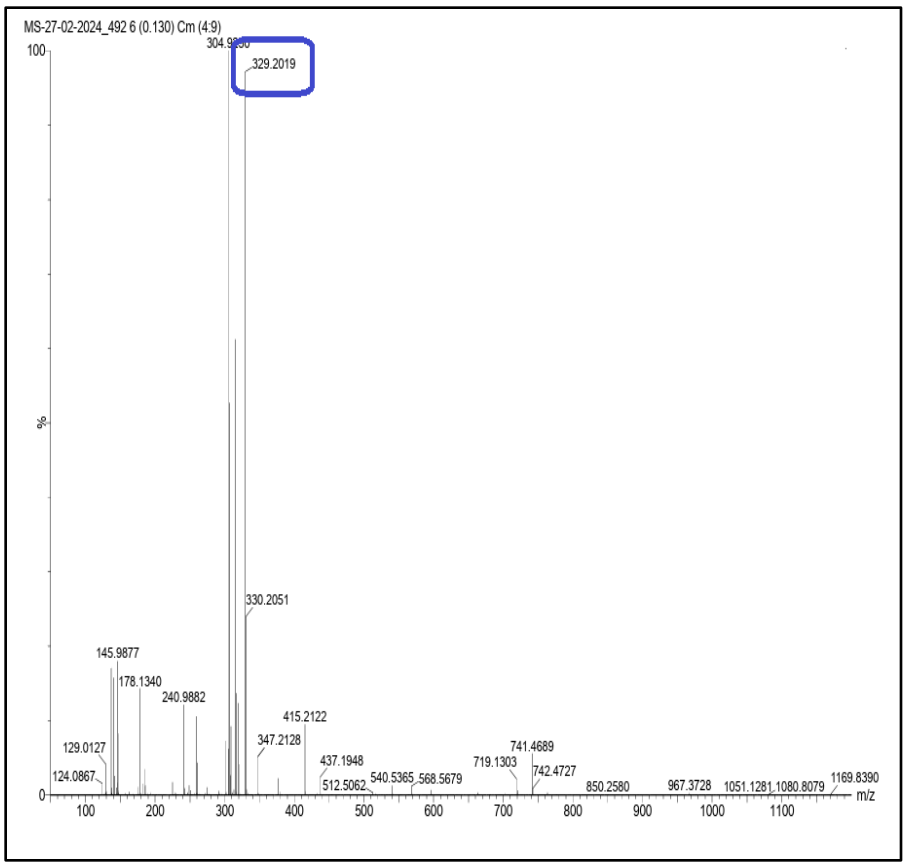

Figure 8.4.7: Mass spectrometry of complex [Zn(bptsc)] **43**

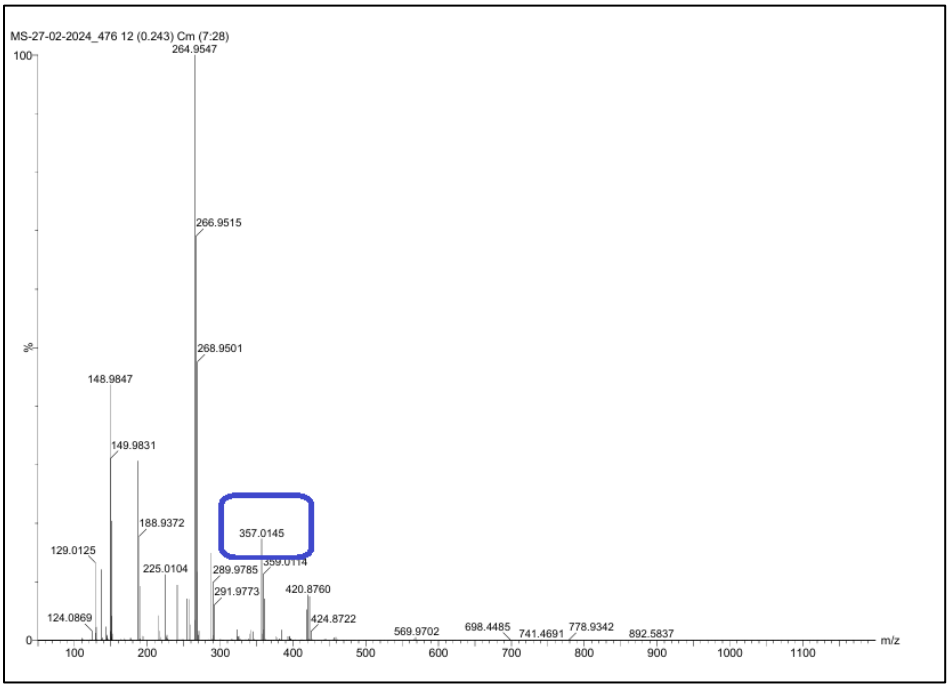

Figure 8.4.8: Mass spectrometry of complex [Zn(bptsc,N-Me)] **44**

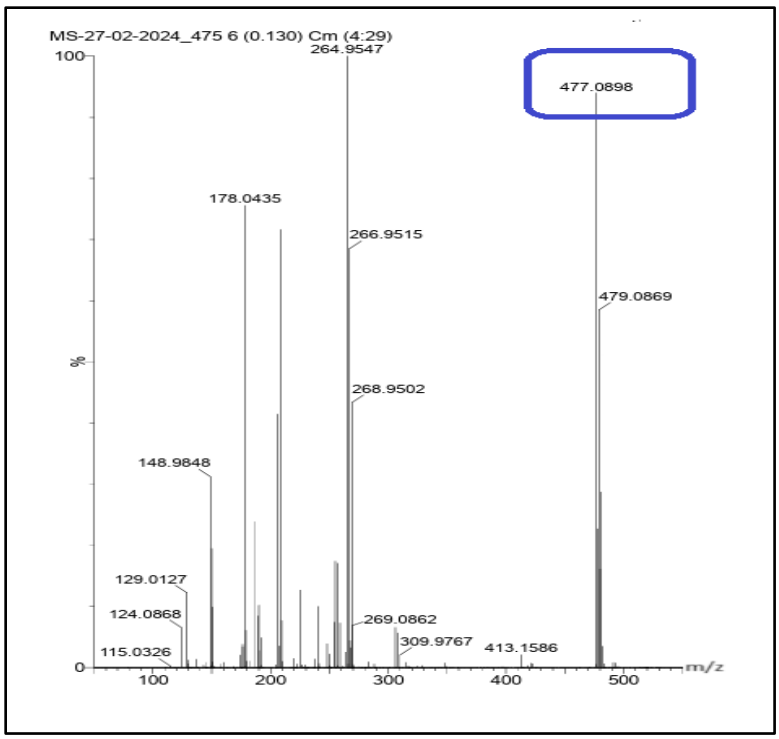

Figure 8.4.9: Mass spectrometry of complex [Zn(bptsc,N-Ph)] **45**

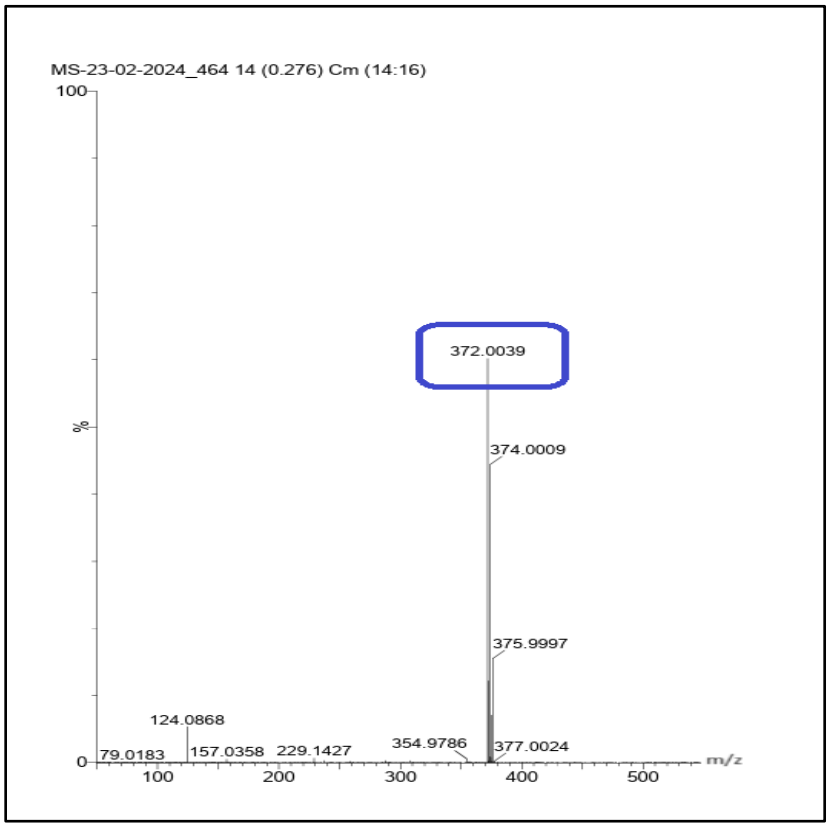

Figure 8.4.10: Mass spectrometry of complex [Zn(bdptsc)] **46**

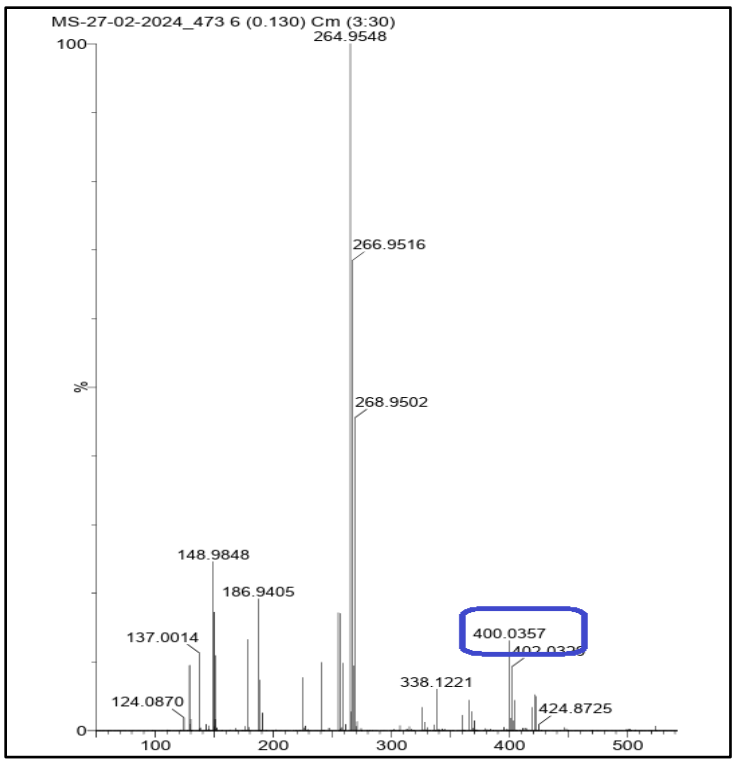

Figure 8.4.11: Mass spectrometry of complex [Zn(bdptsc,N-Me)] **47**

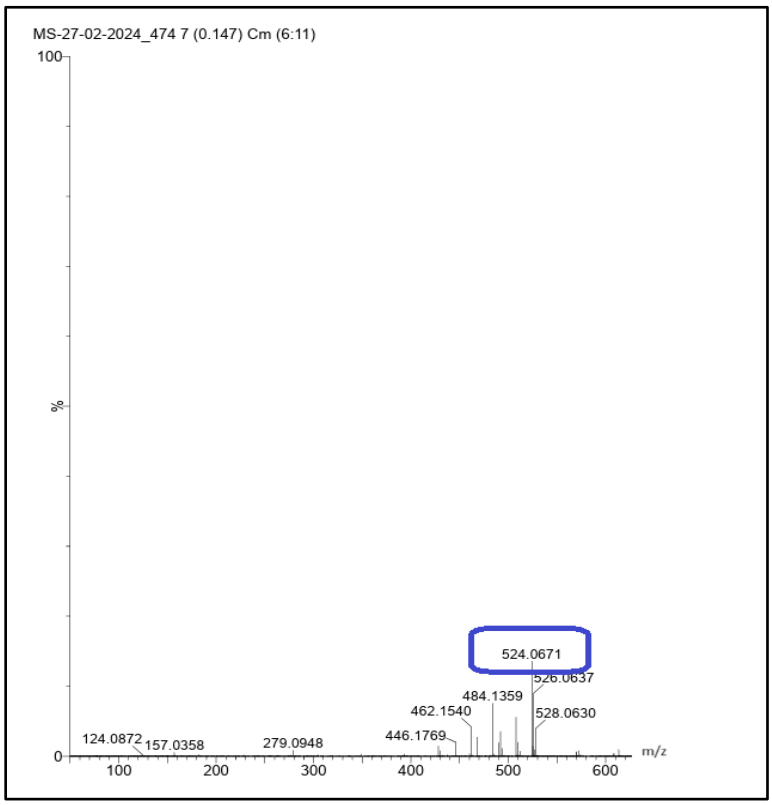

Figure 8.4.12: Mass spectrometry of complex [Zn(bdptsc,N-Ph)

8.5 XRD studies:

X-ray diffraction (XRD) is a strong analytical technique for determining the atomic or molecular structure of crystalline materials. The diffraction pattern formed by X-rays interacting with the crystal lattice provides a lot of information about the material's structural features. When electromagnetic radiation interacts with an ordered periodic structure, diffraction occurs. X-rays are electromagnetic waves with extremely short wavelengths of a few angstroms (1 Angstrom =0.1nm), equal to the distance between two successive planes in a crystal. The short wavelength of X-rays reveals their tremendous energy value. Diffraction occurs when an electromagnetic wave bends around the corners of an obstacle, as if the size of the aperture or obstacle matches the wavelength of the wave. For diffraction to occur, the incident radiation's wavelength must match the periodic structure's repeat distance. In crystalline substances, inter-atomic distances range from 1-10 Angstrom, making X-rays suitable for diffraction from the atoms. This characterisation approach relies on constructive interference in cathode ray tubes, resulting in a monochromatic stream of X-rays from the crystalline sample. X-ray diffraction (XRD) is a non-destructive method for studying X-ray interactions with materials. Elastic diffusion, also known as Rayleigh diffusion, is when a monochromatic X-ray beam interacts with an object and scatters in random directions with the same energy as the input photons. This characterisation approach only applies to crystalline or semi-crystallized materials. If the sample has a regular arrangement of atoms, dispersed light will be oriented in specific directions based on X-ray wavelength, crystal lattice dimensions, and orientation [220]. Bragg's condition states that constructive interference of rays from planes results in a diffracted beam from a crystalline material. To determine the X-ray pattern of a material, measure its intensity as a function of angle [2θ].

The powder X-ray diffraction patterns of the complexes were recorded in the range of 2θ = 10-60° to obtain additional details regarding the crystalline structure of the metal-ligand complexes. All the complexes showed strong sharp peaks in XRD graphs indicates crystalline behaviour of the complexes (**37-48**). The powder XRD analysis of the complexes are shown in Figures 8.5.1-8.5.10 and the XRD parameters of complexes **37-48** are given in Tables 8.5.1-8.5.10. The diffraction of X-rays from crystalline planes is described by William H. and W. Lawrence Bragg in their law known as Bragg's Law [221]. It clarifies the relationship between the

wavelength used for X-rays and the angle at which a beam diffracts from a crystalline surface. The interplanar spacing (d) can be calculated using (Equation -12) according to Bragg's rule [222].

$$d = \frac{n\lambda}{2sin\theta} \qquad \text{…….. (12)}$$

where λ = 1.5406 Å denotes the X-ray wavelength, n is the diffraction peak order, and θ is Bragg's angle. The d-spacing values for the prepared samples acquired are given in Table 8.14.

To determine the average crystalline size, Debye-Scherer's (Equation -13) is used.

$$D = \frac{\lambda}{\beta\cos(\theta)} \qquad \text{…….……. (13)}$$

Where, D is the Size of crystals, λ is the X-ray wavelength, β = Full width at the diffraction peak's half maximum, θ stands for Bragg's angle. The crystal size, crystal system, space group and cell parameters of complexes are given in Table 8.5.11.

The average crystal size of the complexes was calculated using the equation-13. The complexes **37-48** have different crystal sizes as 25.95 **37**, 53.74 **38**, 53.74 **39**, 0.993 **41**, 5.77 **42**, 8.2 **42**, 15.23 **43**, 16.65 **44**, 13.10 **45**, 42.34 **46**, 23.22 **47**, 38.96 **48**. It was observed that crystalline complexes (**37-39,43-48**) has good crystal size as compared to amorphous complexes (**40,42**) and belongs to different crystal system. The crystal structure of complexes can vary depending on the type of the ligands (ionic, covalent, or π-acceptor), as well as their sizes and forms. Bulky ligands or ligands with flexible binding sites can cause distortion in metal-ligand interactions and change how metal complexes pack together. Bulky ligands, for example, may hinder close packing, resulting in more open or asymmetrical crystal formations. Large ligands or substituents on ligands can cause steric hindrance, pushing the complex to form a certain arrangement that may depart from ideal geometry. Furthermore, Steric conflicts can change the relative orientation of molecules in the crystal lattice, resulting in distinct unit cells and symmetries. The spectra of amorphous complexes (**40,42**) are given after crystalline complexes.

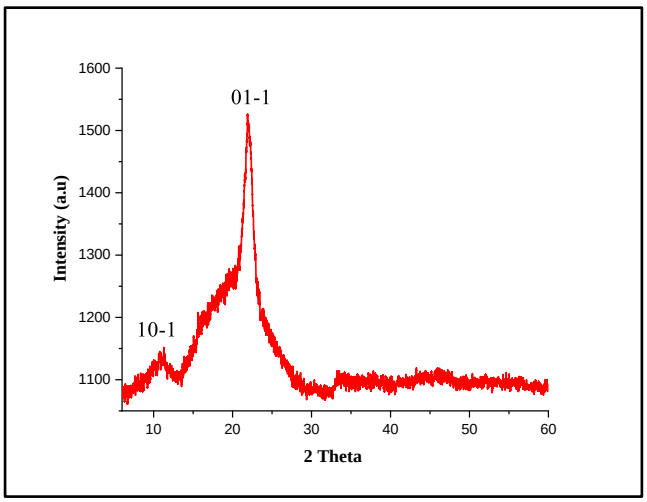

Figure 8.5.1: XRD Spectra of [Zn(bttsc)] **37**

Table 8.5.1: XRD parameters of [Zn(bttsc,N-Me)] **37**

Peaks	2θ	θ	Sinθ	$d^{(Calcd)}$	$d^{(obsd)}$	hkl
1.	12.28	6.14	0.106	7.26	7.19	10-1
2.	22.06	11.03	0.191	4.03	4.02	01-1
3.	28.90	14.45	0.249	3.09	3.08	100

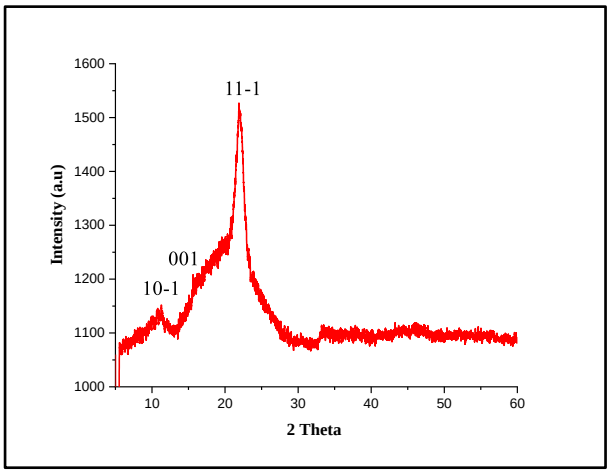

Figure 8.5.2: XRD Spectra of [Zn(bttsc,N-Me)] **38**

Table 8.5.2: XRD parameters of [Zn(bttsc,N-Me)] **38**

Peaks	2θ	θ	Sinθ	$d^{(Calcd)}$	$d^{(obsd)}$	hkl
1.	12.28	6.14	0.106	7.26	7.19	10-1
2.	16.18	8.09	0.140	5.50	5.47	001
3.	22.017	11.00	0.190	4.05	4.03	11-1

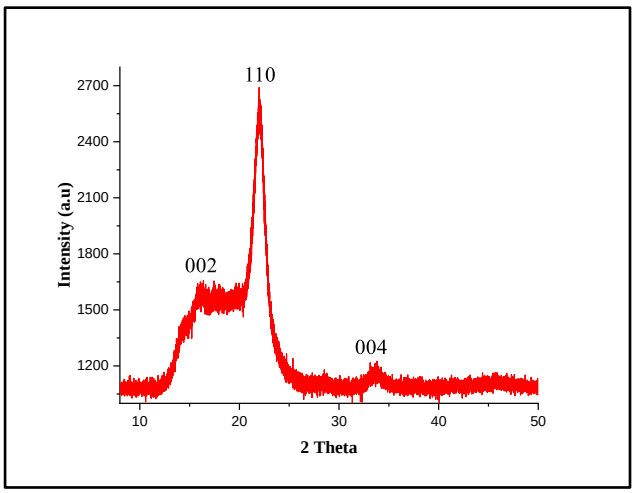

Figure 8.5.3: XRD Spectra of [Zn(bttsc,N-Ph)] **39**

Table 8.5.3: XRD parameters of [Zn(bttsc,N-Ph)] **39**

Peaks	**2θ**	**θ**	**Sinθ**	**d(Calcd)**	**d(obsd)**	**hkl**
1.	16.10	8.05	0.140	5.50	5.49	002
2.	22.06	11.03	0.191	4.05	4.03	110
3.	33.57	16.78	0.288	2.67	2.68	004

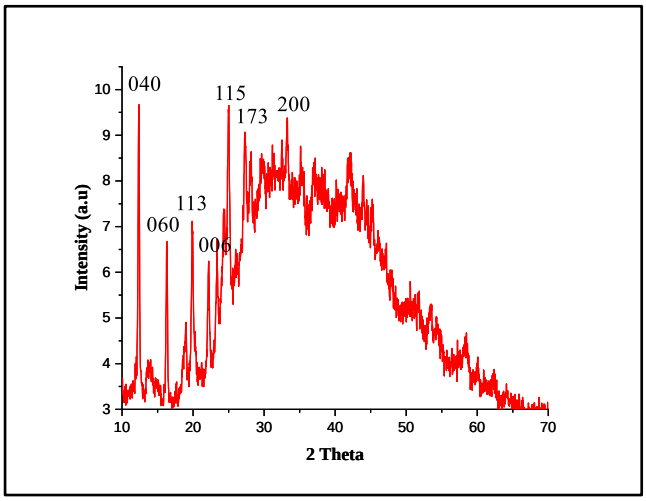

Figure 8.5.4: XRD Spectra of [Zn(bitsc,N-Me)] **41**

Table 8.5.4: XRD parameters of [Zn(bitsc,N-Me)] **41**

Peaks	**2θ**	**θ**	**Sinθ**	**d(Calcd)**	**d(obsd)**	**hkl**
1.	12.39	6.19	0.107	7.19	6.93	040
2.	16.38	8.19	0.142	5.42	5.66	060
3.	20.02	10.01	0.173	4.45	4.42	113
4.	22.10	11.05	0.191	4.03	4.01	006
5.	25.14	12.57	0.217	3.54	3.56	115
6.	27.08	13.54	0.234	3.29	3.28	173
7.	33.39	16.69	0.287	2.68	2.68	200

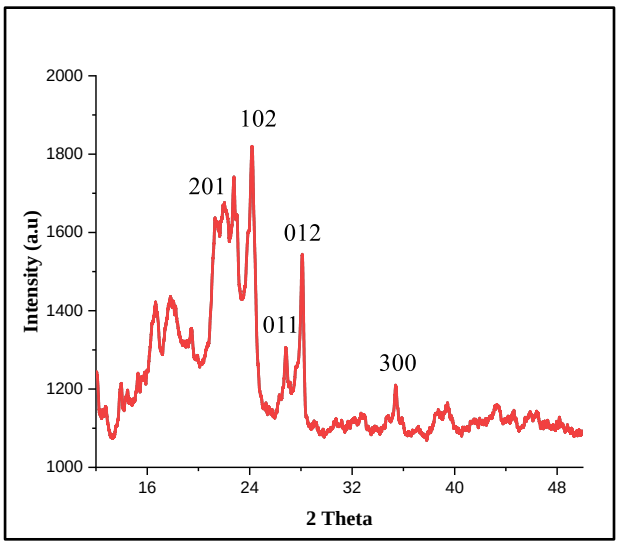

Figure 8.5.5: XRD spectra of [Zn(bptsc)] **43**

Table 8.5.5: XRD parameters of [Zn(bptsc)] **43**

Peaks	2θ	θ	Sinθ	$d^{(Calcd)}$	$d^{(obsd)}$	hkl
1.	22.91	11.45	0.198	3.89	3.87	201
2.	24.15	12.06	0.208	3.68	3.68	102
3.	26.91	13.45	0.232	3.32	3.29	011
4.	28.12	14.06	0.242	3.17	3.17	012
5.	35.41	17.70	0.304	2.53	2.52	300

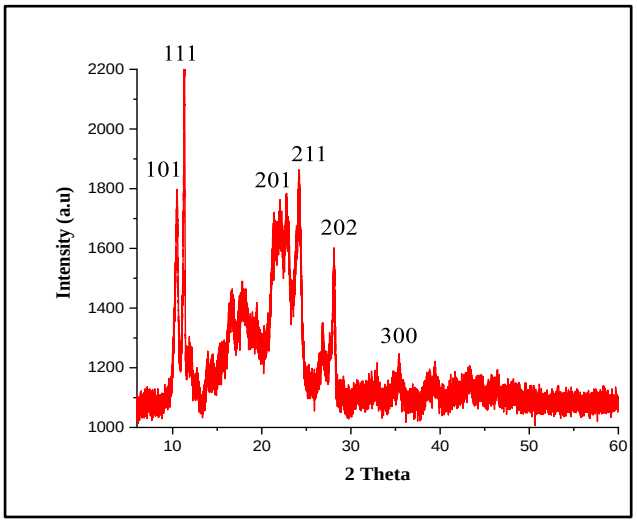

Figure 8.5.6: XRD spectra of [Zn(bptsc,N-Me)] **44**

Table 8.5.6: XRD parameters of [Zn(bptsc,N-Me)] **44**

Peaks	2θ	θ	Sinθ	$d^{(Calcd)}$	$d^{(obsd)}$	hkl
1.	10.49	5.24	0.091	8.46	8.42	101
2.	11.35	5.67	0.098	7.86	7.78	111
3.	22.91	11.45	0.198	3.89	3.87	201
4.	24.23	12.11	0.209	3.67	3.66	211
5.	28.14	14.07	0.243	3.16	3.17	202
6.	35.41	17.70	0.304	2.53	2.52	300

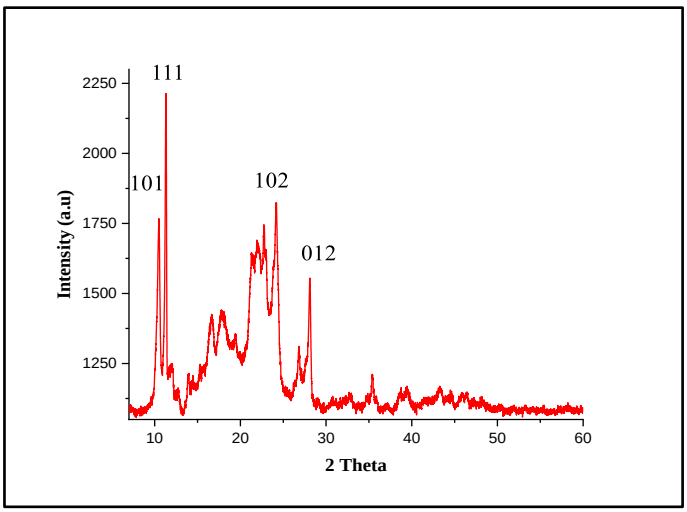

Figure 8.5.7: XRD spectra of [Zn(bptsc,N-Ph)] **45**

Table 8.5.7: XRD parameters of [Zn(bptsc,N-Ph)] **45**

Peaks	2θ	θ	Sinθ	$d^{(Calcd)}$	$d^{(obsd)}$	hkl
1.	10.49	5.24	0.091	8.46	8.42	101
2.	11.35	5.67	0.098	7.86	7.78	111
3.	24.15	12.06	0.208	3.68	3.68	102
4.	28.12	14.06	0.242	3.17	3.17	012

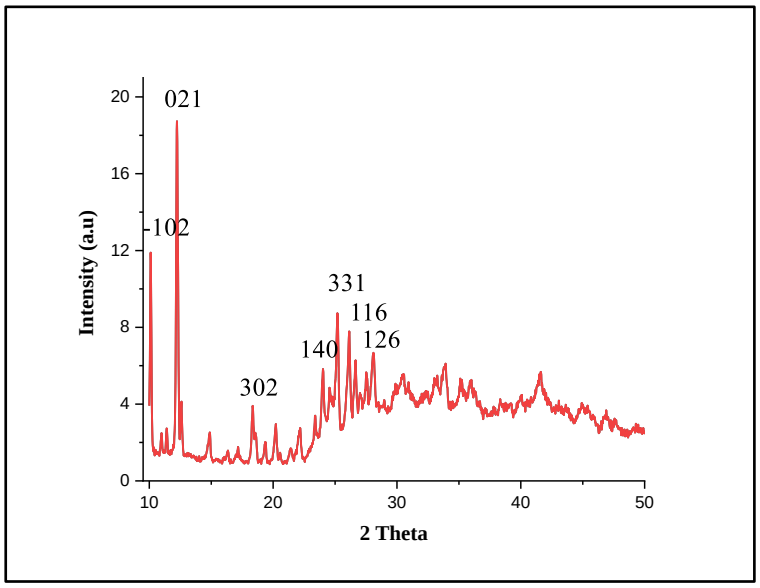

Figure 8.5.8: XRD Spectra of [Zn(bdptsc)] **46**

Table 8.5.8: XRD parameters of [Zn(bdptsc)] **46**

Peaks	2θ	θ	Sinθ	$d^{(Calcd)}$	$d^{(obsd)}$	hkl
1.	10.17	5.08	0.088	8.75	8.74	-102
2.	12.31	6.15	0.107	7.19	7.10	021
3.	20.03	10.01	0.173	4.53	4.54	302
4.	24.21	12.10	0.209	3.68	3.65	140
5.	25.42	12.71	0.220	3.50	3.50	331
6.	26.27	13.13	0.227	3.42	3.39	116
7.	28.19	14.09	0.243	3.16	3.16	126

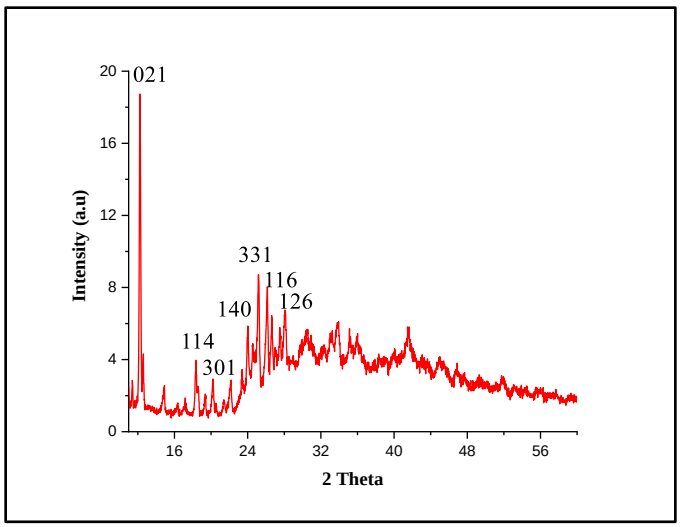

Figure 8.5.9: XRD Spectra of [Zn(bdptsc,N-Me)] **47**

Table 8.5.9: XRD parameters of [Zn(bdptsc,N-Me)] **47**

Peaks	2θ	θ	Sinθ	$d^{(Calcd)}$	$d^{(obsd)}$	hkl
1.	12.31	6.15	0.107	7.199	7.104	021
2.	18.47	9.23	0.160	4.81	4.88	114
3.	20.03	10.01	0.173	4.53	4.54	302
4.	24.21	12.10	0.209	3.68	3.65	140
5.	25.42	12.71	0.220	3.50	3.50	331
6.	26.27	13.13	0.227	3.42	3.39	116
7.	28.19	14.09	0.243	3.16	3.16	126

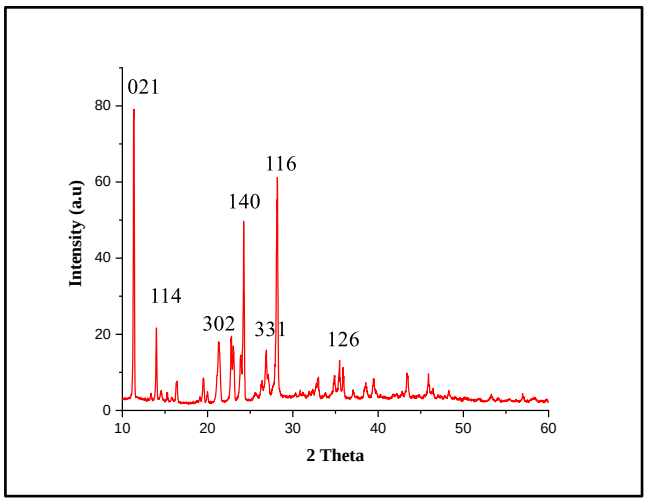

Figure 8.5.10: XRD Spectra of [Zn(bdptsc, N-Ph)] **48**

Table 8.5.10: XRD parameters of [Zn(bdptsc,N-Ph)] **48**

Peaks	2θ	θ	Sinθ	$d^{(Calcd)}$	$d^{(obsd)}$	hkl
1.	12.31	6.15	0.107	7.199	7.104	021
2.	18.47	9.23	0.160	4.81	4.88	114
3.	20.03	10.01	0.173	4.53	4.54	302
4.	24.21	12.10	0.209	3.68	3.65	140
5.	25.42	12.71	0.220	3.50	3.50	331
6.	26.27	13.13	0.227	3.42	3.39	116
7.	28.19	14.09	0.243	3.16	3.16	126

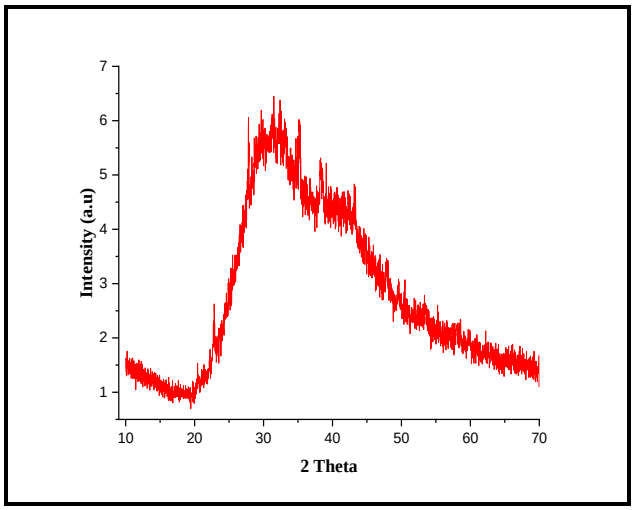

Figure 8.5.11: XRD Spectra of [Zn(bitsc)] **40**

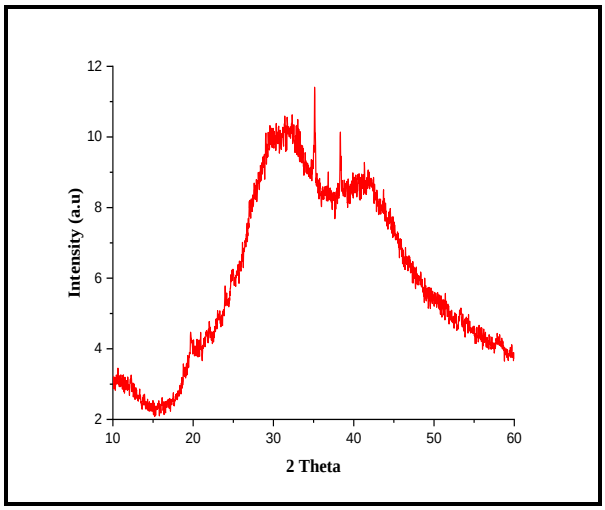

Figure 8.5.12: XRD Spectra of [Zn(bitsc,N-Ph)] **42**

Table 8.5.11: Crystal system, crystallite size, space group and cell parameters of complexes **(37-48)**

Complex No.	**Crystal system**	**Crystallite size (nm)**	**Space group**	**Cell parameters(Å)**
37	Triclinic	25.95	P-1 (2)	a= 2.95390 b= 4.84300 c= 5.58800
38	Monoclinic	53.74	P-1 21/m 1 (11)	a= 13.36500 b= 5.09700 c= 6.63800
39	Tetragonal	7.96	I 4/m m m(139)	a= 5.49300 c= 10.97000
40	Hexagonal	10.99	P-3 1 m (162)	a= 6.64000 c= 39.75000
41	Orthorhombic	5.77	F m m m (69)	a= 5.36710 b= 33.97190 c= 24.07220

42	Monoclinic	8.2	P n m a (62)	a= 6.19647 b= 8.74999 c= 6.22045
43	Hexagonal	15.23	P 63 m c (186)	a= 5.47000 c= 8.92000
44	Cubic	16.65	P 41 3 2 (213)	a= 6.93520 Å
45	Hexagonal	13.10	P 63 m c (186)	a= 5.47000 c= 8.92000
46	Monoclinic	42.34	P 1 2/c 1 (13)	a= 13.06020 b= 12.07450 c= 15.71140
47	Monoclinic	23.22	P 1 c 1 (7)	a= 15.05020 b= 15.05450 c= 21.51140
48	Monoclinic	38.96	P 1 2/c 1 (13)	a= 10.02000 b= 11.50100 c= 16.28600

8.6 Anti-tuberculosis activity:

All the ligands **($^{1}H_2L$-$^{12}H_2L$)** and their Zinc(II) complexes **(37-48)** were evaluated and is given in Table 8.6.1 [179]. No particular structure-activity relationship has been observed. The anti-T.B activity of ligands generally gets enhanced upon complexation. It was found from the experimental data that the activity of ligand **2,5 H_2bttsc N-Ph ($^{3}H_2L$), and 2,5 H_2bptsc ($^{7}H_2L$)** has no change on complexation and exhibited maximum anti-T.B activity (MIC = 1.6µg/ml), even same to standard drugs Rifampicin or Streptomycin (MIC = 1.6µg/ml). The anti-TB activity of ligands $^{1}H_2L$, $^{2}H_2L$, $^{12}H_2L$ **(**MIC = 6.25 $^{1}H_2L$**;** 3.12 $^{2}H_2L$**,** 12.5 $^{12}H_2L$ µg/ml) didn't get enhanced on complexation with Zinc(II) (MIC = 25 **37**; 12.5 **38**; 50 **12** µg/ml). Whereas, the anti-TB activity of ligands $^{4}H_2L$, $^{5}H_2L$, **(**MIC=50 $^{4}H_2L$,$^{10}H_2L$,$^{11}H_2L$;100$^{5}H_2L$;100 $^{6}H_2L$;3.12 $^{8}H_2L$,$^{9}H_2L$; µg/ml) gets enhanced upon complexation (MIC = 12.5 **40, 47;** 25 **41,46;** 1.6 **42;** 0.8 **44,45** µg/ml). Chelation of ligand with cobalt (II) may have resulted in increase of its retention time on bio-membrane to allow longer interaction at target site. The possible interactions of ligand as well as

complexes have been studied using molecular docking for most potent ligand **2,5 H_2bptsc (^7H_2L)** and its **[Zn(2,5 bptsc)] 43** complex.

Table 8.6.1: Anti-T.B activity of bisthiosemicarbazones (**^1H_2L-$^{12}H_2L$)** and complexes **(37-48)**

		MIC (µg /mL)							
S. No	**Compound**	*100*	*50*	*25*	*12.5*	*6.25*	*3.12*	*1.6*	*0.8*
1.	**2,5 H_2bttsc (^1H_2L)**	S	S	S	S	S	R	R	R
2.	**[Zn(2,5 bttsc)] 37**	S	S	S	R	R	R	R	R
3.	**2,5H_2bttsc N-Me (^2H_2L)**	S	S	S	S	S	S	S	R
4.	**[Zn(2,5 bttsc N-Me)] 38**	S	S	S	S	R	R	R	R
5.	**2,5 H_2bttsc N-Ph (^3H_2L)**	S	S	S	S	S	S	S	R
6.	**[Zn(2,5 bttsc N-Ph)] 39**	S	S	S	S	S	S	S	R
7.	**2,3 H_2bitsc (^4H_2L)**	S	S	R	R	R	R	R	R
8.	**[Zn(2,3 bitsc)] 40**	S	S	S	S	R	R	R	R
9.	**2,3 H_2bitsc-N^1-Me (^5H_2L)**	S	R	R	R	R	R	R	R
10.	**[Zn(2,3 bitsc-N^1-Me)] 41**	S	S	S	R	R	R	R	R
11.	**2,3 H_2bitsc-N^1-Ph (^6H_2L)**	S	R	R	R	R	R	R	R
12.	**[Zn(2,3 bitsc-N^1-Ph)] 42**	S	S	S	S	S	S	S	R
13.	**2,5 H_2bptsc (^7H_2L)**	S	S	S	S	S	S	S	R
14.	**[Zn(2,5 bptsc)] 43**	S	S	S	S	S	S	S	S
15.	**2,5 H_2bptsc, N-Me (^8H_2L)**	S	S	S	S	S	S	R	R
16.	**[Zn(2,5 bptsc, N-Me)] 44**	S	S	S	S	S	S	S	S
16.	**2,5 H_2bptsc, N-Ph (^9H_2L)**	S	S	S	S	S	S	R	R
17.	**[Zn(2,5 bptsc, N-Ph)] 45**	S	S	S	S	S	S	S	S
19.	**2,5 H_2bdptsc ($^{10}H_2L$)**	S	S	R	R	R	R	R	R

20.	**[Zn(2,5 bdptsc)] 46**	S	S	S	R	R	R	R	R
21.	**2,5 H_2bdptsc, N-Me ($^{11}H_2L$)**	S	S	R	R	R	R	R	R
22.	**[Zn(2,5 bdptsc, N-Me)] 47**	S	S	S	S	R	R	R	R
23.	**2,5 H_2bdptsc, N-Ph ($^{12}H_2L$)**	S	S	S	S	R	R	R	R
24.	**[Zn(2,5 bdptsc, N-Ph)] 48**	S	S	R	R	R	R	R	R

8.7 Human Serum Albumin binding studies:

Interactions of HSA with most potent ligand **2,5 H_2bptsc, N-Ph ($^{9}H_2L$)** and its complex **[Zn(2,5 bptsc, N-Ph)] 45** has been studied through UV-visible spectroscopy.

8.7.1 UV-visible spectroscopic study

Interactions of HSA with ligand **2,5 H_2bptsc, N-Ph ($^{9}H_2L$)** and its complex **[Zn(2,5 bptsc, N-Ph)] 45** has been studied using UV-visible absorption of HSA (7μM) in the absence and incremental additions of **$^{9}H_2L$** (0-5 μM) and **45** (0-6 μM). UV-visible spectrum of HSA gives absorption peak at 280 nm). Significant, increase in absorbance at 280 nm of HSA (57% for ligand **$^{9}H_2L$** and 48% for **45** on elevated ligand concentrations **$^{9}H_2L$** and complex **45** showed agitations in the microenvironment of protein's chromophores due to the interaction of HSA with ligand and its complex. The binding constants for interactions of the ligand-HSA and complex-HSA system were calculated using Equation-2 (Benesi-Hildebrand) [195] and initiated to be (3.13×10^{5}) M^{-1} and (9.34×10^{5}) M^{-1}, respectively (Figure 8.7.1.1). The strong binding affinities (high binding constant) indicate the effective transport of ligand **$^{9}H_2L$** and complex **45** to their target sites.

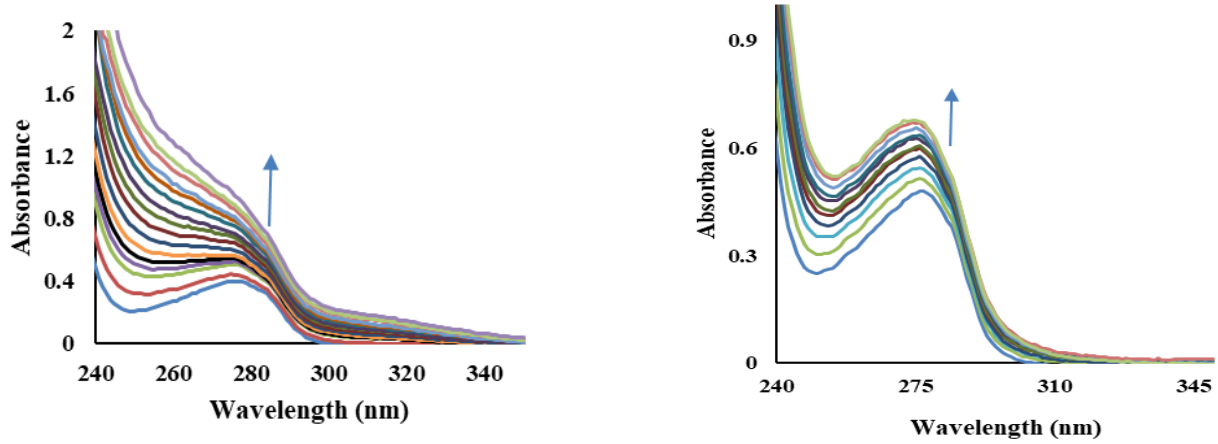

Figure 8.7.1.1: UV-visible absorption of HSA with incremental additions of ligand **2,5 H_2bptsc,N-Ph** (a) and **[Zn(2,5 bptsc,N-Ph)]** (b)

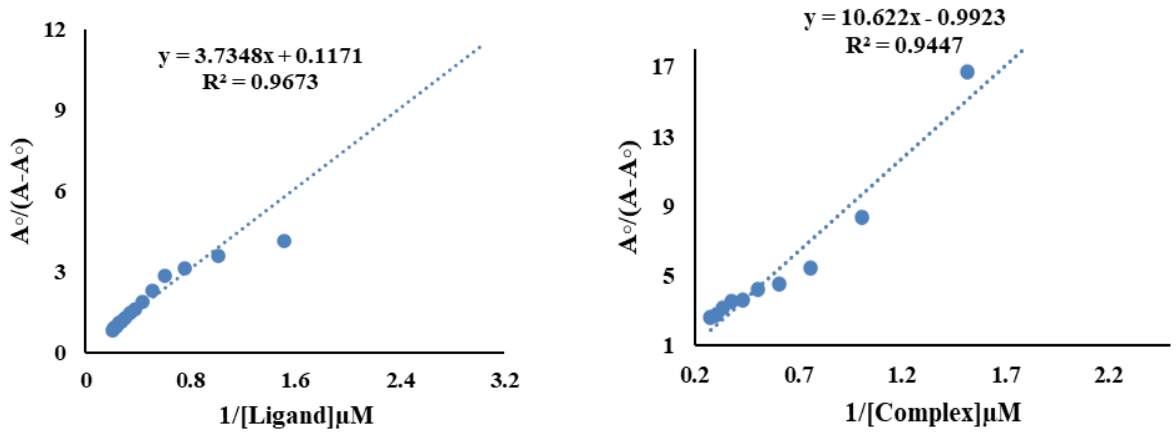

Figure 8.7.1.2: Benesi-Hildebrand plot {$A_o/(A-A_o)$ vs. 1/[ligand or complex]} for binding studies of HSA with ligand **2,5 H_2bptsc,N-Ph** (a) and **[Zn(2,5 bptsc, N-Ph)]** (b)

8.8 Docking studies:

The interactions of the potent ligand 2,5 H_2bptsc, N-Ph (**^9H_2L**) and their Zinc complex [Zn(2,5bptsc,N-Ph)] **45** have been studied by molecular modelling using Autodock 4.0 in order to corroborate and explain the experimental results [46]. Docking of ligand 2,5 H_2bptsc,N-Ph and their Zinc complex [Zn(2,5bptsc,N-Ph)] with mycobacterium tuberculosis enoyl reductase yielded minimal binding energies of -9.1 and -12.4 Kcal/mol, respectively. The results show that the strongest binding with the target was exhibited by (**^9H_2L**) and its complex **45**. It is evident from the binding energy statistics that complexes **45** gets more firmly bound in comparison to free ligands with mycobacterium tuberculosis enoyl reductase. For complex **45** a higher binding energy

(negative) denotes stable structure in the docked state. This corresponds to the same order as the experimental data showed.

The docking analysis of interactions between ligand (**$^{9}H_2L$**) and its complex **45** with mycobacterium tuberculosis enoyl reductase revealed that the ligand (**$^{9}H_2L$**) had interactions (hydrogen bonding) with oxygen atom of amino acid residue of (LYS 164) (d = 3.022 Å), and (GLY95) (d =3.07, 2.48 and 2.64 Å) and (SER 93) of chain A. The ligand **$^{10}H_2L$** interacts with amino acid residues (PHE148 and PHE 40), (PHE148), (ILE 121 and ILE94), of chain A via hydrophobic and other interactions. The complex **45** interacts with the target by hydrogen bonding with (TYR 158) (d = 2.63 Å), and (GLY 96) (d = 2.66 and 2.79 Å) amino acid residue of chain A. The complex **45** also interacts with amino acid residues (ILE 122), (MET 199 and MET 147), phenylalanine (PHE 97 and PHE 41), (ILE 95) and (ALA 191) amino acid residues of the chain A via hydrophobic and other interaction (Figure 6.8.1)

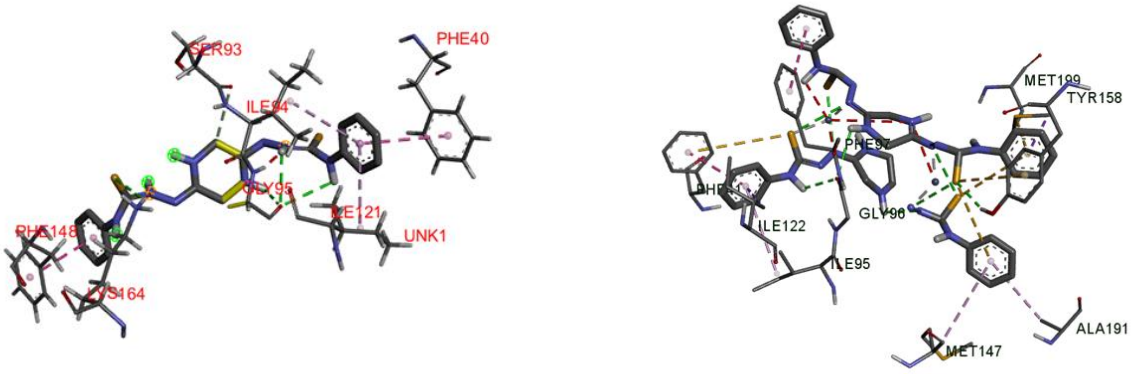

(a) (b)

Figure 6.8.1: 3D representation of interactions of ligand **$^{9}H_2L$** (a) and its complex **45** (b) with mycobacterium tuberculosis enoyl reductase

8.9 <u>Conclusion</u>: Reaction of Zinc(II) acetate with ^{1}**H$_2$L-^{12}H$_2$L** yielded complexes of stoichiometry, [Zn(L)] 37-48 in molar ratio 1:1. All the compounds were characterized using FTIR, Mass, U.V visible and XRD studies. Ligands ^{1}**H$_2$L-^{12}H$_2$L**, along with their complexes (37-48), were subjected to evaluation for anti-tuberculosis activity. The following conclusion has been drawn from results obtained:

1. All the complexes have m/z values in well agreement with proposed stoichiometry.
2. It was observed that crystalline complexes (**37-39,43-48**) has good crystal size as compared to amorphous complexes (**40-42**) and belongs to different crystal system.
3. The anti-T.B activity of ligands generally get enhanced upon complexation. It has been observed that with the increase of hydrophobicity of ligand due to substituent present at N^1 atom, mostly the anti-TB activity gets increased. Also, the anti-TB activity of ^{9}**H$_2$L** (MIC = 3.12µg/ml) get more enhanced-on complexation with Zn(II) **45** (MIC=0.8µg/ml).
4. Low binding energy obtained from molecular modelling (-9.1) ^{1}**H$_2$L**, (-12.4) **1** Kcal/ mol, indicate strong interaction, which also supports the experimental data.
5. The ligand ^{9}**H$_2$L** and complex (**45)** exhibited highest value of binding constant i.e., (3.13×10^5) M^{-1} and (9.34×10^5) M^{-1}, respectively and showed strong binding interactions with HSA.

CHAPTER -9

CONCLUSION

Conclusion and Future look:

Bisthiosemicarbazones emerges as an important category of N, S- donor ligands due to their variable bonding modes and various biological activities. All known bisthiosemicarbazones in each category are compiled, and they are categorised based on the linkage between two thio-moieties. It has been explored how the coordination chemistry of bisthiosemicarbazones with transition and representative elements work together. By choosing a different aldehyde or ketone to produce the ligand, coordination chemistry can be further investigated. The denticity of the ligand can be changed by changing the bond between two thio- moieties. In most circumstances, all of the donor atoms bond to a single metal ion to form mononuclear complexes. However, in a small number of cases, binding of one arm of the bisthiosemicarbazone with one metal and the second arm with a second metal is seen, which results in the creation of dinuclear complexes. Polynuclear complexes of bisthiosemicarbazone are not common. The primary purpose of studying bisthiosemicarbazones and their complexes is to determine their anticancer properties. since they are able to permeate the cell lines semi-permeable barrier. By altering the substituents on the C-C backbone or the amino nitrogen of either or both arms, a structure-activity link can be established. Any component that increases the lipophilicity of the ligands can boost its anticancer activity. The terephthaldehyde bisthiosemicarbazone palladium complex has demonstrated strong catalytic activity for the aryl chloride and olefin Mizoroki-Heck cross-coupling reaction, suggesting that it may function as a homogeneous catalyst and serve as a useful platform for further research. Reaction of cobalt (II) acetate with $^{1}\mathbf{H_2L}$-$^{12}\mathbf{H_2L}$ in molar ratio in 1:1 yielded complexes of stoichiometry, [Co(L)] **1-12**. Each complex was characterized by means of FTIR, Mass, U.V visible and ESR spectroscopy. Ligands ($^{1}\mathbf{H_2L}$ -$^{12}\mathbf{H_2L}$) and their corresponding compounds (**1-12**) were assessed for their anti-tuberculosis efficacy. All the complexes have m/z values in well agreement with proposed stoichiometry. In ESR spectroscopy, a greater $g_{\parallel}$ value compared to $g_{\perp}$ confirms the presence of free electrons in the ground state $d_{x^2-y^2}$ orbital within a tetrahedral structure. The anti-T.B activity of ligands generally get enhanced upon complexation. It has been observed that the anti-tuberculosis activity generally increases with the hydrophobicity of the ligand, which is influenced by the substituents present at the N^1 atom. The anti-TB activity of $^{1}\mathbf{H_2L}$ (MIC = 6.25µg/ml) get more enhanced on complexation with Co(II) **1** (MIC=1.6µg/ml). However, it has been observed that certain ligands are better than others or respective metal complexes. The anti-TB activity of compounds (ligands/complexes) depends upon number of factors like i) the

increase in the stability of complexes due to chelation of metal by ligands; ii) increase in hydrophilicity of ligands and iii) increased time of interaction between complex and target site thus sometime variation in the anti-TB activity within ligands or ligand and metal complexes were observed. The ligand ^{1}**H$_2$L** and complex (**1)** were also evaluated for protein binding interaction and exhibited highest value of binding constant i.e., 7.14×10^{5} M^{-1} and 15.07×10^{5} M^{-1} and showed strong binding interactions with HSA. The binding sites (n) for the binding of ligand (**^{1}H$_2$L)** and complex **(1)** with HSA obtained from modified Stern-Volmer equation were found to be 1.21 and 1.37. Furthermore, the binding interaction of ligand with Co(II) was supported by molecular modelling low binding energy obtained (-5.8) ^{1}**H$_2$L**, (-6.68) **1** Kcal/ mol, indicate strong interaction, which also supports the experimental data. Reaction of Nickel (II) acetate with ^{1}**H$_2$L**-^{12}**H$_2$L** in molar ratio 1:1 yielded complexes of stoichiometry, [Ni(L)] **13-24**. Each complex was characterized by means of FTIR, Mass, UV-Visible, and ESR spectroscopy. The ligands (^{1}**H$_2$L**-^{12}**H$_2$L**) and their respective complexes (**13-24**) were assessed for their anti-tuberculosis activity. All the complexes have m/z values in well agreement with proposed stoichiometry. The magnetic moment found experimentally was in the range of 2.8-4.62 B.M for complexes (**13-24)** confirms the tetrahedral geometry. The anti-T.B activity of ligands generally get enhanced upon complexation. Also, the anti-TB activity of ^{10}**H$_2$L** (MIC = 50µg/ml) get more enhanced-on complexation with Ni(II) **34** (MIC=12.5µg/ml). The ligand ^{10}**H$_2$L** and complex (**34)** exhibited high binding interactions with HSA having highest value of binding constant i.e., (6.4×10^{5}) M^{-1} and (5.2×10^{5}) M^{-1} respectively. Substantial intermolecular interactions of these compounds were observed, with minimal binding energy being achieved (-6.4) ^{10}**H$_2$L**, (-7.0) **34** Kcal/ mol by docking studies, indicate strong interaction which also supports the experimental data. Reaction of copper(II) acetate with ^{1}**H$_2$L**-^{12}**H$_2$L** in molar ratio 1:1 yielded complexes of stoichiometry, [Cu(L)] **25-36**. Each complex of this series was characterized using FTIR, Mass, U.V visible and ESR spectroscopy. Ligands (^{1}**H$_2$L** -^{12}**H$_2$L**) and their complexes (**25-36**) were assessed for anti-tuberculosis activity. All the complexes have m/z values in well agreement with proposed stoichiometry. All complexes exhibit two distinct g values: $g_{\parallel}$ ranging from 2.48 to 2.15 and $g_{\perp}$ ranging from 2.14 to 2.09, suggesting axial symmetry. The dominance of $g_{\parallel}$ over $g_{\perp}$ confirms the presence of free electrons in the ground term $d_{x^2-y^2}$ within a square planar structure. Ligands (^{1}**H$_2$L** – ^{12}**H$_2$L**) and their complexes (**25-36**) were also evaluated for anti-tuberculosis activity. Also, anti-T.B activity of ^{2}**H$_2$L** and ^{4}**H$_2$L** (MIC = 3.12, 50µg/ml) get enhanced on complexation

with Cu(II) (MIC=1.6, 25µg/ml). Substantial intermolecular interaction of compounds was revealed by molecular modeling studies with least binding energy -5.8 (^{2}**H$_2$L**), -7.6(^{4}**H$_2$L**), -6.6 (**26**) and -8.7 (**28**) Kcal/ mol, which also are in support of our experimental data. The ligand ^{2}**H$_2$L,** ^{4}**H$_2$L** and complex **26,28** having highest values of binding constant i.e., (4.24 ×10^5) M^{-1} and (4.92 ×10^5) M^{-1} and (4.90×10^5) M^{-1} and (6.09×10^5) M^{-1} indicates significant binding interaction with HSA, respectively and showed high binding interactions with HSA. The binding sites (n) for the binding of ligand (**^{2}H$_2$L)** and complex **(26)** with HSA was found to be 1.02 and 1.21, and for ligand (**^{4}H$_2$L)** and complex **(28)** with HSA was 1.10 and 1.25 respectively. Reaction of Zinc(II) acetate with ^{1}**H$_2$L-^{12}H$_2$L** in molar ratio 1:1 yielded complexes of stoichiometry, [Zn(L)] **37-48**. Each of the complex of this series was characterized by means of FTIR, Mass, U.V visible and XRD studies. The ligands (^{1}**H$_2$L-^{12}H$_2$L**) and their complexes (**37-48**) were assessed for anti-tuberculosis. All the complexes have m/z values in well agreement with proposed stoichiometry. It was observed that crystalline complexes (**37-39,43-48**) has good crystal size as compared to amorphous complexes (**40-42**) and belongs to different crystal system. The anti-T.B activity of ligands generally get enhanced upon complexation. It has been observed the anti-TB activity of ^{9}**H$_2$L** (MIC = 3.12µg/ml) get more enhanced-on complexation with Zn(II) **45** (MIC=0.8µg/ml). Low binding energy obtained from molecular modelling (-9.1) ^{1}**H$_2$L**, (-12.4) **1** Kcal/ mol, indicate strong interaction, which also supports the experimental data. The ligand ^{9}**H$_2$L** and complex (**45)** exhibited binding constant of (3.13× 10^5) M^{-1} and (9.34×10^5) M^{-1} and exhibited high binding interactions with HSA.

REFERENCES

[1] James E. Huheey, "Inorganic Chemistry, Principle of structure and reactivity," (1983)

[2] W.S. Sheldrick, R. Knorr, H. Polzer, Bis{ *N* -[3-(4-chlorophenylimino)-2-phenyl-1-propenyl]-4-chloroanilinato- *N* , *N* '}nickel(II), Acta Crystallogr B Struct Sci 35 (1979) 739–741. https://doi.org/10.1107/S0567740879004611.

[3] S.K. K, P.C. Varma, R. V N, K.K. Aravindakshan, Cytotoxic, Antitumor And Antimicrobial Studies Of An Oxygen And Nitrogen Donor, Novel Schiff Base Ligand, Acetoacetanilide-(1,2-Ethylenediimine) Ethylacetoacetate And Its Transition Metal Complexes, Int. Res. J. Pharm. 8 (2017) 160–166. https://doi.org/10.7897/2230-8407.0810201.

[4] H. Torayama, T. Nishide, H. Asada, M. Fujiwara, T. Matsushita, Preparation and characterization of novel cyclic tetranuclear manganese (III) complexes: MnIII4(X-salmphen)6 (X-salmphenH2 = N,N′-di-substituted-salicylidene-1,3-diaminobenzene (X = H, 5-Br), Polyhedron 16 (1997) 3787–3794. https://doi.org/10.1016/S0277-5387(97)00148-4.

[5] T. Punniyamurthy, S.J.S. Kalra, J. Iqbal, Cobalt(II) catalyzed biomimetic oxidation of hydrocarbons in the presence of dioxygen and 2-methylpropanal, Tetrahedron Letters 36 (1995) 8497–8500. https://doi.org/10.1016/0040-4039(95)01780-L.

[6] L.M.N. Saleem, *trans – cis* Isomerization of schiff's bases (*N* -benzylideneanilines) on addition of lanthanide shift reagents, Org. Magn. Reson. 19 (1982) 176–180. https://doi.org/10.1002/mrc.1270190403.

[7] J. Bernstein, Y.M. Engel, A.T. Hagler, An *abinitio* study of the conformational energetics of *N* -benzylideneaniline, The Journal of Chemical Physics 75 (1981) 2346–2353. https://doi.org/10.1063/1.442296.

[8] M.D. Cohen, S. Flavian, Topochemistry. Part XXIV. The luminescence properties of N-salicylideneaniline and related anils in solution, J. Chem. Soc., B: (1967) 317. https://doi.org/10.1039/j29670000317.

[9] H.E. Smith, R. Records, Optically active amines—V, Tetrahedron 22 (1966) 813–824. https://doi.org/10.1016/0040-4020(66)80052-2.

[10] M. Kobayashi, M. Yoshida, H. Minato, Configuration of the photoisomers of benzylideneanilines, J. Org. Chem. 41 (1976) 3322–3324. https://doi.org/10.1021/jo00882a026.

[11] M. Tyagi, S. Chandra, Synthesis, characterization and biocidal properties of platinum metal complexes derived from 2,6-diacetylpyridine (bis thiosemicarbazone), Open Journal of Inorganic Chemistry 2 (2012) 41–48. https://doi.org/10.4236/ojic.2012.23007.

[12] D. Mishra, S. Naskar, M.G.B. Drew, S.K. Chattopadhyay, Synthesis, spectroscopic and redox properties of some ruthenium(II) thiosemicarbazone complexes: Structural description of four of these complexes, Inorganica Chimica Acta 359 (2006) 585–592. https://doi.org/10.1016/j.ica.2005.11.001.

[13] S.A. Patil, V.H. Naik, A.D. Kulkarni, P.S. Badami, DNA cleavage, antimicrobial, spectroscopic and fluorescence studies of Co(II), Ni(II) and Cu(II) complexes with SNO donor coumarin Schiff bases, Spectrochim Acta A Mol Biomol Spectrosc 75 (2010) 347–354. https://doi.org/10.1016/j.saa.2009.10.039.

[14] J.L. Dearling, J.S. Lewis, G.E. Mullen, M.J. Welch, P.J. Blower, Copper bis(thiosemicarbazone) complexes as hypoxia imaging agents: structure-activity relationships, J Biol Inorg Chem 7 (2002) 249–259. https://doi.org/10.1007/s007750100291.

[15] A. Obata, E. Yoshimi, A. Waki, J.S. Lewis, N. Oyama, M.J. Welch, H. Saji, Y. Yonekura, Y. Fujibayashi, Retention mechanism of hypoxia selective nuclear imaging/radiotherapeutic agent Cu-diacetyl-bis(N 4-methylthiosemicarbazone) (Cu-ATSM) in tumor cells, Ann Nucl Med 15 (2001) 499–504. https://doi.org/10.1007/BF02988502.

[16] K. Wada, Y. Fujibayashi, N. Tajima, A. Yokoyama, Cu-ATSM, an Intracellular-Accessible Superoxide Dismutase (SOD)-Like Copper Complex: Evaluation in an Ischemia-Reperfusion Injury Model., Biological & Pharmaceutical Bulletin 17 (1994) 701–704. https://doi.org/10.1248/bpb.17.701.

[17] C. Stefani, Z. Al-Eisawi, P.J. Jansson, D.S. Kalinowski, D.R. Richardson, Identification of differential anti-neoplastic activity of copper bis(thiosemicarbazones) that is mediated by intracellular reactive oxygen species generation and lysosomal membrane permeabilization, Journal of Inorganic Biochemistry 152 (2015) 20–37. https://doi.org/10.1016/j.jinorgbio.2015.08.010.

[18] M.A. Cater, H.B. Pearson, K. Wolyniec, P. Klaver, M. Bilandzic, B.M. Paterson, A.I. Bush, P.O. Humbert, S. La Fontaine, P.S. Donnelly, Y. Haupt, Increasing Intracellular Bioavailable Copper Selectively Targets Prostate Cancer Cells, ACS Chem. Biol. 8 (2013) 1621–1631. https://doi.org/10.1021/cb400198p.

[19] D. Denoyer, H.B. Pearson, S.A.S. Clatworthy, Z.M. Smith, P.S. Francis, R.M. Llanos, I. Volitakis, W.A. Phillips, P.M. Meggyesy, S. Masaldan, M.A. Cater, Copper as a target for prostate cancer therapeutics: copper-ionophore pharmacology and altering systemic copper distribution, Oncotarget 7 (2016) 37064–37080. https://doi.org/10.18632/oncotarget.9245.

[20] A.E. Liberta, D.X. West, Antifungal and antitumor activity of heterocyclic thiosemicarbazones and their metal complexes: current status, Biometals 5 (1992) 121–126. https://doi.org/10.1007/BF01062223.

[21] Q.U. Ain, I. Singh, R. Carmieli, A. Savci, K. Paul, R. Sharma, Substituted 2,5 thiophene dicarboxaldehyde bisthiosemicarbazones and their copper(II) complexes: Synthesis, structure elucidation, HSA binding, biological activities and docking studies, Journal of Molecular Structure 1291 (2023) 135996. https://doi.org/10.1016/j.molstruc.2023.135996.

[22] T.S. Lobana, R. Sharma, G. Bawa, S. Khanna, Bonding and structure trends of thiosemicarbazone derivatives of metals—An overview, Coordination Chemistry Reviews 253 (2009) 977–1055. https://doi.org/10.1016/j.ccr.2008.07.004.

[23] M.J.M. Campbell, Transition metal complexes of thiosemicarbazide and thiosemicarbazones, Coordination Chemistry Reviews 15 (1975) 279–319. https://doi.org/10.1016/S0010-8545(00)80276-3.

[24] T. Rosu, S. Pasculescu, V. Lazar, C. Chifiriuc, R. Cernat, Copper(II) Complexes with Ligands Derived from 4-Amino-2,3-dimethyl-1-phenyl-3-pyrazolin-5-one: Synthesis and Biological Activity, Molecules 11 (2006) 904–914. https://doi.org/10.3390/11110904.

[25] J.S. Casas, A. Castiñeiras, M.C. Rodríguez-Argüelles, A. Sánchez, J. Sordo, A. Vázquez-López, E.M. Vázquez-López, Reactions of diorganotin(IV) oxides with isatin 3- and 2-thiosemicarbazones and with isatin 2,3-bis(thiosemicarbazone): influence of diphenyldithiophosphinic acid (isatin = 1H-indole-2,3-dione), J. Chem. Soc., Dalton Trans. (2000) 4056–4063. https://doi.org/10.1039/b005103i.

[26] J.S. Casas, M.S. García-Tasende, J. Sordo, Structural aspects of the coordination chemistry of organothallium(III) and organomercury(II) derivatives, Coordination Chemistry Reviews 193–195 (1999) 283–359. https://doi.org/10.1016/S0010-8545(99)00087-9.

[27] R.K. Mahajan, T.P.S. Walia, Sumanjit, T.S. Lobana, Cyclopentanone Thiosemicarbazone, a New Complexing Agent for Copper Determination in Biological Samples by Adsorptive Stripping Voltammetry, ANAL. SCI. 22 (2006) 389–392. https://doi.org/10.2116/analsci.22.389.

[28] R. Mahajan, A mercury(II) ion-selective electrode based on neutral salicylaldehyde thiosemicarbazone, Talanta 59 (2003) 101–105. https://doi.org/10.1016/S0039-9140(02)00473-3.

[29] R. Mahajan, T. Walia, T. Lobana, The versatility of salicylaldehyde thiosemicarbazone in the determination of copper in blood using adsorptive stripping voltammetry, Talanta 67 (2005) 755–759. https://doi.org/10.1016/j.talanta.2005.03.024.

[30] A. Castiñeiras, N. Fernández-Hermida, I. García-Santos, L. Gómez-Rodríguez, Neutral NiII, PdII and PtII ONS-pincer complexes of 5-acetylbarbituric-4N-dimethylthiosemicarbazone: synthesis, characterization and properties, Dalton Trans. 41 (2012) 13486. https://doi.org/10.1039/c2dt31753b.

[31] A. Khan, K. Paul, I. Singh, J.P. Jasinski, V.A. Smolenski, E.P. Hotchkiss, P.T. Kelley, Z.A. Shalit, M. Kaur, S. Banerjee, P. Roy, R. Sharma, Copper(I) and silver(I) complexes of anthraldehyde thiosemicarbazone: synthesis, structure elucidation, *in vitro* anti-tuberculosis/cytotoxic activity and interactions with DNA/HSA, Dalton Trans. 49 (2020) 17350–17367. https://doi.org/10.1039/D0DT03104F.

[32] Ş. Güveli, S. Agopcan Çınar, Ö. Karahan, V. Aviyente, B. Ülküseven, Nickel(II)–PPh_3 Complexes of *S* , *N* -Substituted Thiosemicarbazones – Structure, DFT Study, and Catalytic Efficiency, Eur J Inorg Chem 2016 (2016) 538–544. https://doi.org/10.1002/ejic.201501227.

[33] S. Priyarega, P. Kalaivani, R. Prabhakaran, T. Hashimoto, A. Endo, K. Natarajan, Nickel(II) complexes containing thiosemicarbazone and triphenylphosphine: Synthesis, spectroscopy, crystallography and catalytic activity, Journal of Molecular Structure 1002 (2011) 58–62. https://doi.org/10.1016/j.molstruc.2011.06.046.

[34] U. Abram, K. Ortner, R. Gust, K. Sommer, Gold complexes with thiosemicarbazones: reactions of bi- and tridentate thiosemicarbazones with dichloro[2-(dimethylaminomethyl)phenyl-C 1,N]gold(III), [Au(damp-C 1,N)Cl2], J. Chem. Soc., Dalton Trans. (2000) 735–744. https://doi.org/10.1039/a908712e.

[35] N.C. Kasuga, K. Onodera, S. Nakano, K. Hayashi, K. Nomiya, Syntheses, crystal structures and antimicrobial activities of 6-coordinate antimony(III) complexes with tridentate 2-acetylpyridine thiosemicarbazone, bis(thiosemicarbazone) and semicarbazone ligands, Journal of Inorganic Biochemistry 100 (2006) 1176–1186. https://doi.org/10.1016/j.jinorgbio.2006.01.037.

[36] C. Biswas, A. Chatterjee, S. Bhattacharya, D.P. Mandal, S. Bhattacharjee, R. Ghosh, Synthesis, X-ray structures and cytotoxic effects of a Cu(II)- and a Zn(II) thiosemicarbazones on human epidermoid carcinoma cell A431, J Chem Sci 133 (2021) 45. https://doi.org/10.1007/s12039-021-01906-5.

[37] D.X. West, J.S. Ives, J. Krejci, M.M. Salberg, T.L. Zumbahlen, G.A. Bain, A.E. Liberta, J. Valdes-Martinez, S. Hernandez-Ortiz, R.A. Toscano, Copper(II) complexes of 2-benzoylpyridine 4N-substituted thiosemicarbazones, Polyhedron 14 (1995) 2189–2200. https://doi.org/10.1016/0277-5387(95)00010-P.

[38] J. García-Tojal, L. Lezama, J.L. Pizarro, M. Insausti, M.I. Arriortua, T. Rojo, Spectroscopic and magnetic properties of copper(II) complexes derived from pyridine-2-carbaldehyde thiosemicarbazone. Structures of [Cu(NO3)(C7H8N4S)(H2O)](NO3) and [{Cu(NCS)(C7H7N4S)}2], Polyhedron 18 (1999) 3703–3711. https://doi.org/10.1016/S0277-5387(99)00310-1.

[39] R. Anjum, D. Palanimuthu, D.S. Kalinowski, W. Lewis, K.C. Park, Z. Kovacevic, I.U. Khan, D.R. Richardson, Synthesis, Characterization, and in Vitro Anticancer Activity of Copper and Zinc Bis(Thiosemicarbazone) Complexes, Inorg. Chem. 58 (2019) 13709–13723. https://doi.org/10.1021/acs.inorgchem.9b01281.

[40] M.T.H. Tarafder, T.-J. Khoo, K.A. Crouse, A.M. Ali, B.M. Yamin, H.-K. Fun, Coordination chemistry and bioactivity of some metal complexes containing two isomeric bidentate NS Schiff bases derived from S-benzyldithiocarbazate and the X-ray crystal structures of S-benzyl-β-N-(5-methyl-2-furylmethylene)dithiocarbazate and bis[S-benzyl-β-N-(2-

furylmethylketone)dithiocarbazato]cadmium(II), Polyhedron 21 (2002) 2691–2698. https://doi.org/10.1016/S0277-5387(02)01272-X.

[41] L. Subramanyam Sarma, J. Rajesh Kumar, C. Jaya Kumar, A. Varada Reddy, A Sensitive Extractive Spectrophotometric Determination of Cobalt(II) in Real Samples Using Pyridoxal-4-phenyl-3-thiosemicarbozone, Analytical Letters 36 (2003) 605–618. https://doi.org/10.1081/AL-120018251.

[42] K.J. Reddy, J.R. Kumar, C. Ramachandraiah, T. Thriveni, A.V. Reddy, Spectrophotometric determination of zinc in foods using N-ethyl-3-carbazolecarboxaldehyde-3-thiosemicarbazone: Evaluation of a new analytical reagent, Food Chemistry 101 (2007) 585–591. https://doi.org/10.1016/j.foodchem.2006.02.018.

[43] M.A. Akl, M.E. Khalifa, S.E. Ghazy, M.M. Hassanien, Selective Flotation-Separation and Spectrophotometric Determination of Cadmium Using Phenanthraquinone Monophenythiosemicarbazone, ANAL. SCI. 18 (2002) 1235–1240. https://doi.org/10.2116/analsci.18.1235.

[44] M. Joseph, M. Kuriakose, M.R.P. Kurup, E. Suresh, A. Kishore, S.G. Bhat, Structural, antimicrobial and spectral studies of copper(II) complexes of 2-benzoylpyridine N(4)-phenyl thiosemicarbazone, Polyhedron 25 (2006) 61–70. https://doi.org/10.1016/j.poly.2005.07.006.

[45] D.X. West, Y. Yang, T.L. Klein, K.I. Goldberg, A.E. Liberta, J. Valdes-Martinez, S. Hernandez-Ortega, Dinuclear nickel(II) complexes of 2-hydroxyacetophenone 4N-substituted thiosemicarbazones, Polyhedron 14 (1995) 3051–3060. https://doi.org/10.1016/0277-5387(95)00105-2.

[46] D. Kovala-Demertzi, Platinum(II) complexes with 2-acetyl pyridine thiosemicarbazone Synthesis, crystal structure, spectral properties, antimicrobial and antitumour activity, Journal of Inorganic Biochemistry 86 (2001) 555–563. https://doi.org/10.1016/S0162-0134(01)00224-0.

[47] D. Kovala-Demertzi, A. Boccarelli, M.A. Demertzis, M. Coluccia, In vitroAntitumor Activity of 2-Acetyl Pyridine 4N-Ethyl Thiosemicarbazone and Its Platinum(II) and Palladium(II) Complexes, Chemotherapy 53 (2007) 148–152. https://doi.org/10.1159/000099986.

[48] D. Sharma, J.P. Jasinski, V.A. Smolinski, M. Kaur, K. Paul, R. Sharma, Synthesis and structure of complexes (NiII, AgI) of substituted benzaldehyde thiosemicarbazones and antitubercular activity of NiII complex, Inorganica Chimica Acta 499 (2020) 119187. https://doi.org/10.1016/j.ica.2019.119187.

[49] F.A. Beckford, G. Leblanc, J. Thessing, M. Shaloski, B.J. Frost, L. Li, N.P. Seeram, Organometallic ruthenium complexes with thiosemicarbazone ligands: Synthesis, structure and cytotoxicity of [(η6-p-cymene)Ru(NS)Cl]+ (NS=9-anthraldehyde thiosemicarbazones), Inorganic Chemistry Communications 12 (2009) 1094–1098. https://doi.org/10.1016/j.inoche.2009.08.034.

[50] M. Belicchi Ferrari, F. Bisceglie, G. Gasparri Fava, G. Pelosi, P. Tarasconi, R. Albertini, S. Pinelli, Synthesis, characterization and biological activity of two new polymeric copper(II) complexes with α-ketoglutaric acid thiosemicarbazone, Journal of Inorganic Biochemistry 89 (2002) 36–44. https://doi.org/10.1016/S0162-0134(01)00371-3.

[51] T.S. Lobana, G. Bawa, R.J. Butcher, C.W. Liu, Thiosemicarbazonates of Ruthenium(II): Crystal Structures of [Bis(triphenylphosphine)][bis(*N* -phenyl-pyridine-2-carbaldehyde Thiosemicarbazonato)]ruthenium(II) and [Bis(diphenylphosphino)butane][bis(salicylaldehyde Thiosemicarbazonato)]ruthenium(II), Zeitschrift Anorg Allge Chemie 635 (2009) 355–360. https://doi.org/10.1002/zaac.200800380.

[52] S. Halder, S.-M. Peng, G.-H. Lee, T. Chatterjee, A. Mukherjee, S. Dutta, U. Sanyal, S. Bhattacharya, Synthesis, structure, spectroscopic properties and cytotoxic effect of some thiosemicarbazone complexes of palladium, New J. Chem. 32 (2008) 105–114. https://doi.org/10.1039/B707448D.

[53] R. Sharma, T.S. Lobana, A. Castineiras, R.J. Butcher, T. Akitsu, The influence of substituents at C2/N1 atoms of pyridine-2-formaldeyhde-/benzaldehyde-N1-substituted thiosemicarbazones on the type of copper(I) complexes, Polyhedron 158 (2019) 449–457. https://doi.org/10.1016/j.poly.2018.11.034.

[54] T.S. Lobana, R.J. Butcher, Metal–thiosemicarbazone interactions. Synthesis of an iodo-bridged dinuclear [diiodobis(pyrrole-2-carbaldehydethiosemicarbazone)dicopper(I)] complex, Transition Metal Chemistry 29 (2004) 291–295. https://doi.org/10.1023/B:TMCH.0000020371.72284.4d.

[55] T.S. Lobana, Rekha, R.J. Butcher, A. Castineiras, E. Bermejo, P.V. Bharatam, Bonding Trends of Thiosemicarbazones in Mononuclear and Dinuclear Copper(I) Complexes: Syntheses, Structures, and Theoretical Aspects, Inorg. Chem. 45 (2006) 1535–1542. https://doi.org/10.1021/ic051018j.

[56] J.S. Casas, E.E. Castellano, M.D. Couce, J. Ellena, A. Sánchez, J. Sordo, C. Taboada, A gold(I) complex with a vitamin K3 derivative: Characterization and antitumoral activity, Journal of Inorganic Biochemistry 100 (2006) 1858–1860. https://doi.org/10.1016/j.jinorgbio.2006.07.006.

[57] J.S. Casas, A. Castiñeiras, M.C. Rodríguez-Argüelles, A. Sánchez, J. Sordo, A. Vázquez López, S. Pinelli, P. Lunghi, P. Ciancianaini, A. Bonati, P. Dall'Aglio, R. Albertini, Synthesis, structure, spectroscopic properties and biological activity of mixed diorganotin(IV) complexes containing pyridine-2-carbaldehyde thiosemicarbazonato and diphenyldithiophosphinato ligands, Journal of Inorganic Biochemistry 76 (1999) 277–284. https://doi.org/10.1016/S0162-0134(99)00185-3.

[58] A. Khan, J.P. Jasinski, V.A. Smolenski, E.P. Hotchkiss, P.T. Kelley, Z.A. Shalit, M. Kaur, K. Paul, R. Sharma, Enhancement in anti-tubercular activity of indole based thiosemicarbazones on complexation with copper(I) and silver(I) halides: Structure elucidation, evaluation and molecular modelling, Bioorganic Chemistry 80 (2018) 303–318. https://doi.org/10.1016/j.bioorg.2018.06.027.

[59] L.J. Ashfield, A.R. Cowley, J.R. Dilworth, P.S. Donnelly, Functionalized Thiosemicarbazone Clusters of Copper(I) and Silver(I), Inorg. Chem. 43 (2004) 4121–4123. https://doi.org/10.1021/ic035451+.

[60] Z. Lu, C. White, A.L. Rheingold, R.H. Crabtree, Deprotonated thioamides as thiolate S-donor ligands with a high tendency to avoid M-S-M bridge formation: crystal and molecular structure of bis(2-hydroxy-5-methylacetophenone N,N-dimethylthiosemicarbazonato)dinickel, Inorg. Chem. 32 (1993) 3991–3994. https://doi.org/10.1021/ic00071a006.

[61] P. McQuade, K.E. Martin, T.C. Castle, M.J. Went, P.J. Blower, M.J. Welch, J.S. Lewis, Investigation into 64Cu-labeled Bis(selenosemicarbazone) and Bis(thiosemicarbazone) complexes as hypoxia imaging agents, Nuclear Medicine and Biology 32 (2005) 147–156. https://doi.org/10.1016/j.nucmedbio.2004.10.004.

[62] A. Pérez-Rebolledo, G.M. De Lima, N.L. Speziali, O.E. Piro, E.E. Castellano, J.D. Ardisson, H. Beraldo, Tin(IV) complexes obtained by reacting 2-benzoylpyridine-derived thiosemicarbazones with SnCl4 and Ph2SnCl2, Journal of Organometallic Chemistry 691 (2006) 3919–3930. https://doi.org/10.1016/j.jorganchem.2006.05.046.

[63] T.S. Lobana, R. Sharma, G. Bawa, S. Khanna, Bonding and structure trends of thiosemicarbazone derivatives of metals—An overview, Coordination Chemistry Reviews 253 (2009) 977–1055. https://doi.org/10.1016/j.ccr.2008.07.004.

[64] J.K. Swearingen, D.X. West, [No title found], Transition Metal Chemistry 25 (2000) 241–246. https://doi.org/10.1023/A:1007095116629.

[65] M.E. Hossain, M.N. Alam, M.A. Ali, M. Nazimuddin, F.E. Smith, R.C. Hynes, The synthesis, characterization and bioactivities of some copper(II) complexes of the 2-acetylpyridine schiff bases of s-methyl- and s-benzyldithiocarbazate, and the x-ray crystal structure of the nitrato(s-benzyl-β-n-(2-acetylpyridyl) methylenedithiocarbazato)copper(II) complex, Polyhedron 15 (1996) 973–980. https://doi.org/10.1016/0277-5387(95)00310-X.

[66] S. Padhye, Z. Afrasiabi, E. Sinn, J. Fok, K. Mehta, N. Rath, Antitumor Metallothiosemicarbazonates: Structure and Antitumor Activity of Palladium Complex of Phenanthrenequinone Thiosemicarbazone, Inorg. Chem. 44 (2005) 1154–1156. https://doi.org/10.1021/ic048214v.

[67] M. Christlieb, J.R. Dilworth, Ligands for Molecular Imaging: The Synthesis of Bis(thiosemicarbazone) Ligands, Chem. Eur. J. 12 (2006) 6194–6206. https://doi.org/10.1002/chem.200501069.

[68] R. Hueting, M. Christlieb, J.R. Dilworth, E.G. Garayoa, V. Gouverneur, M.W. Jones, V. Maes, R. Schibli, X. Sun, D.A. Tourwé, Bis(thiosemicarbazones) as bifunctional chelators for the room temperature 64-copper labeling of peptides, Dalton Trans. 39 (2010) 3620. https://doi.org/10.1039/b925128f.

[69] R.S. Nyholm, Magnetism and inorganic chemistry, Q. Rev., Chem. Soc. 7 (1953) 377. https://doi.org/10.1039/qr9530700377.

[70] A. Bagchi, P. Mukherjee, A. Raha, A REVIEW ON TRANSITION METAL COMPLEX-MORDERN WEAPON IN MEDICINE, (n.d.).

[71] J. Takaya, Catalysis using transition metal complexes featuring main group metal and metalloid compounds as supporting ligands, Chem. Sci. 12 (2021) 1964–1981. https://doi.org/10.1039/D0SC04238B.

[72] U. Sandbhor, S. Padhye, D. Billington, D. Rathbone, S. Franzblau, C.E. Anson, A.K. Powell, Metal complexes of carboxamidrazone analogs as antitubercular agents, Journal of Inorganic Biochemistry 90 (2002) 127–136. https://doi.org/10.1016/S0162-0134(02)00406-3.

[73] S.S. Kanwar, K. Lumba, S.K. Gupta, V.M. Katoch, P. Singh, A.K. Mishra, S.B. Kalia, Synthesis and mycobactericidal properties of metal complexes of isonicotinoyldithiocarbazic acid, Biotechnol Lett 30 (2008) 677–680. https://doi.org/10.1007/s10529-007-9601-5.

[74] R. Maccari, R. Ottanà, B. Bottari, E. Rotondo, M.G. Vigorita, In vitro advanced antimycobacterial screening of cobalt(II) and copper(II) complexes of fluorinated isonicotinoylhydrazones, Bioorganic & Medicinal Chemistry Letters 14 (2004) 5731–5733. https://doi.org/10.1016/j.bmcl.2004.09.052.

[75] B. Bottari, R. Maccari, F. Monforte, R. Ottanà, E. Rotondo, M.G. Vigorita, Isoniazid-related copper(II) and nickel(II) complexes with antimycobacterial in vitro activity. Part 9, Bioorganic & Medicinal Chemistry Letters 10 (2000) 657–660. https://doi.org/10.1016/S0960-894X(00)00058-5.

[76] M.C. Mandewale, B. Thorat, D. Shelke, R. Yamgar, Synthesis and Biological Evaluation of New Hydrazone Derivatives of Quinoline and Their Cu(II) and Zn(II) Complexes against *Mycobacterium tuberculosis*, Bioinorganic Chemistry and Applications 2015 (2015) 1–14. https://doi.org/10.1155/2015/153015.

[77] Q.U. Ain, I. Singh, R. Carmieli, A. Savci, K. Paul, R. Sharma, Substituted 2,5 thiophene dicarboxaldehyde bisthiosemicarbazones and their copper(II) complexes: Synthesis, structure elucidation, HSA binding, biological activities and docking studies, Journal of Molecular Structure 1291 (2023) 135996. https://doi.org/10.1016/j.molstruc.2023.135996.

[78] P.J. Blower, T.C. Castle, A.R. Cowley, J.R. Dilworth, P.S. Donnelly, E. Labisbal, F.E. Sowrey, S.J. Teat, M.J. Went, Structural trends in copper(II) bis(thiosemicarbazone) radiopharmaceuticals, Dalton Trans. (2003) 4416–4425. https://doi.org/10.1039/B307499D.

[79] J.L. Dearling, J.S. Lewis, G.E. Mullen, M.J. Welch, P.J. Blower, Copper bis(thiosemicarbazone) complexes as hypoxia imaging agents: structure-activity relationships, J Biol Inorg Chem 7 (2002) 249–259. https://doi.org/10.1007/s007750100291.

[80] F.A. French, B.L. Freedlander, A. Hosking, J. French, Carcinostatic activity of some dicarbonyl compounds and their bis-hydrazones, Acta Unio Int Contra Cancrum 16 (1960) 614–624.

[81] S.R. Bayly, R.C. King, D.J. Honess, P.J. Barnard, H.M. Betts, J.P. Holland, R. Hueting, P.D. Bonnitcha, J.R. Dilworth, F.I. Aigbirhio, M. Christlieb, In Vitro and In Vivo Evaluations of a Hydrophilic ^{64} Cu-Bis(Thiosemicarbazonato)–Glucose Conjugate for Hypoxia Imaging, J Nucl Med 49 (2008) 1862–1868. https://doi.org/10.2967/jnumed.108.054015.

[82] J.P. Holland, F.I. Aigbirhio, H.M. Betts, P.D. Bonnitcha, P. Burke, M. Christlieb, G.C. Churchill, A.R. Cowley, J.R. Dilworth, P.S. Donnelly, J.C. Green, J.M. Peach, S.R. Vasudevan, J.E. Warren, Functionalized Bis(thiosemicarbazonato) Complexes of Zinc and Copper: Synthetic Platforms Toward Site-Specific Radiopharmaceuticals, Inorg. Chem. 46 (2007) 465–485. https://doi.org/10.1021/ic0615628.

[83] B.M. Paterson, P.S. Donnelly, Copper complexes of bis(thiosemicarbazones): from chemotherapeutics to diagnostic and therapeutic radiopharmaceuticals, Chem. Soc. Rev. 40 (2011) 3005. https://doi.org/10.1039/c0cs00215a.

[84] J.S. Lewis, R. Laforest, T.L. Buettner, S.-K. Song, Y. Fujibayashi, J.M. Connett, M.J. Welch, Copper-64-diacetyl-bis(N^4 -methylthiosemicarbazone): An agent for radiotherapy, Proc. Natl. Acad. Sci. U.S.A. 98 (2001) 1206–1211. https://doi.org/10.1073/pnas.98.3.1206.

[85] H.M. Betts, P.J. Barnard, S.R. Bayly, J.R. Dilworth, A.D. Gee, J.P. Holland, Controlled Axial Coordination: Solid-Phase Synthesis and Purification of Metallo-Radiopharmaceuticals, Angewandte Chemie 120 (2008) 8544–8547. https://doi.org/10.1002/ange.200801936.

[86] Z.-L. Guo, D.R. Richardson, D.S. Kalinowski, Z. Kovacevic, K.C. Tan-Un, G.C.-F. Chan, The novel thiosemicarbazone, di-2-pyridylketone 4-cyclohexyl-4-methyl-3-thiosemicarbazone (DpC), inhibits neuroblastoma growth in vitro and in vivo via multiple mechanisms, J Hematol Oncol 9 (2016) 98. https://doi.org/10.1186/s13045-016-0330-x.

[87] Z. Kovacevic, S. Chikhani, D.B. Lovejoy, D.R. Richardson, Novel Thiosemicarbazone Iron Chelators Induce Up-Regulation and Phosphorylation of the Metastasis Suppressor N-myc Down-Stream Regulated Gene 1: A New Strategy for the Treatment of Pancreatic Cancer, Mol Pharmacol 80 (2011) 598–609. https://doi.org/10.1124/mol.111.073627.

[88] H. Beraldo, L.P. Boyd, D.X. West, [No title found], Transition Metal Chemistry 23 (1997) 67–71. https://doi.org/10.1023/A:1006958018049.

[89] C.R. Kowol, P. Heffeter, W. Miklos, L. Gille, R. Trondl, L. Cappellacci, W. Berger, B.K. Keppler, Mechanisms underlying reductant-induced reactive oxygen species formation by anticancer copper(II) compounds, J Biol Inorg Chem 17 (2012) 409–423. https://doi.org/10.1007/s00775-011-0864-x.

[90] L.J. Farrugia, *WinGX* suite for small-molecule single-crystal crystallography, J Appl Crystallogr 32 (1999) 837–838. https://doi.org/10.1107/S0021889899006020.

[91] D.B. Lovejoy, P.J. Jansson, U.T. Brunk, J. Wong, P. Ponka, D.R. Richardson, Antitumor Activity of Metal-Chelating Compound Dp44mT Is Mediated by Formation of a Redox-Active Copper Complex That Accumulates in Lysosomes, Cancer Research 71 (2011) 5871–5880. https://doi.org/10.1158/0008-5472.CAN-11-1218.

[92] D.B. Lovejoy, D.M. Sharp, N. Seebacher, P. Obeidy, T. Prichard, C. Stefani, M.T. Basha, P.C. Sharpe, P.J. Jansson, D.S. Kalinowski, P.V. Bernhardt, D.R. Richardson, Novel Second-Generation Di-2-Pyridylketone Thiosemicarbazones Show Synergism with Standard Chemotherapeutics and Demonstrate Potent Activity against Lung Cancer Xenografts after Oral and Intravenous Administration in Vivo, J. Med. Chem. 55 (2012) 7230–7244. https://doi.org/10.1021/jm300768u.

[93] H.G. Petering, H.H. Buskirk, G.E. Underwood, The Anti-Tumor Activity of 2-Keto-3-ethoxybutyraldehyde Bis(thiosemicarbazone) and Related Compounds, (n.d.).

[94] C. Shipman, S.H. Smith, J.C. Drach, D.L. Klayman, Thiosemicarbazones of 2-acetylpyridine, 2-acetylquinoline, 1-acetylisoquinoline, and related compounds as inhibitors of herpes simplex virus in vitro and in a cutaneous herpes guinea pig model, Antiviral Research 6 (1986) 197–222. https://doi.org/10.1016/0166-3542(86)90002-1.

[95] S.I. Pascu, P.A. Waghorn, T.D. Conry, H.M. Betts, J.R. Dilworth, G.C. Churchill, T. Pokrovska, M. Christlieb, F.I. Aigbirhio, J.E. Warren, Designing Zn(ii) and Cu(ii)

derivatives as probes for in vitro fluorescence imaging, Dalton Trans. (2007) 4988. https://doi.org/10.1039/b705227h.

[96] S.I. Pascu, P.A. Waghorn, T.D. Conry, B. Lin, H.M. Betts, J.R. Dilworth, R.B. Sim, G.C. Churchill, F.I. Aigbirhio, J.E. Warren, Cellular confocal fluorescence studies and cytotoxic activity of new Zn(ii) bis(thiosemicarbazonato) complexes, Dalton Trans. (2008) 2107. https://doi.org/10.1039/b802806k.

[97] J. Burt, J.W. Emsley, W. Levason, G. Reid, I.S. Tinkler, Systematics of BX_3 and BX_2^+ Complexes (X = F, Cl, Br, I) with Neutral Diphosphine and Diarsine Ligands, Inorg. Chem. 55 (2016) 8852–8864. https://doi.org/10.1021/acs.inorgchem.6b01375.

[98] D.X. West, A.E. Liberta, S.B. Padhye, R.C. Chikate, P.B. Sonawane, A.S. Kumbhar, R.G. Yerande, Thiosemicarbazone complexes of copper(II): structural and biological studies, Coordination Chemistry Reviews 123 (1993) 49–71. https://doi.org/10.1016/0010-8545(93)85052-6.

[99] The Wide Pharmacological Versatility of Semicarbazones, Thiosemicarbazones and Their Metal Complexes, MRMC 4 (2004) 31–39. https://doi.org/10.2174/1389557043487484.

[100] D.X. West, S.B. Padhye, P.B. Sonawane, Structural and physical correlations in the biological properties of transition metal heterocyclic thiosemicarbazone and S-alkyldithiocarbazate complexes, in: Complex Chemistry, Springer Berlin Heidelberg, Berlin, Heidelberg, 1991: pp. 1–50. https://doi.org/10.1007/3-540-53499-7_1.

[101] J.R. Dilworth, R. Hueting, Metal complexes of thiosemicarbazones for imaging and therapy, Inorganica Chimica Acta 389 (2012) 3–15. https://doi.org/10.1016/j.ica.2012.02.019.

[102] S.B. Maity, S. Banerjee, K. Sunwoo, J.S. Kim, P.K. Bharadwaj, A Fluorescent Chemosensor for Hg^{2+} and Cd^{2+} Ions in Aqueous Medium under Physiological pH and Its Applications in Imaging Living Cells, Inorg. Chem. 54 (2015) 3929–3936. https://doi.org/10.1021/acs.inorgchem.5b00106.

[103] X.-J. Jiang, M. Li, H.-L. Lu, L.-H. Xu, H. Xu, S.-Q. Zang, M.-S. Tang, H.-W. Hou, T.C.W. Mak, A Highly Sensitive C_3-Symmetric Schiff-Base Fluorescent Probe for Cd^{2+}, Inorg. Chem. 53 (2014) 12665–12667. https://doi.org/10.1021/ic501279y.

[104] M. Colilla, M.A. Mendiola, J.R. Procopio, M.T. Sevilla, Application of a Carbon Paste Electrode Modified with a Schiff Base Ligand to Mercury Speciation in Water, Electroanalysis 17 (2005) 933–940. https://doi.org/10.1002/elan.200403198.

[105] T. Chatterjee, S. Areti, M. Ravikanth, Synthesis, Structure, and Hg^{2+} -Ion-Sensing Properties of Stable Calixazasmaragdyrins, Inorg. Chem. 54 (2015) 2885–2892. https://doi.org/10.1021/ic503028k.

[106] Y.S. Rao, B. Prathima, S.A. Reddy, K. Madhavi, A.V. Reddy, Complexes of Cu(II) and Ni(II) with Bis(Phenylthiosemicarbazone): Synthesis, Spectral, EPR and *in Vitro* -Antibacterial and Antioxidant Activity, J Chinese Chemical Soc 57 (2010) 677–682. https://doi.org/10.1002/jccs.201000094.

[107] T.S. Lobana, Activation of C–H bonds of thiosemicarbazones by transition metals: synthesis, structures and importance of cyclometallated compounds, RSC Adv. 5 (2015) 37231–37274. https://doi.org/10.1039/C5RA03333K.

[108] V. Ruangpornvisuti, A DFT study of molecular structures and tautomerizations of 2-benzoylpyridine semicarbazone and picolinaldehyde N-oxide thiosemicarbazone and their complexations with Ni(II), Cu(II), and Zn(II), Struct Chem 18 (2007) 977–984. https://doi.org/10.1007/s11224-007-9258-7.

[109] V. Ruangpornvisuti, K. Supakornchailert, C. Tungchitpienchai, B. Wanno, A DFT investigation on molecular structures of semicarbazone complexes with Co(II), Ni(II) and Zn(II) and reaction energies of their complexation, Struct Chem 17 (2006) 27–34. https://doi.org/10.1007/s11224-006-9027-z.

[110] A.S. El-Tabl, M.M.A. El-wahed, A.M.S.M. Rezk, Cytotoxic behavior and spectroscopic characterization of metal complexes of ethylacetoacetate bis(thiosemicarbazone) ligand, Spectrochimica Acta Part A: Molecular and Biomolecular Spectroscopy 117 (2014) 772–788. https://doi.org/10.1016/j.saa.2013.04.014.

[111] A.P. King, H.A. Gellineau, J.-E. Ahn, S.N. MacMillan, J.J. Wilson, Bis(thiosemicarbazone) Complexes of Cobalt(III). Synthesis, Characterization, and Anticancer Potential, Inorg. Chem. 56 (2017) 6609–6623. https://doi.org/10.1021/acs.inorgchem.7b00710.

[112] N.P. Prajapati, H.D. Patel, Novel thiosemicarbazone derivatives and their metal complexes: Recent development, Synthetic Communications (2019) 1–38. https://doi.org/10.1080/00397911.2019.1649432.

[113] S. Sarpaki, F. Cortezon-Tamarit, R.M. Exner, K. Song, S.R.M.M. De Aguiar, H. Ge, C. Pourzand, S.J. Paisey, G. Kociok-Köhn, J.R. Dilworth, L. Carroll, S.I. Pascu, Functional, Aromatic, and Fluorinated Monothiosemicarbazones: Investigations into Their Structures

and Activity toward the Gallium-68 Incorporation by Microwave Irradiation, ACS Omega 7 (2022) 13750–13777. https://doi.org/10.1021/acsomega.1c07396.

[114] P. Munín, F. Lucio, A. Fernandez-Figueiras, F. Reigosa, J. Vila, M. Pereira, J. Ortigueira, Study, preparation and characterization of thiosemicarbazone ligands and their compounds, in: Proceedings of The 20th International Electronic Conference on Synthetic Organic Chemistry, MDPI, Sciforum.net, 2016: p. a051. https://doi.org/10.3390/ecsoc-20-a051.

[115] B. Shakya, P.N. Yadav, Thiosemicarbazones as Potent Anticancer Agents and their Modes of Action, MRMC 20 (2020) 638–661. https://doi.org/10.2174/1389557519666191029130310.

[116] M. Rani, J. Devi, B. Kumar, Thiosemicarbazones-based Co(II), Ni(II), Cu(II) and Zn(II) complexes: synthesis, structural elucidation, biological activities and molecular docking, Chem. Pap. 77 (2023) 6007–6027. https://doi.org/10.1007/s11696-023-02917-x.

[117] S. Priyarega, J. Haribabu, R. Karvembu, Development of thiosemicarbazone-based transition metal complexes as homogeneous catalysts for various organic transformations, Inorganica Chimica Acta 532 (2022) 120742. https://doi.org/10.1016/j.ica.2021.120742.

[118] S. Gupta, N. Singh, T. Khan, S. Joshi, Thiosemicarbazone derivatives of transition metals as multi-target drugs: A review, Results in Chemistry 4 (2022) 100459. https://doi.org/10.1016/j.rechem.2022.100459.

[119] I.D. Kostas, B.R. Steele, Thiosemicarbazone Complexes of Transition Metals as Catalysts for Cross-Coupling Reactions, Catalysts 10 (2020) 1107. https://doi.org/10.3390/catal10101107.

[120] J. Devi, B. Kumar, A. Dubey, A. Tufail, A. Boora, Exploring the antimalarial and antioxidant efficacy of transition metal(II) chelates of thiosemicarbazone ligands: spectral investigations, molecular docking, DFT, MESP and ADMET, Biometals 37 (2024) 247–265. https://doi.org/10.1007/s10534-023-00546-1.

[121] A. Panja, C. Campana, C. Leavitt, M.J.V. Stipdonk, D.M. Eichhorn, Iron and cobalt complexes of 2,6-diacetylpyridine-bis(R-thiosemicarbazone) (R=H, phenyl) showing unprecedented ligand deviation from planarity, Inorganica Chimica Acta 362 (2009) 1348–1354. https://doi.org/10.1016/j.ica.2008.06.031.

[122] G. Vuckovic, V. Stanic, S. Sovilj, M. Antonijevic-Nikolic, J. Mrozynski, Cobalt(II) complexes with aromatic carboxylates and N-functionalized cyclam bearing 2-

pyridylmethyl pendant arms, J Serb Chem Soc 70 (2005) 1121–1129. https://doi.org/10.2298/JSC0509121V.

[123] D. Palanimuthu, S.V. Shinde, K. Somasundaram, A.G. Samuelson, In Vitro and in Vivo Anticancer Activity of Copper Bis(thiosemicarbazone) Complexes, J. Med. Chem. 56 (2013) 722–734. https://doi.org/10.1021/jm300938r.

[124] T.K. Venkatachalam, P.V. Bernhardt, G.K. Pierens, D.H.R. Stimson, R. Bhalla, D.C. Reutens, Synthesis and Characterisation of Indium(III) Bis-Thiosemicarbazone Complexes: 18F Incorporation for PET Imaging, Aust. J. Chem. 72 (2019) 383. https://doi.org/10.1071/CH18559.

[125] E. López-Torres, A.R. Cowley, J.R. Dilworth, Reactivity of bisthiosemicarbazones with Sn(II) and Sn(IV): The synthesis and structure of an eight-coordinate complex with two bis(thiosemicarbazone) ligands, Inorganic Chemistry Communications 10 (2007) 724–727. https://doi.org/10.1016/j.inoche.2007.03.002.

[126] M.A. Green, D.L. Klippenstein, J.R. Tennison, Copper(II) Bis(thiosemicarbazone) Complexes as Potential Tracers for Evaluation of Cerebral and Myocardial Blood Flow with PET, (n.d.).

[127] M. Ghaemy, H. Mighani, H. Behmadi, Synthesis and characterization of novel Schiff-base polyamides from copper/benzil bisthiosemicarbazone complexes, J of Applied Polymer Sci 109 (2008) 2388–2394. https://doi.org/10.1002/app.28244.

[128] J.K. Lim, C.J. Mathias, M.A. Green, Mixed Bis(thiosemicarbazone) Ligands for the Preparation of Copper Radiopharmaceuticals: Synthesis and Evaluation of Tetradentate Ligands Containing Two Dissimilar Thiosemicarbazone Functions, J. Med. Chem. 40 (1997) 132–136. https://doi.org/10.1021/jm9605703.

[129] E. López-Torres, M.A. Mendiola, Orthometallated versus coordination compounds for reactions of platinum(II) and palladium(II) with the ligand benzil bis(4-methyl-3-thiosemicarbazone), Inorganica Chimica Acta 363 (2010) 1735–1740. https://doi.org/10.1016/j.ica.2010.03.014.

[130] J.K. Bilyj, J.R. Harmer, P.V. Bernhardt, Copper Complexes of Benzoylacetone Bis-Thiosemicarbazones: Metal and Ligand Based Redox Reactivity, Aust. J. Chem. 74 (2021) 34. https://doi.org/10.1071/CH20210.

[131] S.N. Pandeya, D. Sriram, G. Nath, E. DeClercq, Synthesis, antibacterial, antifungal and anti-HIV activities of Schiff and Mannich bases derived from isatin derivatives and N-[4-(4′-chlorophenyl)thiazol-2-yl] thiosemicarbazide, European Journal of Pharmaceutical Sciences 9 (1999) 25–31. https://doi.org/10.1016/S0928-0987(99)00038-X.

[132] A.R. Jalilian, M. Sadeghi, Y. Yari Kamrani, Development of [^{103} Pd]-labeled- *bis* (N^{4} -methylthiosemicarbazone) complexes as possible therapeutic agents, Radiochimica Acta 94 (2006) 865–869. https://doi.org/10.1524/ract.2006.94.12.865.

[133] H. Luo, P.E. Fanwick, M.A. Green, Synthesis and Structure of a Novel Cu(II) Complex with a Monoprotic Tetradentate Schiff Base Ligand, Inorg. Chem. 37 (1998) 1127–1130. https://doi.org/10.1021/ic9708632.

[134] A. Castiñeiras, E. Bermejo, L.J. Ackerman, H. Beraldo, D.X. West, Structural and spectral characterization of two bis{N(4)-alkylthiosemicarbazones} of 1-phenylglyoxal, Journal of Molecular Structure 477 (1999) 1–6. https://doi.org/10.1016/S0022-2860(98)00609-7.

[135] B.N. Bottenus, P. Kan, T. Jenkins, B. Ballard, T.L. Rold, C. Barnes, C. Cutler, T.J. Hoffman, M.A. Green, S.S. Jurisson, Gold(III) bis-thiosemicarbazonato complexes: synthesis, characterization, radiochemistry and X-ray crystal structure analysis, Nuclear Medicine and Biology 37 (2010) 41–49. https://doi.org/10.1016/j.nucmedbio.2009.08.003.

[136] C. González-García, C. García-Pascual, R. Burón, D.G. Calatayud, J. Perles, M.A. Mendiola, E. López-Torres, Structural variety, fluorescence and photocatalytic activity of dissymmetric thiosemicarbazone complexes, Polyhedron 223 (2022) 115945. https://doi.org/10.1016/j.poly.2022.115945.

[137] B.L. Geoghegan, J.K. Bilyj, P.V. Bernhardt, S. DeBeer, G.E. Cutsail, X-ray absorption and emission spectroscopy of $N_2S_2Cu(II)/(III)$ complexes, Dalton Trans. 53 (2024) 7828–7838. https://doi.org/10.1039/D4DT00085D.

[138] H.S. Seleem, B.A. El-Shetary, S.M.E. Khalil, M. Mostafa, M. Shebl, Structural diversity in copper(II) complexes of bis(thiosemicarbazone) and bis(semicarbazone) ligands, Journal of Coordination Chemistry 58 (2005) 479–493. https://doi.org/10.1080/00958970512331334269.

[139] A.A. Abou-Hussen, N.M. El-Metwally, E.M. Saad, A.A. El-Asmy, Spectral, magnetic, thermal and electrochemical studies on phthaloyl bis(thiosemicarbazide) complexes,

Journal of Coordination Chemistry 58 (2005) 1735–1749. https://doi.org/10.1080/00958970500262270.

[140] F.N. Akladios, S.D. Andrew, C.J. Parkinson, Cytotoxic activity of expanded coordination bis-thiosemicarbazones and copper complexes thereof, J Biol Inorg Chem 21 (2016) 931–944. https://doi.org/10.1007/s00775-016-1390-7.

[141] R.L. Arrowsmith, P.A. Waghorn, M.W. Jones, A. Bauman, S.K. Brayshaw, Z. Hu, G. Kociok-Köhn, T.L. Mindt, R.M. Tyrrell, S.W. Botchway, J.R. Dilworth, S.I. Pascu, Fluorescent gallium and indium bis(thiosemicarbazonates) and their radiolabelled analogues: Synthesis, structures and cellular confocal fluorescence imaging investigations, Dalton Trans. 40 (2011) 6238. https://doi.org/10.1039/c1dt10126a.

[142] A.I. Matesanz, J.M. Pérez, P. Navarro, J.M. Moreno, E. Colacio, P. Souza, Synthesis and characterization of novel palladium(II) complexes of bis(thiosemicarbazone). Structure, cytotoxic activity and DNA binding of Pd(II)-benzyl bis(thiosemicarbazonate), Journal of Inorganic Biochemistry 76 (1999) 29–37. https://doi.org/10.1016/S0162-0134(99)00105-1.

[143] S.A. Reddy, K.J. Reddy, S.L. Narayana, Y. Sarala, A.V. Reddy, Synthesis of New Reagent 2,6-Diacetylpyridine Bis-4-Phenyl-3-Thiosemicarbazone (2,6-DAPBPTSC): Selective, Sensitive and Extractive Spectrophotometric Determination of Co(II) in Vegetable, Soil, Pharmaceutical and Alloy Samples, Jnl Chinese Chemical Soc 55 (2008) 326–334. https://doi.org/10.1002/jccs.200800049.

[144] G.F.D. Sousa, V.M. Deflon, E. Niquet, A. Abras, Synthesis and characterization of heptacoordinated tin(IV) complexes. X-ray crystal structure of [nBu2Sn(dappt)]·(Me 2CO)0.5 [H2dappt = 2,6-diacetylpyridine bis(4-phenylthiosemicarbazone)], J. Braz. Chem. Soc. 12 (2001) 493–498. https://doi.org/10.1590/S0103-50532001000400009.

[145] K. Alomar, A. Landreau, M. Allain, G. Bouet, G. Larcher, Synthesis, structure and antifungal activity of thiophene-2,3-dicarboxaldehyde bis(thiosemicarbazone) and nickel(II), copper(II) and cadmium(II) complexes: Unsymmetrical coordination mode of nickel complex, Journal of Inorganic Biochemistry 126 (2013) 76–83. https://doi.org/10.1016/j.jinorgbio.2013.05.013.

[146] M. Maji, S. Ghosh, S.K. Chattopadhyay, [No title found], Transition Metal Chemistry 23 (1997) 81–85. https://doi.org/10.1023/A:1006914203028.

[147] P. Banerjee, O.P. Pandey, S.K. Sengupta, Microwave-assisted synthesis, spectroscopy and biological aspects of binuclear titanocene chelates of isatin-2,3-bis(thiosemicarbazones), Appl. Organometal. Chem. 23 (2009) 19–23. https://doi.org/10.1002/aoc.1464.

[148] D.-H. Lee, N.N. Murthy, K.D. Karlin, Copper(I)/Dioxygen Reactivity with Dinuclear Compounds: Catalytic Oxygenation and Oxo-Transfer to a Ketone, Inorg. Chem. 35 (1996) 804–805. https://doi.org/10.1021/ic951490c.

[149] A.I. Matesanz, C. Hernández, P. Souza, New bioactive 2,6-diacetylpyridine bis(p -chlorophenylthiosemicarbazone) ligand and its Pd(II) and Pt(II) complexes: Synthesis, characterization, cytotoxic activity and DNA binding ability, Journal of Inorganic Biochemistry 138 (2014) 16–23. https://doi.org/10.1016/j.jinorgbio.2014.04.017.

[150] B.S. Garg, V.K. Jain, Analytical applications of thiosemicarbazones and semicarbazones, Microchemical Journal 38 (1988) 144–169. https://doi.org/10.1016/0026-265X(88)90017-3.

[151] A.J.M. Al-Karawi, W. Clegg, R.W. Harrington, R.A. Henderson, Synthetic, structural and kinetic studies on the binding of cyclohexane-1,2-bis(4-methyl-3-thiosemicarbazone) to divalent metal ions (Co, Ni, Cu, Zn or Cd), Dalton Trans. (2009) 564–570. https://doi.org/10.1039/B814852J.

[152] A.I. Matesanz, P. Albacete, J. Perles, P. Souza, A structural and biological study on the new 3,5-diacetyl-1,2,4-triazol bis(p-chlorophenylthiosemicarbazone) ligand and its bimetallic complexes, Inorg. Chem. Front. 2 (2015) 75–84. https://doi.org/10.1039/C4QI00128A.

[153] N. Arefyeva, A. Sandleben, A. Krest, U. Baumann, M. Schäfer, M. Kempf, A. Klein, [2 × 2] Molecular Grids of Ni(II) and Zn(II) with Redox-Active 1,4-Pyrazine-Bis(thiosemicarbazone) Ligands, Inorganics 6 (2018) 51. https://doi.org/10.3390/inorganics6020051.

[154] R.N. Prabhu, R. Ramesh, Catalytic application of dinuclear palladium(II) bis(thiosemicarbazone) complex in the Mizoroki-Heck reaction, Tetrahedron Letters 53 (2012) 5961–5965. https://doi.org/10.1016/j.tetlet.2012.08.120.

[155] M. Jurić, B. Perić, N. Brničević, P. Planinić, D. Pajić, K. Zadro, G. Giester, B. Kaitner, Supramolecular motifs and solvatomorphism within the compounds $[M(bpy)_3]_2[NbO(C_2O_4)_3]Cl\cdot nH_2O$ ($M = Fe^{2+}$, Co^{2+}, Ni^{2+}, Cu^{2+} and Zn^{2+}; n = 11, 12). Syntheses,

structures and magnetic properties, Dalton Trans. (2008) 742–754. https://doi.org/10.1039/B707937K.

[156] L.J. Ackerman, P.E. Fanwick, M.A. Green, E. John, W.E. Running, J.K. Swearingen, J.W. Webb, D.X. West, Structural and spectral studies of copper(II) and nickel(II) complexes of pyruvaldehyde mixed bis{N(4)-substituted thiosemicarbazones}, Polyhedron 18 (1999) 2759–2767. https://doi.org/10.1016/S0277-5387(99)00173-4.

[157] M.L. Grieve, P.R.W.J. Davey, C.M. Forsyth, B.M. Paterson, The Synthesis of a Bis(thiosemicarbazone) Macrocyclic Ligand and the Mn(II), Co(II), Zn(II) and 68Ga(III) Complexes, Molecules 26 (2021) 3646. https://doi.org/10.3390/molecules26123646.

[158] R. Bhalla, J. Burt, A.L. Hector, W. Levason, S.K. Luthra, G. McRobbie, F.M. Monzittu, G. Reid, Complexes of aluminium, gallium and indium trifluorides with neutral oxygen donor ligands: Synthesis, properties and reactions, Polyhedron 106 (2016) 65–74. https://doi.org/10.1016/j.poly.2015.12.032.

[159] R. Pedrido, M.R. Bermejo, M.J. Romero, M. Vázquez, A.M. González-Noya, M. Maneiro, M.J. Rodríguez, M.I. Fernández, Syntheses and X-ray characterization of metal complexes with the pentadentate thiosemicarbazone ligand bis(4-N-methylthiosemicarbazone)-2,6-diacetylpyridine. The first pentacoordinate lead(II) complex with a pentagonal geometry, Dalton Trans. (2005) 572–579. https://doi.org/10.1039/B416296J.

[160] A. Guzman-Perez, R.T. Wester, M.C. Allen, J.A. Brown, A.R. Buchholz, E.R. Cook, W.W. Day, E.S. Hamanaka, S.P. Kennedy, D.R. Knight, P.J. Kowalczyk, R.B. Marala, C.J. Mularski, W.A. Novomisle, R.B. Ruggeri, W.R. Tracey, R.J. Hill, Discovery of zoniporide: A potent and selective sodium–hydrogen exchanger type 1 (NHE-1) inhibitor with high aqueous solubility, Bioorganic & Medicinal Chemistry Letters 11 (2001) 803–807. https://doi.org/10.1016/S0960-894X(01)00059-2.

[161] A.E.-G.E. Amr, N.A. Abdel-Latif, M.M. Abdalla, Synthesis and antiandrogenic activity of some new 3-substituted androstano[17,16-c]-5′-aryl-pyrazoline and their derivatives, Bioorganic & Medicinal Chemistry 14 (2006) 373–384. https://doi.org/10.1016/j.bmc.2005.08.024.

[162] V. Varun, S. Sonam, R. Kakkar, Isatin and its derivatives: a survey of recent syntheses, reactions, and applications, Med. Chem. Commun. 10 (2019) 351–368. https://doi.org/10.1039/C8MD00585K.

[163] K.S. Bose, R.H. Sarma, Delineation of the intimate details of the backbone conformation of pyridine nucleotide coenzymes in aqueous solution, Biochem Biophys Res Commun 66 (1975) 1173–1179. https://doi.org/10.1016/0006-291x(75)90482-9.

[164] W.A. Hendrickson, K.B. Ward, Atomic models for the polypeptide backbones of myohemerythrin and hemerythrin, Biochemical and Biophysical Research Communications 66 (1975) 1349–1356. https://doi.org/10.1016/0006-291X(75)90508-2.

[165] J.C. Cassatt, C.P. Marini, J.W. Bender, Reversible reduction of horse metmyoglobin by the iron(II) complex of trans-1,2-diaminocyclohexane-N,N,N',N'-tetraacetate, Biochemistry 14 (1975) 5470–5475. https://doi.org/10.1021/bi00696a014.

[166] F.E. Anderson, C.J. Duca, J.V. Scudi, Some Heterocyclic Thiosemicarbazones, J. Am. Chem. Soc. 73 (1951) 4967–4968. https://doi.org/10.1021/ja01154a501.

[167] S.G. Franzblau, R.S. Witzig, J.C. McLaughlin, P. Torres, G. Madico, A. Hernandez, M.T. Degnan, M.B. Cook, V.K. Quenzer, R.M. Ferguson, R.H. Gilman, Rapid, Low-Technology MIC Determination with Clinical *Mycobacterium tuberculosis* Isolates by Using the Microplate Alamar Blue Assay, J Clin Microbiol 36 (1998) 362–366. https://doi.org/10.1128/JCM.36.2.362-366.1998.

[168] A.S. Kolyva, P.C. Karakousis, Old and New TB Drugs: Mechanisms of Action and Resistance, (n.d.).

[169] G.S. Timmins, V. Deretic, Mechanisms of action of isoniazid, Molecular Microbiology 62 (2006) 1220–1227. https://doi.org/10.1111/j.1365-2958.2006.05467.x.

[170] H. Muğlu, Synthesis, characterization, and antioxidant activity of some new N4-arylsubstituted-5-methoxyisatin-β-thiosemicarbazone derivatives, Res Chem Intermed 46 (2020) 2083–2098. https://doi.org/10.1007/s11164-020-04079-x.

[171] S.A. Ross, G. Lowe, Downfield displacement of the NMR signal of water in deuterated dimethylsulfoxide by the addition of deuterated trifluoroacetic acid, Tetrahedron Letters 41 (2000) 3225–3227. https://doi.org/10.1016/S0040-4039(00)00355-5.

[172] G.R. Fulmer, A.J.M. Miller, N.H. Sherden, H.E. Gottlieb, A. Nudelman, B.M. Stoltz, J.E. Bercaw, K.I. Goldberg, NMR Chemical Shifts of Trace Impurities: Common Laboratory Solvents, Organics, and Gases in Deuterated Solvents Relevant to the Organometallic Chemist, Organometallics 29 (2010) 2176–2179. https://doi.org/10.1021/om100106e.

[173] P. Kaur, B. Lal, N. Kaur, G. Singh, A. Singh, G. Kaur, J. Singh, Selective two way Cd(II) and Co(II) ions detection by 1,2,3–triazole linked fluorescein derivative, Journal of Photochemistry and Photobiology A: Chemistry 382 (2019) 111847. https://doi.org/10.1016/j.jphotochem.2019.05.010.

[174] P. Saini, Sushma, G. Singh, G. Kaur, J. Singh, H. Singh, Copper (I)-catalyzed 'Quick Click' generated 1,2,3-triazole anthraquinone linkers for selective detection of Fe (II) ions, Inorganic Chemistry Communications 141 (2022) 109524. https://doi.org/10.1016/j.inoche.2022.109524.

[175] P. Banerjee, O.P. Pandey, S.K. Sengupta, Microwave-assisted synthesis, spectroscopy and biological aspects of binuclear titanocene chelates of isatin-2,3-bis(thiosemicarbazones), Applied Organometallic Chemistry 23 (2009) 19–23. https://doi.org/10.1002/aoc.1464.

[176] P. Banerjee, O.P. Pandey, S.K. Sengupta, Microwave-assisted synthesis, spectroscopy and biological aspects of binuclear titanocene chelates of isatin-2,3-bis(thiosemicarbazones), Applied Organom Chemis 23 (2009) 19–23. https://doi.org/10.1002/aoc.1464.

[177] S. Tripathi, A. Dey, M. Shanmugam, R.S. Narayanan, V. Chandrasekhar, Cobalt(II) Complexes as Single-Ion Magnets, in: V. Chandrasekhar, F. Pointillart (Eds.), Organometallic Magnets, Springer International Publishing, Cham, 2018: pp. 35–75. https://doi.org/10.1007/3418_2018_8.

[178] I. Ejidike, Cu(II) Complexes of 4-[(1E)-N-{2-[(Z)-Benzylidene-amino]ethyl}ethanimidoyl]benzene-1,3-diol Schiff Base: Synthesis, Spectroscopic, In-Vitro Antioxidant, Antifungal and Antibacterial Studies, Molecules 23 (2018) 1581. https://doi.org/10.3390/molecules23071581.

[179] M.C.S. Lourenço, M.V.N. de Souza, A.C. Pinheiro, M. de L. Ferreira, R.S.B. Gonçalves, T.C.M. Nogueira, M.A. Peralta, Evaluation of anti-tubercular activity of nicotinic and isoniazid analogues, Arkivoc 2007 (2007) 181–191. https://doi.org/10.3998/ark.5550190.0008.f18.

[180] J.A. Molina-Bolívar, F. Galisteo-González, C. Carnero Ruiz, M. Medina-O´ Donnell, A. Parra, Spectroscopic investigation on the interaction of maslinic acid with bovine serum albumin, Journal of Luminescence 156 (2014) 141–149. https://doi.org/10.1016/j.jlumin.2014.08.011.

[181] E. Guercia, C. Forzato, L. Navarini, F. Berti, Interaction of coffee compounds with serum albumins. Part II: Diterpenes, Food Chemistry 199 (2016) 502–508. https://doi.org/10.1016/j.foodchem.2015.12.051.

[182] G. Wang, D. Wang, X. Li, Y. Lu, Exploring the binding mechanism of dihydropyrimidinones to human serum albumin: Spectroscopic and molecular modeling techniques, Colloids and Surfaces B: Biointerfaces 84 (2011) 272–279. https://doi.org/10.1016/j.colsurfb.2011.01.016.

[183] J. Wang, C. Xiang, F.-F. Tian, Z.-Q. Xu, F.-L. Jiang, Y. Liu, Investigating the interactions of a novel anticancer delocalized lipophilic cation and its precursor compound with human serum albumin, RSC Adv. 4 (2014) 18205. https://doi.org/10.1039/c3ra46997b.

[184] A. Sułkowska, Interaction of drugs with bovine and human serum albumin, Journal of Molecular Structure 614 (2002) 227–232. https://doi.org/10.1016/S0022-2860(02)00256-9.

[185] M.R. Eftink, C.A. Ghiron, Fluorescence quenching studies with proteins, Analytical Biochemistry 114 (1981) 199–227. https://doi.org/10.1016/0003-2697(81)90474-7.

[186] I. Parveen, P. Khan, S. Ali, Md.I. Hassan, N. Ahmed, Synthesis, molecular docking and inhibition studies of novel 3-N-aryl substituted-2-heteroarylchromones targeting microtubule affinity regulating kinase 4 inhibitors, European Journal of Medicinal Chemistry 159 (2018) 166–177. https://doi.org/10.1016/j.ejmech.2018.09.030.

[187] P. Bourassa, S. Dubeau, G.M. Maharvi, A.H. Fauq, T.J. Thomas, H.A. Tajmir-Riahi, Locating the binding sites of anticancer tamoxifen and its metabolites 4-hydroxytamoxifen and endoxifen on bovine serum albumin, European Journal of Medicinal Chemistry 46 (2011) 4344–4353. https://doi.org/10.1016/j.ejmech.2011.07.005.

[188] R. Singh, G. Singh, N. George, G. Singh, P. Malik, H. Singh, G. Kaur, J. Singh, Unveiling the ion sensing capabailities of ‘click’ derived chalcone-tailored 1,2,3-triazolic isomers for Pb(II) and Cu(II) ions: DFT analysis, RSC Adv. 14 (2024) 15374–15390. https://doi.org/10.1039/D4RA01471E.

[189] I. Song, P. Torawane, J.-S. Lee, S.D. Warkad, A. Borase, S.K. Sahoo, S.B. Nimse, A. Kuwar, The detection of Al^{3+} and Cu^{2+} ions using isonicotinohydrazide-based chemosensors and their application to live-cell imaging, Mater. Adv. 2 (2021) 6306–6314. https://doi.org/10.1039/D1MA00564B.

[190] G. Singh, B. Lal, R. Singh, N. George, G. Singh, Diksha, G. Kaur, H. Singh, R.K. Tittal, G. Kaur, J. Singh, Ampyrone appended 1,2,3-triazole as selective fluorescent Cu(II) ion sensor: DFT and docking findings, Spectrochimica Acta Part A: Molecular and Biomolecular Spectroscopy 302 (2023) 123163. https://doi.org/10.1016/j.saa.2023.123163.

[191] K. Kaur, H. Mahajan, A. Sharma, I. Mohammaed, A.K. Srivastava, D. Basandrai, Manganese doped cobalt–nickel spinel ferrite via. sol–gel approach: Insight into structural, morphological, magnetic, and dielectric properties, Journal of Materials Research 38 (2023) 3837–3849. https://doi.org/10.1557/s43578-023-01119-1.

[192] I. Mohammed, J. Mohammed, A. Sharma, H. Mahajan, S. Sharma, M. Thakur, A. Kaur, N. Aggarwal, A.K. Srivastava, Structural, morphological, optical, magnetic, and microwave properties of La3+- Mn2+ substituted Zn2-Y-type barium-strontium hexaferrite, Chinese Journal of Physics 78 (2022) 377–390. https://doi.org/10.1016/j.cjph.2022.06.025.

[193] N. Sarı, S.Ç. Şahin, H. Öğütcü, Y. Dede, S. Yalcin, A. Altundaş, K. Doğanay, Ni(II)-tetrahedral complexes: Characterization, antimicrobial properties, theoretical studies and a new family of charge-transfer transitions, Spectrochimica Acta Part A: Molecular and Biomolecular Spectroscopy 106 (2013) 60–67. https://doi.org/10.1016/j.saa.2012.12.078.

[194] L.M. Venanzi, Tetrahedral complexes of nickel (II) and the factors determining their formation, Journal of Inorganic and Nuclear Chemistry 8 (1958) 137–142. https://doi.org/10.1016/0022-1902(58)80175-X.

[195] H.A. Benesi, J.H. Hildebrand, A Spectrophotometric Investigation of the Interaction of Iodine with Aromatic Hydrocarbons, J. Am. Chem. Soc. 71 (1949) 2703–2707. https://doi.org/10.1021/ja01176a030.

[196] G. Singh, Priyanka, A. Singh, P. Satija, Sushma, Pawan, Mohit, J. Singh, J. Singh, Schiff base-functionalized silatrane-based receptor as a potential chemo-sensor for the detection of Al^{3+} ions, New J. Chem. 45 (2021) 7850–7859. https://doi.org/10.1039/D1NJ00943E.

[197] G. Singh, J. Singh, S.S. Mangat, A. Arora, Synthetic approach towards ‘click’ modified chalcone based organotriethoxysilanes; UV-Vis study, RSC Adv. 4 (2014) 60853–60865. https://doi.org/10.1039/C4RA08724K.

[198] P. Saini, Sonika, G. Singh, G. Kaur, J. Singh, H. Singh, Robust and Versatile Cu(I) metal frameworks as potential catalysts for azide-alkyne cycloaddition reactions: Review, Molecular Catalysis 504 (2021) 111432. https://doi.org/10.1016/j.mcat.2021.111432.

[199] P. Kalra, R. Kaur, G. Singh, H. Singh, G. Singh, Pawan, G. Kaur, J. Singh, Metals as "Click" catalysts for alkyne-azide cycloaddition reactions: An overview, Journal of Organometallic Chemistry 944 (2021) 121846. https://doi.org/10.1016/j.jorganchem.2021.121846.

[200] G. Singh, Sushma, A. Singh, P. Satija, Shilpy, Mohit, Priyanka, J. Singh, A. Khosla, Schiff base derived bis-organosilanes: Immobilization on silica nanosphere and Cu2+ and Fe3+ dual ion sensing, Inorganica Chimica Acta 514 (2021) 120028. https://doi.org/10.1016/j.ica.2020.120028.

[201] G. Singh, J. Singh, S.S. Mangat, J. Singh, S. Rani, Chalcomer assembly of optical chemosensors for selective Cu^{2+} and Ni^{2+} ion recognition, RSC Adv. 5 (2015) 12644–12654. https://doi.org/10.1039/C4RA14329A.

[202] G. Singh, A. Majeed, R. Singh, N. George, G. Singh, S. Gupta, H. Singh, G. Kaur, J. Singh, CuAAC ensembled 1,2,3-triazole linked nanogels for targeted drug delivery: a review, RSC Adv. 13 (2023) 2912–2936. https://doi.org/10.1039/D2RA05592A.

[203] G. Singh, N. George, R. Singh, G. Singh, J.D. Kaur, G. Kaur, H. Singh, J. Singh, CuAAC-Derived Selective Fluorescent Probe as a Recognition Agent for Pb(II) and Hg(II): DFT and Docking Studies, ACS Omega 7 (2022) 39159–39168. https://doi.org/10.1021/acsomega.2c05050.

[204] P. Kaur, B. Lal, N. Kaur, G. Singh, A. Singh, G. Kaur, J. Singh, Selective two way Cd(II) and Co(II) ions detection by 1,2,3–triazole linked fluorescein derivative, Journal of Photochemistry and Photobiology A: Chemistry 382 (2019) 111847. https://doi.org/10.1016/j.jphotochem.2019.05.010.

[205] N. George, G. Singh, R. Singh, G. Singh, Priyanka, H. Singh, G. Kaur, J. Singh, Click modified bis-appended Schiff base 1,2,3-triazole chemosensor for detection of Pb(II)ion and computational studies, Journal of Molecular Structure 1288 (2023) 135666. https://doi.org/10.1016/j.molstruc.2023.135666.

[206] P. Saini, Sonika, G. Singh, G. Kaur, J. Singh, H. Singh, Robust and Versatile Cu(I) metal frameworks as potential catalysts for azide-alkyne cycloaddition reactions: Review, Molecular Catalysis 504 (2021) 111432. https://doi.org/10.1016/j.mcat.2021.111432.

[207] S.I. Hazarika, G. Mahata, P. Pahari, N. Pramanik, A.K. Atta, A simple triazole-linked bispyrenyl-based xylofuranose derivative for selective and sensitive fluorometric detection

of Cu2+, Inorganica Chimica Acta 507 (2020) 119582. https://doi.org/10.1016/j.ica.2020.119582.

[208] R. Selwin Joseyphus, M. Sivasankaran Nair, Synthesis, characterization and biological studies of some Co(II), Ni(II) and Cu(II) complexes derived from indole-3-carboxaldehyde and glycylglycine as Schiff base ligand, Arabian Journal of Chemistry 3 (2010) 195–204. https://doi.org/10.1016/j.arabjc.2010.05.001.

[209] I.M. Procter, B.J. Hathaway, P. Nicholls, The electronic properties and stereochemistry of the copper(II) ion. Part I. Bis(ethylenediamine)copper(II) complexes, J. Chem. Soc., A (1968) 1678. https://doi.org/10.1039/j19680001678.

[210] B.J. Hathaway, D.E. Billing, The electronic properties and stereochemistry of mono-nuclear complexes of the copper(II) ion, Coordination Chemistry Reviews 5 (1970) 143–207. https://doi.org/10.1016/S0010-8545(00)80135-6.

[211] U. Sakaguchi, A.W. Addison, Spectroscopic and redox studies of some copper(II) complexes with biomimetic donor atoms: implications for protein copper centres, J. Chem. Soc., Dalton Trans. (1979) 600. https://doi.org/10.1039/dt9790000600.

[212] D.E. Nikles, M.J. Powers, F.L. Urbach, Copper(II) complexes with tetradentate bis(pyridyl)-dithioether and bis(pyridyl)-diamine ligands. Effect of thio ether donors on the electronic absorption spectra, redox behavior, and EPR parameters of copper(II) complexes, Inorg. Chem. 22 (1983) 3210–3217. https://doi.org/10.1021/ic00164a009.

[213] L. Latheef, M.R.P. Kurup, Spectral and structural studies of copper(II) complexes of thiosemicarbazones derived from salicylaldehyde and containing ring incorporated at N(4)-position, Spectrochimica Acta Part A: Molecular and Biomolecular Spectroscopy 70 (2008) 86–93. https://doi.org/10.1016/j.saa.2007.07.015.

[214] E.B. Seena, M. Sithambaresan, S. Vasudevan, M.R.P. Kurup, Structural and spectral characterization of Cu(II) complexes of N(4)-substituted thiosemicarbazones derived from 2-hydroxyacetophenone: Crystal structure of a dinuclear Cu(II) complex, J Chem Sci 132 (2020) 149. https://doi.org/10.1007/s12039-020-01845-7.

[215] M.R. Eftink, C.A. Ghiron, Fluorescence quenching studies with proteins, Analytical Biochemistry 114 (1981) 199–227. https://doi.org/10.1016/0003-2697(81)90474-7.

[216] P. Bourassa, S. Dubeau, G.M. Maharvi, A.H. Fauq, T.J. Thomas, H.A. Tajmir-Riahi, Locating the binding sites of anticancer tamoxifen and its metabolites 4-hydroxytamoxifen

and endoxifen on bovine serum albumin, European Journal of Medicinal Chemistry 46 (2011) 4344–4353. https://doi.org/10.1016/j.ejmech.2011.07.005.

[217] J.A. Molina-Bolívar, F. Galisteo-González, C. Carnero Ruiz, M. Medina-O´ Donnell, A. Parra, Spectroscopic investigation on the interaction of maslinic acid with bovine serum albumin, Journal of Luminescence 156 (2014) 141–149. https://doi.org/10.1016/j.jlumin.2014.08.011.

[218] M.R. Eftink, C.A. Ghiron, Fluorescence quenching studies with proteins, Analytical Biochemistry 114 (1981) 199–227. https://doi.org/10.1016/0003-2697(81)90474-7.

[219] G. Singh, R. Singh, N. George, G. Singh, Sushma, G. Kaur, G. Kaur, H. Singh, J. Singh, 'Click'-synthesized PET based fluorescent sensor for Hg(II), Pb(II) and Cr(III) recognition: DFT and docking studies, Journal of Photochemistry and Photobiology A: Chemistry 441 (2023) 114741. https://doi.org/10.1016/j.jphotochem.2023.114741.

[220] N.M. Mohd Shahrani, R.S. Azis, M. Hashim, H. Jumiah, Z. Azmi, N. Daud, Effect of Variation Sintering Temperature on Magnetic Permeability and Grain Sizes of $Y_3Fe_5O_{12}$ via Mechanical Alloying Technique, MSF 846 (2016) 395–402. https://doi.org/10.4028/www.scientific.net/MSF.846.395.

[221] T. Arun, M. Vairavel, S. Gokul Raj, R. Justin Joseyphus, Crystallization kinetics of Nd-substituted yttrium iron garnet prepared through sol–gel auto-combustion method, Ceramics International 38 (2012) 2369–2373. https://doi.org/10.1016/j.ceramint.2011.10.090.

[222] Synthesis, characterization, molecular docking and antibacterial activities of Bis-[(E)-3{2-(1-4-chlorophenyl) ethylidiene}hydrazinyl]-N-(4-methylphenyl)-3-oxopropanamideZinc (II) complex, IJBB (2022). https://doi.org/10.56042/ijbb.v59i1.41323.

LIST OF PUBLICATIONS

(1) Ain, Q. U.; Sharma, R. Structure and Bonding Trends of Bisthiosemicarbazones: An Overview. *Applied Organom Chemis* **2023**, *37* (6), e7100. https://doi.org/10.1002/aoc.7100.

(2) Ain, Q. U.; Singh, I.; Carmieli, R.; Savci, A.; Paul, K.; Sharma, R. Substituted 2,5 Thiophene Dicarboxaldehyde Bisthiosemicarbazones and Their Copper(II) Complexes: Synthesis, Structure Elucidation, HSA Binding, Biological Activities and Docking Studies. *Journal of Molecular Structure* **2023**, *1291*, 135996. https://doi.org/10.1016/j.molstruc.2023.135996.

(3) Ain, Q. U.; Singh, A.; Singh, I.; Carmieli, R.; Sharma, R. Synthesis, Characterization and Anti-Tubercular Activities of Copper(II) Complexes of Substituted 2,3-Isatin Bisthiosemicarbazones: An Experimental and Theoretical Approach. *Results in Chemistry* **2023**, *6*, 101171. https://doi.org/10.1016/j.rechem.2023.101171.

(4) Ain, Q. U.; Insha, S.; Sharma, R. Synthesis, Characterization and Anti-Tubercular Activity of Substituted Thiosemicarbazones and Their Ni(II) Complexes. *Clinical Medicine* **2021**, *08* (03).

LIST OF CONFERENCES

1. Q.U.Ain, R.Sharma. Cobalt(II) complexes of heterocyclic 2,5 thiophene dicarboxaldehyde bisthiosemicarbazones as potential anti-tubercular agents. **5th International Conference on Recent Advances in Fundamental and Applied Sciences (**19th-20th, April 2024 | Lovely Professional University, Punjab).

2. Q.U.Ain, R.Sharma. Synthesis, spectroscopy and evaluation of biological activities of substituted 2,3 isatin bisthiosemicarbazones with Copper(II) complexes. **4th International Conference on Recent Advances in Fundamental and Applied Sciences (**24th-25th, March 2023 | Lovely Professional University, Punjab).

3. Q.U.Ain, R.Sharma. Structural and spectral studies of cobalt(II) and copper(II) complexes of substituted 2,3-isatin bisthiosemicarbazones. **International Conference on Feminine Hygiene Management- Beyond Taboo (**25th-26th, November 2022 | Lovely Professional University, Punjab).

4. Q.U.Ain, R.Sharma. Synthesis and Structural Characterization of metal complexes of heterocyclic based ligand bisthiosemicarbazones. **International Conference on Emerging Materials for sustainable development** (9th-11th, October 2022 | CSIR- CSIO, Chandigarh).

5. Q.U.Ain, R.Sharma. Synthesis and Spectroscopic Characterization of Substituted Isatin Bisthiosemicarbazones. **International Conference on Materials for Emerging Technologies** (18th-19th, February 2022 | Lovely Professional University, Punjab).